UNIVERSITÀ DELLA
CALABRIA

UNIVERSITA' DELLA CALABRIA

Dipartimento di Farmacia e Scienze della Salute e della Nutrizione

Dottorato di Ricerca in

Medicina Traslazionale

CICLO

XXXIII

TITOLO TESI

APPLICATION OF COMPUTATIONAL METHODOLOGIES
TOWARD THE IDENTIFICATION OF NOVEL THERAPEUTICS
AND PHOTODEGRADATION STUDIES
FOR THE DESIGN OF LIGHT-STABLE FORMULATIONS

Settore Scientifico Disciplinare CHIM/08

Coordinatore: Prof. Sebastiano Andò

Supervisori: Dott.ssa Fedora Grande

Dott.ssa Giuseppina Ioele

Dottoranda: Dott.ssa Maria Antonietta Occhiuzzi

CONTENTS

PREFACE

Despite the remarkable progress made in the fields of biology, chemistry and pharmacology during the past years, there is still a lasting need to develop effective therapeutics for the treatment of several diseases such as cancer, cardiovascular or metabolic disorders. Collaborative, multidisciplinary research has led to new concepts to design newer pharmaceutical agents with high potency, hight light-stability and few side effects. The discovery of a new drug is thus a consequence of the combination of several convergent approaches such as SAR studies, development of synthetic and biological procedures, and also serendipitous factors. In addition, computational techniques are nowdays of great help in the discovery process of new clinical drug candidates. It is therefore possible, for example, to *in silico* establish the modalities of interaction, in terms of affinity, for a small molecule to bind to a macromolecule.

The overall goals of part of the herein reported research work have been the design and synthesis of small molecules and the identification of compounds of either natural or synthetic origin endowed with pharmacologic activity, with the help of computational studies. Photodegradation studies aimed to the evaluation of drug stability under different conditions represent another topic herein developed.

The project thus resulted in the synergy of medicinal and analytical chemistry techniques. In particular, during the first year of the doctorate course, advanced computational techniques have been applied toward the identification of novel antiviral compounds. Part of these studies have been carried out at the molecular modeling laboratory of the School of Pharmacy and Pharmaceutical Sciences at Cardiff University, UK. The second and third year were focused on the development of simple and innovative methods for the synthesis of novel compounds endowed with anti-inflammatory activity, useful for topical application after their inclusion into specific photoprotective delivery systems. The capability of small molecules of natural origin to interact with selected targets implicated in different pathologies were also evaluated through molecular docking studies.

Accordingly, this thesis includes three main chapters:

- Application of advanced computational techniques toward the identification of natural and synthetic compounds and investigation of their mechanism of action. This topic resulted in five papers published on peer-reviewed journals and further computational experiments will be reported in a paper under preparation.

- Photodegradation studies of newly synthesized compounds and known photosensitive drugs and application of supramolecular system for their photoprotection. This chapter includes three papers published on peer-reviewed journals.

- Study of small molecules endowed with biological properties. In this chapter are reported five papers published on peer-reviewed journals.

CHAPTER 1

APPLICATION OF ADVANCED COMPUTATIONAL TECHNIQUES TOWARD THE IDENTIFICATION OF NATURAL AND SYNTHETIC COMPOUNDS AND INVESTIGATION OF THEIR MECHANISM OF ACTION

1. Introduction

The search to find a pharmacological remedy usually consists in developing a way to regulate the function of a molecular target whose activity is altered, restoring in this way the physiological conditions [1–3].

The molecular targets of drugs are essentially represented by nucleic acids and proteins. The latters, however, are the most common ones due to their catalytic properties able to properly regulate most functions of the body [4–7].Once a relation between an altered molecule function and a disease has been established, the next step of the drug discovery process consists in the search for a compound capable of binding the target and modifying its activity without significantly altering any other cellular property [8]. This compound is called "hit", and its identification usually requires the screening of a huge number of compounds (high-throughput assays) from either natural and synthetic products or virtual databases. The identified "hit" thus become "lead compound" that is in turn chemically modified to improve pharmacokinetics and pharmacodynamic properties. At this point, the compound is subjected to various phases of preclinical and clinical experimentation in order to hopefully become a drug.

Unfortunately, the discovery of a drug is far from being a simple process and the whole path presents many pitfalls. In fact, the development of a new drug, starting from target identification till the approval for marketing, is a high-risk, cost and time demanding enterprise (more than 95% of the developed substances fail to reach the market as a new medicine). The entire process, which involves a variety of scientific disciplines, including biology, chemistry and pharmacology, usually takes over 12 years or longer, and the cost has been estimated to be around 2.6 billion of dollars [9,10]. One of the major hurdles in a drug discovery program remains the identification of a drug candidate able to selectively interact with a specific molecular target to achieve the desired therapeutic action, while minimizing potential side effects.

The considerable advances made in recent years by genomics and proteomics have allowed the discovery and characterization of many biological macromolecules involved in the emergence and progression of diseases and have provided bases for a rational approach to drug development. One of the most interesting aspects of modern research is the attempt to effectively integrate conventional approaches with new computational methodologies in order to make the drug discovery process more efficient in terms of cost and time.

The improvement in technologies related to crystallography, combinatorial chemistry, and high-performance screening procedures, has made possible to get an ever-increasing number of three-dimensional structures of molecular targets as well as many libraries of chemical compounds. Furthermore, through computational studies, it is possible to virtually anticipate the three-dimensional structure of an intermolecular complex between a potential drug and its therapeutic target, also defining which of the possible conformations is the most effective. This helps to establish whether a therapeutic action is plausible, as the drug-target interaction is necessary for the physiological response.

The technologies currently available provide reliable theoretical calculations to estimate the binding affinity of a ligand within a target biomacromolecule. However, although the affinity of a compound for a target molecule is a prerequisite of an effective interaction, it is not a condition sufficient to guarantee a therapeutic effect.

Therefore, theoretical predictions always need to be proved by biological experiments to confirm the action and the mechanism for an active compound.

2. Methods

2.1. Molecular Docking

During the first phase of a drug discovery project, virtual screening is a valid, alternative or complementary approach to high-throughput screening, to rapidly analyze many (even millions) compounds. It is particularly useful for the identification of molecules able to interact with new targets for which no leads are yet available [11]. On the other hand, molecular docking is a computational procedure that became more and more useful over time due to the availability of an increasing number and an improved resolution of 3D X-ray and NMR structures of molecular targets, now reported in the Protein Data Bank (PDB) [12]. These techniques in combination aim to predict the behaviour of small molecules in the binding pockets of target proteins, determining the most favorable orientation of the ligand toward the macromolecular target in together form a stable complex, and also predicting the binding affinity. The determination of the correct conformation of a small molecule ligand interacting with a target macromolecule is the first step of the drug design process and the study of the mechanism of action for a drug candidate.

Docking methods fit a ligand into a binding site by combining and optimizing variables like steric, hydrophobic and electrostatic complementarity, and also estimating the energy of binding (scoring). Based on the types of molecules involved, docking can be classified as protein–small molecule, protein–nucleic acid or protein–protein docking.

Protein–small molecule docking represents the simplest approach and there are many available and efficient computational programs that are useful to predict whether a compound is able to bind a macromolecule or not. The theoretical assumption is that the recognition of a ligand by a receptor relies on their spatial shape matching and a favourable binding energy [13].

The first step consists of the X-ray structure selection of the target from the PDB, where the protein is usually co-crystallized with a known ligand, or alternatively it can be obtained from molecular dynamics simulations or through the use of specific modelling software. The successive step is to determine the set of all possible conformations and orientations of the ligand in the complex, and calculate the interactions by a scoring function [14]. The accuracy of the prediction of the interaction mode between a ligand and the target molecule is crucial for the quality and the relevance of data that will be obtained.

One of the main goals of molecular docking is the identification of the most energetically favourable conformation of a ligand in the binding site of the target molecule. The stability of a complex depends on the number and type of interactions that occur between a ligand and its target. Furthermore, the more negative the binding energy, the better is the ligand interaction.

However, it must be considered that the target macromolecule in molecular docking is implicitly considered as a rigid model, and this generally represents one of the main limitations of the currently available computational techniques. In fact, proteins are not static models, but they possess their own non-random internal dynamics. As a consequence, the presence and the interaction with a ligand can induce conformational modifications of the macromolecule to better accommodate the ligand itself. However, for practical purposes, it is assumed that the protein has a rigid structure, while changes in the degrees of freedom are taken into account for the ligand, resulting in variations of dihedral angles around the different chemical bonds that allow rotation. All the conformations obtained for the ligand anchored to the receptor are called "poses".

Therefore, to guarantee a computational efficiency, while the structure of the small molecule ligand can freely change conformation, the target macromolecules is maintained rigid (or at least only a few of its rotatable amino acid residues are considered) [15].

The intermolecular interactions accounted as significant in the evaluation of the affinity between a ligand and its target are of different types and include:

- hydrogen bonds;
- ion and dipole interactions;
- van der Waals forces;
- hydrophobic interactions.

The basic principle of molecular docking methods thus consists in placing a ligand into a binding site of a target macromolecule by combining and optimizing several variables such as steric, hydrophobic and electrostatic complementarity, and giving an approximate estimation of the binding free energy [16]. Accordingly, a docking program is based on two main components: i) the sampling algorithm, to generate the highest number of conformations of the ligand compatible with the receptor structure, ii) the scoring function, to evaluate in terms of binding energy all the ligand-target virtual conformations. The latter helps to identify the better conformation able to fit into the receptor structure and to evaluate the affinity between the target and the ligand. Over the past years, several sampling algorithms have been developed. The main difference among them consists of the number of degrees of freedom ignored and the time required to identify a conformation that best matches in the receptor structure of millions of compounds in a given computational time. These algorithms are supplemented by scoring functions that estimate the binding energy in the formation of the complex by means of different assumptions and simplifications. This aim to get a value very close to the real binding energy in a time as short as possible. The most common scoring functions are based on an adequate balance between accurate estimation of binding energy and computational cost in terms of time [17]. From the analysis of the simulation data, it is possible to predict the docked orientation which most accurately represents the "true" structure of the intermolecular complex and thus which is the most plausible mode of interaction between a ligand and a target macromolecule.

From this consideration, it becomes possible to hypothesize a biological activity of the ligand: if a compound is able to bind the active site or an allosteric site of a molecule involved in a specific disorder, this capability could suggest its potential as a drug candidate [18].

2.2. Virtual screening

Virtual screening (VS) is a set of computational methods referring to protein based *in silico* screening procedures widely used toward the rationalization of the drug discovery process. The main goal of VS consists in the reduction of the huge quantity of small molecules to be synthesized or screened from large libraries of chemical structures, that are most likely to bind to a specific target protein, leading to a limited number of leads with a high chance to become drug candidates.

VS is based on a multistep screening computational approach to filter compound libraries according to several parameters including structural features, drug likeness, pharmacokinetic profile, availability of pharmacophore models and capability of compounds to bind a target protein calculated by automated docking procedures [19].

There are two main approaches of VS: ligand-based virtual screening (LBVS) and structure-based virtual screening (SBVS).

LBVS relies on the statement that molecules sharing a similar chemical skeleton, may have a comparable biological activity on the same target [20]. The molecule can be considered within its 2D or 3D structure. Thus, the technique based on the QSAR (quantitative structure activity relationship) considers 2D similarity between a significant set of ligands with known activity, that is compared with a statistical model to predict the activity of new compounds.

Another technique is the generation of a 3D pharmacophore model, which is built by exploring the minimum necessary structural features that a potential analog must possess to bind the biological target. The pharmacophore model concerns the position of important functional groups in the space, as well as the interatomic distances between these functional groups and the type of non-covalent interactions. It can be built by an approach based on the chemical structure of the ligand or by mapping the active site of a co-crystallised protein, after evaluating the interactions between the ligand and the protein. The latter method is generally preferred to perform the shape-based virtual screening.

SBVS relies on the knowledge of the crystal structure of the biological target. The identification of the protein binding siteis the first step of SBVS. The binding site can be more easily identified when a ligand has already been co-crystallised with the protein. After the identification of the active site, a library of compounds is docked into it. Along with the prediction of the binding mode, SBVS provides a ranking of dockable molecules. Since several structures of a target macromolecule can be available, the selection of the most suitable one is mostly based on the conformational changes that may occur when a ligand is co-crystallised with the protein, comparing this structure with the one of the wild-type protein. Then, the selected structure undergoes several procedures to properly be considered for the molecular docking studies. Afterwards, the database compounds are docked into the protein binding site and screened according to software algorithms based on energetic parameters. Compounds with a high scoreare then selected as potential ligands.

Finally, throught the visual inspection of the docking results, starting from hundreds or thousands of small molecules it is possible to select a final limited number of possible hit-like compounds to be screened in *in vitro* tests. However, this last step, crucial to rationalize the analysis and the screening of hit compounds, mostly depend on chemical intuition, knowledge and experience of the operator.

In conclusion, although as already mentioned the activity of a compound against off-target proteins predicted in *in silico* screens needs to be confirmed by biological trials, the numerous advantages of computational techniques in the drug discovery process cannot be neglected playing a pivotal role in rationalizing the route towards drug design and development [21].

3. Results Summary

This first part of the thesis describes the results obtained through molecular docking studies. Selected compounds of natural or synthetic origin have been investigated, in order to establish their capability to interact with specific biological targets, involved in different pathologies.

In particular, in the first paper, two structurally related homoisoflavones isolated from *Leopoldia comosa* (L.) Parl. (*L. comosa*), a perennial bulbous plant similar to a small wild onion, have been studied as potential hormonal substitutes or complements for cancer treatment. Together with a preliminary assessment of the biological properties of the selected compounds, their capability to interact with the active site of estrogen receptors has been investigated through molecular docking studies. The results provide evidence of the potential of these compounds to bind both the two different estrogen receptor (ER) subtypes mainly expressed in mammals, ERα and ERβ, by forming significant interactions with key residues of the protein active sites.

These evidences suggest that these compounds represent suitable leads for the development of novel probes to be used in studies aimed at dissecting ERs signalling toward the development of new pharmacological tools useful in hormone-sensitive cancers treatment.

In a second work, the antioxidant potential of the extract of Tacle®, a hybrid citrus species, has been investigated. This fruit, obtained from the crossbreeding of Clementine and Tarocco tetraploids, recently gained an increasing interest due to its commercial value and nutraceutical properties. In fact, the high content in polyphenols confers to its extracts a protective activity against oxidative agents involved in several degenerative disorders. The extracts are in fact rich in naringin and hesperidin, whose antioxidant, lipid lowering and hypoglycemic activities are well known. In the study, the properties of Tacle pulp, peels and leaves extracts were tested in order to evaluate not only the nutraceutical potential of the edible fraction of the fruits, but also the potential utility of the waste left after agro-food procedures.

The antioxidant activity of Tacle extracts, as well as the inhibitory activity against human amilase and lipase enzymes involved in the metabolism of carbohydrates and lipids, respectively, have been proved in specific *in vitro* assay. These particular features could be ascribed to the relevant content in naringin and hesperidin glycosides. The corresponding aglycones, naringenin and hesperetin, have been investigated for the determination of their binding mode within the pancreatic amilase and pancreatic enzymes active site by molecular docking, on the basis of some available crystallographic enzyme structures.

The overall results showed a peculiar nutraceutical profile of Tacle, suggesting that a dietary enrichment with its extracts could be useful in the complementary treatment of metabolic disorders such as obesity and diabetes, as assessed by *in vivo* experiments on rats, after an accurate standardization in their polyphenol content. Furthermore, assays performed on leaves and peel of the fruit proved that active phytochemicals, to be included into nutraceutical formulations, could be recovered with a high yield, after simple extraction procedures from agro-food processes waste.

In a third paper, describing a part of research focused on the identification of natural compounds as drug leads, the capability of cryptotanshinone and tanshinone IIA, two compounds isolated from *Salvia miltiorrhiza* Bunge, has been investigated by *in vitro* biological assay as inhibitors of pancreatic lipase enzyme. This property has been confirmed by *in silico* studies. Docking experiments, carried out on the crystallographic structure of the enzyme, demonstrated that both compounds were able to interact with the key residues of the protein active site, therefore they should be able to prevent the access of the natural ligand to the catalytic site.

All these findings provided new insights into the understanding of the interactions between natural constituents of *S. miltiorrhiza* extract and pancreatic lipase. The studied compounds could then represent suitable leads for the development of new effective inhibitors useful for the management of obesity and related disorders.

Other studies have been carried out on compounds of synthetic origin as potential ligands and modulators of proteins involved in human disorders.

Accordingly, in a fourth paper, the anticancer potential of a new class of benzothienoquinazolinone compounds using Ellipticine as a lead was investigated. The carbazole moiety and the pyridine ring present in the reference compound have been replaced by a dibenzothiophene and a pyrimidine, respectively, leading to the new series of benzothienoquinazolinones. The synthesized compounds were investigated for their anticancer activity against two breast cancer cell lines. Two of the new compounds exerted an interesting antitumor profile against MDA-MB-231 cancer cells, without any cytotoxic effect on healthy cells, and have been selected for further investigation. These compounds

were proved to act as dual inhibitors of tubulin and human topoisomerase enzyme, as predicted by *in silico* studies.

A fifth paper included in this section describes the physiological and biochemical properties of Cateslytin (Ctl), an endogenous antimicrobial peptide, on H9c2 cardiomyocytes exposed to lipopolysaccharide infection. Both enantiomers of Cateslytin significantly increased cardiomyocytes viability following infection, the *L* isomer being more effective than the *D* one. Molecular analyses indicated that *L*-Ctl enantiomer directly binds the partner protein MD-2*L*-Ctl, modulating TLR4 activity. Overall, the results obtained suggest that Ctl could be considered as a plausible candidate for the development of new antimicrobials strategies in the treatment of myocarditis.

Finally, in the last paragraph, the results of computational experiments focusing on the identification, throughout VS approach, of compounds able to bind the NS5 polymerase protein of Tick-borne Encephalitis Virus (TBE) are described. In this study, through the application of advanced computational techniques, the polymerase protein model has been developed through the application of advanced computational tecniques. High-throughput virtual screening (HTVS) docking procedures were then applied to screen several compound libraries (90 milions compounds), leading to 17 thousand compounds. Successively, visual inspection allows the selection of 25 compounds as potential anti-TBEV agents. Biological *in vitro* studies are undergoing to assess the biological properties of the selected molecules.

References

[1] Zhong, H.; Neubig, R.R. Regulator of G protein signaling proteins: Novel multifunctional drug targets. *J. Pharmacol. Exp. Ther.* 2001, *297*, 837–845.

[2] Gershell, L.J.; Atkins, J.H. A brief history of novel drug discovery technologies. *Nat. Rev. Drug Discov.* 2003, *2*, 321–327, doi:10.1038/nrd1064.

[3] Zheng, C.J.; Han, L.Y.; Yap, C.W.; Xie, B.; Chen, Y.Z. Trends in exploration of therapeutic targets. *Drug News Perspect.* 2005, *18*, 109–127.

[4] Swinney, D.C. Biochemical mechanisms of drug action: What does it take for success? *Nat. Rev. Drug Discov.* 2004, *3*, 801–808, doi:10.1038/nrd1500.

[5] Cohen, P. Protein kinases - The major drug targets of the twenty-first century? *Nat. Rev. Drug Discov.* 2002, *1*, 309–315, doi:10.1038/nrd773.

[6] Lappano, R.; Maggiolini, M. G protein-coupled receptors: Novel targets for drug discovery in cancer. *Nat. Rev. Drug Discov.* 2011, *10*, 47–60.

[7] Santos, R.; Ursu, O.; Gaulton, A.; Bento, A.P.; Donadi, R.S.; Bologa, C.G.; Karlsson, A.; Al-Lazikani, B.; Hersey, A.; Oprea, T.I.; et al. A comprehensive map of molecular drug targets. *Nat. Rev. Drug Discov.* 2016, *16*, 19–34, doi:10.1038/nrd.2016.230.

[8] Muntha, P. Drug Discovery & Development - A Review. *Res. Rev. Pharm. Pharm. Sci.* 2016, *5*, 135–142.

[9] DiMasi, J.A.; Grabowski, H.G.; Hansen, R.W. Innovation in the pharmaceutical industry: New estimates of R&D costs. *J. Health Econ.* 2016, *47*, 20–33, doi:10.1016/j.jhealeco.2016.01.012.

[10] Tufts CSDD Cost to Develop and Win Marketing Approval for a New Drug Is $2.6 Billion. *Tufts CSDD* 2014, *19*, 1–7.

[11] Alvarez, J.C. High-throughput docking as a source of novel drug leads. *Curr. Opin. Chem. Biol.* 2004, *8*, 365–370.

[12] Berman, H.M.; Westbrook, J.; Feng, Z.; Gilliland, G.; Bhat, T.N.; Weissig, H.; Shindyalov, I.N.; Bourne, P.E. The Protein Data Bank. *Nucleic Acids Res.* 2000, *28*, 235–242.[

[13] Rizzuti, B.; Grande, F. Virtual screening in drug discovery: a precious tool for a still-demanding challenge. In *Protein Homeostasis Diseases*; Elsevier, 2020; pp. 309–327.

[14] Understanding the Basics of QSAR for Applications in Pharmaceutical Sciences and Risk Assessment - 1st Edition Available online: https://www.elsevier.com/books/understanding-the-basics-of-qsar-for-applications-in-pharmaceutical-sciences-and-risk-assessment/roy/978-0-12-801505-6 (accessed on Apr 16, 2021).

[15] Friesner, R.A.; Murphy, R.B.; Repasky, M.P.; Frye, L.L.; Greenwood, J.R.; Halgren, T.A.; Sanschagrin, P.C.; Mainz, D.T. Extra precision glide: Docking and scoring incorporating a model of hydrophobic enclosure for protein-ligand complexes. *J. Med. Chem.* 2006, *49*, 6177–6196, doi:10.1021/jm051256o.

[16] Diller, D.J.; Merz, K.M. High throughput docking for library design and library prioritization. *Proteins Struct. Funct. Genet.* 2001, *43*, 113–124, doi:10.1002/1097-0134(20010501)43:2<113::AID-PROT1023>3.0.CO;2-T.

[17] Liao, C.; Sitzmann, M.; Pugliese, A.; Nicklaus, M.C. Software and resources for computational medicinal chemistry. *Future Med. Chem.* 2011, *3*, 1057–1085.

[18] Lin, X.; Li, X.; Lin, X. A review on applications of computational methods in drug screening and design. *Molecules* 2020, *25*.

[19] Tondi, D.; Slomczynska, U.; Costi, M.P.; Watterson, D.M.; Ghelli, S.; Shoichet, B.K. Structure-based discovery and in-parallel optimization of novel competitive inhibitors of thymidylate synthase. *Chem. Biol.* 1999, *6*, 319–331, doi:10.1016/S1074-5521(99)80077-5.

[20] Ripphausen, P.; Nisius, B.; Bajorath, J. State-of-the-art in ligand-based virtual screening. *Drug Discov. Today* 2011, *16*, 372–376.

[21] Sethi, A.; Joshi, K.; Sasikala, K.; Alvala, M. Molecular Docking in Modern Drug Discovery: Principles and Recent Applications. In *Drug Discovery and Development - New Advances*; IntechOpen, 2020.

I. IDENTIFICATION BY MOLECULAR DOCKING OF HOMOISOFLAVONES FROM *LEOPOLDIA COMOSA* AS LIGANDS OF ESTROGEN RECEPTORS

Fedora Grande [1]; Bruno Rizzuti [2]; Maria Antonietta Occhiuzzi [1]; Giuseppina Ioele [1]; Teresa Casacchia [1]; Fabrizio Gelmini [3]; Rita Guzzi [2,4]; Antonio Garofalo [1]; Giancarlo Statti [1]

[1] Department of Pharmacy, Health and Nutritional Sciences, University of Calabria, Ampl. Polifunzionale, Via P. Bucci, 87036 Rende (CS), Italy;
[2] CNR-NANOTEC, Licryl-UOS Cosenza and CEMIF.Cal, Department of Physics, University of Calabria, Via P. Bucci, 87036 Rende (CS), Italy;
[3] Department of Environmental Science and Policy–ESP, University of Milan, Via Celoria 2, 20133 Milan, Italy;
[4] Department of Physics, University of Calabria, Via P. Bucci, 87036 Rende (CS), Italy.

Abstract:
The physiological responses to estrogen hormones are mediated within specific tissues by at least two distinct receptors, ERα and ERβ. Several natural and synthetic molecules show activity by interacting with these proteins. In particular, a number of vegetal compounds known as phytoestrogens shows estrogenic or anti-estrogenic activity. The majority of these compounds belongs to the isoflavones family and the most representative one, genistein, shows antiproliferative effects on various hormone-sensitive cancer cells, including breast, ovarian and prostate cancer. In this work we describe the identification of structurally related homoisoflavones isolated from *Leopoldia comosa* (L.) Parl. (*L. comosa*), a perennial bulbous plant, potentially useful as hormonal substitutes or complements in cancer treatments. Two of these compounds have been selected as potential ligands of estrogen receptors (ERs) and the interaction with both isoforms of estrogen receptors have been investigated through molecular docking on their crystallographic structures. The results provide evidence of the binding of these compounds to the target receptors and their interactions with key residues of the active sites of the two proteins, and thus they could represent suitable leads for the development of novel tools for the dissection of ER signaling and the development of new pharmacological treatments in hormone-sensitive cancers.

Keywords: natural compounds; molecular docking; estrogen receptors; ligand interactions.

1. Introduction

The estrogen receptors (ERs), members of the nuclear receptor family, are ligand-inducible intracellular transcription factors and are involved in the regulation of several physiological processes, including cell growth, survival and differentiation [1-3].
In mammals, cellular responses to estrogens are mainly mediated by two different estrogen receptor subtypes, ERα and ERβ, which exhibit variable expression and distribution levels, as well as distinct signaling responses. ERα is predominantly expressed in female reproductive organs, breast, kidney, bone, white adipose tissue and liver, whereas ERβ has

been found in several tissues of both male and female bodies including the central nervous system, colon, lung, kidney, male reproductive organs, and cardiovascular and immune systems. As members of the nuclear receptor protein family, ERs are located in the nucleus, even if they are also present in the cytoplasm and mitochondria [4].

The activities of ERs are modulated by a variety of natural and synthetic ligands. The activated ligand-ER homodimer complex binds to specific DNA sequences EREs (estrogen-response elements) and regulates transcription activity throughout interactions with specific transcription modulators. In some cases, ERα and ERβ could form heterodimers, and experimental evidence suggests that in this form they can induce activation of target genes that are different from those induced by homodimers [5-8].

Extensive data [9–13] have been recently published on the ER structures, their intra- and intermolecular interactions, and related post-translational modifications. These proteins are the natural target of estrogens, such as 17β-estradiol (**E**) (Figure 1), which are steroid hormones biosynthesized initially from cholesterol. ERα is expressed only in a low fraction of cells in healthy breast epithelium, whereas its expression significantly increases (up to 80% of cells) in breast cancer. On the other hand, more than 80% of normal breast epithelial cells express ERβ whereas its presence is reduced or completely suppressed during breast cancer emergence and progression. Accordingly, antihormonal therapy is commonly adopted for the treatment of breast cancer in patients that show an over-expression of such a receptor.

A number of chemical compounds derived from plants, known as phytoestrogens, demonstrates the ability to bind to the estrogen receptors, producing estrogenic or anti-estrogenic activity. Their potential anti-proliferative effects could be useful for the formulation of nutraceuticals or pharmaceutics. Tamoxifen (**TX**), a selective estrogen-receptor modulator (SERM), is nowadays the most effective and widely used anti-estrogen drug used for this purpose. However, several patients treated with **TX** develop a rapid onset of resistance [4]. Thus, the identification of novel anti-estrogen compounds able to overcome resistance onset is still demanding.

Several natural compounds have shown interesting estrogenic activity, the majority of them belonging to the isoflavones family. The most representative one, genistein (**G**) (Figure 4), has shown anti-proliferative effects on various hormone-sensitive cancer cells including breast, ovarian and prostate cells [16-18]. The structure of **G** has many points of similarity to E, and this could explain its capability in binding the estrogen receptors within the same active site.
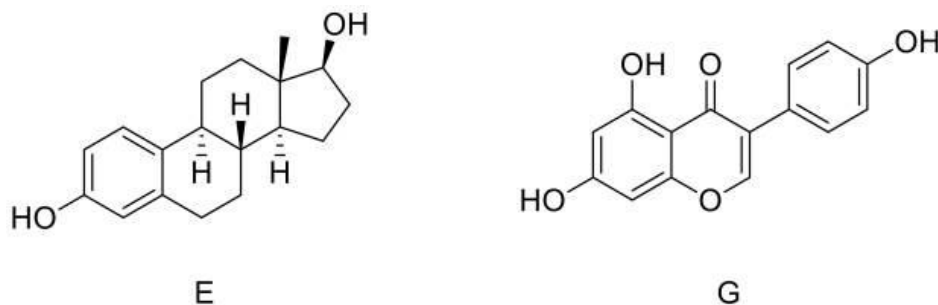
Figure 1. *Structures of 17β-estradiol (E) and genistein (G).*

The increasing interest of the scientific community in the health benefits of the Mediterranean diet led us to investigate the estrogenic activity of homoisoflavones structurally related to **G** and isolated from *Leopoldia comosa* (L.) Parl., (ex Muscari), a perennial bulbous plant that is endemic in southern Italy. A number of ethnobotanical

investigations demonstrated a wide use of *L. comosa* bulbs in traditional cooking recipes and in the formulation of remedies useful for the treatment of toothache and skin spots [19–21]. Earlier studies demonstrated the anti-oxidant, anti-inflammatory, diuretic, and anti-obesity properties of *L. comosa* extracts mainly due to the considerable presence of homoisoflavones [22–25]. These natural anti-oxidants were also found endowed with cytotoxic properties in a panel of *in vitro* human cancer models at low micromolar-range concentrations [22,26]. This study describes the identification of two homoisoflavones isolated from *L. comosa* as ER ligands, thus useful as hormonal substitutes or complements in breast cancer treatments. Molecular docking studies on the crystallographic structures of ERs have been carried out to investigate the binding mode of these homoisoflavones on both receptors. The results indicate that the two novel molecules can effectively bind ERs in the same binding site of both **E** and **G**. Furthermore, they show a greater conformational adaptability in their binding geometry compared to **G**, within both ERα and ERβ, thus proving that they could be of interest for the development of selective agents useful in the treatment of hormone-sensitive cancers.

2. Results and discussion

2.1. Homoisoflavones from Leopoldia Comosa

Several phenolic compounds based on a 3-benzylchroman-4-one skeleton and termed homoisoflavones have been isolated from various genres of the Hyacinthaceae plants family [27]. These compounds are generally classified in three small groups: 3-benzyl-4-cromanones, 3- benzylidene-4-cromanones and scillascylinoid homoisoflavones [28,29]. Although these compounds are considered as a sub-class of the extensively studied flavonoids, some steps in their biosynthetic pathways still need to be elucidated and, therefore, further studies are necessary to fully establish their chemical origin and biological properties [30]. Homoisoflavonoids are biosynthesized from cinnamic acid derivatives along with malonyl-CoA sub-units through the shikimato route by following the polyketide pathway. In a following step, phenylalanine is formed from prephenate and leads to a C-4, C-3, C-9 backbone, to which another ring is added from the acetate/mevalonate pathway [31]. Geopedological aspects and agronomic techniques have a significant influence on the polyphenol content and related biological activity of the plant extracts [32]. In the genus *L.*, two different classes of homoisoflavonoids have been identified: 3-benzylchroman-4-one containing compounds and scillascillin derivatives (Figure 2).
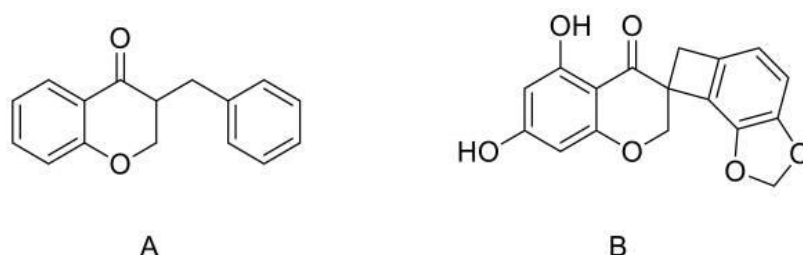
Figure 2. *Structures of 3-benzylchroman-4-one (A) and scillascillin (B).*

In this study, bulbs of *L. comosa* were collected in the fields of the Sila Massif, Calabria, southern Italy. The bulbs were opportunely stored in a cool and dry environment and successively separated from roots and soil residues. The bulbs were then subjected to extraction with a water/ethanol mixture. The total phenol and the total flavonoid content of the whole extract was determined using the Folin–Ciocalteu reagent and chlorogenic acid as

standard [33], and with the AlCl₃ colorimetric method [34], respectively, following known procedures [23]. The phytochemical identification of homoisoflavones present in the total extract of the bulbs was conducted through semi-preparative high-performance liquid chromatography (HPLC) and gas chromatography–mass spectrometry (GC–MS) (Figure 3), after functionalization of the whole extract. Comparison of the results obtained with the two applied techniques allowed the recognition of two compounds, **N1** (5,7-dihydroxy-3-(4-hydroxy-3-methoxybenzyl) chroman-4-one) and **N2** (5,7-dihydroxy-3-(4-hydroxybenzyl)-8- methoxychroman-4-one), belonging to the 3-benzylchroman-4-one class (Figure 4).
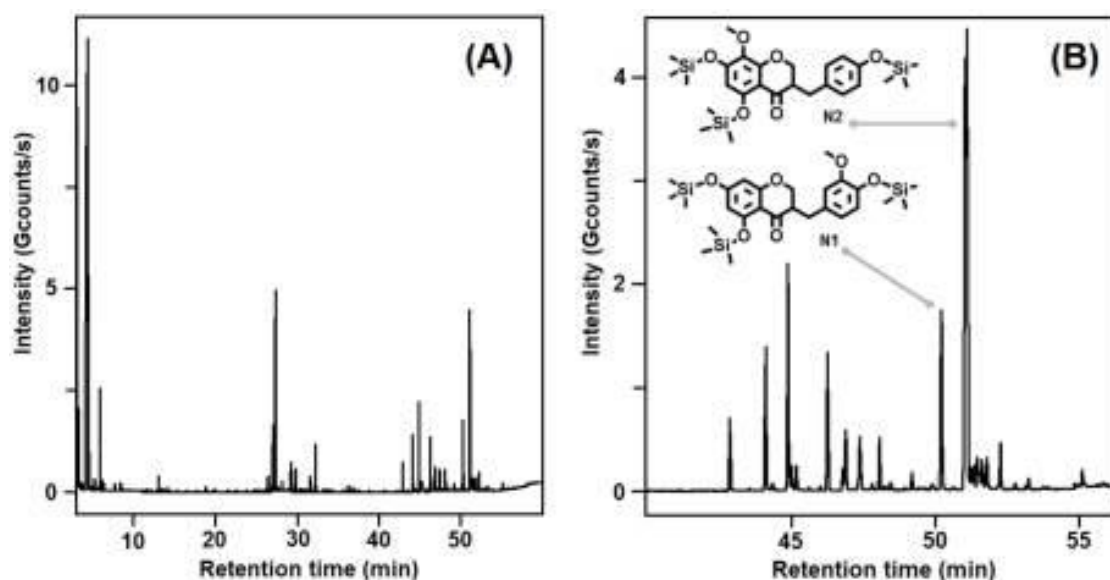
Figure 3. *Gas chromatography–mass spectrometry (GC–MS) analysis of the hydroalcoholic extract of L. comosa bulbs: (A) chromatographic profile (total ion current, TIC); (B) detail of the chromatogram including indication of the peaks of the two silyl-functionalized homoisoflavones **N1** and **N2**.*
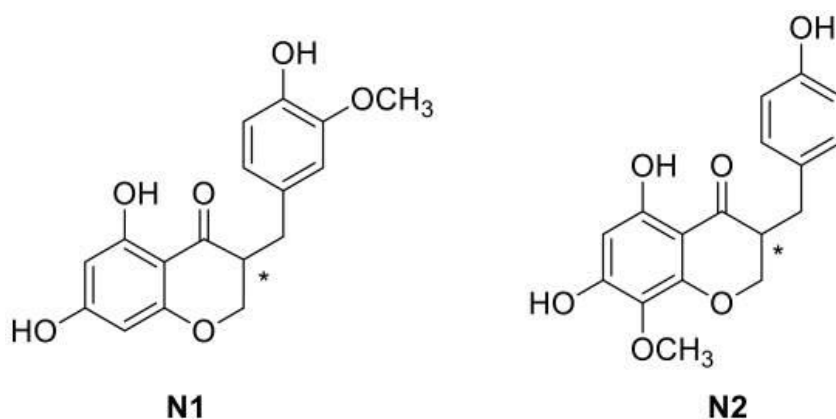
Figure 4. *Structures of the identified homoisoflavones **N1** and **N2**.*

2.2. Binding to Estrogen Receptor (ER) Proteins

Molecular docking is a useful technique to investigate the association of ligands to a target protein, and it has already been applied to elucidate details of the binding properties of ERs

[35–38]. Accordingly, after identification of the two naturally occurring homoisoflavones **N1** and **N2**, molecular docking studies were performed to investigate their binding to the active site of both ERs. To this aim, the binding modes and affinities of these two compounds were compared to those obtained for known ligands of ERs, E and **G**. In particular, we investigated whether the replacement of the appended substituted phenyl ring of G with a substituted benzyl of **N1** and **N2** was consistent with a retained affinity within the active site of the receptors. Such an alteration confers a higher degree of flexibility to the whole molecular asset and, on the other hand, keeps aromatic moieties slightly farther from each other with respect to their position in **G**. As a result, the calculated distance between 3- and 17-OH of E and the corresponding groups in G (7- and phenolic-OH) remains almost unchanged between 7-OH and phenolic-OH in **N1** and **N2**. Furthermore, the presence of a stereocenter in both compounds (Figure 4) led to enantiomers, which could differently accommodate into the receptor's active site. In order to evaluate the influence of chirality to the interaction with the key residues of the active site of ERs, molecular docking studies were performed on both enantiomers of each compound. The availability of several ER models allowed us to pursue a structure-based approach to characterize the interaction of isolated homoisoflavones within the ligand-binding pocket of the receptors. The ligands were docked into the crystallographic structures of both ERα and ERβ, obtained from the Protein Data Bank (PDB) [39]. The crystallographic structures selected for this study include three ERα-**E** and two ERα-**G** complexes, as well as one ERβ-**E** and two ERβ-**G** complexes. In some of these complexes the receptor is represented as a monomer (1X7R [40] and 2OCF [41] for ERα, and 1QKM [42] for ERβ) and in other as homodimer (2QA8 [43], 1A52 [44] and 1GWR [45] for ERα, and 1X7J [40] and 5TOA [46] for ERβ).

In a first step, the crystallographic structures of both ERs in complex with E and G were considered, and their shape complementarity, hydrogen-bonding network, and van der Waals clashes with the ligands were thoroughly analyzed. The crystal structures of the receptors showed the presence of a compact ellipsoid cavity, where ligands are surrounded by a hydrophobic environment. Within this pocket, OH groups of **E** at positions 3 and 17, as well as the hydroxyl groups of **G** at position 7 and phenolic-OH and a further OH group at position 5, play an important role in orienting the ligand within the active site. For evaluating the binding affinity of the ligands in their anchoring location, the scoring function of AutoDock Vina [47] was used with a re-docking of the crystallographic binding poses in their exact crystallographic position, without performing any search within the protein volume. The resulting binding energies, reported in Table 1, ranged from −9.4 to −10.0 kcal/mol for E (−9.7 kcal/mol on average), and from −7.8 to −9.6 kcal/mol for G (−8.9 kcal/mol on average). These findings point to a preference in the binding of E compared to G, although the variability obtained in the binding values of the latter is higher (standard deviations were 0.2 and 0.7 kcal/mol for **E** and **G**, respectively). In contrast, no significant differences were found between ERα and ERβ in the binding values for these two ligands. We also tested the ability of the docking engine to identify the ligand-binding site in a blind search performed on the protein volume. To this end, docking simulations were carried out with the unliganded receptors (i.e., the protein structures with the ligand taken away), considering again the binding of the two crystallographic ligands. As shown in Figures 5 and 6, both **E** and **G** were found to bind within the ER site in the same position determined in crystallography, with a root mean square displacement ≤1 Å. The complexes obtained were further refined in an energy minimization procedure by using a molecular mechanics protocol [48] to mimic the refinement process commonly adopted in crystallography [49,50]

and for a more direct comparison with the protocol that we later used for testing the binding of our compounds (see below).

The affinities obtained for **E** and **G** (see Table 1) were on average −9.8 and −8.8 kcal/mol, respectively, confirming a preference in the binding of the former ligand by 1 kcal/mol. The deviation in the variability of the binding energies were 0.3 kcal/mol for both ligands, proving that the energetic preference in the binding of **E** is significant. As in the case of the re-docking of the crystallographic ligands without performing any search, differences between ERα and ERβ in the binding of these ligands were found to be negligible. We also noted that, although the binding energies found with the two procedures (i.e., either re-docking the binding modes in their exact crystallographic position or performing a blind search followed by an energy minimization) were not identical in general, their average value and dispersion were the same. Thus, the values obtained for **E** and **G**, reported above, can be considered as references to compare the binding affinity of other compounds to the same receptors.
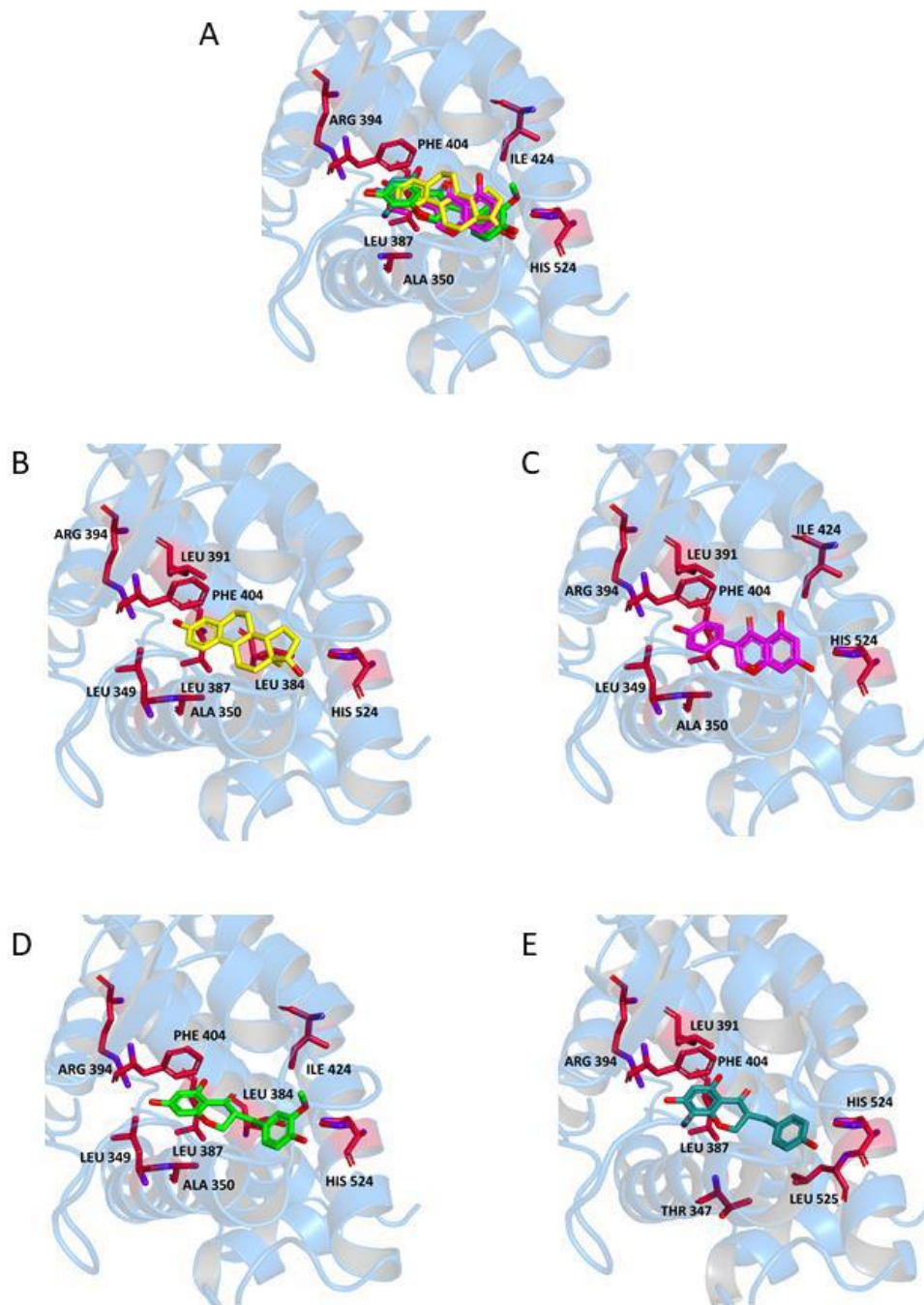
Figure 5. *Ligand-binding pocket of the active site of ERα; ribbons representing protein structural elements are also shown. (A) Superimposed binding modes of all the four ligands: E (yellow), G (magenta), (R)-**N1** (green), and (R)-**N2** (cyan); the key residues are also indicated in the specific binding mode of (B) E; (C) G; (D) (R)-N1; and (E) (R)-N2.*
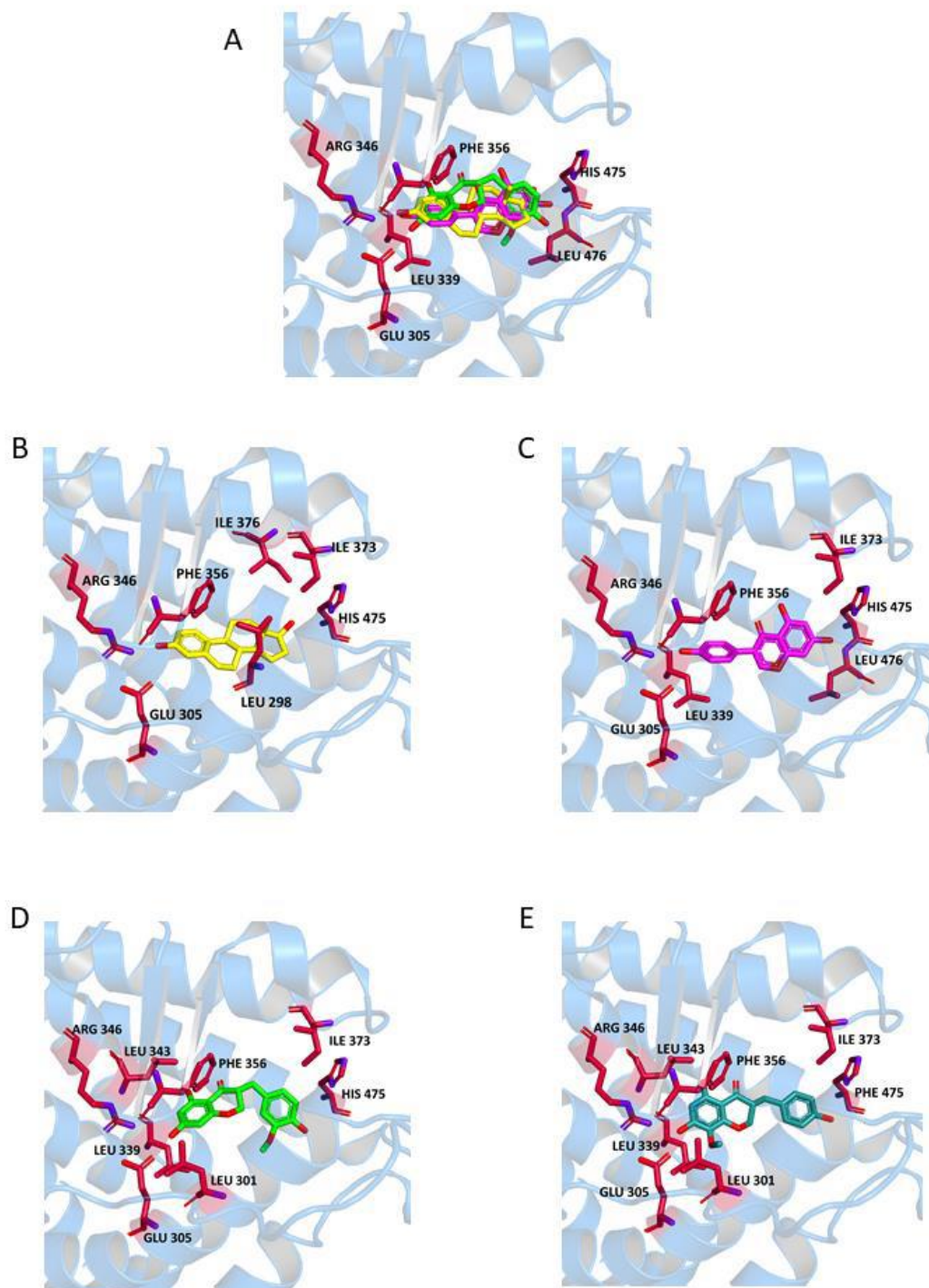
Figure 6. *Ligand-binding pocket of the active site of ERβ; ribbons representing protein structural elements are also shown. (A) Superimposed binding modes of all the four ligands: E (yellow), G (magenta), (R)-**N1** (green), and (R)-**N2** (cyan); the key residues are also indicated in the specific binding mode of (B) E; (C) G; (D) (R)-**N1**; and (E) (R)-**N2**.*

Table 1. *Binding energies for **E** and **G** complexed with ERα and ERβ. Energetic evaluation isperformed by using the scoring function of AutoDock Vina, either without any search (score-only assessment for the crystallographic poses of the ligands) or exploring the whole receptor (volumesearch on the protein structure) followed by a minimization refinement for the complex obtained. Results for receptors in dimeric form are reported with two values corresponding to chain A and B, respectively.*

Protein Data Bank (PDB) Entry	Receptor	Ligand	Binding Energy (kcal/mol)	
			Score-Only	Volume-Search
1A52	ERα	E	−9.7/−9.8	−9.5/−9.8
1GWR	ERα	E	−9.7/−10.0	−10.3/−10.1
2OCF	ERα	E	−9.4	−9.7
2QA8	ERα	G	−8.6/−9.6	−8.7/−8.7
1X7R	ERα	G	−7.8	−8.5
5TOA	ERβ	E	−9.7/−9.9	−9.5/−9.5
1X7J	ERβ	G	−9.2/−8.6	−8.6/−8.8
1QKM	ERβ	G	−9.5	−9.4

After assessing the binding of known ligands to the receptors, we proceeded in the estimate of the binding properties of our new compounds. The results of molecular docking performed using the crystallographic structures of the ERα and ERβ showed in all cases association of the compounds within the same binding sites as **E** and **G**. These binding modes were obtained for the ligand docked to rigid receptors, and did not include any re-accommodation of the protein structure. Thus, the complexes obtained were further refined with the same energy-minimization process previously used in the case of the blind docking of the crystallographic ligands. The binding scores found at the end of the refinement procedure are reported in Table 2. The binding energy values were −8.8 ± 0.3, −8.6 ± 0.4, −8.6 ± 0.4 and −8.7 ± 0.6 kcal/mol for **(R)-N1**, **(S)-N1**, **(R)-N2** and **(S)-N2**, respectively. These values are similar to those obtained in the binding of the crystallographic ligand **G**, i.e., −8.9 ± 0.7 and −8.8 ± 0.3 kcal/mol in both cases previously discussed (i.e., without or with blind search, respectively).

These results strongly suggest that our compounds are able to accommodate in both enantiomeric forms into the active site of ERs with the same affinity of **G**, and with only a slightly lower affinity compared to **E**.

Table 2. *Binding energies for **N1** and **N2** in both enantiomeric forms complexed with ERα and ERβ. Docking performed by using AutoDock Vina [31], followed by a minimization refinement for the complex obtained. Results for receptors in dimeric form are reported with two values corresponding to chain A and B, respectively.*

PDB Entry	Receptor	Binding Energy (kcal/mol)			
		(R)-N1	(S)-N1	(R)-N2	(S)-N2
1A52	ERα	−8.4/−8.5	−8.2/−8.2	−8.2/−8.9	−9.2/−9.3
1GWR	ERα	−8.4/−8.6	−8.3/−8.5	−8.6/−8.6	−8.9/−9.2
2OCF	ERα	−8.6	−8.9	−9.4	−8.6
2QA8	ERα	−8.8/−9.1	−8.9/−9.5	−8.8/−9.0	−8.0/−8.3
1X7R	ERα	−9.1	−8.4	−8.1	−8.5
5TOA	ERβ	−8.4/−8.6	−8.2/−8.4	−8.2/−8.7	−7.2/−8.7
1X7J	ERβ	−9.2/−9.2	−8.4/−8.9	−8.5/−8.7	−8.8/−9.0
1QKM	ERβ	−9.2	−9.0	−8.8	−8.8

We completed our analysis by investigating the protein residues involved in the ligand-receptor binding within the active site of the two types of receptors in the case of homoisoflavones **N1** and **N2**. Resulting interactions are reported (Table 3) for both the (R) and (S) enantiomers, and are compared with those established by ligands E and G in the binding sites of the crystallographic structures. It can be clearly seen that not only the binding energies are similar for the two enantiomers of both **N1** and **N2** (see Table 2), but also the interacting protein residues are the same with only a few exceptions (indicated with the labels ′(R)′ and ′(S)′ in Table 3). This observation confirms that our ligands are able to bind both ERs with a larger variety of conformational possibilities compared to **E** and **G**.

Table 3. Key protein residues of estrogen receptors (ERs) interacting with the ligands. Interactions identified with protein–ligand interaction profiler (PLIP) [51]: HI = hydrophobic interaction; HB = hydrogen bond; π-st. = π-stacking. Interactions with residues in Italics are unique to only one out of the four ligands. (R) or (S) indicate that the interaction in solely formed by either of the two enantiomers of N1/N2.

	Interacting Residues					
Ligand	**ERα**			**ERβ**		
	HI	HB	π-st.	HI	HB	π-st.
E	Leu349 Ala350 Leu384 Leu387 Leu391	Leu387 Arg394 His524	Phe404	*Leu298* Ile373 Ile376	Glu305 Arg346 His475	Phe356
G	Leu349 Leu387 Leu391 Ile424	*Ala350* Leu387 Arg394 His524	Phe404	Leu339 Ile373 Leu476	Glu305 Arg346 His475	Phe356
N1	Leu349 (S) Ala350 (S) Leu384 Ile 424 Leu525 [*1] (R)	Leu387 Arg394 His524	Phe404	Leu301 [*2] (R) Leu339 *Leu343* [*3] Ile373 *His475* [*4] (S)	*Leu298* *Leu339* [*5] *Leu343* [*3] Arg346 His475	Phe356
N2	Leu349 (S) Leu387 Leu391 Leu525 [*1] (R)	*Thr347* Leu387 Arg394 His524	Phe404	Leu301 [*2] Leu339	Arg346 *Phe356* [*6] His475	Phe356

Notes: [*1] corresponds to Leu476 in ERβ that forms HI with G; [*2] corresponds to Leu349 in ERα that forms HI with all the ligands; [*3] corresponds to Leu391 in ERα that forms HI with E, G and **N2**; [*4] forms HI solely with **N1**, but forms HB with all the ligands; [*5] corresponds to Leu387 in ERα that forms HI with E and G; [*6] forms HI solely with **N2**, but forms HB with all the ligands.

Visual inspection provided further details on the binding modes of **N1** and **N2** within the ERs; due to the similarities of the binding energies and anchoring residues discussed above for their two enantiomers, in the following we will show models representing only the (R) form, although the discussion will regard both forms. In the binding pocket of ERα (Figure 5, Panels A–E), both 17-OH of E and 7-OH of G interact with His524 through formation of a hydrogen bond. An equivalent interaction is formed by the phenolic-OH group of **N1** and **N2**. Moreover, 7-OH of **N1** and **N2** is involved in further hydrogen bonds with Arg394 and Leu387, similarly to the 3-OH of E and the phenolic-OH of G. Additional stabilization of the complex results from a π-stacking interaction between Phe404 and the aromatic ring of E or the appended phenyl of G. The same interaction could be established between the aromatic amino acid and the benzo-fused ring of **N1** and **N2**. The ligand receptor complex

is further stabilized for **N1** and **N2** by hydrophobic interactions with Ala350, Ile424, and a number of Leu residues. In ERβ (Figure 6), all ligands are involved in a hydrogen bond with His475 and a π-stacking interaction with Phe356. In particular, an interaction with Hys475 is established by 17-OH of E, 7-OH of G and the phenolic-OH of **N1** and **N2**. A π-stacking interaction with Phe356 involves the aromatic ring of E or the appended phenyl of G. Similarly, to ERα, this interaction is established by the benzofused moiety of **N1** and **N2**. For this receptor, a hydrogen bond formation was observed between Arg346 and the 3-OH of E, the phenolic-OH of G, and the 7-OH of **N1** and **N2**. The ligand-receptor complex is further stabilized in the presence of **N1** and **N2** by hydrophobic interactions with Leu301 and Leu339, along with some other interactions specific for each ligand. The presence of the extra carbon atom between the two cyclic portions of the molecule in **N1** and **N2** is compatible with their accommodation into the active site of both receptors, although the two fused ring systems of **N1** and **N2** are in a reversed orientation with respect to **G**.

In summary, our data suggest that the described compounds are sterically compatible and form binding interactions with the key residues of the active site of both ERα and ERβ. It is interesting to note that, besides the conformations of **N1** and **N2** described above, which closely resemble those of the crystallographic ligand E and G, we also observed some alternative orientations of our ligands with slightly lower or even comparable energies. This observation is perhaps not surprising, since **N1** and **N2** possess a larger conformational freedom compared to the structure of both E and G. Although this possibility does not affect our docking results in terms of binding energy, it could be exploited in the use of these homoisoflavones as leading compounds for further optimization, with the aim of designing ligands with enhanced affinity toward ERs.

3. Materials and Methods

3.1. Plant Material and Phytochemical Profile

Bulbs of *L. comosa* were collected in the fields of the Sila Massif (39°40′27.34″ N, 16°46′79.24″ E– 39°40′9.20″ N, 16°46′84.91″ E), Calabria, southern Italy. The bulbs were stored in a cool and dry environment and subsequently separated from roots and cleaned of soil residues. The bulbs (580 g) were used for an extraction with a water/ethanol mixture (1:1 *v/v*) using a Naviglio® extractor (Atlas Filtri S.r.L., Limena, PD, Italy) according to previously reported procedures [23]. The total phenol content of the whole extracts was determined using Folin–Ciocalteu reagent and chlorogenic acid as a standard [33]. The total flavonoid content of the crude extract was determined by the $AlCl_3$ colorimetric method on the same extracts used for total phenol determination [34]. The phytochemical composition of the hydroalcoholic extract was investigated by high-performance liquid chromatography coupled to ultraviolet diode array detection (HPLC–UVDAD) and by gas chromatography coupled with mass spectrometric detection (GC–MS) after derivatization (silanization) of the sample as previously described [23].

3.2. Molecular Docking

Eight crystallographic structures of ERs [40–46] including five in dimeric form, were obtained from the PDB, and consisted of the protein in complex with either **E** or **G**. The structures of both **E** and **G** were extracted from the crystallographic complexes, while the structures of **N1** and **N2**, considered in either (R) or (S) structural conformations, were built by using the modeling software Avogadro [52]. Molecular docking was performed by using AutoDock Vina 1.1.2 (the Scripps Research Institute, La Jolla, CA, USA) [47]. A preliminary conversion of the structures from the PDB format was performed by using the graphical interface AutoDock Tools 1.5.6 (the Scripps Research Institute, La Jolla, CA,

USA) [53]. During the conversion, polar hydrogens were added for the crystallographic ligands, and apolar hydrogens of **N1** and **N2** were merged to the carbon atom they are attached to. To account for the binding in any possible internal pocket of ERs, a search volume including the whole protein was considered, with a grid space of 1 Å. Full flexibility was guaranteed to all the ligands, resulting in two active torsions for **E** (the two hydroxyls) and four for **G** (three hydroxyls, plus the bond connecting the phenol group to the rest of the molecule). Six rotations around dihedral angles were allowed for both **N1** and **N2** molecules. A single run was carried out at very high exhaustiveness (16 times larger than the default value) in each case. Re-docking experiments were also performed as score-only assessment without any search. Refinement of the complex structures was performed by energy minimization using the web server AMMOS2 [48], which employs the universal force field (UFF) potential set [54] and AMBER partial charges [55] with a conjugate gradient optimization. Intermolecular interactions were evaluated by using the automated protein–ligand interaction profiler (PLIP) [51].

4. Conclusions

In this work we have investigated the capability of newly identified homoisoflavones to form complexes with ER proteins. Our results confirm that these compounds are sterically compatible to accommodation within the active site occupied by previously known ligands, **E** and **G**, and interact with the same key protein residues of both the isoforms of ERs. Because of the known anti-tumor effect of the parent compound, i.e. the isoflavone **G**, and due to the possibility of using other natural homoisoflavones or employing these compounds as lead drugs for optimization through a rational design, this study could be considered the starting point for the identification of novel tools in the treatment of estrogen-sensitive breast-cancer. Further studies will be performed successively in order to assess the agonistic or antagonistic activity for these homoisoflavone compounds.

References

[1] Wang, P.; McInnes, C.; Zhu, B.T. Structural characterization of the binding interactions of various endogenous estrogen metabolites with human estrogen receptor α and β subtypes: A molecular modelling study. PLoS ONE 2013, 8, e74615.

[2] Sukocheva, O.A. Estrogen, estrogen receptors, and hepatocellular carcinoma: Are we there yet? World J. Gastroenterol. 2018, 24, 1–4.

[3] Guillaume, M.; Montagner, A.; Fontaine, C.; Lenfant, F.; Arnal, J.F.; Gourdy, P. Nuclear and membrane actions of estrogen receptor alpha: contribution to the regulation of energy and glucose homeostasis. Adv. Exp. Med. Biol. 2017, 1043, 401–426.

[4] Jia, M.; Dahlman-Wright, K.; Gustafsson, J.A. Estrogen receptor alpha and beta in health and disease. Best Pract. Res. Clin. Endoc. Metab. 2015, 29, 557–568.

[5] Pettersson, K.; Delaunay, F.; Gustafsson, J.A. Estrogen receptor beta acts as a dominant regulator of estrogen signaling. Oncogene 2000, 19, 4970–4978.

[6] Paech, K.; Webb, P.; Kuiper, G.G.; Nilsson, S.; Gustafsson, J.; Kushner, P.J.; Scanlan, T.S. Differential ligand activation of estrogen receptors ERalpha and ERbeta at AP1 sites. Science 1997, 277, 1508–1510.

[7] Cowley, S.M.; Parker, M.G. A comparison of transcriptional activation by ER alpha and ER beta. J. Steroid Biochem. Mol. Biol. 1999, 69, 165–175.

[8] Chakraborty, S.; Willett, H.; Biswas, P.K. Insight into estrogen receptor beta-beta and alpha-beta homo- and heterodimerization: A combined molecular dynamics and sequence analysis study. Biophys. Chem. 2012, 170, 42–50.

[9] Farzaneh, S.; Zarghi, A. Estrogen Receptor Ligands: A Review (2013–2015). Sci. Pharm. 2016, 84, 409–427.

[10] Paterni, I.; Granchi, C.; Katzenellenbogen, J.A.; Minutolo, F. Estrogen receptors alpha (ERalpha) and beta (ERbeta): Subtype-selective ligands and clinical potential. Steroids 2014, 90, 13–29.

[11] Kumar, R.; Zakharov, M.N.; Khan, S.H.; Miki, R.; Jang, H.; Toraldo, G.; Singh, R.; Bhasin, S.; Jasuja, R. The dynamic structure of the estrogen receptor. J. Amino Acids 2011, 2011, 812540.

[12] Traboulsi, T.; El Ezzy, M.; Gleason, J.L.; Mader, S. Antiestrogens: Structure-activity relationships and use in breast cancer treatment. J. Mol. Endocrinol. 2017, 58, R15–R31.

[13] Ascenzi, P.; Bocedi, A.; Marino, M. Structure-function relationship of estrogen receptor alpha and beta: Impact on human health. Mol. Asp. Med. 2006, 27, 299–402.

[14] Huang, B.; Omoto, Y.; Iwase, H.; Yamashita, H.; Toyama, T.; Coombes, R.C.; Filipovic, A.; Warner, M.; Gustafsson, J.A. Differential expression of estrogen receptor α, $\beta1$, and $\beta2$ in lobular and ductal breast cancer. Proc. Natl. Acad. Sci. USA 2014, 111, 1933–1938.

[15] Zhao, C.; Lam, E.W.; Sunters, A.; Enmark, E.; de Bella, M.T.; Coombes, R.C.; Gustafsson, J.A.; Dahlman- Wright, K. Expression of estrogen receptor beta isoforms in normal breast epithelial cells and breast cancer: Regulation by methylation. Oncogene 2003, 22, 7600–7606.

[16] Lee, J.Y.; Kim, H.S.; Song, Y.S. Genistein as a potential anticancer agent against ovarian cancer. J. Tradit. Complement. Med. 2012, 2, 96–104.

[17] Zhang, L.L.; Li, L.; Wu, D.P.; Fan, J.H.; Li, X.; Wu, K.J.; Wang, X.Y.; He, D.L. A novel anti-cancer effect of genistein: Reversal of epithelial mesenchymal transition in prostate cancer cells. Acta Pharmacol. Sin. 2008, 29, 1060–1068.

[18] Peterson, G.; Barnes, S. Genistein inhibition of the growth of human breast cancer cells: independence from estrogen receptors and the multi-drug resistance gene. Biochem. Biophys. Res. Commun. 1991, 179, 661–667.

[19] Lentini, F.; Venza, F. Wild food plants of popular use in Sicily. J. Ethnobiol. Ethnomed. 2007, 3, 15.

[20] Pieroni, A.; Nebel, S.; Santoro, R.F.; Heinrich, M. Food for two seasons: culinary uses of non-cultivated local vegetables and mushrooms in a south Italian village. Int. J. Food Sci. Nutr. 2005, 56, 245–272.

[21] Pieroni, A.; Nebel, S.; Quave, C.; Munz, H.; Heinrich, M. Ethnopharmacology of liakra: Traditional weedy vegetables of the Arbereshe of the Vulture area in southern Italy. J. Ethnopharmacol. 2002, 81, 165–185.

[22] Lin, L.G.; Liu, Q.Y.; Ye, Y. Naturally occurring homoisoflavonoids and their pharmacological activities. Planta Med. 2014, 80, 1053–1066.

[23] Casacchia, T.; Scavello, F.; Rocca, C.; Granieri, M.C.; Beretta, G.; Amelio, D.; Gelmini, F.; Spena, A.; Mazza, R.; Toma, C.C.; et al. Leopoldia comosa prevents metabolic disorders in rats with high-fat diet-induced obesity. Eur. J. Nutr. 2018, 1–15, doi:org/10.1007/s00394-018-1609-1.

[24] Nirmal, N.P.; Rajput, M.S.; Prasad, R.G.; Ahmad, M. Brazilin from Caesalpinia sappan heartwood and its pharmacological activities: A review. Asian Pac. J. Trop. Med. 2015, 8, 421–430.

[25] Loizzo M.R.; Tundis, R.; Menichini, F.; Pugliese, A.; Bonesi, M.; Solimene, U.; Menichini, F. Chelating, antioxidant and hypoglycaemic potential of Muscari comosum (L.) Mill. bulb extracts. Int. J. Food Sci. Nutr. 2010, 61, 780–791.

[26] Dai, Y.; Harinantenaina, L.; Brodie, P.J.; Goetz, M.; Shen, Y.; TenDyke, K.; Kingston, D.G. Antiproliferative homoisoflavonoids and bufatrienolides from Urginea depressa. J. Nat. Prod. 2013, 76, 865–872.

[27] Mulholland, D.A.; Schwikkard, S.L.; Crouch, N.R. The chemistry and biological activity of the Hyacinthaceae. Nat. Prod. Rep. 2013, 30, 1165–1210.

[28] Du Toit, K.; Elgorashi, E.E.; Malan, S.F.; Drewes, S.E.; van Staden, J.; Crouch, N.R.; Mulholland, D.A. Antiinflammatory activity and QSAR studies of compounds isolated from Hyacinthaceae species and Tachiadenus longiflorus Griseb. (Gentianaceae). Bioorg. Med. Chem. 2005, 13, 2561–2568.

[29] Abegaz, B.M.; Mutanyatta-Comar J.N. Naturally occurring homoisoflavonoids: Phytochemistry, biological activities and synthesis. Nat. Prod. Commun. 2007, 2, 475–498.

[30] Castelli, M.V.; López, S.N. Homoisoflavonoids: Occurrence, biosynthesis, and biological activity. In Studies in Natural Products Chemistry; Elsevier: Amsterdam, Netherlands, 2017, Volume 54, pp. 315–354.

[31] Mann, J.; Davidson, R.S.; Hobbs, J.B.; Banthorpe, D.V.; Harbome, J. B. Natural products: Their chemistry and biological significance. In Longman Scientific and Technical; Harlow, E., Ed; Longman Group UK Ltd.: Harlow, UK, 1994, p. 372.

[32] De Vincenzi, S.; Lupattelli, M.; Cestola, E.; Liponi, G.B. Effect of variety and agronomical conditions on the level of polyphenols and antinutritional factors of Vicia Faba Minor. Vet. Res. Commun. 2006, 30, 371–374.

[33] Casacchia, T.; Sofo, A.; Casaburi, I.; Marrelli, M.; Conforti, F.; Statti, G.A. Antioxidant, enzyme-inhibitory and antitumor activity of the wild dietary plant Muscari comosum (L.). Int. J. Plant Biol. 2017, 8, 6895.

[34] Marrelli, M.; Cristaldi, B.; Menichini, F.; Conforti, F. Inhibitory effects of wild dietary plants on lipid peroxidation and on the proliferation of human cancer cells. Food Chem. Toxicol. 2015, 86, 16–24.

[35] Martinez-Archundia, M.; Garcia-Vazquez, J.B.; Colin-Astudillo, B.; Bello, M.; Prestegui-Martel, B.; Chavez-Blanco, A.; Duenas-Gonzalez, A.; Fragoso-Vazquez, M.J.; Mendieta-Wejebe, J.; Abarca-Rojano, E.; et al. Computational study of the binding modes of diverse DPN analogues on estrogen receptors (ER) and the biological evaluation of a new potential antiestrogenic ligand. Anticancer Agents Med. Chem. 2018.

[36] Yugandhar, P.; Kumar, K.K.; Neeraja, P.; Savithramma, N. Isolation, characterization and *in silico* docking studies of synergistic estrogen receptor a anticancer polyphenols from Syzygium alternifolium (Wt.) Walp. J. Intercult. Ethnopharmacol. 2017, 6, 296–310.

[37] Muchtaridi, M.; Syahidah, H.N.; Subarnas, A.; Yusuf, M.; Bryant, S.D.; Langer, T. Molecular docking and 3D-pharmacophore modeling to study the interactions of chalcone derivatives with estrogen receptor alpha. Pharmaceuticals 2017, 10, 81.

[38] Manas, E.S.; Unwalla, R.J.; Xu, Z.B.; Malamas, M.S.; Miller, C.P.; Harris, H.A.; Hsiao, C.; Akopian, T.; Hum, W.T.; Malakian, K.; et al. Structure-based design of estrogen receptor-beta selective ligands. J. Am. Chem. Soc. 2004, 126, 15106–15119.

[39] Berman, H.M.; Westbrook, J.; Feng, Z.; Gilliland, G.; Bhat, T.N.; Weissig, H.; Shindyalov, I.N.; Bourne, P.E. The Protein Data Bank. Nucleic Acids Res. 2000, 28, 235–242.

[40] Manas, E.S.; Xu, Z.B.; Unwalla, R.J.; Somers, W.S. Understanding the selectivity of genistein for human estrogen receptor-beta using X-ray crystallography and computational methods. Structure 2004, 12, 2197–2207.

[41] Koide, A.; Abbatiello, S.; Rothgery, L.; Koide, S. Probing protein conformational changes in living cells by using designer binding proteins: application to the estrogen receptor. Proc. Natl. Acad. Sci. USA 2002, 99, 1253–1258.

[42] Pike, A.C.; Brzozowski, A.M.; Hubbard, R.E.; Bonn, T.; Thorsell, A.G.; Engstrom, O.; Ljunggren, J.; Gustafsson, J.A.; Carlquist, M. Structure of the ligand-binding domain of oestrogen receptor beta in the presence of a partial agonist and a full antagonist. Embo J. 1999, 18, 4608–4618.

43. Nettles, K.W.; Bruning, J.B.; Gil, G.; Nowak, J.; Sharma, S.K.; Hahm, J.B.; Kulp, K.; Hochberg, R.B.; Zhou, H.; Katzenellenbogen, J.A.; et al. NFkB selectivity of estrogen receptor ligands revealed by comparative crystallographic analyses. Nat. Chem. Biol. 2008, 4, 241–247.

[44] Tanenbaum, D.M.; Wang, Y.; Williams, S.P.; Sigler, P.B. Crystallographic comparison of the estrogen and progesterone receptor's ligand binding domains. Proc. Natl. Acad. Sci. USA 1998, 95, 5998–6003.

[45] Warnmark, A.; Treuter, E.; Gustafsson, J.A.; Hubbard, R.E.; Brzozowski, A.M.; Pike, A.C. Interaction of transcriptional intermediary factor 2 nuclear receptor box peptides with the coactivator binding site of estrogen receptor alpha. J. Biol. Chem. 2002, 277, 21862–21868.

[46] Souza, P.C.T.; Textor, L.C.; Melo, D.C.; Nascimento, A.S.; Skaf, M.S.; Polikarpov, I. An alternative conformation of ERbeta bound to estradiol reveals H12 in a stable antagonist position. Sci. Rep. 2017, 7, 3509.

[47] Trott, O.; Olson, A.J. AutoDock Vina: Improving the speed and accuracy of docking with a new scoring function, efficient optimization, and multithreading. J. Comput. Chem. 2010, 31, 455–461.

[48] Labbè, C.M.; Pencheva, T.; Jereva, D.; Desvillechabrol, D.; Becot, J.; Villoutreix, B.O.; Pajeva, I.; Miteva, M.A. AMMOS2: A web server for protein-ligand-water complexes refinement via molecular mechanics. Nucleic Acids Res. 2017, 45, W350–W355.

[49] Summa, C.M.; Levitt, M. Near-native structure refinement using in vacuo energy minimization. Proc. Natl. Acad. Sci. USA 2007, 104, 3177–3182.

[50]. Rizzuti, B.; Daggett, V. Using simulations to provide the framework for experimental protein folding studies. Arch. Biochem. Biophys. 2013, 531, 128–135.

[51] Salentin, S.; Schreiber, S.; Haupt, V.J.; Adasme, M.F.; Schroeder, M. PLIP: Fully automated protein-ligand interaction profiler. *Nucleic Acids Res.* 2015, *43*, W443–W447.

[52] Hanwell, M.D.; Curtis, D.E.; Lonie, D.C.; Vandermeersch, T.; Zurek, E.; Hutchison, G.R. Avogadro: An advanced semantic chemical editor, visualization, and analysis platform. *J. Cheminform.* 2012, *4*, 17.

[53] Morris, G.M.; Goodsell, D.S.; Halliday, R.S.; Huey, R.; Hart, W.E.; Belew, R.K.; Olson, A.J. Automated docking using a Lamarckian genetic algorithm and an empirical binding free energy function. *J. Comput. Chem.* 1998, *19*, 1639–1662.

[54] Rappé, A.K.; Casewit, C.J.; Colwell, K.S.; Goddard, W.A. UFF, a full periodic table force field for molecular mechanics and molecular dynamics simulations. *J. Am. Chem. Soc.* 1992, *114*, 10024–10035.

[55] Weiner, S.J.; Kollman, P.A.; Nguyen, D.T.; Case, D.A. An all atom force field for simulations of proteins and nucleic acids. *J. Comput. Chem.* 1986, *7*, 230–252.

II. A PILOT STUDY ON THE NUTRACEUTICAL PROPERTIES OF THE *CITRUS* HYBRID TACLE® AS A DIETARY SOURCE OF POLYPHENOLS FOR SUPPLEMENTATION IN METABOLIC DISORDERS

Teresa Casacchia [a]; Maria Antonietta Occhiuzzi [a]; Fedora Grande [a]; Bruno Rizzuti [b]; Maria Concetta Granieri [c]; CarmineRocca [c]; Alfonsina Gattuso [c]; Antonio Garofalo [a]; Tommaso Angelone [c]; Giancarlo Statti [a.]

[a] Department of Pharmacy, Health and Nutritional Sciences, University of Calabria, Via P. Bucci, 87036 Rende, CS, Italy
[b] CNR-NANOTEC, Licryl-UOS Cosenza and CEMIF.Cal, Department of Physics, University of Calabria, Via P. Bucci, 87036 Rende, CS, Italy
[c] Department of Biology, Ecology and Earth Sciences, University of Calabria, Via P. Bucci, 87036 Rende, CS, Italy

Abstract:

Tacle® is a citrus variety obtained from the crossbreeding of Clementine and Tarocco tetraploids. This new fruit recently gained an increasing interest due to its commercial value and nutraceutical properties. A high content in polyphenols confers to its extracts a protective activity against oxidative agents involved in several degenerative disorders. In this study, we investigated the antioxidant potential of Tacle and its inhibitory activity against human amilase and lipase *in vitro*. These particular features could be ascribed to the relevant content in naringin and hesperidin glycosides and the corresponding aglycones have been *in silico* demonstrated able to bind the active site of both enzymes. The overall results showed an enhanced nutraceutical profile of Tacle with respect to citrus parents, suggesting that a dietary enrichment with its extracts could be useful in the complementary treatment of metabolic disorders such as obesity and diabetes, as assessed by *in vivo* experiments on rats.

Keywords: Glycosides, Human pancreatic amylase, Human pancreatic lipase, Anthropometric parameters, Molecular docking.

1. Introduction

Obesity and its associated disorders, including insulin resistance and type 2 diabetes as well as cardiovascular diseases and cancer, represent major risk factors for human health and are a leading cause of death in Western countries (Fan, Song, Chen, Hui, & Zhang, 2013). Obesity is mainly due to a long term energy imbalance between energy intake and calories expense, thus a therapeutic strategy for its treatment could reside in the reduction of carbohydrate and lipid absorption in the gastrointestinal tract (Maida, Se Balaji, Divakar, & Geetha, 2017). Flavon derivatives strongly inhibit (Xiao, Capanoglu, Jassbi, & Miron, 2016) the absorption of sugars within the duodenal tract, the enteric portion mainly involved in this process. Flavones and other structurally related molecules are abundant in *Citrus*, a genus of plants widely distributed in sub-tropical areas. This genus belongs to the rue family, Rutaceae and it is placed in the order Sapindales. It is of great economic value in warm temperate climates due to its numerous edible fruits, including tangerine (*Citrus reticulate* Blanco), sweet orange (*Citrus sinensis* L. Osbeck), grapefruit (*Citrus paradisi* Macf.), lemon (*Citrus limon* L. Burm.), lime (*Citrus aurantifolia* Christm. Swingle) and several hybrid

varieties (Tacle® (TC), Mandalate®, Clara®) (Rapisarda, Bellomo, Fabroni, & Russo, 2008). *Citrus* fruits could be eaten as such, drunk in the form of juice, or employed for the preparation of several manufactured foods. They are considered as a major source of vitamin C (Magiorkinis, Beloukas, & Diamantis, 2011), folic acid, potassium, pectins and flavonoids. The latter include various derivatives endowed with remarkable antioxidant properties and are involved in a number of physiological and pathological processes (Anagnostopoulou, Kefalas, Papageorgiou, Assimopoulou, & Boskou, 2006; Gorinstein et al., 2004; Khettal et al., 2017; Proteggente, Saija, De Pasquale, & Rice-Evans, 2003). In recent years, several studies focused on the antioxidant activity of *Citrus* fruits and their role in the prevention and treatment of various chronic and degenerative human diseases (Zou, Xi, Hu, Nie, & Zhou, 2016). In particular, a number of studies demonstrated the beneficial effects of supplements based on *Citrus* leaf, peel and pulp extracts on the control of body weight and anthropometric parameters (Hossain et al., 2016; Khettal et al., 2017; Muthiah, Umamaheswari, & Asokkumar, 2012; Rampersaud & Valim, 2017). Several evidences demonstrated that the administration of different *Citrus* extracts could lead to lipid-lowering and hypoglycemic effects, reaching a similar effectiveness of wellknown drugs, such as atorvastatin and metformin.

While the hypoglycemic activity seems due to the inhibition of human pancreatic amylase (HPA), an endoglycosidase responsible for food starches digestion (Parmar & Kar, 2008; Shen, Xu, & Lu, 2012), the lipid-lowering action appears to be mainly related to an inhibitory activity on the human pancreatic lipase (HPL), involved in the lipid absorption (Cho, Kim, Andrade, Burgess, & Kim, 2011; Ding et al., 2012; Fukuchi et al., 2008; Kang et al., 2012; Kim et al., 2016; Mallick & Khan, 2016; Pu et al., 2012). HPL modulates lipids absorption by catalysing their hydrolysis to glycerol and fatty acids within the intestine. Thus, pancreatic lipase inhibitors could reduce fat absorption and related metabolic disorders. Orlistat (tetrahydrolipostatin), an analog of the known HPL inhibitor lipostatin, is the only remedy acting peripherally approved by the Food and Drug Administration (FDA) for longterm management of obesity. Despite its considerable lipid lowering properties, orlistat shows unwanted side effects, such as steatorrhea, fecal incontinence and abdominal colic. This observation has encouraged the identification of alternative agents able to inhibit HPL, but with a lower occurrence of side effects.

Hesperedin and naringin represent the most abundant flavonoid component isolated from various parts of plants belonging to *Citrus* genus and seem to be responsible for a potent antioxidant and anti-inflammatory property *in vitro* and *in vivo*. Hesperidin is constituted by the aglycone hesperetin and the disaccharide rutinose, whereas naringin is a flavanone-7-O-glycoside that derives from the combination of the flavanone naringenin and the disaccharide neohesperidose (Figure 1) (Mishra, Kumar, & Pandey, 2013).

Citrus extracts, being rich in naringin and hesperidin, are useful dietary supplements that may relieve several cardiovascular disorders, in particular during the treatment of hypertension (Agrawal et al., 2014; Alam, Kauter, & Brown, 2013; Ikemura, Sasaki, Giddings, & Yamamoto, 2012; Reshef et al., 2005; Yamamoto, Jokura, Suzuki, Hase, & Shimotoyodome, 2013). Further studies on rats demonstrated how naringenin is able to affect adipocyte differentiation (Cho et al., 2011) and to reduce LDL, HDL and the plasmatic concentration of triglycerides (Pu et al., 2012). This compound was shown to act by limiting the absorption of fatty acids, preventing their accumulation in the body (Birari & Bhutani, 2007). Dietary hesperidin supplementation in induced-diabetes rats causes the normalization of plasma-levels of lipids and adiponectin, a hormone that promotes the fatty acid catabolism and reduces the glucose release from liver (Akiyama et al., 2010). Further studies on the glycemic modulation by naringin and naringenin demonstrated that such flavanones possess an inhibitory activity against α-glycosidase and α-amilase, causing a lowering of the glucose

plasma levels and a remarkable increase of insulin and glycogen (Choi, Yokozawa, & Oura, 1991; Mulvihill et al., 2009; Priscilla, Roy, Suresh, Kumar, & Thirumurugan, 2014; Revathy, Srinivasan, Abdullah, &Udaiyar, 2018). Some pharmacological interactions have also been observed during the simultaneous administration of naringenin and pioglitazone, a full agonist of peroxisome proliferator-activated receptor gamma (PPARγ) that represents an alternative agent for the treatment of type-2 diabetes (Yoshida et al., 2017). In this study, we have investigated the antioxidant, lipid-lowering and hypoglycemic activities of the extracts from three *Citrus* plants, namely Tarocco (TR), Clementina (CL), and their crossbred Tacle (TC), largely farmed in the Sibari plane, southern Italy. In particular, TC is a Tangerine-like citrus endowed with some peculiar characters such as the absence of seeds, easy peeling, and medium-early maturing (December-January). When mature, it develops a noticeable anthocyanin content and acquires a particularly pleasant taste due to a balanced sugar-acid ratio. The biological profiles of the extracts of pulp, peels and leaves of the three above-mentioned cultivars have been assessed by *in vitro* and *in vivo* assays. This choice was made in order to evaluate not only the nutraceutical potential of the edible fraction of the fruits (pulp), but also the residual utility of the waste left after agrofood procedures (peels, leaves). Particular attention was paid to the new specie TC in order to verify whether this hybrid, beside an improved nutritional profile, was also endowed with an increased biological potential when compared to parent cultivars. The antioxidant activity was assessed by a free radical scavenging assay and a β-carotene bleaching (BCB) test, whereas HPA and HPL inhibition was measured by specific antienzymatic assays. The biological properties of the extracts are attributable mainly to the flavone components of the glycosides hesperidin and naringin. The corresponding aglycones, hesperetin and naringenin, have been investigated for determining their binding mode within the HPA and HPL active site by molecular docking, on the basis of some available crystallographic enzyme structures. Finally, after obtaining encouraging *in vitro* and *in silico* results, studies were undertaken *in vivo* in order to determine the influence of TC extracts on a rat obesity model by evaluating specific anthropometric values and blood parameters of glucose and lipid metabolism.
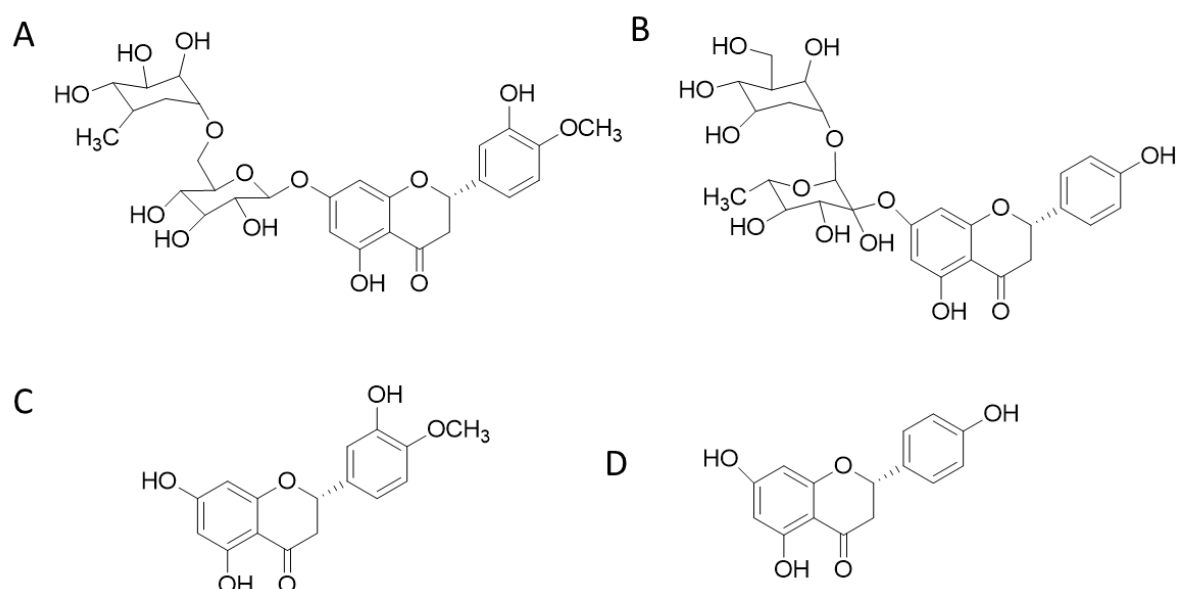
Figure 1. Chemical structure of hesperidin (A), naringin (B), hesperetin (C), naringenin (D).

2. Materials and methods

2.1. Samples

Citrus spp. All the samples were collected during the 2015–2016 winter in the regional company for the development of agriculture, ARSAC, located in Mirto-Crosia (geographical coordinates: 39.606803;16.763717), Calabria. All the plants had a similar irrigation treatment and were exposed to the same climate, grown in a ground with a pH ranging in between 7.9 and 8.2. The three varieties studied were CL *(Citrus clementina* Hort. ex. Tanaka), TR *(Citrus sinensis* L. Osbeck) and TC. The latter is a triploid hybrid obtained by the crossbreed of Monreal CL and TR. TC was also subjected to long-term phytochemical content evaluation (0, 6, 8 weeks at 1 °C and 90–95% relative humidity). Leaves were cleaned of soil residues and stored in a dry and cool place and kept at constant weight. Fruits were cut longitudinally and deprived of the two covers. Peels (flavedo) and pulp were separated from residues of the white portion (albedo). The pulp was deprived of the segment membrane and weighed. Samples were extracted by a Naviglio® apparatus (Atlas Filtri SRL, Limena, Italy), using a water-ethanol (1/1, v/v) solution (Toma, Casacchia, Don, D'Ippolito, & Statti, 2017).

2.2. Total polyphenol content determination

The total phenol content of the total extracts was determined using Folin–Ciocalteu reagent and chlorogenic acid as a standard, modified as previously reported (Casacchia et al., 2017). The total flavonoid content of the crude extract was determined by the $AlCl_3$ colorimetric method on the same extracts used for total phenol determination (Marrelli, Cristaldi, Menichini, & Conforti, 2015). Briefly, 20 mg of extract were dissolved in 10 μ of a mixture of ethanol/HCl (95:5), kept at 60 °C for 1 h and successively cooled to room temperature and homogenized. An amount of 200 μL (three replicates) was introduced into test tubes, followed by addition of 1.0 mL of Folin–Ciocalteu reagent and, after 3 min, 1.0 mL of $Na2CO_3$ (7.5%, v/v). The tubes were vortexed and heated at 40 °C (water bath) for 30 min. The calibration curve was determined by using seven standards with concentrations ranging from 50 to 1200 μg/mL. The absorption at 726 nm was measured (Perkin-Elmer Lambda 40 UV/VIS spectrophotometer) and the total phenol content expressed as mg of chlorogenic acid equivalents (CAE) per g of fresh weight (FW) material. Chlorogenic acid (10–1000 μg/mL) was used as a standard to obtain the calibration curve (y=0.0015x+0.3701, r^2=0,996).

2.3. Total flavonoid content determination

The total flavonoid content was determined using a colorimetric assay based on the formation of a flavonoid-aluminum complex, showing a λ_{max} absorption at 430 nm (Quettier-Deleu et al., 2000). Briefly, 2 mg of each TC extract were mixed with 1 mL of ethanol. After 5 min incubation, a 2% aqueous solution of $AlCl_3$ was added and the whole sample was left for 15 min in the dark. The calibration curve was determined by seven standard concentrations (25–900 μg/mL) of chlorogenic acid. The total flavonoid content was expressed as mg of quercetin equivalent (QE) per g of FW. The equation for the calibration curve was y=0.0018x+0.2974, with r^2=0.996.

2.4. Phytochemical profile determination by HPLC-DAD

The phytochemical composition of the *Citrus* hydroalcoholic extract was investigated by high-performance liquid chromatography coupled to ultraviolet detection (HPLC–UV–DAD) by using a DGU-14A Shimadzu (Kyoto, Japan) equipped with a pump (LC-10AT-VP model). The Shimadzu software was used to calculate the area of the surfaces under the

peaks. The compounds were separated on a Spherisorb ODS1 column (Waters Instruments, MA, USA). Solvent system: (A) 2%. aqueous acetic acid, (B) acetonitrile. Gradient program: 0–15 min, A=100%; 15–45 min, B=0–30%; 45–60 min, B=30–100%. Flow was 1 mL/min (XRs column), and volume of injection was 20 μL of extract solution. The detection wavelength was fixed at 285 nm. The retention times (RT) of naringin (32.5 min) and hesperidin (33.5 min) were similar to those already reported in other studies (Gorinstein et al., 2006). Standards of naringin, naringenin and hesperedin were measured under the same conditions.

2.5. Vitamin C determination
The vitamin C content was determined by the method of Nzewe and coworkers (Nweze, Abdulganiyu, & Erhabor, 2015). Titrations were performed in triplicate. The concentration of vitamin C for each 100 mL sample was calculated as % vitamin C concentration (mg/100 mL) = [standard concentration (mg/mL)/sample weight (g)]×1000.

2.6. Antioxidant activity: DPPH method
The 1,1-diphenyl-2-picryl-hydrazyl radical (DPPH) assay was adapted as previously described (Marrelli et al., 2014). *Citrus* extracts at different concentrations were added to an ethanol solution of DPPH radical (final concentration: 1.0×10^{-4} mol/L). The absorbance of the resulting solutions was measured at 517 nm. The DPPH solution without the sample solution was used as control. Trolox (Sigma-Aldrich St. Louis, USA) was used as the positive control. Decreasing absorbance values of the DPPH solutions indicated an increase of DPPH radical scavenging activity. Such activity was calculated as: % DPPH radical scavenging = (absorbance control−absorbance sample)/absorbance control×100.

2.7. Antilipoperoxidation activity
The antilipoperoxidation activity was measured using the BCB test (Marrelli et al., 2014). The solutions were obtained by adding 0.04 mL of linoleic acid, 0.4 mL of Tween 20 and 1.5 mL of a β-carotene solution in chloroform (0.5 mg/mL). The solvent was then evaporated under reduced pressure at 40 °C for 10 min through a rotary evaporator and the dry residue was immediately diluted with 150 mL of distilled water. Water was slowly added to the mixture and vigorously stirred to form an emulsion. Then, 0.2 mL of sample solutions at different concentrations (120, 60, 30, 15, 8, 4, 2, 0.5 mg/mL) were added to 5 mL of the emulsion.
Trolox was used as positive control after water solubilization at the same sample concentration. The absorbance was detected at λ=470 nm at both t_0 (the starting incubation time) and t=30 min. The antioxidant activity (AA) was calculated as: AA=[1−(A_0−A_t)/($A_0°$−$A_t°$)]×100, where A_0 and $A_0°$ are the absorbance values measured at t=0 min for sample standard and control, respectively, and A_t and $A_{t°}$ are the absorbance values measured in the sample standard and control at t=30 min, respectively (Kumazawa et al., 2002).

2.8. Pancreatic lipase inhibition assay
The porcine pancreatic lipase activity was assayed using p-nitrophenyl-octanoate (NPO) as substrate and spectrophotometrically recorded at λ=412 nm. A water solution (3 mg/mL) was prepared from type II crude porcine pancreatic cells (Conforti et al., 2012). Then, a 7.5 mmol/L solution of NPO in DMSO was prepared. The composition of the reaction mixture was the following: 100 μL of 7.5 mmol/L NPO, 4 mL of Tris–HCl buffer (pH=8.5), 100 μL of extract (concentration 400, 250, 100, 55, 30, 15, 5, 2, 0.8, 0.20, 0.05 mg/mL) and 100 μL of enzyme solution. The mixture was incubated at 37 °C. In the control, the extract was replaced with the same volume of DMSO. A blank sample without

the enzyme was prepared for each extract. Orlistat was used as positive control. The pancreatic inhibitory activity I was calculated as: I (%) = [1−(A$_c$−A$_s$)/A0]×100, where A$_c$ is the absorbance of the substrate of the porcine enzyme in the presence of the sample, As the absorbance of the porcine enzyme with the sample without substrate, and A$_0$ the absorbance at 100% enzyme activity on the substrate (without sample).

2.9. α-Amylase inhibition assay

Inhibition of the α-amylase enzyme was evaluated using a modified version of the method suggested by Kwon et al. (Kwon, Apostolidis, Kim, & Shetty, 2007). Sample solutions of 100 µL (with concentration 400, 250, 100, 55, 30, 15, 5, 2, 0.8, 0.20, 0.05 mg/mL) were added to 500 µL of a 0.5 mg/mL enzyme solution in cold distilled water and to 500 µL of a 1% (v/v) starch solution in 0.01 mol/L phosphate buffer at pH 7.0. The reaction mixture was incubated at 37 °C for 5 min; the reaction was stopped after the addition of 1 mL of the reagent dye DNS (3,5-dinitrosalicylic acid and 1% potassium sodium tartrate in 2% NaOH 0.4 mol/L). The reaction mixture was incubated at 100 °C for 5 min and the absorbance measured at 540 nm. The α-amylase inhibitory activity was calculated as: I(%)=[(A$_1$−A$_0$)/A$_1$]×100, where A$_0$ is defined as the absorbance at 100% enzyme activity (without sample) and A$_1$ as the absorbance of a test sample (with enzyme). The concentration of acarbose and of plant extracts that are required to inhibit 50% of α-amylase activity under these conditions was defined as the IC$_{50}$ value. The α-amylase inhibitory activity of the plant extracts and of acarbose was calculated, and IC$_{50}$ values were determined (Casacchia, Scavello, Rocca, Granieri, Beretta, Amelio, et al., 2018).

2.10. Molecular Docking

Molecular docking was performed on the crystallographic structures of HPA and HPL, corresponding to the entries 4GQR (Williams, Li, Withers, & Brayer, 2012) and 1LPB (Egloff et al., 1995) in the Protein Data Bank (PDB), respectively. Molecular structures of naringenin and hesperetin, both in the naturally occurring S enantiomeric form, were built by using the modeling software Avogadro (Hanwell et al., 2012). Docking calculations were performed by using AutoDock Vina 1.1.2 (Trott & Olson, 2010). Preliminary conversion of the structures from the PDB format was performed by using the graphical interface AutoDock Tools 1.5.6 (Morris et al., 1998). During the conversion, polar hydrogens were added for the crystallographic enzymes, and apolar hydrogens of naringenin and hesperetin were merged to the carbon atom they are attached to. Full flexibility was guaranteed for the ligands, resulting in four active torsions for naringenin (three hydroxyls, plus the bond connecting the phenol group to the rest of the molecule) and five for hesperetin (three hydroxyls, plus the two bonds connecting the phenol and methoxy group). A single simulation run was carried out in each case at very high exhaustiveness, 16 times larger than the default value.

2.11. In vivo study design

The *in vitro* anti-enzymatic activity of our extract, expressed as IC$_{50}$, was very close to that of Orlistat, used as positive control. Since Ferraz et al. determined that the effective dose of Orlistat to be administered to obtain significant pancreatic lipase inhibition in mice was 20 mg/day, we used an equivalent amount of extract in our *in vivo* assay. (Ferraz, Tiselius, & Heilberg, 2004). The study was conducted on Wistar rats (Envigo-Udine, Italy), which were individually housed in cages under controlled light (12 h light/dark cycle) and temperature (23–25 °C; 50–55% humidity) conditions with free access to food and water. Experiments were performed in accordance with the Declaration of Helsinki, the Italian law (D.L. 26/2014), the Guide for the Care and Use of Laboratory Animals published by the US

National Institutes of Health (2011) and the Directive 2010/63/EU of the European Parliament on the protection of animals used for science. The project was approved by the Italian Ministry of Health, Rome, and by the ethics review board. Diets used for the present study were provided by Envigo (Udine, Italy). Normolipidic (Diet 2018, used as standard diet, and indicated as SD; 6.2% kcal fat, 18.6% kcal protein, and 44.2% kcal carbohydrate) and hypercaloric (Teklad Diet TD 06414, used as high fat diet, and indicated as HFD; 60% kcal fat, 18.3%, kcal protein and 21.7% kcal carbohydrate) diets were administered as previously described (Casacchia et al., 2018). Rats were randomly assigned to three different experimental groups: (1) Group SD (fed with SD); (2) Group HFD (fed with HFD); (3) Group HFD+TC (fed with HFD plus 20 mg of extracts from edible part of TC, orally administered every day throughout the entire course of the treatment). The extracts were orally administered to each rat by using a syringe containing the daily dose, by holding the rat and letting the animal swallow the extract suspension (Kuster et al., 2012). During the procedure, complete ingestion was ensured, eliminating risks of variability in the intake among individual animals. In control rats, the same volume of filtered water has been administered. The experimental groups were subjected to the specific diet for 12 weeks.

2.12. "Anthropometric" variables determination and blood biochemical measurements

At the end of treatments, rats were anesthetized with ethyl carbamate (2 g/kg body weight, i.p.) and sacrificed. Subsequently, plasma was obtained by blood centrifugation at 4 °C for 15 min at 4000 g within 30 min from its collection. Immediately after sacrifice, hearts, livers and abdominal fats were collected and weighed. All "anthropometric" parameters (body weight, m waist circumference, body mass index, BMI and cardiac somatic index (CSI), the latter defined as the ratio between the heart weight and the animal weight multiplied by 100) and plasma analyses for biochemical determination indicated in the present work were performed as previously described (Casacchia et al., 2018). In particular, glycaemia was determined using a glucometer (ACCUCHEK, Roche Diagnostics, Germany); total cholesterol, HDL cholesterol, LDL cholesterol and triglycerides were determined using specific kits from PKL® POKLER ITALY; oxidized LDL cholesterol (LDL cholesterol-Ox) and insulin were evaluated by using enzymelinked immunosorbent assay kits (Elabscience Biotechnology, WuHan, China for LDL cholesterol-Ox and Millipore, St. Charles, MO, USA for insulin).

2.13. Liver triglycerides determination

The triglycerides quantitative determination in liver samples was performed by using a colorimetric assay kit from PKL® POKLER ITALY as follows: the liver of each experimental group was homogenized with an Ultra-Turrax® in phosphate buffered saline, PBS (137mM NaCl, 2.7mM KCl, 10mM Na_2HPO_4, 1.8mM KH_2PO_4; pH 7.4) plus a mixture of protease inhibitors (1 mmol/L aprotinin, 20 mmol/L phenylmethylsulfonyl fluoride, and 200 mmol/L sodium orthovanadate) and centrifuged at 15000 g for 20 min (4 °C). The supernatants were then assayed with the kit. The assay started with the enzymatic hydrolysis of the triglycerides by lipoprotein lipase to produce glycerol and free fatty acids. The glycerol released was then measured by a coupled enzymatic reaction system with a colorimetric readout at 540 nm. Results were expressed as mg triglycerides per g of liver tissue.

2.14. HOMA-IR (Homeostatic Model Assessment-estimated Insulin Resistance) index

HOMA index was calculated according to Matthews et al. (1985) and Cacho, Sevillano, de Castro, Herrera, and Ramos (2008).

2.15. Statistical analysis

Statistical analysis for *in vivo* study was performed by using the GraphPad Prism Software$^{®}$ (version 5.0; GraphPad Software, San Diego, CA, USA). Data were expressed as the mean ± SEM. Oneway ANOVA (analysis of variance) Newman-Keuls multiple comparison test was used. Statistically significant differences: *$p \leq 0.05$, **$p \leq 0.01$, ***$p \leq 0.001$.

3. Results and discussion

3.1. Antioxidant activity evaluation

The antioxidant activity of *Citrus* extracts is in a direct relationship with the content of polyphenols and their chemical properties. The activity strongly depends on the capability of polyphenols to act as reducing agents or hydrogen atom donors (Rodrigues et al., 2013). On the other hand, the antioxidant activity is hard to be unambiguously defined, since the polyphenol content depends on several factors such as variability in the extract composition, environmental conditions during the plant growth, origin of the starting materials, as well as the different techniques adopted for the polyphenol determination (Floegel, Kim, Chung, Koo, & Chun, 2011). Three different *Citrus* cultivars TR, CL and TC were considered in this study, especially focusing on the latter because, being a hybrid of the two former cultivars, could represent an improvement in terms of nutritional potential and possible source of active molecules. Moreover, the research was conducted not only on the edible part of the fruits, but also on leaves and peels, which represent a waste material left out after specific agro-food manufacturing, but still rich in antioxidant agents.

The first step of the research process consisted in the hydro-alcoholic digestion of natural solid materials by using the method already described (Toma et al., 2017), in order to optimize the polyphenol fraction extraction avoiding any stress to thermo-sensitive components. The successive step was the determination of the total polyphenol content of the extracts and the subsequent measurement of the amount of flavonoids. Both determination, as well as that of the antioxidant activity of the extracts, were performed on fresh TC and on the parent cultivar extracts. The former was further assayed after 6- and 8-week storage periods (Table 1). The polyphenol and flavonoid content was higher for the pulp of TR (207 mgCAE/gFW and 85 mgQE/gFW, respectively) compared to CL and TC, whereas radical scavenging activity was higher for the pulp of CL (IC_{50}=100.5 mg/mL). On the other hand, the leaf and peel extracts showed an overall higher value for TC compared to the other two cultivars. Due to the high commercial and nutritional interest of TC, the amount of antioxidants was also monitored for this cultivar after a 6- and 8-week storage period on both pulp and leaves. Quite surprisingly, a slight increase was detected for the overall content of polyphenols and flavonoids, besides a negligible variation of the antioxidant activity after the storage lapse. The antioxidant properties for the pulp extract were unchanged and seem to be related to both the vitamin C content, which was almost constant after storage (40.23 ± 0.02, 40.03 ± 0.05 and 40.01 ± 0.01 mg/100 mL for the fresh extract and after 6- and 8- week storage, respectively), and the polyphenol fraction, which slightly increased with time. Taking into consideration the overall results obtained, it can be deduced that the antioxidant activity of TC leaf extract (IC_{50}=67.2 μg/ mL) was higher than that observed for the remaining parts of the fruit. At the same time, activity of peel extract (IC_{50}=55.7 μg/mL) was comparable to that of pulp (IC_{50}=57.5 μg/mL). These results proved that peels and leaves, both considered as waste during the manufacturing processes, could be further exploited as starting material for the preparation of dietetic supplements or cosmetic preparations.

3.2. HPLC determination of naringin, naringenin and hesperidin

Based on the above results, further investigation was planned in order to assess the variability of flavonoids content of peel and pulp TC extracts. The amount of hesperidin, naringin and naringenin after 8- week storage (1 °C e 90–95% RH) significantly increased in both extracts, as determined by HPLC technique. As a result, a significant increase for all the three flavonoids was detected. In particular, an almost four-fold increase in peel and a three-fold increase in pulp extracts were recorded (Table 2). These results are in accordance with other studies performed on non-climateric *Citrus* fruits subjected to storage and refrigeration (Amarowicz et al., 2009; Crifo, Petrone, Lo Cicero, & Lo Piero, 2012; Crifo, Puglisi, Petrone, Recupero, & Lo Piero, 2011).

3.3. Enzymatic assays: Inhibition of HPA and HPL

HPA is a key enzyme in the starch digestion process and it is responsible for the transformation of starch to malto-oligosaccharides, and then to glucose. On the other hand, HLP is of great importance for the digestion and absorption of lipids, since it is able to hydrolyze fats to glycerol and fatty acids. Therefore, both enzymes represent attractive therapeutic targets for the treatment of metabolic disorders such as diabetes and obesity. The antienzymatic activity of different *Citrus* variety had been assessed in previous studies and it was shown to be related to specific parts of the plant (Shen et al., 2012; Uddin et al., 2014). In this study, the inhibitory activity of selected *Citrus* cultivars was accordingly evaluated on both enzymes. The antienzymatic tests have been carried out on pulp, peel and leaf extracts, which represent the final product and waste after agro-food manufacturing. In particular, samples of CL, TR and TC have been investigated in order to compare the inhibitory activity of the hybrid TC with its parent cultivars. The activity exerted on HPA was higher for the pulp extract of TC (IC_{50}=44.28 ± 0.65 μg/mL). This extract showed the best result also in the HLA inhibition test (IC_{50}=67.20 ± 0.30 μg/mL). A similar outcome was obtained for the HPA inhibition with TC peel extract (IC_{50}=41.23 ± 0.25 μg/mL), which was equipotent to CL, but still more potent than TR. Again, the highest activity for leaf extracts on HPA and HPL was exerted by TC (IC_{50}=54.27 ± 0.28 and 63.30 ± 0.09 μg/mL, respectively). In conclusion, it can be deduced that the performance of the hybrid was more favorable with respect to its parents in almost all the assays attempted, thus confirming that TC is worthy of further investigations to be used as a supplement in the treatment of metabolic disorders (Table 3). After these preliminary results, we also investigated TC activity after 6- and 8-week storage under controlled ambient conditions (1 °C and 90–95% RH). Accordingly, referring to peel extract, both HPA and HPL inhibitory activities were monitored and, despite the increase in the flavonoid content, the best result was achieved after a 6-week lapse, whereas a decrement was observed for the longer storage time. Conflicting results were obtained from assays on pulp extract. It was noticed that the HPA inhibitory activity decreases with time, whereas the HPL inhibitory activity remains almost unchanged after storage. From the results above reported, it can be hypothesized that the increased HPA and HPL inhibition after fruit storage could be due to the induction of genes expression promoted by stressing conditions, which could influence the plant defense pathways with an increase in the amount of biologically active secondary metabolites.

Table 1: *Total polyphenol content, total flavonoid content and antioxidant activity (DPPH test) in pulp, peels and leaves of CL, TR and TC. Values are expressed as means ± standard deviations on three measurements. CAE and QE indicate chlorogenic acid and quercetin equivalents, respectively. Results were reported as mean ± SD. Different letters (a, b, c) in the same column indicate significant differences among extracts (P < 0,05) according to Student's t-test. Statistically significant differences among pulp, peel and leaves of each Citrus specie are indicated by $^{\S,*,\wedge}$. Trolox was used as positive control in the DPPH test.*

Samples	Pulp			Peels			Leaves		
	Polyphenols (mgCAE/gFW)	Flavonoids (mgQE/gFW)	DPPH (IC$_{50}$) (µg/mL)	Polyphenols (mgCAE/gFW)	Flavonoids (mgQE/gFW)	DPPH (IC$_{50}$) (µg/mL)	Polyphenols (mgCAE/gFW)	Flavonoids (mgQE/gFW)	DPPH (IC$_{50}$) (µg/mL)
CL	90.01 ± 0.65^{c*}	41.3 ± 0.52^{c*}	100.3 ± 0.08^{c}	109.86 ± 0.72^{c*}	61.3 ± 0.60^{c§}	96.7 ± 0.31^{c*}	137.29 ± 0.89^{c§}	58.6 ± 0.65^{c*}	56.6 ± 0.09^{a§}
TR	207.69 ± 0.13^{a*}	85.9 ± 0.21^{a§}	85.1 ± 0.18^{b*}	177.16 ± 0.46^{b*}	65.9 ± 0.50^{b*}	86.9 ± 0.75^{b*}	209.27 ± 0.56^{b§}	65.2 ± 0.50^{b*}	76.8 ± 0.05^{c§}
TC	201.23 ± 0.95^{b*}	67.2 ± 0.99^{c*}	57.5 ± 0.08^{a§}	201.23 ± 0.93^{a*}	77.2 ± 0.49^{a§}	55.7 ± 0.88$^{a\wedge}$	214.17 ± 0.88^{a§}	67.2 ± 0.49^{a*}	67.2 ± 0.08^{b*}
TC (6 weeks)	205.64 ± 0.56^{b*}	75.2 ± 0.50^{b*}	49.4 ± 0.05^{a§}	367.31 ± 0.36^{b§}	85.1 ± 0.20^{b§}	57.4 ± 0.02^{b*}			
TC (8 weeks)	228.95 ± 0.88^{a*}	87.2 ± 0.49^{a§}	49.3 ± 0.08^{a§}	372.11 ± 0.28^{a§}	87.3 ± 0.99^{a§}	56.3 ± 0.05^{a*}			

Table 2: *Hesperedin, naringenin and naringin content in TC peel and pulp extracts after storage (1 °C, 90–95% RH). Values are expressed as means ± standard deviations on three measurements. Results were reported as mean ± SD. Different letters (a, b, c) in the same column indicate significant differences among extracts (P < 0,05) according to Student's t-test. Statistically significant differences among pulp, peel and leaves of each Citrus specie are indicated by $^{\S,*,\wedge}$.*

Citrus	Pulp			Peels		
	Hesperedin (ppm)	Naringin (ppm)	Naringenin (ppm)	Hesperedin (ppm)	Naringin (ppm)	Naringenin (ppm)
TC	86.8 ± 0.05^{c*}	87.69 ± 0.04^{c§}	107 ± 0.05^{c§}	193.3 ± 0.05^{c§}	63.69 ± 0.05^{c*}	89 ± 0.03^{c*}
TC (6 weeks)	162.8 ± 0.09^{b*}	185.0 ± 0.05^{b§}	306 ± 0.05^{b§}	631.9 ± 0.03^{b§}	112.00 ± 0.05^{b*}	298 ± 0.025^{b*}
TC (8 weeks)	241.1 ± 0.08^{a*}	205.8 ± 0.03^{a*}	307 ± 0.06^{a*}	775.1 ± 0.08^{a§}	209.5 ± 0.06^{a§}	323 ± 0.05^{a§}

Table 3: *Antienzymatic activity of Citrus extracts. IC$_{50}$ is the in vitro concentration required to decrease to 50% the reactivity of the studied reactive species (mean ± standard error of the mean; three measurements). Different letters (a, b, c) in the same column indicate significant differences among extracts (P < 0,05) according to Student's t-test. *Acarbose was used as a positive control (IC$_{50}$=36.50 ± 0.32 µg/mL). **Orlistat was used as a positive control (IC5$_{0}$=57.20 ± 0.19 µg/mL). Statistically significant differences among pulp, peel and leaves of each Citrus specie are indicated by $^{\S,\#,\wedge}$.*

Samples	Pulp		Peels		Leaves	
	HPA (IC$_{50}$)*	HPL (IC$_{50}$)**	HPA (IC$_{50}$)*	HPL (IC$_{50}$)**	HPA (IC$_{50}$)*	HPL (IC$_{50}$)**
CL	99.66 ± 0.36$^{c\wedge}$	86.30 ± 0.45$^{b\#}$	49.86 ± 0.02^{c§}	61.30 ± 0.50^{c§}	97.29 ± 0.89$^{c\#}$	98.60 ± 0.55^{c}
TR	57.12 ± 0.63^{b§}	105.90 ± 0.20$^{c\wedge}$	77.16 ± 0.16$^{b\#}$	85.90 ± 0.20$^{b\#}$	89.21 ± 0.06$^{b\wedge}$	85.20 ± 0.05^{b§}
TC	44.28 ± 0.65$^{a\#}$	67.20 ± 0.30$^{a\#}$	41.23 ± 0.25^{a§}	67.20 ± 0.29$^{a\#}$	54.27 ± 0.28$^{a\wedge}$	63.30 ± 0.09^{a§}
TC (6 weeks)	44.28 ± 0.65^{a§}	67.2 ± 0.30$^{a\#}$	57.16 ± 0.90$^{c\#}$	65.7 ± 0.50^{b§}		
TC (8 weeks)	57.16 ± 0.90$^{c\#I}$	65.7 ± 0.50^{b§}	55.1 ± 0.03^{b§}	67.9 ± 0.25$^{a\#}$		

3.4. Molecular docking

In order to verify whether the inhibitory activity could be attributed to the direct interaction of naringenin and hesperetin with HPA and HPL, molecular docking was performed by using the crystallographic enzyme structures withdrawn from the PDB. Only aglycones naringenin and hesperetin were tested, and not the corresponding native glycosides naringin and hesperidin, because it has long been suggested that sugar molecules of a glycoside can only influence pharmacokinetics into the body, whereas the receptor activity is confined to the

aglyconic portion. Moreover, the majority of flavonoid glycosides are hydrolyzed at an intestinal or hepatic level by the action of a lactase phloridzin hydrolase or a β-glucosidase, so that only the free aglycones are able to reach the systemic bloodstream (Day et al., 1998, 2000; Ioku et al., 1998). The mode of interactions of each compound with the active site of both enzymes was predicted by a protein-based docking approach, using a protocol already adopted for the study of other polyphenol (Grande et al., 2018). Although both naringenin and hesperetin could each exist in two enantiomeric configurations, only the S isomer has been taken into consideration for the computational studies, because such form is the only one present in nature (Dewick, 2009). Since 67 different HPA and 7 different HPL crystallographic structures have been deposited to the PDB, a selection of suitable models was carried out for both proteins. The 4GQR entry (Williams et al., 2012) was chosen for HPA because in this structure the protein is complexed with the flavonol myricetin, an analogue of our compounds. Furthermore, the most recent 1LPB entry (Egloff et al., 1995) was adopted for HPL. Three distinct domains can be recognized in the crystallographic structure of HPA. The active site is located to one end of a triosephosphate isomerase barrel and three carboxylic acid residues (i.e., Asp197, Glu233 and Asp300) have been shown to be essential for catalysis. As shown in Figure 2A and B, in our docking experiments the two flavonoids adopt an orientation similar to that observed in the binding of myricetin (Williams et al., 2012). Furthermore, both naringenin and hesperetin interact with the three catalytic residues in the enzyme active site. In particular, Asp197 is the key residue for the nucleophilic hydrolytic catalysis of HPA on starch polymers (Rydberg et al., 2002; Zhang et al., 2009). The interaction with Glu233 precludes its catalytic function as acid-base promoter of hydrolysis, while the binding with Asp300 prevents the correct orientation of starch molecule into the active site. The binding energies calculated for naringenin and hesperetin were −8.1 and −7.7 kcal/mol, respectively, indicating a good affinity for the protein. These values are comparable to the one obtained after the re-docking of myricetin in the crystallographic position, −7.8 kcal/mol, further suggesting that all these molecules can bind to HPA. The crystallographic structure of HPL includes three structural domains: a N-terminal domain containing the active site, a non-catalytic C-terminus encompassing a colipase binding site, and a lid loop that regulates the ligand entry into the active site. A catalytic triad (Ser152, Asp176 and Hys263) actively participates to lipid hydrolysis in the active site. As shown in Figure 2C and D, both naringenin and hesperetin were found to interact with all these residues, therefore preventing the substrate access. The two molecules accommodate with the same orientation into the protein active site, showing in both cases a binding affinity of −9.6 kcal/mol, strongly supporting the anchoring to HPL.
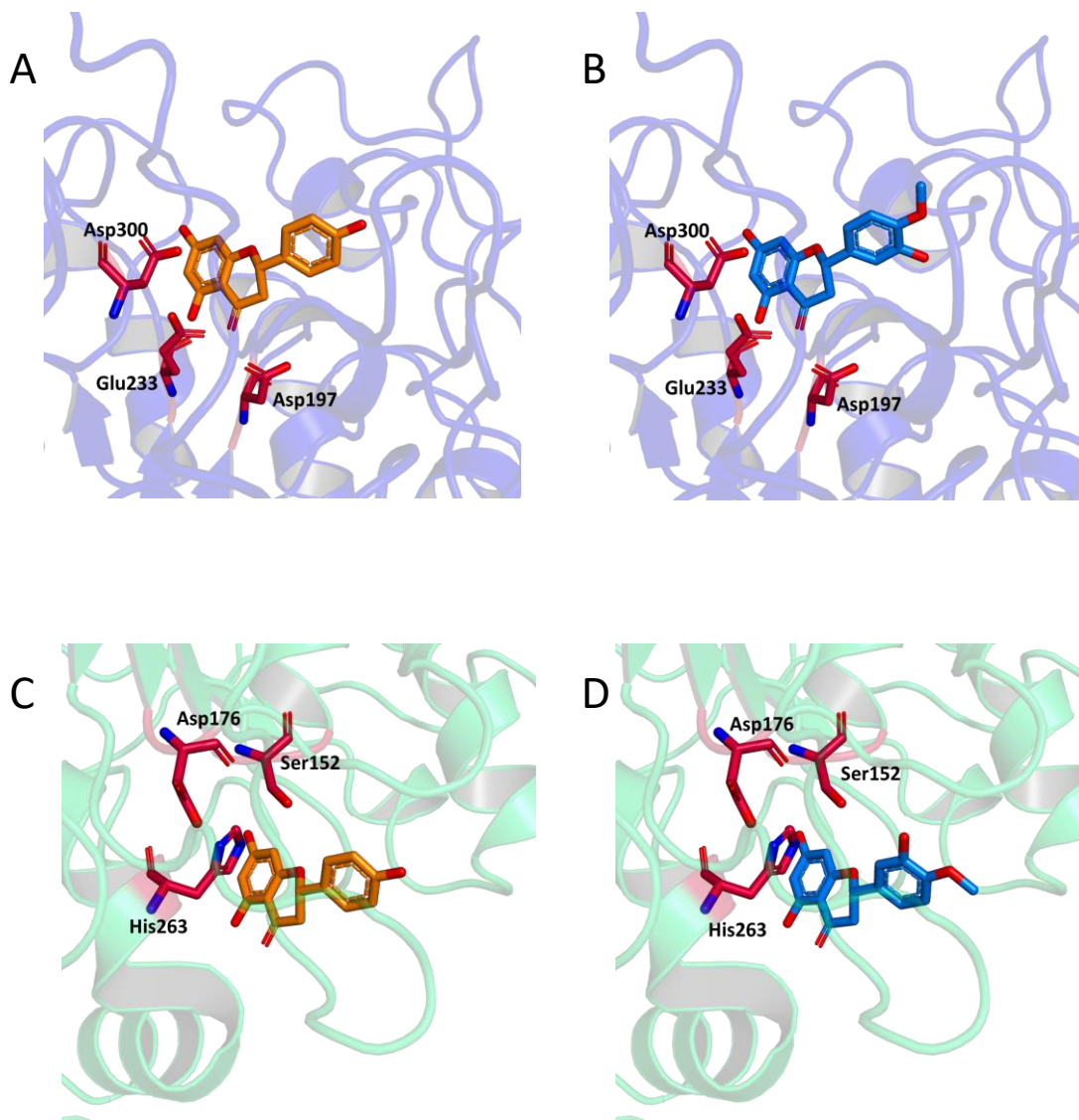
Figure 2. Docking poses of the ligands within the protein active sites: (A) naringenin (yellow) and B) hesperetin (blue) bound to the catalytic pocket of HPA, and the same two compounds (C and D, respectively) anchored within the binding site of HPL.

3.5. In vivo studies

3.5.1. "Anthropometric" and metabolic parameters

Firstly, no significant differences were observed for the anthropometric and metabolic parameters in the SD+TC pulp (20 mg of extracts) group (data not shown), suggesting that this extract does not exert effects in normolipidic condition. After 12 weeks of treatment, the mean body weight of rats fed with HFD was higher than those fed with SD (Figure 3A); in the HFD+TC group, the mean body weight significantly decreased with respect to the group fed with HFD. A similar trend was observed in the measurements of BMI and waist circumference (Figures 3B and C). As showed in Figure 3D, the abdominal fat deposition was significantly higher in HFD rats with respect to the SD control counterpart and to the HFD+TC group. Several studies indicate that the value of BMI and fat mass deposition represent important indicators of adiposity, and the latter also seems to be a critical factor in

the development of insulin resistance (Virtue & Vidal-Puig, 2010). Both these factors are widely used, together with a metabolic health assessment, as a useful population-level measure of overweight and obesity (Goossens, 2017) which represent important risk factors for the development of pathological conditions (Kopelman, 2000). Our results indicate that the addition of TC moderately opposes the increase of the considered parameters, Interestingly, the experimental groups showed differences in the food intake, daily recorded during treatments. In particular, the HFD group showed a significantly higher daily caloric intake compared to SD group (58 ± 2 kcal/day for the SD *vs* 117 ± 3 kcal/day for the HFD). In contrast, TC extracts affected the caloric intake since it significantly decreased with respect to the HFD counterpart (117 ± 3 kcal/day for the HFD *vs* 107 ± 1 kcal/day for HFD+TC). Furthermore, the weight reduction, observed in HFD fed rats treated with TC extracts, may be also due to ability to influence the food intake control. In fact, several observations regarding the effects of specific polymethoxylated flavones on appetite suppression and regulation are reported (Kim & Park, 2011). Particularly, some *Citrus* flavonoids (including naringenin and hesperetin) act as appetite suppressants by targeting specific signaling hormones that control caloric intake and by activating selective receptors and proteins involved in the increase of energy expenditure in heat-producing, brown adipose tissue (Kim & Park, 2011). It has been observed that obesity is associated with hemodynamic alterations of the cardiovascular function and thus with cardiac structural changes in terms of left ventricular hypertrophy (Kopelman, 2000; Lauer, Anderson, Kannel, & Levy, 1991). Accordingly, in the present study, the heart weight (Figure 3E) and the cardiac somatic index (CSI) (Figure 3F), an index of cardiac hypertrophy (Flanagan et al., 2008), were found to be higher in HFD fed animals with respect to the SD group; in contrast, the administration of TC in HFD rats significantly inverted these alterations (Figure 3E and F), providing indications on the role of these extracts in the abnormal heart growth induced by obesity. In fact, in the HFD-treated rats the heart weight was greater either in absolute and in the heart/body weight ratio values. Since obesity presents an augmented risk in the development of nonalcoholic fatty liver disease (NAFLD), associated with several alterations in glucose, fatty acid and lipoprotein metabolism (Fabbrini, Sullivan, & Klein, 2010), we investigated the TC extract effects on the hepatic function. A significant reduction of the liver weight (Fig. 3G) and hepatic levels of triglycerides (Figure 3H) was recorded for obese rats orally supplemented with *Citrus* solution with respect to the HFD group (Figure 3H and G). This prompts to hypothesize that the extract is able to counteract the hepatic alteration related to the increased liver weight and to the intrahepatic triglycerides accumulation induced by obesity. The plasma determination of specific analytes showed a significant increase of total cholesterol (Figure 4A), LDL cholesterol (Figure 4B), oxidized LDL cholesterol (Figure 4C) and triglycerides (Figure 4D) levels after HFD diet, whereas in the HFD+TC group they were significantly reduced (Figure 4A–D). An opposite trend was observed for HDL cholesterol plasma levels (Figure 4E). Accordingly, these measurements indicate that *Citrus* might globally reduce the cardiovascular risk dependent from the alteration of the plasma lipid profile associated with obesity (Klop, Elte, & Cabezas, 2013). Interestingly, TC also decreased the circulating oxidized LDL, a marker of oxidative stress, strongly associated in adults with obesity, insulin resistance, metabolic syndrome and cardiovascular disease (Reilly & Kelly, 2011). Finally, the metabolic analysis regarding the insulin sensitivity assessment indicated a significant increase of insulin (Figure 4F), basal glucose plasma levels (Figure 4G) and, consequently, of the HOMA index (Figure 4H) in the HFD group with respect to SD group. HOMA index is widely used to easily estimate the whole body insulin sensitivity. This index has a variability and discriminant power comparable to those of other more complex and invasive methods, and it can be applied also in animal models, providing a useful tool for assessing the metabolic state related to the

glucose homeostasis and insulin efficiency (Cacho et al., 2008; Matthews et al., 1985). Compared to HFD fed animals, the treatment with *Citrus* was able to significantly reduce these parameters. The beneficial effects mediated by the extract on these factors, which represent important predictors of insulin resistance in the early stage of diabetes (Cacho et al., 2008; Matthews et al., 1985), indicate that TC might improve the insulin sensitivity and glucose tolerance, thus being potentially useful in the control of altered metabolic above condition.
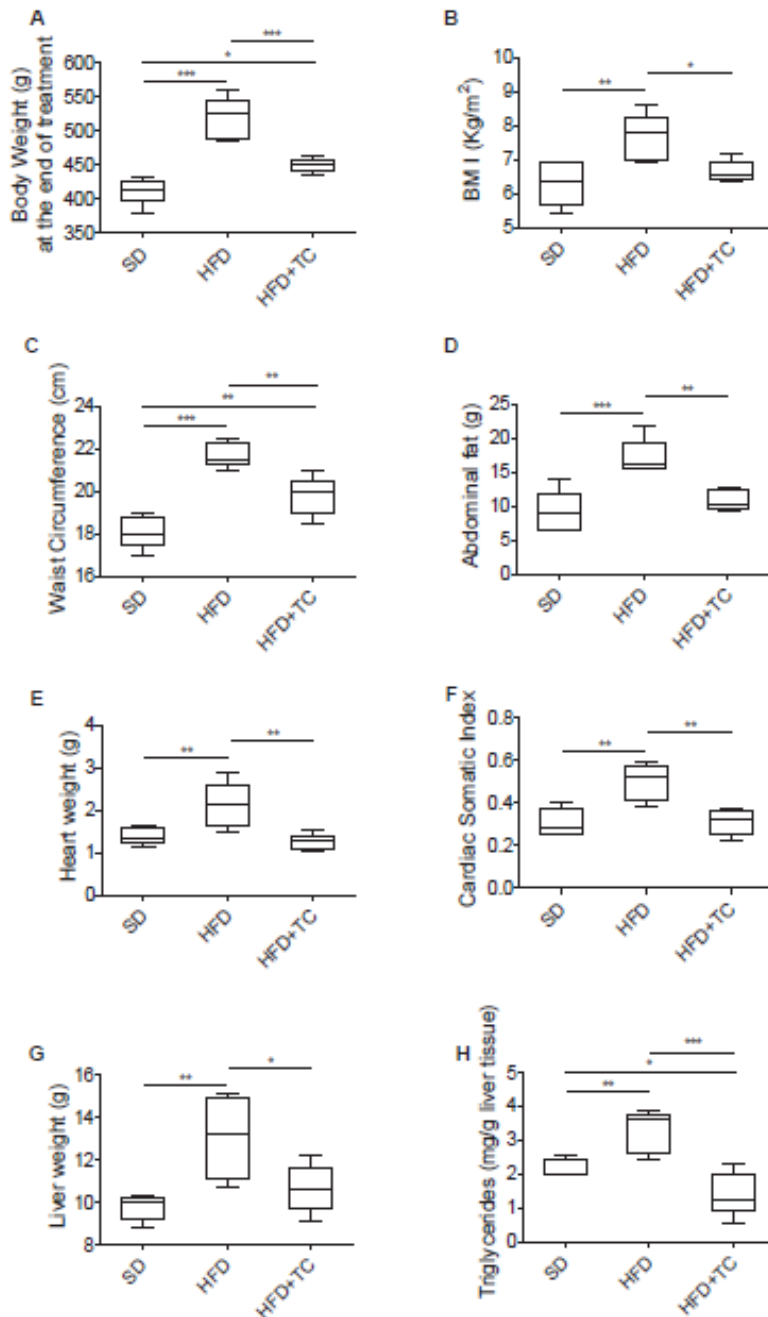
Figure 3. Body weight (A), BMI (B), waist circumference (C), abdominal fat (D), heart weight (E), cardiac somatic index (CSI) (F), liver weight (G) and hepatic triglycerides (expressed as mg/g tissue) of rats fed with SD, HFD, or HFD+TC (20 mg of extract), recorded at the end of the treatment (5 rats for each group); significance of difference: oneway ANOVA, non-parametric Newman-Keuls multiple comparison test (for post-ANOVA comparisons). *P < 0.05, **P < 0.01, ***P < 0.001.
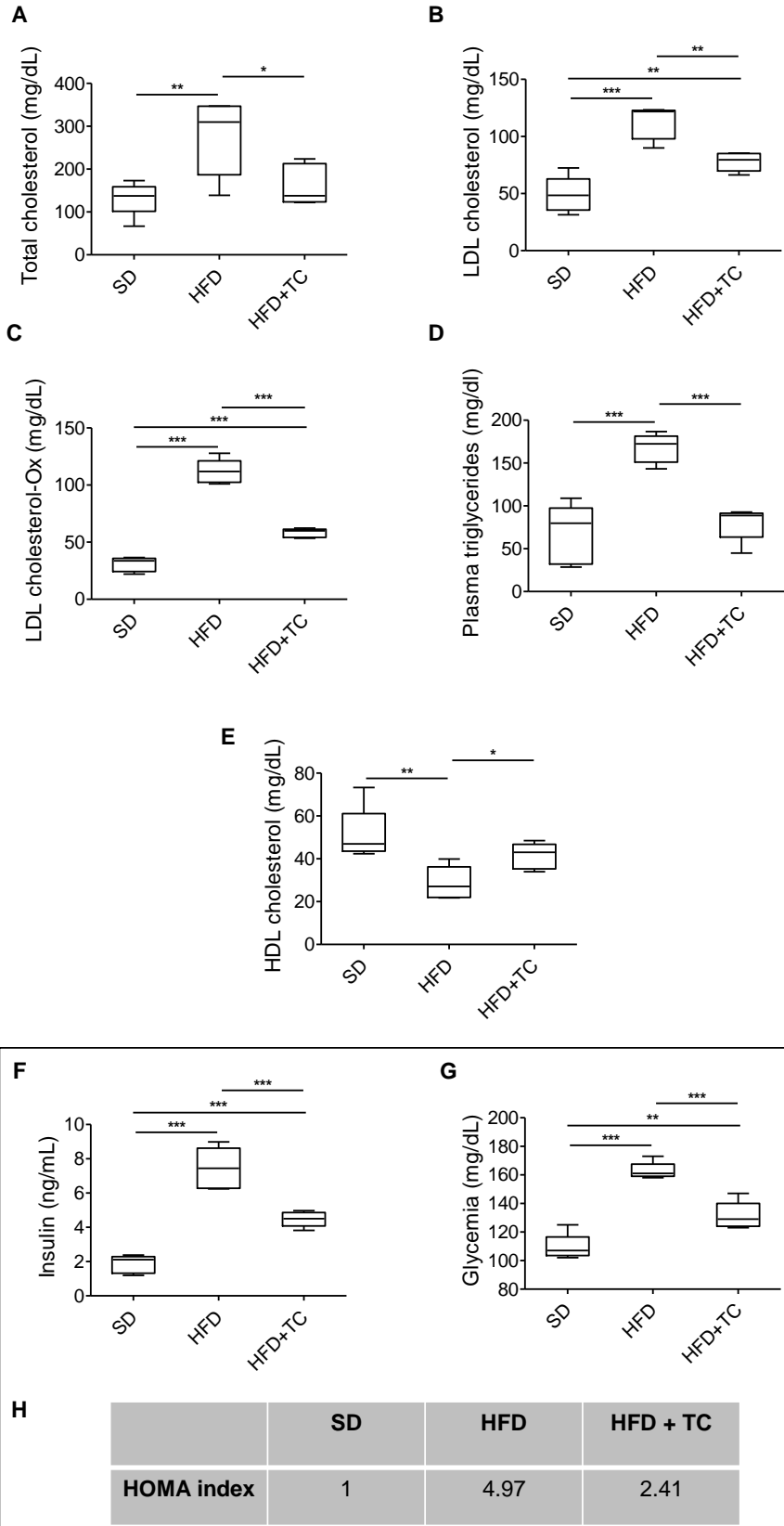
Figure 4. *Plasma levels of total cholesterol (A), LDL cholesterol (B), oxidized-LDL cholesterol (C), triglycerides (D), HDL cholesterol (E), insulin (F), glucose (G) and HOMA index (H) on rats fed with SD, HDF or HDF+TC (20 mg of extract), recorded at the end of the treatment. (5 rats for each group); significance of difference: oneway ANOVA, non-parametric Newman-Keuls multiple comparison test (for post-ANOVA comparisons). *P < 0.05, **P < 0.01, ***P < 0.001.*

4. Conclusions

The *Citrus* hybrid TC has been selected for the determination of its nutraceutical potential with respect to its parent cultivars, TR and CL. Besides a profitable economic interest, this *Citrus* variety seems endowed with interesting biological features due to the remarkable polyphenol content. In particular, the extracts were rich in naringin and hesperidin, the antioxidant, lipid lowering and hypoglycemic activities of which are well known. A significant antioxidant and HPA/HPL inhibitory activity has been demonstrated by specific *in vitro* assays on different TC extracts. Moreover, favorable interactions with protein key residues were found for the two corresponding aglycones, naringenin and hesperetin, that have been docked into active site of the two enzymes. The influence of TC extracts dietary administration on anthropometric values, lipid and glucose metabolism on a rat model of obesity and metabolic syndrome was measured by *in vivo* studies. All the collected results indicate that, after an accurate standardization in their polyphenol content, the TC extracts could be included in dietary supplements for the management of metabolic disorders. Furthermore, assays performed on *Citrus* leaves and peel proved that active phytochemicals, to be included into nutraceutical formulations, could be recovered with a high yield, after simple extraction procedures on agrofood processes waste.

References

Agrawal, Y. O., Sharma, P. K., Shrivastava, B., Ojha, S., Upadhya, H. M., Arya, D. S., & Goyal, S. N. (2014). Hesperidin produces cardioprotective activity via PPAR-gamma pathway in ischemic heart disease model in diabetic rats. PLoS ONE, 9(11), e111212.

Akiyama, S., Katsumata, S., Suzuki, K., Ishimi, Y., Wu, J., & Uehara, M. (2010). Dietary hesperidin exerts hypoglycemic and hypolipidemic effects in streptozotocin-induced marginal type 1 diabetic rats. Journal of Clinical Biochemistry and Nutrition, 46(1), 87–92.

Alam, M. A., Kauter, K., & Brown, L. (2013). Naringin improves diet-induced cardiovascular dysfunction and obesity in high carbohydrate, high fat diet-fed rats. Nutrients, 5(3), 637–650.

Amarowicz, R., Carle, R., Dongowski, G., Durazzo, A., Galensa, R., Kammerer, D., ... Piskula, M. K. (2009). Influence of postharvest processing and storage on the content of phenolic acids and flavonoids in foods. Molecular Nutrition & Food Research, 53(Suppl 2), S151–S183.

Anagnostopoulou, M. A., Kefalas, P., Papageorgiou, V. P., Assimopoulou, A. N., & Boskou, D. (2006). Radical scavenging activity of various extracts and fractions of sweet orange flavedo (Citrus sinensis). Food Chemisty, 94, 19–25.

Birari, R. B., & Bhutani, K. K. (2007). Pancreatic lipase inhibitors from natural sources: Unexplored potential. Drbug Discovery Today, 12(19–20), 879–889.

Cacho, J., Sevillano, J., de Castro, J., Herrera, E., & Ramos, M. P. (2008). Validation of simple indexes to assess insulin sensitivity during pregnancy in Wistar and Sprague-Dawley rats. American Journal Physiology Endocrinology Metabolism, 295(5), E1269–E1276.

Casacchia, T., Scavello, F., Rocca, C., Granieri, M. C., Beretta, G., Amelio, D., ... Pasqua, T. (2018). Leopoldia comosa prevents metabolic disorders in rats with high-fat dietinduced obesity. European Journal of Nutrition.

Casacchia, T., Sofo, A., Casaburi, I., Marrelli, M., Conforti, F., & Statti, G. (2017). Antioxidant, enzyme-inhibitory and antitumor activity of the wild dietary plant Muscari comosum (L.) Mill. International Journal of Plant Biology, 8, 6895.

Cho, K. W., Kim, Y. O., Andrade, J. E., Burgess, J. R., & Kim, Y. C. (2011). Dietary naringenin increases hepatic peroxisome proliferators-activated receptor alpha protein expression and decreases plasma triglyceride and adiposity in rats. European Journal of Nutrition, 50(2), 81–88.

Choi, J. S., Yokozawa, T., & Oura, H. (1991). Improvement of hyperglycemia and hyperlipemia in streptozotocin-diabetic rats by a methanolic extract of Prunus davidiana stems and its main component, prunin. Planta Medica, 57(3), 208–211.

Conforti, F., Perri, V., Menichini, F., Marrelli, M., Uzunov, D., Statti, G. A., & Menichini, F. (2012). Wild Mediterranean dietary plants as inhibitors of pancreatic lipase. Phytotherapy Research, 26(4), 600–604.

Crifo, T., Petrone, G., Lo Cicero, L., & Lo Piero, A. R. (2012). Short cold storage enhances the anthocyanin contents and level of transcripts related to their biosynthesis in blood oranges. Journal of Agriculture and Food Chemistry, 60(1), 476–481.

Crifo, T., Puglisi, I., Petrone, G., Recupero, G. R., & Lo Piero, A. R. (2011). Expression analysis in response to low temperature stress in blood oranges: Implication of the flavonoid biosynthetic pathway. Gene, 476(1–2), 1–9.

Day, A. J., Canada, F. J., Diaz, J. C., Kroon, P. A., McLauchlan, R., Faulds, C. B., ... Williamson, G. (2000). Dietary flavonoid and isoflavone glycosides are hydrolysed by the lactase site of lactase phlorizin hydrolase. FEBS Letters, 468(2–3), 166–170.

Day, A. J., DuPont, M. S., Ridley, S., Rhodes, M., Rhodes, M. J., Morgan, M. R., & Williamson, G. (1998). Deglycosylation of flavonoid and isoflavonoid glycosides by human small intestine and liver beta-glucosidase activity. FEBS Letters, 436(1), 71–75.

Dewick, P. M. (2009). Medicinal natural products a biosynthetic approach (3rd ed.).

Ding, X., Fan, S., Lu, Y., Zhang, Y., Gu, M., Zhang, L., ... Huang, C. (2012). Citrus ichangensis peel extract exhibits anti-metabolic disorder effects by the inhibition of PPARgamma and LXR signaling in high-fat diet-induced C57BL/6 mouse. Evidence-Based Complementary and Alternative Medicine, 2012, 678592.

Egloff, M. P., Marguet, F., Buono, G., Verger, R., Cambillau, C., & van Tilbeurgh, H. (1995). The 2.46 a resolution structure of the pancreatic lipase-colipase complex inhibited by a C11 alkyl phosphonate. Biochemistry, 34(9), 2751–2762.

Fabbrini, E., Sullivan, S., & Klein, S. (2010). Obesity and nonalcoholic fatty liver disease: Biochemical, metabolic, and clinical implications. Hepatology, 51(2), 679–689.

Fan, J., Song, Y., Chen, Y., Hui, R., & Zhang, W. (2013). Combined effect of obesity and cardio-metabolic abnormality on the risk of cardiovascular disease: A meta-analysis of prospective cohort studies. International Journal of Cardiology, 168(5), 4761–4768.

Ferraz, R. R., Tiselius, H. G., & Heilberg, I. P. (2004). Fat malabsorption induced by gastrointestinal lipase inhibitor leads to an increase in urinary oxalate excretion. Kidney International, 66(2), 676–682.

Flanagan, E. T., Buckley, M. M., Aherne, C. M., Lainis, F., Sattar, M., & Johns, E. J. (2008). Impact of cardiac hypertrophy on arterial and cardiopulmonary baroreflex control of renal sympathetic nerve activity in anaesthetized rats. Experimental Physiology, 93(9), 1058–1064.

Floegel, A., Kim, D., Chung, S., Koo, S. I., & Chun, O. K. (2011). Comparison of ABTS/ DPPH assays to measure antioxidant capacity in popular antioxidantrich US foods. Journal of Food Composition and Analysis, 24, 1043–1048.

Fukuchi, Y., Hiramitsu, M., Okada, M., Hayashi, S., Nabeno, Y., Osawa, T., & Naito, M. (2008). Lemon polyphenols suppress diet-induced obesity by up-regulation of mRNA levels of the enzymes involved in beta-oxidation in mouse white adipose tissue. Journal of Clinical Biochemistry and Nutrition, 43(3), 201–209.

Goossens, G. H. (2017). The metabolic phenotype in obesity: Fat mass, body fat distribution, and adipose tissue function. Obesity Facts, 10(3), 207–215.

Gorinstein, S., Cvikrova, M., Machackova, I., Haruenkit, R., Park, Y. S., Jung, S. T., & Trakhtenberg, S. (2004). Characterization of antioxidant compounds in Jaffa sweeties and white grapefruits. Food Chemistry, 84, 503–510.

Gorinstein, S., Huang, D., Leontowicz, H., Leontowicz, M., Yamamoto, K., Soliva-Fortuny, R., & Trakhtenberg, S. (2006). Determination of naringin and hesperidin in citrus fruit by high-performance liquid chromatography. The antioxidant potential of citrus fruit. Acta Chromatographica, 17, 108–124.

Grande, F., Rizzuti, B., Occhiuzzi, M. A., Ioele, G., Casacchia, T., Gelmini, F., ... Statti, G. (2018). Identification by molecular docking ofhomoisoflavones from leopoldia comosa as ligands of estrogen receptors. Molecules, 23(4).

Hanwell, M. D., Curtis, D. E., Lonie, D. C., Vandermeersch, T., Zurek, E., & Hutchison, G. R. (2012). Avogadro: An advanced semantic chemical editor, visualization, and analysis platform. The Journal of Cheminformatics, 4(1), 17.

Hossain, M. K., Dayem, A. A., Han, J., Yin, Y., Kim, K., Saha, S. K., ... Cho, S. G. (2016). Molecular mechanisms of the anti-obesity and anti-diabetic properties of flavonoids. International Journal of Molecular Sciences, 17(4), 569.

Ikemura, M., Sasaki, Y., Giddings, J. C., & Yamamoto, J. (2012). Preventive effects of hesperidin, glucosyl hesperidin and naringin on hypertension and cerebral thrombosis in stroke-prone spontaneously hypertensive rats. Phytotherapy Research, 26(9), 1272–1277.

Ioku, K., Pongpiriyadacha, Y., Konishi, Y., Takei, Y., Nakatani, N., & Terao, J. (1998). Beta-glucosidase activity in the rat small intestine toward quercetin monoglucosides. Bioscience, Biotechnology, and Biochemistry, 62(7), 1428–1431.

Kang, S. I., Shin, H. S., Kim, H. M., Hong, Y. S., Yoon, S. A., Kang, S. W., ... Kim, S. J. (2012). Immature Citrus sunki peel extract exhibits antiobesity effects by beta-oxidation and lipolysis in high-fat diet-induced obese mice. Biological and Pharmaceutical Bulletin, 35(2), 223–230.

Khettal, B., Kadri, N., Tighilet, K., Adjebli, A., Dahmoune, F., & Maiza-Benabdeslam, F. (2017). Phenolic compounds from citrus leaves: Antioxidant activity and enzymatic browning inhibition. Journal of Complementary & Integrative Medicine, 14(1).

Kim, K. H., & Park, Y. (2011). Food components with anti-obesity effect. The Annual Review of Food Science and Technology, 2, 237–257.

Kim, G. N., Shin, M. R., Shin, S. H., Lee, A. R., Lee, J. Y., Seo, B. I., ... Roh, S. S. (2016). Study of antiobesity effect through inhibition of pancreatic lipase activity of Diospyros kaki fruit and citrus unshiu Peel. Biomed Research International, 2016, 1723042.

Klop, B., Elte, J. W., & Cabezas, M. C. (2013). Dyslipidemia in obesity: Mechanisms and potential targets. Nutrients, 5(4), 1218–1240.

Kopelman, P. G. (2000). Obesity as a medical problem. Nature, 404(6778), 635–643.

Kumazawa, S., Taniguchi, M., Suzuki, Y., Shimura, M., Kwon, M. S., & Nakayama, T. (2002). Antioxidant activity of polyphenols in carob pods. Journal of Agriculture and Food Chemistry, 50(2), 373–377.

Crifo, T., Petrone, G., Lo Cicero, L., & Lo Piero, A. R. (2012). Short cold storage enhances the anthocyanin contents and level of transcripts related to their biosynthesis in blood oranges. Journal of Agriculture and Food Chemistry, 60(1), 476–481.

Kuster, T., Zumkehr, B., Hermann, C., Theurillat, R., Thormann, W., Gottstein, B., & Hemphill, A. (2012). Voluntary ingestion of antiparasitic drugs emulsified in honey represents an alternative to gavage in mice. Journal of the American Association for Laboratory Animal Science, 51(2), 219–223.

Kwon, Y. I., Apostolidis, E., Kim, Y. C., & Shetty, K. (2007). Health benefits of traditional corn, beans, and pumpkin: In vitro studies for hyperglycemia and hypertension management. Journal of Medicinal Food, 10(2), 266–275.

Lauer, M. S., Anderson, K. M., Kannel, W. B., & Levy, D. (1991). The impact of obesity on left ventricular mass and geometry. The Framingham Heart Study JAMA, 266(2), 231–236.

Magiorkinis, E., Beloukas, A., & Diamantis, A. (2011). Scurvy: Past, present and future. The European Journal of Internal Medicine, 22(2), 147–152.

Maida, E., Se Balaji, B., Divakar, S., & Geetha, G. (2017). Ligand based pharmacophore modeling, virtual screening and molecular docking studies to design novel pancreatic lipase inhibitors. Internetation Journal of pharmacy and pharmaceutical sciences, 9(4), 48–64.

Mallick, N., & Khan, R. A. (2016). Antihyperlipidemic effects of Citrus sinensis, Citrus paradisi, and their combinations. Journal of Pharmacy and Bioallied Sciences, 8(2), 112–118.

Marrelli, M., Conforti, F., Toniolo, C., Nicoletti, M., Statti, G., & Menichini, F. (2014). Hypericum perforatum: Influences of the habitat on chemical composition, photoinduced cytotoxicity, and antiradical activity. Pharmaceutical Biology, 52(7), 909–918.

Marrelli, M., Cristaldi, B., Menichini, F., & Conforti, F. (2015). Inhibitory effects of wild dietary plants on lipid peroxidation and on the proliferation of human cancer cells. Food and Chemical Toxicology, 86, 16–24.

Matthews, D. R., Hosker, J. P., Rudenski, A. S., Naylor, B. A., Treacher, D. F., & Turner, R. C. (1985). Homeostasis model assessment: Insulin resistance and beta-cell function from fasting plasma glucose and insulin concentrations in man. Diabetologia, 28(7), 412–419.

Mishra, A., Kumar, S., & Pandey, A. K. (2013). Scientific validation of the medicinal efficacy of Tinospora cordifolia. Scientific World Journal, 2013, 292934.

Morris, G. M., Goodsell, D. S., Halliday, R. S., Huey, R., Hart, W. E., Belew, R. K., & Olson, A. J. (1998). Automated docking using a Lamarckian genetic algorithm and an empirical binding free energy function. Journal of Computational Chemistry, 19, 1639–1662.

Mulvihill, E. E., Allister, E. M., Sutherland, B. G., Telford, D. E., Sawyez, C. G., Edwards, J. Y., ... Huff, M. W. (2009). Naringenin prevents dyslipidemia, apolipoprotein B overproduction, and hyperinsulinemia in LDL receptor-null mice with diet-induced insulin resistance. Diabetes, 58(10), 2198–2210.

Muthiah, P., Umamaheswari, M., & Asokkumar, K. (2012). *In vitro* antioxidant activities of leaves, fruits and peel extracts of Citrus. International Journal of Phytopharmacy, 13–20.

Nweze, C. C., Abdulganiyu, M. G., & Erhabor, O. G. (2015). Comparative analysis of vitamin c in fresh fruits juice of Malus domestica, Citrus sinensi, Ananas comosus and Citrullus lanatus BY iodometric titration. International Journal of Science, Environment and Technology, 4, 17–22.

Parmar, H. S., & Kar, A. (2008). Antiperoxidative, antithyroidal, antihyperglycemic and cardioprotective role of Citrus sinensis peel extract in male mice. Phytotherapy Research, 22(6), 791–795.

Priscilla, D. H., Roy, D., Suresh, A., Kumar, V., & Thirumurugan, K. (2014). Naringenin inhibits alpha-glucosidase activity: A promising strategy for the regulation of postprandial hyperglycemia in high fat diet fed streptozotocin induced diabetic rats. Chemico-Biological Interactions, 210, 77–85.

Proteggente, A. R., Saija, A., De Pasquale, A., & Rice-Evans, C. A. (2003). The compositional characterisation and antioxidant activity of fresh juices from sicilian sweet orange (Citrus sinensis L. Osbeck) varieties. Free Radical Research, 37(6), 681–687.

Pu, P., Gao, D. M., Mohamed, S., Chen, J., Zhang, J., Zhou, X. Y., ... Jiang, H. (2012). Naringin ameliorates metabolic syndrome by activating AMP-activated protein kinase in mice fed a high-fat diet. Archives of Biochemistry and Biophysics, 518(1), 61–70.

Quettier-Deleu, C., Gressier, B., Vasseur, J., Dine, T., Brunet, C., Luyckx, M., ... Trotin, F. (2000). Phenolic compounds and antioxidant activities of buckwheat (Fagopyrum esculentum Moench) hulls and flour. Journal of Ethnopharmacology, 72(1–2), 35–42.

Rampersaud, G. C., & Valim, M. F. (2017). 100% citrus juice: Nutritional contribution, dietary benefits, and association with anthropometric measures. Critical Reviews in Food Science and Nutrition, 57(1), 129–140.

Rapisarda, P., Bellomo, S. E., Fabroni, S., & Russo, G. (2008). Juice quality of two new mandarin-like hybrids (Citrus clementina Hort. ex Tan x Citrus sinensis L. Osbeck) containing anthocyanins. Journal of Agriculture and Food Chemistry, 56(6), 2074–2078.

Reilly, J. J., & Kelly, J. (2011). Long-term impact of overweight and obesity in childhood and adolescence on morbidity and premature mortality in adulthood: Systematic review. International Journal of Obesity (London), 35(7), 891–898.

Reshef, N., Hayari, Y., Goren, C., Boaz, M., Madar, Z., & Knobler, H. (2005). Antihypertensive effect of sweetie fruit in patients with stage I hypertension. American Journal of Hypertension, 18(10), 1360–1363.

Revathy, J., Srinivasan, S., Abdullah, S. H. S., & Udaiyar, M. (2018). Antihyperglycemic effect of hesperetin, a citrus flavonoid, extenuates hyperglycemia and exploring the potential role in antioxidant and antihyperlipidemic in streptozotocin-induced diabetic rats. Biomedicine & Pharmacotherapy, 97, 98–106.

Rodrigues, F., Palmeira-de-Oliveira, A., das Neves, J., Sarmento, B., Amaral, M. H., & Oliveira, M. B. (2013). Medicago spp. extracts as promising ingredients for skin care products. Industrial Crops and Products, 49, 634–644.

Rydberg, E. H., Li, C., Maurus, R., Overall, C. M., Brayer, G. D., & Withers, S. G. (2002). Mechanistic analyses of catalysis in human pancreatic alpha-amylase: Detailed kinetic and structural studies of mutants of three conserved carboxylic acids.m Biochemistry, 41(13), 4492–4502.

Shen, W., Xu, Y., & Lu, Y. H. (2012). Inhibitory effects of Citrus flavonoids on starch digestion and antihyperglycemic effects in HepG2 cells. Journal of Agriculture and Food Chemistry, 60(38), 9609–9619.

Toma, C. C., Casacchia, T., Don, I., D'Ippolito, C., & Statti, G. A. (2017). New extraction technologies for syringa vulgaris (Oleaceae) Meristematic Extracts. Revista de Chemie, 68(8), 1796–1798.

Trott, O., & Olson, A. J. (2010). AutoDock Vina: Improving the speed and accuracy of docking with a new scoring function, efficient optimization, and multithreading. Journal of Computational Chemistry, 31(2), 455–461.

Uddin, N., Hasan, M. R., Hossain, M. M., Sarker, A., Hasan, A. H., Islam, A. F., ... Rana, M. S. (2014). *In vitro* alpha-amylase inhibitory activity and *in vivo* hypoglycemic effect of methanol extract of Citrus macroptera Montr. fruit. Asian Pacific Journal of Tropical Biomedicine, 4(6), 473–479.

Virtue, S., & Vidal-Puig, A. (2010). Adipose tissue expandability, lipotoxicity and the Metabolic Syndrome–An allostatic perspective. Biochimica et Biophysica Acta, Gene Regulatory Mechanisms, 1801(3), 338–349.

Williams, L. K., Li, C., Withers, S. G., & Brayer, G. D. (2012). Order and disorder: Differential structural impacts of myricetin and ethyl caffeate on human amylase, an antidiabetic target. Journal of Medicinal Chemistry, 55(22), 10177–10186.

Xiao, J., Capanoglu, E., Jassbi, A. R., & Miron, A. (2016). Advance on the Flavonoid Cglycosides and Health Benefits. Critical Reviews in Food Science and Nutrition, 56(Suppl 1), S29–S45.

Yamamoto, M., Jokura, H., Suzuki, A., Hase, T., & Shimotoyodome, A. (2013). Effects of continuous ingestion of hesperidin and glucosyl hesperidin on vascular gene expression in spontaneously hypertensive rats. Journal of Nutritional Science and Vitaminology (Tokyo), 59(5), 470–473.

Yoshida, H., Tsuhako, R., Atsumi, T., Narumi, K., Watanabe, W., Sugita, C., & Kurokawa, M. (2017). Naringenin interferes with the anti-diabetic actions of pioglitazone via pharmacodynamic interactions. Journal of Natural Medicines, 71(2), 442–448.

Zhang, R., Li, C., Williams, L. K., Rempel, B. P., Brayer, G. D., & Withers, S. G. (2009). Directed "in situ" inhibitor elongation as a strategy to structurally characterize the covalent glycosyl-enzyme intermediate of human pancreatic alpha-amylase. Biochemistry, 48(45), 10752–10764.

Zou, Z., Xi, W., Hu, Y., Nie, C., & Zhou, Z. (2016). Antioxidant activity of Citrus fruits. Food Chemistry, 196, 885–896.

III. CRYPTOTANSHINONE AND TANSHINONE IIA FROM *SALVIA MILTHORRHIZA* BUNGE (DANSHEN) AS A NEW CLASS OF POTENTIAL PANCREATIC LIPASE INHIBITORS

Mariangela Marrelli [a]; Fedora Grande [a]; Maria Antonietta Occhiuzzi [a]; Francesco Maione [b]; Nicola Mascolo [b]; Filomena Conforti [a].

[a] Department of Pharmacy Health and Nutritional Sciences, University of Calabria, Rende, Italy;
[b] Department of Pharmacy School of Medicine and Surgery, University of Naples Federico II, Naples, Italy

Abstract:

Salvia miltiorrhiza Bunge extract was investigated for the first time for its inhibitory activity against pancreatic lipase (PL), an important enzyme involved in the digestion of dietary fats. It showed a concentration-dependent activity with an IC_{50} value of 3.54 ± 0.22 mg/mL. Two compounds, cryptotanshinone and tanshinone IIA (the major lipophilic constituents of S. miltiorrhiza), have been selected as potential ligands of PL. Cryptotanshinone showed a higher lipase inhibitory activity ($IC_{50} = 6.86 \pm 0.43$ mM) compared to the parent tanshinone IIA (Figure 1). Molecular docking studies were undertaken to establish whether a direct interaction of the principal constituents of the S. miltiorrhiza extract with the human pancreatic lipase could be evoked. All these findings provided new insights into the understanding of the interactions between natural constituents of *S. miltiorrhiza* extract and PL, also suggesting that cryptotanshinone could be used as lead compound for the development of efficacious PL inhibitors.

Keywords: *Salvia miltiorrhiza* Bunge, Lamiaceae, pancreatic Lipase inhibitors, tanshinones, molecular docking.

1. Introduction

Obesity is characterized by an exceeding adipose biomass and adipose tissue expansion, so reducing the absorption of carbohydrates and lipids in the digestive system using anti-obesity drugs, has been considered as an effective therapeutic approach (Apovian 2016). An important enzyme involved in the digestion of dietary fats is pancreatic lipase (PL), a triacylglycerol acyl hydrolase, that is responsible for the hydrolysis of almost 60% triacylglycerides in the gastrointestinal tract (Wang et al. 2013). Natural products have been considered a source of safe and promising anti-obesity drugs (Marrelli et al. 2016). *Salvia miltiorrhiza* Bunge (Danshen) belongs to the Lamiaceae family. It has been widely used in Asian countries for treating different diseases and early pharmacological studies demonstrated its multiple bioactivities: cardiovascular and cerebrovascular effects as well as antioxidant, anti-inflammatory and anti-tumor properties (Jianping et al. 2018). These activities are due to the presence of lipophilic tanshinones (Li et al. 2018). In the present study S. miltiorrhiza extract and the major lipophilic compounds, cryptotanshinone and tanshinone IIA, were investigated for the first time as lipase inhibitors. Molecular docking studies on the crystallographic structures of pancreatic lipase have been carried out to investigate the binding mode of the compounds with the enzyme binding site.

2. Results and discussion

The lyophilized extract of S. miltiorrhiza (E.S. 1% tanshinones) showed a lipase inhibitory activity with an IC_{50} value of 3.54 ± 0.22 mg/ml (Figure S1, Table S1).
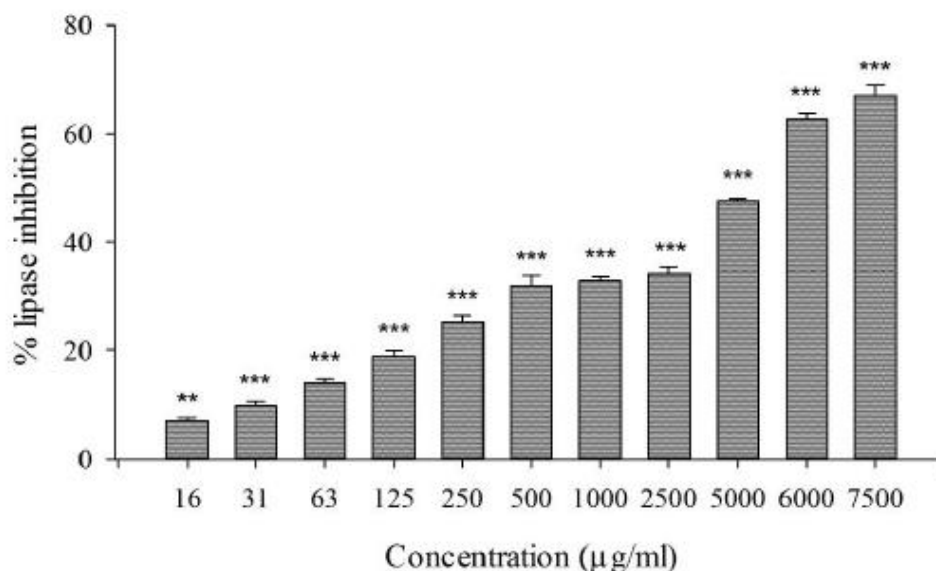
Figure S1. *Pancreatic lipase inhibition activity of S. miltiorrhiza extract. Data were expressed as means ± S. E. (n = 3). Mean values of samples showing significant difference from the control was denoted with * p < 0.05, ** p < 0.01, *** p < 0.001 in one-way ANOVA followed by Dunnett's test.*

Table S1. *Inhibition of pancreatic lipase induced by tanshinones from S. miltiorrhiza.*

Sample	IC_{50} (µM)
Cryptotanshinone	6.860 ± 0.43 ***
Tanshinone IIA	n.d.
Rutin	163.000 ± 7.24
Orlistat	0.036 ± 0.002

*Data are expressed as mean ± S.E.M. (n=3). Rutin was chosen as natural reference compound. Orlistat was used as positive control. The statistical difference between cryptotanshinone and both rutin and orlistat was determined by t-test (***P < 0.001).*

The potential contribution of tanshinone IIA (**1**) and cryptotanshinone (**2**) (Figure S2) was evaluated.
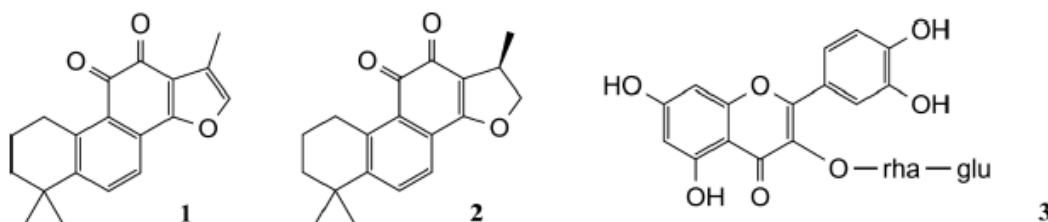
Figure S2. *Chemical structures of Tanshinone IIA (**1**), Cryptotanshinone (**2**) and rutin (**3**).*

Pancreatic lipase activity was significantly affected by **1** at the three highest concentration tested (∗∗∗ p<0.001, Dunnett's multiple comparison test) (Figure 1). Compound **2** effectively inhibited pancreatic lipase activity at all the concentrations tested, with an IC_{50} value of $6.86 \pm 0.43 \mu M$ (Table S1). Even if there was a significant difference between the biological activity of this compound and the positive control orlistat (IC_{50} value = 0.036 ± 0.002 µM, *** P<0.001, t-test), the biological activity of cryptotanshinone was significantly higher than those of rutin, chosen as natural reference compound (IC_{50} value = 163.00 ± 7.24 µM, *** P<0.001, t-test).
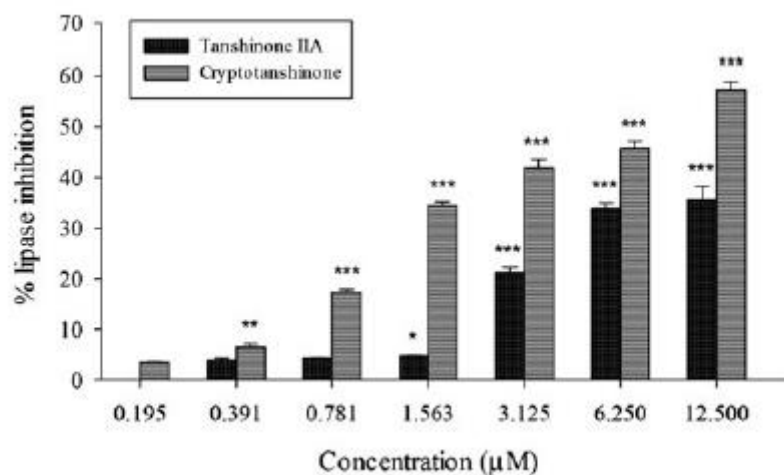

Figure 1. *Pancreatic lipase inhibition induced by cryptotanshinone and tanshinone IIA. Data were expressed as means ± S. E. (n=3). Mean values of samples showing significant difference from the control was denoted with *P<0.05, ** P<0.01, *** P<0.001 in one-way ANOVA followed by Dunnett's test.*

Various pharmacological properties have been ascribed to cryptotanshinone in particular it is able to inhibit in a concentration dependent manner the rat platelet aggregation (Maione et al. 2015). Our data are in accordance with previous studies that showed that cryptotanshinone is able to reduce the concentration of body fat, serum cholesterol and triglyceride levels in mice (Kim et al. 2007). Subsequent studies also showed that cryptotanshinone can effectively inhibit adipogenesis (Rahman et al. 2016).

In order to verify whether the inhibitory activity of *S. miltiorrhiza* extract could be attributed to the direct interaction of **1** and **2** with the enzyme, molecular docking was performed by using a pancreatic lipase structure withdrawn from the Protein Data Bank (PDB). Different pancreatic lipase crystallographic structures have been deposited to the PDB, the most recent 1LPB entry was adopted. In this structure pancreatic lipase is complexed with two molecules of a C11 alkyl phosphonate inhibitor MUP. The crystallographic structure of pancreatic lipase includes three structural domains: a N-terminal domain containing the active site characterized by a Ser152-Asp176-Hys263 catalytic triad, a non-catalytic C-terminus surrounding a colipase binding site, and a lid-loop modulating the ligand entry into the active site. During docking experiments, the agliconic portion of Rutin (**3**) (Figure S2) was used as an anti-pancreatic lipase reference compound. Docking experiments showed that compounds 1–3 were able to interact with the enzyme accommodating in the same binding site of the crystallographic ligand, therefore they should be able to prevent the access of the natural ligand to the catalytic site. All the three molecules were find able to bind the protein active domain with comparable affinities ranging from -9.9 to −11.1 kcal/mol (Table S2).

PDB Entry	Binding Energy (kcal/mol)		
1LPB	1	2	3
	-10.9	-11.1	-9.9

Furthermore, as easily hypothesized, compounds 1 and 2 interact with the catalytic core in a very similar way (Figure 2) since the structural differences present on the furan moiety do not significantly influence the overall interaction of ligands with the enzyme. In particular, the interaction with PL of both compounds 1 and 2 is made favorable by two H-bonds: O atoms at position 10 and 11, acting as H-acceptors, interact with the side chain of His263 and Ser152, respectively.
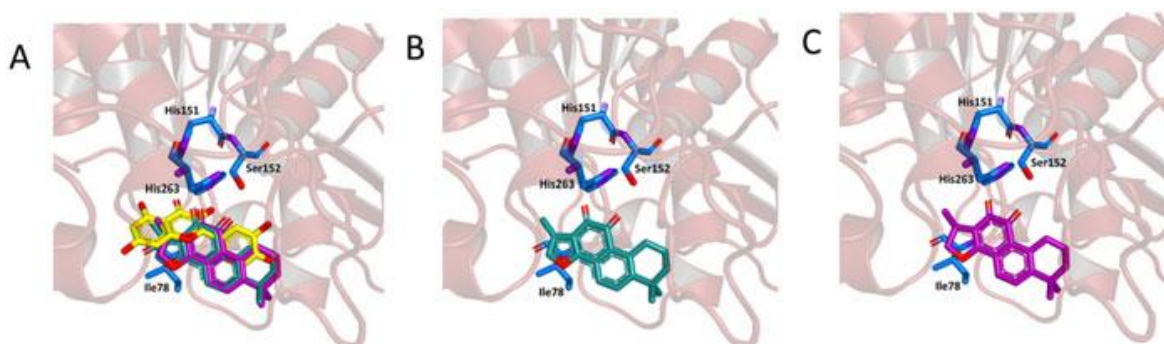
*Figure 2. Ligand-binding pocket of the active site of HPL; protein structural elements are represented as ribbons. (a) Superimposed binding modes of the agliconic portion of Rutin, **3** (yellow); Tanshinone IIA, 1 (cyan); Cryptotanshinone, 2 (magenta). The key residues are also indicated in the specific binding mode of (b) **1** and (c) **2**.*

Moreover, several hydrophobic interactions contribute to the complex stability. Here, for the first time, we have investigated the inhibitory effects of *S. miltiorrhiza* extract and its reference compounds, tanshinone IIA and cryptotanshinone, on pancreatic lipase. The results showed that the extract possesses moderate inhibitory effects on pancreatic lipase.
Molecular docking simulations demonstrated that selected compounds were able to interact with the catalytic site of pancreatic lipase and can act as valuable enzyme ligands. All these findings provided new insights into the deep understanding of the interactions between natural constituents in S. miltiorrhiza extract and pancreatic lipase also suggesting that cryptotanshinone (**2**) could represent a suitable lead compound for the development of new pancreatic lipase inhibitors useful for the management of obesity and related disorders.

References

Apovian CM. 2016. Obesity: definition, comorbidities, causes, and burden. Am J Manag Care. 22(7 Suppl):s176–s185.

Jianping X, Kunhua W, Guojun Z, Lujing L, Dawei Y, Wenle W, Qiheng H, Yuan X, Yaqiong B, Min Y, Minhui L. 2018. Ethnopharmacology, phytochemistry, and pharmacology of Chinese Salvia species: A review. J Ethnopharmacol. 225:18–30.

Kim EJ, Jung SN, Son KH, Kim SR, Ha TY, Park MG, Jo IG, Park JG, Choe W, Kim SS, Ha J. 2007. Antidiabetes and antiobesity effect of cryptotanshinone via activation of AMP-activated   protein kinase. Mol Pharmacol. 72(1):6272.

Li ZM, Xu SW, Liu PQ. 2018. Salvia miltiorrhiza Bunge (Danshen): A golden herbal medicine in cardiovascular therapeutics. Acta Pharmacol Sin. 39(5):802–824.

Maione F, Cantone V, Chini MG, De Feo V, Mascolo N, Bifulco G. 2015. Molecular mechanism of tanshinone IIA and cryptotanshinone in platelet anti-aggregating effects: an integrated study of pharmacology and computational analysis. Fitoterapia. 100:174–178.

Marrelli M, Conforti F, Araniti F, Statti GA. 2016. Effects of saponins on lipid metabolism: a review of potential health benefits in the treatment of obesity. Molecules. 21(10):1404.

Rahman N, Jeon M, Song HY, Kim YS. 2016. Cryptotanshinone, a compound of Salvia miltiorrhiza inhibits pre-adipocytes differentiation by regulation of adipogenesis-related genes expression via STAT3 signaling. Phytomedicine. 23(1):58–67.

Wang TY, Liu M, Portincasa P, Wang DQ. 2013. New insights into the molecular mechanism of intestinal fatty acid absorption. Eur J Clin Invest. 43(11):1203–1223.

IV. BENZOTHIENOQUINAZOLINONES AS NEW MULTI-TARGET SCAFFOLDS: DUAL INHIBITION OF HUMAN TOPOISOMERASE I AND TUBULIN POLYMERIZATION

Jessica Ceramella [a]; Anna Caruso [a]; Maria Antonietta Occhiuzzi [a]; Domenico Iacopetta [a]; Alexia Barbarossa [a]; Bruno Rizzuti [b]; Patrick Dallemagne [c]; Sylvain Rault [c]; Hussein El-Kashe [d]; Carmela Saturnino [e], Fedora Grande [a]; Maria Stefania Sinicropi [a].

[a] Department of Pharmacy, Health and Nutritional Sciences, University of Calabria, 87036, Arcavacata di Rende, CS, Italy
[b] CNR-NANOTEC, Licryl-UOS Cosenza and CEMIF. Cal, Dep. of Physics, University of Calabria, Via P. Bucci, 87036, Rende, CS, Italy
[c] Centre d'Etudes et de Recherche sur le Medicament de Normandie, Normandie Univ, UNICAEN, CERMN, 14000, Caen, France
[d] Chemistry Department, Faculty of Science, Assiut University, 71516, Assiut, Egypt
[e] Department of Science, University of Basilicata, Potenza, Italy

Abstract:

3-(Alkyl(dialkyl)amino)benzothieno[2,3-*f*]quinazolin-1(2H)-ones (4-9) have been designed using Ellipticine structure as a model, replacing the carbazole core and the pyridine ring with a dibenzothiophene and a pyrimidine moiety, respectively. New benzothienoquinazolinones (4-9) have been synthesized by a simple one-pot reaction employing 3-aminodibenzothiophene as starting material. The benzothienoquinazolinones obtained (4-9), were evaluated for their anticancer activity against two breast cancer cell lines, MDA-MB-231 and MCF-7. The results revealed that compounds 4 and 7 presented a good antitumor activity toward the triple negative MDA-MB-231, without cytotoxicity against non-tumoral cells. Furthermore, the compounds 4 and 7 can be considered important molecular multi-target tools for their dual inhibition of different cellular proteins, i.e. Tubulin and human Topoisomerase I, involved in relevant cellular processes, as predicted by *in silico* studies and demonstrated by *in vitro* assays (for compound 4).

Keywords: Tubulin, Cytoskeleton, Breast cancer, Docking study, Benzothienoquinazolinones.

1. Introduction

Ellipticine (Figure 1) is a naturally occurring alkaloid, which belongs to the 6H-pyridocarbazole family. This compound and its derivatives are endowed with antitumor activities due to their DNA intercalating capacity and their high DNA binding affinity, responsible in part for these pharmacological properties [1-4]. This compound may be qualified as a pro-drug and its ability, resulting from cytochrome P450 (CYP)- and/or peroxidase metabolism, to form adducts binding DNA plays a fundamental role for its pharmacological activity and/or side effects [5]. Additionally, Ellipticine has been shown to interfere with biotransformation or metabolism of different enzymes. Treatment of human breast cancer cells MCF-7 and MDA-MB-231, leukemia HL-60 and CCRFCEM

neuroblastoma IMR-32, UKF-NB-3 and UKF-NB-4, glioblastoma U87MG, and other various cells with Ellipticine resulted in inhibition of their growth and proliferation [6-9]. These effects were associated with the formation of two covalent Ellipticinederived DNA adducts, identical to those formed by 13-hydroxyand 12-hydroxyellipticine. Therefore, DNA adducts formation in the most of the aforementioned cancer cell lines tested might be one of the causes of their sensitivity to Ellipticine treatment [10]. Furthermore, Ellipticine is considered a multi-target compound, interacting with different proteins involved in DNA replication and cellular proliferation such as Telomerases, Topoisomerases I and II, Tubulin, Kinases, and possibly others [11-14].

However, because of the onset of several side effects the therapeutic applications of this compound and its derivatives still remain limited [15]. In order to overcome these limitations, the search for new Ellipticine derivatives and analogs having a potent antitumor activity and less side effects is always demanded. To this aim, several libraries of carbazole derivatives and isosteres (such as pyrimidocarbazoles, pyrrolopyrazinocarbazoles, benzofuropyrroloquinoxalines, pyridazinocarbazoles, benzofurophtalazines, benzothienoquinolines, benzofuroquinolines, benzothieno-, benzofuropyrrolopyrazines-, pyrido[3,2-b]carbazoles, and many others) have been reported [16-20].
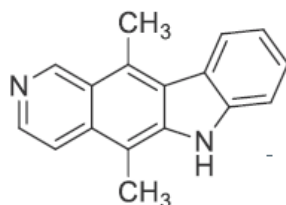
Figure1. Ellipticine structure.

More recently, a large number of Ellipticine derivatives have been synthesized and tested for their antitumor activity in preclinical models [21-25]. Considering that benzofuran was a promising scaffold for the synthesis of anticancer agents [26], in our previous paper [27], we have described an efficient and simple synthesis of a series of 3-(alkyl(dialkyl)amino)benzofuro[2,3-f]quinazolin-1(2H)-ones, and evaluated their biological activities on two models of breast cancer. The encouraging results obtained, together with other data previously reported [28,29], prompted us to extend the synthetic methodology to the synthesis of their thiophenic isosteres (Figure 2).
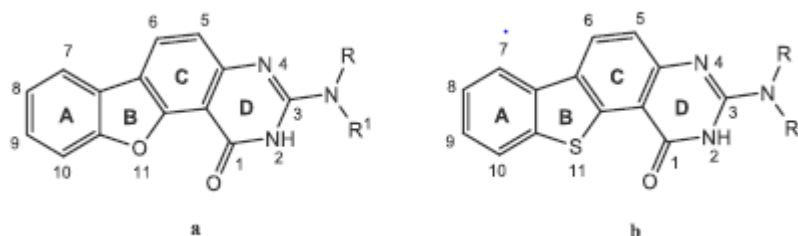
Figure 2. Structure of benzofuroquinazolinone (a) and benzothienoquinazolinone (b) derivatives

Herein, we reported the synthesis of a series of planar fused tetracyclic heterocyclic compounds, as new Ellipticine analogues and structurally correlated to 3-(alkyl(dialkyl)amino)benzofuro [2,3-f]quinazolin-1(2H)-ones [27], namely 3-(alkyl(dialkyl)amino) benzothieno[2,3-f]quinazolin-1(2H)-ones 4e9 (Table 1).

Table 1. *3-(Alkyl(dialkyl)amino)benzothieno[2,3-f]quinazolin-1(2H)-ones 4e9*.

4-9

Compounds	R	R^1
4	H	$(CH_2)_2CH_3$
5	H	$(CH_2)_3CH_3$
6	H	Cyclopentyl
7	$(CH_2)_2CH_3$	$(CH_2)_2CH_3$
8	$(CH_2)_4CH_3$	$(CH_2)_4CH_3$
9	Morpholin-1-yl	_

The series has been evaluated for its antitumor activity toward two human breast cancer cell lines: ERa-positive MCF-7 and triple negative MDA-MB-231 [30]. Compounds 4 and 7 exhibited a good antitumor activity, mostly against aggressive and highly metastatic MDA-MB-231 cells (IC$_{50}$ = 3.88 μM and 4.69 μM, respectively), without affecting non-tumoral MCF-10A cells growth. With the aim of investigating the molecular mechanism of action of synthetized compounds, we performed *in silico* studies on all of them as new human Topoisomerases I and II and Tubulin inhibitors. These simulations revealed that the most active compounds, **4** and **7**, obtained the higher scores as possible inhibitors of both enzymes, with a good bond affinity. These data have been confirmed by enzymatic assays performed on the aforementioned proteins and shed light on the versatility of this new class of molecules.
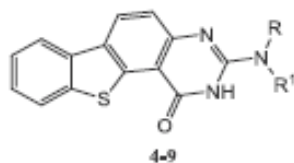
Indeed, the use of molecular multi-targeted therapies represents an advantage in terms of efficacy and toxicity, arising from the need to have the highest activity and to overcome the onset of undesired side effects or drug-resistance. For this reason, the new benzothieno[2,3-f]quinazolin-1(2H)-ones 4-9 can be considered promising candidates for next studies aiming at the development of new agents useful to limit aggressive pathologies, such as breast cancer, the commonest malignancy in women with 1 million new cases in the world each year [31,32].

2. Results and Discussion

2.1. Chemistry

3-Aminodibenzothiophene **1** was used as starting material in the synthesis of a series of new 3-(alkyl(dialkyl)amino)benzothieno [2,3-f]quinazolin-1(2*H*)-ones **4-9** by a one-pot three-component reaction (Scheme 1, Table 1) [16,19,22,27,33]. Compound **1** was prepared following a previously described synthetic route [34].

The amino derivative **1** was reacted with ethoxycarbonylisothiocyanate to give the thiourea intermediate **2**, which was in turn converted into the ethoxycarbonylguanidine intermediates **3** after the reaction with a proper alkyl- or dialkylamine in presence of HgCl$_2$. Derivatives **3** were cyclized at 160° C in the same reaction medium and 3-

(alkyl(dialkyl)amino)benzothieno[2,3-f]quinazolin-1(2H)-ones **4-9** were recovered after filtration of the by-product HgS. This sequential one-pot three-component synthesis proved to be rapid, simple and efficient representing a suitable synthetic methodology in order to obtain a pyrimidinone moiety from an aromatic ring carrying an amino group. It is important to underline that the mercury was totally removed as black precipitate of HgS, as confirmed by mass spectrometry.
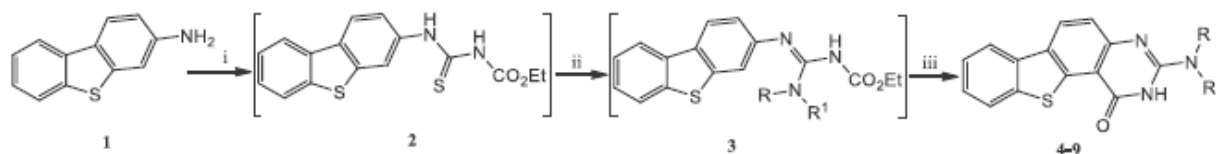
Scheme 1. *Reagents: (i) EtOCONCS (1 eq.), DMF, 4 h, rt; (ii) alkylamines or dialkylamines (3 eq.), HgCl$_2$ (1 eq.), 10 min, 0 °C, then 18 h, rt; (iii) 2 h, 160 °C.*

2.2. Antitumor activity

The ability of all synthetized compounds to inhibit the cells growth was evaluated toward two breast cancer cell lines, the ER-α positive MCF-7 and triple negative MDA-MB-231 cells. This evaluation was conducted using 3-(4,5-dimethylthiazol-2-y1)-2,5-diphenyltetrazolium (MTT) assay [35] and Ellipticine as reference drug. As reported in Table 2, the most active compounds resulted **4** and **7**, particularly against the highly aggressive MDA-MB-231 cell line (IC$_{50}$ =3.88 ± 0.81 μM and 4.69 ± 1.00 μM, respectively). Compounds **4** and **7** are decorated with one or two propylic groups at the nitrogen in C-3, respectively. On the contrary, the elongation of the alkylic chain, as for compounds **5** and **8**, led to a drastic decrease of their activity (IC$_{50}$ = 38.90 ± 1.22 μM and 42.35 ± 1.63 μM, respectively). Replacement of linear amines with a cyclic amine (cyclopentyl amine) was well tolerated; in fact, compound 6 exhibited a good antitumor activity toward MDA-MB-231 with an IC$_{50}$ value of 5.59 ± 0.90 μM. Finally, when a morfolinic group was present at C-3 (compound 9), the activity was slightly decreased (IC$_{50}$ = 9.43 ± 1.44 μM). MCF-7 cell line was less sensitive to all the tested derivatives. Moreover, all compounds were also tested on non-tumoral human mammary epithelial MCF-10A cells and no cytotoxic effects were noticed, at least at the concentrations used in these assays. The reference molecule, Ellipticine, even if demonstrated a better activity than compounds 4-9 (IC50 values for MDA MB-231 and MCF-7 cells equal to 1.85 ± 0.28 μM and 1.25 ± 0.35 μM, respectively), exhibited also a strong cytotoxicity against non-tumoral MCF-10A cells (IC$_{50}$ =1.20 ± 0.26 μM). We also evaluated the Vinblastine effects on the viability of the cell lines used in the previous experiments, noticing a scarce selectivity between the tumoral and non-tumoral cells.

Table 2. *IC₅₀ values of benzothienoquinazolinones (4-9) and Ellipticine, expressed in μM. The means ± standard deviations are shown.*

IC₅₀ (μM)			
Compound	MDA-MB-231	MCF-7	MCF-10A
4	3.88 ± 0.81	40.70 ± 0.23	>100
5	38.90 ± 1.22	74.46 ± 1.52	>100
6	5.59 ± 0.90	45.61 ± 0.23	>100
7	4.69 ± 1.00	41.99 ± 0.51	>100
8	42.35 ± 1.63	75.23 ± 0.93	>100
9	9.43 ± 1.44	21.17 ± 1.18	>100
Ellipticine	1.85 ± 0.28	1.25 ± 0.35	1.20 ± 0.26
Vinblastine	31.64 ± 0.86	15.00 ± 1.41	25.86 ± 1.33

2.3. Molecular docking

In order to predict the molecular mechanism that could be responsible for the antitumor activity, molecular docking of compounds **4** and **7** was performed on the crystallographic structures of Tubulin, Topoisomerase I and Topoisomerase II, obtained from the Protein Data Bank (PDB). The 1SA0 entry [36] was chosen for Tubulin because in this structure the protein is complexed with Colchicine, a known powerful inhibitor [37]. Similarly, the entry 1K4T [38] was selected for Topoisomerase I because in this case the protein is bound with the antitumor drug Topotecan. Finally, in the entry 5GWI [39], Topoisomerase II is complexed with the inhibitor Etoplatin N2β.

Within the structure of Tubulin, Colchicine is bound inside the stathmin-like domain, in a region essential for catalysis that is located in the b subunit and surrounded by residues Ala180, Cys241, Leu248, Ala250, Met259 and Ala316. Ligands able to bind to this region induce a structural modification that prevents an interaction between subunits α and β, inhibiting the enzyme. As shown in Figure 3, in our docking experiments, the two benzothienoquinazolinone derivatives may adopt two different orientations, but in both cases they shared the same position occupied by Colchicine in the crystallographic complex. Furthermore, both 4 and **7** interacted with the catalytic residue in the enzyme active site. In particular, **7** binds with its pentacyclic moiety to the sidechain of the protein residue Leu248 through a π-hydrogen interaction with a typical distance of 3.9 Å, whereas 4 forms a hydrogen bond having the N atoms of the appended aliphatic chain as a donor and the backbone O of Asn349 as acceptor, with a bond distance of 2.94 Å and interaction energy -2.7 kcal/mol. Overall, the binding energies estimated for 4 and 7 to Tubulin were -8.1 and -7.3 kcal/mol, respectively, indicating a good affinity for the protein. These values are comparable to the one obtained after the re-docking of Colchicine in the crystallographic position, -7.9 kcal/mol, further confirming that these molecules can bind Tubulin with a very good affinity.

57
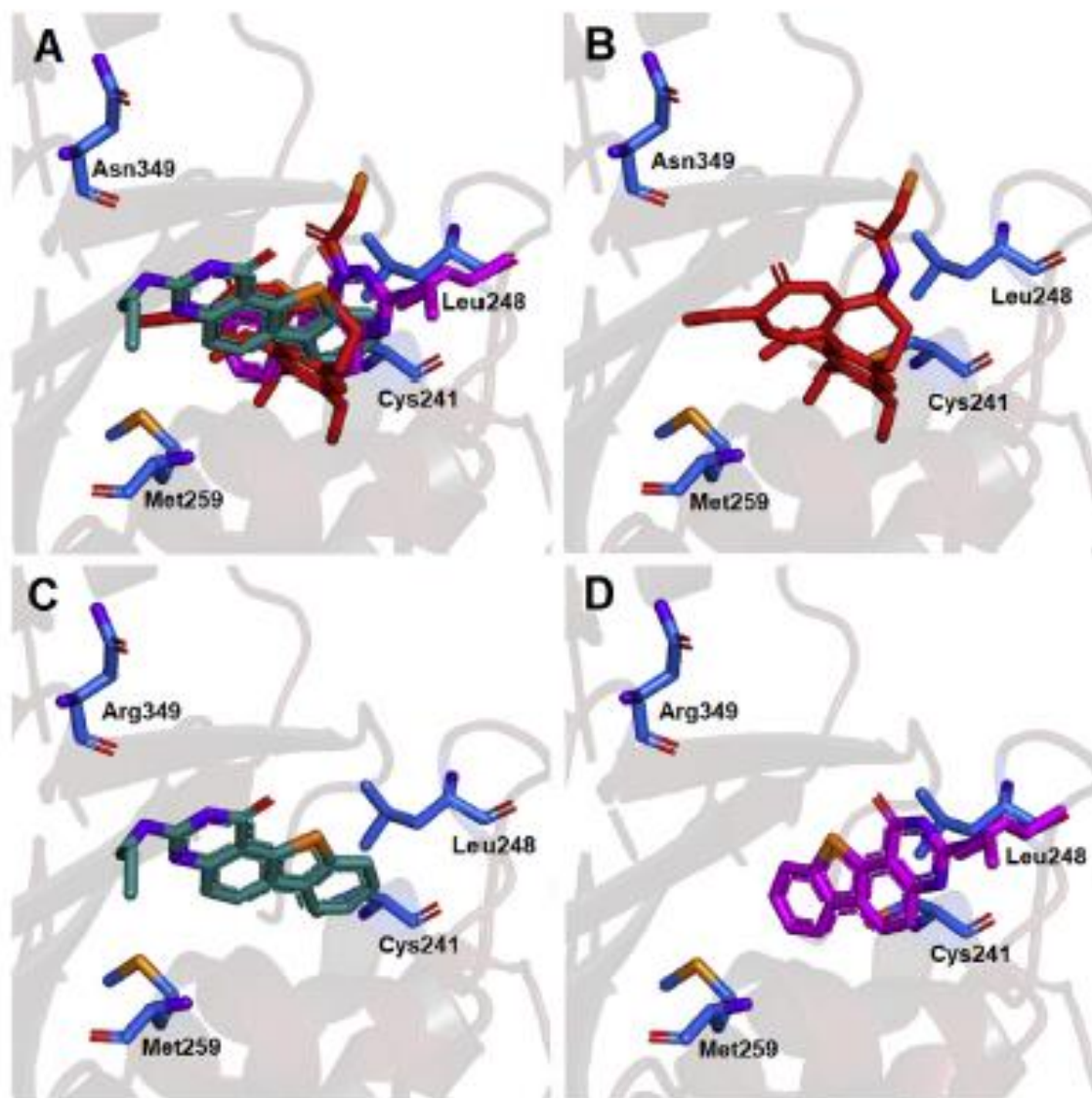
Figure 3. *Ligand-binding pocket of the active site of Tubulin. Protein backbone is represented in background as ribbons, and key protein residues are in blue. (A) Superimposed binding modes of the Colchicine (red), **4** (cyan) and **7** (magenta). The ligands are also shown separately: (B) Colchicine, (C) compound **4**, and (D) compound **7**. (For interpretation of the references to colour in this figure legend, the reader is referred to the Web version of this article.)*

In the ternary Topoisomerase I-DNA-Topotecan complex, the drug intercalates at the site of DNA cleavage and is stabilized by base-stacking interactions with both the +1 (upstream) and +1 (downstream) base pairs [38]. In addition to interaction with the DNA bases, Topotecan binds to residues Asp533, Arg364 and Asn722 of the protein. We used the Topotecan binding site as a reference for docking of the benzothienoquinazolinones and, as show in Figure 4, both **4** and **7** attached to the same binding site of the crystallographic ligand.

Figure 4. *Ligand-binding pocket of the active site of Topoisomerase I-DNA complex. Protein backbone is represented in background as ribbons, and key protein residues are in blue. (A) Superimposed binding modes of the Topotecan (green),* ***4*** *(cyan) and* ***7*** *(magenta). The ligands are also shown separately: (B) Topotecan, (C) compound* ***4****, and (D) compound* ***7****. (For interpretation of the references to colour in this figure legend, the reader is referred to the Web version of this article.)*

Also in this case, as for Tubulin, the binding energies of the two ligands are highly favourable: -10.3 kcal/mol for **4** and -10.2 kcal/mol for **7**. These values are only slightly less favourable with respect to the one obtained after the re-docking of Topotecan in the crystallographic position, -11.5 kcal/mol. A large number of specific interactions with the enzyme-bound DNA contribute to such very favourable binding affinity, as reported in Table 3.

Table 3. *DNA bases involved in aromatic (π−π) interactions for Topoisomerase I complexed with **4** or **7**. Nucleobases follow the numbering in the crystallographic structures [38], and rings of **4** or **7** are labelled (either A, B, C or D) as shown in Figure 2.*

COMPOUND	ring	Topoisomerase I DNA nucleobase Pyrimidine ring	Distance (Å)	Imidazole ring	Distance (Å)
4	**C**	A113	3.61	A113	3.87
		G11	3.62		
	D	A113	3.67	−	−
		G11	3.72		
7	**C**	A113	3.92	A113	3.63
		G11	3.67		
	D	A113	3.67	−	−
		G11	3.64		

In particular, both **4** and **7** form several aromatic π−π interactions with two bases (G11 and A113, according to the base numbering in the crystallographic structure) [38]. A relatively weak hydrogen bond (energy -2.2 kcal/mol) is also formed with the protein, with one of the terminal N atoms in the side chain of Arg364 acting as donor, and the N at position 4 of the quinazolinone moiety of the ligands as acceptor.

Human type II Topoisomerase isoforms, hTop2α and hTop2β, are targeted by some of the most successful anticancer drugs. The binding domain in hTop2β is located among residues Met782, Gln778 and Tyr821, and the ligand forms steric contacts also with two bases (A12 and G13, following the base numbering of the x-ray structure) of the bound DNA [40]. As shown in Figure 5, in our docking experiments both benzothienoquinazolinone derivatives bind in the enzyme active site.
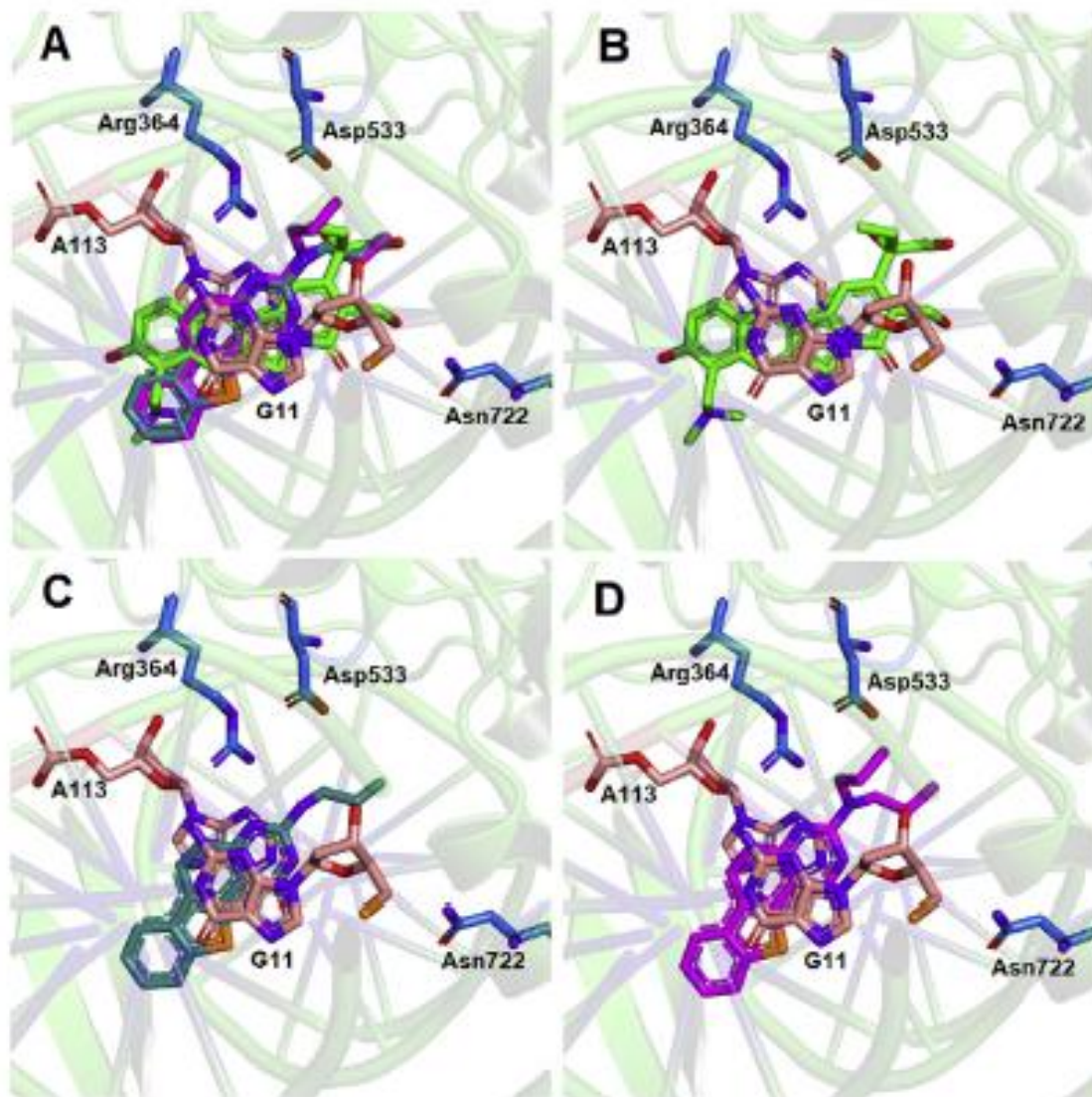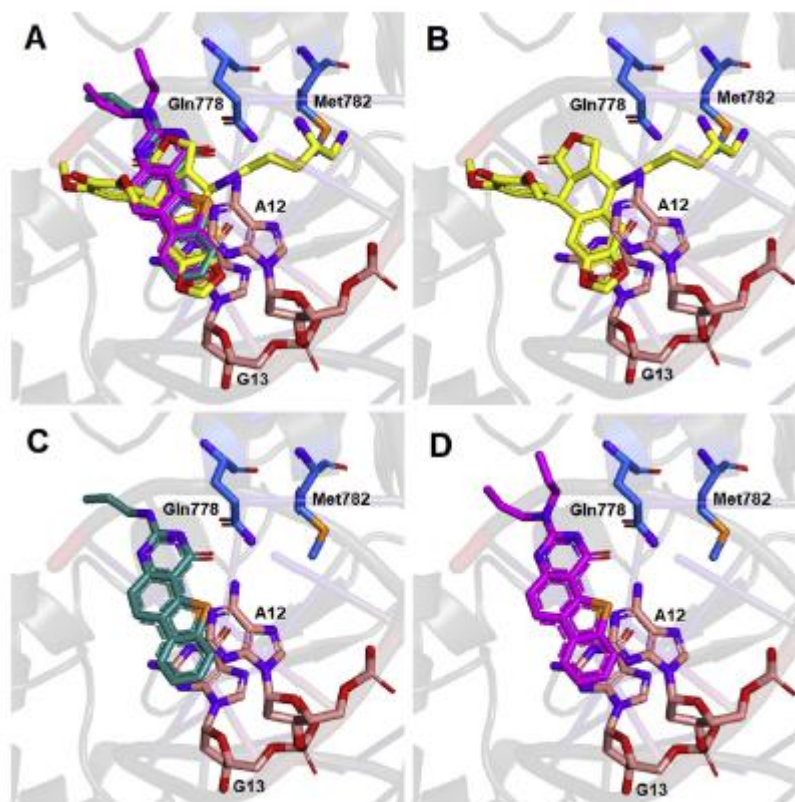

Figure 5. *Ligand-binding pocket of the active site of Topoisomerase II-DNA complex. Protein backbone is represented in background as ribbons, and key protein residues are in blue. (A) Superimposed binding modes of Etoplatin N2β (yellow), **4** (cyan) and **7** (magenta). The ligands are also shown separately: (B) Etoplatin N2β (yellow), (C) compound **4**, and (D) compound **7**. (For interpretation of the references to colour in this figure legend, the reader is referred to the Web version of this article.)*

Again in this case, as it happened for Topoisomerase I, several aromatic π–π interactions are formed with the DNA (Table 4). In addition, both benzothienoquinazolinones form a hydrogen-p interaction between the S atom of pentacyclic moiety of the ligand and the 5-embered ring of an adenine base (A12). The binding energy obtained for **4** and **7** are, respectively, -7.9 and -7.3 kcal/mol, and can be compared to the value obtained in the re-docking of the crystallographic ligand (Etoplatin), -8.7 kcal/mol. This result indicates that Topoisomerase II is likely, although it is possibly less favourable compared to the binding of other known drugs.

Table 4. *DNA bases involved in aromatic (π–π) interactions for Topoisomerase II complexed with **4** or **7**. Nucleobases follow the numbering in the crystallographic structures [39], and rings of **4** or **7** are labelled (either A, B, C or D) as shown in Figure 2. (*) Hydrogen-π interaction with the atom 10 of both ligands.*

| COMPOUND | ring | Topoisomerase II | | | |
| | | DNA nucleobase | | | |
		Pyrimidine ring	Distance (Å)	Imidazole ring	Distance (Å)
4	A	G13	3.80	A12 (*)	3.54
				G13	3.74
	B	G13	3.78	–	–
7	A	G13	3.79	A12 (*)	3.56
				G13	3.75
	B	G13	3.89	–	–

2.4. Compounds *4* and *7* are tubulin polymerization inhibitors

Literature studies classified Ellipticine and derivatives with a carbazolic moiety as hopeful tools for the fight against cancer. The anti-proliferative activity of these molecules is mostly associated with their capacity to interfere with different proteins involved in DNA replication and cellular growth such as Telomerases, Topoisomerases I and II, Tubulin, Kinases, and so on [12,14].

Considering the therapeutic interest played by Taxanes and Vinca Alkaloids, well known for they ability to interact with microtubules dynamics, research efforts are concentrated on developing new cytoskeleton-targeted compounds [41,42].

Cytoskeleton is an important structure of eukaryotic cells formed by three main molecules: microtubules, intermediate filaments and microfilaments. In particular, microtubules, biopolymers composed of α- and β-tubulin heterodimers, play a key role in the main cell functions, such as mitosis, maintaining of cell shape, cell division, intracellular transport and chromosome segregation [43-45]. The impairment of this normal cellular balance can cause an abnormal cell behaviour, including uncontrolled proliferation and migration and can be considered one of the principal factors for cancer development. Moreover, the relevance of microtubules in apoptosis induction and in mitosis makes them an important target for anticancer drug design [46].

Microtubule-targeting agents can be classified into two different families: microtubule-stabilizing agents that bind to the tubulin polymer and stabilize microtubules (like Paclitaxel) and microtubule-destabilizing agents that bind to the tubulin dimers and destabilize microtubules (like Vinca Alkaloid) [47,48].

With the aim to establish whether the most active compounds **4** and **7** could be inhibitors of the tubulin polymerization, we carried out an *in vitro* tubulin-polymerization inhibition assay, a well-established test that allow to evaluate tubulin polymerization through the measuring of turbidity variation at 350 nm. To perform the test, we used a vehicle (DMSO) control, compounds **4** and **7** and two well-known microtubules targeting agents, Paclitaxel and Vinblastine, as reference molecules, at the 10 μM concentration.

As it can be seen in Figure 6, in the control reaction (vehicle, DMSO) tubulin heterodimers self-assemble, as indicated by the turbidity increase in a time-dependent manner, reaching the steady state after about 15 min and with a final optical density value at 350nm (OD_{350}) of about 0.47. As expected, the microtubule-stabilizing agent Paclitaxel caused a similar behaviour but with a higher rate and amount of tubulin heterodimers assembly (OD_{350} of about 0.52), reaching the plateau after about 10 min. On the contrary, Vinblastine was able to block strongly the tubulin polymerization, as indicated by the reaching of the steady state only after about 40 min and by the lower final turbidity value, less than the half of the control reaction (OD_{350} of about 0.2). The exposure of tubulin to compounds **4** and **7** influences the tubulin polymerization reaction as well, even if in a lesser extent compared to Vinblastine. Particularly, compounds **4** and **7** presented the same behaviour of Vinblastine in the first **7** min after the reaction start, and then the curves reached the steady state at 15 and 30 min, respectively. Even though Vinblastine is a faster inhibitor with respect to compounds **4** and **7**, it should be noticed that the final OD_{350} values for compounds **4** and **7** (OD_{350} of about 0.24 and 0.26, respectively) are similar to that of Vinblastine. Thus, our outcomes demonstrate that compounds **4** and **7** are valid tubulin polymerization inhibitors, a bit less powerful than Vinblastine but with the very important advantage of lack of cytotoxic effects on non-tumoral cell lines (Table 2, comparing IC_{50} values of compounds **4**, **7** and Vinblastine for MCF-10A cells).
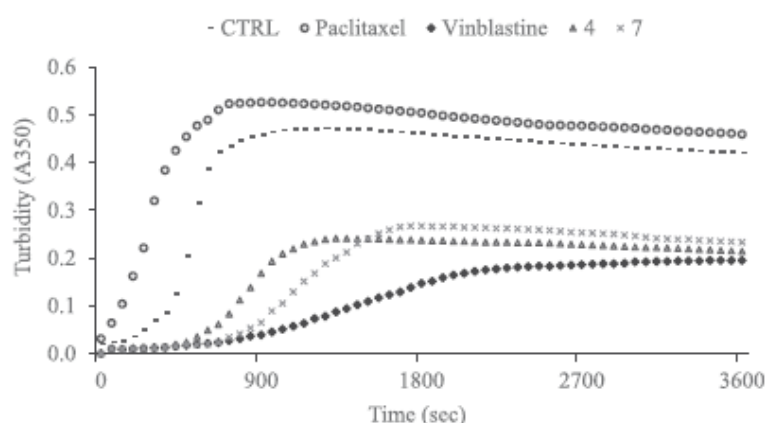
Figure 6. *Tubulin polymerization assay. Tubulin heterodimers polymerization into microtubules was determined by measuring the turbidity at 350nm for 3600 s at 37°C. The effect of compounds **4** and **7** (10 μM) on tubulin polymerization in vitro was examined. DMSO was used as a negative control. Tubulin-targeting agent Paclitaxel (10 μM) and Vinblastine (10 μM) were used as tubulin-stabilizing and tubulin-destabilizing reference agents, respectively.*

2.5. Compounds 4 and 7 are selective human Topoisomerase I inhibitors

DNA Topoisomerases are one of the major topic on the road towards combating cancer. Among the main functions of Topoisomerases there is the capability to prevent the excessive DNA's supercoiling. DNA supercoiled affects some important cellular events such as DNA transcription and replication, chromosome segregation, chromatin assembly and maintaining of genomic stability. However, Topoisomerases are often over-expressed in cancer cells, allowing an uncontrolled proliferation. As consequence, many researchers have focused on the study of new Topoisomerases targeting drugs in order to inhibit the tumour growth. Considering these relevant observations, we evaluated whether our most active compounds 4 and 7 could be able to inhibit the human topoisomerases I (hTopo I) and II (hTopo II) in a cell free system, as predicted by previous *in silico* studies.

For hTopo I inhibition assay, we incubated the enzyme with Ellipticine, compounds **4** and **7** at 50 μM final concentration for 1h at 37 °C and processed the samples, as detailed in the Experimental section. The obtained data, reported in Figure 7, highlighted that compound **4** was able to inhibit hTopo I; indeed a single band at the bottom of the gel (lane 4) represents the uncleaved plasmid pHOT1. On the contrary, compound **7** did not exhibit any inhibitory activity, at least under the conditions and at the concentration used in this assay. In fact, multiple bands due to plasmidic DNA cleavage are visible (lane 5), as in the control (lane 2), where enzyme was exposed only to vehicle (DMSO). Ellipticine, used as reference molecules, exhibits the already known effect, being able to inhibit hTopo I enzyme and capable to shift the super coiled plasmid DNA electrophoretic migration [5,27] (Figure 7, lane 3).
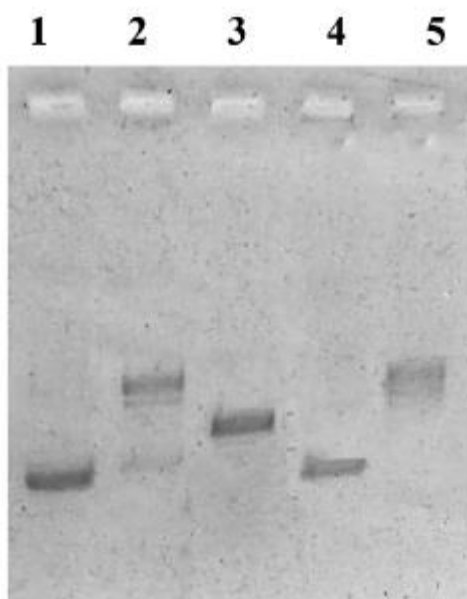
Figure 7. *hTopoI assay. Supercoiled DNA was incubated without or with human topo I in the absence or presence of the test compounds at 50 μM: lane 1, super coiled DNA, lane 2, vehicle (DMSO), lane 3, Ellipticine, lane 4, compound **4**, lane 5, compound **7**.*

Next, we evaluated the inhibitory activity of **4** and **7** toward human Topoisomerase II (hTopo II), exposing it to our compoundsat a concentration equal to 50 μM for 1 h at 37 °C (for more details see Experimental section). In this case, both the compounds **4** and **7** were not able to inhibit hTopo II activity, even raising the concentration up to 100 μM (data not shown). Summing up, the two most active compounds, **4** and **7**, displayed a different behavior regarding their biological effects. The most active one (4) exerted its antitumor properties targeting two different cellular proteins, i.e. tubulin and hTopoI, whereas compound **7** seems to inhibit only tubulin polymerization. These data set the compounds **4** as a good lead for the development of drugs targeting different cellular proteins/enzymes.

3. Conclusions

In the past decade, numerous drugs have been designed, synthesized and successful studied for their biological activities. Most of these new molecules have been screened for a single cellular target, showing high selectivity and less side effects. This effort provided several potential therapeutic approaches for many diseases, but the bottleneck lies in the area of the treatment of complex or multifactorial diseases, such cardiovascular or neurological ones

and, most importantly, for cancer treatment. Additionally, clinical experiences reinforce the idea that a single-target drug could not always produce the desired effect, first because of the ability of the organism to activate compensatory ways. Thus, very recently the multi-target drug design concept represents the current trend for future drug research and development. With this in mind, we designed and synthesized new carbazole-related compounds, i.e. thiophenic isosteres, which have been studied in two models of breast cancer cell lines, in order to individuate the potential biological targets. The preliminary evaluation of their antitumor properties served us to select the most active compounds, which have undergone to *in silico* studies, aimed at individuating some important targets for the cancer treatment, particularly tubulin and human topoisomerases. Our simulation results showed that the two ligands investigated (compounds **4** and **7**) are both predicted to bind the enzymes with a relatively high affinity, at least in the low micromolar range. The affinity is even more favourable in the case of the binding with the Topoisomerase I-DNA complex, where it is predicted to be in the nanomolar range.

Besides a high probability in the binding indicated by the docking scores obtained in the *in silico* experiments, in one case (**4** bound to Tubulin) the predicted energy was more favourable than the one obtained in the re-docking of the crystallographic ligand (i.e., Colchicine) in the known binding position. These results allow us to conclude that the two benzothienoquinazolinone derivatives (**4** and **7**) are able to interact with the complexes, and can be reasonably expected to inhibit (or at last interfere with) their function. Next, we performed *ad hoc* studies with the aim to confirm the potential biological activity towards tubulin polymerization and human Topoisomerases. Our outcomes undoubtedly show that the most active one (compound **4**) is able to target at least two not strictly related cellular targets, namely tubulin and hTopoI, a feature that is very important for a potential success in cancer treatment because of the complexity and heterogeneity of mechanisms involved in tumor onset and development. We believe that compound **4** may represent a good lead for the development of new multi-target drugs and, as well, for next studies aimed at the individuation of new cellular targets.

4. Experimental section

4.1. Synthesis and characterization

General chemical information is reported in a previous work [27], and 3-Aminodibenzothiophene (1) was prepared as already described [34].

4.1.1. General procedure for the preparation of 3-(alkyl(dialkyl) amino)benzothieno[2,3-f]quinazolin-1(2H)-ones (4-9)

3-Aminodibenzothiophene (**1**) (1.56 mmol) in DMF (40 mL) was mixed with a solution of ethoxycarbonylisothiocyanate (1.56 mmol) and the obtained mixture was stirred at room temperature (rt) for 4 h and then cooled down to 0 °C. Then, alkyl(- dialkyl)amine (4.70 mmol) and $HgCl_2$ (1.56 mmol) were added and the resulting mixture was stirred at rt for 18 h. Then it was heated at 160 °C for 2 h, cooled, filtered through a celite pad and concentrated in vacuum. The crude solid was crystallized from acetonitrile to give pure benzothienoquinazolinones (**4-9**).

4.1.1.1. 3-(Propylamino)benzothieno[2,3-f]quinazolin-1(2H)-one (4)

Brown powder (41% yield). Mp > 260 °C. IR (KBr) (cm^{-1}): 3264 (ν NH), 2957 (ν CH arom.), 871 (ν CH aliph.), 1715 (ν C=O), 1636 (ν C=N), 1520 (ν C=C), 1458 (ν C=C), 1300, 1186, 829, 753. ^{1}H NMR (400 MHz, DMSO-d$_6$): δ 0.87-0.98 (t, 3H, CH$_3$), 1.58-1.68 (m, 2H,

CH$_2$CH$_2$CH$_3$), 3.40-3.60 (m, 2H, CH$_2$CH$_2$CH$_3$), 6.50 (br, 1H, NH), 7.44-7.55 (m, 3H, Ar), 7.99 (δ, 1H, J = 8.0 Hz, Ar), 8.30 (δ, 1H, J = 8.8 Hz, Ar), 9.80 (δ, 1H, J ¼=8.3 Hz, Ar), 11.10 (br, 1H, NH). ^{13}C NMR (100 MHz, DMSO-d$_6$): 160.23, 153.41, 143.67, 140.59, 136.61, 134.48, 133.25, 128.83, 124.55, 124.17, 123.82, 123.37, 120.64, 118.41, 41.58, 24.61, 12.32. MS (EI) m/z (%): 309 (M$^{+\cdot}$, 100), 267 (99) (M$^{+\cdot}$-CH$_2$CH$_2$CH$_3$). Anal. Calcd for C$_{17}$H$_{15}$N$_3$OS: C, 66.00; H, 4.89; N, 13.58. Found: C, 65.98; H, 4.91; N, 13.60.

4.1.1.2. 3-(Butylamino)benzothieno[2,3-f]quinazolin-1(2H)-one (**5**)

Brown powder (35% yield). Mp > 260 °C. IR (KBr) (cm^{-1}): 3261 (ν NH), 3044 (ν CH arom.), 2954 (ν CH aliph.), 2868 (ν CH aliph.), 1706 (ν C=O), 1636 (ν C=N), 1457 (ν C=C), 1300, 1029, 757. ^{1}H NMR (400 MHz, DMSO-d$_6$): δ 0.65-0.75 (t, 3H, CH$_3$), 1.11-1.27 (m, 2H, CH$_2$CH$_3$), 1.28-1.40 (m, 2H, CH$_2$CH$_2$CH$_2$CH$_3$), 3.18-3.30 (m, 2H, NCH$_2$(CH$_2$)$_2$CH$_3$), 7.00 (br, 1H, N*H*), 7.20-7.48 (m, 3H, Ar), 7.85 (d, 1H, J = 7.8 Hz, Ar), 8.10 (d, 1H, J =8.4 Hz, Ar), 9.58 (d, 1H, J =8.1 Hz, Ar),11.30 (br,1H, NH). ^{13}C NMR (100 MHz, DMSO-d$_6$): 160.51,153.78, 143.24, 140.12, 136.37, 134.29, 133.17, 128.34, 124.72, 124.46, 123.54, 123.19, 120.28, 119.16, 42.68, 33.47, 20.61, 14.51. MS (EI) m/z (%): 323 (M$^{+\cdot}$, 100), 267 (90) (M$^{+\cdot}$ e CH$_2$CH2CH$_2$CH$_3$). Anal. Calcd for C$_{18}$H$_{17}$N$_3$OS: C, 66.85; H, 5.30; N, 12.99. Found: C, 66.87; H, 5.33; N, 13.02.

4.1.1.3. 3-(Cyclopenthylamino)benzothieno[2,3-f]quinazolin-1(2H)- one (**6**)

Ligth brown powder (40% yield). Mp > 260 °C. IR (KBr) (cm^{-1}): 3419 (ν NH), 3078 (ν CH arom.), 2954 (n CH aliph.), 1705 (ν C=O), 1628 (ν C=N), 1460 (n C=C), 1301, 824, 758. 1H NMR (400 MHz, DMSO-d$_6$): δ 1.50-2.10 (m, 8H, CH$_2$), 4.30-4.40 (m, 1H, CH), 6.00 (br, 1H, N*H*), 7.42-7.66 (m, 3H, Ar), 8.00 (δ, 1H, J = 7.8 Hz, Ar), 8.30 (d, 1H, J = 8.8 Hz, Ar), 9.70 (d, 1H, J = 8.3 Hz, Ar), 11.10 (br, 1H, NH). ^{13}C NMR (100 MHz, DMSO-d$_6$): 161.09, 153.59, 142.04, 140.54, 136.31, 133.73, 133.26, 128.57, 124.51, 124.15, 123.62, 123.09, 119.89,117.91, 54.38, 33.24, 24.15.MS (EI) m/z (%): 335 (M$^{+\cdot}$, 53), 267 (100) (M$^{+\cdot}$-cyclopentyl). Anal. Calcd for C$_{19}$H$_{17}$N3OS: C, 68.03; H, 5.11; N, 12.53. Found: C, 68.05; H, 5.09; N, 12.51.

4.1.1.4. 3-(Dipropylamino)benzothieno[2,3-f]quinazolin-1(2H)-one (**7**)

Green powder (40% yield). Mp =234 °C. IR (KBr) (cm^{-1}): 3435 (n NH), 3166 (ν CH arom.), 2962 (ν CH aliph.), 1637 (ν C=O), 1581 (ν C=C), 1455 (ν C=C), 1302, 785, 503. ^{1}H NMR (400 MHz, DMSO-d$_6$): δ 0.83-0.93 (t, 6H, CH$_3$), 1.53-1.66 (m, 4H, CH$_2$CH$_3$), 3.46-3.56 (m, 4H, NCH$_2$CH$_2$CH$_3$), 7.40-7.52 (m, 3H, Ar), 7.98 (d, 1H, J =7.8 Hz, Ar), 8.15 (d, 1H, J = 8.8 Hz, Ar), 9.80 (d, 1H, J = 7.8 Hz, Ar), 11.20 (br, 1H, NH). ^{13}C NMR (100 MHz, DMSO-d$_6$): 160.51, 153.68, 143.61, 140.29, 136.73, 134.61, 133.43, 128.91, 124.68, 124.54, 123.62, 123.21, 120.79, 118.54, 41.72, 24.75, 13.18. MS (EI) m/z (%): 351 (M$^{+\cdot}$, 93), 267 (100). Anal. Calcd for C$_{20}$H$_{21}$N$_3$OS: C, 68.35; H, 6.02; N, 11.96. Found: C, 68.37; H, 6.01; N, 11.94.

4.1.1.5. 3-(Dipentylamino)benzothieno[2,3-f]quinazolin-1(2H)-one (**8**)

Yellow powder (44% yield). Mp > 200 °C. IR (KBr) (cm^{-1}): 3435 (ν NH), 3043 (CH arom.), 2954 (CH aliph.), 2927 (CH aliph.), 1635 (ν C=O), 1600 (n C=C), 1456 (ν C=C), 1307, 1132, 827, 729, 624. ^{1}H NMR (400 MHz, DMSO-d$_6$): d 0.82e0.97 (t, 6H, (CH$_2$)$_4$CH$_3$), 1.20-1.38 (m, 8H, (CH$_2$)$_2$CH$_2$ CH$_2$CH$_3$), 1.50-1.58 (m, 4H, CH$_2$CH$_2$(CH$_2$)$_2$CH$_3$), 3.46-3.56 (m, 4H, NCH$_2$(CH$_2$)$_3$CH$_3$), 7.40-7.50 (m, 3H, Ar), 8.00 (d, 1H, J = 7.8 Hz, Ar), 8.15 (d, 1H, J

=8.8 Hz, Ar), 9.80 (d, 1H, J =7.5 Hz, Ar), 11.20 (br, 1H, NH). 13C NMR (100 MHz, DMSO-d_6): 160.72, 153.37 143.51, 140.41, 136.82, 134.67, 133.58, 129.07, 124.82, 124.61, 123.74, 123.53, 121.12, 118.67, 49.85, 30.61, 23.42, 21.19, 14.48. MS (ESI$^+$): 408 (M$^+$ +1). Anal. Calcd for $C_{24}H_{29}N3OS$: C, 70.73; H, 7.17; N, 10.31. Found: C, 70.71; H, 7.20; N, 10.33.

4.1.1.6. 3-(Morpholin-1-yl)benzothieno[2,3-f]quinazolin-1(2H)-one (9)

Green powder (50% yield). Mp > 260 °C. IR (KBr) (cm^{-1}): 3649 (ν NH), 3056 (CH arom.), 2960 (ν CH aliph.), 1647 (ν C=O), 1581 (ν C=C), 1456 (ν C=C), 1115, 1065, 884, 775. 1H NMR (400 MHz, DMSO-d_6): δ 3.50-3.62 (m, 8H, CH2 morpholine), 7.30-7.42 (m, 3H, Ar), 7.92 (d, 1H, J ¼ 7.8 Hz, Ar), 8.11 (d, 1H, J ¼ 8.7 Hz, Ar), 9.68 (d, 1H, J = 9.0 Hz, Ar), 11.35 (br, 1H, NH). 13C NMR (100 MHz, DMSO-d_6): 161.25, 153.87 143.83, 140.75, 137.11, 135.21, 133.81, 129.15, 125.06, 124.96, 123.89, 123.78, 121.57, 118.07, 67.29, 50.64. MS (EI) m/z (%): 337 (M$^{+\cdot}$, 100). Anal. Calcd for $C_{18}H_{15}N_3O_2S$: C, 64.08; H, 4.48; N, 12.45. Found: C, 64.06; H, 4.50; N, 12.47.

4.2. Molecular Docking

Molecular docking of 4 and 7 was carried out on the crystallographic structures of Tubulin, Topoisomerase I and Topoisomerase II, corresponding to entries 1SA0 [36], 1K4T [38] and 5GWI [40] of the PDB, respectively. Molecular structures of the ligands were built by using the modeling software Avogadro [49]. Preliminary conversion of the structures from the PDB format was carried out by using the graphical interface AutoDock Tools 1.5.6 [50]. During the conversion, polar hydrogens were added for the crystallographic enzymes (including DNA, when present), and apolar hydrogens of **4** and **7** were merged to the carbon atom they were attached to.

Docking calculations were performed by using AutoDock Vina 1.1.2 [51], either exploring the search volume that included each protein structure or, alternatively, by performing a score-only assessment without any search in the case of re-docking of the crystallographic ligands in their known binding pose. In the former case a very high exhaustiveness of search was used, 8 times larger than the default value [52], facilitated by the relatively small number of active torsions around bond dihedral angles necessary to give full flexibility to the two ligands (three degrees of freedom for **4**, and five for **7**). The binding modes of the ligands were analysed through visual inspection, and interactions energies and distances were quantified by using Molecular Operating Environment (MOE) 2018.01 [53]. The Molecular Graphics System PyMOL has been used to visualize protein structure and ligand binding [54].

4.3. Biological methods

4.3.1. Cell cultures and viability

The three cell lines used for this work were purchased from American Type Culture Collection (ATCC, Manassas, VA, USA). Human estrogen receptor (ER)-positive MCF-7, triple negative MDAMB-231 were cultured in DMEM-F12 medium containing 2 mmol/mL L-glutamine, 1 mg/mL penicillin-streptomycin and 5% Newborn Calf Serum (NCS) or 5% Fetal Bovine Serum (FBS), respectively. MCF-10A human mammary epithelial cells were cultured in DMEM/F12 medium, supplemented with 5% horse serum,100 mg/mL penicillinstreptomycin, 0.5 mg/mL hydrocortisone, 20 ng/mL hEGF,10 mg/mL insulin and 0.1 mg/mL cholera enterotoxin. Cells were maintained at 37 °C in a humidified atmosphere of 95% air and 5% CO_2 [12,55].

To assess the cells viability, all cell lines were seeded in 48 well plates and cultured for 24 h in full medium. Next, cells were serumstarved for 24 h and the effect of the different concentrations of each compound was measured using 3-(4,5-dimethylthiazol-2-yl)- 2,5-diphenyl tetrazolium bromide (MTT) assay, as previously described [30]. Each experiment was performed in triplicate, using six molecules concentrations (0.1, 1, 10, 20, 40 and 100 mM) and the absorbance was measured at 570 nm using a microplate reader (Micro-plate reader, Synergy, BioTek). Results are represented as percent (%) of basal and the IC_{50} values were calculated using GraphPad Prism 6 (GraphPad Software, La Jolla, CA, USA).

4.3.2. In vitro tubulin polymerization assay

Tubulin polymerization inhibition was measured using *in vitro* Tubulin Polymerization Assay Kit purchased from EMD Millipore Corporation using the manufacturer's instructions. Polymerization reaction occurs in 70 mL final volume, with 60 mM tubulin in 1x PBGTP and each compound at a concentration of 10 mM. Both Paclitaxel and Vinblastine (used as control) were dissolved in DMSO and used at final concentration of 10 mM. The mixturewere combined in a 96-well plate and readings were performed using a Tecan microplate reader (37 °C, 10 s shaking before each reading) and the turbidity variation was measured every 30 s at 350nm for 90 min.

4.3.3. Human topoisomerase I relaxation assay

hTopo I relaxation assays have been performed in a final volume of 20 μL, as reported by Iacopetta et al. [12,56], incubating 0.25 μg of supercoiled pHOT1 in TE buffer (TopoGEN, Port Orange, FL, USA) with tested compounds and recombinant hTopo I (2 units) (Topo-GEN, Port Orange, FL, USA) for 1h at 37 °C. The final solution has been loaded onto a 1% agarose gel containing 1x TAE buffer without ethidium bromide (EB). At the end, 1x TAE buffer containing EB (0.5 μg/mL) has been used to stain agarose gel for 30 min and after wash with distilled water for 15 min it has been visualized by using a UV transilluminator. The experiment was repeated three times.

4.3.4. Human topoisomerase II decatenation assay

hTopo II decatenation assays were performed in a final volume of 20 mL, as reported by Iacopetta et al. [12,56], using 0.2 mg of kinetoplast DNA (kDNA) (topoGEN, Port Orange, FL, USA), tested compounds and 3 units of hTopo II (topoGEN, Port Orange, FL, USA). Reaction products were analyzed by agarose gel electrophoresis with ethidium bromide (EB). At the end the gel was washed with distilled water and observed using a UV transilluminator. The experiment was repeated three times.

References

[1] A. Caruso, A. Chimento, H. El-Kashef, J.C. Lancelot, A. Panno, V. Pezzi, C. Saturnino, M.S. Sinicropi, R. Sirianni, S. Rault, Antiproliferative activity of some 1,4-dimethylcarbazoles on cells that express estrogen receptors: part I, J. Enzym. Inhib. Med. Chem. 27 (2012) 609e613.

[2] C. Saturnino, A. Caruso, P. Longo, A. Capasso, A. Pingitore, M.C. Caroleo, E. Cione, M. Perri, F. Nicolo, V.M. Nardo, L.M. Scolaro, M.S. Sinicropi, M.R. Plutino, H. El-Kashef, Crystallographic study and biological evaluation of 1,4-dimethyl-N-alkylcarbazoles, Curr. Top. Med. Chem. 15 (2015) 973e979.

[3] M.S. Sinicropi, R. Lappano, A. Caruso, M.F. Santolla, A. Pisano, C. Rosano, A. Capasso, A. Panno, J.C. Lancelot, S. Rault, C. Saturnino, M. Maggiolini, (6- Bromo-1,4-dimethyl-9H-carbazol-3-yl-methylene)-hydrazine (carbhydraz) acts as a GPER agonist in breast cancer cells, Curr. Top. Med. Chem. 15 (2015) 1035e1042.

[4] T. Isah, Rethinking Ginkgo biloba L.: medicinal uses and conservation, Pharmacogn. Rev. 9 (2015) 140e148. [5] M. Stiborova, E. Frei, Ellipticines as DNA-targeted chemotherapeutics, Curr. Med. Chem. 21 (2014) 575e591.

[6] O.I. Parisi, C. Morelli, F. Puoci, C. Saturnino, A. Caruso, D. Sisci, G.E. Trombino N. Picci, M.S. Sinicropi, Magnetic molecularly imprinted polymers (MMIPs) for carbazole derivative release in targeted cancer therapy, J. Mater. Chem. B. 2 (2014) 6619e6625.

[7] C. Saturnino, A. Caruso, D. Iacopetta, C. Rosano, J. Ceramella, N. Muia, A. Mariconda, M.G. Bonomo, M. Ponassi, G. Rosace, M.S. Sinicropi, P. Longo, Inhibition of human topoisomerase II by N,N,N-trimethylethanammonium iodide alkylcarbazole derivatives, ChemMedChem 13 (2018) 2635e2643.

[8] M.S. Sinicropi, D. Iacopetta, C. Rosano, R. Randino, A. Caruso, C. Saturnino, N. Muia, J. Ceramella, F. Puoci, M. Rodriquez, P. Longo, M.R. Plutino, N-thioalkylcarbazoles derivatives as new anti-proliferative agents: synthesis, characterisation and molecular mechanism evaluation, J. Enzym. Inhib. Med. Chem. 33 (2018) 434e444.

[9] J. Lin, M. Tang, R. Zhao, Q. Du, L. Shen, G. Du, Y. Zhang, Y. Li, X. Pan, Synthetic optimization of ellipticine and antitumor activity of novel hexacyclic derivatives of ellipticine, Curr. Pharmaceut. Des. 25 (2019) 1e12.

[10] M. Stiborova, J. Poljakova, E. Martinkova, L. Borek-Dohalska, T. Eckschlager, R. Kizek, E. Frei, Ellipticine cytotoxicity to cancer cell lines - a comparative study, Interdiscip. Toxicol. 4 (2011) 98e105.

[11] C. Saturnino, C. Palladino, M. Napoli, M.S. Sinicropi, A. Botta, M. Sala, A.C. de Prati, E. Novellino, H. Suzuki, Synthesis and biological evaluation of new Nalkylcarbazole derivatives as STAT3 inhibitors: preliminary study, Eur. J. Med. Chem. 60 (2013) 112e119.

[12] D. Iacopetta, C. Rosano, F. Puoci, O.I. Parisi, C. Saturnino, A. Caruso, P. Longo, J. Ceramella, A. Malzert-Freon, P. Dallemagne, S. Rault, M.S. Sinicropi, Multifaceted properties of 1,4-dimethylcarbazoles: focus on trimethoxybenzamide and trimethoxyphenylurea derivatives as novel human topoisomerase II inhibitors, Eur. J. Pharm. Sci. 96 (2017) 263e272.

[13] S. Ghosh, A. Kar, S. Chowdhury, D. Dasgupta, Ellipticine binds to a human telomere sequence: an additional mode of action as a putative anticancer agent? Biochemistry 52 (2013) 4127e4137.

[14] A. Zabka, K. Winnicki, J.T. Polit, J. Maszewski. The effects of anti-DNA topoisomerase II drugs, etoposide and ellipticine, are modified in root meristem cells of Allium cepa by MG132, an inhibitor of 26S proteasomes, Plant Physiol. Biochem. 96 (2015) 72e82.

[15] S. Sumalatha, V. Namrata, M. Lakshmi, G. Sridhar, Synthesis and anticancer activity of oxadiazole incorporated ellipticine derivatives, Russ. J. Gen. Chem. 89 (2019) 505e510.

[16] A. Caruso, J. Lancelot, H. El-Kashef, M.S. Sinicropi, R. Legay, R. Lesnard, S. Rault, A rapid and versatile synthesis of novel pyrimido[5,4-b]carbazoles. Tetrahedron 65 (2009) 10400e10405.

[17] A. Caruso, A.S. Voisin-Chiret, J.C. Lancelot, M.S. Sinicropi, A. Garofalo, S. Rault, Novel and efficient synthesis of 5,8-dimethyl-9h-carbazol-3-ol via a hydroxydeboronation reaction, Heterocycles 71 (2007) 2203e2210.

[18] A. Caruso, A.S. Voisin-Chiret, J.C. Lancelot, M.S. Sinicropi, A. Garofalo, S. Rault, Efficient and simple synthesis of 6-Aryl-1,4-dimethyl-9H-carbazoles, Molecules 13 (2008) 1312e1320.

[19] A. Caruso, J.C. Lancelot, H. El-Kashef, A. Panno, M.S. Sinicropi, R. Legay, A. Lesnard, A. Lepailleur, S. Rault, Four partners, three-step, one-pot reaction for a library of new 2-Alkyl(dialkyl)aminoquinazolin-4(3H)-ones, J. Heterocycl. Chem. 51 (2014) E282eE293.

[20] A. Panno, M.S. Sinicropi, A. Caruso, H. El-Kashef, J.C. Lancelot, G. Aubert, A. Lesnard, T. Cresteil, S. Rault, New trimethoxybenzamides and trimethoxyphenylureas derived from dimethylcarbazole as cytotoxic agents. Part I, J. Heterocycl. Chem. 51 (2014) E294eE302.

[21] C. Saturnino, M. Buonerba, G. Boatto, M. Pascale, O. Moltedo, L. De Napoli, D. Montesarchio, J.C. Lancelot, P. de Caprariis, Synthesis and preliminary biological evaluation of a new pyridocarbazole derivative covalently linked to a thymidine nucleoside as a potential targeted antitumoral agent. I, Chem. Pharm. Bull. 51 (2003) 971e974.

[22] A. Caruso, M.S. Sinicropi, J.C. Lancelot, H. El-Kashef, C. Saturnino, G. Aubert, C. Ballandonne, A. Lesnard, T. Cresteil, P. Dallemagne, S. Rault, Synthesis and evaluation of cytotoxic activities of new guanidines derived from carbazoles, Bioorg. Med. Chem. Lett 24 (2014) 467e472.

[23] F.M. Deane, E.C. O'Sullivan, A.R. Maguire, J. Gilbert, J.A. Sakoff, A. McCluskey, F.O. McCarthy, Synthesis and evaluation of novel ellipticines as potential anticancer agents, Org. Biomol. Chem. 11 (2013) 1334e1344.

[24] C.M. Miller, E.C. O'Sullivan, K.J. Devine, F.O. McCarthy, Synthesis and biological evaluation of novel isoellipticine derivatives and salts, Org. Biomol. Chem. 10 (2012) 7912e7921.

[25] T.T. Bui, F. Goubard, M. Ibrahim-Ouali, D. Gigmes, F. Dumur, Recent advances on organic blue thermally activated delayed fluorescence (TADF) emitters for organic light-emitting diodes (OLEDs), Beilstein J. Org. Chem. 14 (2018) 282e308.

[26] G. Khodarahmi, P. Asadi, F. Hassanzadeh, E. Khodarahmi, Benzofuran as a promising scaffold for the synthesis of antimicrobial and antibreast cancer agents: a review, J. Res. Med. Sci. 20 (2015) 1094e1104.

[27] P. Rizza, M. Pellegrino, A. Caruso, D. Iacopetta, M.S. Sinicropi, S. Rault, J.C. Lancelot, H. El-Kashef, A. Lesnard, C. Rochais, P. Dallemagne, C. Saturnino, F. Giordano, S. Catalano, S. Ando, 3-(Dipropylamino)-5-hydroxybenzofuro [2,3-*f*]quinazolin-1(2H)-one (DPA-HBFQ-1) plays an inhibitory role on breast cancer cell growth and progression, Eur. J. Med. Chem. 107 (2016) 275e287.

[28] B.L. Yu, B.M. Dietz, T. Dunlap, I. Kastrati, D.D. Lantvit, C.R. Overk, P. Yao, Z.H. Qin, J.L. Bolton, G.R.J. Thatcher, Structural modulation of reactivity/activity in design of improved benzothiophene selective estrogen receptor modulators: induction of chemopreventive mechanisms, Mol. Cancer Ther. 6 (2007) 2418e2428.

[29] J.D. Koruznjak, M. Grdisa, N. Slade, B. Zamola, K. Pavelic, G. Karminski-Zamola, Novel derivatives of benzo[b]thieno[2,3-c]quinolones: synthesis, photochemical synthesis, and antitumor evaluation, J. Med. Chem. 46 (2003) 4516e4524.

[30] D. Iacopetta, A. Carocci, M.S. Sinicropi, A. Catalano, G. Lentini, J. Ceramella, R. Curcio, M.C. Caroleo, Old drug scaffold, new activity: thalidomidecorrelated compounds exert different effects on breast cancer cell growth and progression, ChemMedChem 12 (2017) 381e389.

[31] K. McPherson, C.M. Steel, J.M. Dixon, ABC of breast diseases. Breast cancerepidemiology, risk factors, and genetics, Br. Med. J. 321 (2000) 624e628.

[32] M. Ghoncheh, Z. Pournamdar, H. Salehiniya, Incidence and mortality and epidemiology of breast cancer in the world, Asian Pac. J. Cancer Prev. APJCP 17 (2016) 43e46.

[33] C. Siciliano, R. De Marco, L.E. Guidi, M. Spinella, A. Liguori, A one-pot procedure for the preparation of N-9-fluorenylmethyloxycarbonyl-alpha-amino diazoketones from alpha-amino acids, J. Org. Chem. 77 (2012) 10575e10582.

[34] Y.C. Wu, J.C. Li, J.J. Wu, P. Morgan, X. Xu, F. Rancati, S. Vallese, L. Raveglia, R. Hotchandani, N. Fuller, J. Bard, K. Cunningham, S. Fish, R. Krykbaev, S. Tam, S.J. Goldman, C. Williams, T.S. Mansour, E. Saiah, J. Sypek, W. Li, Discovery of potent and selective matrix metalloprotease 12 inhibitors for the potential treatment of chronic obstructive pulmonary disease (COPD), Bioorg. Med. Chem. Lett 22 (2012) 138e143.

[35] E. Sirignano, A. Pisano, A. Caruso, C. Saturnino, M.S. Sinicropi, R. Lappano, A. Botta, D. Iacopetta, M. Maggiolini, P. Longo, Different 6-aryl-fulvenes exert anti-proliferative effects on cancer cells, Anti Cancer Agents Med. Chem. 15 (2015) 468e474.

[36] R.B. Ravelli, B. Gigant, P.A. Curmi, I. Jourdain, S. Lachkar, A. Sobel, M. Knossow, Insight into tubulin regulation from a complex with colchicine and a stathmin-like domain, Nature 428 (2004) 198e202.

[37] E. Chosson, F. Santoro, C. Rochais, J.S.D. Santos, R. Legay, S. Thoret, T. Cresteil, M.S. Sinicropi, T. Besson, P. Dallemagne, Synthesis of novel 7-oxo and 7- hydroxy trifluoroallocolchicinoids with cytotoxic effect, Bioorg. Med. Chem. 20 (2012) 2614e2623.

[38] B.L. Staker, K. Hjerrild, M.D. Feese, C.A. Behnke, A.B. Burgin Jr., L. Stewart, The mechanism of topoisomerase I poisoning by a camptothecin analog, Proc. Natl. Acad. Sci. U.S.A. 99 (2002) 15387e15392.

[39] Y.R. Wang, S.F. Chen, C.C. Wu, Y.W. Liao, T.S. Lin, K.T. Liu, Y.S. Chen, T.K. Li, T.C. Chien, N.L. Chan, Producing irreversible topoisomerase II-mediated DNA breaks by site-specific Pt(II)-methionine coordination chemistry, Nucleic Acids Res. 45 (2017) 10861e10871.

[40] Y.R. Wang, S.F. Chen, C.C. Wu, Y.W. Liao, T.S. Lin, K.T. Liu, Y.S. Chen, T.K. Li, T.C. Chien, N.L. Chan, Producing irreversible topoisomerase II-mediated DNA breaks by site-specific Pt(II)-methionine coordination chemistry, Nucleic Acids Res. 45 (2017) 10861e10871.

[41] M. Abal, J.M. Andreu, I. Barasoain, Taxanes: microtubule and centrosome targets, and cell cycle dependent mechanisms of action, Curr. Cancer Drug Targets 3 (2003) 193e203.7

[42] M.A. Jordan, L. Wilson, Microtubules as a target for anticancer drugs, Nat. Rev. Cancer 4 (2004) 253e265.

[43] P.P. Gan, J.A. McCarroll, S.T. Po'uha, K. Kamath, M.A. Jordan, M. Kavallaris, Microtubule dynamics, mitotic arrest, and apoptosis: drug-induced differential effects of betaIII-tubulin, Mol. Cancer Ther. 9 (2010) 1339e1348.

[44] G.J. Brouhard, L.M. Rice, The contribution of alphabeta-tubulin curvature to microtubule dynamics, J. Cell Biol. 207 (2014) 323e334.

[45] S. Banerjee, D.J. Hwang, W. Li, D.D. Miller, Current advances of tubulin inhibitors in nanoparticle drug delivery and vascular disruption/angiogenesis. Molecules 21 (2016) 1468e1504.

[46] R. Kaur, G. Kaur, R.K. Gill, R. Soni, J. Bariwal, Recent developments in tubulin polymerization inhibitors: an overview, Eur. J. Med. Chem. 87 (2014) 89e124.

[47] Y. Zhao, X. Mu, G. Du, Microtubule-stabilizing agents: new drug discovery and cancer therapy, Pharmacol. Ther. 162 (2016) 134e143.

[48] D. Fanale, G. Bronte, F. Passiglia, V. Calo, M. Castiglia, F. Di Piazza, N. Barraco, A. Cangemi, M.T. Catarella, L. Insalaco, A. Listi, R. Maragliano, D. Massihnia, A. Perez, F. Toia, G. Cicero, V. Bazan, Stabilizing versus destabilizing the microtubules: a double-edge sword for an effective cancer treatment option? Anal. Cell. Pathol. (Amst). 2015 (2015), 690916-690974.

[49] M.D. Hanwell, D.E. Curtis, D.C. Lonie, T. Vandermeersch, E. Zurek, G.R. Hutchison, Avogadro: an advanced semantic chemical editor, visualization, and analysis platform, J. Cheminf. 4 (2012) 17e32.

[50] G.M. Morris, D.S. Goodsell, R.S. Halliday, R. Huey, W.E. Hart, R.K. Belew, A.J. Olson, Automated docking using a Lamarckian genetic algorithm and an empirical binding free energy function, J. Comput. Chem. 19 (1998) 1639e1662.

[51] O. Trott, A.J. Olson, AutoDock Vina: improving the speed and accuracy of docking with a new scoring function, efficient optimization, and multithreading, J. Comput. Chem. 31 (2010) 455e461.

[52] F. Grande, B. Rizzuti, M.A. Occhiuzzi, G. Ioele, T. Casacchia, F. Gelmini, R. Guzzi, A. Garofalo, G. Statti, Identification by molecular docking of homoisoflavones from leopoldia comosa as ligands of estrogen receptors, Molecules 23 (2018) 894e916.

[53] Chemical Computing Group ULC, 1010 Sherbooke St. West, Suite #910, Montreal, QC, Canada, H3A 2R7 in, 2018.

[54] PyMOL Molecular Graphics System, Version 1.2r3pre, Schrodinger, LLC., in.

[55] R. Tundis, D. Iacopetta, M.S. Sinicropi, M. Bonesi, M. Leporini, N.G. Passalacqua, J. Ceramella, F. Menichini, M.R. Loizzo, Assessment of antioxidant, antitumor and pro-apoptotic effects of salvia fruticosa mill. subsp. thomasii (lacaita) brullo, guglielmo, pavone & terrasi (lamiaceae), Food Chem. Toxicol. 106 (2017) 155e164.

[56] A. Chimento, C. Saturnino, D. Iacopetta, R. Mazzotta, A. Caruso, M.R. Plutino, A. Mariconda, A. Ramunno, M.S. Sinicropi, V. Pezzi, P. Longo, Inhibition of human topoisomerase I and II and anti-proliferative effects on MCF-7 cells by new titanocene complexes, Bioorg. Med. Chem. 23 (2015) 7302e7312.

V. CATESLYTIN ABROGATES LIPOPOLYSACCHARIDE-INDUCED CARDIOMYOCYTE INJURY BY REDUCING INFLAMMATION AND OXIDATIVE STRESS THROUGH TOLL LIKE RECEPTOR 4 INTERACTION

Carmine Rocca [a]; Anna De Bartolo [a,b]; Fedora Grande [c], Bruno Rizzuti [d], Teresa Pasqua [a,e], Francesca Giordano [b], Maria Concetta Granieri [a], Maria Antonietta Occhiuzzi [c], Antonio Garofalo [c], Nicola Amodio [f], Maria Carmela Cerra [g], Francis Schneider [h,i], Maria Luisa Panno [b], Marie H´el`ene Metz-Boutigue [i,j], Tommaso Angelone [a,k] Angelone, T.;

[a] Laboratory of Cellular and Molecular Cardiovascular Pathophysiology, Department of Biology, E and E.S., University of Calabria, Rende, CS, Italy
[b] Department of Pharmacy, Health and Nutritional Sciences, University of Calabria, Rende, CS, Italy
[c] Laboratory of Medicinal and Analytical Chemistry, Department of Pharmacy, Health and Nutritional Sciences, University of Calabria, Rende, Italy
[d] CNR-NANOTEC, Licryl-UOS Cosenza and CEMIF.Cal, Department of Physics, University of Calabria, Rende, Italy
[e] Department of Health Science, University of Catanzaro Magna Graecia, 88100 Catanzaro, Italy
[f] Department of Experimental and Clinical Medicine, Magna Graecia University of Catanzaro, Catanzaro, Italy
[g] Laboratory of Organ and System Physiology, Department of Biology, E and E.S., University of Calabria, Rende, CS, Italy
[h] Department of Intensive Care, Hospital Hautepierre, University of Strasbourg, Strasbourg, France
[i] Inserm UMR 1121, Fédération de Médecine Translationnelle, University of Strasbourg, Strasbourg, France
[j] Faculty of Odontology, University of Strasbourg, Strasbourg France
[k] National Institute of Cardiovascular Research (INRC), Bologna, Italy

Abstract:

Global public health is threatened by new pathogens, antimicrobial resistant microorganisms and a rapid decline of conventional antimicrobials efficacy. Thus, numerous medical procedures become life-threating. Sepsis can lead to tissue damage such as myocardium inflammation, associated with reduction of contractility and diastolic dysfunction, which may cause death. In this perspective, growing interest and attention are paid on host defence peptides considered as new potential antimicrobials. In the present study, we investigated the physiological and biochemical properties of Cateslytin (Ctl), an endogenous antimicrobial chromogranin A42 derived peptide, in H9c2 cardiomyocytes exposed to lipopolysaccharide (LPS) infection. We showed that both Ctl (L and D) enantiomers, but not their scrambled counterparts, significantly increased cardiomyocytes viability following LPS, even if L-Ctl was effective at lower concentration (1 nM) compared to D-Ctl (10 nM). L-Ctl mitigated LPS-induced LDH release and oxidative stress, as visible by a reduction of MDA and protein carbonyl groups content, and by an increase of SOD activity. Molecular docking simulations strongly suggested that L-Ctl modulates TLR4 through a direct binding to the partner protein MD-2. Molecular analyses indicated that the protection mediated by L-Ctl against LPS-evoked sepsis targeted the TLR4/ERK/JNK/p38-MAPK pathway, regulating NFkB p65, NFkB p52 and COX2 expression and repressing the mRNA expression levels of the LPS-induced proinflammatory factors IL- 1β, IL- 6, TNF- α and iNOS. These findings indicate that Ctl could be considered as a possible candidate for the

development of new antimicrobials strategies in the treatment of myocarditis. Interestingly, L-enantiomeric Ctl showed remarkable properties in strengthening the anti-inflammatory and anti-oxidant effects on cardiomyocytes.

1. Introduction

Evidences from epidemiological studies conducted on post-mortem individuals identified myocarditis as a 68 significant cause of unexpected death, representing a major reason of cardiovascular events. Myocarditis is potentially life-threatening disease and mostly occurs in young and adult people [1]. Accordingly, biopsy proven myocarditis was reported in 9–16% of adult patients and a prevalence of myocarditis of 2-42% of cases in young people was registered [1 and references therein]. Several viral and bacterial infections represent etiological agents of myocarditis. Among them, the severe acute respiratory syndrome coronavirus 2 (SARS CoV-2) can cause myocarditis as evinced by numerous recent investigations reporting cases of acute myocarditis or myocardial inflammation in coronavirus disease 2019 (COVID-19) [2,3 and references therein]. Also, direct infection of the heart muscle by bacteria and bacteria-produced toxins can be responsible of myocarditis and severe myocardial damage. Bacterial myocarditis is usually observed in the context of a severe sepsis, such as an infection induced by Gram-negative bacteria, that can lead to multi-organ failure, including heart dysfunction and arrhythmias that can occur in around 60% of septic patients [4]. Clinical and experimental studies have extensively reported how decreased contractility and impaired myocardial compliance constitute major factors causing myocardial dysfunction in sepsis [5]. Lipopolysaccharide (LPS) represents the major component of the outer membrane of Gram-negative bacteria that belongs to the pathogen-associated molecular patterns (PAMPs). During myocardial inflammation, LPS interacts with the key member of pattern-recognition receptors (TLRs), the toll-like receptor 4 (TLR4), expressed on the surface of host cardiomyocyte, stimulating the innate immune system and inducing the inflammatory response [6]. TLR4 activation by LPS induces the myeloid differentiation factor 88 (Myd88)- dependent pathway, converging on nuclear transcription factors activation, such as nuclear factor-kB (NFkB). This, in turn, induces the production of pro-inflammatory cytokines leading to inflammatory cascades that are associated with several cardiovascular diseases, including myocarditis and heart failure [7 and references therein]. The identification of new classes of drugs to include in the therapeutic options for inflammatory dilated cardiomyopathy and myocarditis, for which the availability of specific treatment remains limited, is of crucial clinical interest. This is particularly important also given the global increasing impact of antibiotic-resistant infections on health and economic outcomes [8]. In this context, antimicrobial peptides (AMPs) are antimicrobial agents active against infections that do not show the typical disadvantages of more conventional antibiotics related to possible gastrointestinal or allergic reactions, and associated to antibiotic-resistant bacteria [9].
Chromogranin A (CgA), a member of the chromogranin/secretogranin family, is a pro-hormone localized in the secretory vesicles of neurons, neuroendocrine cells, granulocytes, immune cells and cardiomyocytes [10-12]The intravesicular proteolytic processing of CgA under physiological or stress conditions generates several protein fragments with different biological activities [12], ranging from the regulation of innate immunity, antimicrobial activities and inflammation to neuroprotection and cardiovascular protection [13,14,15]. One of the CgA cleavage products, the bioactive peptide Catestatin (Cst, human

CgA352−372) was initially described as a potent inhibitor of catecholamines release via the nicotinic receptor [16]. Experimental evidences report that Cst may affect the heart function and the blood pressure both directly and indirectly, playing a crucial regulatory role in cardiovascular system under physiological and pathological conditions [13,17]. Accordingly, Cst is able to counteract the cardiac effects following adrenergic stimulation, and to protect the heart against ischemia/reperfusion injury, acting as a post-conditioning protective agent [13]. It is also known that Cst contributes to the immune system regulation and can mitigate severe inflammatory response, thus preserving tissues function [17].

In addition to several other AMPs resulting from the natural processing of CgA, such as vasostatin-1, the core sequence of Cst, Cateslytin (Ctl; bovine CgA344–358, with sequence RSMRLSFRARGYGFR), can also act as host defense peptides (HDPs), due to its antimicrobial activities against a wide number of pathogens [18]. In addition, compared to other CgA fragments with antimicrobial properties, Ctl is able to resist to the degradation when treated with bacterial supernatants [19] and it is unable to induce resistance for the host [20].

Based on these knowledges, the present work was undertaken to explore: i) the ability of the two enantiomers of the Ctl (*L* or *D* amino acids) to mitigate the cardiomyocyte injury evoked by LPS infection; ii) the potential ability of *L*-Ctl to affect TLR4 through interaction with the partner protein MD-2; iii) the molecular mechanism of action underlying the effect of *L*-Ctl in the presence of LPS in H9c2 cardiomyocytes.

2.Material & methods

2.1. Peptides and chemicals

L-Ctl (CgA$_{344–358}$, RSMRLSFRARGYGFR) and its derivate D-Ctl were synthesized by roteogenix SAS (Schiltigheim, France) according to the Merrifield Technique, a stepwise solid-phase peptide synthesis approach with FMOC chemistry, and purified to >95% by using reverse phase high-performance liquid chromatography (RP-HPLC) and controlled by MALDI-TOF mass spectrometry. As negative controls, the scrambled LCtl and D-Ctl (FMRLRYRSSAFGGRR, in L-and D-aminoacid forms, respectively) have been used. Both L-Ctl and D-Ctl were dissolved in sterile water before use (UltraPure RNase/DNase-free distilled water, Invitrogen, California, USA). Lipopolysaccharides (LPS) from Escherichia coli O55:B5, sodium pyruvate and β-nicotinamideadenine dinucleotide disodium salt, 2,4 dinitrophenylhydrazine (DNPH), 2-thiobarbituric acid (TBA), bovine serum albumin (BSA), butanol-1, butylated hydroxyanisole, diethyl ether, ethylenediaminetetraacetic acid (disodium salt), streptomycin sulfate, tween-20 and urea were obtained from Sigma Aldrich (St. Louis, MO, USA). Dimethyl sulfoxide (DMSO) was purchased from PanReac AppliChem (Glenview, Illinois, USA). Absolute ethanol, ethyl acetate, hydrochloric acid, methanol and trichloroacetic acid were purchased from Carlo Erba Reagents (Cornaredo, MI, Italy).

2.2. Cell culture

H9c2 cells (rat embryonic cardiomyocytes) were obtained from American Type Culture Collection (ATCC, Manassas, VA, USA) (Cat# CRL-1446_H9c2, RRID: CVCL_0286) and maintained in Dulbecco's Modified Eagle Medium/Nutrient Mixture F-12 (DMEM/F-12, Gibco, Thermo Fisher Scientific, Waltham, MA, USA) containing 10% fetal bovine serum (FBS, Gibco), supplemented with 1% penicillin/streptomycin (Thermo Fisher Scientific), and incubated at 37 ∘C in humidified atmosphere with 5% CO2 [21]. When the cells reached a density of 80% in 100-mm dishes, they were digested using 0.25% Trypsin-EDTA (1X)

(Gibco) according to a 1:2 ratio following manufacturer's instructions (ATCC). For each experiment, cells were seeded and incubated for 48 h at 37 °C, 95% O_2 and 5% CO_2.

2.2.1. Cell viability assay

H9c2 cell viability was evaluated by 3-(4,5-dimethylthiazol-)2,5- diphenyl tetrazonium bromide (MTT) assay, as previously described [21]. Cells were seeded at a density of 5×10^3 cells/well in 96-well plate and exposed to the following treatments: Control (vehicle), L-Ctl (from 1 to 100 nM), D-Ctl (from 1 to 100 nM), LPS (10 μg/mL) alone, LPS + L-Ctl (from 1 to 100 nM), LPS + D-Ctl (from 1 to 100 nM), LPS+ scrambled LCtl (from 1 to 100 nM) and scrambled L-Ctl (from 1 to 100 nM) for 6 h [22]. The control was treated with the vehicle (UltraPure RNase/DNasefree distilled water). At the end of the treatments, the cell culture medium was replaced with 100 μl of 2 mg/ml MTT solution (Sigma Aldrich) and cells were incubated for 4 h at 37 ∘C, 5% CO2. After incubation, the solution was removed and the formazan crystals were solubilized by adding 100 μl of DMSO for 30 min. The absorbance was measured using a Multiskan EX Microplate Reader Lab (Thermo Fisher Scientific) at 570 nm. The means of absorbance values of six wells in each experimental group were expressed as the percentage of cell viability. The experiment was repeated three independent times. Cell viability was reported as percentage of cells survival relative to control cells.

2.2.2. Biochemical analyses of H9c2 cells

2.2.2.1. Lactate dehydrogenase (LDH) activity determination.

The structural integrity of cultured H9c2 cardiomyocytes was evaluated by determining the level of LDH released in the culture supernatant. To this aim, cells were seeded in a 24-well plate at a density of 1×10^5 cell/ml and treated with vehicle (control), LPS (10 μg/mL), LPS + *L*-Ctl (1 nM) and *L*-Ctl (1 nM) alone for 24 h. 100 μl of the culture supernatant per well was used for LDH activity determination. The enzyme activity was evaluated spectrophotometrically (GENESYS 20 spectrophotometer, Thermo Fisher Scientific), following the method of McQueen (1972) [23]. After incubation of reagents, absorbance at 340 nm was recorded every min until steady-state was reached. The reaction velocity was determined by a decrease in absorbance at 340 nm, resulting from the oxidation of NADH indicative of LDH activity, that was expressed in IU/ L [24].

2.2.2.2. Evaluation of malondialdehyde (MDA) concentration.

The concentration of MDA (as an indicator of lipid peroxidation following ROS generation) in H9c2 cell lysates was determined by thiobarbituric acid reactive substances (TBARS) assay, as previously described [25–27]. Cells were seeded in a 24-well plate at a density of 1×10^5 cell/ml and treated as described above for 6 h. Subsequently, cells were washed with cold phosphate buffered saline (PBS), centrifuged at 300g for 10 min and the supernatant was removed. The precipitate obtained was resuspended in 1 mL of a cold sodium phosphate buffer 10 mM (containing 1 mM ethylenediaminetetraacetic acid and 1 mM butylated hydroxyanisole in 0.15% ethanol), pH = 7.2 and crushed by ultrasonic wave. MDA concentration was estimated spectrophotometrically (GENESYS 20 spectrophotometer, Thermo Fisher Scientific). The absorbance differences A (535–600 nm) was converted to MDA equivalents using the extinction coefficient for MDA 1.55×10^5 M^{-1} cm^{-1}. Lipid peroxidation was expressed in mM MDA.

2.2.2.3. Estimation of protein carbonyl content.

The assessment of the protein carbonyl content (as an indicator of protein damage following oxidative stress) was evaluated in H9c2 cells by 2,4 dinitrophenylhydrazine (DNPH) assay, following the method of Reznick and Packer (1994) [28] and as previously described [26,27]. Cells were seeded in a 24-well plate at a density of 1×10^5 cell/ml and treated as described above for 6 h. Subsequently, they were washed with cold PBS, centrifuged at 300g for 10 min and the supernatant was removed. The precipitate obtained was resuspended in 1 mL of a cold phosphate buffer 50 mM, pH 6.7, containing 1 mM ethylenediaminetetraacetic acid and crushed by ultrasonic wave. The protein carbonyl content (expressed in μM) was evaluated spectrophotometrically (GENESYS 20 spectrophotometer, Thermo Fisher Scientific) by absorbance detected at 375 nm, using the extinction coefficient for DNPH (22 mM^{-1} cm^{-1}).

2.2.2.4. Superoxide dismutase (SOD) enzyme activity assay.

SOD activity was determined by measuring the inhibition of pyrogallol autoxidation following the method of Marklund S. and Marklund G. (1974) [29] and as previously described [30]. Cells were seeded in a 24-well plate at a density of 1×10^5 cell/ml and treated as described above for 6 h. Subsequently, the cells were washed with cold PBS, centrifuged at $300 \times g$ for 10 min and the supernatant was removed. The precipitate obtained was resuspended in Tris buffer 50 mM, pH 8.2, containing 100 mM ethylenediaminetetraacetic acid and the reaction was initiated by adding 8 mM pyrogallol (prepared in 1 mM HCl). The SOD activity in the cell extract was measured by monitoring the autoxidation of pyrogallol for 5 min at room temperature using a GENESYS 20 spectrophotometer (Thermo Fisher Scientific) at 420 nm. SOD activity was assessed as the degree of inhibition of the pyrogallol autoxidation rate.

2.2.3. Western blot

At the end of treatments with vehicle (control), LPS (10 μg/mL), LPS + L-Ctl (1 nM) and L-Ctl (1 nM) alone, H9c2 cardiomyocytes were washed with DPBS (Gibco) and the proteins were extracted using RIPA lysis buffer (Sigma Aldrich) suitably supplemented with a mixture of protease inhibitors [(aprotinin 20 μg/mL, phenylmethylsulfonyl fluoride 1%, sodium orthovanadate 2 μM (Sigma-Aldrich)]. Cells were scraped and transferred in microcentrifuge tubes, incubated on ice for 30 min with intermittent mixing, and then centrifugated at 12,000g for 15 min at 4 ∘C. The supernatant was collected for protein concentration determination by Bradford reagent using bovine serum albumin (BSA) as a standard. Equal amounts of protein (30 μg) were loaded on 10% SDS-PAGE gel [for toll like receptor 4 (TLR4), phospho-extracellularsignal- regulated kinase 1/2 (p-ERK1/2), ERK1/2, phospho-c-Jun Nterminal kinase 1/2 (p-JNK1/2), JNK1/2, p-p38 mitogen-activated protein kinase (p-p38 MAPK), nuclear factor kappa-light-chainenhancer of activated B cells (NFkB) p52, p-NFkB p65, NFkB p65 and cyclooxygenase-2 (COX2)], exposed to electrophoresis, and transferred to polyvinyl difluoride membranes (GE Healthcare, Chicago, USA). Membranes were blocked in 5% non-fat dried milk at room temperature for 1 h, and then incubated overnight at 4 ∘C with primary antibodies specific for the above antigens diluted 1:1000 (for TLR4, p-ERK1/2 and ERK1/2) or 1:500 (for p-JNK1/2, JNK1/2, p-NFkB p65, NFkB p65, NFkB p52 and COX2) in tris-buffered saline containing 0.2% Tween 20 (TBST) and 5% BSA.

Antibodies against β-actin, ERK1/2, JNK1/2, p38-MAPK and NFkB p65 were used as internal controls. Following incubation with primary antibodies, all membranes were washed three times with TBST for 5 min and then incubated with secondary antibodies at room temperature for 2 h (anti-mouse and anti-rabbit peroxidase-linked, Santa Cruz Biotechnology, California, USA), diluted 1:2000 in TBST containing 5% non-fat dried milk. Immunodetection was carried out using the enhance chemiluminescence kit (GE Healthcare). Membranes were exposed to Xray films (Hyperfilm ECL, Amersham), the densitometric analyses of the bands areas and the pixel intensity were performed and the background was subtracted. The analyses were carried out using ImageJ 1.6 (National Institutes of Health, Bethesda, Maryland) as previously described [31,32].

2.2.4. Molecular docking

The molecular docking engine Autodock Vina [33] was used to simulate the binding of L-Ctl to the myeloid differentiation protein 2 (MD-2), the partner protein of TLR4. The structure of MD-2 was extracted from the entry 4G8A of the Protein Data Bank [34], which reports the crystallographic conformation of the complex with human TLR4 (polymorphic variant D299G and T399I) and with several ligand species in the binding site. All these molecules, including crystallographic waters, were not considered in the docking. Human Ctl (sequence SSMRLSFRARGYGFR, L-enantiomeric form) was built in extended conformation by using UCSF Chimera [35].

Since the conformational space of Ctl is too large to be explored in a single simulation run, the search was performed in a simplified way, in analogy with a protocol already described for simulating the docking of peptides [36,37]. Full flexibility was guaranteed to seven consecutive residues [38], and the internal degrees of freedom of the other eight were inhibited. The flexible region was then systematically varied along the peptide sequence, from the N to the C terminus (SSMRLSF, SMRLSFR, …, ARGYGFR), for a total of nine distinct simulations. The search was performed in a volume (40 Å × 40 Å × 40 Å) larger than the binding site of MD-2, and with exhaustiveness much greater (8–32 times larger) than the default value [39,40].

2.2.5. Quantitative Reverse-Transcription Real-Time PCR (qRT-PCR)

H9c2 cells were grown in 6-well plate to 70–80% confluence and then treated with vehicle (control), LPS (10 μg/mL), LPS + L-Ctl (1 nM) and L-Ctl (1 nM) alone. Total RNA from cells was isolated using TRIzol reagent (Invitrogen, Life Technologies, Carlsbad, CA, USA) according to the manufacturer's protocol. The purity and integrity of RNA were confirmed by spectrophotometric analysis.

1 μg of total RNA was reverse transcribed to provide complementary DNA (cDNA) using High-Capacity cDNA Reverse Transcription Kit (Applied Biosystems™, Thermo Fisher Scientific). The cDNA was amplified by qRT-PCR using SYBR™ Select Master Mix (Thermo Fisher Scientific) according to the manufacturer's instructions on Applied Biosystems™ QuantStudio™ 5 Real-Time PCR System apparatus (Thermo Fisher Scientific). Samples were analyzed in triplicate (n = 3 independent experiments) and the relative mRNA expression levels of the different genes were normalized to rRNA18S and calculated on the basis of the $2^{-\Delta\Delta}$ Ct method [41,42].

Primers used for the amplification were: forward 5′-CCCAGGACATGCTAGGGAGCC-3′ and reverse 5′-AGGCAGGGAGGGAAACACACG-3′ (IL-1β); forward 5′-GGAGTTCCGTTTCTACCTGG-3′ and reverse 5′ - GGTCCTTAGCCACTCCTTCTGT-3′ (IL-6); forward 5′-CACCACGCTCTTCTGTCTACTG-3′ and reverse 5′-

GCTACGGGCTTGTCACTCG-3′ (TNF-α); forward 5′-AGCCCTCACCTACTTCCTGG-3′ and reverse 5′-CTCTGCCTGTGCGTCTCTTC-3′ (NOS2); forward 5′-GCAATTATTCCCCATGAACG-3′ and reverse 5′-GGCCTCACTAAACCATCCAA-3′ (18S).

2.2.6. Statistical analysis

Data, expressed as mean ± SEM, were analysed by one-way ANOVA and the non-parametric Newman-Keuls Multiple Comparison Test (for post-ANOVA comparisons) and one-way ANOVA followed by Dunnett's Multiple Comparison Test when appropriate. Values of $*p =<0.05$, $**p=<0.01$, $***p =<0.001$ were considered statistically significant. The statistical analysis was carried out using Graphpad Prism 5 (GraphPad Software, La Jolla, California, USA).

3. Results

3.1. Effect of L-Ctl and D-Ctl on cell proliferation in H9c2 cardiomyocytes

In order to evaluate the effects of catestatin-derived peptides, *L*-Ctl and *D*-Ctl, on cell viability, H9c2 cells were exposed to increasing concentrations of either peptides and MTT was performed. As shown in (Figure 1A), *L*-Ctl induced a significant increase in cell proliferation at each concentration tested (1–100 nM), while *D*-Ctl produced a significant increase in cardiac cell viability only at 5 nM, 10 nM and 100 nM (Figure 1B).
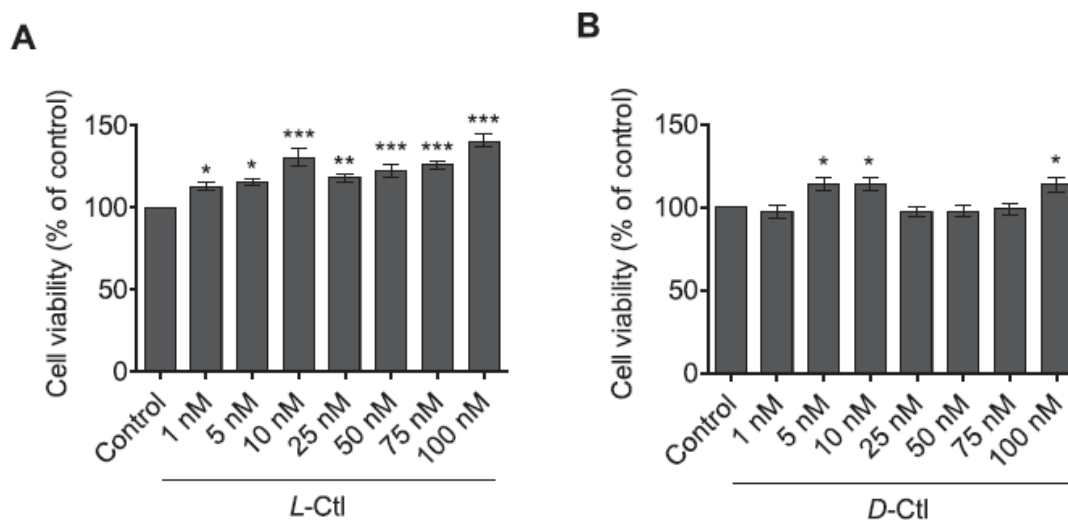

Figure 1. Effects of L-cateslytin (L-Ctl) and D-cateslytin (D-Ctl) on cell viability in H9c2 cardiomyocytes. H9c2 cardiomyocytes were treated with vehicle (Control) or increasing concentration of A) L-Ctl (1–100 nM) or B) D-Ctl (1–100 nM) for 6 h. Cell viability was determined using MTT assay and was expressed as the percentage of control cells only exposed to vehicle (indicated as Control). Results are represented as mean ± SEM (n = 6 per group). Significant differences were detected by one-way ANOVA followed by Dunnett's test, p < 0.05 (*); p < 0.01 (**) and p < 0.001 (***) vs Control group.

3.2. Action of L-Ctl and D-Ctl on LPS-induced damage in H9c2 cells

The action of L-Ctl or D-Ctl on LPS-induced injury in H9c2 cardiac cells was then investigated. To this aim, cells were treated with LPS alone or in combination with increasing concentrations of L-Ctl or D-Ctl, and cell viability was evaluated (Figure 2). MTT revealed that the treatment with LPS was able to significantly reduce cardiomyocytes viability; however, the cytotoxic effect exerted by LPS was reversed by both L-Ctl (Figure 2A) and D-Ctl (Figure 2B). In particular, L-Ctl induced beneficial effects on LPS-dependent cytotoxicity starting from 1 nM, and its effect was significant at each concentration tested (up to 100 nM) (Figure 2A). In contrast, D-Ctl reduced H9c2 mortality when co-administered with LPS, only at the concentration range 10–100 nM (Figure 2B). Scrambled L-Ctl and D-Ctl were used as negative controls. Figure 3 indicates that scrambled L-Ctl was inactive, since no significant effects have been observed on viability of H9c2 cells at the concentrations range of 1–100 nM, in the absence (Figure 3A) or in the presence of LPS (Figure 3B). Comparable data were obtained with the scrambled D-Ctl (data not shown).
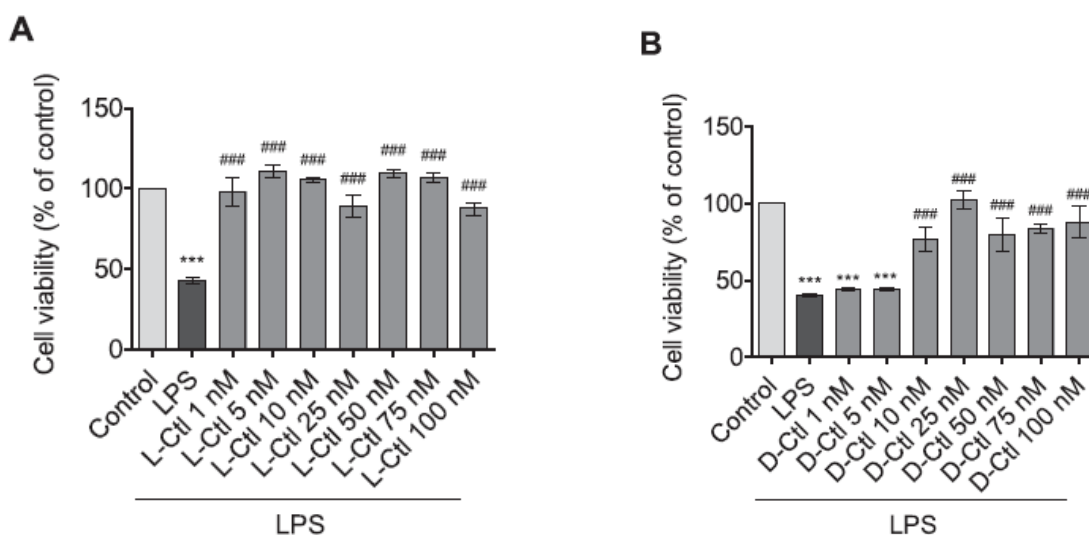

Figure 2. *Effects of L-Ctl and D-Ctl in the presence of lipopolysaccharide (LPS) on H9c2 cardiomyocytes viability. H9c2 cardiomyocytes were treated with vehicle (Control) or LPS (10 µg/mL) alone and in co-treatment with increasing concentration of A) L-Ctl (1–100 nM) or B) D-Ctl (1–100 nM) for 6 h. Cell viability was determined using MTT assay and was expressed as the percentage of control cells only exposed to vehicle (indicated as Control). Results are represented as mean ± SEM (n = 6 per group). Significant differences were detected by one-way ANOVA and Newman-Keuls multiple comparison test. P < 0.001 (***) vs Control group; p < 0.001 (###) vs LPS group.*
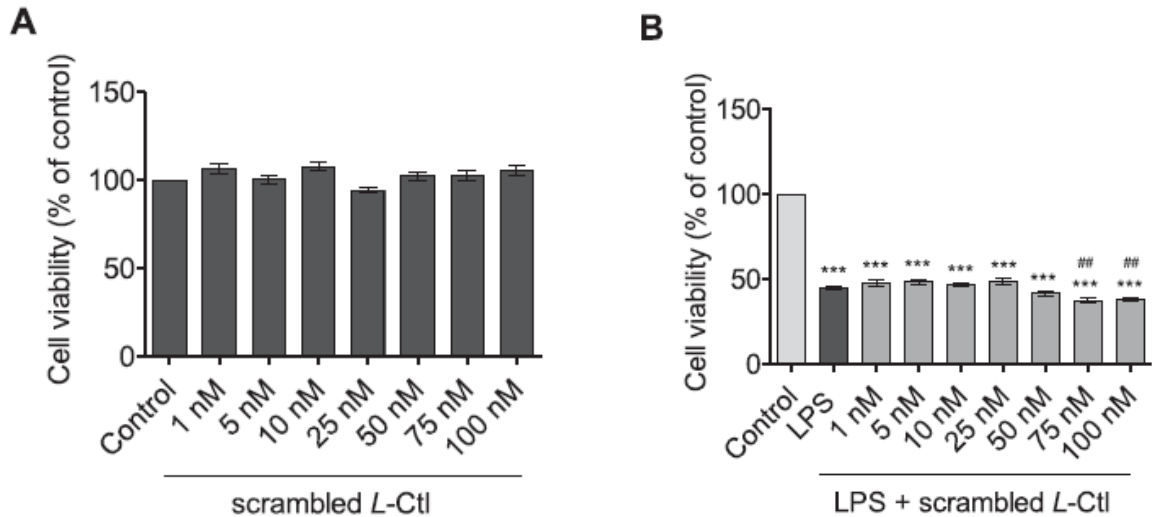
Figure 3. *Effect of scrambled L-Ctl in the absence or in the presence of LPS on H9c2 cardiomyocytes viability. H9c2 cardiomyocytes were treated with vehicle (Control) or increasing concentration of scrambled L-Ctl (1–100 nM) for 6 h A) Cell viability was determined using MTT assay and was expressed as the percentage of control cells only exposed to vehicle (indicated as Control). Results are represented as mean ± SEM (n = 6 per group). Statistical analysis was carried out by one-way ANOVA followed by Dunnett's test. H9c2 cardiomyocytes were treated with vehicle (Control) or LPS (10 µg/mL) alone and in co-treatment with increasing concentration of scrambled L-Ctl (1–100 nM) for 6 h B) Significant differences were detected by one-way ANOVA and Newman-Keuls multiple comparison test. p < 0.001 (***) vs Control group; p < 0.01 (##) vs LPS group.*

3.3. Influence of L-Ctl on TLR4 expression in LPS-stimulated H9c2

Among the two Ctl enantiomers, L-Ctl resulted to be more active (1 nM, that is referred to the first effective concentration) compared to DCtl (10 nM, that is referred to the first effective concentration) in the presence of LPS. Therefore, the cardiac molecular mechanism of L-Ctl was investigated. Western blot and densitometric analyses of cell extracts showed that TLR4 expression was significantly increased in LPStreated cells with respect to the control group, whereas in the LPS + L-Ctl group the protein expression was reduced (Figure 4).
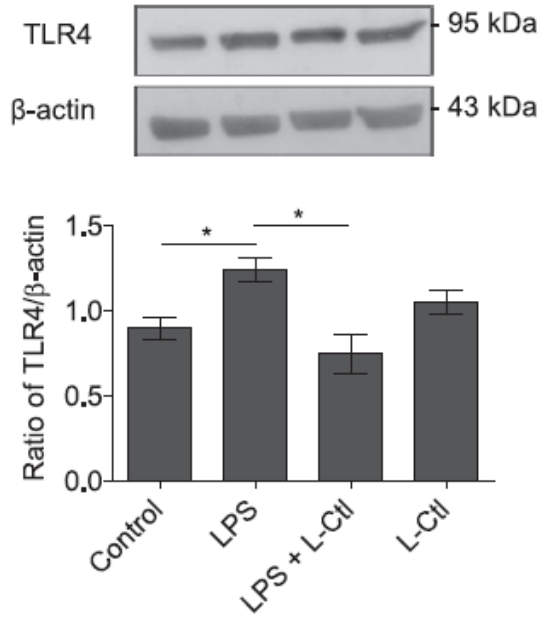
Figure 4. Influence of L-Ctl on toll like receptor 4 (TLR4) expression in H9c2 cardiomyocytes stimulated with LPS. Western blot analysis of TLR4 in H9c2 cardiomyocytes exposed to vehicle (indicated as Control), LPS (10 µg/mL), LPS + L-Ctl (1 nM) (n = 3 independent experiments) [mouse monoclonal antibody against TLR4 (Cat# sc-293072, RRID: AB_10611320) and β-actin (Cat# sc- 69879, RRID: AB_1119529) Santa Cruz Biotechnology (Dallas, Texas, USA)]. Histograms represent the ratio of densitometric analysis of protein: loading control. Significant differences were detected by one-way ANOVA and Newman-Keuls multiple comparison test. p < 0.05 (*).

3.4. Molecular docking

Molecular docking was used to investigate whether the presence of LCtl can affect TLR4. Bacterial lipopolysaccharide and its precursor lipid A, as well as peptidomimetics with no structural similarity to the physiological ligands of TLR4, do not bind this protein directly but anchor in the relatively large binding site of its co-receptor MD-2 [34,43]. The conformation of MD-2 is similar in all these complex, and they only differ by the molecular contacts formed with the various ligands. Thus, we performed the molecular docking of L-Ctl to a monomer of MD-2 extracted from a complex with human TLR4 [34], and isolated from any other molecular species.

Ctl possesses 15 amino acid residues and 64 rotatable dihedral angles, which is a number far too large to be exhaustively explored in a single molecular docking run. Therefore, the conformational space of the peptide was explored in a simplified way, by allowing rotations in the main and side chains of seven consecutive residues while the other eight residues were considered rigid, and systematically varying such flexible region along the whole peptide sequence.

The results indicated that the central region of L-Ctl (sequence fragment LSFRARG) has the most favorable affinity for MD-2, with a predicted binding energy of -10 kcal/mol. In contrast, the two peptide endings showed a comparatively lower binding score, with -8 kcal/mol for the N-terminal region and - 8.5 kcal/mol for the C-terminal one. Due to the fact that the rigid portion of peptide structure was not optimized in the simulations, these values should be considered as an upper limit for the (negative) binding energy, and may reflect an

even more favorable binding. The overall findings suggest a high affinity of L-Ctl for MD-2, with a binding equilibrium constant in the nanomolar range. Figure 5 shows the structure or the most favorable docking pose of L-Ctl to MD-2 obtained in the simulations. The peptide is deeply inserted in the core of the protein binding site, and its position mostly overlaps with the location of the physiological ligands [34] in the original crystallographic complex.
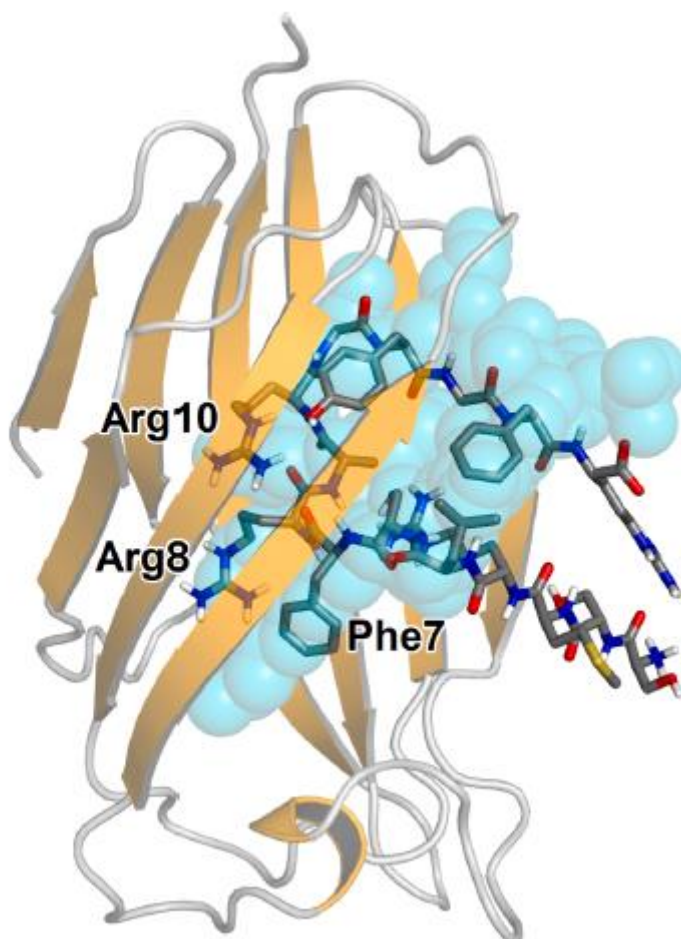

Figure 5. Binding of Ctl to myeloid differentiation factor 2 (MD-2). Most favorable structure of Ctl (stick representation, with colored atoms) bound in the binding site of MD-2 (yellow cartoon representation), superimposed to the volume occupied in the same pocket by physiological ligands (cyan spheres) in the crystallographic structure of the protein [34]. Image created with PyMol [69].

3.5. Involvement of inflammatory pathways in L-Ctl mechanism of action

Western blot and densitometric analyses were carried out to determine the expression levels of p-ERK1/2 (Figure 6A), p-JNK1/2 (Figure 6B), pp38 MAPK (Figure 6C), NFkB p65 (Figure 6D), NFkB p52 (Figure 6E) and COX2 (Figure 6F) in H9c2 cells treated with LPS in the presence or absence of LCtl. The expression of all the above proteins significantly increased following LPS treatment and significantly decreased in the cells treated with LPS + L-Ctl (Figure 6).
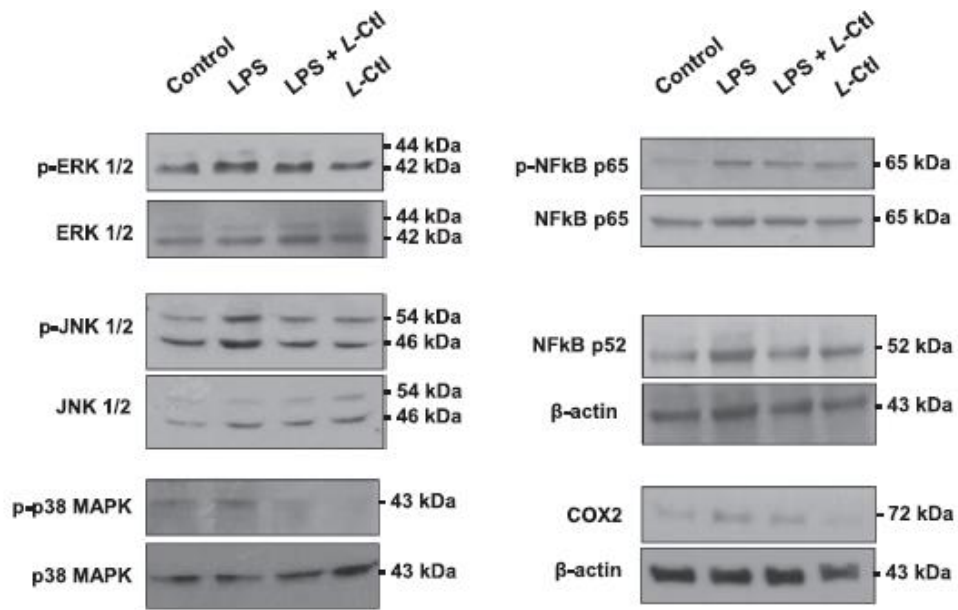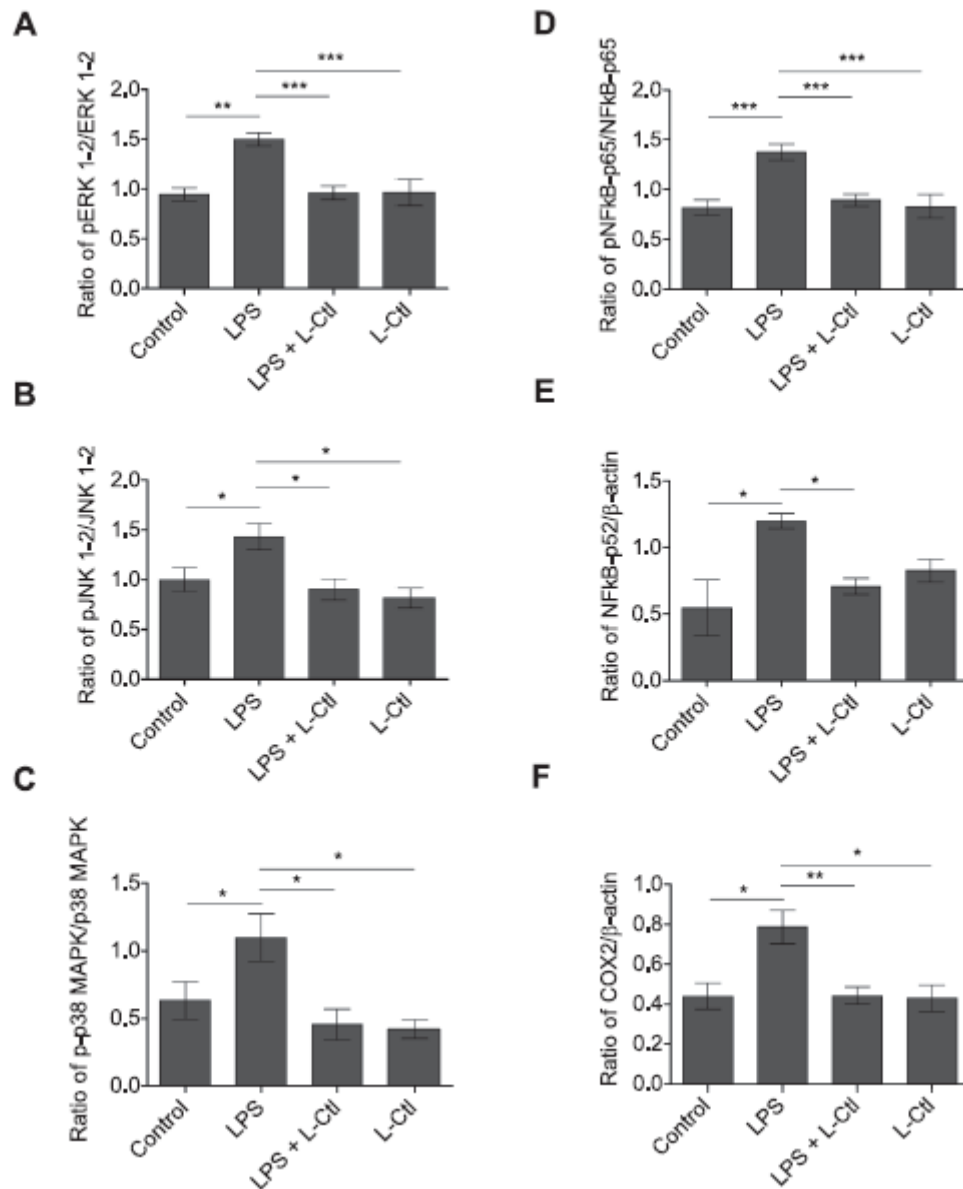
Figure 6. *Molecular mechanism activated by L-Ctl in H9c2 cardiomyocytes. Western blot analysis of A) phospho- extracellular-signal-regulated kinase 1/2 (p-ERK1/2), B) phospho-c-JunN-terminal kinase 1/2 (p-JNK1/2), C) phospho-p38 mitogen-activated protein kinase (p38 MAPK), D) nuclear factor kappa-lightchain- enhancer of activated B cells (NFkB) p65 (p-NFkB p65), E) NFkB p52 and F) cyclooxygenase-2 (COX2) in H9c2 cardiomyocytes exposed to vehicle (indicated as Control), LPS (10 μg/mL), LPS + L-Ctl (1 nM) and L-Ctl (1 nM) (n = 3 independent experiments) for 6 h [mouse monoclonal antibodies against p-ERK1/ 2 (Cat# sc-7383), ERK1/2 (Cat# sc-514302), NFkB p65 (Cat# sc-8008), NFkB p52 (Cat# sc-7386, RRID: AB_2267131) Santa Cruz Biotechnology (Dallas, Texas, USA), p-NFkB p65 (#13346), Cell Signaling Technology, Inc, (Danvers, Massachusetts, USA), or rabbit polyclonal antibodies against p-SAPK/JNK (#9251), SAPK/JNK (#9252), p-p38 MAPK (#9211) or p38 MAPK (#9218), Cell Signaling Technology, or COX2 (Cat# TA313292), OriGene Technologies (Rockville, Maryland, USA)]. Histograms represent the ratio of densitometric analysis of protein: loading control. Significant differences were detected by one-way ANOVA and Newman-Keuls multiple comparison test. p < 0.05 (*); p < 0.01 (**); p < 0.001 (***).*

3.6. Effect of L-Ctl on mRNA expression levels of inflammatory mediators

L-Ctl molecular effect on the LPS-injured H9c2 cells was further investigated by assessing the mRNA expression levels of selective inflammatory mediators. qRT-PCR analysis of cell extracts revealed that the proinflammatory factors IL-1β (Fig. 7A), IL-6 (Figure 7B), TNF-α (Figure 7C) and NOS2 (Figure 7D) were significantly upregulated in LPSstimulated H9c2 cells compared to the control group. On the contrary, the mRNA expression levels of the above markers were significantly reduced in LPS + L-Ctl experimental group (See Figure 7).
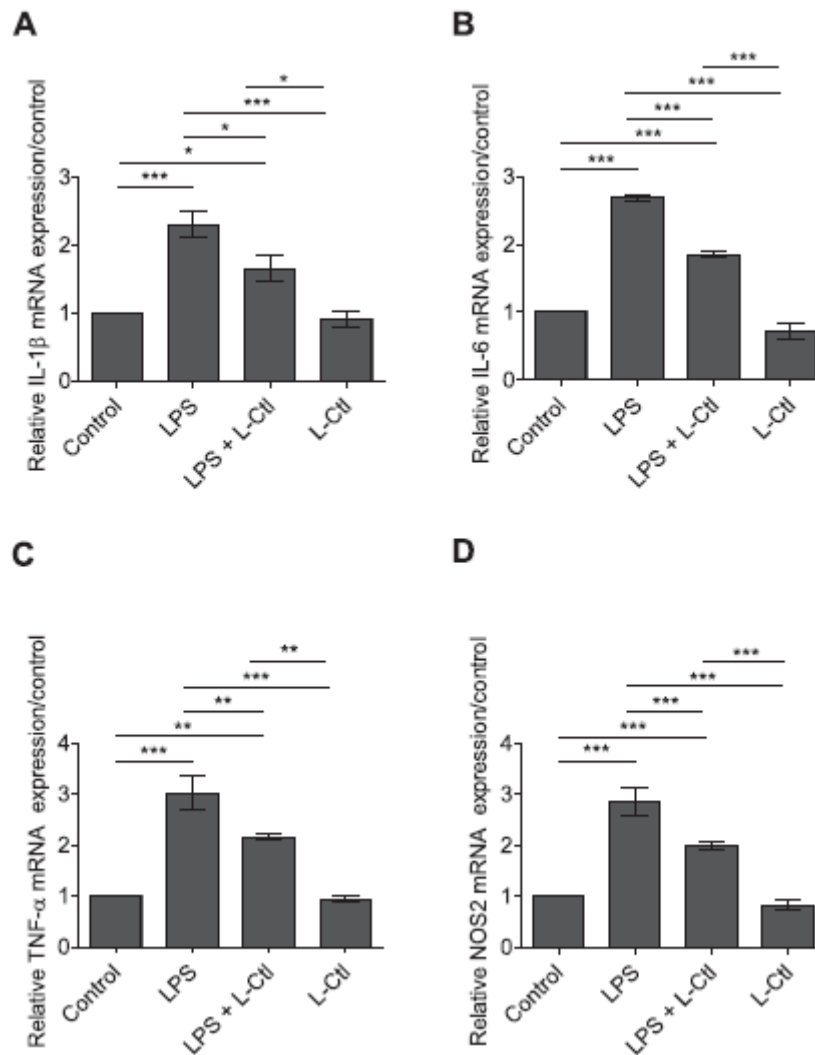

Figure 7. *Effects of L-Ctl on the LPS-induced mRNA expression of inflammatory mediators in H9c2 cells. Evaluation of mRNA expression levels of A) interleukin (IL)-1β, B) IL-6, C) tumor necrosis factor (TNF)-α, and D) nitric oxide synthase (NOS) 2 (inducible) by quantitative reverse-transcription real-time PCR (qRT-PCR) in H9c2 cardiomyocytes exposed to vehicle (indicated as Control), LPS (10 μg/mL), LPS + L-Ctl (1 nM) and L-Ctl (1 nM) for 6 h. Samples were analyzed in triplicate, the relative mRNA expression levels of the different genes were normalized to rRNA18S and calculated on the basis of the $2^{-\Delta\Delta Ct}$ method. Data are expressed as the mean ± SEM of 3 separate experiments. Significant differences were detected by one-way ANOVA and Newman-Keuls multiple comparison test. $p < 0.05$ (*); $p < 0.01$ (**); $p < 0.001$ (***).*

3.7. Effect of L-Ctl on oxidative stress-related markers, SOD activity and LDH release in H9c2 exposed to LPS

To determine whether *L*-Ctl could affect the cellular oxidative balance under LPS treatment, oxidative stress-related markers and the activity of the antioxidant enzyme SOD were measured. The MDA production and the content of protein carbonyl groups, used as lipid peroxidation and protein damage markers, respectively, were assayed in H9c2 cell lysates. Figure 8 shows that protein carbonyl groups content (Figure 8A) and MDA concentration (Figure 8B) were significantly increased in LPS group compared to the control, while they were significantly decreased in the LPS + *L*-Ctl co-treatment. On the contrary, the percentage of pyrogallol autoxidation (i.e. index of SOD activity) was significantly decreased in LPS-exposed H9c2, and significantly increased in the LPS + *L*-Ctl group (Figure 8C). *L*-Ctl alone did not exert significant effects on the above parameters compared to the vehicle exposed cells (Figure 8A-C). As depicted in Figure 8D, LPS treatment also significantly increased LDH, whose release in the H9c2 culture medium is considered an indicator for cell membrane damage, whereas the co-treatment with *L*-Ctl reversed, to a significant extent, the enzyme concentration released in response to LPS. *L*-Ctl treatment alone did not induce significant effect in the LDH release compared to the control group (Figure. 8D).
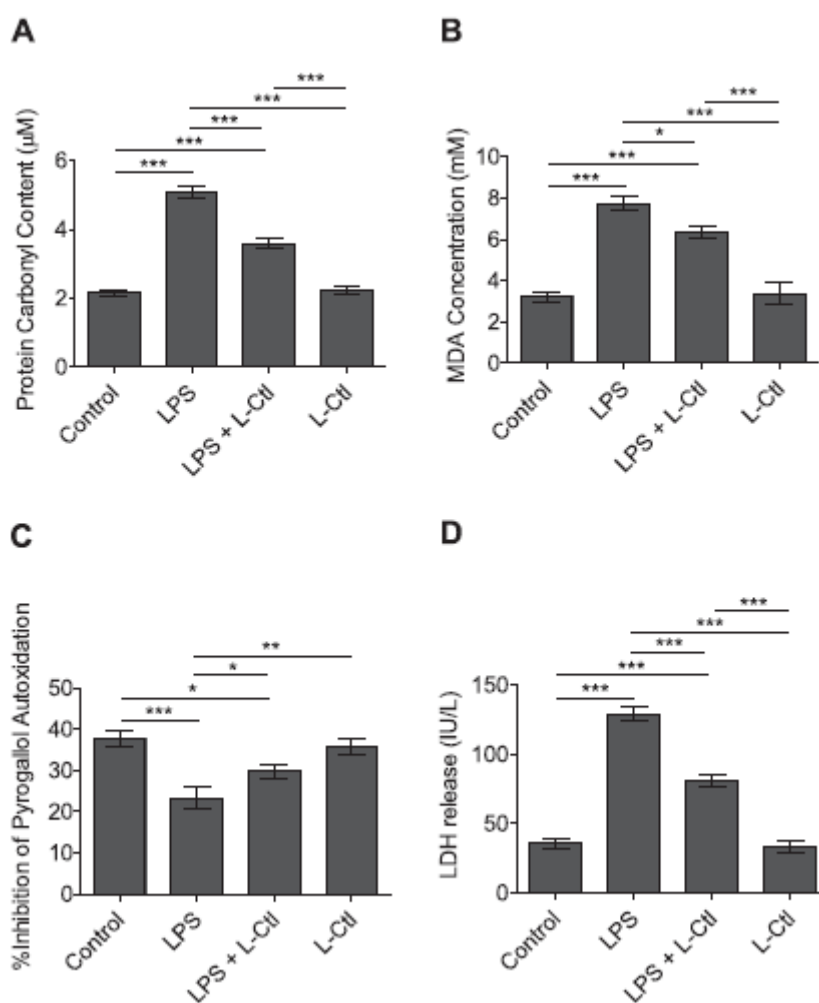

Figure 8. *Effect of L-Ctl on malondialdehyde (MDA) levels, protein carbonyl groups content, superoxide dismutase (SOD) activity and lactate dehydrogenase (LDH) release in LPS-treated*

87

H9c2 cells. MDA concentration A), protein carbonyl groups content B) and SOD activity C) in lysates of H9c2 cardiomyocytes treated with vehicle (Control), LPS (10 µg/mL), LPS + L-Ctl (1 nM) and L-Ctl (1 nM) for 6 h. MDA concentration was expressed as mmol/L, protein carbonyl groups content was expressed as µmol/L and SOD activity was expressed as percentage of inhibition of the pyrogallol autoxidation rate. Data are expressed as the mean ± SEM of six separate experiments. Significant differences were detected by one-way ANOVA and Newman-Keuls multiple comparison test. $p < 0.05$ (*); $p < 0.01$ (**); $p < 0.001$ (***). LDH release in the supernatant of H9c2 cardiomyocytes treated with vehicle (Control), LPS (10 µg/mL), LPS + L-Ctl (1 nM) and L-Ctl (1 nM) for 24 h D). The result of LDH activity was expressed as IU/L. Data are expressed as the mean ± SEM of six separate experiments. Significant differences were detected by one-way ANOVA and Newman-Keuls multiple comparison test. $p < 0.001$ (***).

4. Discussion

The present study aimed to investigate the protective effects of Ctl in LPS-stimulated H9c2 cardiomyocytes. For the first time, we demonstrated that both L-Ctl and D-Ctl significantly increase cell viability under LPS stimulation. Since the L-enantiomeric form of the peptide resulted more effective, it was used for the subsequent analyses of the underlying mechanism of action. Our simulation results suggested that Ctl may influence the biological activity of TLR4 through a direct binding to the partner protein MD-2. In addition, molecular analyses showed that L-Ctl mitigates the LPS-dependent oxidative stress, the reduction of SOD activity and the release of LDH in the cell medium. The peptide was also able to decrease the expression of inflammatory signaling molecules (IL-1β, IL-6, TNF-α, NOS2) and the activation of important inflammatory mediators (p-ERK 1/2, p-JNK, p-p38 MAPK, p- NFkB p65, p-NFkB p52, COX2). These data are of interest in the context of myocarditis and in the field of antimicrobial peptides (AMPs) in regard to their capability to counteract antibiotic resistance.

Antibiotic resistance, primarily due to the overuse of these drugs, has emerged as a severe worldwide health problem, as every year millions of people are affected by multi-drug resistant bacteria resulting in a high case-fatality ratio. For this reason, growing energies and efforts are invested in this field trying to reduce antibiotic prescription and to identify or design alternative drugs able to overcome resistance. Among the molecules currently considered as novel anti-infective agents [44], a prominent position is occupied by AMPs, major players in the innate defense, since they have a relatively low chance to establish resistance [45]. AMPs exist across all major lineages, they represent highly conserved forms of innate immunity and are active against numerous pathogens [46]. Their short amphipathic -cationic conformation seems to be a key component of their antimicrobial activity, since it promotes the disruption of microbial membranes [47]. In particular, mammalian AMPs are able to directly kill the microbe and activate rapidly the immune response [48].

Ctl, the shorter and active arginine rich N-terminus fragment of CgAderived Cst peptide, can be fully included among AMPs, being effective against many microbial strains [18–20]. In the present study we tested on an *in vitro* model of myocarditis, i.e. LPS-stimulated H9c2 cells [49], both the naturally occurring enantiomeric species L-Ctl and its derived epipeptide D-Ctl, where all L-amino acids have been replaced by D-amino acids. In this regard, it is known that LPS, expressed on the external membrane of Gram-negative bacteria, represents a powerful inducer of immunity responses through the modulation of toll-like receptors 4 (TLR4) [7]; for this reason, it is widely used to reproduce inflammatory diseases, such as myocarditis [50]. Myocarditis, or inflammatory cardiomyopathy, is an inflammatory condition of the myocardium that, if prolonged, leads to cardiac injury, cardiac dysfunction, cardiomyocytes death [49] and resistance of the infectious agents to therapies [51].

In our experimental model, both L-Ctl and D-Ctl were able to improve cell viability, alone or when administered together with LPS, while their scrambled L-Ctl and D-Ctl counterparts were unable to significantly affect cell viability. Indeed, according to previous data [52], LPS alone reduces cell viability and induces a significant release of LDH (an indicator of cytotoxicity) in the culture medium, indicating that the model of myocarditis has been successfully established. Of note, L-Ctl showed greater effectiveness with respect to the D-enantiomeric form in increasing cell viability and in relieving LPS effects at all the tested concentrations. D-Ctl was produced, starting from its natural peptide, to promote the stability of the peptide against bacterial proteases and, at variance with our results, it was much more effective against microbial strains and more resistant to proteolytic degradation than L-Ctl [18,20].

Nevertheless, our study did not include a microbiology approach but aimed to analyze an *in vitro* model of myocarditis and this may account for the different potency observed for D-Ctl and L-Ctl in these diverse experimental sets. Moreover, it is conceivable that, from a physiological point of view, H9c2 cells establish a more favorable interaction with the natural occurring L-Ctl, since molecular chirality is a key feature in molecular host–guest recognition [53]. Results have been further corroborated by the use of a scrambled peptide. Thus, we focused on the anti-bacterial/anti-inflammatory role of LCtl possibly mediated via the TLR4 pathway. It is well established that LPS activates TLR4 and its downstream cascade by the interaction with its essential accessory protein, namely MD-2 [54]. LPS binds the hydrophobic pocket of MD-2 through 5 of its acyl chains, allowing the engagement and the dimerization of TLR4 and the generation of the activated LPS-MD2-TLR4 complex [54]. The crucial role of MD-2 in TLR4 inflammatory responses has been supported by studies performed on MD-2 knockout mice, that showed hypo-responsiveness to LPS and higher rate of survival to endotoxic shock [55]. Confirming previous experimental evidences, in our model LPS induces an increase in TLR4 protein expression, generally regulated by transcriptional and posttranscriptional mechanisms [56]. This supports the important contribution of TLR4 to the relationship existing between inflammation and cardiovascular disorders. Since L-Ctl was able to mitigate the LPSdependent upregulation of TLR4, it is conceivable that a regulation of its expression at the MD-2 level may exist. Accordingly, the molecular docking analysis clearly supported the interaction between the peptide and MD-2, the TLR4 partner protein. Indeed, the results of our computational studies suggest a high affinity of L-Ctl for MD-2, with a predicted binding energy of at least -10 kcal/mol. The peptide deeply plunged into the protein binding site with residues Phe7, Arg8 and Arg10. It is likely that the energetic penalty due to the desolvation of the arginine side chains buried into the protein pocket was adequately compensated by electrostatic and entropic effects at the peptide termini, which are exposed and relatively free to fluctuate in the solvent, although such effects cannot be directly assessed by using molecular docking. A number of interactions stabilized the anchoring of the peptide into MD-2, including electrostatic attraction with the charged residue Glu92 of the protein, and hydrophobic interactions with several phenylalanine isoleucine residues. Thus, our simulation results strongly suggest the possibility that Ctl may influence the biological activity of TLR4 through a direct binding to the partner protein MD-2. Both the interaction energy and the predicted location of binding of Ctl are fully consistent with an anchoring in the protein pocket, similar to the one observed in the experiment for physiological ligands bound to MD-2. The interaction between Ctl and MD-2 could thus represent the mechanism used by the peptide to suppress LPS inflammation, since a competitive antagonism on this site can be postulated.

It is widely accepted that the activation of TLR4, such as under LPS stimulation, induces the downstream MAPKs cascade converging on NFkB, lastly able to promote the expression of pro-inflammatory actors, including IL-1β, IL-6, TNF-α, NOS$_2$ [57,58]. Of note, Ctl

downregulates the expression of these proteins corroborating its supposed anti-inflammatory action via TLR4 inhibition.

Moreover, it is known that NFkB importantly participates in immune responses [59] and its overactivation contributes to the long-term inflammation responsible for acute myocardial lesions [60]. Indeed, NFkB is a well established downstream player of LPS/TLR4, MAPKs and JNK activation [56,61,62], and a positive regulator of COX2 expression, a key enzyme of inflammatory pathways [63]. Accordingly, our results showed an increase of p-ERK 1/2, p-JNK, p-NFkB p65, p-NFkB p52, and inducible COX under LPS stimulation, reversed by the addition of L-Ctl to the medium. Therefore, it is plausible that L-Ctl, by reducing the LPS-induced NFkB expression, may also prevent the production and the release of proinflammatory cytokines in cardiac myocytes [64], as showed in our experimental set. This finding can be further supported by evidence indicating the ability of another CgA-derived peptide (chromofungin, CgA 47–66) to exert antiinflammatory effects by inhibiting the NFkB-mediated transcription [65]. Interestingly, in our LPS-stimulated model p38 MAPK is more phosphorylated, according to the increased expression of NFkB, conversely to what happens under Ctl treatment. Being NFkB a crucial target for MAP-kinases, such as p38 MAPK that is strongly involved in cardiac pathologies [66] and references therein], this result may be useful in the view of future frontiers in therapeutics.

Another important aspect regards the well established ROS production, and its resulting oxidative stress, detectable in septic myocardial inflammation [67,68]. According to these data, in our model LPS is a strong stimulus for oxidative stress as visible by the increase of MDA and of protein carbonylation (used as markers of lipid peroxidation and protein damage secondary to oxidative stress, respectively) and by the reduction of SOD activity. The amelioration of oxidative balance following L-Ctl treatment, further describes the peptide as a novel candidate in the treatment of septic cardiomyopathy. Moreover, in line with our results, LPS-induced oxidative stress may additionally contribute to the activation of NFkB that, in turn, may further impact the cardiomyocytes inflammation that is finally mitigated/abolished by Ctl.

5. Conclusions

Taken together our results describe Ctl as a potential anti-inflammatory/anti-microbial therapeutic agent, and its inhibition of TLR4 by targeting MD-2 could represent an effective tool to counteract sepsis and septic shock induced by Gram negative bacteria in addition to its interesting and protective antioxidant properties. These data are of interest considering that Ctl efficacy and resistance have been extensively demonstrated in several microbial strains. Moreover, being a short and linear peptide, stable in a wide range of pH and temperature, Ctl would be easily synthesized at a minimal cost making it an excellent candidate for future drug development.

References

[1] S.P. Caforio, E. Arbustini, C. Basso, J. Gimeno-Blanes, S.B. Felix, M. Fu, T. Heli¨o, S. Heymans, R. Jahns, K. Klingel, A. Linhart, B. Maisch, W. McKenna, J. Mogensen, Y.M. Pinto, A. Ristic, H.P. Schultheiss, H. Seggewiss, L. Tavazzi, G. Thiene, A. Yilmaz, P. Charron, P.M. Elliott, Current state of knowledge on aetiology, diagnosis, management, and therapy of myocarditis: a position statement of the European Society of Cardiology Working Group on Myocardial and Pericardial Diseases, Eur. Heart J. (2013) 2636–2648.

[2] V.O. Puntmann, M.L. Carerj, I. Wieters, M. Fahim, C. Arendt, J. Hoffmann, A. Shchendrygina, F. Escher, M. Vasa-Nicotera, A.M. Zeiher, M. Vehreschild, E, Nagel, 2020. Outcomes of Cardiovascular Magnetic Resonance Imaging in Patients Recently Recovered From Coronavirus Disease 2019 (COVID-19). JAMA Cardiol., e203557.

[3] F. Moccia, A. Gerbino, V. Lionetti, M. Miragoli, L.M. Munaron, P. Pagliaro, T. Pasqua, C. Penna, C. Rocca, M. Samaja, T. Angelone, COVID-19-associated cardiovascular morbidity in older adults: a position paper from the Italian Society of Cardiovascular Researches, Geroscience (2020) 1–29.

[4] A. Vieillard-Baron, V. Caille, C. Charron, G. Belliard, B. Page, F. Jardin, Actual incidence of global left ventricular hypokinesia in adult septic shock, Crit. Care Med. (2008) 1701–1706.

[5] M.W. Merx, C. Weber, Sepsis and the heart, Circulation (2007) 793–802, https:// doi.org/10.1161/CIRCULATIONAHA.106.678359.

[6] S. Frantz, L. Kobzik, Y.D. Kim, R. Fukazawa, R. Medzhitov, R.T. Lee, R.A. Kelly, Toll4 (TLR4) expression in cardiac myocytes in normal and failing myocardium, J. Clin. Invest. (1999) 271–280.

[7] Y. Yang, J. Lv, S. Jiang, Z. Ma, D. Wang, W. Hu, C. Deng, C. Fan, S. Di, Y. Sun, W. Yi, The emerging role of Toll-like receptor 4 in myocardial inflammation, Cell Death Dis. 7 (5) (2016), e2234.

[8] R.N. Naylor, R. Atun, N. Zhu, K. Kulasabanathan, S. Silva, A. Chatterjee, G. M. Knight, J.V. Robotham, Estimating the burden of antimicrobial resistance: a systematic literature review, Antimicrob. Resist. Infect. Control. 7 (2018) 58.

[9] M. Mateescu, S. Baixe, T. Garnier, L. Jierry, V. Ball, Y. Haikel, M.H. Metz-Boutigue, M. Nardin, P. Schaaf, O. Etienne, P. Lavalle, Antibacterial peptide- based gel for prevention of medical implanted-device infection, PLoS ONE 10 (12) (2015), e0145143.

[10] D. Zhang, P. Shooshtarizadeh, B.J. Laventie, D.A. Colin, J.F. Chich, J. Vidic, J. de Barry, S. Chasserot-Golaz, F. Delalande, A. Van Dorsselaer, F. Schneider, K. Helle, D. Aunis, G. Pr´evost, M.H. Metz-Boutigue, Two chromogranin A-derived peptides induce calcium entry in human neutrophils by calmodulin-regulated calcium independent phospholipase A2, PLoS ONE 4 (2) (2009), e4501.

[11] E. Glattard, T. Angelone, J.M. Strub, A. Corti, D. Aunis, B. Tota, M.H. Metz- Boutigue, Y. Goumon, Characterization of natural vasostatin-containing peptides in rat heart, FEBS J. (2006) 3311–3321.

[12] K.B. Helle, M.H. Metz-Boutigue, M.C. Cerra, T. Angelone, Chromogranins: from discovery to current times, Pflugers Arch (2018) 143–154.

[13] T. Pasqua, C. Rocca, A. Spena, T. Angelone, M.C. Cerra, Modulation of the coronary tone in the expanding scenario of Chromogranin-A and its derived peptides, Future Med. Chem. 11 (12) (2019) 1501–1511.

[14] T. Pasqua, A. Corti, S. Gentile, L. Pochini, M. Bianco, M.H. Metz-Boutigue, M. C. Cerra, B. Tota, T. Angelone, Full-length human chromogranin-A cardioactivity: myocardial, coronary, and stimulus-induced processing evidence in normotensive and hypertensive male rat hearts, Endocrinology 154 (9) (2013) 3353–3365.

[15] J. Troger, M. Theurl, R. Kirchmair, T. Pasqua, B. Tota, T. Angelone, M.C. Cerra, Y. Nowosielski, R. Mˇatzler, J. Troger, J.R. Gayen, V. Trudeau, A. Corti, K.B. Helle, Granin-derived peptides, Prog Neurobiol. 154 (2017) 37–61.

[16] L. Taupenot, S.K. Mahata, M. Mahata, R.J. Parmer, D.T. O'Connor, Interaction of the catecholamine release-inhibitory peptide catestatin (human chromogranin A (352–372)) with the chromaffin cell surface and Torpedo electroplax: implications for nicotinic cholinergic antagonism, Regul. Pept. (2000) 9–17.

[17] E.M. Muntjewerff, G. Dunkel, M.J.T. Nicolasen, S.K. Mahata, G. van den Bogaart, Catestatin as a target for treatment of inflammatory diseases, Front. Immunol. 9 (2018) 2199.

[18] P. Dartevelle, C. Ehlinger, A. Zaet, C. Boehler, M. Rabineau, B. Westermann, J. M. Strub, S. Cianferani, Y. Haïkel, M.H. Metz-Boutigue, C. Marban, D-Cateslytin: a new antifungal agent for the treatment of oral Candida albicans associated infections, Sci. Rep. 18 (2018) 9235.

[19] R. Aslam, M. Atindehou, T. Lavaux, Y. Haïkel, F. Schneider, M.H. Metz-Boutigue, Chromogranin A-derived peptides are involved in innate immunity, Curr. Med. Chem. (2012) 4115–4123.

[20] A. Zaet, P. Dartevelle, F. Daouad, C. Ehlinger, F. Quil`es, G. Francius, C. Boehler, C. Bergthold, B. Frisch, G. Pr´evost, P. Lavalle, F. Schneider, Y. Haïkel, M.H. Metz- Boutigue, C. Marban, D-Cateslytin, a new antimicrobial peptide with therapeutic potential, Sci. Rep. 15199 (2017).

[21] C. Rocca, S. Femmin`o, G. Aquila, M.C. Granieri, E.M. De Francesco, T. Pasqua, D. C. Rigiracciolo, F. Fortini, M.C. Cerra, M. Maggiolini, P. Pagliaro, P. Rizzo, T. Angelone, C. Penna, Notch1 mediates preconditioning protection induced by GPER in normotensive and hypertensive female rat hearts, Front. Physiol. (2018) 9–521.

[22] Y. Zheng, S. Li, R. Hu, F. Cheng, L. Zhang, GFI-1 protects against lipopolysaccharide-induced inflammatory responses and apoptosis by inhibition of the NF-κB/TNF-α pathway in H9c2 cells, Inflammation (2020) 74–84.

[23] M.J. McQueen, Optimal assay of LDH and α-HBD at 37 ◦C, Ann. Clin. Biochem. 9 (1972) 2.

[24] C. Rocca, F. Scavello, B. Colombo, A.M. Gasparri, A. Dallatomasina, M.C. Granieri, D. Amelio, T. Pasqua, M.C. Cerra, B. Tota, A. Corti, T. Angelone, Physiological levels of chromogranin A prevent doxorubicin-induced cardiotoxicity without impairing its anticancer activity, FASEB J. (2019) 7734–7747.

[25] S.F. Assimakopoulos, C.E. Vagianos, G. Zervoudakis, K.S. Filos, C. Georgiou, V. Nikolopoulou, C.D. Scopa, Gut regulatory peptides bombesin and neurotensin reduce hepatic oxidative stress and histological alterations in bile duct ligated rats, Regul. Pept. (2004) 185–193.

[26] M.R. Preetha Rani, N. Anupama, M. Sreelekshmi, K.G. Raghu, Chlorogenic acid attenuates glucotoxicity in H9c2 cells via inhibition of glycation and PKC α upregulation and safeguarding innate antioxidant status, Biomed. Pharmacother. (2018) 467–4777.

[27] T. Pasqua, C. Rocca, F.R. Lupi, N. Baldino, D. Amelio, O.I. Parisi, M.C. Granieri, A. De Bartolo, A. Lauria, M. Dattilo, I.D. Perrotta, F. Puoci, M.C. Cerra, D. Gabriele, T. Angelone, Cardiac and metabolic impact of functional foods with antioxidant properties based on whey derived proteins enriched with hemp seed oil, Antioxidants 9 (11) (2020) 1066.

[28] A.Z. Reznick, L. Packer, Oxidative damage to proteins: spectrophotometric method for carbonyl assay, Methods Enzymol. (1994) 357–363.

[29] S. Marklund, G. Marklund, Involvement of the superoxide anion radical in the autoxidation of pyrogallol and a convenient assay for superoxide dismutase, Eur. J. Biochem. (1974) 469–474.

[30] A. Thakur, J. Alam, M.R. Ajayakumar, S. Ghaskadbi, M. Sharma, S.K. Goswami, Norepinephrine-induced apoptotic and hypertrophic responses in H9c2 cardiac myoblasts are characterized by different repertoire of reactive oxygen species generation, Redox Biol. (2015) 243–252.

[31] C. Rocca, L. Boukhzar, M.C. Granieri, I. Alsharif, R. Mazza, B. Lefranc, B. Tota, J. Leprince, M.C. Cerra, Y. Anouar, T. Angelone, A selenoprotein T-derived peptide protects the heart against ischaemia/reperfusion injury through inhibition of apoptosis and oxidative stress, Acta Physiol. 223 (4) (2018), e13067.

[32] C. Rocca, F. Scavello, M.C. Granieri, T. Pasqua, N. Amodio, S. Imbrogno, A. Gattuso, R. Mazza, M.C. Cerra, T. Angelone, Phoenixin-14: detection and novel physiological implications in cardiac modulation and cardioprotection, Cell. Mol. Life Sci. (2018) 743–756.

[33] O. Trott, A.J. Olson, AutoDock Vina: improving the speed and accuracy of docking with a new scoring function, efficient optimization, and multithreading, J. Comput. Chem. (2010) 455–461.

[34] U. Ohto, N. Yamakawa, S. Akashi-Takamura, K. Miyake, T. Shimizu, Structural analyses of human Toll-like receptor 4 polymorphisms D299G and T399I, J. Biol. Chem. (2012) 40611–40617.

[35] E.F. Pettersen, T.D. Goddard, C.C. Huang, G.S. Couch, D.M. Greenblatt, E.C. Meng, T.E. Ferrin, UCSF Chimera – a visualization system for exploratory research and analysis, J. Comput. Chem. (2004) 1605–1612.

[36] P. Santofimia-Casta~no, B. Rizzuti, ´A.L. Pey, P. Soubeyran, M. Vidal, R. Urrutia, J. L. Iovanna, J.L. Neira, Intrinsically disordered chromatin protein NUPR1 binds to the C-terminal region of Polycomb RING1B, PNAS (2017) 6332–6341.

[37] R. Lappano, C. Mallet, B. Rizzuti, F. Grande, G.R. Galli, C. Byrne, I. Broutin, L. Boudieu, A. Eschalier, Y. Jacquot, M. Maggiolini, The peptide ERα17p Is a GPER inverse agonist that exerts antiproliferative effects in breast cancer cells, Cells 590 (2019.

[38] M. Sugawara, J.M. Resende, C. Mendonca de Moraes, J.F. Chich, A. Marquette, M. H. Metz-Boutigue, B. Bechinger, Membrane structure and interactions of human Catestatin by multidimensional solution and solid-state NMR spectroscopy, FASEB J. (2010) 1737–1746.

[39] F. Grande, B. Rizzuti, M.A. Occhiuzzi, G. Ioele, T. Casacchia, F. Gelmini, R. Guzzi, A. Garofalo, G. Statti, Identification by molecular docking of homoisoflavones from Leopoldia comosa as ligands of estrogen receptors, Molecules 23 (2018) 894.

[40] T. Casacchia, M.A. Occhiuzzi, F. Grande, B. Rizzuti, M.C. Granieri, C. Rocca, A. Gattuso, A. Garofalo, T. Angelone, G. Statti, A pilot study on the nutraceutical properties of the Citrus hybrid Tacle® a dietary source of polyphenols for supplementation in metabolic disorders, J. Funct. Foods (2019) 370–381.

[41] T. Angelone, E. Filice, A.M. Quintieri, S. Imbrogno, N. Amodio, T. Pasqua, D. Pellegrino, F. Mul`e, M.C. Cerra, Receptor identification and physiological characterisation of glucagon-like peptide-2 in the rat heart, Nutr. Metab. Cardiovasc. Dis. (2012) 486–494.

[42] I.C. Nettore, C. Rocca, G. Mancino, L. Albano, D. Amelio, F. Grande, F. Puoci, T. Pasqua, S. Desiderio, R. Mazza, D. Terracciano, A. Colao, F. B`eguinot, G. L. Russo, M. Dentice, P.E. Macchia, M.S. Sinicropi, T. Angelone, P. Ungaro, Quercetin and its derivative Q2 modulate chromatin dynamics in adipogenesis and Q2 prevents obesity and metabolic disorders in rats, J. Nutr. Biochem. 69 (2019) 151–162.

[43] Y. Wang, L. Su, M.D. Morin, B.T. Jones, L.R. Whitby, M.M.R.P. Surakattula, H. Huang, H. Shi, J.H. Choi, K. Wang, E.M.Y. Moresco, M. Berger, X. Zhan, H. Zhang, D.L. Boger, B. Beutler, TLR4/MD-2 activation by a synthetic agonist with no similarity to LPS, PNAS (2016) 884–893.

[44] Z. Golkar, O. Bagasra, D.G. Pace, Bacteriophage therapy: a potential solution for the antibiotic resistance crisis, J. Infect. Dev. Ctries. (2014) 129–136.

[45] M. Mahlapuu, J. Håkansson, L. Ringstad, C. Bj¨orn, Antimicrobial peptides: an emerging category of therapeutic agents, Front. Cell. Infect. Microbiol. 6 (2016) 194.

[46] R.E. Hancock, H.G. Sahl, Antimicrobial and host-defense peptides as new antiinfective therapeutic strategies, Nat. Biotechnol. (2006) 1551–1557.

[47] M.R. Yeaman, N.Y. Yount, Mechanisms of antimicrobial peptide action and resistance, Pharmacol. Rev. (2003) 27–55.

[48] M.H. Metz-Boutigue, A.E. Kieffer, Y. Goumon, D. Aunis, Innate immunity: involvement of new neuropeptides, Trends Microbiol. (2003) 585–592.

[49] Q. Su, J. Yao, C. Sheng, Geniposide attenuates LPS-induced injury via up-regulation of miR-145 in H9c2 cells, Inflammation (2018) 1229–1237.

[50] R. Wang, D. Li, J. Ouyang, X. Tian, Y. Zhao, X. Peng, S. Li, G. Yu, J. Yang, Leonurine alleviates LPS-induced myocarditis through suppressing the NF-κB signaling pathway, Toxicology 422 (1–13) (2019).

[51] T.H. Htwe, N.M. Khardori, Cardiac emergencies: infective endocarditis, pericarditis, and myocarditis, Med. Clin. North Am. (2012) 1149–1169.

[52] R. Hao, G. Su, X. Sun, X. Kong, C. Zhu 2, G. Su, Adiponectin attenuates lipopolysaccharide-induced cell injury of H9c2 cells by regulating AMPK pathway. Acta Biochim Biophys Sin (Shanghai) (2019), 51(2):168-177.

[53] N.H. Evans, Chiral catenanes and rotaxanes: fundamentals and emerging applications, Chemistry (2018) 3101–3112.

[54] L. Chen, W. Fu, L. Zheng, Y. Wang, G. Liang, Recent progress in the discovery of myeloid differentiation 2 (MD2) modulators for inflammatory diseases, Drug Discov. Today (2018) 1187–1202.

[55] Y. Nagai, S. Akashi, M. Nagafuku, M. Ogata, Y. Iwakura, S. Akira, T. Kitamura, A. Kosugi, M. Kimoto, K. Miyake, Essential role of MD-2 in LPS responsiveness and TLR4 distribution, Nat. Immunol. (2002) 667–672.

[56] Y.C. Lu, W.C. Yeh, P.S. Ohashi, LPS/TLR4 signal transduction pathway, Cytokine (2008) 145–151.

[57] J.L. Lai, Y.H. Liu, C. Liu, M.P. Qi, R.N. Liu, X.F. Zhu, Q.G. Zhou, Y.Y. Chen, A. Z. Guo, C.M. Hu, Indirubin inhibits LPS-induced inflammation via TLR4 abrogation mediated by the NF-kB and MAPK signaling pathways, Inflammation 1 (2017) 1–12.

[58] Y.J. Choi, W.S. Lee, E.G. Lee, M.S. Sung, W.H. Yoo, Sulforaphane inhibits IL-1beta-induced proliferation of rheumatoid arthritis synovial fibroblasts and the production of MMPs, COX-2, and PGE2, Inflammation (2014) 1496–1503.

[59] B. Hoesel, J.A. Schmid, The complexity of NF-kappaB signaling in inflammation and cancer, Mol. Cancer 12 (2013) 86.

[60] A. Valaperti, Drugs targeting the canonical NF-κB pathway to treat viral and autoimmune myocarditis, Curr. Pharm. Des. (2016) 440–449.

[61] T. Yu, D. Dong, J. Guan, J. Sun, M. Guo, Q. Wang, Alprostadil attenuates LPSinduced cardiomyocyte injury by inhibiting the Wnt5a/JNK/NF-kappaB pathway. Herz (2020), (Suppl 1):130-138.

[62] C. Huang, Y. Zhang, H. Qi, X. Xu, L. Yang, J. Wang, Myc is involved in Genistein protecting against LPS-induced myocarditis *in vitro* through mediating MAPK/JNK signaling pathway, Biosci Rep 40(6):BSR20194472 (2020.

[63] R.M. Guo, W.M. Xu, J.C. Lin, L.Q. Mo, X.X. Hua, P.X. Chen, K. Wu, D.D. Zheng, J. Q. Feng, Activation of the p38 MAPK/NF-κB pathway contributes to doxorubicininduced inflammation and cytotoxicity in H9c2 cardiac cells, Mol. Med. Rep. (2013) 603–608.

[64] S.F. Liu, A.B. Malik, NF-kappa B activation as a pathological mechanism of septic shock and inflammation, Am. J. Physiol. Lung Cell. Mol. Physiol. (2006) 622–645.

[65] F. Schneider, C. Marban, G. Ajob, S. Helle, M. Guillot, A. Launoy, Q. Maestraggi, F. Scavello, O. Rohr, M.H. Metz-Boutigue. In trauma patients, the occurrence of early-onset nosocomial

infections is associated with increased plasma concentrations of chromogranin A, Shock (2018) 522–528.

[66] Y.C. Tien, J.Y. Lin, C.H. Lai, C.H. Kuo, W.Y. Lin, C.H. Tsai, F.J. Tsai, Y.C. Cheng, W. H. Peng, C.Y. Huang, Carthamus tinctorius L. prevents LPS-induced TNFalpha signaling activation and cell apoptosis through JNK1/2-NFkappaB pathway inhibition in H9c2 cardiomyoblast cells, J. Ethnopharmacol. (2010) 505–513.

[67] H. Yuan, C.N. Perry, C. Huang, E. Iwai-Kanai, R.S. Carreira, C.C. Glembotski, R. A. Gottlieb, LPS-induced autophagy is mediated by oxidative signaling in cardiomyocytes and is associated with cytoprotection, Am. J. Physiol. Heart Circ. Physiol. (2009) 470–479.

[68] S. Lei, Y. Zhang, W. Su, L. Zhou, J. Xu, Z.Y. Xia, Remifentanil attenuates lipopolysaccharide-induced oxidative injury by downregulating PKCβ2 activation and inhibiting autophagy in H9C2 cardiomyocytes. Life Sci. (2018),109-115.

[69] W.L. DeLano, The PyMOL molecular graphics system. DeLano Scientific, Palo Alto, (2002).

VI. VIRTUAL SCREENING APPLICATION TOWARD THE IDENTIFICATION OF TBEV INHIBITION

1. Introduction

The screening of large and chemically diverse compound libraries is one of the most widespread strategies in drug discovery to identify novel lead compounds targeting biologically active macromolecules [1]. By docking a large library of compounds into one or more structures of the target receptor, a few compounds can be selected and evaluated for their effective interaction. The factors that influence the execution and the results of the virtual screening (VS) are various: the availability of structural data of the biological target, the existence of at least one molecule that can interact unequivocally with the target, the number and type of compounds to be screened and the software used. VS strategies fall into two main types: ligand-based approach and structure-based approach. Generally, the choice of the method depends on whether the ligands or the structure of the target are known. When possible, virtual screening studies can combine the two methods for more reliable results [2]. These experimental procedures have been applied in ordert to identify compouds able to inhibit crucial proteins involved in the replication cycle of tick-borne encephalitis virus (TBEV). The latter is a single-stranded RNA flavivirus within the family *Flaviviridae* and belongs to arthropod-borne viruses, known as arboviruses. TBEV is widespread across large parts of Europe and Asia and constitutes the etiological agent of tick-borne encephalitis, a human viral infectious disease involving the central nervous system, leading to permanent neurological complications or death.

Since TBEV infection is constantly rising, the identification of compounds able to inhibit its replication is demanding.

Accordingly, this study has been carried out in order to identify:
- potential targets necessary to TBEV replication;
- potential structural homologies with other flaviviruses (DENV, WNV, ZIKV etc.);
- non-nucleoside potential inhibitors.

2. Methods

The crystallographic structure of RNA dependent RNA polymerase domain of west nile virus (PDB code 2HCN_A) [3] was used as a template to create the protein model of TBEV polymerase. The model was built using MOE program. High-throughput virtual screening (HTVS) docking was performed through Maestro Schrödinger software on three different libraries (Specs, ChemDiv and Life Chemical) for a total of 90.000.000 compounds. The 10% of the best poses obtained was selected to perform the docking using Glide Standard precision (SP) function. All the resulting poses were subsequently rescored using other three different docking programs: XP (extra precision), FlexX and Plants. Applying an internal consensus score procedure, the values of the three different scoring functions for each docking pose were analysed. Then, a database containing all the results of rescoring was created. The resulted set of compounds has been refined according to the following parameters:
- sum >3 (sum of function sign)
- structural cluster
- logP>1

- logP<6

The selected compounds were further subjected to a final screeening through visual inspection using MOE program and according to the following criteria:
- ability of a compound to overall occupy the binding site;
- number of interactions formed between the compound and the target protein (H-bonds, π-π interactions, etc.).

3. Results and discussion

The TBEV genome consist of approximately 11 kb positive-sense single-stranded RNA, which encodes one single open reading frame (ORF) of about 3400 amino acids, flanked by 5′ and 3′ non-coding regions (NCRs), three structural proteins; envelope (E), precursor membrane (PrM) and capsid (C), and seven non-structural proteins (NS1, NS2A, NS2B, NS3, NS4A-2K-4B complex and NS5) [4] (Figure1).
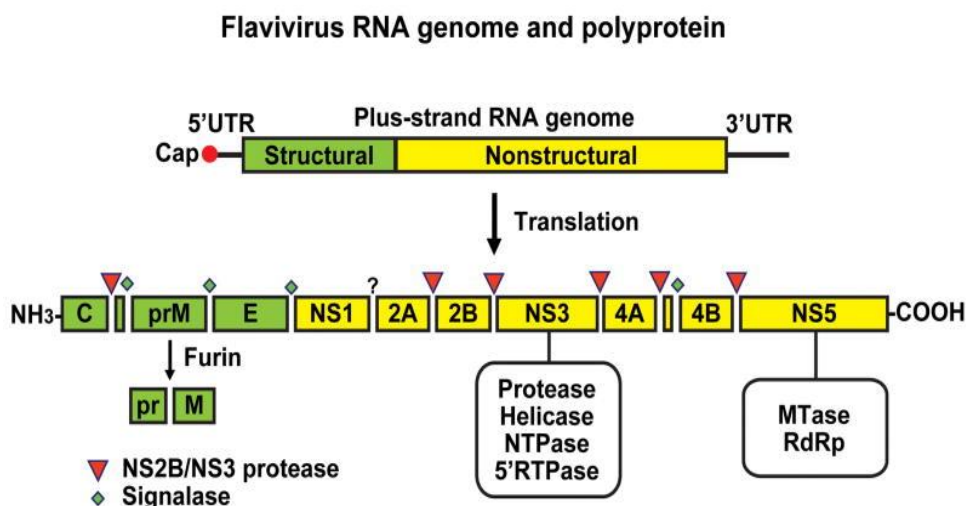
Flavivirus RNA genome and polyprotein

Figure 1. *Representation of the viral RNA of TBEV*

NS5 are polymerase proteins that play a crucial role in TBEV replication, thus have been selected as targets for the development of novel drugs to prevent or slow the viral infection.

The catalytic domain Rdrp (RNA dependent RNA polymerase), consisting in a fragment of 150 RNA replicase protein residues, is available on the UniProt website. A possible sequence homology was searched using the UniProt BLAST function by choosing the PDB database and 61% homology was obtained with the PDB code 2HCN _A (chain A crystal structure of the West Nile Virus RdRp domain [3]. This crystallographic structure was then used as a template to create a protein model using the appropriate function of the MOE program (Figure 2).
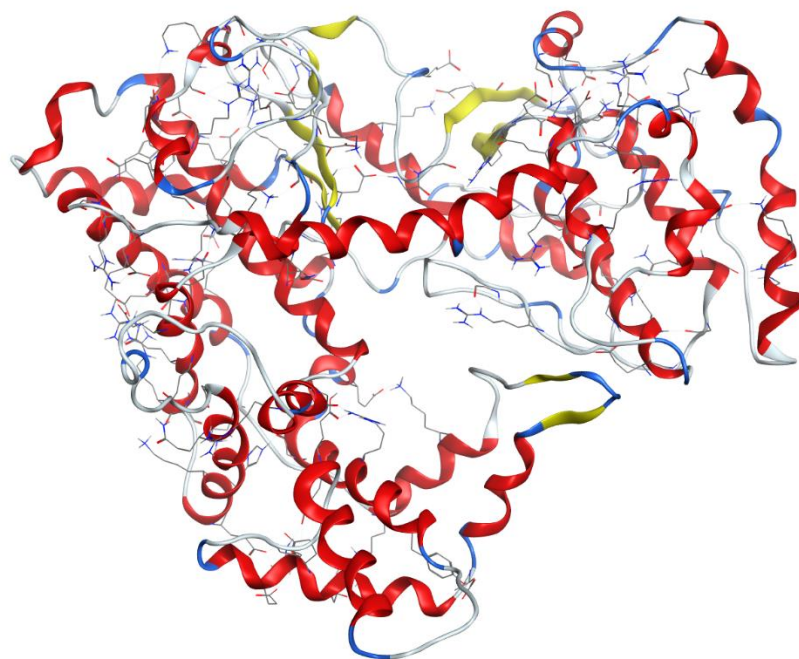
Figure 2. *Protein model obtained using West Nile virus NS5 polymerase as template.*

Successively, in order to identify a possible binding pocket, alignments and overlaps were made between the model created and the polymerases of different *Flaviviruses* in a complex with at least one inhibitor.

After identifying a potential binding pocket, a High-throughput Virtual Screening (HTVS) was performed using various libraries (Specs, ChemDiv, Enamine and Life Chemical) containing approximately 90.000.000 compounds.
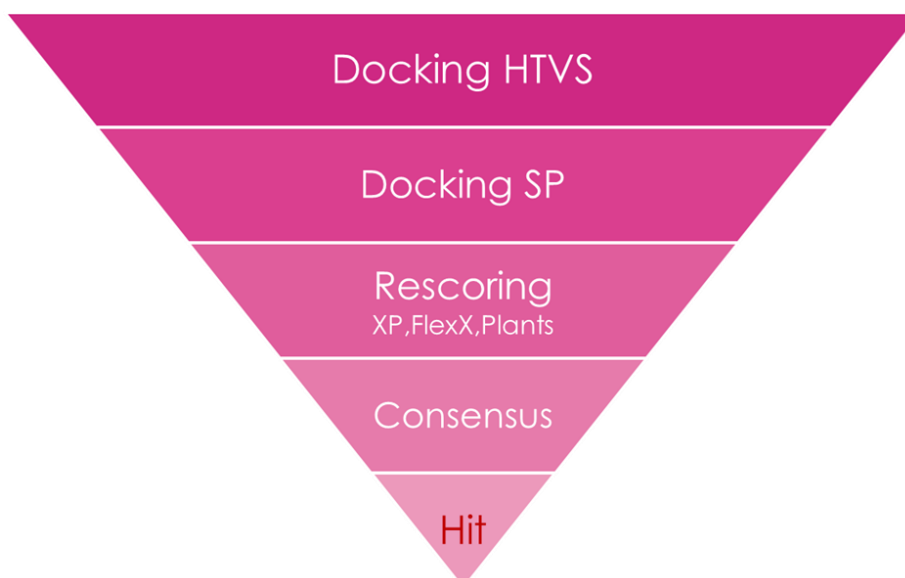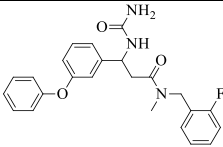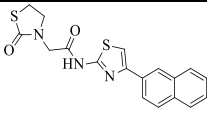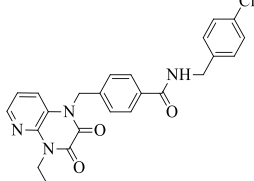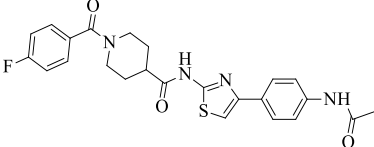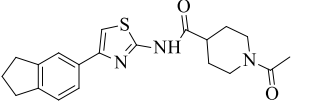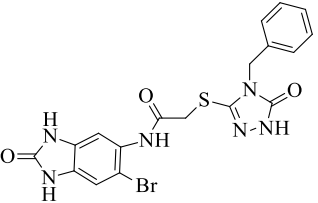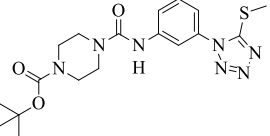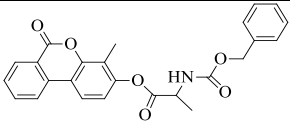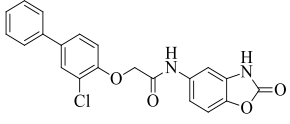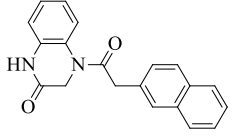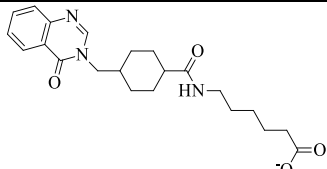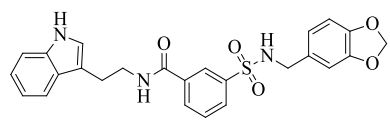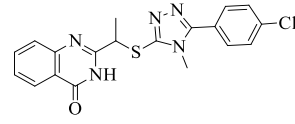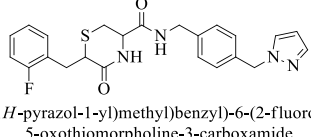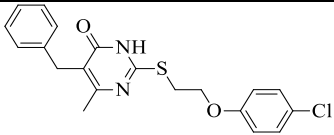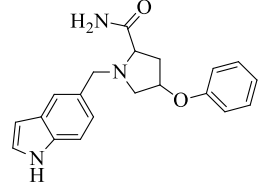

Figure 3. *Representative phases of virtual screening*
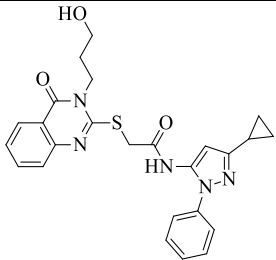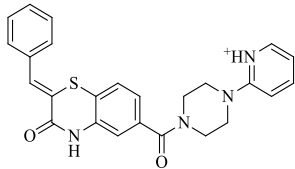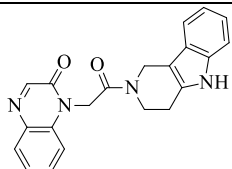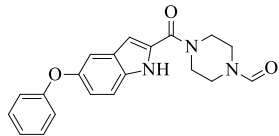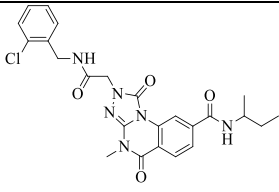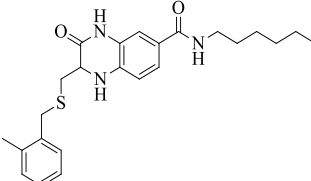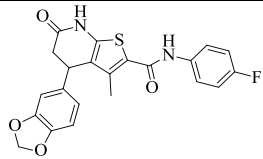
The last phase of the virtual screening was the selection of the compounds that were more favorable, by means of visual inspection. About 17.220 compounds were visualized, and
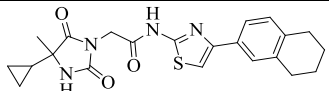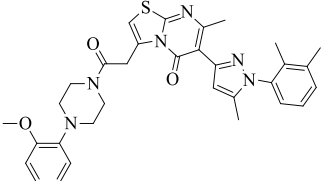
following the previously described procedure (Figure 3), 25 were selected as potential anti-TBEV agents (Table 1).

Table 1. *Chemical strusctures of selected compounds as potential anti-TBEV agents*

CPD	CODE	CHEMICAL STRUCTURE	N.I.	H-I	HY-I			I-I
					πι-πι	πι-H	H-πι	
1	Z26576487	*N*-(2-fluorobenzyl)-*N*-methyl-3-(3-phenoxyphenyl)-3-ureidopropanamide	5	Ala 409 Ser 406 Ala 409 Val 404	Trp 479			
2	Z28636182	*N*-(4-(naphthalen-2-yl)thiazol-2-yl)-2-(2-oxothiazolidin-3-yl) acetamide	5	Lys 403 Ser 406 Ala 409 Ala 409		Ala 409		
3	F704-0088	*N*-(4-chlorobenzyl)-4-((4-ethyl-2,3-dioxo-3,4-dihydropyrido[2,3-*b*]pyrazin-1(2*H*)-yl)methyl)benzamide	5	Val 606 Val 607 Gnl 600	Trp 479	Arg 483		
4	Z27057384	*N*-(4-(4-acetamidophenyl)thiazol-2-yl)-1-(4-fluorobenzoyl) piperidine-4-carboxamide	4	Lys403 Ser 406 Ala 409 Ala 409				
5	Z28889153	1-acetyl-*N*-(4-(2,3-dihydro-1*H*-inden-5-yl)thiazol-2-yl) piperidine-4-carboxamide	4	Lys 403 Ser 406 Ala 409 Ala 409				
6	Z112629622	2-((4-benzyl-5-oxo-4,5-dihydro-1*H*-1,2,4-triazol-3-yl)thio)-*N*-(6-bromo-2-oxo-2,3-dihydro-1*H*-benzo[*d*]imidazol-5-yl)acetamide	4	Ala 409 Val 607 Gly 411		Val 606		
7	Z413812828	tert-butyl 4-((3-(5-(methylthio)-1H-tetrazol-1-yl)phenyl) carbamoyl)piperazine-1-carboxylate	4	Arg 483 Val 606 Gly 411		Arg 483		

#	ID	Structure / Name					
8	Y041-4631	4-methyl-6-oxo-6*H*-benzo[*c*]chromen-3-yl 2-(((benzyloxy)carbonyl)amino)propanoate	4	Val 606 Leu 410 Gly 411		Arg 483	
9	Z319332718	2-((3-chloro-[1,1'-biphenyl]-4-yl)oxy)-*N*-(2-oxo-2,3-dihydrobenzo[*d*]oxazol-5-yl)acetamide	4	Ser 406 Leu 410 Gly 411		Val 404	
10	Z33397508	4-(2-(naphthalen-2-yl)acetyl)-3,4-dihydroquinoxalin-2(1*H*)-one	4	Ala 409 Ala 409		Arg 483 Arg 483	
11	Y040-8576	6-(4-((4-oxoquinazolin-3(4*H*)-yl)methyl)cyclohexanecarboxamido)hexanoate	4	Arg 793 Leu 410			Arg 793 Arg 793
12	Z32439691	*N*-(2-(1*H*-indol-3-yl)ethyl)-3-(*N*-(benzo[*d*][1,3]dioxol-5-ylmethyl)sulfamoyl)benzamide	4	Leu 410 Gly 411		Gly 411 Arg 483	
13	Z15836284	2-(1-((5-(4-chlorophenyl)-4-methyl-4*H*-1,2,4-triazol-3-yl)thio)ethyl)quinazolin-4(3*H*)-one	3	Ala 409 Leu 410 Gly 411			
14	Z298299390	*N*-(4-((1*H*-pyrazol-1-yl)methyl)benzyl)-6-(2-fluorobenzyl)-5-oxothiomorpholine-3-carboxamide	3	Leu 410 Gly 411 Ala 409			
15	D058-0083	5-benzyl-2-((2-(4-chlorophenoxy)ethyl)thio)-6-methylpyrimidin-4(3*H*)-one	3	Ala 409 Ala 409 Gly 411			
16	S720-2191	1-((1*H*-indol-5-yl)methyl)-4-phenoxypyrrolidine-2-carboxamide	3	Val 404 Ser 406 Ala 409			

17	Z297824504	*N*-(3-cyclopropyl-1-phenyl-1*H*-pyrazol-5-yl)-2-((3-(3-hydroxypropyl)-4-oxo-3,4-dihydroquinazolin-2-yl)thio)acetamide	3	Gln 605 Leu 410 Arg 793			
18	K788-9530	(*Z*)-2-(4-(2-benzylidene-3-oxo-3,4-dihydro-2*H*-benzo[*b*][1,4]thiazine-6-carbonyl)piperazin-1-yl)pyridin-1-ium	3	Ala 409 Ala 409		Trp 479	
19	Z225652666	1-(2-(3,4-dihydro-1*H*-pyrido[4,3-*b*]indol-2(5*H*)-yl)-2-oxoethyl)quinoxalin-2(1*H*)-one	3	Ala 409 Val 606	Arg 483		
20	F019-1745	4-(5-phenoxy-1*H*-indole-2-carbonyl)piperazine-1-carbaldehyde	3	Ala 409 Gly 411		TRP 479	
21	F470-0703	*N*-(*sec*-butyl)-2-(2-((2-chlorobenzyl)amino)-2-oxoethyl)-4-methyl-1,5-dioxo-1,2,4,5-tetrahydro-[1,2,4]triazolo[4,3-*a*]quinazoline-8-carboxamide	3	Val 406 Gly 411	Val 404		
22	K784-1583	*N*-hexyl-2-(((2-methylbenzyl)thio)methyl)-3-oxo-1,2,3,4-tetrahydroquinoxaline-6-carboxamide	3	Ala 409 Ala 409		Trp 479	
23	8019-7948	4-(benzo[*d*][1,3]dioxol-5-yl)-*N*-(4-fluorophenyl)-3-methyl-6-oxo-4,5,6,7-tetrahydrothieno[2,3-*b*]pyridine-2-carboxamide	3	ALA 409 ALA 409		Trp 479	
24	Z51854797		4	Lys 403 Ser 406 Ala 409 Ala 409			

		 2-(4-cyclopropyl-4-methyl-2,5-dioxoimidazolidin-1-yl)- *N*-(4-(5,6,7,8-tetrahydronaphthalen-2-yl) thiazol-2-yl)acetamide						
25	V004-5552	 6-(1-(2,3-dimethylphenyl)-5-methyl-1*H*-pyrazol-3-yl)- 3-(2-(4-(2-methoxyphenyl)piperazin-1-yl)-2-oxoethyl)- 7-methyl-5*H*-thiazolo[3,2-*a*]pyrimidin-5-one	4	Gln 600 Gln 600		Trp 479 Val 606		

Notes: NI: Number of Interaction; H-I: Hydrogen Interaction; Hy-I: Hydrophobic Interaction; I-I; Ionic Interaction

4. Conclusions

TBE is an important tick-borne central nervous system infection in Europe and Asia. It is a spherical lipid-enveloped RNA virus, a member of genus *Flavivirus* within the *Flaviviridae* family. In this study, focused the attention as NS5 polymerase protein involved in the viral replication. In particular, through application of advanced computational techniques, has been identified the polymerase protein model. Successively was carried out HTVS docking using all the libraries available (Specs, ChemDiv and Life Chemical). According to the certain parameters of refine, was obtained 17220 compounds. The last phase of virtual screening made it possible to select 25 compounds as potential anti- TBEV agents.
Biological *in vitro* studies are undergoing to assess the biological properties of the selected molecules. Preliminary results seem to confirm the capability of some of them as potent NS5 inhibitors.
Regarding this point, the results need to be still organized and will be published afterwards.

References

[1] B.K. Shoichet, Virtual screening of chemical libraries, Nature. 432 (2004) 862–865.

[2] T. Seidel, O. Wieder, A. Garon, T. Langer, Applications of the Pharmacophore Concept in Natural Product inspired Drug Design, Mol. Inform. 39 (2020) 2000059.

[3] H. Malet, M.P. Egloff, B. Selisko, R.E. Butcher, P.J. Wright, M. Roberts, A. Gruez, G. Sulzenbacher, C. Vonrhein, G. Bricogne, J.M. Mackenzie, A.A. Khromykh, A.D. Davidson, B. Canard, Crystal structure of the RNA polymerase domain of the West Nile virus non-structural protein 5, J. Biol. Chem. 282 (2007) 10678–10689.

[4] K.M. Paulsen, A. Lamsal, S. Bastakoti, J.H.O. Pettersson, B.N. Pedersen, K. Stiasny, M. Haglund, T. Smura, O. Vapalahti, R. Vikse, K. Alfsnes, Å.K. Andreassen, High-throughput sequencing of two European strains of tick-borne encephalitis virus (TBEV), Hochosterwitz and 1993/783, Ticks Tick. Borne. Dis. 12 (2021).

CHAPTER 2

PHOTODEGRADATION AND PHOTOSTABILIZATION STUDIES OF NEWLY SYNTHESIZED COMPOUNDS AND KNOWN PHOTOSENSITIVE DRUGS

1. Introduction

A further goal of the overall project has been the design of light-stable formulations of newly synthesized derivatives active as anti-inflammatory agents or T-type calcium channel blockers.

Chemical structural alterations to known compounds were performed in order to maintain the structural features associated with the biological activity but removing the functional groups possibly responsible for photosensitivity and side effects. Nowadays, light has been recognized as one of the most significant external factors affecting drug stability, thus, the study of photosensitivity of a drug is essential for design proper formulation and packaging. Drug degradation not only can lead to the reduction of biological activity, but in several cases the formation of toxic byproducts can even occur. A basic protocol for testing the photostability of new drugs is described in the ICH (International Conference on Harmonization) guidelines, as a part of the full rational program containing rules for the drug stability control [1]. The intrinsic photostability characteristics of new drugs should be evaluated to demonstrate that, as appropriate, light exposure does not result in unacceptable changes. The impurities from synthesis and degradation need to be identified and quantified and their limits must be established. During production, packaging and consumer handling, pharmaceutical products can be exposed to light coming by different sources, ranging from natural sunlight to a variety of artificial light conditions.

The majority of drug formulations result in solid phase or solution pharmaceutical forms. Literature data indicate that liquid preparations are usually less stable under light radiation than solids. Generally, photodegradation rate decreases when the drug concentration in a specific formulation increase.

Several approaches can be adopted to prevent drug photodegradation. A drug can be protected from light by simply selecting an appropriate opaque container or maintaining an inert atmosphere to minimize the absorbance of specific wavelengths and limiting oxygen catalysed reactions.

The formulation in presence of different and appropriate excipients able to increase the drug photochemical stability is widely adopted to stabilize pharmaceutical preparations. The design of photoprotective pharmaceutical systems presents the twofold advantage to keep unaltered the drug concentration, in order to guarantee the therapeutic effect, and to avoid the formation of photo-byproducts.

Anyway, the incorporation of photosensitive compounds into supramolecular systems represents one of the most effective approach to overcomes several drawbacks related to drug instability and unfavourable pharmacokinetics.

2. Methods

2.1. Chemistry

The new compounds were prepared by modification of previously described synthetic routes.

In particular, regarding NSAIDs derivatives, a Nabumetone derivative has been prepared in good yield and high purity by polyphosphoric acid catalysed Friedel-Crafts intramolecular cyclization of 3-(6-methoxynaphthalen-2-yl)propanoic acid [2] in order to replace the butanone chain of the reference compound with a condensed cyclic ketone moiety.

1,4-Dihydropyridine (DHP) derivatives were instead prepared in good yield following a modified Hantzsch reaction procedure in collaboration with the Department of Pharmaceutical Chemistry, Faculty of Pharmacy, Hacettepe University, Ankara, Turkey [3,4].

2.2 Photostability studies

Photodegradation experiments were performed in accordance with the ICH recommendations for the drug stability tests. These tests were performed by using the light cabinet Suntest CPS+ (Figure 1), that provides information about the long-term response of the product exposed to light, particularly solar radiation. Photostability test can be performed by using two different sources light:

Option 1: the samples have to be irradiated under a light source producing an output similar to the D65/ID65 emission standard. An artificial daylight fluorescent lamp combining visible and ultraviolet (UV) outputs, xenon, or metal halide lamp are suitable for this test. D65 is the internationally recognized standard for outdoor daylight as defined in ISO 10977 (1993). ID65 is the equivalent indoor indirect daylight standard. If necessary, appropriate filters must provide to eliminate the radiations below 320 nm.

Option 2: a cool white fluorescent and a near ultraviolet lamp are both required. The first must produce an output similar to that specified in ISO 10977 (1993); the second lamp must furnish a spectral distribution from 320 nm to 400 nm with a maximum energy emission between 350 nm and 370 nm.

This accurate definition of the light sources has been helpful to avoid different procedures in the photostability tests. Whatever the option is chosen, the operator should mind maintaining an appropriate control of the temperature to minimize the effect of localized temperature changes caused by the light sources.

The device is equipped with an electronic system (CPS, Controlled Power System) that offers constant control over irradiation, allowing a good reliability in providing a reproducible test.

Figure 1. *Suntest CPS+*

During a photodegradation experiments, the compounds formulated in solutions or in gels were exposed to light and drug content was measured at several exposure times by spectrophotometry.

Spectral data were elaborated by Multivariate Curve Resolution (MCR) technique, able to estimate spectra and concentration profiles of the components involved in the studied system. This chemometric procedure decomposes the spectral data into the contributions due to the pure components of the system following a bilinear model derived from the generalized Lambert-Beer's absorption law.

$$\mathbf{D}_{(r\,x\,c)} = \mathbf{C}_{(r\,x\,n)}\,\mathbf{S^T}_{(n\,x\,c)} + \boldsymbol{E}_{(r\,x\,c)} \qquad \text{Equation 1}$$

where **C** is the concentration matrix of n components and ST is the matrix of their spectra. **E** represents the unexplained variance in the data set. In MCR methods, the first step is the estimation of the number of involved components (n) in the kinetic system, which is initially obtained by application of singular value decomposition (SVD). Moreover, iterative MCR methods, like MCR-ALS (Alternative Least Squares), need a preliminary estimation of $\mathbf{S^T}$ or **C**, calculated either by evolving factor analysis (EFA), by selection of the pure variables, or by any previously estimation of them. These initial estimates are used to start the ALS constrained optimization through an iterative process. At each cycle, a new estimation of $\mathbf{S^T}$ and **C** is calculated by solving alternatively the two following least-squares matrix equations, according to the scheme:

$$\mathbf{S^T} = (\mathbf{C})^{+}\mathbf{D} \qquad \text{Equation 2}$$
$$\mathbf{C} = \mathbf{D}(\mathbf{S^T})^{+} \qquad \text{Equation 3}$$

where $(\mathbf{S^T})^{+}$ and $(\mathbf{C})^{+}$ are the pseudoinverses of the $\mathbf{S^T}$ and **C** matrices, respectively [5-7]. At every iteration, constraints like non-negativity, unimodality and concentration closure are applied to drive the optimization process towards a final solution with chemical meaning fulfilling the applied constraints . This iteration procedure is stopped when convergence is achieved, by fixing a preselected number of cycles or when the value of lack of fit (% LOF) does not change significantly between consecutive iterations:

$$\%\,LOF = 100 \times \sqrt{\frac{\sum_{ij}(d_{ij} - d_{ij}^*)^2}{\sum_{ij} d_{ij}^2}} \qquad \text{Equation 4}$$

where d_{ij} and d_{ij}^* were respectively the experimental and calculated (by MCR-ALS) absorbance values. A different parameter used to indicate the quality of MCR-ALS modelling results is the percentage of explained variance (r^2):

$$\%\,r^2 = 100 \times \frac{\sum_{ij} d_{ij}^{2*}}{\sum_{ij} d_{ij}^2} \qquad \text{Equation 5}$$

Another important feature of the MCR-ALS method is its possibility to perform the simultaneous analysis of multiple data sets coming from more than one experiment, using different experimental conditions and/or conducted by different analytical techniques. The whole set of photodegradation experiments performed at different NFZ initial concentrations exposed under different illuminance power conditions were arranged in a column-wise augmented data matrix and analyzed using MCR-ALS according to the extended bilinear model equation

$$\mathbf{D}_{Aug.} = \mathbf{C}_{Aug.}\mathbf{S}^T + \mathbf{E}_{Aug.} = [\mathbf{D_1}; \mathbf{D_2};\dots; \mathbf{D_N}] = [\mathbf{C_1}; \mathbf{C_2};\dots; \mathbf{C_N}]\,\mathbf{S}^T + [\mathbf{E_1};\mathbf{E_2};\dots;\mathbf{E_N}]\ \text{Equation 6}$$

In this matrix equation, column wise matrix augmentation is indicated using MATLAB notation '**;**', which indicates that every individual data block obtained in a single kinetic experiment is set on top of the other, with the same number of columns (wavelengths) in common, and consequently increasing the number of rows of the corresponding augmented matrix. As indicated in this equation, the same spectral matrix $\mathbf{S}^T$ is resolved for all $\mathbf{D_i}$, i=1,..,$\mathbf{N}$ matrices, i.e. the same pure spectra are resolved for the common species in the different experiments. On the contrary, the concentration profiles of the different resolved components in $\mathbf{C_i}$ matrices are allowed to be different for the different kinetic experiments. This is in agreement with the possibility of having degradation (concentration) profiles with different shapes in the different experimental data matrices obtained at different initial NFZ concentration and power irradiances. These degradation profiles will follow different patterns which cannot be described by the same set of concentration profiles. In contrast, however, the same chemical species will have the same characteristic UV spectrum in the different kinetic experiments. In conclusion, the model proposed in Equation 6 will fit well with the expected behaviour of the measured system if the generalized bilinear Beer's Lambert law of UV absorption holds for the system under investigation.

3. Results Summary

Non-steroidal anti-inflammatory drugs (NSAIDs) have been marketed in topical preparations for about 40 years with the aim to avoid part of the side effects developed after systemic administration. In addition, the absence of a first pass metabolism could contribute to better control the plasmatic concentration of the drug. Unfortunately, most of the NSAIDs are not easily absorbed after transdermal application, this drawback being exacerbate by the hydrophilic nature of many dermal preparations. Despite their wide use, another important limit of several NSAIDs is their easy chemical degradation under several physical or chemical conditions leading to the appearence of various impurities.

Accordingly, the first work of this section describes, photostability studies applied on aqueous solutions of Nabumetone (NA), a non-acidic anti-inflammatory prodrug, confirmed

a marked light sensitivity for this compound. Accordingly, the stability of NA-cyclodextrin (CD) complexes was investigated in gels potentially suitable as sustained-release formulations, under various experimental conditions.

In a second work, in view of the metabolic transformation and photostability profile of NA, a new tricyclic analog was synthesized by including part of the too light-sensitive side chain in an additional fused ring. This alteration was performed to enhance light stability, while maintaining the capability to undergo a metabolic activation similar to that of NA.

Photoprotection methodologies have been applied on both NA and the new derivative in order to design topical light-stable formulations, including entrapment of the compounds into microemulsions. Very satisfactory results in term of degradation time and photoprotection were achieved for both compounds when formulated in microemulsion included in gel.

Another project focused on the stabilization of newly synthesized DHP derivatives, an important class of L- and T-type calcium channel blockers widely used in clinic. Several chemical modifications on the DHP scaffold led to new derivatives active on T-type calcium channels and others, which have recently attracted interest due to their role in chronic pain onset. The study focused on the development of light-stable liquid and gel formulations for the incorpotation of newly synthesized active compounds. Photodegradation studies were performed in different experimental conditions.

References

[1] ICH harmonized tripartite guideline, Federal Register. Photostability testing of new drug substance and products. European Medicines Agency: London, UK, 1997; Volume 62.

[2] Mimori, S.; Koshikawa, Y.; Mashima, Y.; Mitsunaga, K.; Kawada, K.; Kaneko, M.; Okuma, Y.; Nomura, Y.; Murakami, Y.; Kanzaki, T.; et al. Evaluation of synthetic naphthalene derivatives as novel chemical chaperones that mimic 4-phenylbutyric acid. Bioorg. Med. Chem. Lett. 2015, 25, 811–814.

[3] Schaller, D.; Gunduz, M.G.; Zhang, F.X.; Zamponi, G.W.; Wolber, G. Binding mechanism investigations guiding the synthesis of novel condensed 1,4-dihydropyridine derivatives with L-/T-type calcium channel blocking activity. Eur. J. Med. Chem. 2018, 155, 1–12.

[4] Cevher, H.A.; Schaller, D.; Gandini, M.A.; Kaplan, O.; Gambeta, E.; Zhang, F.X.; Çelebier, M.; Tahir, M.N.; Zamponi, G.W.; Wolber, G.; et al. Discovery of Michael acceptor containing 1,4-dihydropyridines as first covalent inhibitors of L-/T-type calcium channels. Bioorg. Chem. 2019, 91, 103187.

[5] Golub, G.H. and Van Loan, C.F. Matrix Computations, 2nd Ed., The John Hopkins University Press, London (1989)

[6] Tauler, R., Chemom. Intell. Lab. Syst.1995, 30, 133-146.

[7] Tauler, R., Smilde, A.K., Kowalski, B.R., J. Chemom.1995, 931-58.

I. CYCLODEXTRINS IN TOPICAL GEL FORMULATION AS PHOTOPROTECTIVE SYSTEM FOR NABUMETONE

Maria Antonietta Occhiuzzi; Fedora Grande; Michele De Luca; Gaetano Ragno, Antonio Garofalo; Giuseppina Ioele.

Department of Pharmacy, Health and Nutritional Sciences, University of Calabria, 87036 Arcavacata di Rende (CS) – Italy

Abstract:

Photostability studies applied on aqueous solutions of Nabumetone, an anti-inflammatory drug used in the treatment of osteoarthritis and rheumatoid arthritis, have confirmed the sensitivity to light of this compound, revealing the 6-methoxy-naphthalenealdehyde as the main photoproduct. In this work, the stability of NA-cyclodextrin (CD) complexes was investigated in gel formulation potentially suitable as sustained-release systems. The photodegradation experiments were realized under stressed conditions according to the ICH rules and monitored by spectrophotometry. The spectral data were processed by Multivariate Curve Resolution (MCR), able to estimate spectra and concentration profiles of the components involved in the kinetic process. NA entrapped in cyclodextrin and formulated in solution and gel preparations were exposed to an irradiance power of 350 W/m^2.

Encapsulation percentage of the drug in several cyclodextrins was measured, recording an increase of the water solubility in the order hpβCD>mβCD>βCD. No significant photoprotection of NA was measured in aqueous solution. On the contrary, the gel containing the hpβCD-complex showed relevant stability. The photoprotective ability of this formulation was further increased by adding ascorbic acid 2%, still detecting 90% of the starting concentration after 90 min of light exposure.

1. Introduction

The safety of the drugs, during production, storage, distribution and use by patients, is affected by exposure to several causes of degradation, including temperature and light [1]. In particular, the exposure to light could affect the physicochemical properties of either a pure compound or a pharmaceutical formulation. A great amount of liquid or in topical gel preparations, liquid or in gel, are classified as sensitive to light in the U.S. and European Pharmacopeia [2], consequently, the development of advanced photoprotective systems is still demanding. Furthermore, the use of appropriate protective containers or packaging may also be involved in the photostabilization strategies of the drugs [3]. When the pharmacokinetic behavior of a drug is not favorable and the absorption through the skin take too long, an active compound should be also protected after application, allowing a prolonged exposure to sunlight. In these cases, several approaches of encapsulation into supramolecular systems have been proposed, very often supported by the addition of antioxidants and solar filters [4-7]. In the pharmaceutical field, cyclodextrin (CD) complexes represent the most used encapsulation matrices to realize photoprotective carriers [8]. These cyclic oligosaccharides can incorporate lipophilic drugs into the hydrophobic cavities by non-covalent complexation [9]. Moreover, the variety of available CDs, both natives and modified, allows the incorporation of drugs with different size.

In this work, the light stability of Nabumetone (4-(6-methoxy-2-naphthyl)butan-2-one) (NA) was investigated in solution and gel formulations. Photoprotection of NA was performed after entrapping the drug into CD matrices. According to the ICH rules, the photodegradation tests were made in an appropriate standard irradiation chamber on drug solutions and CD complexes in solution and gel formulations.

The photodegradation profiles were monitored by spectrophotometry and the spectral data were processed by Multivariate Curve Resolution (MCR). This chemometric procedure was chosen because particularly suitable for following transformation kinetic processes as it is able to estimate spectra and concentration profiles of the components involved [10-13].

2. Materials and methods

2.1. Chemicals, Instruments and Software

NA, ascorbic acid (AA), propylene glycol, microcrystalline cellulose, βCD, mβCD, and hpβCD were purchased from Sigma-Aldrich (Milan, Italy). Ethanol and methanol were from J.T. Baker (Holland).

UV spectra were recorded by using a Perkin-Elmer Lambda 40P Spectrophotometer by setting the following instrumental conditions: λ range 200–450 nm, scan rate 1 nm/s; time response 1 s; spectral band 1 nm. Spectral acquisition and elaboration were made by using the dedicate software UV WinLab® (Perkin-Elmer, Waltham, MA).

A light cabinet Suntest CPS+ (Heraeus, Milan, Italy) equipped with a Xenon lamp was used to perform the photodegradation experiments. The ID65 standard filter was set to simulate sunlight in a spectral range between 300 and 800 nm.

Multivariate analysis was performed by the software Matlab® computer environment (Mathwork Inc., version 7).

2.2. Sample Preparation

NA standard solutions were prepared in ethanol at the concentration of 5.0 μg/ml in consideration of the low solubility of the drug in water. CD-complexes were prepared by dissolving an excess of NA (25 mg) in 10 ml of cyclodextrin solution (10mM) and 10.0 ml of Britton-Robinson buffer pH 6.57 (0.04 M phosphoric acid; 0.04 M acetic acid; 0.04 M boric acid; 0.2 M NaOH) under stirring for 20 h at 37° C. Four series of samples (4 x 5) were prepared by using βCD, mβCD, and hpβCD. All the samples were stored for 4 days at 4° C and then filtered through a 0.45 μm membrane. Spectrophotometric measurements were performed after dilution 1:10 of the samples in ethanol. For the solubility tests, the drug content was added to each cyclodextrin solution with concentrations of 1, 5, 7.5 and 10 μM in 10 ml buffer.

Gel formulation (20 g) was prepared according to the European Pharmacopoeia [14]. NA 0.20 g (1% w/w) was emulsified in propylene glycol 2 g under continuous stirring for 15 minutes. 0.60 g of microcrystalline cellulose (gelling agent) and 17.2 g of water were then added and the final emulsion was stirred for 50 min getting a homogeneous white gel.

The gel formulation containing the complex CD-drug was prepared by adding 17.2 g of the CD complex solution to propylene glycol and microcrystalline cellulose.

A last sample was prepared by adding AA to the CD-drug complex before the preparation of the gel, in such a way to obtain a percentage concentration of 2%.

2.3. Photodegradation test

The photodegradation tests were made on all the prepared liquid and gel formulations under the following conditions: irradiation power 450 W/m², corresponding to 27 kJ/m2 min,

temperature 25 °C. The samples were analysed just after preparation (t= 0 min) and at the several exposure times (10-30-50-70-100-130-150-210-270-300 min) by UV spectrophotometry. All laboratory experiments were carried out in a dark room to minimize drug photodegradation. The drug content in gel along the photodegradation experiments was measured by MCR applied to the UV data of the methanol extracts. At this aim, gel 0.5 g was uniformly stratified on a glass plate to form a layer thickness of 0.25 mm and then exposed to forced irradiation. After each irradiation dose, the glass plate was sonicated in acetonitrile 25 mL for 10 min at room temperature. 10 ml of the obtained suspension were centrifuged at 5000 rpm for 10 min and the supernatant was analysed after 1:10 dilution with methanol.

3. Results and discussion

3.1. Photodegradation of NA solutions
An ethanol solution of NA 5.0 μg/ml was subdued to forced photodegradation, under the standard conditions above reported. The spectra, depicted in Figure 1, were recorded just after the preparation and at several exposure times up to five hours.
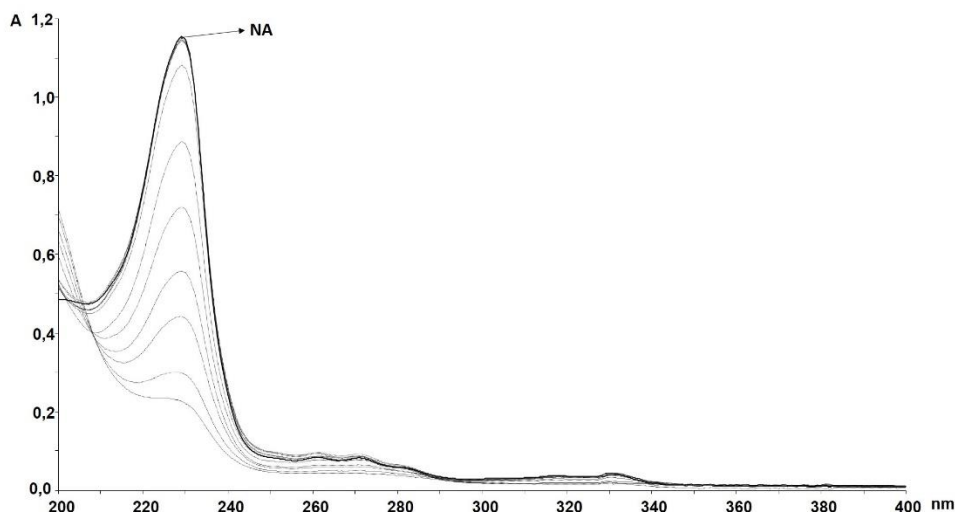
Figure 1. *Absorbance spectra recorded for the ethanol solution of NA at several exposure times.*

The spectral data, as an average of five experiments collected during the photodegradation tests, were used to construct the data matrix to be analysed by MCR-ALS. The results reported in Figure 2 showed the photodegradation profiles of NA and its photoproducts (A) and the respective absorbance spectra (B).
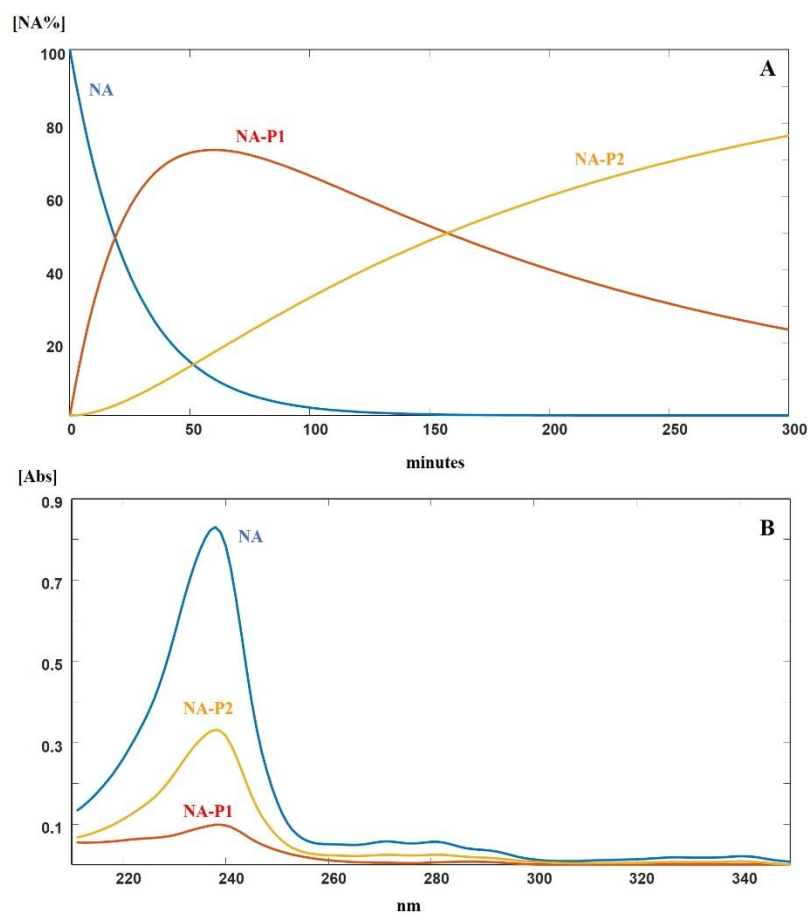
Figure 2. *Photodegradation profiles of NA and its photoproducts (A) and their absorbance spectra (B).*

In accordance with the results reported in the literature, data elaboration confirmed the formation of one major photoproduct (NA-P1) and traces of another by-product (NA-P2). [15] reported the photooxidation of the side chain to 6-methoxy-2-naphthaldehyde, as a major product, in butanol solution and the formation of the (4-(6-methoxy-2-naphthyl)-3-buten-2-one) (Figure 3).

NA

4-(6-methoxynaphthalen-2-yl)butan-2-one

NA-P1   **NA-P2**

6-methoxy-2-naphthaldehyde   (*E*)-4-(6-methoxynaphthalen-2-yl)but-3-en-2-one
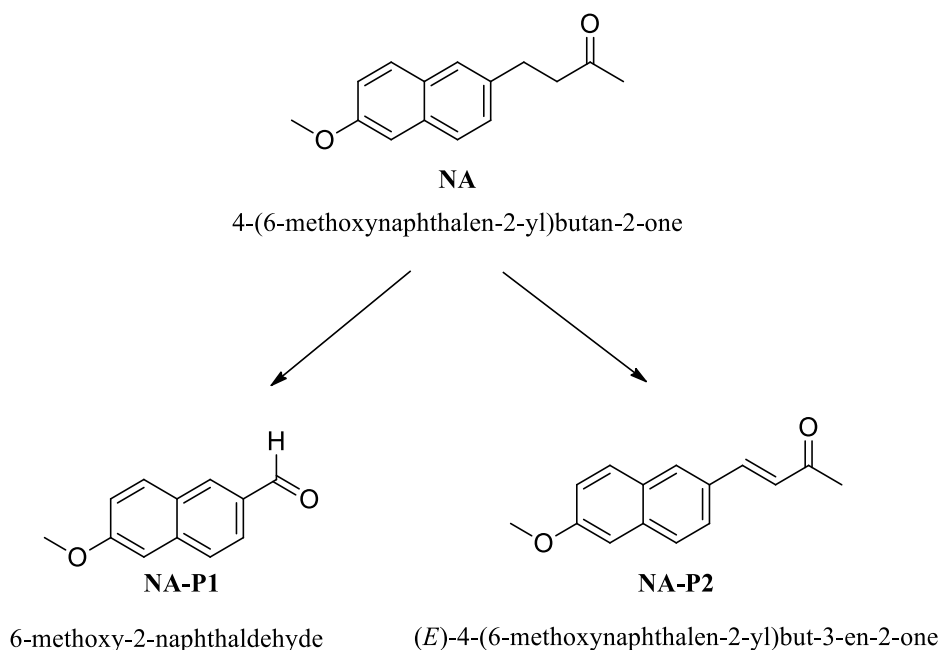
Figure 3. *Chemical Structures of NA and its photoproducts NA-P1 and NA-P2.*

This photodegradation process followed the first-order kinetics. In the used solvent, the process seemed to be more efficient than in water [16]. In our experiment, the full degradation of the drug was observed after about 30 min. The degradation process proceeded via first-order kinetics, described by the equation:

$$\ln [\%NA] = - k \cdot t + 4.6$$

where %NA was the percentage of residual drug, k the photodegradation rate constant, t the time (min), and 4.6 the logarithm of the starting concentration (100%).

The parameter $t_{0.1}$ (time to cause 10% degradation) was chosen as a criterion to compare the degradation behaviour of the tested samples. This parameter is conventionally adopted because a drug could no longer be used when its purity falls below 90%. The value of k was 0.0482 and $t_{0.1}$ resulted in being 2.08 min, as reported in Table 1.

Table 1. *Degradation kinetic parameters calculated for NA in different solutions*

Samples	Entrapment efficiency (%)	K x 10^{-3}	$t_{0.1}$ (min)	R^2
NA-free	-	48.2	2.08	0.999
NA-βCD	14	23.9	4.18	0.965
NA-mβCD	15	20.6	4.85	0.970
NA-hpβCD	88	4.20	23.8	0.987
NA-gel	-	23.4	4.27	0.977
NA- hpβCD gel	-	1.99	50.25	0.999
NA- hpβCD AA gel	-	1.11	90.09	0.922

In order to minimize light degradation, the stability of NA was investigated by entrapping the drug in cyclodextrin matrices. The CD systems can also enhance the solubility of the drugs in water. In fact, the influence of several cyclodextrins on the solubility of NA has been tested, as described by [17].

A set of NA aqueous solutions was prepared as above described by using βCD, mβCD, and hpβCD, respectively. The most effective cyclodextrin in increasing the solubility of NA resulted in being hpβCD. The incorporation percentage was measured by spectrophotometry as 88, 15 and 14% for hpβCD, mβCD and βCD, respectively. The best performance of hpβCD can be explained by a better fitting of the drug molecule in the cavity of this CD. All the prepared complexes were exposed to light. Figure 4 shows the photodegradation profiles of NA in the different CDs and Table 1 lists the kinetics parameters calculated by MCR.

All the used CDs increased the stability to light of the NA. In particular, the hpβCD-complex showed a $t_{0.1}$ value of 23.9 min, better than that for the simple solution but still unsatisfactory for the goals we had set.
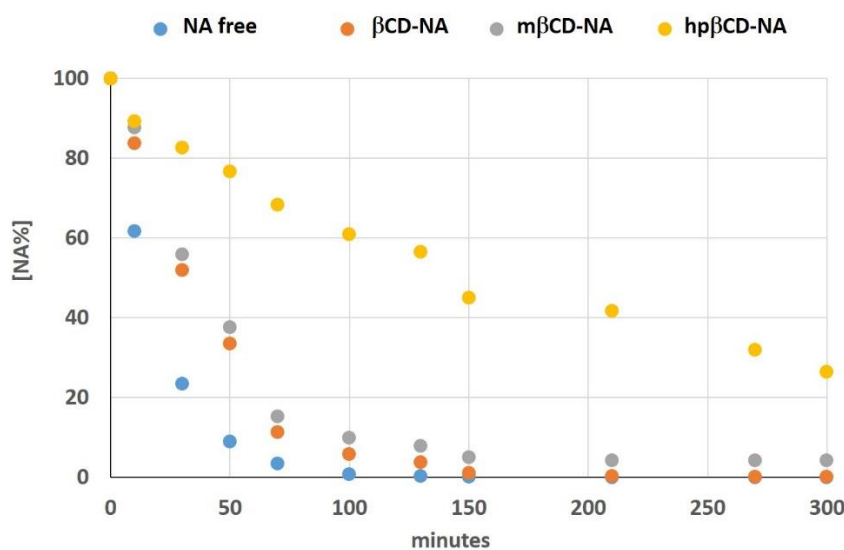
Figure 4. Photodegradation profiles of NA in the different CDs compared with the ethanol solution.

3.2. Photodegradation of NA in gel

Photodegradation tests were then applied to the above-described formulations prepared in gel. Firstly, gel formulation was made with 1% of the pure drug and exposed to light. The data obtained from the photodegradation experiments were processed by MCR method and the kinetics parameters are listed in Table 1. Also, in this formulation, the drug resulted very sensitive to light showing a $t_{0.1}$ value of 4.27 min.

A promising result was obtained when the complex hpβCD-NA was emulsified in gel. In this case, a clear decrease in NA degradation was measured, with a very successful $t_{0.1}$ value of 50.25 min. The good performance of this formulation in terms of photostabilization could be attributed to a dualaction of the CD complex: real physical protection of the entrapped drug by means of a molecular shield aided by the increase of the drug solubility in this matrix.

The light-stable formulation was optimized by adding the antioxidant ascorbic acid (2%) to the complex hpβCD-NA in gel, showing a very high increase of the stability with a $t_{0.1}$ value of 90.09 min. The photodegradation profile of this formulation hpβCD-NA-AA followed the first-order kinetics and was compared in Figure 5 to that of NA 1%, as gel control, and hpβCD-NA gel. Table 1 summarizes the degradation rate constants and the values of $t_{0.1}$ for all the studied matrices.
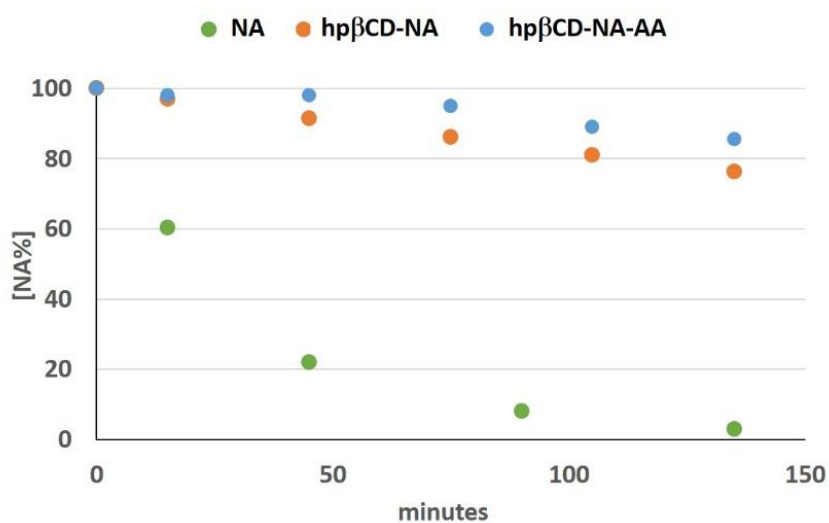
Figure 5. Photodegradation profiles of NA, hpβCD-NA complex and hpβCD-NA-AA formulated in gel.

4. Conclusions

In this work, the anti-inflammatory drug Nabumetone, either in solution or in gel formulations, was demonstrated to undergo photodegradation. The study was performed by adopting photostability tests defined by international rules. In particular, under an irradiance power of 350 W m^{-2}, corresponding to 21 kJ m^{-2} min and at a constant temperature of 25° C, the drug resulted degraded of 10% in only 2.08 and 4.27 min, in ethanol and gel, respectively. The design of photoprotective pharmaceutical matrices for topical application is particularly important due to the greater probability of light exposure that can cause a lower bioavailability of the drug and, at the same time, an increase of the risk of formation of toxic

photoproducts. The entrapping of the drug into cyclodextrins and the addition of an antioxidant agent was the adopted approach to reduce drug photodegradation. The addition of ascorbic acid to the hpβCD-NA gel complex gave good results with a considerable increase of the drug photostability, reaching a very satisfactory value of 90.09 min for $t_{0.1}$. The proposed system which has been shown to be particularly effective in reducing the photodegradation of the drug could be considered a valuable starting point for the development of innovative pharmaceutical formulations for topical use of Nabumetone.

References

[1] Tonnesen H H 2001 Formulation and stability testing of photolabile drugs *Int.J. Pharm.* 225 (1-2) 1-14.

[2] Baertschi S W, Clapham D, Foti C, Kleinman M H, Kristensen S, Reed R A, Templeton A C and Tonnesen H H 2015 Implications of In-Use Photostability: Proposed Guidance for Photostability Testing and Labeling to Support the Administration of Photosensitive Pharmaceutical Products *J Pharm. Sci.* Part 2: Topical Drug Product 104(9) 2688-2701.

[3] De Luca M, Ioele G, Spatari C and Ragno G 2016 Photostabilization studies of antihypertensive 1,4-dihydropyridines using polymeric containers *Int.J. Pharm.* 505(1-2) 376-382.

[4] Ragno G, Risoli A, Ioele G, Cione E and De Luca M 2006 Photostabilization of 1,4-dihydropyridine antihypertensives by incorporation into β-cyclodextrin and liposomes *J. Nanosci. Nanotechnol.* 6 2979-2985.

[5] Ragno G, Cione E, Garofalo A, Genchi G, Ioele G, Risoli A and Spagnoletta A 2003 Design and monitoring of photostability systems for amlodipine dosage forms *Int.J. Pharm.* 265(1-2) 125-132.

[6] Ioele G, De Luca M and Ragno G 2014 Photostability of barnidipine in combined cyclodextrin-in-liposome matrices *Future Med. Chem*. 6(1) 35-43.

[7] Ioele G, De Luca M, Garofalo A and Ragno G 2017 Photosensitive drugs: a review on their photoprotection by liposomes and cyclodextrins *Drug deliv.* 24 (sup1) 33-44.

[8] Coelho L, Almeida I F, Sousa Lobo J M and Sousa E S J P 2018 Photostabilization strategies of photosensitive drugs *Int. J. Pharm.* 541(1-2) 19-25.

[9] Scalia S, Casolari A., Iaconinoto A and Simeoni S 2002 Comparative studies of the influence of cyclodextrins on the stability of the sunscreen agent, 2-ethylhexyl-p-methoxycinnamate *J. Pharmaceut. Biomed.* 30(4) 1181-1189.

[10] Ragno G, Vetuschi C, Risoli A and Ioele G 2003 Application of a classical least-squares regression method to the assay of 1,4-dihydropyridine antihypertensives and their photoproducts *Talanta* 59 (2) 375-782.

[11] De Juan A, Rutan S C, Maeder M and Tauler R 2009 *Comp. Chem*. Vol. 2 (Oxford, U.K.: Elsevier) pp 207-558.

[12] De Luca M, Mas S, and Tauler R 2010 Kinetic studies of nitrofurazone photodegradation by multivariate curve resolution applied to UV-spectral data *Int.J. Pharm.* 386(1-2) 99-107.

[13] De Luca M, Tauler R, Ioele G and Ragno G 2013 Study of photodegradation kinetics of melatonin by multivariate curve resolution (MCR) with estimation of feasible band boundaries *Drug Test. Anal.* 5(2) 96-102.

[14] *Council of Europe,* 2010 *European pharmacopoeia* (Strasbourg, France: 9 th Edition).

[15] Valero M 2004 Photodegradation of Nabumetone in n-butanol solutions *J. Photochem. Photobiol. A: Chemistry* 163(1-2) 159-164.

[16] Valero M and Costa S M B 2003 Photodegradation of Nabumetone in aqueous solutions *J. Photochem. Photobiol. A: Chemistry* 157(1, 21) 93-101.

[17] Higuchi T and Connors K 1985 Phase solubility techniques *Adv. Anal. Chem. Instr.* 4 127-212.

II. GEL FORMULATION OF NABUMETONE AND A NEWLY SYNTHESIZED ANALOG: MICROEMULSION AS A PHOTOPROTECTIVE TOPICAL DELIVERY SYSTEM

Fedora Grande; Gaetano Ragno; Rita Muzzalupo; Maria Antonietta Occhiuzzi; Elisabetta Mazzotta; Michele De Luca; Antonio Garofalo; Giuseppina Ioele.

Department of Pharmacy, Health and Nutritional Sciences; University of Calabria, 87036 Rende (CS), Italy;

Abstract:

Photostability studies were performed on topical formulations containing the anti-inflammatory drug Nabumetone and an analog newly synthesized in order to achieve better photostability and pharmacokinetic profile. Stability tests, according to the International Conference on Harmonization rules, were applied on ethanol solutions and topical gel formulations of both compounds. The photodegradation profiles were monitored by Multivariate curve resolution applied to the UV spectral data. The inclusion of the compounds in microemulsion was investigated to improve light stability and, at the same time, to ensure a sustained release system for skin delivery. All the formulations in solution, gel, microemulsion, and microemulsion-in-gel were exposed to a forced irradiation of 350 W/m^2, corresponding to a 21 kJ/m^2 min, for up to 300 min.

Photostability increased significantly for both drugs in the liquid microemulsion and microemulsion-in-gel, compared to the ethanol solution and plain gel, reaching a residual drug of 97% and 98% for Nabumetone and analog in microemulsion-in-gel, respectively. Permeation experiments on the microemulsion-in-gel showed a better performance of the analog formulated at 0.2%, compared to the same formulation of Nabumetone at 0.7%. These results highlight the potential of the designed matrices as delayed drug delivery systems along with the use of lower drug doses leading to reduced side effects.

Keywords: anti-inflammatory drugs; nabumetone; photostability; microemulsion-in-gel; multivariate curve resolution.

1. Introduction

Nabumetone (4-(6-methoxy-2-naphthyl)butan-2-one) (NA), based on a 2,6-disubstituted naphthyl-alkanone structure, is a non-acidic nonsteroidal anti-inflammatory drug (NSAID) which is rapidly metabolized in the liver to the major active metabolite 6-methoxy-2-naphthyl acetic acid (6- MNA) [1]. The side effects of this drug are well known [2,3] as well as its sensitivity to light [4].

Actually, the photo-oxidation of the side chain to 6-methoxy-2-naphthaldehyde, as a major product, and the formation of the (4-(6-methoxy-2-naphthyl)-3-buten-2-one) have been already reported [4,5].

Photosensitivity represents an important limit throughout the various stages of production, storage and distribution as well as during clinical application, particularly in local skin formulations [6]. It seems necessary to develop new strategies aimed at preventing or

minimizing photodegradation of NA, also considering that the use of protective containers or packaging has proved to be insufficient to guarantee light stability [7–9].

For this aim, structural modifications on NA were attempted to improve drug stability and pharmacokinetics and reduce side effects. Accordingly, a new derivative A was designed in which the butanone chain was replaced by a condensed cyclic ketone moiety (Figure 1). This analog was designed considering the characteristics of the receptor binding-site, with the aid of computerassisted approaches, thanks to the availability of several data on the crystal structure of the cyclooxygenase-2 protein [10]. Furthermore, a calculated log P of 2.4 for compound A reflects a hydrophobicity adequate to allow good absorption and permeation after local administration [11].

NA

4-(6-methoxynaphthalen-2-yl)butan-2-one

A

7-methoxy-2,3-dihydro-1*H*-cyclopenta[*b*]naphthalen-1-one
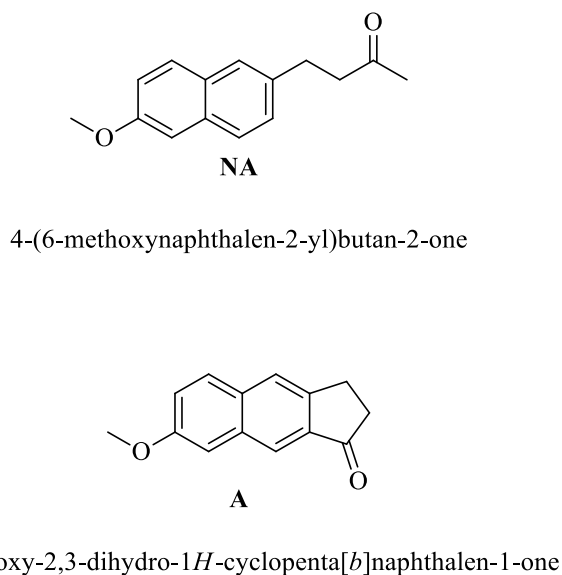
Figure 1. Chemical structures of Nabumetone (4-(6-methoxy-2-naphthyl)butan-2-one) (NA) and its analog A.

Furthermore, when the pharmacokinetics of a drug is not favorable and at the same time the absorption through the skin is slow, a system to protect the drugs from prolonged sun exposure after application should be designed. Some examples are proposed in the studies of incorporation into supramolecular systems, such as cyclodextrins, liposomes, and niosomes, often supported by the addition of antioxidants and solar filters [12–17]. Recent investigations suggest the use of microemulsions (ME) as dispersion systems to realize photoprotective carriers for drugs [18–20].

These systems are solutions optically isotropic and thermodynamically stable with droplet size in the submicron range. Usually, they consist of oil phase and aqueous phase with the addition of surfactants and cosurfactants. Some advantages offered by ME include high drug solubilisation capacity, enhancement of skin permeation for both hydrophobic and hydrophilic drugs, easy manufacturing, and a prolonged shelf life [21,22]. In 2018, the entrapping of NA in ME has been proposed by Jagdale et al. [23] to optimize transdermal micro-emulgel delivery of the drug for the treatment of arthritis.

In this work, the light stability of NA and its analog A were investigated in solution and gel formulations, according to the international International Conference on Harmonization (ICH) rules [24]. Photoprotection studies were performed by entrapping the compounds into liquid ME, solution and gel formulation (MEG). The photodegradation profiles of the species in the photodegradation experiments were monitored by UV spectrophotometry and

the spectral data were processed by Multivariate Curve Resolution (MCR). This chemometric procedure was chosen because particularly suitable to follow the kinetic processes of a chemical transformation, allowing to estimate spectra and concentration profiles of the components involved [25–30]. The delivering behavior of the novel gel formulations was investigated by ex-vivo permeation studies using rabbit ear skin and vertical Franz diffusion cells. The transdermal administration represents an attractive and accessible route for testing drug absorption overcoming problems associated with oral or parenteral administration, such as a low bioavailability due to first-pass metabolism.

Topical NSAIDs represent the main clinical device to treat the inflammatory status and are often used in the therapy of rheumatic and non-rheumatic diseases of the muscle-skeletal system, such as accidents during sport activities. The most important advantage of topical NSAIDs is the lack of serious adverse effects associated with systemic NSAIDs, particularly in elderly patients. Oral treatment with NSAIDs has been in fact associated with increased gastrointestinal (GI), renal, and cardiovascular toxicity [31]. Evidence indicates that topical formulations can achieve therapeutic drug concentrations in localized tissues by keeping serum drug levels low and potentially avoiding systemic toxicity [32]. In this context, the development of photostable formulations for topical use of newly synthesized NSAIDs could lead to the availability of drugs with effective biological activity, high stability, and reduced side effects.

2. Materials and methods

2.1. Chemicals, Instruments and Software

NA, propylene glycol, microcrystalline cellulose, Brij® 97, and isopropyl myristate were purchased from Sigma-Aldrich (Milan, Italy). Ethanol and methanol were from J.T. Baker (Deventer, Holland).

UV spectra were recorded by using a Perkin-Elmer Lambda 40P Spectrophotometer by setting the following instrumental conditions: λ range 200–450 nm, scan rate 1 nm/s; time response 1 s; spectral band 1 nm. Spectral acquisition and elaboration were made by using the dedicate software UV WinLab® (Perkin-Elmer, Waltham, MA, USA). A light cabinet Suntest CPS+ (Heraeus, Milan, Italy) equipped with a Xenon lamp was used to perform the photodegradation experiments. The ID65 standard filter was set to simulate sunlight in a spectral range between 300 and 800 nm. Multivariate analysis was performed by the software Matlab® computer environment (Mathwork Inc., version 7, Torino, Italy).

2.2. Chemistry

Compound A was prepared in good yield and high purity by polyphosphoric acid catalysed Friedel-Crafts intramolecular cyclization of 3-(6-methoxynaphthalen-2-yl)propanoic acid [33].

In detail, a mixture of 3-(6-methoxynaphthalen-2-yl)propanoic acid (100 mg, 0.43 mmol) and polyphosphoric acid (1 g) was heated to 110 °C for 1 h. After cooling, the mixture was poured into cold water and stirred for an additional 30 min before extraction with ethyl acetate. The organic layer was successively washed with $NaHCO_3$ saturated solution, water and brine then dried over magnesium sulfate. The evaporation of the solvent left a residue which was purified by column hromatography on silica gel (n-hexane/ethyl acetate 6:1, as eluent) to give 73 mg (79% yield) of pure compound A.

2.3. Sample Preparation

A calibration set, including ten standard one-component solutions of NA and A in ethanol in a concentration range of 0.5–10.0 µg/mL, was prepared and used to establish the mathematical relationships between concentration and respective analytical signals. Thus, different MCR procedures were applied to the spectrophotometric data of these solutions. A set of five ethanol solutions (prediction set) containing NA or A in the same concentration range used for the calibration set, was prepared in order to apply the analytical methods defined and used to calculate statistical effectiveness of the methods in terms of accuracy and precision. A last set of diluted solutions was prepared to measure the Limit of Detection (LOD) and the Limit of Quantitation (LOQ) of the chemometric procedures in calculating the concentration of NA and A in all the samples.

Photodegradation test was performed on standard solutions of NA and A, prepared in ethanol at the concentration of 5.0 µg/mL, in consideration of the low solubility of the compounds in water.

According to the European Pharmacopoeia procedures [34], gel formulation (20 g) of both compounds were prepared by emulsifying the drug 0.20 g (1% *w/w*) in propylene glycol 2 g under continuous stirring for 15 min. 0.60 g of microcrystalline cellulose (gelling agent) and 17.2 g of water were then added, and the final emulsion was stirred for 50 min getting a homogeneous white gel.

ME composition was established by considering the ternary diagram phase Brij 97—isopropyl myristate-H_2O, in absence of a cosurfactant, as reported by Wang et al. [35]. In this diagram, five single-phase regions are identified, in which two regions correspond to sotropic solution phases, one is an anisotropic lamellar liquid crystalline phase, one is an anisotropic hexagonal liquid crystalline phase and one is an isotropic micellar cubic liquid crystalline phase. In consideration of the used water content, between 65.5 and 90.5 wt. %, the prepared ME is an isotropic solution phase, i.e., an O/W microemulsion [36,37]. In the first step, the oil phase (isopropyl myristate, 0.25 g) and the Brij 97 surfactant (0.95 g) were mixed and heated at 70 °C for 3 min. The drug was solubilized in this mixture and then added to water (3.80 g) dropwise. Finally, the samples were subjected to several centrifugation cycles at 3500 rpm for 10 min, followed by 4 min of vortex mixing at 2200 rpm. The formation of ME was confirmed by the appearance of a clear and transparent isotropic solution. The final drug concentration in ME formulation was 0.7 wt. %.

In order to make ME suitable for topical application, it was incorporated into a gel matrix (MEG).

The formulation was prepared by the following procedure: 4.46 g of drug-ME were added to 0.65 g of propylene glycol and 0.15 g of cellulose and stirred magnetically up to 15 min to get an opalescent homogenous gel.

2.4. Size and Distribution Analysis

The mean diameter of the micro-emulsion oil droplets was measured by dynamic light scattering (DLS) using a 90 Plus Particle Size Analyzer (Brookhaven Instruments Corporation, New York, NY, USA) at 25.0 ± 0.1 °C. Before measurement, micro-emulsions were appropriately diluted in distilled water and the results were directly obtained from instrument data fitting through the inverse "Laplace transformation" and the Contin methods [38]. The polydispersity index (PDI) was used as a measure of the width of size distribution. The PDI values lower than 0.3 indicated a homogenous population for colloidal systems. All the measures were done in triplicate and expressed as mean ± standard deviation.

2.5. Photodegradation Test

The photodegradation tests were made on all the prepared liquid and gel formulations under the following conditions: irradiation power 350 W/m2, corresponding to 21 kJ/m2 min, temperature 25 °C. The samples were analyzed just after preparation (t = 0 min) and at several exposure times (10, 30, 50, 70, 100, 130, 150, 210, 270, 300 min) by UV spectrophotometry. All laboratory experiments were carried out in a dark room to minimize additive light interferences.

Drug content in liquid samples was calculated by MCR applied on the UV spectral data recorded along the photodegradation experiments. MCR methods were previously elaborated on the NA and A ethanol solutions (calibration sets) prepared as above described. The robustness of the chemometric methods was determined by predicting the concentration of other five samples prepared in the same concentration range (prediction set). The parameter lack of fit (% lof), used to indicate the fit quality of the MCR results, was below 5% in all the experiments. LOD was calculated to be 0.0081 and 0.0093 µg/mL for NA and A, respectively. LOQ was in the range 0.078–14.3 µg/mL for NA and 0.089–13.5 µg/mL for A.

ME formulations were previously diluted with ethanol to obtain a drug concentration of 5 µg/mL at zero time. Gel formulations (0.5 g) were uniformly stratified on a glass plate to form a layer thickness of 0.25 mm and then exposed to forced irradiation. After each irradiation dose, the glass plate was sonicated in acetonitrile 25 mL for 10 min at room temperature. Then, 10 mL of the obtained suspension was centrifuged at 5000 rpm for 10 min and the supernatant was analyzed after 1:10 dilution with methanol.

2.6. Ex-Vivo Permeation Studies

Ex-vivo permeation studies were carried out using rabbit ear skin obtained from local slaughterhouse and vertical diffusion Franz cells for 7 h at 37 °C. This temperature value was selected according to the results reported in literature [39,40]. The receptor solutions were maintained at 37 °C in order to assure a temperature of skin surface loaded in diffusion cell in the range 32–35 °C.

The skin, previously frozen at −18 °C, was pre-equilibrated in physiological solution at room temperature for 2 h before the experiments. A circular piece of skin was placed between the receptor and donor compartment with the dermal side in contact with the receiver medium and the epidermis side in contact with the donor chamber (contact area = 0.416 cm^2). The donor compartment was charged with an appropriate volume of sample to keep constant the drug molar concentration in particular, the amount of drug loaded in the donor compartment was 1.00×10^{-6} moles for the samples containing 0.2% of drug and 2.98×10^{-6} moles for the ones at 0.7%. The receptor compartment was filled with 5.5 mL of fresh hydroalcoholic solution (water:ethanol 1:1), maintained at 37 ± 0.5 °C and stirred by a magnetic bar. At regular time points up to 7 h, the receptor solution was removed for analysis and replaced with an equal volume of a pre-thermostated (37 ± 0.5 °C) fresh one.

The drug content in the samples was calculated by spectrophotometry. Each experiment was carried out in triplicate and the results agreed within ± standard deviation.

3. Results

3.1. Micro-emulsion characterization

Incorporation of the drugs into ME was set at 0.2% due to the limited solubility of A. However, a further formulation with 0.7% NA concentration was needed to reach a comparable permeation rate through the skin.

ME loaded with NA or A appeared as an isotropic and translucent solution. According with the results provided by Ingvar Danielsson and Bjorn Lindman in 1981, the prepared ME is a mixture of water, oil and surfactant resulting in an liquid isotropic system, fluid, transparent and thermodynamically stable [41]. Actually, the samples were very stable, similar size and PDI and no sedimentation, creaming or flocculation were observed for 6 months. The average oil droplet size, diameter in the range 13–23 nm, and the polydispersity index of micro-emulsions are reported in Table 1, after 1 day and six months from preparation. The loading of the drug 0.2% resulted in a decrease of mean oil droplet size, whereas the same trend was not observed in the 0.7% formulation.

This behavior was probably due to the drug which at low concentrations acts as an emulsifying agent capable of reducing the oil droplet size, as described in a previous work [42]. The polydispersity index of the samples was in the range between 0.153 and 0.214, indicating a narrow oil droplet size distribution and, consequently, that the formulations had relatively homogenous dimensions.

Table 1. Oil droplet size and polydispersity index (PDI) of NA and A in a microemulsions (ME) at different drug concentrations, after 1 day and 6 months after preparation, at 25 °C. Values are expressed as mean ± S.D. (n = 3).

Samples	Diameter Droplet (nm)	PDI	Diameter Droplet (nm)	PDI
	After 1 day		After 6 months	
ME	20.16 ± 1.70	0.214	20.87 ± 1.05	0.223
NA-ME 0.2%	13.17 ± 0.50	0.158	13.01 ± 0.65	0.163
NA-ME 0.7%	23.64 ± 3.21	0.169	24.52 ± 2.74	0.175
A-ME 0.2%	13.71 ± 0.32	0.153	13.54 ± 0.45	0.162

3.2. Photodegradation of Liquid Formulations

The ethanol solutions of the compounds at a concentration of 5.0 mg/mL were subjected to forced photodegradation, under the conditions above reported. The spectra, shown in Figure 2, were recorded just after the preparation and at several exposure times up to 300 min.
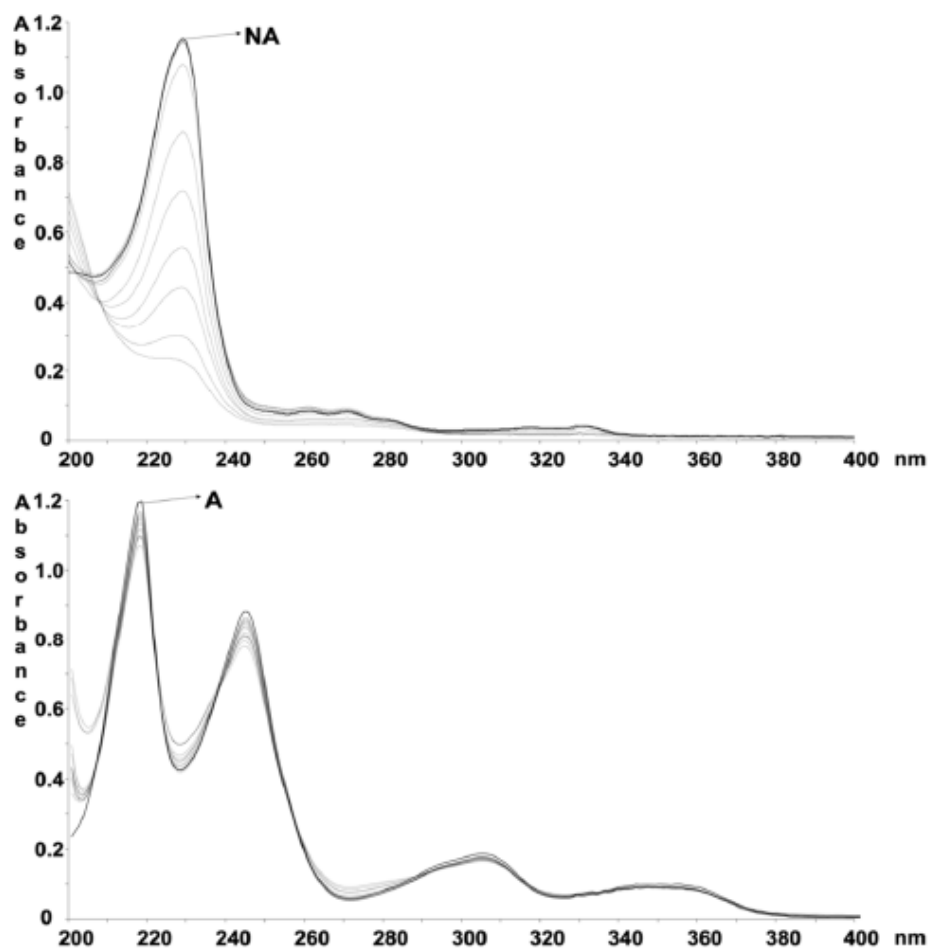
Figure 2. *Absorbance spectra recorded on the ethanol solution of NA and A at the following exposure times: 0, 10, 30, 50, 70, 100, 130, 150, 210, 270, 300 min.*

The spectral data, as averages collected during five photodegradation experiments, were used to build the data matrix to be analyzed by MCR. All the measured relative standard deviation values fell within the range: 1.36%–4.79%. Figure 3 showed the photodegradation profiles of NA and A and the predicted absorbance spectra of their photoproducts.
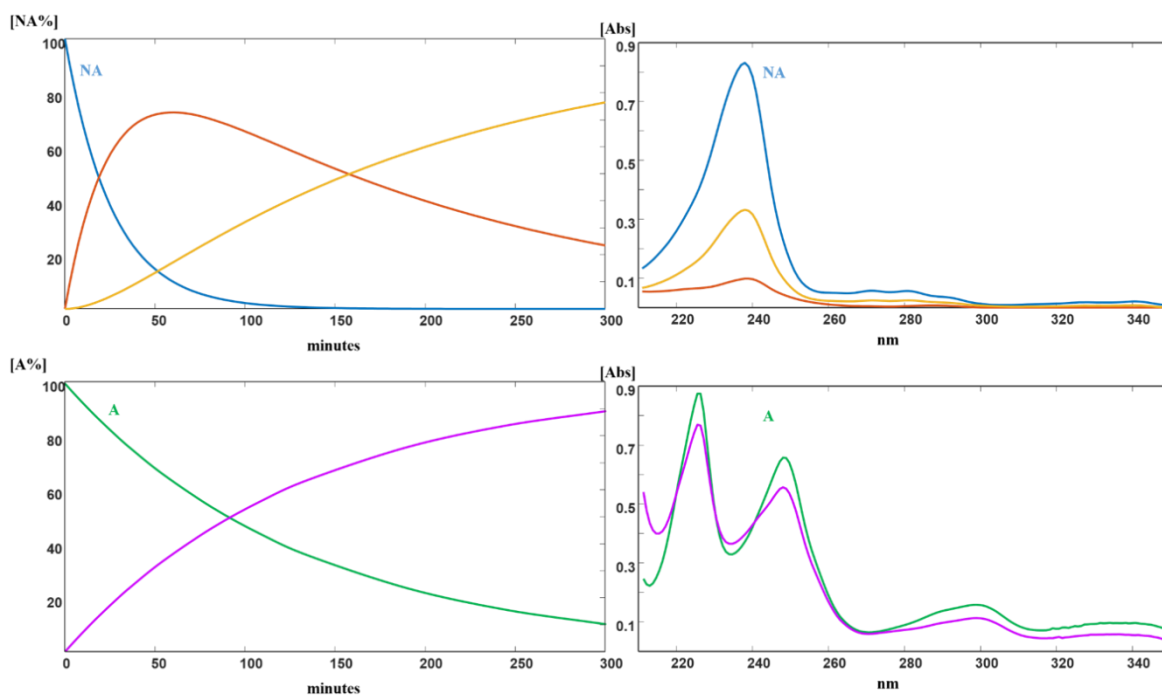
Figure 3. *Photodegradation of NA and A: kinetic profiles and absorbance spectra of the pure compounds and respective photodegradation products.*

The degradation process proceeded via a first-order kinetics described by the Equation:

$$\ln[\%DRUG]=-kt + 4.6 \qquad (1)$$

where % DRUG was the percentage of residual drug, k the photodegradation rate constant, t the time (min), and 4.6 the logarithm of the starting concentration (100%). The parameters $t_{0.1}$ (time to cause 10% degradation) and $t_{0.5}$ (time to cause 50% degradation) were used to compare the degradation behavior of the tested formulations.

ME formulations of each drug were prepared as above described and subdued to photodegradation test. The kinetic profiles were calculated also in these experiments. Table 2 lists the kinetics parameters calculated for both compounds in solution and ME liquid formulations.

Table 2. *Degradation kinetic parameters calculated for NA and A in different samples.*

Samples		$K \times 10^{-3}$	$t_{0.1}$ (min)	$t_{0.5}$ (min)	R^2
NA liquid formulations	NA-free	48.2	2.08	14.31	0.999
	NA-ME	0.20	500.95	-	0.910
NA semisolid formulations	NA-gel 0.2%	23.4	4.27	29.49	0.977
	NA-gel 0.7%	22.9	4.37	30.56	0.985
	NA-MEG	0.005	-	-	0.947
A liquid formulations	A-free	6.9	14.49	100.00	0.903
	A-ME	0.2	500.00	-	0.945
A semisolid formulations	A-gel	2.6	38.46	265.40	0.951
	A-MEG	0.07	-	-	0.924

3.3. Photodegradation of Gel Formulations

Photodegradation tests were applied on the gel formulations prepared as above described. Gel formulations were made with 0.2 and 0.7% of pure NA and 0.2% of pure A. All the prepared systems were exposed to light.

The stability of the compounds was also investigated by preparing the ME-drug in gel with 0.2% of the drug. The data obtained from the photodegradation experiments were processed by MCR and the kinetics parameters were calculated. The photodegradation profiles of these formulations followed a first-order kinetics. Table 2 summarizes the degradation rate constants and the values of $t_{0.1}$ and $t_{0.5}$ for the tested matrices. In Figure 4, the photodegradation profile of all the ME and MEG formulations were compared with the ethanol solutions and plain gels for NA and A, respectively.
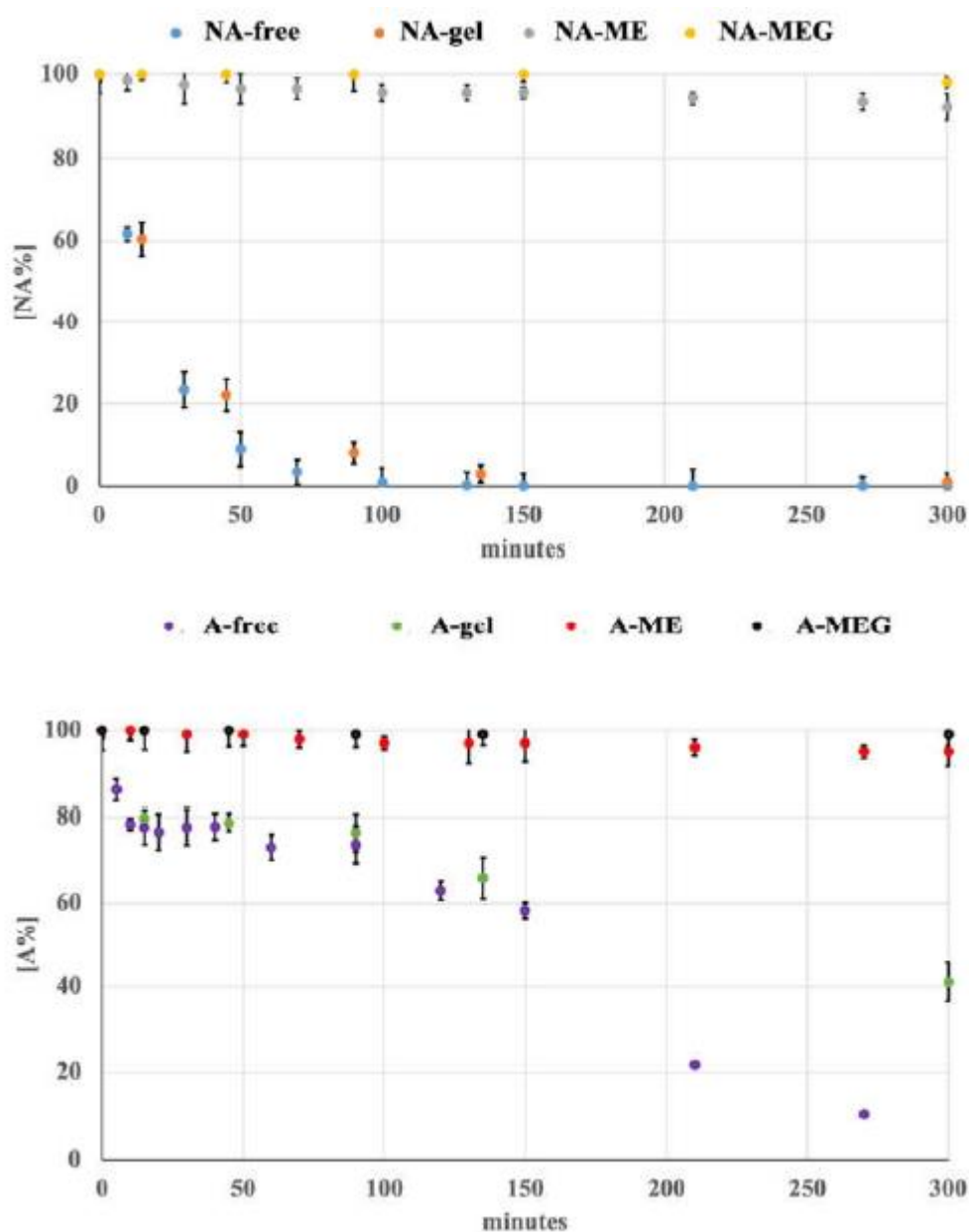
Figure 4. Photodegradation profiles of NA and A in all the tested formulations.

3.4. Ex-Vivo Permeation Studies

In order to evaluate the influence of the different formulations on the drug skin permeation, ex-vivo percutaneous experiments were carried out using a Franz cell diffusion system. The cumulative amounts of NA and its analog A permeated across rabbit ear skin were plotted as a function of time and reported in Figure 5a,b, respectively. Both drugs were able to permeate rabbit ear skin *in vitro* and the cumulative amount of permeated drug increased with the time for all the samples.
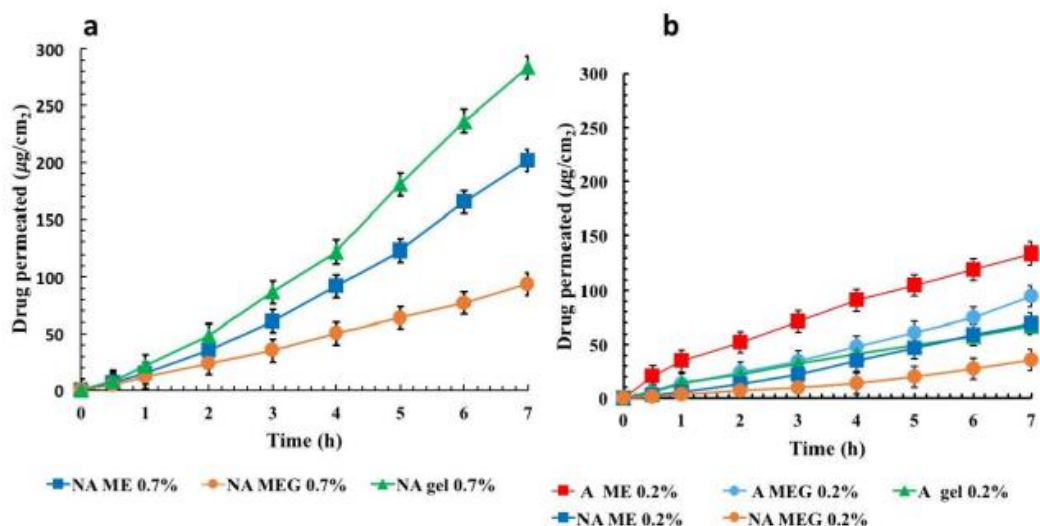
Figure 5. *Cumulative amount of NA (a) and A (b) permeated from different samples through rabbit ear skin at 37 °C: ME (■), MEG (●), plain gel (▲) (mean ± SD; n = 3).*

The skin delivery performance of the different samples was also compared and the results are summarized in Figure 6.

Figure 6. *Amount of drug permeated across rabbit ear skin from different samples after 7 h at 37 °C. Values represent means ± S.D. (n = 3).*

The calculated percentages for the applied dose after 7 h were 30.11%, 21.3%, and 15.16% for AME 0.2%, A-MEG 0.2%, and A gel 0.2%, respectively and 8.35%, 12.30%, and 17.33 % for NA-MEG 0.7%, NA-MEG 0.7%, and NA gel 0.7%.

4. Discussion

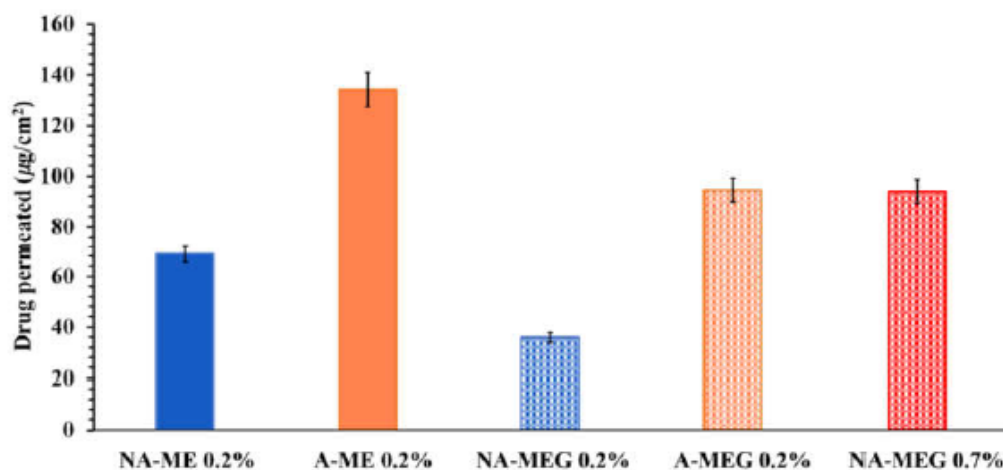In this work, photostability of NA was investigated in liquid and gel formulations. In accordance with the results reported in literature [4,5], the obtained data confirmed the formation of 6-methoxy-2-naphthaldehyde as the major photoproduct and traces of a second by-product, as depicted in Figure 3. When the liquid formulation of NA was exposed in a light cabinet to an irradiance power of 350 W/m^2, a full degradation of the drug was observed after about 30 min. The value of k was 0.0482 and $t_{0.1}$ resulted to be 2.08 min, as reported in Table 2. The gel formulation of the drug containing 0.2% and 0.7% of pure NA also resulted very sensitive to light in both concentrations, showing a rapid degradation of the drug with $t_{0.1}$ values of 4.27 and 4.37 min, respectively. Even in these cases, the formation of the same photoproducts was verified by MCR elaboration.

The photoprotection of the drug was achieved by adopting two different strategies. Firstly, a new analog (A) of NA was designed and synthesized to improve both drug stability and pharmacokinetic profile. NA is a prodrug, which is gradually metabolized to the active metabolite 6-MNA, a quite selective cyclo-oxygenase-2 inhibitor. This drug, as other NSAIDs, exerts analgesic, anti-inflammatory, anti-platelet aggregation and antipyretic activity. Due to its prolonged half-life (up to 74 h), that allows a once-daily administration, NA is one of the most used remedies to reduce pain and inflammation in patients affected by rheumatoid arthritis or osteoarthritis. After the metabolic transformation of NA, 6-MNA does not enter enterohepatic circulation. On the other hand, still active glucuronide-conjugated metabolites are excreted in urine and are present in remarkable amounts in the synovial fluid, which represents the site of action of agents used in the treatment of chronic inflammatory rheumatic diseases [43].

In view of the NA metabolic transformation and photostability profile, showing the formation of active 6-MNA and 6-methoxy-2-naphthaldehyde, respectively, the new analog A was synthesized by including part of the too light-sensitive linear side chain in an additional fused ring. This alteration should enhance light stability, while maintaining the capability to undergo metabolic activation.

Accordingly, a putative mechanism for the Cytochrome P450-catalyzed activation of A is proposed in Figure 7. Similarly to what reported for NA [44,45], compound A would be subjected to oxidative transformation giving rise to the active metabolite 2-(6-methoxynaphthalen-2-yl) acetic acid after a successive double cleavage carbon-carbon bonds, by the release of carbon dioxide [46].
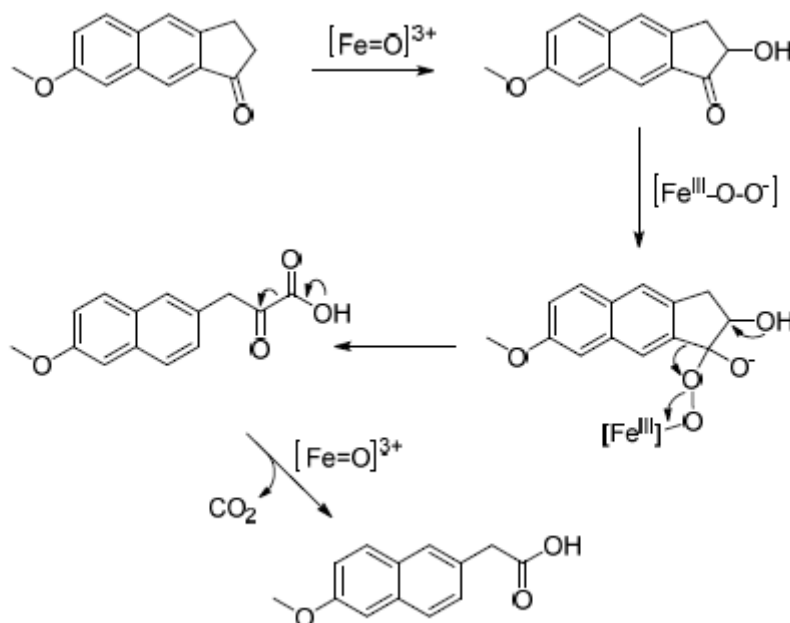
Figure 7. Hypothetic mechanism for the Cytochrome P450-catalyzed metabolism of A.

As expected, the liquid and gel formulation (0.2%) of A showed a far greater light stability than NA, with $t_{0.1}$ values of 14.49 and 38.46 min (2.08 and 4.27 for NA). MCR elaboration (Figure 3), applied on the ethanol solution of A, showed the formation of one photoproduct and a degradation of 50% after about 100 min of light exposure. This photodegradation profile was confirmed also for the gel formulation with a $t_{0.5}$ value of 265.4 min.

After these experiments, which accounted for an overall higher light stability of A, a second strategy to further stabilize the two drug molecules was designed. Accordingly, NA and A were included into suitable protective incorporation systems. The interest of pharmaceutical industry in the design of novel dosage formulations for photosensitive drugs has clearly increased over the last years. The drug incorporation in ME or MEG represents a good approach to increase drug stability and, at once, ensure optimal permeation across the skin. These systems have shown interesting and attractive advantages like high thermodynamic stability, ability to deliver both hydrophilic and lipophilic drug, increase of drug solubility and, not least, a photoprotective capability.

The tested compounds showed a clear decrease of degradation, with a very successful $t_{0.1}$ value of about 500 min in both ME formulations. In addition, when these light-stable formulations were incorporated in gel, complete photoprotection of the drugs was observed, as depicted in Figure 4.

The percutaneous permeation profiles of the photo-stable formulations were thus investigated using Franz diffusion cells systems. As expected, skin permeation of both NA and A by MEG appeared delayed when compared to that obtained by liquid ME. Indeed, the high viscosity of the polymeric network commonly slows the drug diffusion but makes ME suitable for topical use. Different trends related to permeation through the skin were observed for NA and A. In the case of NA, skin permeation through ME systems was lower than the plain gel, which was used as control. It can be assumed that NA located in the inner phase of ME must firstly be partitioned between the oil droplets and the continuous aqueous phase and then on the skin. This led to a delayed drug permeation and higher drug retention capacity compared to plain gel, where the NA is only embedded into polymeric network and so more available. This confirmed the previous results reported in the literature: ME may control and prolong the NA release and create drug reservoir into the skin from which the

drug is released slowly for a long time [42]. Such a behavior suggests that the designed formulations could be used as long-lasting delivery systems of drugs. The creation of a drug reservoir into the skin can reduce the frequency of applications, thus improving patient compliance.

Concerning A, the permeation by ME and MEG was always higher than that obtained with plain gel. Therefore, ME would act as a percutaneous permeation enhancer. This effect could be explained by the different affinity of the drug with the internal phase of ME [47].

As previously mentioned, the chemical modification reduced the hydrophobicity of A and limited its concentration in the ME formulation to a maximum 0.2%. So, the lower hydrophobicity of A influenced its solubility in the external phase and consequently the thermodynamic activity [48], which is the strength of a drug to move from formulation to skin [22]. The compound A probably diffuses more quickly from internal phase to outer phase and, consequently, shows a better partitioning inside the stratum corneum. On the other hand, NA reached a comparable permeation rate at a concentration of 0.7%, so demonstrating that the designed chemical alteration resulted favorable.

As shown in Figure 6, the permeation of A both from ME and MEG 0.2% was found, respectively, 1.94 and 2.64 higher than that obtained for NA. Moreover, a permeation rate of A 0.2% in MEG after 7 h (94.46 $\mu g/cm^2$) was comparable with that recorded for NA 0.7% in the same system (93.87 $\mu g/cm^2$), confirming a better performance of the new compound. This makes possible the use of lower drug doses avoiding more toxic effects.

5. Conclusions

The anti-inflammatory drug Nabumetone, through tests defined by international rules, has been confirmed to undergo extensive photodegradation in both solution and gel formulation. When subjected to an irradiation power of 350 W/m^2, corresponding to 21 kJ/m^2 min, and at a constant temperature of 25 °C, the drug resulted in degradation of 10% in only 2.08 and 4.27 min, in ethanol and gel, respectively. The properties of a new analog A, potentially endowed with higher lightstability and a more favorable pharmacokinetic profile, have been also investigated. Photoprotection approaches have been studied to realize topical light-stable formulations for both compounds, including entrapment into microemulsions. A very satisfactory time of 500 min to detect 10% degradation and an almost complete photoprotection was achieved for both compounds when their microemulsion was included in gel. The obtained results clearly suggest that the proposed microemulsions and microemulsion-in-gel as topical dosage form of Nabumetone may be potentially useful as a long-lasting drug delivery system and could be extended to the analog A for a potential transdermal use of this molecule. The overall data demonstrated that the developed formulations are effective for a controlled topical delivery of the tested compounds and that this approach could be extended for the preparation of innovative local or systemic pharmaceutical formulations.

References

[1] Nobilis, M.; Mikusek, J.; Szotakova, B.; Jirasko, R.; Holcapek, M.; Chamseddin, C.; Jira, T.; Kucera, R.; Kunes, J.; Pour, M. Analytical power of LLE-HPLC-PDA-MS/MS in drug metabolism studies: identification of new nabumetone metabolites. J. Pharmaceut. Biomed. 2013, 80, 164–172.

[2] Blumenthal, K.G.; Lai, K.H.; Huang, M.; Wallace, Z.S.; Wickner, P.G.; Zhou, L. Adverse and Hypersensitivity Reactions to Prescription Nonsteroidal Anti-Inflammatory Agents in a Large Health Care System. J. Allergy Clin. Immunol. Pract. 2017, 5, 737–743.

[3] Kawisha, S.M.; Ahmeda, S.; Gull, A.; Aslam, M.; Pandit, J.; Aqil, M.; Sultana, Y. Development of nabumetone loaded lipid nano-scaffold for the effective oral delivery; optimization, characterization, drug release and pharmacodynamic study. J. Mol. Liq. 2017, 231, 514–522.

[4] Valero, M. Photodegradation of Nabumetone in n-butanol solutions. J. Photoch. Photobio. A 2004, 163 159– 164. 5.

[5] Valero, M.; Costa Brito, S. Photodegradation of Nabumetone in aqueous solutions. J. Photoch. Photobio. A 2003, 157, 93–101.

[6] Tonnesen, H.H. Formulation and stability testing of photolabile drugs. Inter. J. Pharm. 2001, 225, 1–14.

[7] Coelho, L.; Almeida, I.F.; Sousa Lobo, J.M.; Sousa, E.S.J.P. Photostabilization strategies of photosensitive drugs. Inter. J. Pharm. 2018, 541, 19–25.

[8] Ioele, G.; Tavano, L.; Luca, M.; Muzzalupo, R.; Mancuso, A.; Ragno, G. Light-sensitive drugs in topical formulations: stability indicating methods and photostabilization strategies. Future Med. Chem. 2017, 9, 1795–1808.

[9] De Luca, M.; Ioele, G.; Spatari, C.; Ragno, G. Photostabilization studies of antihypertensive 1,4-dihydropyridines using polymeric containers. Inter. J. Pharm. 2016, 505, 376–82

[10] Fiorucci, S.; Antonelli, E. Cyclo-oxygenase isoenzymes. Structural basis for selective inhibition of cyclooxygenases by anti-inflammatory agents. Dig. Liver Dis. 2001, 33 (Suppl. 2), S2–S7. Organic Chemistry Portal. Available online: https://www.organic-chemistry.org/prog/peo/cLogP.html (accessed on 11 February 2019).

[11] Organic Chemistry Portal. Available online: https://www.organic-chemistry.org/prog/peo/cLogP.html (accessed on 11 February 2019).

[12] Ragno, G.; Risoli, A.; Ioele, G.; Cione, E.; De Luca, M. Photostabilization of 1,4-dihydropyridine antihypertensives by incorporation into beta-cyclodextrin and liposomes. J. Nanosci. Nanotechnol. 2006, 6, 2979–2985.

[13] Ioele, G.; De Luca, M.; Ragno, G. Photostability of barnidipine in combined cyclodextrin-in-liposome matrices. Future Med. Chem. 2014, 6, 35–43.

[14] Ioele, G.; De Luca, M.; Garofalo, A.; Ragno, G. Photosensitive drugs: A review on their photoprotection by liposomes and cyclodextrins. Drug Deliv. 2017, 24, (Suppl. 1), 33–44.

[15] Ioele, G.; De Luca, M.; Tavano, L.; Ragno, G. The difficulties for a photolabile drug in topical formulations: the case of diclofenac. Inter. J. Pharm. 2014, 465, 284–290.

[16] Ioele, G.; Tavano, L.; De Luca, M.; Ragno, G.; Picci, N.; Muzzalupo, R. Photostability and ex-vivo permeation studies on diclofenac in topical niosomal formulations. Inter. J. Pharm. 2015, 494, 490–497.

[17] Ioele, G.; Gunduz, M.G.; Spatari, C.; De Luca, M.; Grande, F.; Ragno, G. A New Generation of Dihydropyridine Calcium Channel Blockers: Photostabilization of Liquid Formulations Using Nonionic Surfactants. Pharmaceutics 2019, 11, 28.

[18] Vicentini, F.T.; Fonseca, Y.M.; Pitol, D.L.; Iyomasa, M.M.; Bentley, M.V.; Fonseca, M.J. Evaluation of protective effect of a water-in-oil microemulsion incorporating quercetin against UVB-induced damage in hairless mice skin. J. Pharm. Pharm. Sci. 2010, 13, 274–285.

[19] Patel, M.R.; Patel, R.B.; Parikh, J.R.; Patel, B.G. Improving the isotretinoin photostability by incorporating in microemulsion matrix. ISRN Pharm. 2011, 2011, 838016.

[20] Xia, L.; Zhongxiao, C.; Zhihao, L.; Xiaodong, M.; Ming, X.; Yan, T.; Xinyi, Z.; Bingqing, X.; Jianbin, Z.; Zeyao, T. Improvement of the solubility, photostability, antioxidant activity and UVB photoprotection of transresveratrol by essential oil based microemulsions for topical application. J. Drug Deliv. Sci. Technol. 2018, 48, 346–354.

[21] Nastiti, C.; Ponto, T.; Abd, E.; Grice, J.E.; Benson, H.A.E.; Roberts, M.S. Topical Nano and Microemulsions for Skin Delivery. Pharmaceutics 2017, 9, 37.

[22] Goswami, P.; Choudhury, A.; Kumar, D.B. Microemulsion -A Potential Carrier for Improved Bioavailability. Intern. J. Pharm. Biol. Sci. Arch. 2019, 10, 69–77.

[23] Jagdale, S.C.; Deore, G.K.; Chabukswar, A.R. Development of Microemulsion Based Nabumetone Transdermal Delivery for Treatment of Arthritis. Recent Pat. Drug Deliv. Formul. 2018, 12, 130–149.

[24] ICH harmonized tripartite guideline, Federal Register. Photostability testing of new drug substance and products. European Medicines Agency: London, UK, 1997; Volume 62.

[25] De Luca, M.; Mas, S.; Ioele, G.; Oliverio, F.; Ragno, G.; Tauler, R. Kinetic studies of nitrofurazone photodegradation by multivariate curve resolution applied to UV-spectral data. Inter. J. Pharm. 2010, 386, 99–107.

[26] De Luca, M.; Tauler, R.; Ioele, G.; Ragno, G. Study of photodegradation kinetics of melatonin by multivariate curve resolution (MCR) with estimation of feasible band boundaries. Drug Test. Anal. 2013, 5, 96–102.

[27] De Luca, M.; Ragno, G.; Ioele, G.; Tauler, R. Multivariate curve resolution of incomplete fused multiset data from chromatographic and spectrophotometric analyses for drug photostability studies. Anal. Chim. Acta. 2014, 837, 31–7.

[28] De Luca, M.; Ioele, G.; Mas, S.; Tauler, R.; Ragno, G. A study of pH-dependent photodegradation of amiloride by a multivariate curve resolution approach to combined kinetic and acid-base titration UV data. Analyst 2012, 137, 5428–5435.

[29] Dinç, E.; Ragno, G.; Baleanu, D.; De Luca, M.; Ioele, G. Fractional Wavelet Transform–Continous Wavelet Transform for the Quantification of Melatonin and Its Photodegradation Product. Spectrosc. Lett. 2012, 45, 337–343.

[30] Ragno, G.; Vetuschi, C.; Risoli, A.; Ioele, G. Application of a classical least-squares regression method to the assay of 1,4-dihydropyridine antihypertensives and their photoproducts. Talanta 2003, 59, 375–382.

[31] McPherson, M.L.; Cimino, N.M. Topical NSAID formulations. Pain Med. 2013, 14 (Suppl. 1), S35–S39. 32. Makris, U.E.; Kohler, M.J.; Fraenkel, L. Adverse effects of topical nonsteroidal antiinflammatory drugs in older adults with osteoarthritis: A systematic literature review. J. Rheumatol. 2010, 37, 1236–1243.

[32] Makris, U.E.; Kohler, M.J.; Fraenkel, L. Adverse effects of topical nonsteroidal antiinflammatory drugs in older adults with osteoarthritis: A systematic literature review. J. Rheumatol. 2010, 37, 1236–1243.

[33] Mimori, S.; Koshikawa, Y.; Mashima, Y.; Mitsunaga, K.; Kawada, K.; Kaneko, M.; Okuma, Y.; Nomura, Y.; Murakami, Y.; Kanzaki, T.; et al. Evaluation of synthetic naphthalene derivatives as novel chemical chaperones that mimic 4-phenylbutyric acid. Bioorg. Med. Chem. Lett. 2015, 25, 811–814.

[34] Council of Europe. 2010 European Pharmacopoeia; Council of Europe: Strasbourg, Fance, 2010.

[35] Wang, Z.; Diao, Z.; Liu, F.; Li, G.; Zhang, G. Microstructure and rheological properties of liquid crystallines formed in Brij 97/water/IPM system. J. Colloid Interf. Sci. 2006, 297, 813–818.

[36] Makai, M.; Csanyi, E.; Nemeth, Z.; Palinkas, J.; Eros, I. Structure and drug release of lamellar liquid crystals containing glycerol. Inter. J. Pharm. 2003, 256, 95–107.

[37] Cho, Y.H.; Kim, S.; Bae, E.K.; Mok, C.K.; Park, J. Formulation of a cosurfactant-free O/W microemulsion using nonionic surfactant mixtures. J. Food Sci. 2008, 73, E115–E121.

[38] Provencher, S.W. CONTIN: A general purpose constrained regularization program for inverting noisy linear algebraic and integral equations. Comput. Phys. Commun. 1982, 27, 229–242.

[39] Zhao, Z.; Lian, Y.; Zhu, Y.; Ye, H.; Liu, M.; Lif, J. Depot lidocaine-loaded microemulsion for prolonged local anesthesia: Different efficacy model studies. J. Drug Deliv. Sci. Technol. 2020, 55, 101404.

[40] Jin, S.E.; Kim, C.K. Charge-mediated topical delivery of plasmid DNA with cationic lipid nanoparticles to the skin. Colloids Surf. B Biointerfaces 2014, 116, 582–590.

[41] Danielsson, I.; Lindman, B. The definition of a microemulsion. Colloids Surf. B 1981, 3, 391–392.

[42] Mazzotta, E.; Rossi, C.O.; Muzzalupo, R. Different BRIJ97 colloid systems as potential enhancers of acyclovir skin permeation and depot. Colloid Surf. 2019, 173, 623–631.

[43] Hedner, T.; Samulesson, O.; Wahrborg, P.; Wadenvik, H.; Ung, K.A.; Ekbom, A. Nabumetone: therapeutic use and safety profile in the management of osteoarthritis and rheumatoid arthritis. Drugs 2004, 64, 2315–2343.

[44] Turpeinen, M.; Hofmann, U.; Klein, K.; Murdter, T.; Schwab, M.; Zanger, U.M. A predominate role of CYP1A2 for the metabolism of nabumetone to the active metabolite, 6-methoxy-2-naphthylacetic acid, in human liver microsomes. Drug Metab. Dispos. 2009, 37, 1017–1024.

[45] Varfaj, F.; Zulkifli, S.N.; Park, H.G.; Challinor, V.L.; De Voss, J.J.; Ortiz de Montellano, P.R. Carbon–carbon bond cleavage in activation of the prodrug nabumetone. Drug Metab. Dispos. 2014, 42, 828–838.

[46] Murakami, M.; Takahashi, K.; Amii, H.; Ito, Y. Rhodium(I)-catalyzed successive double cleavage of carbon–carbon bonds of strained spiro cyclobutanones. J. Am. Chem. Soc. 1997, 119, 9307–9308.

[47] De Rosa, F.S.; Tedesco, A.C.; Lopez, R.F.; Pierre, M.B.; Lange, N.; Marchetti, J.M.; Rotta, J.C.; Bentley, M.V. *In vitro* skin permeation and retention of 5-aminolevulinic acid ester derivatives for photodynamic therapy. J. Control. Release 2003, 89, 261–269.

[48] Lopes, L.B. Overcoming the cutaneous barrier with microemulsions. Pharmaceutics 2014, 6, 52–77.

III. USE OF PLURONIC SURFACTANTS IN GEL FORMULATIONS OF PHOTOSENSITIVE 1,4-DIHYDROPYRIDINE DERIVATIVES: A POTENTIAL APPROACH IN THE TREATMENT OF NEUROPATHIC PAIN

Giuseppina Ioele [1]; Rita Muzzalupo [1]; Miyase Gözde Gündüz [2]; Michele De Luca [1]; Elisabetta Mazzotta [1]; Fedora Grande [1]; Maria Antonietta Occhiuzzi [1]; Antonio Garofalo [1]; Gaetano Ragno [1].

[1] Department of Pharmacy, Health and Nutritional Sciences, University of Calabria, 87036 Rende, Italy;
[2] Department of Pharmaceutical Chemistry, Faculty of Pharmacy, Hacettepe University, 06100 Ankara, Turkey.

Abstract:

1,4-Dihydropyridines (DHPs) are the most important class of L-type calcium channel blockers that are employed for the treatment of cardiovascular diseases, particularly hypertension.
Various modifications on this scaffold lead to the discovery of new DHPs blocking different types of calcium channels. Among them, the T-type calcium channel has recently attracted great interest due to its role in chronic pain conditions. In this study, we selected three newly synthesized DHPs (HM8, HM10 and MD20) with different selectivity profiles to the T-type calcium channel and formulated them in micellar solutions and micellar-in-gel matrices to be tested for potential topical use in the treatment of neuropathic pain. To prevent the well-known sensitivity to light of the DHPs, the studied compounds were entrapped in colloidal aggregates obtained by using edible Pluronic® surfactants and adding α-tocopherol as an antioxidant. All the prepared formulations were exposed to stressing light, according to international rules. Along with the degradation experiments, the concentrations of the parent compounds and by-products were calculated by multivariate curve resolution-alternating least squares (MCR-ALS) applied to the spectral data. The defined formulations proved suitable as light-stable matrices for the DHP compounds, showing an increase in stability for HM8 and MD20 and an almost complete photoprotection for HM10, compared to ethanol solutions and standard gel formulations.

Keywords: T-type calcium channel blockers; multivariate curve resolution; drug photostability; Pluronic® surfactants; α-tocopherol.

1. Introduction

Voltage-gated calcium channels mediate calcium influx into the excitable cells of the brain, heart and smooth and skeletal muscle. They regulate a vast variety of physiological functions, including hormone/neurotransmitter release, gene transcription and muscle contraction in the whole body. Through their abilities to control calcium-dependent processes, calcium channels are regarded as druggable targets for the treatment of cardiovascular and neurological disorders [1]. L-type calcium channel ($Ca_v1.2$) is the primary target of 1,4-Dihydropyridines (DHPs), such as nifedipine, amlodipine and isradipine, which are commonly prescribed for controlling hypertension. Subsequently, T-

type calcium channels (Ca$_v$3) were found to control neuronal excitability and are targeted for the therapeutic intervention into neurophysiologic conditions, principally epilepsy and pain. Among the different T-type calcium channel subtypes, the Ca$_v$3.2 isoform regulates pain signals, and thus attracts great interest to bring chronic pain states under control [2]. Within the scope of defining new T-type calcium channel blockers, many compounds of different chemical classes were developed and shown to mediate analgesia [3]. Furthermore, in our previous studies, we synthesized new compounds by introducing a DHP ring into a condensed ring system (hexahydroquinoline) and modifying the alkyl group of the ester side chain, which led to the discovery of novel DHP-based T-type calcium channel blockers with different selectivity profiles over the L-type calcium channel. These derivatives were also demonstrated to be effective at reducing pain signals derived from peripheral inflammation and nerve injury [4,5]. The obtained data suggested that condensed DHPs as T-type calcium channel blockers are novel and promising scaffolds for chronic pain relief.

In this study, we selected three new DHPs (HM8, HM10 and MD20) with different selectivity profiles against the T-type over L-type calcium channels, utilizing the whole-cell patch-clamp technique. Their chemical structures are provided in Figure 1. Among them, HM8 and MD20 were selective blockers of the T-type calcium channel (Cav3.2), with a ~60% inhibition over the L-type calcium channel (Cav1.2) with no significant block [6,7]. Besides them, HM10, carrying the Michael acceptor group in the ester side chain, produced almost complete inhibition (>95%) on Cav3.2, exhibiting low selectivity as it caused moderate inhibition (~50%) on Cav1.2 as well [7].
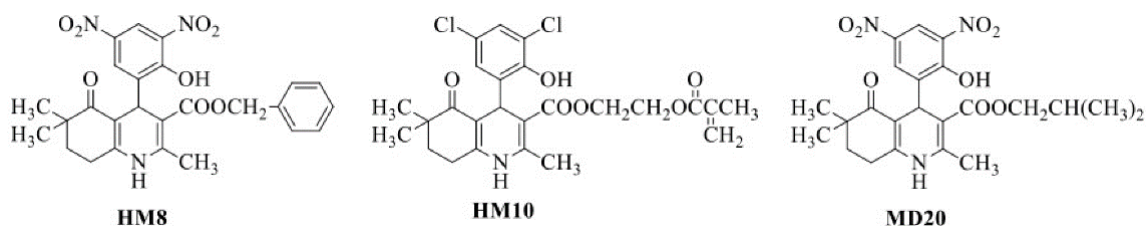

Figure 1. Chemical structures of HM8, HM10, HM20.

The use of DHPs in therapy has always been difficult due to their known sensitivity to light, which leads to the formation of the pyridine by-product as the major photoproduct. DHP drugs are currently formulated mainly in tablets, due to the high light stability in solid form. Several studies have been carried out for defining liquid formulations, providing a valid photoprotection for these drugs [8,9]. The adoption of dark glass containers is the most used method to protect the few available liquid formulations of DHPs today. Alternatively, matrices based on cyclodextrins, liposomes, niosomes or non-ionic surfactants have been studied as photostabilization systems [10,11,12]. Over the past decade, many efforts have been devoted to the development of drug delivery systems based on the use of nanoscale materials, including polymer micelles and polymer–drug conjugates, in which the drugs can simply be entrapped or covalently bound [13,14,15,16,17]. Most of the polymeric micelles, known as Pluronics, consist of triblock PEO–PPO–PEO copolymers: two hydrophilic end-blocks of poly(ethylene oxide) (PEO) and a central hydrophobic block of poly(propylene oxide) (PPO). These copolymers are commercially available in a range of PPO/PEO composition ratios and molecular weights. A relevant number of papers report the application of the Pluronic® surfactants in the preparation of drug delivery systems [18,19,20]. Pluronic smart hydrogel formulations have also been studied for the controlled transport of injectable drugs [13] while other studies have focused on the development of new thermal-sensitive hydrogels for the administration of intranasal vaccines [14]. No paper has reported on their use in protecting drugs from light.

In this work, the use of edible polymer matrices with the addition of antioxidants was investigated as novel photoprotective systems for the preparation of liquid or gel formulations containing the synthesized DHPs. The selected surfactants were Pluronic F-127, which forms micelles consisting of 65 hydrophobic PPO blocks and a corona formed by 200 hydrated PEO blocks, and Pluronic F-108, comprising 50 PPO units and 265 PEO units [15,21]. If the concentration of Pluronics in the aqueous solution exceeds the CMC value, micelles having spherical, cylindrical, lamellar or vesicular morphologies are formed [15].

The study aims to obtain a topical formulation endowed with favorable pharmacokinetic properties to use in the treatment of neuropathic pain that affects a considerable amount of the world population. All the prepared formulations were subjected to photodegradation tests, according to the International Conference on Harmonization (ICH) rules [22]. The photodegradation tests were monitored by spectrophotometry and the kinetic degradation parameters were calculated for all compounds by multivariate curve resolution—alternating least squares (MCR-ALS) [23-27].

2. Material and methods

2.1. Chemicals

HM8 (benzyl 4-(2-hydroxy-3,5-dinitrophenyl)-2,6,6-trimethyl-5-oxo-1,4,5,6,7,8-hexahydroquinoline-3-carboxylate), HM10 (2-(methacryloyloxy)ethyl 4-(3,5-dichloro-2-hydroxyphenyl)-2,6,6-trimethyl-5-oxo-1,4,5,6,7,8-hexahydroquinoline-3-carboxylate) and MD20 (isobutyl 2,6,6-trimethyl-4-(2-hydroxy-3,5-dinitrophenyl)-5-oxo-1,4,5,6,7,8-hexahydroquinoline-3-carboxylate) were synthesized according to modified Hantzsch reactions at the Department of Pharmaceutical Chemistry, Faculty of Pharmacy, Hacettepe University, Ankara, Turkey. Equimolar amounts of 4,4-dimethyl-1,3-cyclohexanedione, 2-hydroxy-3,5-dinitrobenzaldehyde, benzyl (HM8)/isobutyl (MD20) acetoacetate and excess ammonium acetate were dissolved in absolute ethanol and subjected to microwave irradiation (100 W power, constant) for 10 min [6,7]. Upon cooling, the precipitate, obtained by pouring the reaction mixture into ice-water, was filtered and recrystallized from ethanol-water. HM10 was obtained according to the same procedure differently using 3,5-chlorosalicylaldehyde and 2-(methacryloyloxy) ethyl acetoacetate as the aromatic aldehyde and appropriate acetoacetate, respectively [7].

Pluronic® F-127 (MW 12600), F-108 (MW 14600), α-tocopherol and microcrystalline carboxymethylcellulose were purchased from Sigma-Aldrich (Darmstadt, Germany); and ethanol and acetonitrile from J.T. Baker (Deventer, Holland). All chemicals were used without further purification.

2.2. Sample preparation

Due to the almost insolubility of the compounds in water, ten calibration solutions in ethanol were prepared for each compound in concentrations ranging from 5.0 to 30.0 µg mL−1. These solutions were used to establish through MCR the mathematical relationships between the concentration of the compounds and their respective spectrophotometric signals. Likewise, three sets (prediction samples) of five one-component solutions were prepared, containing the compounds in the same concentration range used for the calibration sets. These solutions were used to validate the analytical methods defined and to calculate their statistical effectiveness in terms of accuracy and precision. The micellar solutions were prepared by diluting one compound at a time with Pluronic® surfactant in 10 mL of water. Two of the surfactants tested, namely F-108 and F-127, showed self-aggregation in aqueous solution, forming spherical micelles above a critical micellar concentration (CMC) [15,21].

Therefore, the amount of each surfactant was calculated as an excess of its CMC, measured as 2.30 and 0.43 mol $L^{-1} \times 10^{-3}$, respectively, for F-108 and F-127 [21]. The micellar-in-gel formulation of each compound was prepared by adding carboxymethylcellulose 0.36 g (gelling agent) to the micellar aqueous solution 10.0 mL, prepared as above described [28,29]. The emulsion was stirred at 200 rpm for 50 min at room temperature to obtain a homogeneous transparent gel. The photodegradation profiles of these formulations were compared with the standard gel formulations (5 g) containing the free drugs, in absence of the micelles, but in the same drug concentration measured in the micellar formulation. These gels were prepared by emulsifying about 5.0 mg of each compound with 0.36 g carboxymethylcellulose (gelling agent) and 10.0 mL water [28,29].

2.3. Photodegradation Study

The photodegradation tests were performed by means of a Suntest CPS+ (Heraeus, Milan, Italy), which uses a Xenon lamp as a light source, providing wavelengths in the range 300–800 nm, according to the ID65 standard source of the ICH rules [22]. The irradiation power was set at 350 W m−2, corresponding to 21 kJ m−2·min−1, at a constant temperature of 25 °C. The experiments were carried out in a dark room to avoid any light interference. The UV spectra of the ethanol solutions and micellar matrices were recorded in the λ range 200–450 nm by a Perkin-Elmer Lambda 40P Spectrophotometer (Artisan Technology Group, Mercury Drive Champaign, IL, USA) and acquired by UV WinLab® (Perkin-Elmer, Boston, MA, USA). The analyses were done in triplicate at time 0 and at the sequential time points: 1, 3, 5, 10, 15, 20, 30, 40, 50, 60, 80, 100, 120, 150, 180, 240 and 300 min. The micellar systems were diluted with ethanol, 0.5 to 5 mL. Gel formulations were irradiated at the following exposure times: 0, 5, 15, 20, 40, 60 and 120 min. The photodegradation tests were performed by uniformly layering 0.5 g of the gel on each of seven glass plates with a layer thickness of 0.25 mm. The gel layering was carried out by placing two 0.25-mm-thick aluminum sheets on the glass at a distance of 2 cm and then layering the gel on the aluminum sheets using a steel spatula. The prepared plates were then exposed to forced irradiation. At various irradiation intervals, each glass plate was sonicated in 25 mL acetonitrile for 10 min at room temperature. Then, 10 mL of the suspension obtained were centrifuged at 5000 rpm for 10 min and the supernatant was analyzed after a 1:10 dilution with ethanol.

2.4. MCR Procedure

The MCR algorithm was applied to the spectral data to calculate the drug concentration in the samples using the MATLAB® computer environment software (Mathwork Inc., version 7, Natick, MA, USA). Application of this technique allowed to estimate the number of components, their spectra, the concentration profiles, and the rate constants (k) of the kinetic processes. The MCR methods were elaborated on the standard drug solutions (calibration sets), prepared as above described and validated on external samples with the same concentration range (prediction sets). For each compound, the Limit of Detection (LOD) and Limit of Quantitation (LOQ) were measured.

3. Results

3.1. DLS Analysis

DLS analysis was performed to determine the mean diameter of the micellar systems. The characteristics of the obtained micelles are reported in Table 1.

Table 1. *Characteristics of the Pluronic micellar solutions.*

Compound	Surfactant	Drug: Surfactant Ratio	Micellar Size (nm ± DS)	PDI	Z Potential (mV)	Drug Entrapping %
HM8	F-108	1:10	22.61 ± 0.11	0.218	−12.7 ± 2.44	29.1
	F-127	1:10	54.41 ± 0.63	0.263	−9.89 ± 1.89	69.2
HM10	F-108	1:5	Aggregates	-	−4.78 ± 3.23	20.3
	F-127	1:5	34.75 ± 1.13	0.389	−8.76 ± 2.23	20.9
MD20	F-108	1:10	23.74 ± 2.25	0.382	−9.14 ± 0.08	28.2
	F-127	1:10	Aggregates	-	−4.56 ± 1.25	58.9

The micelle size ranged from 22.61 to 54.41 nm and the coexistence of small micelles and large aggregates was also observed (Figure 2). This trend was widely reported in the literature for Pluronic micelles loaded with a hydrophobic drug: an increased hydrophobicity of the micellar core is associated with a higher presence of colloidal aggregates [19,20]. The use of lipophilic substances influences the evolution of the aggregation characteristics of these systems. This effect is attributed to the increased hydrophobicity of the surfactant molecules by reducing the availability of water around them, thus resulting in a rich set of structural transitions in the surfactant aggregates. In fact, hydrophobic drugs are located in the inner core and corona of the micelles, establishing strong interactions with the polymer chains that lead to a decrease in the intermicellar interaction distance and promote the aggregation process. This effect was predominant when HM10 and MD20 were loaded in the F108 and F127 micelles, respectively, for which only large aggregates were recorded.
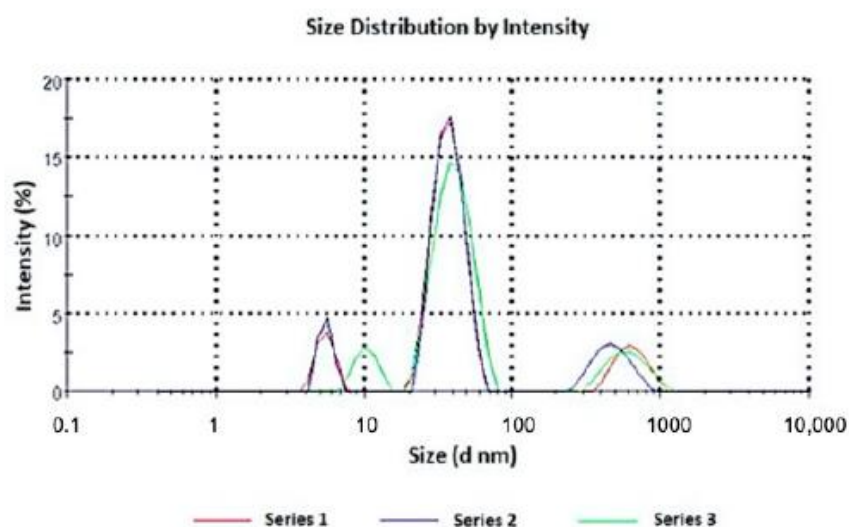

Figure 2. *Size distribution of HM10 loaded in F127 micelles, in triplicate.*

The absence of a chemical interaction between the drugs, the Pluronic surfactant and the carboxymethylcellulose was also demonstrated by FTIR. The typical peaks for each compound were detected in their mixture spectrum, confirming the absence of interactions. A physical-chemical characterization was also performed on the micellar formulations to which 5% α-tocopherol were added, and the obtained data are reported in Table 2.

Table 2. *Characteristics of the Pluronic micellar solutions loaded with 5% α-tocopherol.*

Compound	Surfactant	Z-Potential (mV)	Micellar Size (nm ± DS)	PDI	Drug Entrapping %	α-Tocopherol Entrapping %
HM8	F-108	−5.99 ± 1.05	98.02 ± 5.45	0.521	25.3	31.1
	F-127	−6.89 ± 1.22	157.9 ± 15.19	0.851	61.1	33.9
HM10	F-108	−7.78 ± 1.93	Aggregates	-	18.3	37.6
	F-127	−6.76 ± 2.94	126.0 ± 13.76	0.762	19.1	39.8
MD20	F-108	−7.92 ± 1.76	175.1 ± 8.09	0.382	25.4	35.4
	F-127	−8.76 ± 0.95	Aggregates	-	54.6	37.8

3.2. MCR Processing

Absorbance spectra of the ethanol calibration samples were recorded over the wavelength range 200–450 nm. A first selection of the most useful wavelengths was performed, discarding the wavelengths below 210 nm, which are usually affected by high variability or instrumental noise that can make the model unstable, as well as the wavelengths over 390 nm, due to the absence of signals. Therefore, the MCR elaboration was applied on the spectral data between 210 and 390 nm.

The values of the lack of fit (%LOF), which is an index of the fit quality of the MCR results, was less than 4.5% in all experiments. LOD values calculated were 1.2, 0.99 and 1.1 µg/mL for HM8, HM10 and MD20, respectively. LOQ was in the range 2.4–45.1 µg/mL for HM8, 2.1–46.5 µg/mL for HM10 and 2.5–44.5 µg/mL for MD20.

3.3. Photodegradation of the Ethanol Solutions

Photostability of the DHP compounds was tested by exposing to light the ethanol one-component solutions at a concentration of 20.0 µg mL−1. These solutions were placed in quartz cuvettes and subjected to a photodegradation test as above described. Figure 3 shows the sequences of the absorbance spectra in the range 200–450 nm recorded along the photodegradation tests of HM8, HM10 and MD20 at zero time and at several intervals up to 5 h.
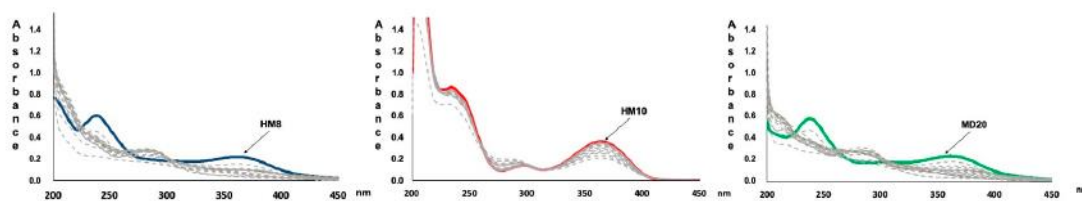

Figure 3. *UV spectra recorded along the photodegradation test on the ethanol solutions of HM8, HM10 and MD20.*

These data were processed by MCR to estimate the number of photoproducts, as well as their spectra and concentration profiles. The photodegradation rate constant (k) was calculated for these experiments, showing in all cases first-order kinetics. The following equation describe the degradation process:

$$\ln[\% \text{ DHP}] = -k \times t + 4.67$$

where % DHP is the percentage concentration of the residual drug; t is the time, expressed in minutes; and 4.67 is the natural logarithm of the starting concentration percentage (100%). Considering that a pharmaceutical formulation whose quantity of active ingredient falls below 90% of the initial value can no longer be used, the parameter $t_{0.1}$ (time to obtain a 10%

degradation) was selected to compare the behavior of the prepared formulations when exposed to light. In addition, the shelf-life of the formulations was also compared by using the parameter $t_{0.5}$ (time to obtain a 50% degradation). The calculated kinetic parameters collected in all the photodegradation experiments are listed in Table 3. The data were the average of three experiments with the values of the relative standard deviation (RSD) for all parameters within the range 1.66–5.04%.

The graphs elaborated from the MCR analysis are shown in Figure 4. For each compound, the absorbance spectra and the concentration profiles of the drugs and relative photoproducts are shown. As reported in our previous works, the oxidation of the dihydropyridine ring to the pyridine-based photoproduct was confirmed for all the tested compounds. Furthermore, the formation of secondary photoproducts for HM8 and MD20 was detected, based on the presence of nitro-groups on the phenyl ring, which accelerates the oxidation process due to the delocalization of the negative charge [30,31].

Table 3. *Degradation kinetic parameters calculated for the HM8, HM10 and MD20 formulations.*

| Compound	Formulation	$k\ (\times 10^{-3})$	$t_{0.1}$ (min)	$t_{0.5}$ (min)	R^2
HM8	Ethanol solution	7.28	0.24	1.59	0.994
	F-108	0.99	1.78	11.71	0.992
	F-127	0.89	1.97	12.96	0.934
	F-108-tocopherol	0.79	2.23	14.65	0.988
	F-127-tocopherol	0.74	2.37	15.61	0.995
	Standard gel	7.04	0.25	1.64	0.912
	F-127-tocopherol gel	0.65	2.69	17.73	0.941
HM10	Ethanol solution	0.17	10.54	69.31	0.974
	F-108	0.06	29.27	192.54	0.957
	F-127	0.10	16.97	111.62	0.940
	F-108-tocopherol	0.00	501.72	-	0.909
	F-127-tocopherol	0.05	34.43	226.52	0.976
	Standard gel	0.15	12.11	79.67	0.996
	F-108-tocopherol gel	0.00	605.52	-	0.975
MD20	Ethanol solution	0.19	9.16	60.27	0.985
	F-108	0.13	13.51	88.87	0.976
	F-127	0.09	20.18	132.79	0.997
	F-108-tocopherol	0.10	17.74	116.69	0.965
	F-127-tocopherol	0.05	38.17	251.14	0.901
	Standard gel	0.18	9.87	64.90	0.955
	F-127-tocopherol gel	0.04	43.90	288.81	0.943
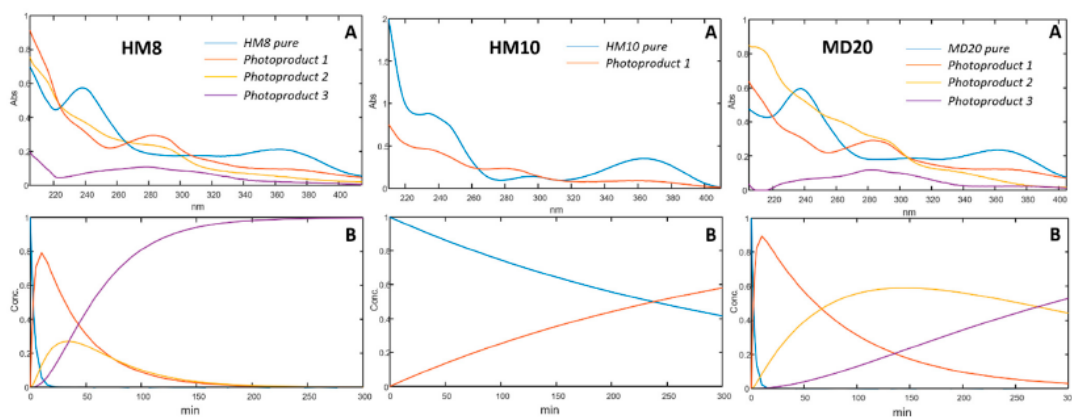
Figure 4. *Spectra (A) and concentration profiles (B) for HM8, HM10 and MD20, and their photoproducts.*

3.4. Photodegradation of Micellar Solutions

Preparation of the micellar solutions containing the studied compounds was optimized by performing various experiments to define the drug: surfactant ratio and the amount of the antioxidant. In this way, an increase in the solubility for the compounds in the micellar solution was obtained.

For each compound, the micellar solutions showing an entrapping percentage higher than 20% (Table 1) were selected to be subjected to the photodegradation test. To these formulations were added 5% α-tocopherol just before the photodegradation test. Figure 5 shows the photodegradation profiles of HM8, HM10 and MD20 in the micellar solutions, compared with those carried out from the ethanol solutions. The kinetic parameters, listed in Table 3, were calculated by applying MCR analysis to the spectral data. These formulations also followed first-order kinetics for the degradation process.
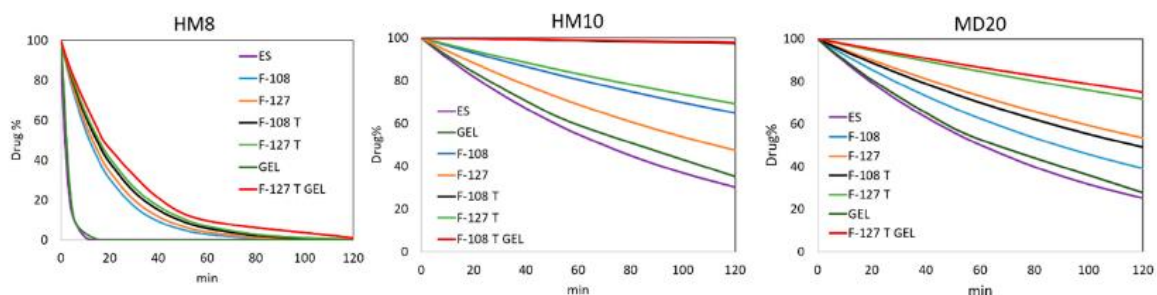

Figure 5. *Photodegradation of HM8, HM10 and MD20 in ethanol, surfactant solutions and gel formulations. ES, ethanol solution; T, α-tocopherol.*

3.5. Photodegradation of the Gel Formulations

The stability of the micellar solutions was also tested in the gel formulation. The micellar systems of the three compounds that showed the best performance, in terms of entrapping percentage and photostability, were formulated in gel, as above described. The photodegradation profiles of these formulations were compared with those of a standard gel prepared in the same conditions and containing the free drugs. Figure 6 compares the photodegradation rates on these samples.
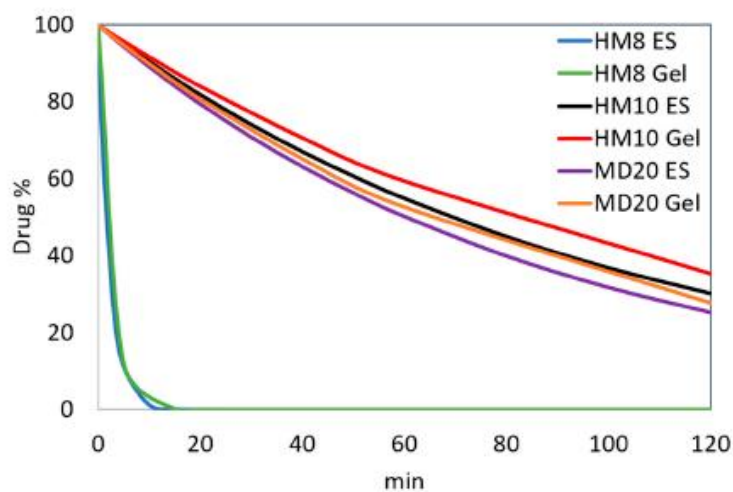

Figure 6. *Comparison of the photodegradation profiles of HM8, HM10 and MD20 in ethanol and gel formulations.*

The kinetic parameters calculated by MCR are listed in Table 3. Figure 5 shows the photodegradation profiles of HM8, HM10 and MD20 in a micellar-gel formulation compared with those of the free compounds in the gel. First-order degradation kinetics were confirmed also for these formulations.

4. Discussion

This paper presents the photodegradation study of newly synthesized DHP-based hexahydroquinolines (HM8, HM10 and MD20) with T-type calcium channel blocking activity (Cav3.2), which is considered a new approach to develop novel analgesics, particularly against neuropathic pain. We formulated them in liquid and gel preparations with the aim of minimizing their sensitivity to light. Photostability of the compounds was first tested in ethanol and gel under standard conditions. The %LOF values, resulting below 4.5% in all the experiments, confirmed the quality and robustness of the MCR data processing from the photodegradation tests.

The sequence of the spectra collected during the photodegradation experiments on the ethanol solutions (Figure 3) showed a decrease of the peak in the 350–390 nm zone for all the compounds, typical of the dihydropyridine structure, and the simultaneous increase of a new peak in the 260–310 nm region. According to our previous studies [30,31], the different chemical groups on the phenyl and dihydropyridine rings lead to different kinetic photodegradation profiles. The presence of chlorine atoms on the phenyl ring of HM10 confers greater stability than the nitro groups in HM8 and MD20. MCR elaboration of the spectral data confirmed this trend, assuming the formation of only the pyridine derivative for HM10 (Figure 4A). Two photoproducts were instead detected during degradation of both HM8 and MD20, corresponding to the pyridine derivatives and to the subsequent reduction of the nitro groups in Positions 3 and 5 on the phenyl ring to nitroso groups. Traces of a third by-product were observed after prolonged exposure to light, but devoid of any characterizing signal. This photodegradation profile was carried out also when the drugs were formulated in gel. As compared in Figure 6, HM8 showed a very fast degradation process in both matrices, with an almost complete disappearance after 10 min of light exposure. In contrast, HM10 and MD20 showed greater stability, with a $t_{0.1}$ value of 10.54 and 9.16 min in ethanol and 12.11 and 9.87 min in gel, respectively.

Due to the marked photosensitivity of the studied molecules, the increase in their photostability was investigated by incorporating the compounds into polymeric micelles.

At first, the use of the Pluronic F-68 surfactant, comprising 29 PPO units and 153 PEO units [15], was tested. Unfortunately, the use of F-68 did not produce satisfactory results, because the entrapping percentage was below 10% in all the experiments, despite several modifications of the experimental conditions. Indeed, difficulties in using Pluronic F-68 in drug formulation have been reported, due to its high CMC, resulting in a low drug load and poor dilution stability [32]. For these reasons, the micellar solutions prepared with this surfactant were eliminated from the subsequent study. The aim of the work was achieved when the compounds were entrapped in micelles formed by using Pluronics F-108 and F-127, showing entrapping percentages above 20% in all formulations. The best results, with values in the range 59–69%, were obtained for HM8 and MD20 entrapped in Pluronic F-127 micelles, whose dimensions were much larger than those formed using Pluronic F-108. HM10, which has a higher molecular weight, formed larger micelles when entrapped in Pluronic F-108. The incorporation percentage of the DHP compounds into the two selected Pluronic surfactants was carried out by spectrophotometry and the values are listed in Table 1. The micellar solutions prepared with F-108 and F-127 were subjected to photodegradation and the spectra recorded along these experiments were processed by MCR. A marked

increase in the light stability was observed for HM10 in both the micelle matrices, showing $t_{0.1}$ values of 29.27 and 16.97 min when using F-108 and F-127, respectively. The formation of the pyridine by-product alone was detected. An almost complete photostability was observed for this compound when 5% α-tocopherol was added to the micellar solutions. As reported in Table 2, α-tocopherol loaded in the micellar systems led to a significant increase in the micelle size. The percentage entrapment of the drugs was slightly decreased and the antioxidant was entrapped at an average of 36%. This behavior did not affect the Z-potential values.

This result demonstrated the importance of the presence of an antioxidant in opposing the photodegradation process of DHP compounds, which mainly involves the oxidation process of the dihydropyridine ring. A clear decrease in the photodegradation rate was shown also for MD20, confirming the validity of the inclusion process in the polymeric micelles. The best results were obtained when this compound was entrapped in the F-127 micelles, showing a $t_{0.1}$ value of 20.18 min. This formulation was analogously added with α-tocopherol, providing a further increasing of light stability, with a t0.1 value of 38.17 min. In contrast, the results from the tests on HM8 were not satisfactory, despite the micellar formulations showing a significant increase in light stability, showing a $t_{0.1}$ value of 1.97 when entrapped in the F-127 micelles and $t_{0.1}$ value of 2.37 min when α-tocopherol was added. The overall t0.1 values are summarized in Table 3.

The most stable micellar sample for each product was finally formulated in a gel matrix and subjected to photodegradation. The experimental procedure, applied in the preparation of the gels, involved the use of plate glasses to be exposed in the irradiation chamber. The use of only seven plates was due to the size of this chamber. Considering that the $t_{0.1}$ value for most of the prepared formulations were less than 45 min, we used shorter irradiation times for the gels than in the experiments performed on the drugs in solution. As shown in Figure 5, the HM8 compound in the micelle-in-gel showed a ten-fold increase in the $t_{0.1}$ value (2.69 min) compared to the standard gel but the photodegradation profile of the micelles-in-gel formulation was like that of the micellar solution. This result was not considered satisfactory for making a light-stable topical formulation. For this compound, the advantage in using the micellar system was limited to improve the water solubility.

Satisfactory results were obtained for MD20, which showed a remarkable increase in light stability, with a $t_{0.1}$ value of 43.90 min. In addition, the light stability was constant for long exposure times, recording a residual concentration of 50% after 288 min. The best result was achieved for the HM10 compound in micelles-in-gel, which maintained a drug concentration of 90% for more than 8 h under stressing light. For these two compounds, UV light likely induced modifications on the polymers and therefore the light exposure of the incorporated drugs was limited. The polymer envelopes were able to isolate the drugs from the surrounding environment and, thus, the UV irradiation did not penetrate below the first molecular layers.

The proposed micelle-in-gel matrices were demonstrated to be able to both entrap water-insoluble drugs and assure high photostability. Furthermore, the polymeric micelles have a high drug-loading capacity and good dispersion characteristics in the body. Based on these results, the study presents some limitations. The proposed formulations for HM8, despite the improved stability compared to the ethanolic solution, showed complete degradation after a short exposure time to light. In addition, our topical gel formulations need to be examined for their analgesic effects to be potential candidates in the treatment of neuropathic pain through blocking T-type calcium channels.

5. Conclusions

A novel approach is proposed for the development of light-stable liquid formulations containing newly synthesized Dihydropyridines with T-type calcium channel blocking activity. Satisfactory results were achieved when two of these compounds were incorporated into micelles formed with Pluronics F-127 and F-108 as surfactants and α-tocopherol as antioxidant. The compounds HM10 and MD20 in micelles-in-gel showed a drug concentration of 90% after 8 and 1 h of light exposure. Furthermore, the use of surfactants greatly favored the solubility in water of all the tested DHP molecules. The proposed matrices demonstrated a remarkable ability in protecting the studied DHPs from light to develop topical formulations. As T-type calcium blockers hold therapeutic value for pain intervention, these formulations can be potential candidates in pain therapy after their analgesic effects are further investigated.

References

[1] Zamponi, G.W.; Striessnig, J.; Koschak, A.; Dolphin, A.C. The Physiology, Pathology, and Pharmacology of Voltage-Gated Calcium Channels and Their Future Therapeutic Potential. *Pharmacol. Rev.* 2015, *67*, 821–870.

[2] Simms, B.A.; Zamponi, G.W. Neuronal Voltage-Gated Calcium Channels: Structure, Function, and Dysfunction. *Neuron* 2014, *82*, 24–45

[3] Snutch, T.P.; Zamponi, G.W. Recent advances in the development of T-type calcium channel blockers for pain intervention. *Br. J. Pharmacol.* 2018, *175*, 2375–2383.

[4] Bladen, C.; Gadotti, V.M.; Gündüz, M.G.; Berger, N.D.; Şimşek, R.; Şafak, C.; Zamponi, G.W. 1,4-Dihydropyridine derivatives with T-type calcium channel blocking activity attenuate inflammatory and neuropathic pain. *Pflug. Arch. Eur. J. Physiol.* 2015, *467*, 1237–1247.

[5] Gadotti, V.M.; Bladen, C.; Zhang, F.X.; Chen, L.; Gündüz, M.G.; Şimşek, R.; Şafak, C.; Zamponi, G.W. Analgesic effect of a broad-spectrum dihydropyridine inhibitor of voltage-gated calcium channels. *Pflüger's Arch. Gesammte Physiol. Menschen Tiere* 2015, *467*, 2485–2493.

[6] Schaller, D.; Gunduz, M.G.; Zhang, F.X.; Zamponi, G.W.; Wolber, G. Binding mechanism investigations guiding the synthesis of novel condensed 1,4-dihydropyridine derivatives with L-/T-type calcium channel blocking activity. *Eur. J. Med. Chem.* 2018, *155*, 1–12.

[7] Cevher, H.A.; Schaller, D.; Gandini, M.A.; Kaplan, O.; Gambeta, E.; Zhang, F.X.; Çelebier, M.; Tahir, M.N.; Zamponi, G.W.; Wolber, G.; et al. Discovery of Michael acceptor containing 1,4-dihydropyridines as first covalent inhibitors of L-/T-type calcium channels. *Bioorg. Chem.* 2019, *91*, 103187.

[8] Ioele, G.; Tavano, L.; De Luca, M.; Muzzalupo, R.; Mancuso, A.; Ragno, G. Light-sensitive drugs in topical formulations: Stability indicating methods and photostabilization strategies. *Future Med. Chem.* 2017, *9*, 1795–1808.
[9] Ioele, G.; De Luca, M.; Garofalo, A.; Ragno, G. Photosensitive drugs: A review on their photoprotection by liposomes and cyclodextrins. *Drug Deliv.* 2017, *24*, 33–44.

[10] Ragno, G.; Risoli, A.; Ioele, G.; Cione, E.; De Luca, M. Photostabilization of 1,4-dihydropyridine antihypertensives by incorporation into beta-cyclodextrin and liposomes. *J. Nanosci. Nanotechnol.* 2006, *6*, 2979–2985.

[11] Ioele, G.; De Luca, M.; Ragno, G. Photostability of barnidipine in combined cyclodextrin-in-liposome matrices. *Futur. Med. Chem.* 2014, *6*, 35–43.

[12] Ioele, G.; Gündüz, M.G.; Spatari, C.; De Luca, M.; Grande, F.; Ragno, G. A New Generation of Dihydropyridine Calcium Channel Blockers: Photostabilization of Liquid Formulations Using Nonionic Surfactants. *Pharmaceutics* 2019, *11*, 28.

[13] Shriky, B.; Kelly, A.; Isreb, M.; Babenko, M.; Mahmoudi, N.; Rogers, S.; Shebanova, O.; Snow, T.; Gough, T. Pluronic F127 thermosensitive injectable smart hydrogels for controlled drug delivery system development. *J. Colloid Interface Sci.* 2020, *565*, 119–130

[14] Pastor, Y.; Ting, I.; Martínez, A.L.; Irache, J.M.; Gamazo, C. Intranasal delivery system of bacterial antigen using thermosensi-tive hydrogels based on a Pluronic-Gantrez conjugate. *Int. J. Pharm.* 2020, *579*, 119154.

[15] Olea, A.F.; Carrasco, H.; Espinoza, L.; Acevedo, B. Solubilization of p-alkylphenols in Pluronics F-68 and F-127 micelles: Par-tition coefficients and effect of solute on the aggregate structure. *J. Chil. Chem. Soc.* 2014, *59*, 2451–2454.

[16] Chatterjee, S.; Chi-leung Hui, P.; Kan, C.; Wang, W. Dual-responsive (pH/temperature) Pluronic F-127 hydrogel drug de-livery system for textile-based transdermal therapy. *Sci. Rep.* 2019, *9*, 1–13.

[17] Bodratti, A.M.; Alexandridis, P. Formulation of Poloxamers for Drug Delivery. *J. Funct. Biomater.* 2018, *9*, 11.

[18] Tavano, L.; Mauro, L.; Naimo, G.D.; Bruno, L.; Picci, N.; Andò, S.; Muzzalupo, R. Further evolution of multifunctional niosomes based on pluronic surfactant: Dual active targeting and drug combination properties. *Langmuir* 2016, *32*, 8926–8933.

[19] Basak, R.; Bandyopadhyay, R. Encapsulation of Hydrophobic Drugs in Pluronic F127 Micelles: Effects of Drug Hydrophobicity, Solution Temperature, and pH. *Langmuir* 2013, *29*, 4350–4356.

[20] Sharma, P.K.; Reilly, M.J.; Jones, D.N.; Robinson, P.M.; Bhatia, S.R. The effect of pharmaceuticals on the nanoscale structure of PEO–PPO–PEO micelles. *Colloid. Surf. B* 2008, *61*, 53–60.

[21] Kozlov, M.Y.; Melik-Nubarov, N.S.; Batrakova, A.E.V.; Kabanov, A.V. Relationship between Pluronic Block Copolymer Structure, Critical Micellization Concentration and Partitioning Coefficients of Low Molecular Mass Solutes. *Macromolecules* 2000, *33*, 3305–3313.

[22] ICH. Photostability testing of new drug substance and products. In *ICH Harmonized Tripartite Guideline, Federal Register*; ICH: Geneva, Switzerland, 1997; Volume 62.

[23] De Luca, M.; Tauler, R.; Ioele, G.; Ragno, G. Study of photodegradation kinetics of melatonin by multivariate curve resolution (MCR) with estimation of feasible band boundaries. *Drug Test. Anal.* 2013, *5*, 96–102.

[24] De Luca, M.; Ragno, G.; Ioele, G.; Tauler, R. Multivariate curve resolution of incomplete fused multiset data from chroma-tographic and spectrophotometric analyses for drug photostability studies. *Anal. Chim. Acta* 2014, *837*, 31–37.

[25] De Luca, M.; Ioele, G.; Mas, S.; Tauler, R.; Ragno, G. A study of pH-dependent photodegradation of amiloride by a multi-variate curve resolution approach to combined kinetic and acid-base titration UV data. *Analyst* 2012, *137*, 5428–5435.

[26] Din, E.; Ragno, G.; Ioele, G.; Baleanu, D. Fractional Wavelet Analysis for the Simultaneous Quantitative Analysis of Lacidipine and Its Photodegradation Product by Continuous Wavelet Transform and Multilinear Regression Calibration. *J. Aoac Int.* 2006, *89*, 1538–1546.

[27] Ragno, G.; Vetuschi, C.; Risoli, A.; Ioele, G. Application of a classical least-squares regression method to the assay of 1,4-dihydropyridine antihypertensives and their photoproducts. *Talanta* 2003, *59*, 375–382.

[28] Ioele, G.; De Luca, M.; Tavano, L.; Ragno, G. The difficulties for a photolabile drug in topical formulations: The case of diclofenac. *Int. J. Pharm.* 2014, *465*, 284–290.

[29] Ioele, G.; Tavano, L.; De Luca, M.; Ragno, G.; Picci, N.; Muzzalupo, R. Photostability and ex-vivo permeation studies on diclofenac in topical niosomal formulations. *Int. J. Pharm.* 2015, *494*, 490–497.

[30] Ragno, G.; Ioele, G.; De Luca, M.; Garofalo, A.; Grande, F.; Risoli, A. A critical study on the application of the zero-crossing derivative spectrophotometry to the photodegradation monitoring of lacidipine. *J. Pharm. Biomed. Anal.* 2006, *42*, 39–45.

[31] Ioele, G.; Oliverio, F.; Andreu, I.; De Luca, M.; Miranda, M.A.; Ragno, G. Different photodegradation behavior of barnidipine under natural and forced irradiation. *J. Photochem. Photobiol. A Chem.* 2010, *215*, 205–213.

[32] Deng, Y.; Song, Y.; Tian, Q.; Huang, Z.; Fan, D.; She, Z.; Liu, X.; Cheng, X.; Yu, B. Self-assembled micelles of novel amphiphilic copolymer cholesterol-coupled F68 containing cabazitaxel as a drug delivery system. *Int. J. Nanomed.* 2014, *9*, 2307–2317.

CHAPTER 3

STUDY OF SMALL MOLECULES ENDOWED WITH BIOLOGICAL PROPERTIES

1. Introduction

Part of this research work focused on the study of small molecules reported in literature as suitable agents targeting macromolecules involved in cellular pathways altered in different diseases.
This approach would provide the basis to discover novel drug targets, identify and optimize lead compounds, to afterward direct toward successive steps of preclinical studies, and better understand the specific responses of molecular targets and pathways to drug exposure.

2. Summary

A first investigated target was represented by the CXCR4 receptor.
CXCR4 (C-X-C Chemokine Receptor type 4) and its natural ligand SDF-1α (Stromal-Derived-Factor-1α) are involved in a number of physiological and pathological processes including cancer spread and progression. Over the past few years, numerous CXCR4 antagonists have been identified and currently are in different development stages as potential agents for the treatment of several diseases involving the CXCR4/SDF-1α axis.
Different classes of CXCR4 inhibitors were analysed: cyclopentapeptides, tripeptidomimetics, indoles, p-xylylenediammine, trisubstituted amines and oxazadiazolepyrimidine derivatives. Among them, cyclopentapeptides and bicyclams appeared as the most promising classes to be investigated in order to select potent candidates for clinical application.
Moreover, CXCR4 act as a co-receptor together with CCR5 (CC-chemokine receptor 5) during HIV entry in the host cell, thus the study of compound able to antagonize the interaction of viral proteins with the host cell membrane receptor CD4 and co-receptors CCR5 and CXCR4 has been carried out. Former selective co-receptor antagonists, were demonstrated able to prevent the viral spread toward AIDS, acting at early stages of infection. Due to the capability of HIV to develop resistance by switching from CCR5 to CXCR4, dual co-receptor antagonists could represent the next generation of AIDS prophylaxis drugs. The identification of selective co-receptor antagonists could be particularly effective in preventing viral infection.
Beside agents able to prevent the viral entry, promising targets of conventional antiviral drugs include specific viral enzymes involved in different phases of HIV replication cycle such as protease (PR), reverse transcriptase (RT) and integrase (IN). Nowadays, HAART (highly active antiretroviral therapy) that includes one or more nucleoside and non-nucleoside reverse transcriptase inhibitors (NRTI and NNRTI, respectively) represents the most useful therapeutic treatment. Despite a high antiviral efficacy, this approach unavoidably shows important clinical drawbacks, such as lifetime administration with a consequent reduced patients' compliance, severe side effects, and quick viral outbreak after drug resistance emergence. This therapeutic strategy is not even capable of stimulating a lasting immune response of memory cells necessary to antagonize the infective agent. Innovative therapeutic approaches based on both the identification of alternative drugs and innovative pharmaceutic formulations still have demanding requirements. Nanotechnologies could help to reach this latter crucial point in order to increase cellular uptake, enhance drug distribution, prolong half-life and reduce side effects depending on the lower drug dosage when included into nanosystems. In particular, application of nanoformulations consisting of a given drug and a supramolecular matrix such as niosomes, liposomes and solid lipid nanoparticles (SLN), already led to some improvements of pharmacokinetics and pharmacodynamic parameters. Very interesting results have been recorded in the anti-cancer

research field where an altered microenvironment of cancer cells facilitates a selective drug delivery. A similar approach could be adopted in the case of cells infected by HIV.

Another target, whose potential ligand have been investigated is represented by the GPER (G protein-coupled estrogen receptor 1 receptor). Different studies have shown that GPER, previously known as GPR30, mediates the multifaceted effects of estrogens in numerous pathophysiological events, including neurodegenerative, immune, metabolic, and cardiovascular disorders and the progression of different types of cancer. In particular, GPER is implicated in hormone-sensitive tumors, albeit diverse issues remain to be more deeply investigated. As such, this receptor may represent an appealing target for therapeutics in different diseases. The yet unavailable complete GPER crystallographic structure and its relatively low sequence similarity with the other members of the G protein-coupled receptor (GPCR) family hamper the possibility to discover compounds able to modulate GPER activity. Consequently, a reliable molecular model of this receptor is required for the design of suitable ligands. To date, convergent approaches involving structure-based drug design and virtual ligand screening have led to the identification of several GPER selective ligands, thus providing important information regarding its mode of action and function.

The last study included in this section focused on polycondensed heterocycles belonging to benzopyrroloxazine class described in papers or patents published during the last decades. The survey has been limited to substances characterized by the presence of a bridgehead N atom, namely a N atom belonging shared by different rings within the same molecule.

Taking into consideration the collected data on all the derivatives examined, it could be deducted that an in-depth investigation of selected classes as well as an optimization of known agents could be desirable in order to identified drug candidates to be developed for clinical application.

I. AN UPDATE ON SMALL MOLECULES TARGETING CXCR4 AS STARTING POINTS FOR THE DEVELOPMENT OF ANTI-CANCER THERAPEUTICS

Fedora Grande [a]; Giancotti Gilda [b]; Giuseppina Ioele [a]; Maria Antonietta Occhiuzzi [a]; Antonio Garofalo [a].

[a] Department of Pharmacy, Health and Nutritional Sciences, University of Calabria, Via P. Bucci, 87036 Rende (CS), Italy
[b] School of Pharmacy and Pharmaceutical Sciences, Cardiff University, King Edward VII Avenue, Cardiff CF10 3NB, UK

Abstract:

CXCR4 (C-X-C Chemokine Receptor type 4) and its natural ligand SDF-1a (Stromal-Derived-Factor-1α) are involved in a number of physiological and pathological processes including cancer spread and progression. Over the past few years, numerous CXCR4 antagonists have been identified and currently are in different development stages as potential agents for the treatment of several diseases involving the CXCR4/SDF-1α axis. Herein, we focus on small molecules reported in literature between 2013 and 2017, claimed as CXCR4 antagonists and potentially useful in the treatment of cancer and other diseases where this receptor is involved. Most of the compounds resulted from a chemical optimization of previously identified molecules and some of them could represent suitable candidates for the development of advanced anticancer agents.

Keywords: CXCR4, Small molecules, Antagonists, Cancer.

1. Introduction

CXCR4 (C-X-C chemokine receptor type 4), also known as cluster of differentiation 184 (CD184) or fusin, belongs to the rhodopsinlike G-protein-coupled receptor family [1,2]. Its structure consists of 352 amino acid residues including a C-terminal domain, seven trans-membrane domains, three extra-cellular and three intracellular loops and a N-terminal domain [3]. The response of CXCR4 to the specific interaction with its natural ligand SDF-1a (Stromal-Derived-Factor-1α, also known as CXCL12), regulates a number of physiological processes. During normal embryogenesis, cells mobility results under the control of several chemokinemediated signaling pathways, of which a pivotal role is played by the SDF-1α/CXCR4 axis. Such a type of control is still operating in adult pluripotent stem cells. Cancer cells invasiveness seems to be modulated by the same migratory pathway. At first CXCR4 was identified as one of the two co-receptors required for Human Immunodeficiency Virus (HIV) cell entry as its involvement is necessary for the fusion between the HIV envelope and the host cell membrane [4-9].
Recent studies confirmed a wide expression of CXCR4 in the hematopoietic and immune systems with a consequent implication of this receptor in a panel of pathological processes such as WHIM (Warts, Hypogammaglobulinemia, Infections, and Myelokathexis) syndrome, SLE (Systemic Lupus Erythematosus), rheumatoid arthritis, pulmonary fibrosis and cancer emergence and progression (Figure 1) [10-22].

The important roles recognized for the SDF-1α/CXCR4 axis in numerous pathogenic pathways make the receptor an attractive target for the development of small-molecule ligands as effective therapeutic agents.
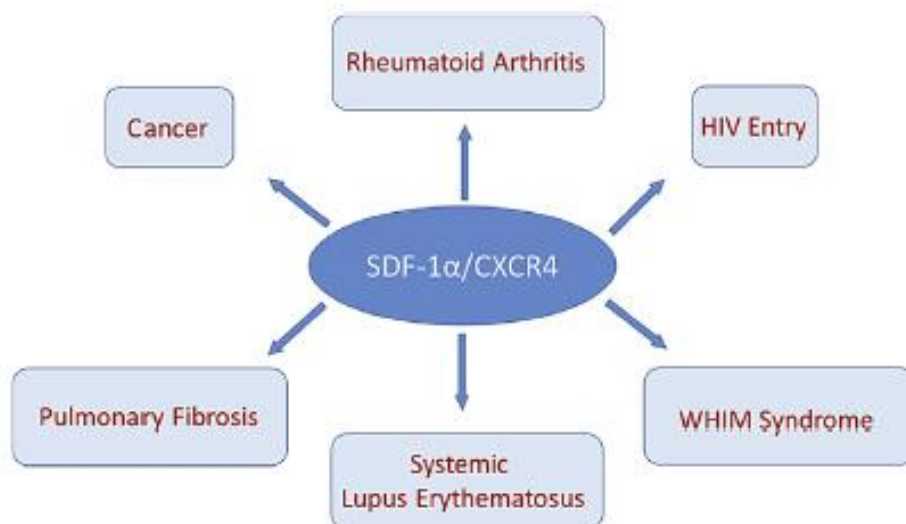

Figure 1. Diseases connected with SDF-1α/CXCR4 axis.

It has been ascertained that certain HIV inhibitors acting on the CXCR4 were also effective on chemokine-mediated processes involved in cancer progression. Thus, several known antagonists have been assayed on both HIV and cancer models, giving rise to converging results [23].

Taking into consideration the key role of SDF-1α/CXCR4 axis in mediating breast and ovarian cancer cell invasion and metastasis, the development of small molecules endowed with antagonistic activity towards the receptor, could lead to effective tools able to inhibit tumor progression, particularly during spreading of aggressive forms of this type of cancer. Targeted therapies based on small molecules antagonists have produced significant progress in experimental models [24].

A potential role of CXCR4 inhibitors was also assessed by a recent study on the PPAR (Peroxisome Proliferator Activated Receptor γ, a member of the nuclear receptor superfamily) downregulation during breast cancer spread and progression [16].

A further possible application for CXCR4 antagonists was also proposed for the treatment of pancreatic cancer, in which the importance of the SDF-1α/CXCR4 axis was also demonstrated using a gemcitabine-resistant tumor model. Matrigel invasion assays and animal studies proved such agents as useful tools for a second-line chemotherapy in pancreatic tumors [25].

Small cell lung carcinoma is known as one of the most aggressive type of cancer with low prognosis success due to rapid metastatic spread and quick emergence of resistance to chemo-agents.

The management of such a disease was achieved by the use of **AMD3100** (Plerixafor, Figure 2), a widely studied CXCR4 antagonist, demonstrating a relevant inhibitory activity in an orthotopic mouse model [26].

In a recent study, this compound and **TN14003** (Figure 2) [27], another known CXCR4 inhibitor, were tested against Herceptinsensitive and Herceptin-resistant HER2 breast cancers, proving a certain differentiated activity in the two cancerous forms. In the case of

the Herceptin-resistant triple negative cancer, the CXCR4 inhibition did not cause reduction of tumor growth besides an unexpected increase in metastatic spread, so limiting benefits of such a therapeutic approach to Herceptin-sensitive form [28].
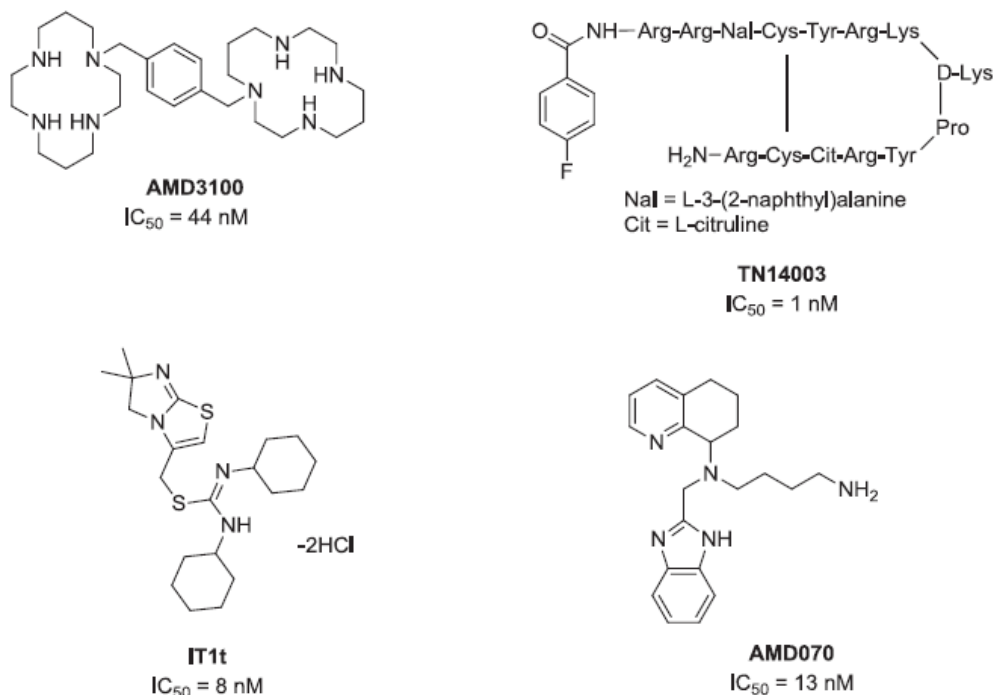

Figure 2. Chemical structures of known antagonists of CXCR4.

In the last few years, the X-ray structure of CXCR4 cocrystallized with various peptide and non-peptide ligands was assessed and used for the development of pharmacophoric models. In particular, the most used ligand for this purpose was **IT1t**, an orally active isothiourea based compound (Figures. 2 and 3) [29].

Several libraries of compounds were accordingly screened and a number of structural requirements have been deducted and taken into consideration for the design of new effective ligands [30-35].
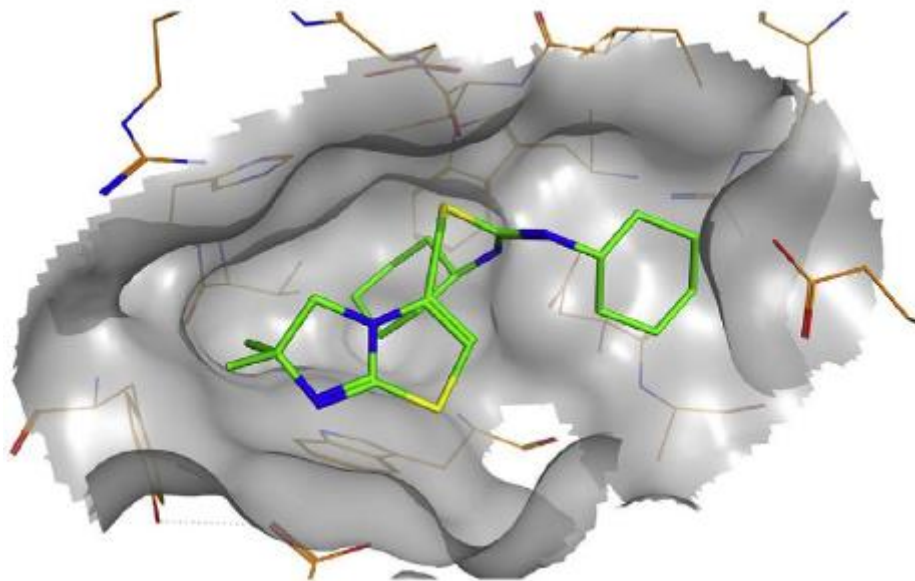
*Figure 3. Co-crystallized structure of CXCR4 with the known ligand **IT1t**.*

2. CXCR4 antagonists

The earlier identified CXCR4 antagonists were positively charged peptides that have been gradually replaced by more manageable downsized derivatives such as cyclic pentapeptides or peptidomimetics. Among the non-peptide ligands, a useful lead namely **AMD3100**, the first CXCR4 antagonist approved by the FDA, was selected within the class of bicyclams (cyclam = 1,4,8,11- tetraazacyclotetradecane), where the two macrocyclic parts are tethered by a *p*-xylylene fragment. The clinical applicability of this compound is however limited by an inadequate bioavailability [36-40]. To reduce the cationic nature as well as the large overall size, one or both cyclam rings have been in turn replaced by smaller moieties leading to still active compounds.

Successively, a tetrahydroquinoline derivative, **AMD070** (Figure 2), was identified as an oral active CXCR4 antagonist with remarkable activity, although its clinical investigation as anti-HIV agent has been now discontinued [6,41,42].

Many others antagonists belonging to more than twenty chemical classes have been so far discovered, even though only a few of them demonstrated features compatible with a possible clinical application.

Until 2012, in addition to the aforementioned bicyclams, the most intriguing active compounds were cyclopentapeptide, indole, tetrahydroquinoline, para-xylylenediamine and guanidine based compounds [15].

All the classes of recently identified antagonists are herein reviewed. However, the antagonists' classification based on a specific chemical feature could result ambiguous, due to the presence of common fragments in the structure of members assigned to distinct classes.

2.1. Cyclopentapeptides

Previous studies led to the discovery of a potent antagonist, **FC131** (cyclo(-Arg1-Arg2-2-Nal3-Gly4-D-Tyr5-), 2-Nal = 3-(2-naphthyl)alanine) (Figure 4), the structure of which was deducted from extensive SAR studies based on a pharmacophore model containing the Arg2-

Nal3-D-Tyr5-Arg14 sequence. More recently, **FC131** has been adopted as a suitable lead for the design of novel CXCR4 antagonists, in which various modifications of both the Nal and Tyr residues were attempted. Moreover, the replacement of Arg1 with the N-methyl-D-arginine led to the most potent derivative **FC122** [43].

A small library of pentapeptide derivatives was accordingly prepared and tested in a functional competitive assay that measured inhibition of SDF-1α-induced activation of human CXCR4. The chemical structures of the most active compounds are reported in Figure 4 (compounds **1-7**). Further development of SAR studies suggested that simpler peptidomimetics CXCR4 antagonists could be designed starting from the Arg2-2-Nal3 fragment [44].
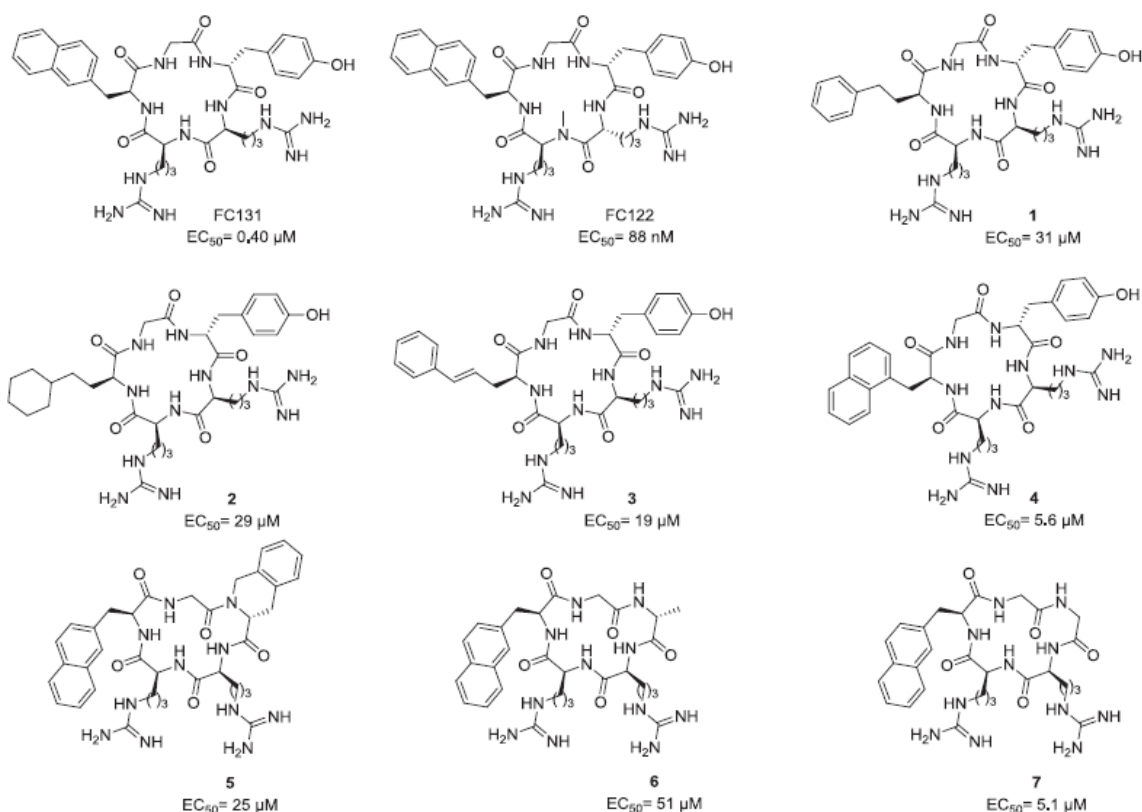
Figure 4. *Structures of **FC131** and most active cyclopentapeptide analogues with relative EC50 calculated by a functional competitive assay against COS-7 cells.*

2.2. Tripeptidomimetics

Successively, in-depth SAR studies on cyclopentapeptide CXCR4 antagonists proved that the tripeptide motif L-/D-Arg1-Arg2-2- Nal3 represents the minimal peptide sequence for the antagonistic activity. Thus, a systematic synthetic elaboration of the sequence led to the identification of a series of constrained tripeptidomimetics, still endowed with CXCR4 antagonist activity.

These compounds were characterized by a dioxohexahydropyrazinothiazine bicyclic central core, bringing two tails ending with a guanidine residue and a third tail containing a naphthyl system (Figure 5, compounds **8** and **9**). Although the potency of such new derivatives resulted lower than the cyclopeptides, as determined by a functional assay, they could

represent suitable starting points for the development of specific and less bulky CXCR4 ligands [45].

A further development of this study focused on the length of the three side chains of these compounds. Itwas demonstrated that the optimal spacer between the central core and both the guanidine moieties consists of a three-carbon atoms chain. On the other hand, the distance between the naphthyl group and the bicyclic core must kept in a two-carbon spacer, whereas a one-carbon spacer is tolerated when a bromine atom was present on the aromatic system, as calculated by functional antagonistic assay on a diastereoisomeric mixture of bromine derivative **10** (Figure 5) [46].
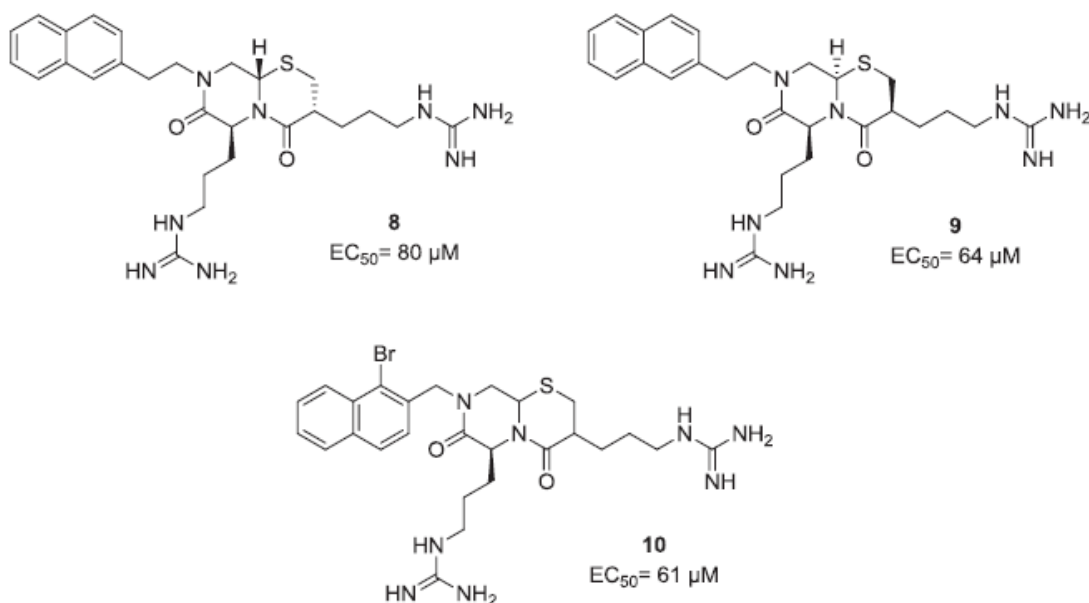
Figure 5. Representative structures of tripeptidomimetics with relative EC$_{50}$ calculated by a functional competitive assay against COS-7 cells.

In a recent study, the binding of a previously described tripeptidomimetic antagonist **KRH1636** to CXCR4 was assessed by the combination of SAR, receptor mapping, and molecular docking studies (Figure 6). Accordingly, a small series of tripeptide analogues has been synthesized and their antagonistic potency was calculated in a functional inhibition assay measuring the SDF-1a mediated activation of CXCR4. As a result, the identification of a binding model resulted from the inspection of interactions with the receptor providing new insight for structure-based design of novel small-molecule CXCR4 antagonists [34]. The chemical structures of the most promising derivatives are depicted in Figure 6 (compounds **11**-**15**).
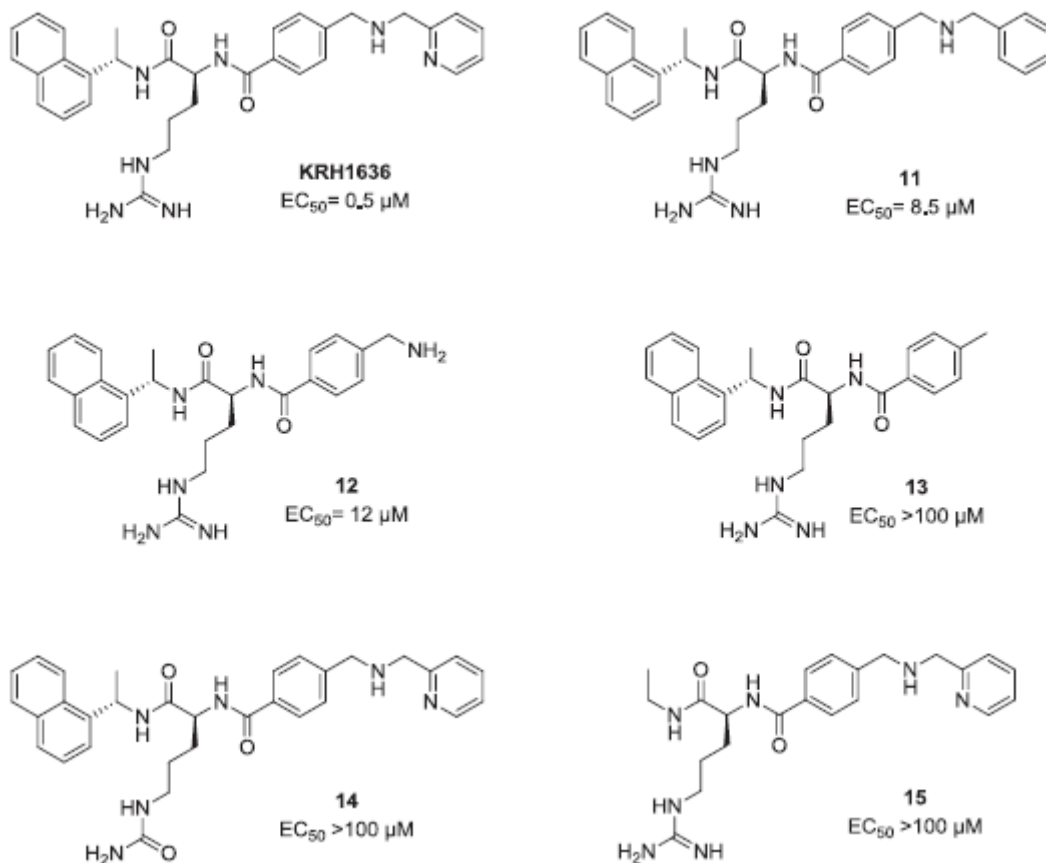
Figure 6. Chemical structures of selected KRH1636 tripeptidomimetic analogues with relative EC₅₀ calculated by a functional competitive assay against COS-7 cells.

2.2. Indoles

A recent approach to identify CXCR4 antagonists was developed using a minimal hybrid ligand/receptor-based pharmacophore model. Such simple approach has been applied to screen a small library of marine natural products. The search led to the identification of Phidianidine A (PHIA, 16), an indole alkaloid isolated from a mollusc, featuring at the same time a guanidine and an indole as the molecules ends and an oxadiazole moiety as the core, resulting in a very flexible structure (Figure 7). It was demonstrated that this compound selectively inhibits SDF-1a/CXCR4 mediated DNA synthesis, cell migration, and ERK1/2 activation, using the CXCR4-expressing/CXCR7-negative GH4C1 cell line. PHIA represents then a new lead for the development of CXCR4 modulators [47].

16
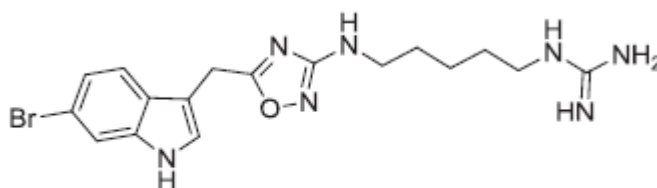
A novel series of indole derivatives was designed by *in silico* analysis of IT1t/CXCR4 complex. A few 2-(1H-indol-1-yl)benzohydrazide derivatives were synthesized and the biological testing revealed their capability to block SDF-1a induced cancer cell motility, proliferation and downstream signaling activation in different experimental models, using MDA-MB-231 and MCF-7 breast cancer cells. A whole cell-based [125I]-SDF-1a ligand binding competition assay confirmed that the mode of action of these compounds consists in a direct interaction with the active site of the receptor. The most active derivative was showed to be compound **17** (Figure 8), with an IC_{50} of 11 nM in the binding assay, while the cell migration inhibition was reached at a concentration lower than 10 nM [48].
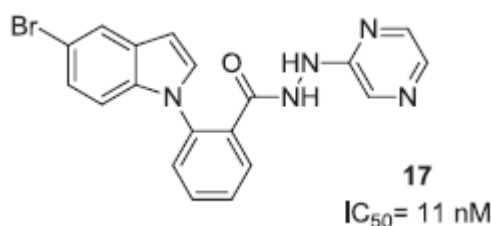

17
$IC_{50}= 11$ nM

Figure 8. Structure of the most active indolbenzohydrazide derivative.

2.4. Tetrahydroquinolines

Among the previous classes of CXCR4 antagonists, a preeminent position was occupied by derivatives based on a 1,2,3,4- tetrahydroquinoline moiety. Recently, a new group of active analogues containing also an additional isoquinoline nucleus was described. These compounds were found to effectively inhibit the receptor function either during CXCR4 mediated HIV attachment (IC_{50} = 5-40 nM, MAGI-HIV1 test) and calcium release (IC_{50} =1-570 nM). The chemical structures of the most active compounds are reported in Figure 9 (compounds **18**-**26**). Furthermore, the most promising compound (18) showed favourable pharmacokinetics, oral bioavailability and the capability of mobilizing white blood cells in a dose-dependent manner [49].
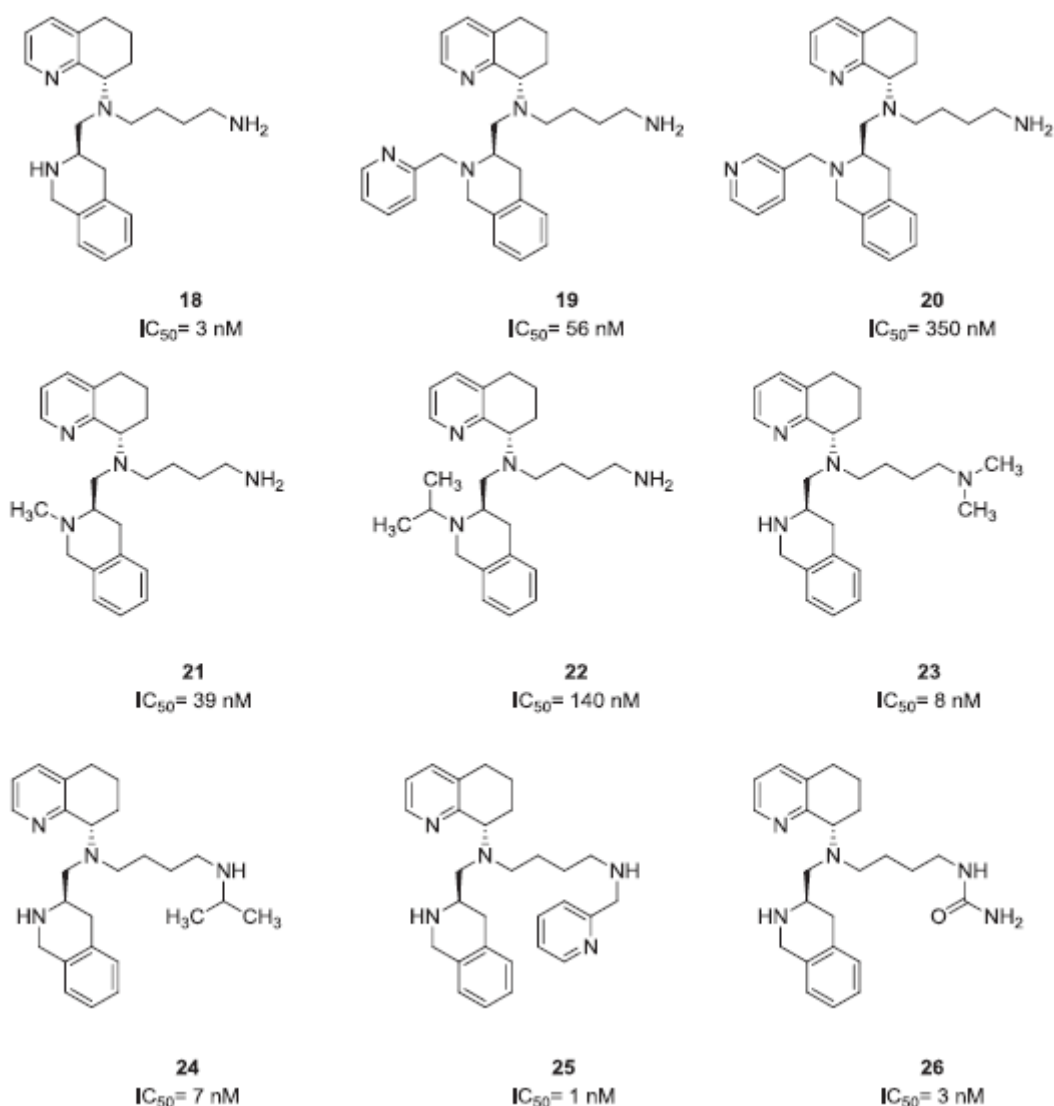
Figure 9. *Structure of the most active tetrahydroquinoline based compounds with relative IC_{50} alculated by a calcium flux/release assay in Chem-1 cells.*

A second series of 1,2,3,4-tetrahydroquinolines, this time combined with a piperazine nucleus, was designed and proved to be active in the same tests above mentioned. One of the new derivatives, compound **27** (Figure 10), beside a pharmacokinetics and an inhibitory potency comparable to the previous isoquinolinecontaining lead (IC_{50} = 20 nM, MAGI-HIV1 test; IC_{50} = 6 nM, calcium release), showed an improved behaviour toward CYP450 and hERG [50].
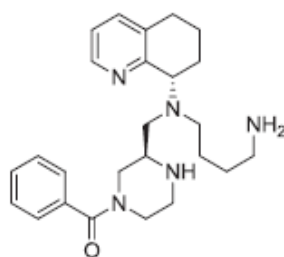
27

Figure 10. *Structure of tetrahydroquinoline 27.*

2.5. p-Xylylenediamine based derivatives

As already mentioned, to improve the pharmacokinetic profile of **AMD3100**, characterized by a p-xylylenediamine tether between two cyclams, intensive studies have been carried out in the search of related simplified active structures. Accordingly, compounds containing a single cyclam connected by a p-xylylenediamine linker to an aromatic or heteroaromatic moiety have been developed and exhibited high antagonistic activity due to their capability to interact similarly to **AMD3100** into the CXCR4 active site [15].

More recently, two monocyclams have been synthesized (Figure 11, compounds **28** and **29**) and in turn linked through the primary amino group to a long linear chain obtained by polymerization of bis-acrilamide. A geometrically defined polymeric structure, necessary for optimal receptor interaction, was obtained by intercalating the cyclams by pharmacologically inert butanol units along the linear chain. Using a receptor redistribution assay based on human osteosarcoma cell line U2OS, widely adopted for screening CXCR4 ligands, it has been demonstrated that the antagonistic activity was considerably improved turning from monomeric structures to polymer. Such macromolecules also showed a remarkable capability to inhibit cancer cells migration and invasiveness at similar concentration of the reference compound **AMD3100**.
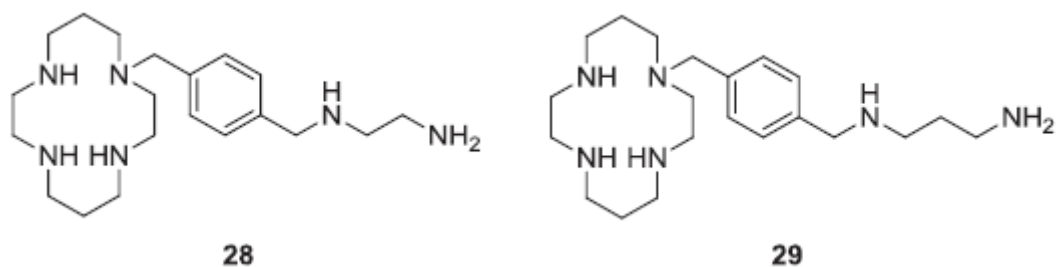

Figure 11. *Monocyclam structures included into polymeric system*

Furthermore, due to their overall positive charge, such polymers resulted able to interact with DNA mediating transfection. The possibility to antagonize CXCR4 function and, at the same time, to deliver nucleic acid makes these systems promising dual-function polymeric drugs for an advanced approach to cancer treatment [51].

More flexible and less bulky structures, with respect to previous described bicyclams or cyclams, have been also taken into consideration. Two series of compounds based on a *p*-xylylen central core, but bearing different cyclic amines at various distances from the phenyl ring on both sides of the molecule, have been prepared and tested in anti-HIV and cytotoxic assays. The series were prepared using a same amine at the same distance from the molecule core or even different amines at variable distances, giving rise to unsymmetrical derivatives. The compounds were tested in an antagonistic assay against MT-4 cells The most active compounds were found to belong to the symmetrical series and bear pyrrolidine, piperidine or 2-methylpiperidine as an amine to both ends of the molecule (Figure 12, compounds **30-38**). The results obtained were confirmed by molecular docking studies [52].
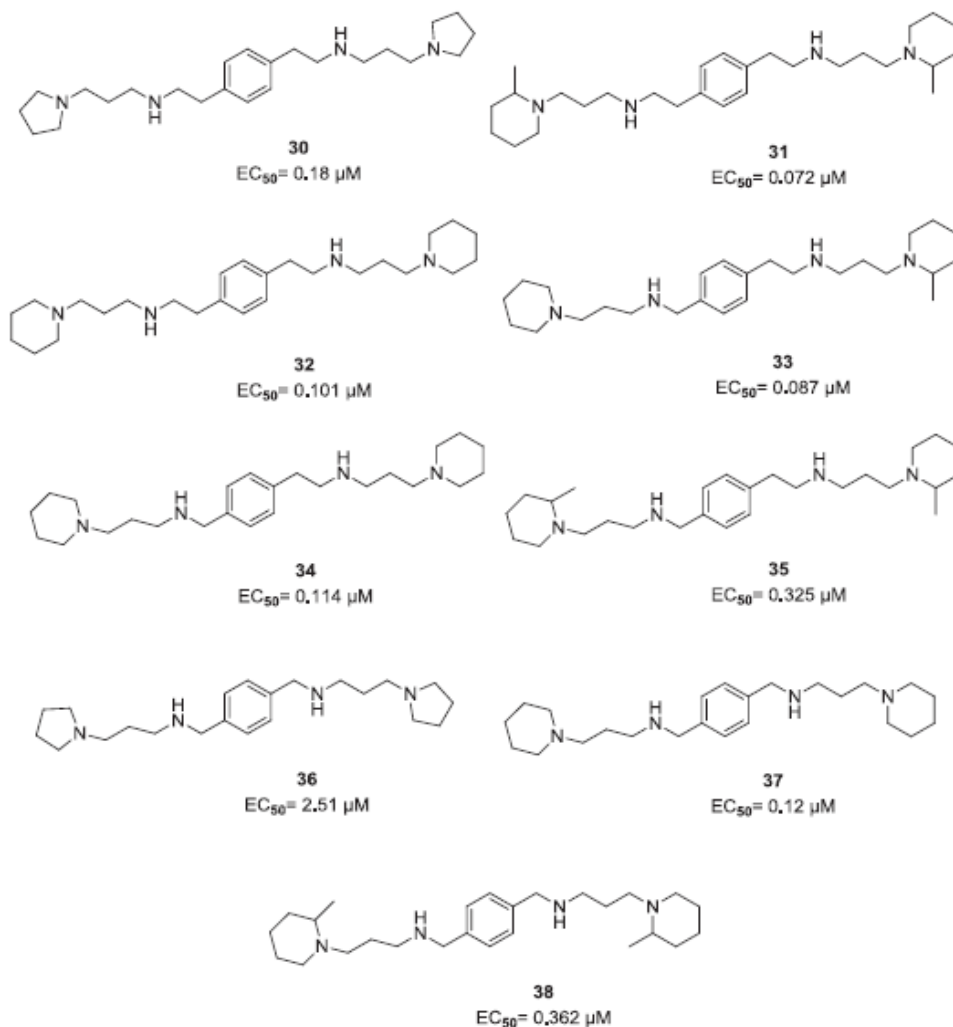
Figure12. Structures of representative examples of symmetrical and unsymmetrical p-xylylenediamine based CXCR4 antagonists with relative EC50 calculated by a MTT assay against MT-4 cells

Starting from compound **WZ811**, a dipyridine derivative, which showed an intriguing biological profile (Figure 13) [53], a new class of benzenesulfonamide analogues, retaining the central phenyl ring was prepared and tested as CXCR4 antagonists. Some of these derivatives were symmetrical compounds with respect to aromatic central core, whilst some others were unsymmetrically substituted.

Chemical structure of all derivatives comprises a sulphonamide moiety on one or both sides of the molecule. Two out of all synthesized compounds, **39** and **40** (Figure 13) resulted particularly active exhibiting IC_{50} values lower than 10 nM in the binding affinity assay and inhibition of invasion higher than 90% in the Matrigel assay.
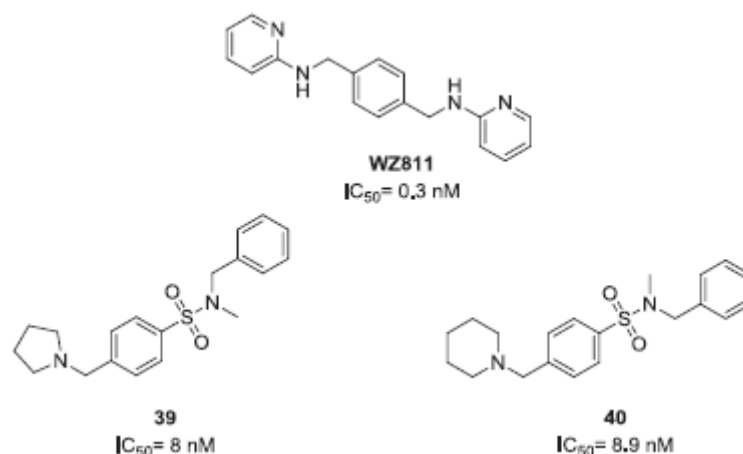
Figure 13. *Structures of* ***WZ811*** *and sulfonamide analogues with relative IC$_{50}$ calculated by a seven- point assay against MDA-MB-231 cells.*

However, authors hypothesized for these two molecules, lacking the whole *p*-xylylene core, a different interaction mode with CXCR4, with respect to the reference compound, as demonstrated by molecular docking studies [54].

In a separate study, structurally related *p*-xylylene derivatives, still containing a sulfonamide moiety, were identified using a computer-aided drug design screening, by a high throughput program named FRESH workflow. From the first 30 prioritized structures, twelve compounds were selected and most of them showed an excellent binding affinity to CXCR4. The amide-sulfamide pharmacophore was confirmed to be a promising scaffold for the development of CXCR4 antagonists.

The chemical structures of the most promising derivatives are depicted in Figure 14 (compounds **41**-**45**) [55].
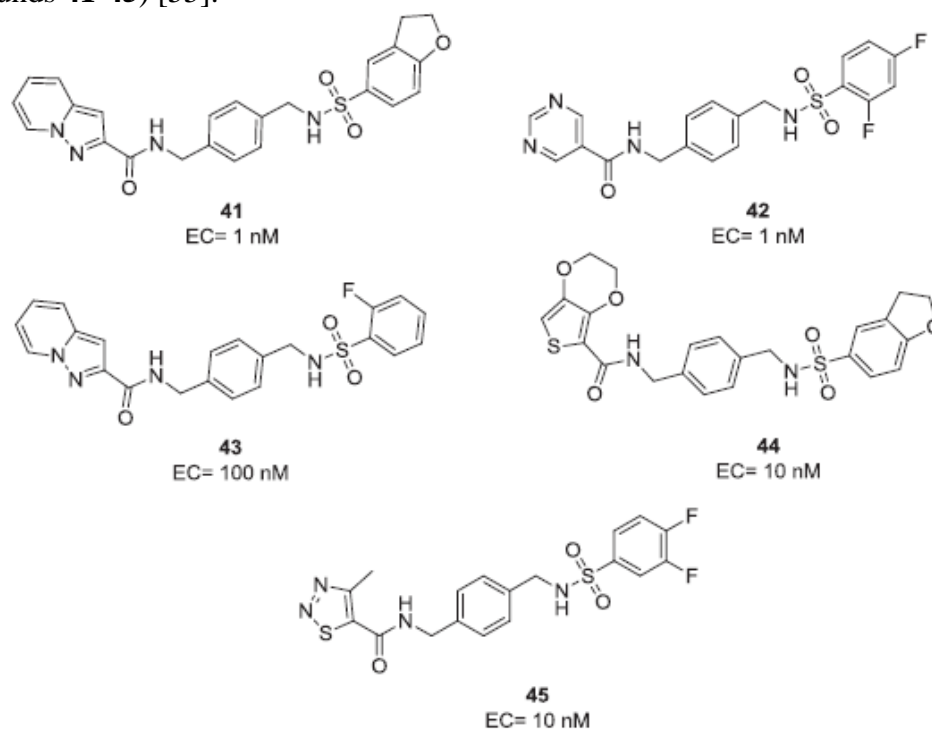

Figure 14. *Structures of selected p-xylylene based CXCR4 antagonists with relative EC calculated by a rhodamine binding assay against MDA-MB-231 breast cancer cells.*

163

The same research group, very recently, published a study in which a new series of *p*-xylylene active unsymmetrical derivatives were obtained. As the sulfonamide group was found to be necessary for activity, in this new series a bioisostere amide group replaced previous imine moiety on the second branch of the molecules, generating the novel amide-sulfamide series of compounds.

This new group of derivatives retains a potent CXCR4 antagonistic activity. A number of selected derivatives showed noteworthy activity in the Matrigel assay preventing invasion for more than 90% cells (Figure 15, compounds **46**-**49**) [56].
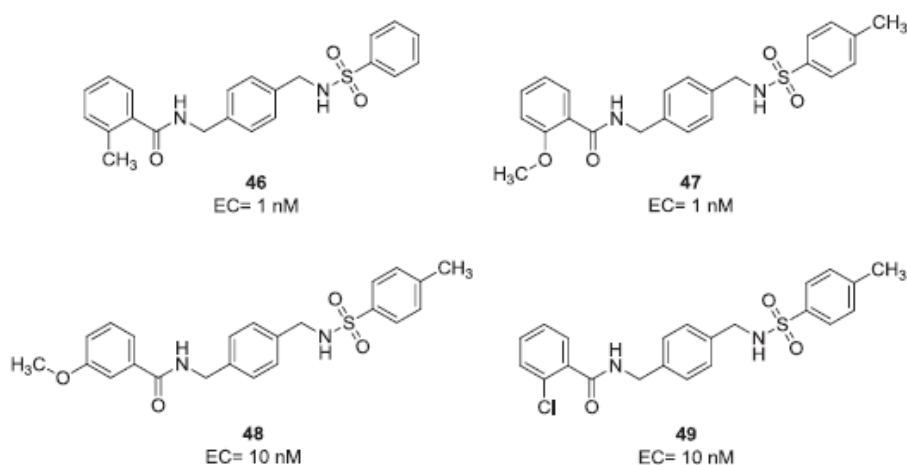

Figure 15. *Structures of the most active sulfonamide derivatives with relative EC calculated by a rhodamine binding assay against MDA-MB-231 breast cancer cells.*

A further modification of previously reported *p*-xylylenediamine derivatives was achieved by replacing the central 1,4- disubstituted phenyl ring with a 2,6-disubstituted pyridine. The resulting compounds were tested using an affinity binding test and the Matrigel invasion assay. Most of the synthesized compounds showed promising results in the binding affinity assay. In particular, the derivative bearing a 3-fluorophenyl fragment on both sides of the molecule and the 4-ethylphenyl analogue resulted as the most interesting derivatives, with an EC value of 10 and 1 nM in the binding affinity assay and 50% and 64% inhibition of invasion, respectively using MDA-MB-231 breast cancer cells (Figure 16, compounds **50** and **51**) [57].
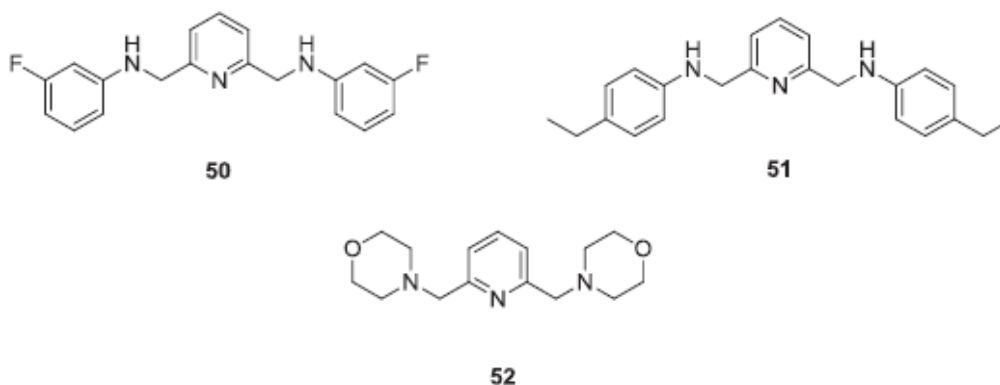

Figure 16. *Selected active pyridine derivatives.*

In a successive study, several new derivatives substituted at positions 2 and 6 or 2 and 5 of the pyridine central ring have been synthesized and tested in a similar CXCR4 binding assay as well as in an invasion inhibition test. Only two compounds, both belonging to the 2,6-substituted series, showed interesting antagonisti properties: the already known derivative **51** and a second one in which the two substituents were replaced by a morpholine (Figure 16, compound **52**). This compound showed an EC value of 10 nM in the binding affinity and 63% inhibition of invasion [58].

Two new series of p-xylylenediamine derivatives were described recently. A first series presents a variously substituted quinazoline system as one side chain, while in the second series the quinazoline was replaced by a substituted purine. The other side of the molecule contains a cyclohexylamine propyl fragment in all the derivatives (Figure 17, compounds **53**-**58**).
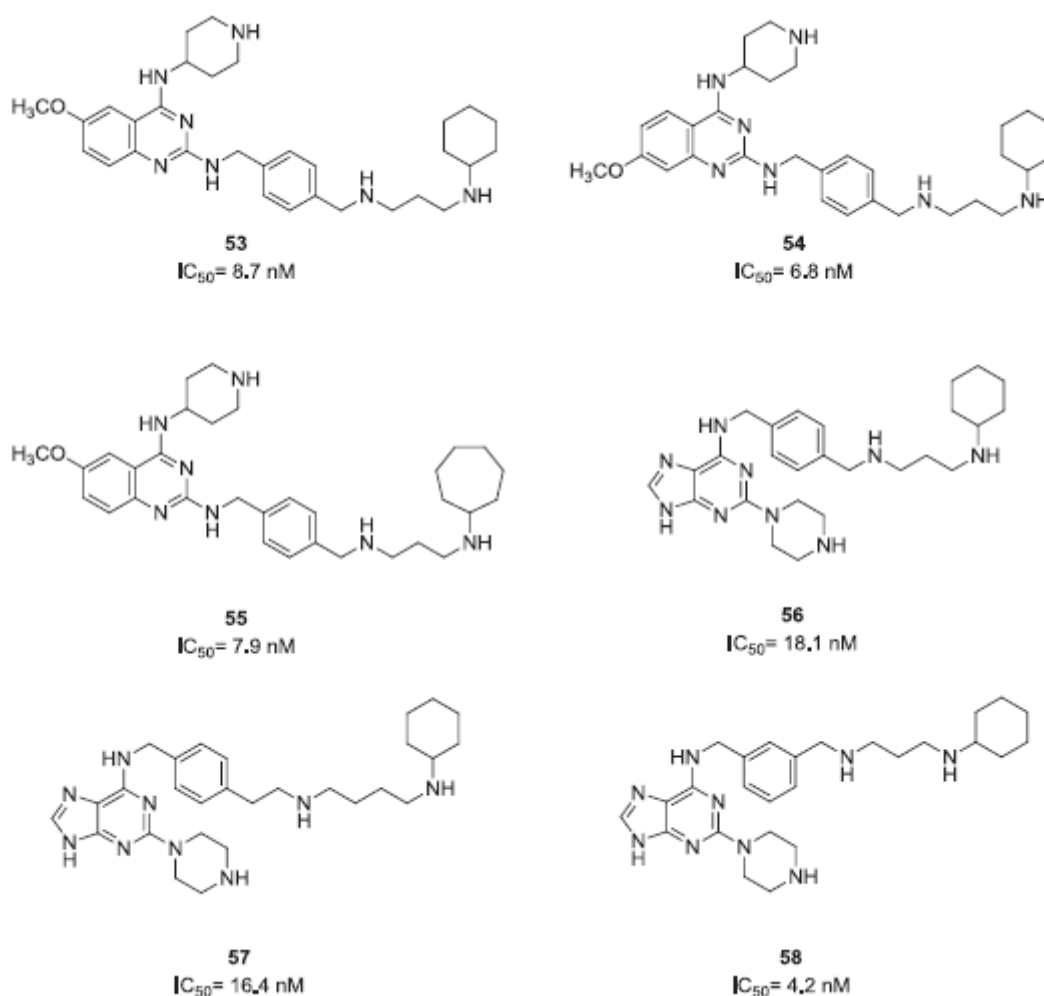

Figure 17. *Quinazoline or purine containing p-xylylene derivatives with relative IC$_{50}$ calculated by a cytotoxic assay against CEM cells*

The most active analogue **58**, belonging to the purine series, showed a remarkable CXCR4 binding affinity with an IC$_{50}$ value of 4.2 nM, thus representing a promising starting point for the development of potent CXCR4 antagonists [59].

The same research group designed and synthesized a series of novel symmetrical compounds characterized by a *p*-xylylene or a 2,6-pyridil central core bearing, as a structural novelty, a tertiary amine on both sides of the molecule. The significant CXCR4 antagonistic effect was

successfully retained, since ten derivatives showed potent binding affinity with EC_{50} values from 1 to 100 nM.

Some of the synthesized compounds were also found to be able to significantly limit tumor cell invasion, with inhibitory rates ranging from 65% to 100%. These results clearly showed that tertiary amines linked to the central core play a crucial role for the interaction with the receptor and thus leading to an improved antagonistic activity.

The chemical structures of the most promising derivatives are depicted in Figure 18 (compounds **59**-**64**) [60].

59
EC= 10 nM

60
EC= 1 nM

61
EC= 10 nM

62
EC= 10 nM

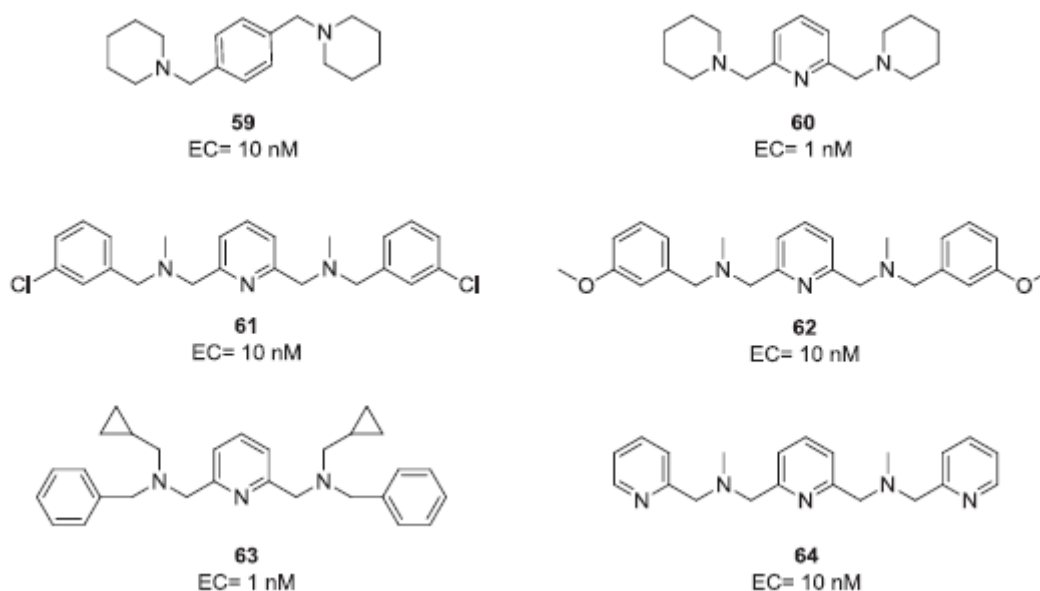**63**
EC= 1 nM

64
EC= 10 nM

Figure 18. *Representative examples of active symmetrical CXCR4 antagonists with relative EC calculated by a rhodamine binding assay in MDA-MB-231 breast cancer cells*

2.6. Trisubstituted amines

Some trisubstituted amine derivatives were known to be capable of inhibiting the SDF-1α/CXCR4 axis provoking different effects on haematopoiesis, stem cells mobilization and cancer. The potent previously mentioned tetrahydroquinoline derivative **AMD070** (Figure 2) is also referable to this class of compounds.

Recently, tris-[2-(dimethylamino)ethyl] amine (**Me6TREN**, Figure 19), a commercially available compound, has been proved as an effective agent able to mobilize hematopoietic stem/progenitor cells by a mechanism involving the inhibition of the SDF-1α/CXCR4 axis. **Me6TREN** promoted a significant inhibition of SDF-1α-einduced chemotaxis in cells based assay (Figure 19) [61].
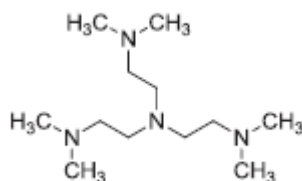

Figure 19. *Structure of **Me6TREN**.*

A trisubstituted amine derivative, 3-((((1-cyclopentylpiperidin- 3-yl)methyl)(2-(piperidin-1-yl)ethyl)amino)methyl)phenol (CX6), was selected after a computational search throughout a library as an ideal small molecule CXCR4 antagonist (Figure 20). The search was conducted on the base of the shape of the known **IT1t** CXCR4 inhibitor (Figure 2) as a reference and employing various algorithms against the IT1t/CXCR4 complex crystal structure. A number of molecules has been accordingly synthesized and tested against U373-MAGI cells leading to compound **CX6** as the most promising candidate. In fact, **CX6** showed to be able to inhibit Ca^{2+} flux elicited
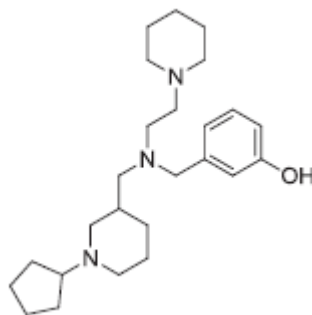by SDF-1a with an IC_{50} value of 92 nM [62].

Figure 20. Structure of CX6.

2.7. Oxadiazolepyrimidine

A new class of small molecule CXCR4 antagonists based on the use of computational modelling studies combined with *in vitro* evaluation of SDF-1α -induced intracellular calcium mobilization, proliferation and chemotaxis was discovered. The lead compound, **ICT5040**, a 2-(pyridin-3-yl)-1,3,4-oxadiazole derivative, was shown to inhibit SDF-1α induced intracellular calcium mobilization, with an IC_{50} value of 3.8 mM, and was opportunely used for chemical optimization. A series of analogues with improved anti-migratory potency was then obtained and the most representative derivative was identified as the soluble analogue 65, which resulted very potent in inhibiting SDF-1α induced intracellular calcium mobilization, as well as cell proliferation and migration. The chemical structures of the most promising derivatives are depicted in Figure 21 (compounds **65-68**) [63].
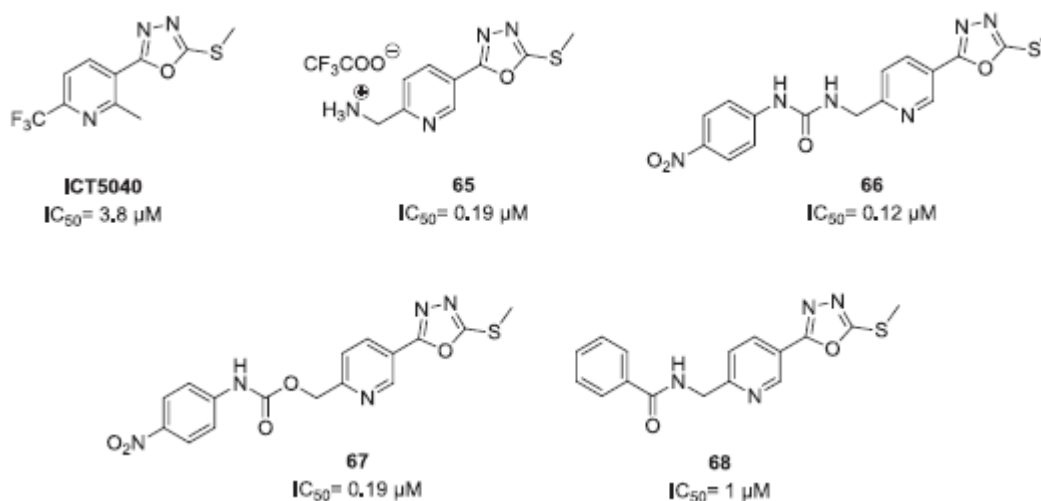

Figure 21. Representative examples of oxadiazolepyrimidine CXCR4 antagonists with relative IC_{50} calculated by MTT assay against U87-MG cells.

3. Conclusion

The role of the SDF-1α/CXCR4 axis has been definitively clarifie as crucial during several physio-pathological events, including spread and mobility of different types of cancer. In particular, hormones sensitive breast and ovarian cancer morbidity seems strictly related to the effects springing from the interaction of SDF- 1α with its receptor. Moreover, reduced survival in breast and ovarian cancer patients was shown to be dependent to an altered SDF-1α expression. Thus, agents able to impair the SDF-1α/CXCR4 axis could represent valuable tools for alternative anti-neoplastic therapies. To date only one CXCR4 antagonist has reached the advanced phases of the clinical trials. As several compounds belonging to distinct chemical classes have been identified as promising antagonists for this process, it seems likely that new small molecules could be shortly developed as therapeutic agents.
Amongst the described compounds, cyclopentapeptides and bicyclams seem the most promising classes to be investigated in order to select potent candidates for clinical application. Both classes of compounds, considered small molecules, show unfavourable pharmacokinetic profiles, which greatly limit a possible use in therapy. *p*-Xylylenediamine and tetrahydroquinoline derivatives are presently widely investigated, even though none of the other described chemical classes has been so far completely abandoned. Herein, the most recent findings in this field have been reviewed. Although most of the active compounds have been at first recognized as feasible anti-HIV agents, all identified antagonists could even act as effective anticancer agents. However, all the examined classes are worth to be in depth investigated in order to generate candidates for a clinical development. In fact, a major goal for medicinal chemists could reside in the identification of orally active and safe CXCR4 antagonists after a comprehensive characterization of long-term toxicity and off-target effects of the most promising candidates. Finally, the possibility to obtain radiolabelled derivatives as potential biomarkers in cancer diagnosis, prevention and drug response, may represent a further applicative development of CXCR4 antagonists.

References

[1] M. Lefrancois, M.R. Lefebvre, G. Saint-Onge, P.E. Boulais, S. Lamothe, R. Leduc, P. Lavigne, N. Heveker, E. Escher, Agonists for the chemokine receptor CXCR4, ACS Med. Chem. Lett. 2 (2011) 597e602.

[2] S.J. Allen, S.E. Crown, T.M. Handel, Chemokine: receptor structure, interactions, and antagonism, Annu. Rev. Immunol. 25 (2007) 787e820.

[3] B. Wu, E.Y. Chien, C.D. Mol, G. Fenalti, W. Liu, V. Katritch, R. Abagyan, A. Brooun, P. Wells, F.C. Bi, D.J. Hamel, P. Kuhn, T.M. Handel, V. Cherezov, R.C. Stevens, Structures of the CXCR4 chemokine GPCR with small-molecule and cyclic peptide antagonists, Science 330 (2010) 1066e1071.

[4] C.C. Bleul, M. Farzan, H. Choe, C. Parolin, I. Clark-Lewis, J. Sodroski, T.A. Springer, The lymphocyte chemoattractant SDF-1 is a ligand for LESTR/ fusin and blocks HIV-1 entry, Nature 382 (1996) 829e833.

[5] A.S. Karaboga, J.M. Planesas, F. Petronin, J. Teixido, M. Souchet, V.I. Perez- Nueno, Highly specific and sensitive pharmacophore model for identifying CXCR4 antagonists. Comparison with docking and shape-matching virtual screening performance, J. Chem. Inf. Model. 53 (2013) 1043e1056.

[6] B. Zhong, Y. Zhen, G. Qin, H. Yang, H. Jiang, G. Chen, K. Yu, Progress in studies of structure, mechanism and antagonists interaction of GPCR co-receptors for HIV, Curr. Pharm. Biotechnol. 15 (2014) 938e950.

[7] H. Zhang, D. Kang, B. Huang, N. Liu, F. Zhao, P. Zhan, X. Liu, Discovery of nonpeptide small molecular CXCR4 antagonists as anti-HIV agents: recent advances and future opportunities, Eur. J. Med. Chem. 114 (2016) 65e78.

[8] F.O. Gombert, D. Obrecht, A. Lederer, J. Zimmermann, C. Oefner, Preparation of b-Hairpin Peptidomimetics as CXCR4 Antagonists for Treatment of HIV Infection, from WO2013182240, 2013.

[9] J.H. Ye, S.M. Zhou, Q. Wang, L. Lu, M.X. Dong, H.B. Chen, S.B. Jiang, Q.Y. Dai, Design, syhthesis and activity evaluation of new anti-HIV-1 CXCR4 inhibitors, Junshi Yixue 38 (2014) 602e607.

[10] L. Portella, R. Vitale, S. De Luca, C. D'Alterio, C. Ierano, M. Napolitano, A. Riccio, M.N. Polimeno, L. Monfregola, A. Barbieri, A. Luciano, A. Ciarmiello, C. Arra, G. Castello, P. Amodeo, S. Scala, Preclinical development of a novel class of CXCR4 antagonist impairing solid tumors growth and metastases, PLoS One 8 (2013) e74548.

[11] H.K. Shu, Y. Yoon, S. Hong, K. Xu, H. Gao, C. Hao, E. Torres-Gonzalez, C. Nayra, M. Rojas, H. Shim, Inhibition of the CXCL12/CXCR4-axis as preventive therapy for radiation-induced pulmonary fibrosis, PLoS One 8 (2013) e79768.

[12] W.T. Choi, Y. Yang, Y. Xu, J. An, Targeting chemokine receptor CXCR4 for treatment of HIV-1 infection, tumor progression, and metastasis, Curr. Top. Med. Chem. 14 (2014) 1574e1589.

[13] A. Zuk, M. Gershenovich, Y. Ivanova, R.T. MacFarland, S.P. Fricker, S. Ledbetter, CXCR (4) antagonism as a therapeutic approach to prevent acute kidney injury, Am. J. Physiol. Ren. Physiol. 307 (2014) F783eF797.

[14] B.S. Cho, Z. Zeng, H. Mu, Z. Wang, S. Konoplev, T. McQueen, M. Protopopova, J. Cortes, J.R. Marszalek, S.B. Peng, W. Ma, R.E. Davis, D.E. Thornton, M. Andreeff, M. Konopleva, Antileukemia activity of the novel peptidic CXCR4 antagonist LY2510924 as monotherapy and in combination with chemotherapy, Blood 126 (2015) 222e232.

[15] B. Debnath, S. Xu, F. Grande, A. Garofalo, N. Neamati, Small molecule inhibitors of CXCR4, Theranostics 3 (2013) 47e75.

[16] D. Rovito, G. Gionfriddo, I. Barone, C. Giordano, F. Grande, F. De Amicis, M. Lanzino, S. Catalano, S. Ando, D. Bonofiglio, Ligand-activated PPARgamma downregulates CXCR4 gene expression through a novel identified PPAR response element and inhibits breast cancer progression, Oncotarget 7 (2016) 65109e65124.

[17] S.H. Chung, K. Seki, B.I. Choi, K.B. Kimura, A. Ito, N. Fujikado, S. Saijo, Y. Iwakura, CXC chemokine receptor 4 expressed in T cells plays an important role in the development of collagen-induced arthritis, Arthritis Res. Ther. 12 (2010). R188.

[18] Wang, P. Guilpain, B.F. Chong, S. Chouzenoux, L. Guillevin, Y. Du, X.J. Zhou, F. Lin, A.M. Fairhurst, C. Boudreaux, C. Roux, E.K. Wakeland, L.S. Davis, F. Batteux, C. Mohan, Dysregulated expression of CXCR4/CXCL12 in subsets of patients with systemic lupus erythematosus, Arthritis Rheumatism 62 (2010) 3436e3446.

[19] Aghamohammadi, H. Abolhassani, J. Puchalka, N. Greif-Kohistani, S. Zoghi, C. Klein, N. Rezaei, Preference of genetic diagnosis of CXCR4 mutation compared with clinical diagnosis of WHIM syndrome, J. Clin. Immunol. 37 (2017) 282e286.

[20] Q. Liu, C. Pan, L. Lopez, J. Gao, D. Velez, S. Anaya-O'Brien, J. Ulrick, P. Littel, J.S. Corns, D.T. Ellenburg, H.L. Malech, P.M. Murphy, D.H. McDermott, WHIM syndrome caused by Waldenstrom's macroglobulinemia-associated mutation CXCR4 (L329fs), J. Clin. Immunol. 36 (2016) 397e405.

[21] T. Pozzobon, G. Goldoni, A. Viola, B. Molon, CXCR4 signaling in health and disease, Immunol. Lett. 177 (2016) 6e15.

[22] K. Rakesh, D.G. Duda, S.V. Kozin, D. Fukumura, Anti-CXCR4 as a Sensitizer to Cancer Therapheutics, from US9155723, 2015.

[23] F. Grande, A. Garofalo, N. Neamati, Small molecules anti-HIV therapeutics targeting CXCR4, Curr. Pharm. Des. 14 (2008) 385e404.

[24] P. Jansa, T. Simon, E. Lansdon, Y.E. Hu, O. Baszczynski, M. Dejmek, R. Mackman, Preparation of Quinazoline Derivatives for the Treatment of HIV Infection, from WO2016105564, 2016.

[25] M. Morimoto, Y. Matsuo, S. Koide, K. Tsuboi, T. Shamoto, T. Sato, K. Saito, H. Takahashi, H. Takeyama, Enhancement of the CXCL12/CXCR4 axis due to acquisition of gemcitabine resistance in pancreatic cancer: effect of CXCR4 antagonists, BMC Cancer 16 (2016).

[26] S. Taromi, G. Kayser, J. Catusse, D. von Elverfeldt, W. Reichardt, F. Braun, W.A. Weber, R. Zeiser, M. Burger, CXCR4 antagonists suppress small cell lung cancer progression, Oncotarget 7 (2016) 85185e85195.

[27] K. Beider, M. Begin, M. Abraham, H. Wald, I.D. Weiss, O. Wald, E. Pikarsky, E. Zeira, O. Eizenberg, E. Galun, I. Hardan, D. Engelhard, A. Nagler, A. Peled, CXCR4 antagonist 4F-benzoyl-TN14003 inhibits leukemia and multiple myeloma tumor growth, Exp. Hematol. 39 (2011) 282e292.

[28] S. Lefort, A. Thuleau, Y. Kieffer, P. Sirven, I. Bieche, E. Marangoni, A. Vincent- Salomon, F. Mechta-Grigoriou, CXCR4 inhibitors could benefit to HER2 but not to triple-negative breast cancer patients, Oncogene 36 (2017) 1211e1222.

[29] G. Thoma, M.B. Streiff, J. Kovarik, F. Glickman, T. Wagner, C. Beerli, H.G. Zerwes, Orally bioavailable isothioureas block function of the chemokine receptor CXCR4 *in vitro* and *in vivo*, J. Med. Chem. 51 (2008) 7915e7920.

[30] S. Costantini, R. Raucci, G. Colonna, F.A. Mercurio, A.M. Trotta, R. Paola, M. Leone, F. Rossi, C. Pellegrino, G. Castello, S. Scala, Peptides targeting chemokine receptor CXCR4: structural behavior and biological binding studies, J. Peptide Sci. Official Publ. Eur. Peptide Soc. 20 (2014) 270e278.

[31] C. Castaldo, T. Benicchi, M. Otrocka, E. Mori, E. Pilli, P. Ferruzzi, S. Valensin, D. Diamanti, W. Fecke, M. Varrone, V. Porcari, CXCR4 antagonists: a screening strategy for identification of functionally selective ligands, J. Biomol. Screen. 19 (2014) 859e869.

[32] B.D. Cox, A.R. Prosser, B.M. Katzman, A.A. Alcaraz, D.C. Liotta, L.J. Wilson, J.P. Snyder, Anti-HIV small-molecule binding in the peptide subpocket of the CXCR4:CVX15 crystal structure, ChemBioChem a Eur. J. Chem. Biol. 15 (2014) 1614e1620.

[33] J. Vabeno, B.E. Haug, M.M. Rosenkilde, Progress toward rationally designed small-molecule peptide and peptidomimetic CXCR4 antagonists, Future Med. Chem. 7 (2015) 1261e1283.

[34] Z.G. Zachariassen, S. Karlshoj, B.E. Haug, M.M. Rosenkilde, J. Vabeno, Probing the molecular interactions between CXC chemokine receptor 4 (CXCR4) and an arginine-based tripeptidomimetic antagonist (KRH-1636), J. Med. Chem. 58 (2015) 8141e8153.

[35] H. Fu, Z. Yan, R. Lin, A. Diao, D. Xiao, Pharmacophore design for non-peptide inhibitors of chemokine acceptor CXCR4, Tianjin Keji Daxue Xuebao 29 (2014) 6e10.

[36] Clinical Trials database: NCT01339039.https://clinicaltrials.gov/ct2/show/ NCT01339039, 2017 (accessed 23.06.2017).

[37] Clinical trials database: NCT01141543. https://clinicaltrials.gov/ct2/show/ NCT01141543, 2014 (accessed 23.06.2017).

[38] Clinical trials database: NCT01373229. https://clinicaltrials.gov/ct2/show/ NCT01373229, 2016 (accessed 23.06.2017).

[39] Clinical trials database: NCT01058993. https://clinicaltrials.gov/ct2/show/ NCT01058993, 2012 (accessed 23.06.2017).

[40] Clinical trials database: NCT01018979. https://clinicaltrials.gov/ct2/show/ NCT01018979, 2015 (accessed 23.06.2017).

[41] T.D. Gaines, S. Reid Mooring, Z. Liang, H. Shim, Synthesis of pyridine and thiophene derivatives as potential antagonists of chemokine receptor type-4, San Francisco (CA), in: 248th ACS National Meeting&Exposition, 2014.

[42] B.N. Naidu, M. Patel, T.P. Connolly, Preparation of Pyridoindazole Compounds as Inhibitors of Human Immunodeficiency Virus Replication, from WO2014159959, 2014.

[43] S. Ueda, S. Oishi, Z.X. Wang, T. Araki, H. Tamamura, J. Cluzeau, H. Ohno, S. Kusano, H. Nakashima, J.O. Trent, S.C. Peiper, N. Fujii, Structure-activity relationships of cyclic peptide-based chemokine receptor CXCR4 antagonists: disclosing the importance of side-chain and backbone functionalities, J. Med. Chem. 50 (2007) 192e198.

[44] J. Mungalpara, Z.G. Zachariassen, S. Thiele, M.M. Rosenkilde, J. Vabeno, Structure-activity relationship studies of the aromatic positions in cyclopentapeptide CXCR4 antagonists, Org. Biomol. Chem. 11 (2013) 8202e8208.

[45] Z.G. Zachariassen, S. Thiele, E.A. Berg, P. Rasmussen, T. Fossen, M.M. Rosenkilde, J. Vabeno, B.E. Haug, Design, synthesis, and biological evaluation of scaffold-based tripeptidomimetic antagonists for CXC chemokine receptor 4 (CXCR4), Bioorg. Med. Chem. 22 (2014) 4759e4769.

[46] M. Baumann, M.M. Hussain, N. Henne, D.M. Garrote, S. Karlshoj, T. Fossen, M.M. Rosenkilde, J. Vabeno, B.E. Haug, Influence of chain length on the activity of tripeptidomimetic antagonists for CXC chemokine receptor 4 (CXCR4), Bioorg. Med. Chem. 25 (2017) 646e657.

[47] R.M. Vitale, M. Gatti, M. Carbone, F. Barbieri, V. Felicita, M. Gavagnin, T. Florio, P. Amodeo, Minimalist hybrid ligand/receptor-based pharmacophore model for CXCR4 applied to a small-library of marine natural products led to the identification of phidianidine a as a new CXCR4 ligand exhibiting antagonist activity, ACS Chem. Biol. 8 (2013) 2762e2770.

[48] F. Grande, I. Barone, F. Aiello, A. Brancale, M. Cancellieri, M. Badolato, F. Chemi, C. Giordano, V. Vircillo, D. Bonofiglio, A. Garofalo, S. Ando, S. Catalano, Identification of novel 2-(1H-indol-1-yl)-benzohydrazides CXCR4 ligands impairing breast cancer growth and motility, Future Med. Chem. 8 (2016) 93e106.

[49] V.M. Truax, H. Zhao, B.M. Katzman, A.R. Prosser, A.A. Alcaraz, M.T. Saindane, R.B. Howard, D. Culver, R.F. Arrendale, P.R. Gruddanti, T.J. Evers, M.G. Natchus, J.P. Snyder, D.C. Liotta, L.J. Wilson, Discovery of tetrahydroisoquinoline-based CXCR4 antagonists, ACS Med. Chem. Lett. 4 (2013) 1025e1030.

[50] H. Zhao, A.R. Prosser, D.C. Liotta, L.J. Wilson, Discovery of novel N-aryl piperazine CXCR4 antagonists, Bioorg. Med. Chem. Lett. 25 (2015) 4950e4955.

[51] Y. Wang, S.T. Hazeldine, J. Li, D. Oupicky, Development of functional poly(- amido amine) CXCR4 antagonists with the ability to mobilize leukocytes and deliver nucleic acids, Adv. Healthc. Mater. 4 (2015) 729e738.

[52] R. Puig de la Bellacasa, A. Gibert, J.M. Planesas, L. Ros-Blanco, X. Batllori, R. Badia, B. Clotet, J. Este, J. Teixido, J.I. Borrell, Nitrogen positional scanning in tetramines active against HIV-1 as potential CXCR4 inhibitors, Org. Biomol. Chem. 14 (2016) 1455e1472.

[53] Z. Liang, W. Zhan, A. Zhu, Y. Yoon, S. Lin, M. Sasaki, J.M. Klapproth, H. Yang, H.E. Grossniklaus, J. Xu, M. Rojas, R.J. Voll, M.M. Goodman, R.F. Arrendale, J. Liu, C.C. Yun, J.P. Snyder, D.C. Liotta, H. Shim, Development of a unique small molecule modulator of CXCR4, PLoS One 7 (2012) e34038.

[54] S.R. Mooring, J. Liu, Z. Liang, J. Ahn, S. Hong, Y. Yoon, J.P. Snyder, H. Shim, Benzenesulfonamides: a unique class of chemokine receptor type 4 inhibitors, ChemMedChem 8 (2013) 622e632.

[55] R. Bai, Q. Shi, Z. Liang, Y. Yoon, Y. Han, A. Feng, S. Liu, Y. Oum, C.C. Yun, H. Shim, Development of CXCR4 modulators by virtual HTS of a novel amidesulfamide compound library, Eur. J. Med. Chem. 126 (2017) 464e475.

[56] R. Bai, Z. Liang, Y. Yoon, E. Salgado, A. Feng, S. Gurbani, H. Shim, Novel antiinflammatory agents targeting CXCR4: design, synthesis, biological evaluation and preliminary pharmacokinetic study, Eur. J. Med. Chem. 136 (2017) 360e371.

[57] S.R. Mooring, T. Gaines, Z. Liang, H. Shim, Synthesis of pyridine derivatives as potential antagonists of chemokine receptor type 4, Heterocycl. Commun. 20 (2014) 149e153.

[58] T. Gaines, D. Camp, R. Bai, Z. Liang, Y. Yoon, H. Shim, S.R. Mooring, Synthesis and evaluation of 2,5 and 2,6 pyridine-based CXCR4 inhibitors, Bioorg. Med. Chem. 24 (2016) 5052e5060.

[59] C.H. Wu, C.J. Wang, C.P. Chang, Y.C. Cheng, J.S. Song, J.J. Jan, M.C. Chou, Y.Y. Ke, J. Ma, Y.C. Wong, T.C. Hsieh, Y.C. Tien, E.A. Gullen, C.F. Lo, C.Y. Cheng, Y.W. Liu, A.A. Sadani, C.H. Tsai, H.P. Hsieh, L.K. Tsou, K.S. Shia, Function-oriented development of CXCR4 antagonists as selective human immunodeficiency virus (HIV)-1 entry inhibitors, J. Med. Chem. 58 (2015) 1452e1465.

[60] R. Bai, Z. Liang, Y. Yoon, S. Liu, T. Gaines, Y. Oum, Q. Shi, S.R. Mooring, H. Shim, Symmetrical bis-tertiary amines as novel CXCR4 inhibitors, Eur. J. Med. Chem. 118 (2016) 340e350.

[61] S. Hosoba, E.K. Waller, New molecule for mobilizing marrow stem cells, Blood 123 (2014) 310e311.

[62] D. Das, K. Maeda, Y. Hayashi, N. Gavande, D.V. Desai, S.B. Chang, A.K. Ghosh, H. Mitsuya, Insights into the mechanism of inhibition of CXCR4: identification of Piperidinylethanamine analogs as anti-HIV-1 inhibitors, Antimicrob. Agents Chemother. 59 (2015) 1895e1904.

[63] V. Vinader, D.S. Ahmet, M.S. Ahmed, L.H. Patterson, K. Afarinkia, Discovery and computer aided potency optimization of a novel class of small molecule CXCR4 antagonists, PLOS ONE 8 (2013) e78744.

II. CCR5/CXCR4 DUAL ANTAGONISM FOR THE IMPROVEMENT OF HIV INFECTION THERAPY

Fedora Grande [1]; Maria Antonietta Occhiuzzi [1]; Bruno Rizzuti [2]; Giuseppina Ioele [1]; Michele De Luca [1]; Paola Tucci [1]; Valentina Svicher[3]; Stefano Aquaro [1]; Antonio Garofalo[1].

[1] Department of Pharmacy, Health and Nutritional Sciences, University of Calabria, Ampliamento Polifunzionale, Via P. Bucci, 87036 Rende (CS), Italy;
[2] CNR-NANOTEC, Licryl-UOS Cosenza and CEMIF.Cal, Department of Physics, University of Calabria,
Via P. Bucci, 87036 Rende (CS), Italy
[3] Department of Experimental Medicine, University of Rome "Tor Vergata", 00133 Rome, Italy;

Abstract:
HIV entry in the host cell requires the interaction with the CD4 membrane receptor, and depends on the activation of one or both co-receptors CCR5 and CXCR4. Former selective co-receptor antagonists, acting at early stages of infection, are able to impair the receptor functions, preventing the viral spread toward AIDS. Due to the capability of HIV to develop resistance by switching from CCR5 to CXCR4, dual co-receptor antagonists could represent the next generation of AIDS prophylaxis drugs. We herein present a survey on relevant results published in the last few years on compounds acting simultaneously on both co-receptors, potentially useful as preventing agents or in combination with classical anti-retroviral drugs based therapy.

Keywords: chemokine receptors; dual drugs; HIV entry; AIDS.

1. Introduction

The most successful treatment of patients infected with HIV-1 (human immunodeficiency virus 1) resides so far in the administration of a combination of antiretroviral agents targeting specific proteins necessary to the viral replication. Such a therapeutic strategy, known as highly active antiretroviral therapy (HAART) [1,2], has shown to be particularly effective during the progression of the full-blown viral infection, whereas the same approach was less applicable in the early stages of the infection when infected people are not warned by specific symptoms. The most common agents included in HAART are inhibitors of viral entry and fusion, or drugs targeting reverse transcriptase, integrase, and protease enzymes. An alternative strategic approach focuses on a multi-target inhibition of the viral entry, before a full spreading of the virus into host cells. The viral entry consists of a complex sequence of events mediated by several viral/cellular membrane proteins, with the interaction between the viral glycoprotein gp120 and CD4 cellular receptor constituting an essential initial step. A further interaction of such glycoprotein with any of the two co-receptors CC-chemokine receptor 5 (CCR5) and CXC-chemokine receptor 4 (CXCR4) is also needed to promote appropriate conformational modifications during such an early stage of the viral cycle [3].
Both CCR5 and CXCR4 are G-protein coupled chemokine receptors determining HIV-1 cellular tropism. In particular, viruses preferentially utilizing CCR5 (R5 strains) are responsible for the primary cell infection, being this co-receptor mainly expressed on

macrophages. On the other hand, the viral replication capacity is attributed to viruses preferentially interacting with CXCR4 (X4 strains), being this second co-receptor mainly expressed on T-lymphocytes. Finally, dual-tropic viruses are defined as those using both co-receptors (Figure 1) [4,5].
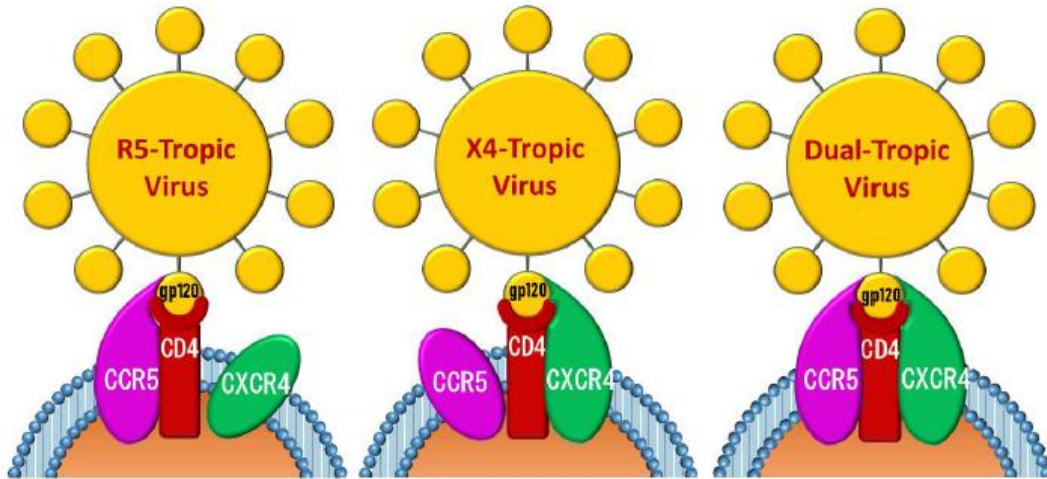

Figure 1. *Schematic representation of chemokine receptors mediating HIV cells entry.*

Whereas a large number of agents acting selectively on either CCR5 or CXCR4 have been described in the literature [6,7], only a few dual antagonists have been so far identified, suggesting that it is possible to simultaneously target the two proteins due to their similarities in the overall structures and in the binding site shapes. In fact, chemokine receptors have a common molecular architecture, which is conserved within the family of G protein-coupled receptors (GPCRs). As members of this unique family, CCR5 and CXCR4 share a structure similarity (Figure 2, top), such as the presence of seven transmembrane domains. Both receptors consist of 352 amino acids with a high number of proline residues, a C-terminal threonine and serine-rich cytoplasmic region, four extracellular loops rich in cysteines and an N-terminal extracellular domain [6,8]. In particular, overlapping regions of the binding pockets of CCR5 and CXCR4 (Figure 2, bottom) may contribute to allow these two proteins to host the same ligand, although not necessarily in the same binding mode and with an identical affinity.
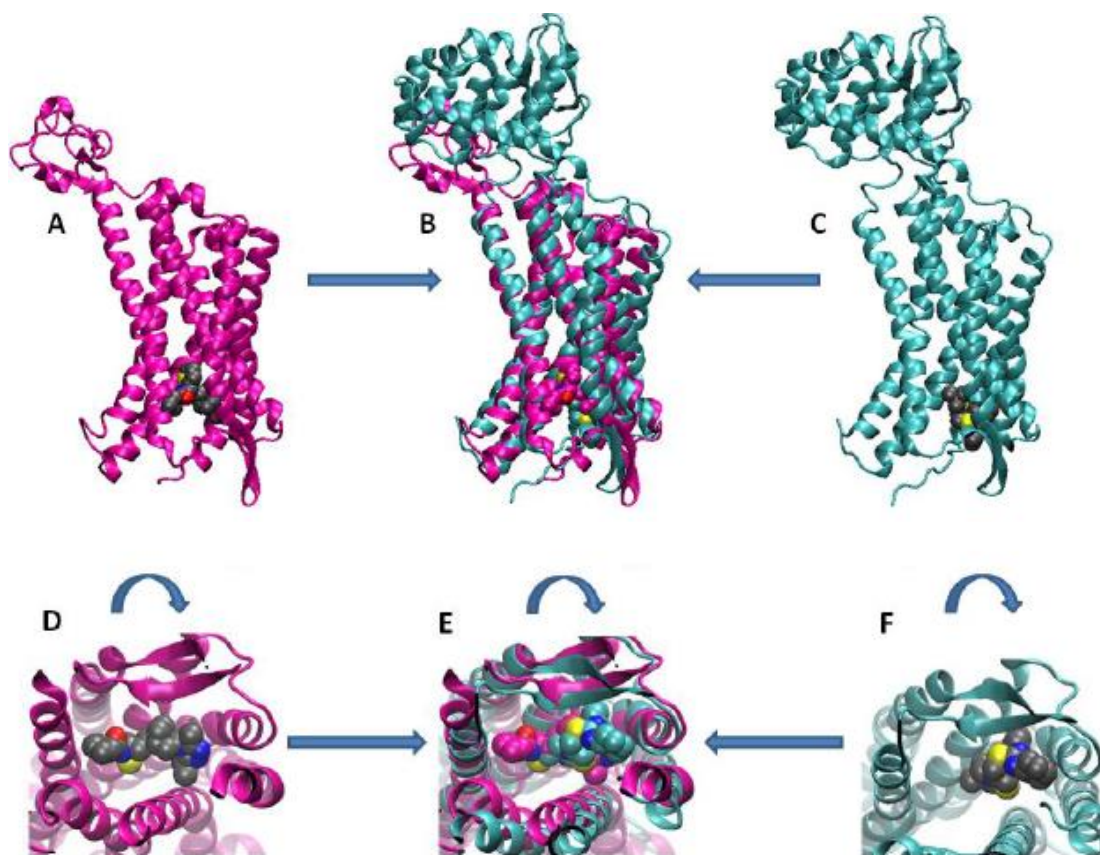
Figure 2. Similarities in the overall structures and binding pockets of CCR5 and CXCR4. Structures of complexes are taken from the Protein Data Bank entry 6AKX (magenta) [9] and 3ODU (cyan) [10] for CCR5 and CXCR4, respectively, and superimposed by least squares fit on protein C atoms. (Top) Overall structure of (A) CCR5, (B) both receptors, and (C) CXCR4; (bottom) detail of the binding site of (D) CCR5, (E) both receptors, and F) CXCR4. The ligands bound to CCR5 and CXCR4 (the 1-heteroaryl-1,3- ropanediamine derivative A4R and the antagonist IT1t, respectively) are shown with atoms in standard colours (C, grey; N, blue; O, red; S, yellow) in panels A, C, D and F, and with atoms in the same colour as their receptor (magenta for A4R, and cyan for IT1t) in panels B and E.

Due to the marked similarities between the active sites of CCR5 and CXCR4, many ligands could be recognized by both receptors. However, RANTES, also known as chemokine ligand 5 (CCL5), was proven to be the natural ligand selective for CCR5 [11], whereas stromal cell derived factor 1 (SDF1) is the natural ligand of CXCR4 [12]. It is well known that the multi-step HIV entry process is not only mediated by the interaction between the viral gp120 with the cellular receptor CD4, but it also requires the activation of one or two chemokine co-receptors. Among these, CCR5 and CXCR4 exhibit this crucial role. The capability of HIV to use either CCR5 or CXCR4, or both at the same time, determines the viral tropism, since, as already stated. In particular, virus strains utilizing CXCR4 or both co-receptors are associated with a higher incidence of AIDS development [13].

From all these considerations, the challenge to discover new CCR5 and CXCR4 antagonists is of paramount importance to improve the therapeutic armamentarium against HIV infection, and the possibility to develop dual co-receptor antagonists appears particularly appealing.

2. CCR5 and CXCR4 Antagonists

2.1. Earlier Co-Receptor Antagonists

Nowadays, the choice for the clinical use of a CCR5 or CXCR4 antagonists is suggested by the identification of viral strain tropism in patients. A rapid resistance onset represents however a limit, since the inhibition of a single co-receptor drives the virus to shift to the more virulent dual tropic strain [14,15]. Among selective and efficacious CCR5 antagonists, Maraviroc (Figure 3, compound **1**) appeared as the most intriguing compound, being the only one already approved by the Food and Drug Administration (FDA), endowed with a favorable resistance profile. On the other hand, Plerixafor (or AMD-3100) (Figure 3, compound **2**) appeared as the most useful CXCR4 antagonist identified during a research program on anti-HIV agents. Although this compound is clinically used for the mobilization of hematopoietic stem cells in cancer patients, it is not yet approved in the treatment of HIV infection due to its severe side effects [16,17].

In particular, AMD3100 was shown to inhibit HIV-1 entry into the target cell by specifically binding to CXCR4 (and not to any other receptor of either CXC- or CC-chemokines). Previous studies had demonstrated that AMD3100 was very active against a broad range of T-tropic HIV-1 and HIV-2 strains at a low nanomolar concentrations [18], and poorly active against M-tropic strains [19]. Furthermore, AMD3100 was shown to inhibit binding of the CXC-chemokine (SDF-1alpha) to CXCR4 and subsequent signal transduction, thus preventing also the functioning of CXCR4 as CXC-chemokine receptor [20].
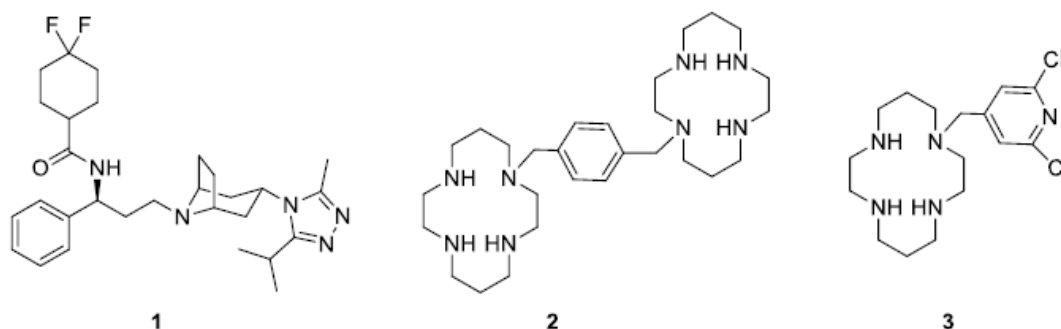

Figure 3. *Chemical structures of Maraviroc (**1**), Plerixafor (**2**), and AMD3451 (**3**).*

In 2004, AMD3451 (Figure 3, compound **3**) was reported as the first dual antagonist of CCR5 and CXCR4 [21]. Although its chemical structure resembles the one of the CXCR4 selective inhibitor AMD3100, it was found to be active also against the CCR5 co-receptor. Its moderate potency did not allow to carry on a proper clinical investigation, but its identification spurred researchers toward the development of more effective dual-tropic CCR5/CXCR4 antagonists [22].

About ten years later it was proven that Maraviroc, initially identified as a selective CCR5 inhibitor, was also an effective therapeutic alternative against dual mixed tropic HIV strains [23]. Antiviral effects of Maraviroc were investigated on U87.CD4 cells expressing wild type or chimeric CCR5 and CXCR4. Furthermore, a direct influence of the drug was observed on the onset of resistance in infected patients [24]. Phase II clinical studies confirmed the susceptibility to Maraviroc of dual mixed tropic viruses, with an activity even higher than that recorded towards pure R5 strains [25].

Nevertheless, Maraviroc is indicated in combination with other antiretroviral agents for the treatment of only CCR5-tropic HIV-1 infection, but not used for dual mixed viruses in the clinic [26].

Around the same time, Hubin and coworkers hypothesized that the simultaneous inhibition of CCR5 and CXCR4 by transition metal complexes based on a tetraazamacrocycle could be particularly effective for the treatment of HIV infection (Figure 4) [27,28]. Thermodynamic properties of bridged and unbridged metal complexants were also compared [29]. In a successive report, the same authors developed alternative synthetic routes to include dichloropyridine moieties into the scaffold of these complexants [28].
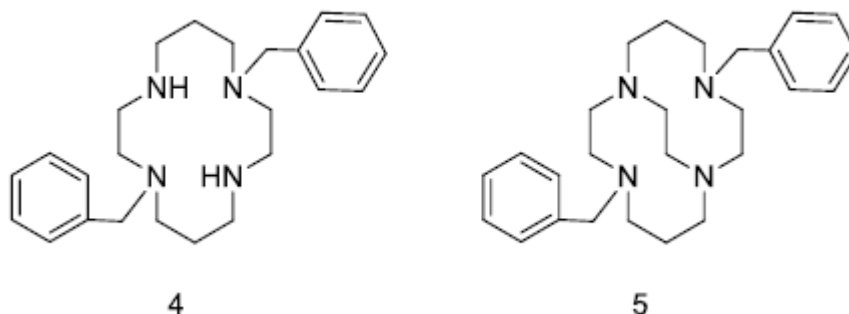

Figure 4. *Example of unbridged (**4**) and cross-bridged (**5**) tetraazamacrocycles.*

2.2. Peptide-Based Antagonists

In a study focusing on the identification of HIV entry inhibitors, peptide triazoles acting as dual antagonists targeting the interaction of gp120 with CD4 and co-receptors CCR5 and CXCR4 were identified. Eleven out of nineteen gp120 alanine mutants were screened by enzyme-linked immunosorbent assay (ELISA), leading to compound KR21 as the most active agent in direct binding and competition experiments (Figure 5, compound **6**). This peptide corresponds to a conserved region of gp120 overlapping with the CD4 binding site. Amino-acid mutation brought to this compound led to a reduction or even complete loss of inhibitory activity. The overall results of this study suggest that KR21 could represent the starting point for the rationale design of smaller dual antagonists [30].
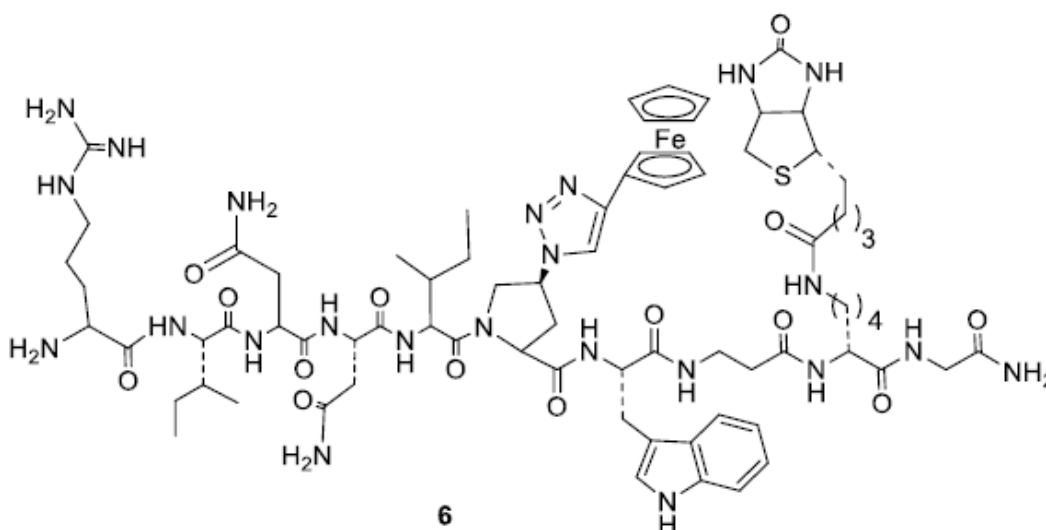

Figure 5. *Chemical structure of KR21 (**6**).*

2.3. Diterpene Derivatives

A new approach to the identification of dual inhibitors was proposed by Gama and coworkers, who described a natural occurring ingenol derivative, a diterpene isolated from the tropical shrub Euphorbia tirucalli (Figure 6, compound **7**) [31]. This compound was further chemically manipulated to give active cynnamic, caproic, and lauric esters (Figure 6, compounds 8–10), which showed promising antiviral activity, likely due to the downregulation of membrane receptors CD4, CCR5, and CXCR4. The compounds were tested against dual tropic HIV-1 strains and the EC_{50} values were found to be comparable to those of commonly used antiretroviral drugs. Moreover, these new derivatives, in particular compound 9, proved to be less toxic than previously discovered ingenol analogs, acting by the modulation of specific protein kinase C isoforms involved in the membrane receptor down-regulation [32].
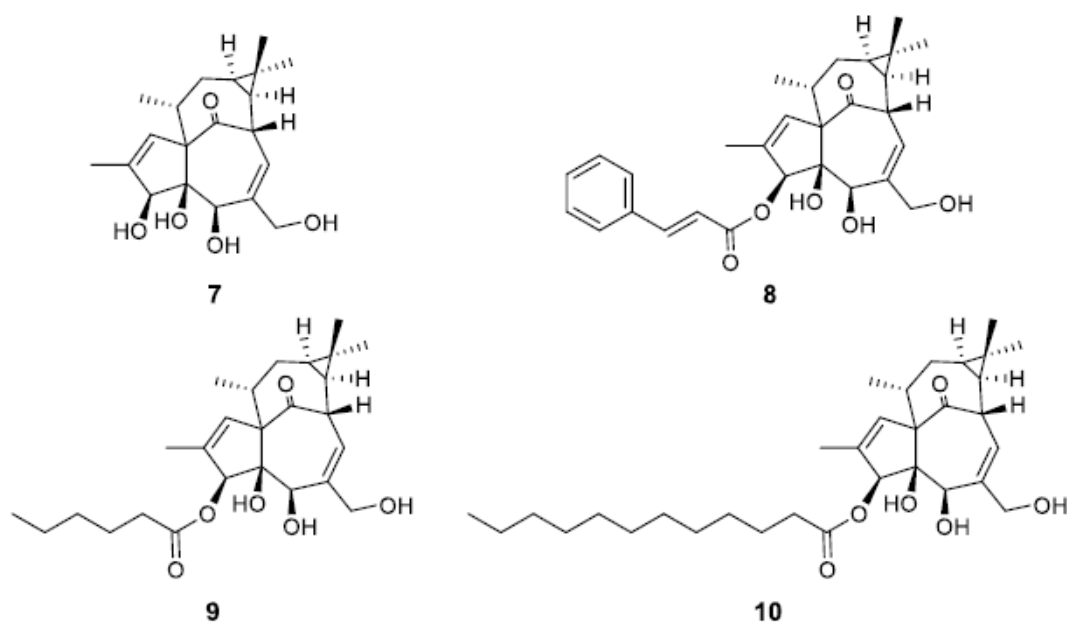

Figure 6. Structure of ingenol **7** and its ester derivatives **8–10**.

2.4. Pyrazole-Based Antagonists

A composite computational study, based on both virtual screening and statistical approach, led to a series of polyheterocyclic derivatives active on both CCR5 and CXCR4. The core structure was represented by a pyrazolo-piperidine nucleus. The most active derivative (Figure 7, compound **11**), bearing a benzyl group appended to the pyrazole and a 4-pyridinemethyl linked to the piperidine, showed an IC_{50} value of 3.8 μM against a CCR5-utilizing HIV-1 strain and an IC_{50} value of 0.8 μM against a CXCR4-utilizing HIV-1 strain, in MAGI assay. This last consists of a high sensitive competitive *in vitro* HIV replication method for quantifying viral infectivity. Whereas the benzyl substituent seems necessary for retaining activity, different bonding mode were tolerated for the pyridine ring (Figure 7, compounds **12** and **13**). These compounds showed an IC_{50} value of 17 and 25 μM in the case of the 3-pyridinemethyl derivative and 16 and 5.8 μM in the case of the 2-pyridinemethyl analog againstn a CCR5- and CXCR4-utilizing HIV-1 strain, respectively. Compound **11** showed also to be active in an assay on Ca^{2+} flux GPCR signaling, therefore allosterically

modulating CXCR4. Furthermore, compound 11 showed to be active against HIV-1 reverse-transcriptase enzyme with an IC$_{50}$ value of 9.0 μM. Moreover, this compound did not result toxic in the same MAGI assay, at a concentration as high as 300 μM. All these data suggest that this lead compound is warranted for further development for the identification of more active dual chemokine receptor inhibitors [33].
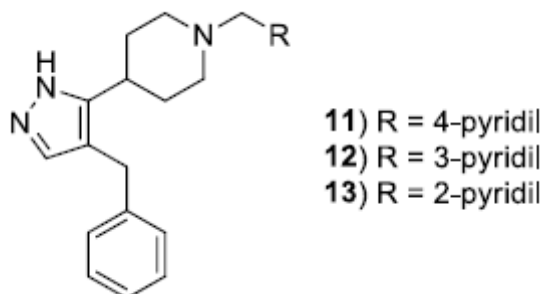

Figure 7. Chemical structure of pyrazolo-piperidine derivatives 11–13.

In a successive computational study, the dynamics of the binding between 11 and both CCR5 and CXCR4 were in depth investigated [34]. The three aromatic rings involved in π-stacking and a positively charged hydrogen bond donor of a piperidine ring were demonstrated to be the main responsible features for the interaction. The replacement of the piperidine ring with a piperazine, leading to a double protonated species interacting with the negatively charged glutamates and aspartates within the active site, was planned in order to strengthen the protein-ligand interaction. Accordingly, compound **14** (Figure 8) was synthesized and demonstrated to have a more favorable interaction compared to 11, after being docked into the active site of both co-receptors [34]. These results suggested that further insights into the molecular dynamics of such compounds and CCR5/CXCR4 could lead to the identification of more effective dual antagonists.
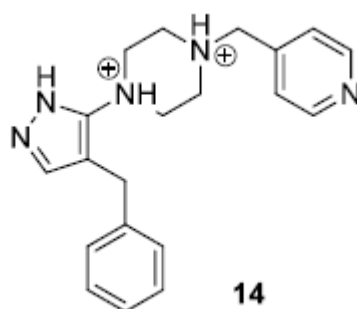

Figure 8. Chemical structure of piperidine derivative 14.

2.5. The Suramin Analog NF279
Inhibition by selective antagonists of P2X1R, a receptor involved in the HIV-1 fusion and replication, could represent an alternative strategy to contrast the viral infection. Compound **15**, also known as NF279 (Figure 9), an analog of the anti-parasite drug suramin, was initially found to be as a selective P2X1 receptor antagonist, and showed a noteworthy antiviral activity [35]. Further studies proved that HIV-1 entry nhibitory of compound **15** was not related to a direct interaction with P2X1R, but rather to the capability of this compound to act ass dual CCR5/CXCR4 co-receptor antagonist. This feature was assessed by the

suppression of cellular calcium responses CCR5/CXCR4 mediated. Thus, NF279 could represent the lead of a new class of dual-coreceptor inhibitors [36].
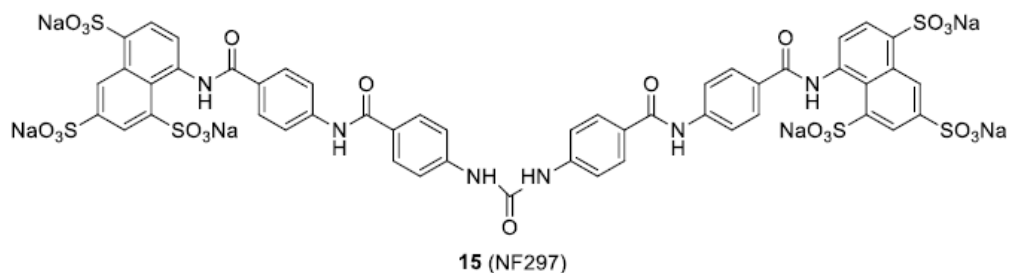

Figure 9. *Chemical structure of compound 15.*

2.6. The Cumarin-Based Ligand GUT-70

It is known that several derivatives of the natural product coumarin are endowed with several pharmacological properties, including anti-viral activity [37]. Compound **16**, a tricyclic coumarin also known as GUT-70 (Figure 10), was demonstrated to be able to reduce cell membrane fluidity by a fluorescent depolarization study conducted onMOLT-4 and PM1-CCR5 T cell lines. This propertywould suggest its potential use against the HIV-1 entry. Furthermore, GUT-70 is capable of down-regulating the expression of CD4, CCR5, and CXCR4 receptors on the cell surface in a dose-dependent manner, therefore representing a starting point for the development of novel tools against HIV-1 infection [38].

However, this compound showed an unfavorable toxicity profile, due to a noteworthy cytotoxicity [39].
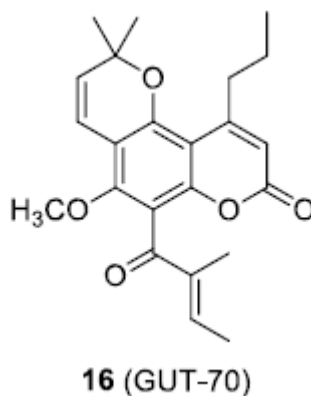

Figure 10. *Chemical structure of compound 16.*

2.7. Penicillixanthone A

It is well known that HIV fusion can be humped by a peptide portion of gp41 (HR2 domain). An antiviral effect has been demonstrated when this peptide portion was conjugated to cell membrane proteins. In particular, a 34 amino acid peptide from HR2 (C34, corresponding to amino acids 628– 661 in HxB2) [40,41] conjugated to the amino termini of CCR5 or CXCR4 exhibited potent and broad inhibition against several HIV-1 strains [42]. Potent anti-HIV-1 activity was showed by penicillixanthone A (PXA, Figure 11, compound **17**), a natural xanthone dimer isolated from the fungus *Aspergillus fumigatus*. The actual mechanism of action of PXA was inferred by molecular modeling studies, which suggested a putative interaction binding mode with both CCR5 and CXCR4 receptors. The IC_{50} values

calculated by *in vitro* studies were 0.36 and 0.26 μM against CCR5- and CXCR4-tropic HIV-1 strains, respectively.

PXA showed only a moderate cytotoxicity evaluated by a colorimetric XTT assay against TZM-bl cells, with an IC_{50} of 20.6 μM. This compound could then represent a lead for the development of HIV-1 dual co-receptor antagonists [43].
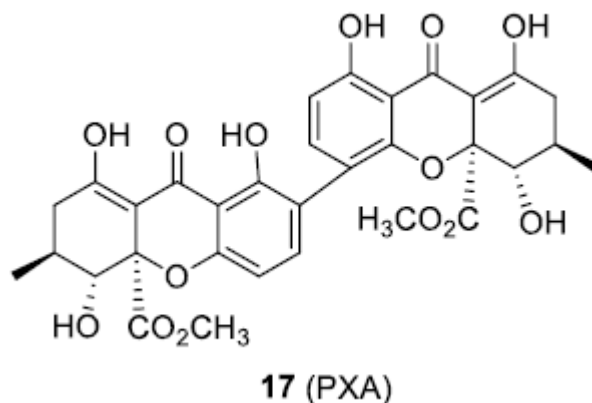

Figure 11. *Chemical structure of compound 17.*

Considering all the above remarks, the identification of dual CCR5/CXCR4 co-receptor antagonists is still an attractive field of anti-HIV research. In fact, the progression of HIV infection is associated with the skill of the virus to switch from one co-receptor to another. Although our understanding of the viral resistance mechanism is not yet complete, the alternative therapeutic option based on the inhibition of membrane co-receptors sounds still appealing. Such an approach could gain particular importance in the case of anti-HIV treatment failure with classic HAART therapy. After the identification of effective antagonists, the next step could reside in the choice of a specific therapy based on the use of selective or dual agents, or even a combination of both types.

3. Conclusions

Successful applications of ligand-based models and recent insights on the mechanism of HIV replication prompted the research of a new strategy aimed at preventing viral adhesion and spread. A promising approach is based on the employment of agents able to antagonize the interaction of viral proteins with the host cell membrane receptor CD4 and co-receptors CCR5 and CXCR4. The viral tropism is in fact thoroughly influenced by the expression of one or both co-receptors. The identification of selective co-receptor antagonists could be particularly effective in preventing viral infection. However, the capability of the virus to switch tropism could reduce drug effectiveness. In this context, the discovery of dual CCR5 and CXCR4 could lead to even more appealing anti-viral agents, able to prevent the replication of the more virulent dual-tropic HIV strains. The studies so far conducted for the identification of dual inhibitors have led to interesting candidates to be further developed, even if several of the identified compounds suffer from an inadequate safety and pharmacokinetics profile.

Most of the analyzed papers deal with *in vitro* and *in silico* evaluations, which often do not reflect therapeutic potentials for a suitable clinical application. Rationale multidisciplinary efforts combining computational and biological techniques are then required for the design of leads to be developed toward clinically useful potent antiviral agents.

References

[1] Cobucci, R.N.; Lima, P.H.; de Souza, P.C.; Costa, V.V.; Cornetta Mda, C.; Fernandes, J.V.; Goncalves, A.K. Assessing the impact of HAART on the incidence of defining and non-defining AIDS cancers among patients with HIV/AIDS: A systematic review. J. Infect. Public Health 2015, 8, 1–10.

[2] Oliva-Moreno, J.; Trapero-Bertran, M. Economic Impact of HIV in the Highly Active Antiretroviral Therapy Era—Reflections Looking Forward. AIDS Rev. 2018, 20, 226–235.

[3] Shepherd, A.J.; Loo, L.; Mohapatra, D.P. Chemokine co-receptor CCR5/CXCR4-dependent modulation of Kv2.1 channel confers acute neuroprotection to HIV-1 glycoprotein gp120 exposure. PLoS ONE 2013, 8, e76698.

[4] Dragic, T.; Litwin, V.; Allaway, G.P.; Martin, S.R.; Huang, Y.; Nagashima, K.A.; Cayanan, C.; Maddon, P.J.; Koup, R.A.; Moore, J.P.; et al. HIV-1 entry into CD4+ cells is mediated by the chemokine receptor CC-CKR- 5. Nature 1996, 381, 667–673. [CrossRef] [PubMed]

[5] Scarlatti, G.; Tresoldi, E.; Bjorndal, A.; Fredriksson, R.; Colognesi, C.; Deng, H.K.; Malnati, M.S.; Plebani, A.; Siccardi, A.G.; Littman, D.R.; et al. *In vivo* evolution of HIV-1 co-receptor usage and sensitivity to chemokine-mediated suppression. Nat. Med. 1997, 3, 1259–1265.

[6] Grande, F.; Garofalo, A.; Neamati, N. Small molecules anti-HIV therapeutics targeting CXCR4. Curr. Pharm. Des. 2008, 14, 385–404.

[7] Singh, I.P.; Chauthe, S.K. Small molecule HIV entry inhibitors: Part II. Attachment and fusion inhibitors: 2004-2010. Expert Opin. Ther. Pat. 2011, 21, 399–416.

[8] Oppermann, M. Chemokine receptor CCR5: Insights into structure, function, and regulation. Cell Signal. 2004, 16, 1201–1210.

[9] Peng, P.; Chen, H.; Zhu, Y.; Wang, Z.; Li, J.; Luo, R.H.; Wang, J.; Chen, L.; Yang, L.M.; Jiang, H.; et al. Structure-Based Design of 1-Heteroaryl-1,3-propanediamine Derivatives as a Novel Series of CC-Chemokine Receptor 5 Antagonists. J. Med. Chem. 2018, 61, 9621–9636.

[10] Wu, B.; Chien, E.Y.; Mol, C.D.; Fenalti, G.; Liu, W.; Katritch, V.; Abagyan, R.; Brooun, A.; Wells, P.; Bi, F.C.; et al. Structures of the CXCR4 chemokine GPCR with small-molecule and cyclic peptide antagonists. Science 2010, 330, 1066–1071.

[11] Chien, H.C.; Chan, P.C.; Tu, C.C.; Day, Y.J.; Hung, L.M.; Juan, C.C.; Tian, Y.F.; Hsieh, P.S. Importance of PLC-Dependent PI3K/AKT and AMPK Signaling in RANTES/CCR5 Mediated Macrophage Chemotaxis. Chin. J. Physiol. 2018, 266–279.

[12] Smith, N.; Pietrancosta, N.; Davidson, S.; Dutrieux, J.; Chauveau, L.; Cutolo, P.; Dy, M.; Scott-Algara, D.; Manoury, B.; Zirafi, O.; et al. Natural amines inhibit activation of human plasmacytoid dendritic cells through CXCR4 engagement. Nat. Commun. 2017, 8, 14253.

[13] Rangel, H.R.; Bello, G.; Villalba, J.A.; Sulbaran, Y.F.; Garzaro, D.; Maes, M.; Loureiro, C.L.; deWaard, J.H.; Pujol, F.H. The Evolving HIV-1 Epidemic in Warao Amerindians Is Dominated by an Extremely High Frequency of CXCR4-Utilizing Strains. AIDS Res. Hum. Retrovir. 2015, 31, 1265–1268.

[14] Gupta, S.; Prosser, A.R.; Cox, B.D.; Wilson, L.J.; Liotta, D. Design and synthesis of dual-tropic HIV entry inhibitors that utilize a homologous CCR5/CXCR4 binding site. In Proceedings of the 249th ACS NationalMeeting & Exposition, Denver, CO, USA, 22–26 March 2015.

[15] Gupta, S.; Prosser, A.R.; Cox, B.D.; Wilson, L.J.; Liotta, D.C. Design and synthesis of Dual Tropic HIV entry inhibitors that utilize a homologous CCR5/CXCR4 binding site. In Proceedings of the 66th Southeast Regional Meeting of the American Chemical Society, Nashville, TN, USA, 16–19 October 2014.

[16] Woollard, S.M.; Kanmogne, G.D. Maraviroc: A review of its use in HIV infection and beyond. Drug Des. Dev. Ther. 2015, 9, 5447–5468.

[17] Grande, F.; Giancotti, G.; Ioele, G.; Occhiuzzi, M.A.; Garofalo, A. An update on small molecules targeting CXCR4 as starting points for the development of anti-cancer therapeutics. Eur. J. Med. Chem. 2017, 139, 519–530.

[18] Schols, D.; Struyf, S.; Van Damme, J.; Este, J.A.; Henson, G.; De Clercq, E. Inhibition of T-tropic HIV strains by selective antagonization of the chemokine receptor CXCR4. J. Exp. Med. 1997, 186, 1383–1388.

[19] Aquaro, S.; Perno, C.F.; Balestra, E.; Balzarini, J.; Cenci, A.; Francesconi, M.; Panti, S.; Serra, F.; Villani, N.; Calio, R. Inhibition of replication of HIV in primary monocyte/macrophages by different antiviral drugs and comparative efficacy in lymphocytes. J. Leukoc. Biol. 1997, 62, 138–143.

[20] Donzella, G.A.; Schols, D.; Lin, S.W.; Este, J.A.; Nagashima, K.A.; Maddon, P.J.; Allaway, G.P.; Sakmar, T.P.; Henson, G.; De Clercq, E.; et al. AMD3100, a small molecule inhibitor of HIV-1 entry via the CXCR4 co-receptor. Nat. Med. 1998, 4, 72–77.

[21] Princen, K.; Hatse, S.; Vermeire, K.; Aquaro, S.; De Clercq, E.; Gerlach, L.O.; Rosenkilde, M.; Schwartz, T.W.; Skerlj, R.; Bridger, G.; et al. Inhibition of human immunodeficiency virus replication by a dual CCR5/CXCR4 antagonist. J. Virol. 2004, 78, 12996–13006.

[22] Kim, M.B.; Giesler, K.E.; Tahirovic, Y.A.; Truax, V.M.; Liotta, D.C.; Wilson, L.J. CCR5 receptor antagonists in preclinical to phase II clinical development for treatment of HIV. Expert Opin. Investig. Drugs 2016, 25, 1377–1392.

[23] Surdo, M.; Balestra, E.; Saccomandi, P.; Di Santo, F.; Montano, M.; Di Carlo, D.; Sarmati, L.; Aquaro, S.; Andreoni, M.; Svicher, V.; et al. Inhibition of dual/mixed tropic HIV-1 isolates by CCR5-inhibitors in primary lymphocytes and macrophages. PLoS ONE 2013, 8, e68076.

[24] Cavarelli, M.; Mainetti, L.; Pignataro, A.R.; Bigoloni, A.; Tolazzi, M.; Galli, A.; Nozza, S.; Castagna, A.; Sampaolo, M.; Boeri, E.; et al. Complexity and dynamics of HIV-1 chemokine receptor usage in a multidrugresistant adolescent. AIDS Res. Hum. Retrovir. 2014, 30, 1243–1250.

[25] Surdo, M.; Alteri, C.; Puertas, M.C.; Saccomandi, P.; Parrotta, L.; Swenson, L.; Chapman, D.; Costa, G. Artese, A.; Balestra, E.; et al. Effect of maraviroc on non-R5 tropic HIV-1: Refined analysis of subjects from the phase IIb study A4001029. Clin. Microbiol. Infect. 2015, 21, 103e1–103e6.

[26] Serrano-Villar, S.; Caruana, G.; Zlotnik, A.; Perez-Molina, J.A.;Moreno, S. Effects ofMaraviroc versus Efavirenz in Combination with Zidovudine-Lamivudine on the CD4/CD8 Ratio in Treatment-Naive HIV-Infected Individuals. Antimicrob. Agents Chemother. 2017, 61, e01763-17.

[7] Hubin, T.J.; Archibald, S.J.; Won, P.; Birdsong, O.C.; Epley, B.M.; Klassen, S.L.; Schols, D. Synthesis and evaluation of transition metal complex dual CXCR4/CCR5 antagonists. In Proceedings of the 245th ACS National Meeting & Exposition, New Orleans, LA, USA, 7–11 April 2013.

[28] Davilla, D.; Birdsong, O.; Schols, D.; Archibald, S.; Hubin, T. Bis- and pendant armed tetraazamacrocycle transition metal complex dual CXCR4/CCR5 antagonists. In Proceedings of the 251st ACS National Meeting & Exposition, San Diego, CA, USA, 13–17 March 2016.

[29] Available online: https://www.swosu.edu/academics/jur/docs/transitionmetals-v1.pdf (accessed on 31 January 2019).

[30] Tuzer, F.; Madani, N.; Kamanna, K.; Zentner, I.; LaLonde, J.; Holmes, A.; Upton, E.; Rajagopal, S.; McFadden, K.; Contarino, M.; et al. HIV-1 Env gp120 structural determinants for peptide triazole dual receptor site antagonism. Proteins 2013, 81, 271–290.

[31] Abreu, C.M.; Price, S.L.; Shirk, E.N.; Cunha, R.D.; Pianowski, L.F.; Clements, J.E.; Tanuri, A.; Gama, L. Dual role of novel ingenol derivatives from Euphorbia tirucalli in HIV replication: Inhibition of de novo infection and activation of viral LTR. PLoS ONE 2014, 9, e97257.

[32] Spina, C.A.; Anderson, J.; Archin, N.M.; Bosque, A.; Chan, J.; Famiglietti, M.; Greene, W.C.; Kashuba, A.; Lewin, S.R.; Margolis, D.M.; et al. An in-depth comparison of latent HIV-1 reactivation in multiple cell model systems and resting CD4+ T cells from aviremic patients. PLoS Pathog. 2013, 9, e1003834.

[33] Cox, B.D.; Prosser, A.R.; Sun, Y.; Li, Z.; Lee, S.; Huang, M.B.; Bond, V.C.; Snyder, J.P.; Krystal, M.; Wilson, L.J.; et al. Pyrazolo-Piperidines Exhibit Dual Inhibition of CCR5/CXCR4 HIV Entry and Reverse Transcriptase. ACS Med. Chem. Lett. 2015, 6, 753–757.

[34] Taylor, C.A.; Miller, B.R., 3rd; Parish, C.A. Design and computational support for the binding stability of a new CCR5/CXCR4 dual tropic inhibitor: Computational design of a CCR5/CXCR4 drug. J.Mol. Graph.Model. 2017, 75, 71–79.

[35] Marin, M.; Du, Y.; Giroud, C.; Kim, J.H.; Qui, M.; Fu, H.; Melikyan, G.B. High-Throughput HIV-Cell Fusion Assay for Discovery of Virus Entry Inhibitors. Assay Drug Dev. Technol. 2015, 13, 155–166.

[36] Giroud, C.; Marin, M.; Hammonds, J.; Spearman, P.; Melikyan, G.B. P2X1 Receptor Antagonists Inhibit HIV-1 Fusion by Blocking Virus-Coreceptor Interactions. J. Virol. 2015, 89, 9368–9382.

[37] Venugopala, K.N.; Rashmi, V.; Odhav, B. Review on natural coumarin lead compounds for their pharmacological activity. BioMed Res. Int. 2013.

[38] Matsuda, K.; Hattori, S.; Kariya, R.; Komizu, Y.; Kudo, E.; Goto, H.; Taura, M.; Ueoka, R.; Kimura, S.; Okada, S. Inhibition of HIV-1 entry by the tricyclic coumarin GUT-70 through the modification of membrane fluidity. Biochem. Biophys. Res. Commun. 2015, 457, 288–294.

[39] Kudo, E.; Taura, M.; Matsuda, K.; Shimamoto, M.; Kariya, R.; Goto, H.; Hattori, S.; Kimura, S.; Okada, S. Inhibition of HIV-1 replication by a tricyclic coumarin GUT-70 in acutely and chronically infected cells. Bioorg. Med. Chem. Lett. 2013, 23, 606–609.

[40] Tozser, J.; Blaha, I.; Copeland, T.D.; Wondrak, E.M.; Oroszlan, S. Comparison of the HIV-1 and HIV-2 proteinases using oligopeptide substrates representing cleavage sites in Gag and Gag-Pol polyproteins. FEBS Lett. 1991, 281, 77–80.

[41] Gorelick, R.J.; Henderson, L.E. Human Retroviruses and AIDS 1994-Part III; Elsevier: Amsterdam, The Netherlands, 2017; p. 9.

[42] Leslie, G.J.; Wang, J.; Richardson, M.W.; Haggarty, B.S.; Hua, K.L.; Duong, J.; Secreto, A.J.; Jordon, A.P.; Romano, J.; Kumar, K.E.; et al. Potent and Broad Inhibition of HIV-1 by a Peptide from the gp41 Heptad Repeat-2 Domain Conjugated to the CXCR4 Amino Terminus. PLoS Pathog. 2016, 12, e1005983.

[43] Tan, S.; Yang, B.; Liu, J.; Xun, T.; Liu, Y.; Zhou, X. Penicillixanthone A, a marine-derived dual-coreceptor antagonist as anti-HIV-1 agent. Nat. Prod. Res. 2017, 1–5.

III. REVERSE TRANSCRIPTASE INHIBITORS NANOSYSTEMS DESIGNED FOR DRUG STABILITY AND CONTROLLED DELIVERY

Fedora Grande; Giuseppina Ioele; Maria Antonietta Occhiuzzi; Michele De Luca; Elisabetta Mazzotta; Gaetano Ragno; Antonio Garofalo; Rita Muzzalupo.

Department of Pharmacy, Health and Nutritional Sciences, University of Calabria, Via P. Bucci.

Abstract:
An in-depth analysis of nanotechnology applications for the improvement of solubility, distribution, bioavailability and stability of reverse transcriptase inhibitors is reported. Current clinically used nucleoside and non-nucleoside agents, included in combination therapies, were examined in the present survey, as drugs belonging to these classes are the major component of highly active antiretroviral treatments. The inclusion of such agents into supramolecular vesicular systems, such as liposomes, niosomes and lipid solid NPs, overcomes several drawbacks related to the action of these drugs, including drug instability and unfavorable pharmacokinetics. Overall results reported in the literature show that the performances of these drugs could be significantly improved by inclusion into nanosystems.

Keywords: HIV; antiretrovirals; nanoformulations; drug degradation; drug protection.

1. Introduction

The human immunodeficiency virus (HIV), belonging to the lentivirus genus of the large family of retroviridae, is the etiological agent of AIDS. The infection causes severe consequences to the immune system including a loss of CD4+T lymphocytes that leads to an increased susceptibility to even fatal opportunistic infections. The identification of various antiretroviral drugs allowed defining e cacious therapeutic regimens for the prevention and treatment of the disease by the combined administration of two, three or more different drugs acting on crucial steps of viral replication. In particular, the targets of conventional drugs are proteins involved in the viral entry or specific enzymes necessary for the virus replication such as protease (PR), reverse transcriptase (RT) and integrase (IN). This approach known as HAART (highly active antiretroviral therapy) nowadays represents the most useful therapeutic treatment, even though it is effected by many drawbacks such as lifetime administration with a consequent reduced patients' compliance, severe side e ects, and quick viral outbreak afterdrug resistance emergence. HAART was demonstrated to be particularly effective in cutting down the overall number of viral particles, but is unable to completely eradicate infection in sanctuary sites, such as the brain, liver and lymphatic system [1–5]. Moreover, HAART always includes one or more nucleoside and non-nucleoside reverse transcriptase inhibitors (NRTI and NNRTI, respectively), which, despite a high antiviral e efficacy, unavoidably show important clinical drawbacks. Relevant information on common RTI is summarized in Table 1 [6,7].

Table 1. *Relevant information of currently used RTI. *Year of FDA approval; LS = Lipid Solubility; OB= Oral Bioavailability; t/2 = Plasma Half-life.*

Drug Class	Name (Acronym)	Year*	LS	OB (%)	t/2 (hours)	Side Effects
NRTIs	Stavudine (STV)	1996	low	86	1.3–1.4	Peripheral neuropathy, pancreatitis, asymptomatic acidosis, lipoatrophy, hepatic steatosis
	Zidovudine (AZT)	1986	low	60	0.5–3	Neutropenia, anemia, nausea, vomiting, asthenia, headache, insomnia, skin hyperpigmentation, acidosis, hepatic steatosis
	Lamivudine (3TC)	1995	low	86	5–7	Cough, diarrhea, fatigue, headache, malaise, nasal symptoms, lactic acidosis, hepatic steatosis
	Abacavir (ABV)	1998	low	83	0.8–1.5	Systemic respiratory hypersensitivity, gastrointestinal symptoms, fever, tiredness, sore throat
	Emtricitabine (FTC)	2006	low	93	8–10	Headache, nausea, upset stomach, diarrhea, trouble sleeping, dizziness, skin rash, strange dreams, cough, runny nose
	Zalcitabine (ZCT)	1992	low	85		Peripheral neuropathy, stomatitis, esophageal ulcerations, acidosis, hepatic steatosis
	Didanosine (DDN)	1991	low	30	2	Gastrointestinal intolerance, peripheral neuropathy, pancreatitis, asymptomatic acidosis, lipoatrophy, hepatic steatosis
	Tenofovir (TDF)	2001	low	25-39	12–15	Nausea, depression, confusion, headache, hitching, weakness, kidneys problems
NNRTIs	Nevirapine (NVR)	1996	moderate	92	25–30	Rash, Stevens-Johnson syndrome, elevated transaminases blood level, hepatitis, severe hypersensitivity reaction
	Efavirenz (EFV)	1998	high	50	40–55	Rash, Stevens-Johnson syndrome, sleep disturbances, dizziness, vertigo, depression, euphoria, difficulty concentrating, hallucination.
	Etravirine (ETV)	2008	high	–	30–40	Rash, Stevens-Johnson syndrome, toxic epidermal necrosis and multiform erythema, hypersensitivity reactions, hepatic failure
	Rilpivirine (RPV)	2011	high	50	19	Rash, depression, liver problems, mood changes

The above therapeutic strategy is not even capable of stimulating a lasting immune response of memory cells necessary to antagonize the infective agent [8]. Even after taking into account all these considerations, innovative therapeutic approaches based on both the identification of alternative drugs and innovative pharmaceutic formulations still have demanding requirements [9–11]. Nanotechnologies could help to reach this latter crucial point in order to increase cellular uptake, enhance drug distribution, prolong half-life and reduce side e_ects depending on the lower drug dosage in the nanosystem. In particular, application of nanoformulations consisting of a given drug and a supramolecular matrix such as niosomes, liposomes and solid lipid nanoparticles (SLN), already led to some improvements of pharmacokinetic and pharmacodynamic parameters. Very interesting results have been recorded in the anti-cancer research field where an altered microenvironment of cancer cells facilitates a selective drug delivery [12]. A similar approach could be adopted in the case of cells infected by HIV [13].

In the light of these findings, the incorporation of new or customary anti-HIV drugs intosupramolecular carriers could be particularly e ective in suppressing viral replication.

This strategy is corroborated by the possibility of encapsulating drugs or genes to not only be delivered next to the infected cells but also to target reservoir tissues to eradicate latent HIV [14]. This innovative strategy is suitable for improving the distribution of both hydrophilic and hydrophobic small molecules, as well as macromolecular drugs, which can be driven toward specific tissues thanks to the reduced size of the nanoscale delivery systems. Antiretroviral drugs can be carried as nanoparticles for their potential to better reach macrophages, CD4+T cells and latent reservoirs organs, such as brain and lymph nodes, that are particularly responsible of viral survival. [15–19]. Drug delivery systems (DDS) for RTI, developed in the last few years, are described in this survey and depicted in Figure 1, while their main properties are summarized in Table 2.
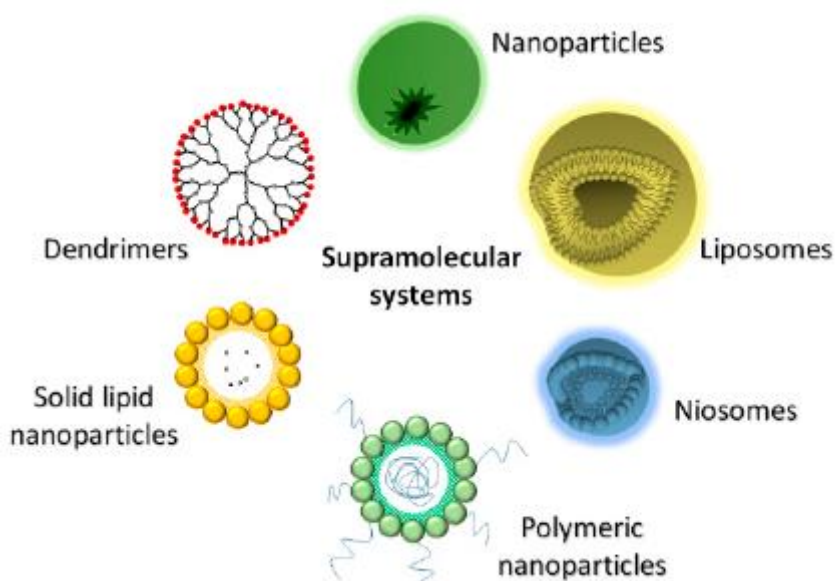

Figure 1. Drug delivery systems for RTI nanoformulations.

Table 2. Targets of DDS designed for anti-HIV therapy.

DDS		TARGET
Matrix	Surface	
Liposome NPs	Mannose	Liver, spleen, lung, brain, macrophages
Liposomes	Galactose	Liver
Chitosan NPs	Glycyrrhizin	Liver
NPs	Transferrin	Brain, endothelial cells
NPs	Serum albumin	Brain, liver, spleen
SLN	Phenylalanine	Blood brain barrier
Polymeric micelles	Anti-GP2 antibody	M-cell of gut-associated lymphoid tissue
Dendrimers	Tuftsin	Macrophages, monocytes, polymorph nuclear leukocytes

Furthermore, some nanomaterials possess themselves favorable biological effects. The nanotechnology approach has been advanced for many aspects dealing with HIV infection, namely theranostic, vaccine prophylaxis and gene therapy. This survey however focuses on studies describing NRTI and NNRTI based nanoformulations for prevention or treatment of

HIV infection. Although these systems allow a remarkable improvement of the pharmacokinetics and pharmacodynamics of RTI, several drawbacks still need to be overcame. The major advantages and limitations of known nanosystems are listed in Table 3.

Table 3. Advantages and limitations of anti-HIV DDS.

DDS	Advantages	Limitations
Liposomes	Co-delivery of hydrophilic and lipophilic drug Selective uptake by mononuclear phagocytes Surface modification with target moiety of virus reservoir	Low drug loading capacity Physical and chemical instability Drug leakage Difficulty in sterilization Short half-life Poor scale up
Niosomes	Chemical stability Protection of drug from degradation Large uptake by mononuclear phagocytes and localization in virus reservoir organs Less expensive respect liposomes Functionalization with target ligand	Physical instability during the storage Difficulty in sterilization Difficulty in large-scale production
Polymeric NPs	High drug loading capacity Co-delivery of different drug for anti-HIV combination therapy Selective uptake by lymphoid organ Prolonged circulation time Surface functionalization with target moiety	Fast burst release Limited safe correlated to polymer toxicity High cost production
SLN	Higher stability and biological compatibility than liposomes and polymeric NPs Increase the bioavailability of poorly water soluble drug Avoidance of organic solvent Slow uptake by the RES Feasible-large scale production and sterilization Less expensive than polymeric and surfactant carriers	Low drug solubility in lipid matrix and loading capacity Drug leakage Particle growth Unpredictable gelation tendency
Dendrimers	Uniform particle size Large surface functional groups for the conjugation with target moieties	Toxicity problems

Several of these clinically used drugs show an undesirable stability profile when exposed to stressing conditions either in solution or in solid form [20,21]. Similarly, stress tests have been performed on supramolecular systems in order to confirm any improved stability, under different conditions [22]. In particular, studies published in the last few years on the RT inhibitors included in combined therapy have been taken into consideration [15,16,23].
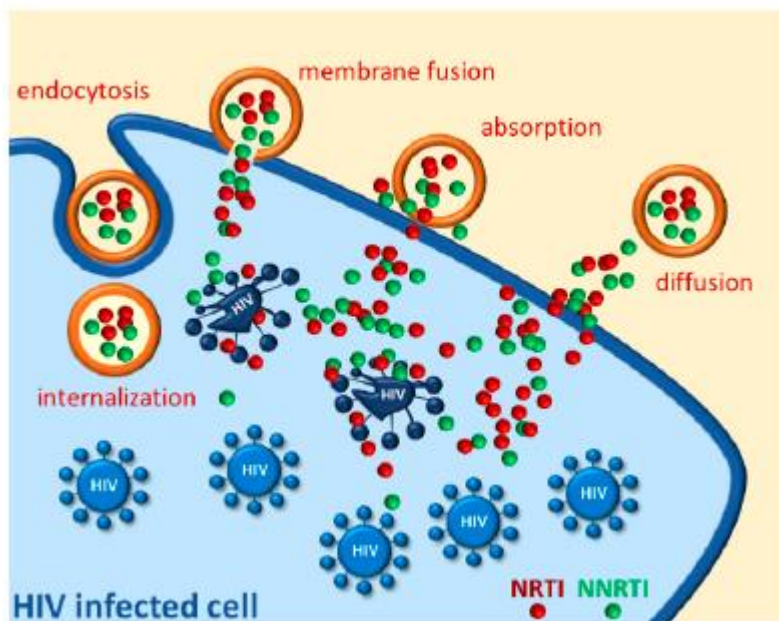
Figure 2. *Representative delivery modalities for NRTI/NNRTI nanosystem to HIV reservoirs.*

2. Drug Protection Nanosystems

Most of the protocols adopted for studying the drug stability are suggested by the ICH (International Conference on Harmonization) guidelines [24]. According to such rules, clearly defined drug storage conditions are required to prevent the degradation e ects related to pH, temperature, light, air and humidity for either solution/suspension or commercial formulations/packaging [25]. The protection of sensitive drugs could often be assured by shielding with an adequate packaging [26]. When this simple precaution showed not to be suffcient, the stability of the drug, exposed to diffrent environmental conditions, could be improved by suitable delivery devices, such as vesicular matrices (i.e., liposomes and niosomes), nanoparticles (NPs), and solid lipid nanoparticles (SLN).

Niosomal and liposomal vesicles consist of amphiphilic molecules and an aqueous compartment and di er for their structural chemical units. Both systems are very versatile. The hydrophilic drugs can be entrapped in their aqueous core while the lipophilic drugs can be partitioned into the bilayer domains. Liposomes are made of natural phospholipids, resulting in a greater stability, a low production cost and reduced toxicity [27–32], while niosomes are prepared by means of synthetic, non-ionic surfactants, as alkyl ethers, alkyl esters and pluronics copolymers, or fatty acid and amino acid compounds [31–33]. The preparation of these vesicles requires a simple procedure based on a gentle agitation or sonication of an aqueous solution of phospholipid/surfactant and drug mixtures taken from an ultracentrifugation or low-pressure gel filtration chromatography to purify the formed systems [34].

More recent SLN have been proposed as alternative formulations for both hydrophilic and hydrophobic drugs. These systems are colloidal carriers based on a solid phase lipid and a surfactant and are characterized by a spherical shape in which the lipid portion is always solid and the surfactant acts as a stabilizing factor [22,35–40]. Fatty acids, monoglycerides, diglycerides, triglycerides, waxes and steroids can be applied in the preparation of SLN in the absence of organic solvent [35]. Low cost, good physical stability, large scale production, no toxicity and high biodegradability represent the greatest advantages in the use of these formulations with respect to the liposomes matrices [41].

Nanoparticles systems are known promising carriers for the improvement of solubility and pharmacokinetics of drugs as well as vaccines, nucleic acids and therapeutic proteins. These delivery devices can influence therapeutic e efficiency of a drug, enhance its protection from degradation and reduce dose-limiting side effects. A variety of hydrophobic or hydrophilic active molecules can be dissolved, encapsulated, absorbed or conjugated to polymeric nanoparticles following different techniques [42]. Several natural and biodegradable materials like chitosan have been proposed for the realization of anti-HIV drug nanosystems. An alternative approach, based on the formation of crystalline complex with a fixed range size, was attempted by inclusion of the pure drug into a hydrophobic synthetic polymer [43]. Polymeric nanoparticles based on poly (lactic acid) (PLA) or poly(lactide-co-glycolide) (PLGA) are reported as ideal delivery systems, showing an improved therapeutic efficacy with lower incidence of side effects [42,44–49].

A higher local concentration of active molecules is often reached by integration of classic antiretroviral drugs in different NPs of metals [50]. According to a relative inertness and low toxicity, silver or gold NPs have been explored in biomedicine as multifunctional scaffold. In particular, the application of gold NPs has been employed to conjugate biomolecules on the outer surface. Alternative inorganic multifunctional materials, such as silver NPs coated with poly(vinyl)pyrrolidone, have also been exploited as drug carriers. [51].

Synthetic well-defined nanopolymers with a three-dimensional architecture, known as dendrimers, have been proposed for the vehiculation of several drugs. Generally, a dendrimer is a symmetric and hyper-branched macromolecule characterized by the presence of reactive groups in the central core, repeated branching units in the interior layers of the core and functional groups spanning from the outer surface. The drug molecule can be either entrapped inside the structure or linked to the external functional groups. This approach was proposed for the carrying of several anti HIV agents [52–55].

Some of these matrices are also able to improve the stability of drugs. Several studies described the use of niosomes, metal based and polymeric NPs to prevent the degradation effects caused by stressing conditions [33,50,56].

3. Nucleoside Reverse Transcriptase Inhibitors Nanosystems

The therapy based on the administration of nucleoside antiviral derivatives such as stavudine, zidovudine, lamivudine and emtricitabine represented a first and e ective approach adopted for the management of HIV infection (Figure 3).
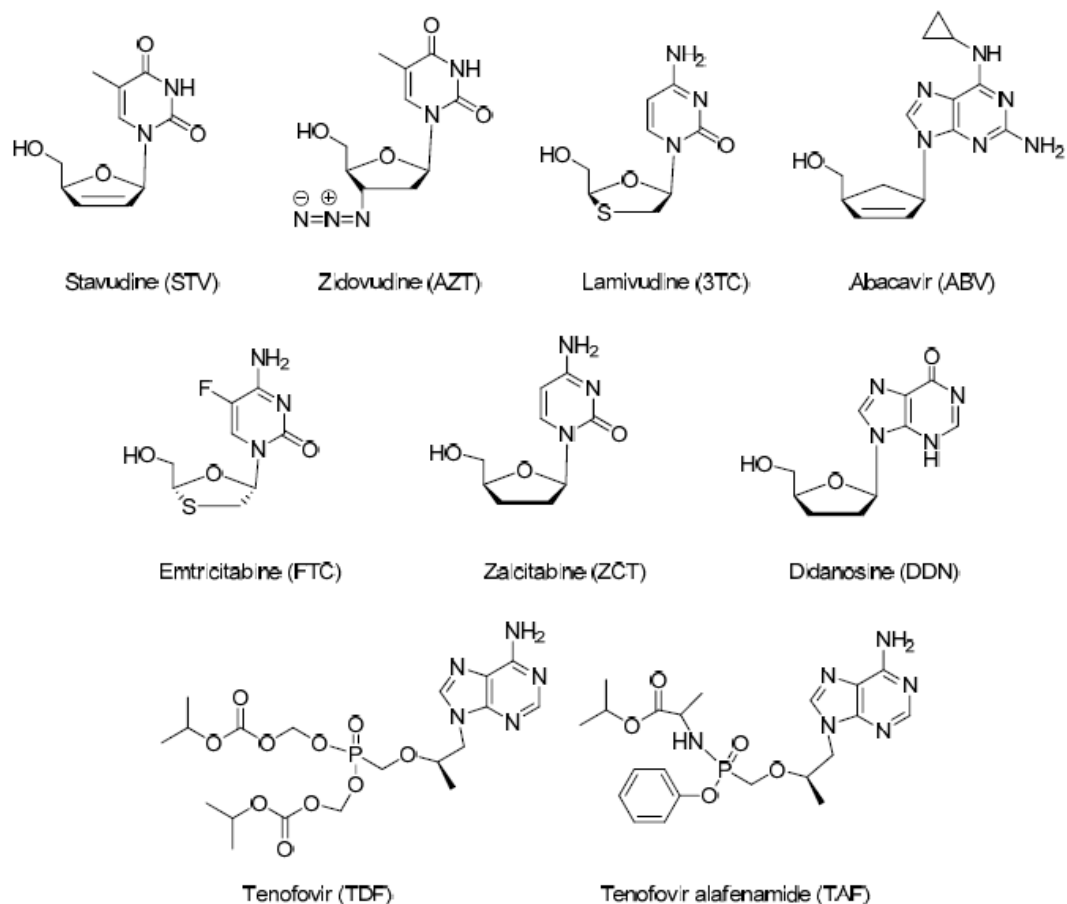
Figure 3. Chemical structures of NRTIs.

Due to the structural similarity to purine or pyrimidine nucleosides, the mode of action of these drugs consists of the competition for the incorporation into viral DNA, catalyzed by RT, so causing chain termination (Figure 4, panel b). Nowadays the most common nucleoside derivatives used in therapy are lamivudine, abacavir, emtricitabine, tenofovir and tenofovir alafenamide [57]. Stavudine and zidovudine, not yet recommended in first-line therapy, were early examples of NRTIs included in nanoformulations designed for limiting their severe side effects and improving pharmacokinetics.
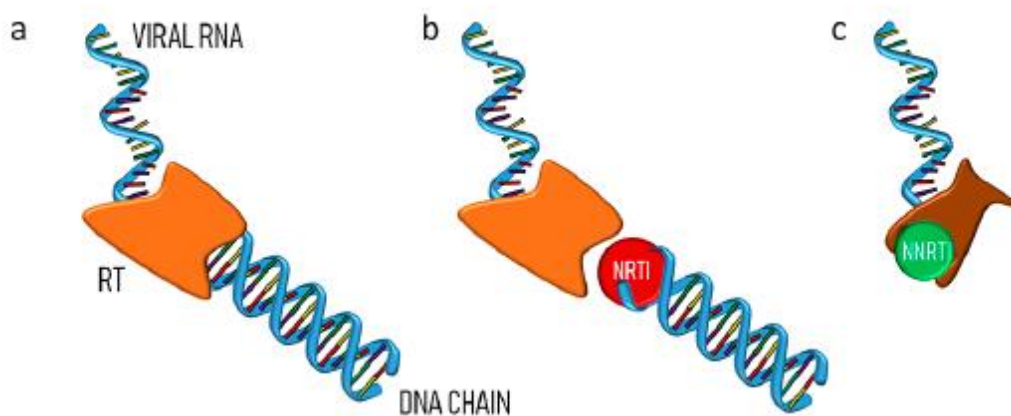

Figure 4. (a) RT catalyzes the conversion of viral RNA into pro-viral DNA before its incorporation into the target cell genome; (b) NRTIs are incorporated into the DNA causing chain termination; (c) NNRTIs bind the enzyme inhibiting its function.

3.1. Stavudine

Stavudine(1-((2R,5S)-5-(hydroxymethyl)-2,5-dihydrofuran-2-yl)-5-methylpyrimidine-2,4 (1H,3H)-dione, STV) is one of the most commonly used forms of NRT approved by FDA in 1996 and its use was recommended in association with other antiretroviral agents. The drug showed major side effects, such as high blood lactate, pancreatitis and hepatomegaly. STV was characterized by a serum half-life of 1h only, while that of its phosphorylated active metabolite was calculated as being 3.5 h [27]. Thus, STV loaded formulations able to concomitantly increase cellular uptake and sustain release should reduce unwanted effects. Accordingly, galactosyl or mannosyl coated liposomes loaded with STV were described. These formulations reached the desired results showing an increased *in vitro* anti-HIV activity together with a remarkable decrease of side effects. The efficacy was tested in a mononuclear phagocyte system, a major reservoir of HIV, proving advantages in terms of bio-stability, site-specific and ligand-mediated delivery, compared to free drug and uncoated liposomes [27,28]. More recently, STV-containing nanoformulations were proposed for the dual utilization to control the residual viremia as well as to target the reservoir sites. To achieve this aim, gelatin nanoformulations containing very low dosage of the drug were prepared through a simple desolvation process and loaded into soya lecithin based liposomes [29]. A study on STV degradation under different stress conditions (hydrolysis, oxidation, photolysis and thermal stress) was initially reported. A stability-indicating reversed-phase HPLC assay method showed the hydrolysis of the drug to thymine in acidic, neutral, alkaline and under oxidative stress conditions [20]. In order to improve the stability of this drug, STV-loaded SLN for intravenous injection were produced by high-pressure homogenization of drug lipid melt dispersed in hot surfactant solution [22]. This SLN formulation was also studied for its active delivery to lymphatic tissues by ex vivo cellular uptake evaluation in macrophages. Reported experiments confirmed an improved cellular uptake together with a prolonged activity next to the delivery site of the formulation compared to the simple drug solution. This could account for an effient and safe therapeutic profile of the drug-carrier system [58].

3.2. Zidovudine

Zidovudine, also known as azidothymidine (1-((2R,4S,5S)-4-azido-5-(hydroxymethyl) tetra hydrofuran-2-yl)-5-methylpyrimidine-2,4(1H,3H)-dione, AZT), the first antiretroviral medication proposed to prevent and treat HIV/AIDS, has been approved in 1986. An extensive first pass metabolism often requires an in vein administration. This feature and a long list of severe side effects limit the use of this drug, which is however still present in many therapeutic anti-HIV regimens. Its incorporation into supramolecular matrices was extensively exploited in order to increase bioavailability and to reduce dose-dependent unwanted effects.

Positively and negatively charged liposomes based on stearylamine and diacetyl phosphate were used as AZT carriers. In order to enhance localization to lynph nodes and spleen, these systems were even coated with a site-specific mannose-terminated stearylamine ligand. Fluorescent microcopy images showed an enhanced uptake and localization localization of these liposomes in the target tissues [59]. In an early paper, a dispersed system comprising polyoxypropylene, polyoxyethylene, oleic acid, water and cetyl alcohol as surfactant, was described as a potential DDS. The release profile experimental analysis showed that the delivery of AZT could be controlled this way, in accordance with a mathematical theoretical approach [60]. This system has been proposed as a carrier, which potentially could overcome the main drawbacks of conventional pharmaceutical formulations [61].

AZT loaded in polymeric NPs based on PLA and poly(L-lactide)poly(ethyleneglycol) (PLA/PEG) were prepared by double emulsion solvent evaporation and thoroughly investigated *in vitro* for uptake into polymorphonuclear leucocytes of rat peritoneal exudate. The cells activation by NPs was assessed by a chemiluminescence assay suggesting a more favorable behavior of PLA vs. PLA/PEG complexes [62]. On the other hand, the drug release increased proportionally to the PEG amount in the blend [63]. AZT was encapsulated in alginate-glutamic acid amide based NPs obtained by an emulsion solvent evaporation method. The polymeric NPs were coated with pluronic F-68 to favour cellular internalization through the endocytosis mechanism. As a result, the antiviral drug loaded in these nanosystems was released in a prolonged manner. Intracellular uptake and cell viability assays also confirmed an effcient uptake of AZT in glioma cell lines [64]. Solid lipid NPs based on modified stearic acid and *Aloe vera* extract were described as an alternative drug delivery carrier for controlled release and targeting of AZT. The plant extract was used because of its high content of polysaccharides that showed synergistic antiretroviral activity with AZT. The described nanocarriers did not interact with plasma proteins and showed high drug loading and entrapment efficiency. Moreover, fluorescent microscopy images suggested that the natural gel facilitated the cellular uptake of AZT in brain cells [36]. The drug proved to decompose when exposed to light or under hydrolytic conditions, while it was more stable toward oxidation agents and thermal stress [65]. In particular, the acid degradation induced the formation of a pyrimidine derivative endowed with higher toxicity when compared to AZT, as demonstrated by a mutagenicity and an aerobic biodegradability assay [21]. Recently, three novel prodrugs of AZT, obtained by functionalization with dicarboxylic acids, were designed in order to enhance pharmacokinetics, chemical stability and affinity for human serum albumin [66].

3.3. Lamivudine

The oral agent lamivudine, (4-amino-1-((2S,5R)-2-(hydroxymethyl)-1,3-oxathiolan-5-yl)pyrimidin-2(1H)-one, 3TC), an analog of nucleoside cytidine, was approved by FDA for the combined therapy with AZT in 1995 and for monotherapy in 2002. However, the emergence of drug resistance, associated to the gene mutation of RT, limited its clinical application [67,68]. Several nanocarriers were prepared by mixing biodegradable networks (i.e. PEG, pluronicpolyethyleneimmine (PEI), glycyrrhizin conjugated chitosan, mannosylated-PLGA) or dendritic networks (i.e. starPEG-PEI, poly(amidoamine)dendrimer-PEI-PEG) or nanogels with AZT or didanosine triphosphates under a freeze-drying method, to specifically deliver the antiviral agent next to macrophages in the CNS. All nano-NRTIs demonstrated high efficacy in inhibiting HIV at low μM drug concentration. The major cause of NRTI neurotoxicity, consisting in the mitochondrial DNA depletion, was also reduced 3-fold compared to uncoated NRTIs [69]. Acid or alkaline conditions as well as an oxidative environment caused the degradation of the drug into five different products. On the other hand, light exposure or thermal stress did not a ect drug stability [70,71].

More recently, a mass spectrometry study evidenced the formation of an additional degradation product when the solid drug was exposed to oxidative conditions [72]. 3TC was incorporated into polymethacrylic acid NPs in different drug/polymer ratio by nanoprecipitation method in order to overcome some drug limitations, such as accumulation during multi dose therapy and poor patient compliance. These polymers offer several advantages, including high stability and simple preparation route compared to remaining colloidal carriers. Moreover, these nanocarriers were shown to increase drug bioavailability and optimize the release time to the target site without significant chemical interactions between the drug and matrix [73]. An alternative encapsulation for 3TC was exploited by

using PLGA NPs coated with bovine serum albumin through a double emulsion procedure. It was then demonstrated that PLGA NPs were rapidly internalized into the human liver cells after oral administration, at different drug concentrations, confirming their high potential as ideal 3TC delivery systems [74]. The PLGA/3TC system was also investigated for the formulation of a thermosensitive vaginal gel. The system was obtained in the form of NPs by the formation of an amide bond between the biodegradable polymer and the free amine group of the drug. An analogue formulation was prepared using emtricitabine as an alternative NRTI. The NPs were finally incorporated into a thermosensitive gel for vaginal administration. The nanoformulations showed to be non-toxic in HeLa cells assay up to a 100 μg/mL concentration. Similar preparations containing fluorescent NPs were found to be active for up to 5 days, suggesting a potential long-lasting application in therapy [75]. A similar approach was adopted for the achievement of transdermal formulation of PLGA/3TC complex. NPs obtained resulted in an ideal spherical shape and an external smooth shell. The high drug entrapment rate resulted in an improved physical stability of the drug together with an efficient delivery after skin permeation.

This last property was enhanced after microneedles skin pre-treatment [76]. Mannosylated-PLGA NPs were prepared to ensure an efficient delivery of 3TC into brain macrophages. The experimental data confirmed the increased drug release from nanocarriers and this effect may be due to the presence of sugar receptors on the luminal surface of blood-brain barrier (BBB) [77]. 3TC was also entrapped into PLA/chitosan (CS) NPs by an emulsion technique. The drug was efficaciously entrapped and protected at low values of pH, while it was rapidly released at higher pH values, thus allowing the drug to be selectively absorbed in the intestinal tract. These NPs were also proven to be non-toxic in a mouse fibroblasts model. Efficient biomedical applications could be accordingly envisaged for such an inclusion system [78].

Similar results were obtained for 3TC-CS NPs prepared by ionic gelation of CS with tripolyphosphate anions. These formulations offer several advantages with respect to conventional dosage forms of the drug, particularly in terms of bioavailability [79]. The CS functionalization with glycyrrhizin was realized for a liver targeting and a 3TC controlled release. In fact, the results of this research confirmed a lower drug release and an augmented level of 3TC in hepatocyte tissues, if compared with CS NPs or the free-drug solution [80]. Successively, 3TC was loaded into poly(□-caprolactone) through a double emulsion spray-drying method giving rise to NPs with spherical morphology. This system also proved to be effective in improving drug bioavailability and reducing side effects [81]. Multiple drugs combined in a single nanosystem showed significant advantages over therapy based on a single drug. Accordingly, an example of polymeric NPs based on methyl methacrylate or ε-caprolactone was designed for the release of four different anti HIV drugs, AZT, 3TC, nevirapine and the IN inhibitor raltegravir [82]. In a recent paper, the incorporation of 3TC into CS with sodium alginate/calcium chloride by the above gelation method, in di erent experimental conditions, was described and showed an impressive drug release rate lasting up to 24 h. The method proved to furnish highly homogenous particles capable of improve bioavailability together with a constant drug release, following a first order mechanism, with diffusion of the drug after swelling of the polymer [83].

Protein-based NPs were prepared using lactoferrin for the controlled release of 3TC combined with AZT and EFV, after its application for a single DDS. The lactoferrin possesses itself antiviral activity and therefore acts synergistically with the entrapped drugs. The assessment of pharmacokinetic profile for each entrapped drug and *in vitro* data suggested that these NPs are able to release drugs intracellularly in a controlled and sustained manner [84,85].

Alternative nanotechnologies used for anti-HIV drugs release included the use of inorganic components such as iron or silica. Preliminary results suggested a potential application for these new formulations. In particular, chemical-physical characterization of SiO_2 NPs coated with magnetic Fe_2O_3 loaded with 3TC were investigated for their pharmacokinetic and cytotoxic profiles showing more favorable features compared to the free drug [86].
A similar preparation was attempted for 3TC and zalcitabine both in form of triphosphates.
Preliminary results showed that these nanosystems of dideoxynucleoside triphosphates/SiO_2 NPs were useful transport systems for delivering these drugs to target cells with increased antiviral efficiency [87].
Moreover, the co-encapsulation of 3TC and AZT, both in form of triphosphates, into iron carboxylate mesoporous NPs gave biocompatible systems endowed with peculiar delivery properties.
In particular, the drugs were released with dierent kinetics: 3TC showed accelerated release, while AZT was released more slowly. This vector protected drug from degradation, conferring at the same time improved *in vitro* anti-HIV activity. In fact, these formulations contribute to stabilizing the drugs since no alterations were detected after two-month storage and freeze-drying reconstitution [50]. High drug bioavailability and patient compliance were recorded after the administration of the of 3TC encapsulated into a new gum odina based biopolymer obtained by a multiple water-in-oil-in-water emulsion approach. The long-term stability study showed the improvement of the stability of the emulsions after a 90-day storage compared to a similar emulsion comprising Tween 80 as a stabilizer [88]. 3TC was also loaded in nanovesicles based on phospholipids or non-ionic surfactants (niosomes and liposomes). The best components and reparation methods able to produce formulations with suitable size, improved drug encapsulation efficiency and release profile were formulated for these systems [89,90].

3.4. Abacavir

Abacavir ((1S,4R)-4-(2-amino-6-(cyclopropylamino)-9H-purin-9-yl)cyclopent-2-en-1-yl)methanol, ABV) introduced in 1998, represented an alternative nucleoside derivative administered orally in solid or solution form for the prevention and treatment of HIV infection. Similarly, to other nucleoside analogs, its use is recommended in combination therapy because of its severe side effects like hypersensitivity, liver damage and lactic acidosis, which all preclude monotherapy. ABV and its congener 3TC, after transformation into the corresponding thiol ending ester derivatives, were conjugated to glucose-coated gold NPs, which were investigated for their pH dependent drug release performances. This drug-delivery system was in turn studied for new multifunctional devices since such gold NPs, themselves endowed with microbicide properties, proved useful for the loading of more than one active agent dierently targeting the viral replication cycle, and therefore representing a multivalent therapeutic approach [51]. Albumin NPs loaded with ABV sulfate were prepared by solvation method and studied for their mechanism of drug release. Results obtained revealed a remarkable drug loading capacity together with a sustained and controlled release within 24 h in HIV reservoir organs [91]. A myristoylated ABV prodrug entrapped into poloxamers was evaluated for the pharmacokinetic properties after injection in mice. Comparison of such nanoformulation with the free drug was performed on human monocyte-derived macrophages by proton nuclear magnetic resonance studies in terms of anti-HIV activity. As a result, an efficacy comparable to that of the native drug was detected for the encased polymer, which showed a two-week lasting release [92]. A detailed study described the formation of innovative nanocarriers named ProTide (PROdrug and nucleoTIDE) obtained by the loading of L-alanine and L-phenylalanine ester phosphoramidates of ABV

into PLGA and poloxamer NPs. Such formulations showed sustained retention and antiretroviral activities for up to one month [93].

3.5. Emtricitabine

Emtricitabine(4-amino-5-fluoro-1-((2S,5R)-2-(hydroxymethyl)-1,3-oxathiolan-5 l)pyrimidin- 2(1H)-one, FTC), is a deoxycytidine nucleoside analog approved in 2006 for anti-HIV therapy. Even if it showed reduced side e ects when compared to other NRTIs, FTC is largely used in triple or quadruple drug combinations.

A customary PLGA nanoformulation of this water soluble drug was achieved through the water-in-oil-in-water emulsion method and showed a sustained release profile in rats, with adequate drug concentration up to two weeks [94,95]. The large volume distribution, beside a short plasma half-life, suggests the use of FTC in alternative formulations, such as PLGA NPs. This particular administration form proved to be able in enhancing drug stability and intracellular retention time, as demonstrated by an ex vivo endosomal assay. A once-biweekly dosing for HIV infection prevention or treatment was accordingly hypothesized [96]. In addition, eight degradation products were separated and characterized by LC–MS/MS from ABV sulfate when subjected to forced degradation under hydrolysis, oxidation, photolysis and thermal stressing conditions [97]. More recently, a solution state study showed the formation of eleven degradation products [98].

The thermal decomposition of FTC was well investigated by applying di erent methods. FTC largely decomposed to small molecules and insoluble substances. A small amount decomposed to 5-fluorocytosine due to an oxidation reaction [99]. When the drug was exposed to the action of acids or bases as well as oxidative stress conditions, an additional degradation product was detected [100].

3.6. Tenofovir

Tenofovir disoproxil fumarate ((R)-(((((1-(6-amino-9H-purin-9-yl)propan-2-yl)oxy)methyl) phosphoryl)bis(oxy))bis(methylene) diisopropyl dicarbonate, TDF) is a more recently approved NRTI (2001) used in the treatment of chronic hepatitis B and in the prevention and treatment of HIV infection. Successively its prodrug tenofovir alafenamide fumarate ((isopropyl2-((((((R)-1-(6-amino-9H-purin-9-yl) propan-2-yl) oxy) methyl)(phenoxy) phosphoryl) amino)propanoate, TAF) was laun-ched in the market due to its more favorable properties after oral administration. TAF has greater antiviral activity and better distribution into lymphoid tissues than TDF. Both drugs are recommended in combination therapy along with other antiretroviral agents.

3.6.1 Tenofovir SLN

Lipid NPs loaded with NRTI and NNRTI agents including TDF or TAF were extensively studied for the improvement of bioavailability and long lasting drug release. Several lipid matrices were designed and showed a very promising behavior under different experimental conditions [37,101,102]. Toxic effects of TDF loaded in nanoemulsions on liver and kidney were assessed using an animal model. Although any behavioral toxicity and mortality were not detected, moderate alterations were however observed on both organs [103]. Extensive chemical-physical studies were performed on hybrid inclusion complexes obtained by encasement of TDF into lipid and polymer matrices by engineered melt emulsification-probe sonication technique. The carrier obtained by combining TDF, lauric acid and pemulen polymer was shown to promote a noteworthy increase of TDF trans-nasal flux, so potentially useful for nasal administration [104]. Nanocarriers based on a hydrogel-core and a lipid-shell were designed for the controlled loading and topical vaginal release of TDF and maraviroc, a virus entry inhibitor. These nanolipogels proved to be efficient systems and

robust carriers for the encapsulation and the prolonged *in vivo* release of antiretroviral drugs, showing solubility concerns that are useful during the prevention and treatment of HIV infection [105].

3.6.2. Tenofovir/Dendrimers Complexes

A drug combination including TDF into dendrimers was designed for the evaluation in an *in vitro* model of semen-enhanced viral infection. The results obtained suggested that this therapeutic strategy could bypass the detrimental e ects of amyloid fibrils, present in semen, which seem responsible of the failure of topical vaginal gels action [54]. An approach to the treatment of neuro-AIDS was based on the use of co-encapsulated drugs into ultra-small iron oxide NPs with the addition of dextran sulfate. The inclusion complex of TDF and vorinostat, a latency-breaking agent, was assembled by magnetically guided layer-by-layer method and a noteworthy blood–brain barrier transmigration of drugs was then observed. This strategy, aimed to the activation of latent virus and its simultaneous killing, would result in a high efficacy to eradicate completely the infection from the CNS [106]. Nanosystems such as carbosilane dendrimers seem themselves able to inhibit HIV replication with a potential as local antiviral agents. Nevertheless, the concomitant administration of specific antiretroviral agents led to a potent synergistic activity. TDF, along with AZT and EFV or with maraviroc was encapsulated into anionic carbosilane dendrimers, bringing sulfated and naphthyl sulfonated groups to generate potential microbicides to prevent the sexual transmission of HIV [55,107–110]. An innovative therapeutic strategy could be based on the TDF prolonged release from NPs obtained by hyaluronic acid (HA) cross-linked with adipic acid dihydrazide. This nanosystem did not show detectable toxicity under the control of hyaluronidase enzyme. Comparative experiments with a simple TDF/HA gel suggested an essential role of the enzyme during the HA degradation and TDF release. The potential of these formulations for topical delivery of antiviral agents for the prevention of sexually transmitted diseases was accordingly hypothesized [111].

3.6.3. Chitosan based TDF Nanoparticles

TDF was also used as a model drug in a CS based nanopreparation coated with sodium acetate, an aggregation-preventing agent, realized by the freeze-drying method. The NPs cytotoxic profile on macrophages was assessed by neutral red, resazurin, nitrite oxide and cytokines assays. Satisfactory encapsulation rate together with a good stability of the colloidal dispersions was observed for the formulation. Moreover, a sustained drug release beside a lack of cytotoxicity and a pro-inflammatory e ect was recorded [112]. Further improvements in terms of mucoadhesive performance were obtained by a formulation based on TDF-loaded CS NPs dispersed in vaginal thermogels [113].

CS based oral NPs loaded with TDF were prepared by the ionic gelation technique and studied for their potential in preventing esterase metabolism and facilitate active transport uptake. Both processes were a effected as confirmed by *in vitro* experiments. Moreover, data obtained suggested that a clathrin-mediated mechanism is involved in the enhancement of drug oral absorption [114].

A triple combination of TDF, FTC and bictegravir, an integrase inhibitor, was loaded into trimethyl CS to generate a nanoconjugate with improved cellular uptake. The efficiency of the nanocarrier was determined by spectrophotometry while XTT and ELISA tests were used to determine cytotoxicity and anti-retroviral efficiency, respectively. As a result, this formulation proved to inhibit viral replication at lower concentrations than the free drugs combination, without a significant cytotoxicity, therefore resulting in a lower drug resistance [115]. Colloids based on polyelectrolyte complexes of CS and chondroitin sulfate were loaded with TDF and examined for the stability at physiological conditions.

This property was assured by the use of Zn(II) throughout the formulation procedure. *In vitro* studies did not reveal toxicity of such NPs on human peripheral blood mononuclear cells, while a remarkable dose-dependent antiretroviral activity was detected [116]. TDF was loaded into thiolated CS core/shell nanofibers in order to investigate the rate of drug loading, mucoadhesion properties and *in vivo* safety.

The formulation was fabricated by assembling poly(ethylene oxide) with the CS component and PLA by a coaxial electrospinning technique. An enhanced drug loading together with a prolonged drug release and an increased mucoadhesion were assessed by *in vitro* studies, whereas a significant toxicity was not detected in neither *in vitro* nor *in vivo* experimental models. These new formulations could be therefore considered promising tools for the local delivery of microbicide agents [117].

3.6.4. Alternative Polymeric TDF NPs

An original formulation to be used for vaginal administration was fabricated by oil-in-water emulsification of the inclusion product of TFV into PLGA and sodium deoxycholate as an ion-pairing agent and a thermosensitive gel. Sustained release properties in humanized BLT mice were shown for these nanoformulations when instilled locally [118]. Similar results were obtained by loading TFV into PLGA/stearylamine and incorporating such NPs into a hydroxypropyl methylcellulose/PVA-based film [119,120]. TAF and FTC entrapped NPs were prepared for subcutaneous administration during pre-exposure prophylaxis. Drugs were included into the PLGA/PVA system and investigated for their long-acting potency detectable even after 14 days by a humanized mice model [121,122]. A similar approach was exploited for the incorporation of TAF and elvitegravir, an integrase inhibitor, during the fabrication of devices to be used during vaginal prevention [123,124]. The drug absorption following oral administration were also positively effected by the use of TAF/PGLA loaded NPs, as highlighted by a statistical model study [125]. Formulations containing mono- or by-layered films of PVA and pectin were coupled with Eudragit NPs loaded with TDF/FTC, by nano spray-drying technique. These systems were designed for vaginal use with a better patient compliance. The time of disintegration and drug release was evaluated in a simulated vaginal fluid, showing favorable results.

The by-layered films equipped with NPs loaded with drugs showed the best performances in terms of drug release delay. Moreover, this topic formulation was shown particularly safe by MTT and lactate dehydrogenase assays using different cervical cell lines [126]. Multifunctional magneto-plasmonic liposomes charged with TDF were obtained with the aim to study guided systems for enhancing efficiency of antiviral treatment. The distribution of such a hybrid system can be monitored by image technique and activated magnetically into the brain. The gold shell of such nanocomplexes can be followed by computed tomography. This way, these particular systems proved to be efficient against HIV in infected microglia cells after adequately crossing the BBB [127]. A nanosuspension of drug combination particles consisting of TDF, ritonavir and lopinavir, two protease inhibitors, and lipids were prepared for the development of innovative topical formulations. This system was highly efficient in targeting lymphocytes during anti-HIV therapy with a long-lasting action after a single subcutaneous administration [128]. Similar results were described after the addition of 3TC to the previously combination to give a four-drug components nanosuspension [129]. Similar results were obtained for alternative combinations of TDF and other RTI. In all cases, a persistent drug concentration was detected after single subcutaneous injection in di erent HIV reservoir cells [130,131].

A stability study was performed on TAF and compared with the stress degradation behavior of TDF. Gastrointestinal stability studies were conducted on both drugs, showing the

formation of six degradation products. These studies revealed a higher stability of TAF, except for with the acid condition, where the drug was extensively degraded [132].

4. Non-Nucleoside Reverse Transcriptase Inhibitors Nanosystems

An alternative approach to anti-HIV treatment with RTIs is represented by the combined therapy using both NRTIs and NNRTIs, exploiting the synergism of the two distinct classes of drugs. Accordingly, the multi-therapy is nowadays the most widely adopted strategy for the treatment of HIV infection in the clinic. NNRTI act directly by binding the enzyme, so preventing its DNA polymerase function. In fact, their heterogeneous structures do not resemble those of nucleobases, the natural substrate of RT (Figure 4, panel c).

After a first generation NNRTI drugs introduced in the 90s (i.e. nevirapine, delavirdine, efavirenz) approved for anti-HIV therapy, recently some new and e ective compounds entered the market (i.e. etravirine, rilpivirine). Some more interesting compounds are currently under clinical investigation. The structures of representative NNTRI are reported in Figure 5.

4.1. Nevirapine

Nevirapine(11-cyclopropyl-4-methyl-5H-dipyrido[3,2-b:20,30-e][1,4]diazepin-6(11H)-one, NVR)was the first NNRTI approved by FDA in 1996 for the treatment of HIV infection. In order to improve the pharmacokinetics of this hydrophobic drug, NVR was loaded into liposomes prepared by thin film hydration and extrusion method to give uniform spherical vesicles. The matrix, obtained from egg phospholipid and cholesterol, proved to release the drug during 22 h at physiological pH values.

The presence of proteins into the medium or the exposition of the system to ultrasounds greatly impair the delivery mode of the drug. However, this encapsulation method could optimize the efficacy of NVR in terms of drug stability and controlled release to the target tissues [30]. Transferrin grafted PLGA NPs have been designed in order to facilitate NVR in crossing vascular endothelial cells of the human brain.

This particular nanosystem allowed a favourable drug loading with a desired controlled release, so proving to act as an efficient carrier to promote vascular diffusion of the compound [133]. Nanoparticles of PLA/PEG, the surface of which was modified with serum albumin, were prepared to improve release of the drug to the target tissues. This favorable feature was measured after i.v. injection in rats, showing an improved bioavailability, cellular uptake and drug accumulation in the brain, liver and spleen, compared to pure drug solution or uncoated nanoformulations. Moreover, no additional cytotoxicity was recorded. The capability to cross the BBB makes these formulations potentially useful for the treatment of AIDS related dementia [134,135]. The stability of NVP was well investigated by a stability-indicating ultra-high performance liquid chromatography (UHPLC) method. Drug product efficacy, safety and quality were verified in different degradation conditions by using acids, bases, water, metal ions, heat, light and oxidation agents. The tests were applied on the pure compound and on its tablet formulation leading to the formation of five degradation products [136]. A physically stable formulation of NVP was prepared by forming a crystalline inclusion complex with biodegradable and hydrophobic poly(ε-caprolactone). Compared to pure NVP crystals, the formulation assured a sustained drug release at physiological conditions in PBS solution up to 6 weeks, due to the reduction of drug solubility [43].
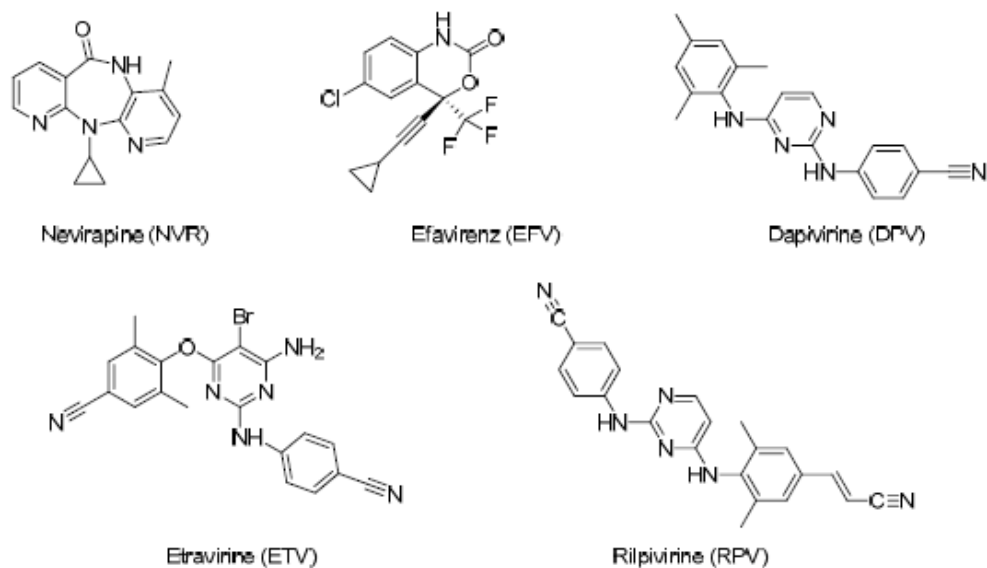
Figure 5. *Chemiical structures of NNRII*

4.2. Efavirenz

Efavirenz, ((S)-6-chloro-4-(cyclopropylethynyl)-4-(trifluoromethyl)-1-*H* benzo[*d*] [1,3] oxazin- 2(4*H*)-one, EFV) was approved in 1998 and is largely utilized with other drugs for anti-HIV association therapies. However, its potential was limited by a low bioavailability due to its high lipophilicity and other drawbacks related to irritant effects on mucosae [137,138]. A strategy devoted to the improvement of EFV pharmacokinetics resides in its incorporation into SLN, which should drive the delivery of the drug next to the lymphoid system and brain [38]. Phenylalanine anchored SLN (PA-SLN) were used to encapsulate EFV and the resulting nanocomplex was tested for its potential to cross BBB. Phenylalanine was chosen in order to exploit the aromatic amino acid transporter active within the barrier. The nanocomplex showed good entrapment e ciency and a favorable drug release, with a remarkable accumulation in brain assuring a long-lasting therapeutic effect [139].

4.2.1. Efavirenz SLN

SLN of selected lipids as matrix medium and EFV were prepared with the addition of a surfactant by high-pressure homogenization technique and evaluated *in vivo* for their enhanced bioavailability and brain targeting. In particular, such properties were assessed after an intranasal administration route, which could be useful for therapy devoted to the complete eradication of HIV [39]. As an example, EFV was loaded into SLN assembled with the use of mono- and tri-glycerides with the aid of a surfactant. This particular formulation allowed the drug to partly by-pass liver metabolism after oral administration and in doing so increasing bioavailability and accumulation into spleen [140]. A prolonged drug release together with a lower incidence of side effects, consequent to a reduced drug dosage, was achieved after EFV incorporation into SLN.

4.4.2. Polymeric EFV NPs

Efavirenz was loaded into NPs based on methacrylate polymers, which conferred an increased drug uptake in monocytes and macrophages [141,142]. Emulsion or nanoprecipitation methods allowed loading EFV into biodegradable PLGA NPs. The effects of the resulting formulations administered in combination with other free or encapsulated

anti-HIV drugs were investigated. As a result, the new formulations proved more efficient compared to the free drugs and also a noteworthy synergistic effect was recorded for encapsulated EFV combined with TDF, a second NRTI [143]. EFV was dispersed with α-tocopherol polyethylene glycol succinate and PVA by an emulsion-templated freeze-drying technique to realize solid inclusion NPs. Dry monoliths charged with these NPs proved to be stable for several months. Their reconstitution in water furnished nanodispersions, which showed reduced cytotoxicity together with an improved bioavailability and pharmacokinetics [49]. A nanoformulation was obtained by combining EFV with cellulose acetate phthalate, acting as an HIV entry inhibitor, by the nanoprecipitation method. The resulting NPs were formulated into a thermosensitive gel, which resulted in an efficient nanomicrobicide for long-term HIV prophylaxis [144]. Polymeric micelles based on pluronic F127 loaded with EFV and bio-conjugated with anti-M-cell-specific antibodies were prepared in order to evaluate their preferential target delivery to gut micro fold cells of lymphoid tissue, one of the major HIV reservoirs in the body. The efficiency of such nanosystem was showed to be higher than the free drug and a possible oral application by enteric-coated capsule was accordingly hypothesized [145]. EFV was loaded into eudragit, pluronic and alginate sodium polymeric based NPs by solvent evaporation method. Cytotoxicity and antiviral characterization was investigated by syncytium inhibition assay. The polymeric nanocarrier was proven to be more effective than the pure free drug by an enhanced drug dissolution and bio-distribution, especially after BBB crossing. A reduced toxicity was also detected [146,147]. NPs to be used during intranasal administration were prepared by the encasement of EFV into CS grafted hydroxypropyl beta cyclodextrin matrices. The results obtained confirmed a better CNS access due to an improved cellular permeation consequent to both a higher drug solubility and a concomitant beneficial action of CS on cell membrane [148].

Rectal polymeric formulations were prepared by incorporation of EFV into PLGA NPs coated with PEG. This particular form assured a prolonged drug residence in the lower colon with a long lasting prophylactic action against HIV transmission [149]. A better BBB crossing together with a reduction of side effects incidence was attempted by the preparation of transferrin functionalized PLGA NPs loaded with EFV. Although a higher deposition rate of the drug to the targeted site was recorded, the formulation did not improve drug membrane permeation [150]. Lactoferrin NPs were fabricated for oral or vaginal administration giving raise to significant results in terms of drug release and bioavailability. A combination of EFV and curcumin was also attempted in order to reach synergism for the two-microbicide agents. The results obtained confirmed an improved pharmacokinetic profile for the drug combination nanoformulation with respect to free drugs [151,152].

4.3.3. Efavirenz/Dendrimer Complexes

EFV was incorporated into t-Boc–glycine and mannose conjugated dendrimer-based poly(propyleneimine) (PPI). These branched three-dimensional polymers were shown to be less toxic than free PPI and could allow the drug to reach monocytes and macrophages, both reservoirs of HIV in the body. In fact, it is known that inhibitors targeting only lymphocytes are ineffective in completely eradicating the infection. These formulations demonstrated tob e particularly effective since they are able to promote a significant increase of EFV cellular uptake [153]. The same authors loaded EFV into dendrimer-based PPI complexed with tuftsin (Tu). This latter is a tetrapeptide coming from the cleavage of immunoglobulin G and showed to be capable of selectively target and activate macrophages, monocytes and polymorph nuclear leukocytes. This strategy would help EFV in avoiding unwanted e ects acting in a synergistic fashion with the peptide. Such an option was suggested by the

fact that the TuPPI complex showed no toxicity and prolonged EFV cellular uptake in HIV infected macrophages with respect to uninfected cells [154].

4.2.4. Alternative Supramolecular EFV NPs

Vesicular systems consisting of gold NPs entrapped inside the aqueous core were loaded with EFV in the bilayer membrane. The niosomes so formed were dispersed in carrageenan/hyaluronic acid/poloxamer based thermogel after coating with an opportunely functionalized mannose, in order to combine the action of the protein and the sugar for an effective prophylactic vaginal application.

A remarkable inhibition of viral transmission as well as a drastic reduction of side e ects was recorded [31]. A soya lecithin/cholesterol and PEG liposomal DDS was designed in order to overcome the limited solubility, dissolution rate and bioavailability of EFV [32]. Similar results were achieved by the entrapment of EFV into boron nitride and carbon nanotubes as delivery vehicles. Both the systems showed a favorable behavior. Between the two distinct formulations, carbon nanotubes assured a higher drug adsorption [155]. Enhanced solubility and dissolution of the drug were also obtained by inclusion complex with hydroxypropyl-β-cyclodextrin. The solubility of the complex was further increased by the addition of l-Arginine [156]. Degradation behavior of the drug in water solution was assessed by HPLC analyses, detecting a total twelve degradation products under acidic conditions.

Alkaline stress resulted in the formation of only two degradation products, whereas oxidative and photolytic conditions did not promote any degradation of the drug. All the degradation derivatives showed remarkable toxicity, including carcinogenicity, mutagenicity and skin irritation, as confirmed by *in silico* experiments [72]. The thermal behavior of glass EFV was evaluated in different experimental conditions, showing a good stability only at room temperature [157].

4.3. Dapivirine

Dapivirine (4-((4-(mesitylamino)pyrimidin-2-yl)amino)benzonitrile, DPV) is a new, sparingly soluble NNRTI, under investigation for vaginal application during the prevention of HIV sexual transmission. This compound was shown to be a noncompetitive inhibitor of RT that is particularly useful for topic treatments. In order to improve efficacy, a microbicide film for vaginal delivery was formulated by loading DPV into PLGA NPs and the nanosystems were in turn coupled to a PVA in a cellulose based platform film using solvent casting technique. TDF was also added to the formulation to achieve a synergist antiviral effects. A rapid release of active principles was accordingly recorded suggesting an ideal behavior of such a formulation as prophylactic microbicide [158,159]. Some advantages were also obtained by alternative formulations of this drug. In particular, surface-engineered poly("-caprolactone) NPs were manufactured and evaluated in pig vaginal and rectal mucosa, resulting in favorable drug release properties [160]. Physical–chemical properties of these nanocarriers were evaluated upon one-year storage to a variable temperature range. Colloidal instability affected the *in vitro* drug release of the NPs, although no detectable degradation was observed for the entrapped drug [56].

4.4. Etravirine

Etravirine (4-((6-amino-5-bromo-2-((4-cyanophenyl)amino)pyrimidin-4-yl)oxy)-3,5-dimethylbenzonitrile, ETV) is a NNRTI approved in 2008 for monotherapy against HIV, also clinically used in combination with other antiviral agents in antiretroviral treatment-experienced adult patients with onset of resistance. A combination of ETV, maraviroc and raltegravir was loaded into PLGA by emulsion-solvent evaporation technique. The antiviral

potency of the resulting NPs was compared to the free triple drug combination in an *in vitro* cells assay and on a macaque cervicovaginal explant model *in vivo*. The nanoformulation provided a prolonged release by extension of the half-life of drugs, leading to an enhanced synergistic antiviral action [161]. An innovative approach for the design of NPs overcoming the drawback, consisting in low drug retention and massive leakage, was undertaken by the preparation of NP-releasing nanofiber vaginal devices. Mucoadhesive PVA fibers coupled to PEGylated NPs should ensure an adequate retention together with a rapid mucus di usion. These composite nanoformulations proved to assure a sustained ETV release for up to seven days [162].

4.5. Rilpivirine

Rilpivirine((E)-4-((4-((4-(2-cyanovinyl)-2,6-dimethylphenyl)amino)pyrimidin-2-yl)amino) benzonitrile, RPV) is a second-generation NNRTI, approved in 2011, possessing increased potency, longer half-life and lesser side-effects with respect to former non-nucleoside agents, today mainly used in combination with other anti-HIV drugs [163]. RPV met therapeutic success either in combination with other anti-HIV agents or in long-acting injectable nanoformulations during maintenance therapy. Its use could also be advantageous for the prophylactic treatment of high-risk uninfected individuals [164,165]. In two separate papers, the potential use of long acting RPV NPs associated with cabotegravir, an HIV integrase inhibitor, was described and an innovative monthly dosing therapeutic regimen was accordingly proposed. Recently, the result of a phase IIb study was reported on the effectiveness of this combination nanoformulation in maintaining adequate drug concentration in plasma or vaginal mucus for up to one month [166–168]. RPV-loaded PLGA NPs were fabricated by emulsion-solvent evaporation method. A sustained release in plasma as well as faster clearance were observed in animal models, suggesting a prophylactic use after the preparation of thermosensitive gels as well as long acting injectable nanosuspensions [169].

Biodistribution of tri-modal theranostic NPs was studied by single-photon emission computed tomography, magnetic resonance imaging and fluorescence techniques. These devices were prepared by the incorporation of Indium radiolabeled, europium doped cobalt-ferrite particles and RPV loaded into a poly("-caprolactone) matrix included into a lipid shell. A sustained drug release and antiretroviral activity were observed in HIV infected macrophages. These multi-functional NPs represent a platform for the monitoring and optimization of the antiretroviral drug pharmacokinetic profile [170].

5. Conclusions

There is a high level of interest in nanotechnologies for their relevant roles in the design and development of innovative anti-HIV formulations either for oral or topical administration. In the first case, a more specific targeted delivery together with a sustained release represents the major goal in the field. Mucoadhesive performance, prolonged retention time and improved patients' compliance were desired for vaginal or rectal application of microbicide nanoformulated antiretroviral agents. A large number of diversely assembled nanocarriers loaded with different classes of antiviral drugs were then developed and deeply investigated to improve both pharmacokinetic characteristics and stability behavior. Overall results demonstrated a potential success of such an approach for monotherapy, even though more profitable applications were recorded for the combination therapy, the most diffused method nowadays. In fact, anti-HIV therapeutic regimens today comprise multiple daily doses of more drugs acting at di erent stages of viral replication, which lead to poor patient compliance. Although the use of protease, integrase and viral entry inhibitors has become

customary, NRTIs and NNRTIs remain pivotal tools during the infection management. In the light of these findings, this overview focuses mainly on the application of nanotechnology applied to RTI as vehicles for challenging virus eradication from depot organs and/or as a platform for the design of modern prophylactic devices for stable or stressing conditions.

References

[1] Vandamme A.M., Van Vaerenbergh K., De Clercq E. Anti-human immunodeficiency virus drug combination strategies. Antivir. Chem. Chemoth. 1998;9:187–203. doi: 10.1177/095632029800900301.

[2] Lisziewicz J., Toke E.R. Nanomedicine applications towards the cure of HIV. Nanomed-Nanotechnol. 2013;9:28–38.

[3] Bangsberg D.R., Hecht F.M., Charlebois E.D., Zolopa A.R., Holodniy M., Sheiner L., Bamberger J.D., Chesney M.A., Moss A. Adherence to protease inhibitors, HIV-1 viral load, and development of drug resistance in an indigent population. Aids. 2000;14:357–366.

[4] Schrager L.K., D'Souza M.P. Cellular and anatomical reservoirs of HIV-1 in patients receiving potent antiretroviral combination therapy. JAMA.

[5] Richman D.D. HIV chemotherapy. Nature. 2001;410:995–1001.

[6] Yilmaz A., Price R.W., Gisslen M. Antiretroviral drug treatment of CNS HIV-1 infection. J. Antimicrob. Chemother. 2012;67:299–311.

[7] Guidelines for the Use of Antiretroviral Agents in Adults and Adolescents with HIV. [(accessed on 10 April 2019)]; Available online: http://aidsinfo.nih.gov/guidelines/html/1/adult-and-adolescent-treatment-guidelines/0.

[8] Rohit S., Ramesh J., Karan G., Raman K., Anil K.S. Nanotechnological interventions in HIV drug delivery and therapeutics. Biointerface Res. Appl. Chem. 2014;4:820–831.

[9] Harrigan P.R., Hogg R.S., Dong W.W., Yip B., Wynhoven B., Woodward J., Brumme C.J., Brumme Z.L., Mo T., et al. Predictors of HIV drug-resistance mutations in a large antiretroviral-naive cohort initiating triple antiretroviral therapy. J. Infect. Dis. 2005;191:339–347.

[10] Chun T.W., Davey R.T., Jr., Engel D., Lane H.C., Fauci A.S. Re-emergence of HIV after stopping therapy. Nature. 1999;401:874–875. doi: 10.1038/44755.

[11] Marsden M.D., Zack J.A. Eradication of HIV: current challenges and new directions. J. Antimicrob. Chemother. 2009;63:7–10.

[12] Nie S., Xing Y., Kim G.J., Simons J.W. Nanotechnology applications in cancer. Annu. Rev. Biomed. Eng. 2007;9:257–288.

[13] Mazzuca P., Caruso A., Caccuri F. HIV-1 infection, microenvironment and endothelial cell dysfunction. New. Microbiol. 2016;39:163–173.

[14] Mahajan S.D., Aalinkeel R., Law W.C., Reynolds J.L., Nair B.B., Sykes D.E., Yong K.T., Roy I., Prasad P.N., Schwartz S.A. Anti-HIV-1 nanotherapeutics: promises and challenges for the future. Int. J. Nanomed. 2012;7:5301–5314.

[15] Vyas T.K., Shah L., Amiji M.M. Nanoparticulate drug carriers for delivery of HIV/AIDS therapy to viral reservoir sites. Expert Opin. Drug Deliv. 2006;3:613–628.

[16] Amiji M.M., Vyas T.K., Shah L.K. Role of nanotechnology in HIV/AIDS treatment: potential to overcome the viral reservoir challenge. Discov. Med. 2006;6:157–162.

[17] Ferrari M. Cancer nanotechnology: opportunities and challenges. Nat. Rev. Cancer. 2005;5:161–171.

[18] Farokhzad O.C. Nanotechnology for drug delivery: the perfect partnership. Expert Opin. Drug Deliv. 2008;5:927–929.

[19] Farokhzad O.C., Langer R. Impact of nanotechnology on drug delivery. ACS Nano. 2009;3:16–20.

[20] Dunge A., Sharda N., Singh B., Singh S. Establishment of inherent stability of stavudine and development of a validated stability-indicating HPLC assay method. J. Pharm. Biomed. Anal. 2005;37:1115–1119.

[21] Devrukhakar P.S., Shiva Shankar M., Shankar G., Srinivas R. A stability-indicating LC-MS/MS method for zidovudine: Identification, characterization and toxicity prediction of two major acid degradation products. J. Pharm. Biomed. Anal. 2017;7:231–236.

[22] Shegokar R., Singh K.K., Muller R.H. Production & stability of stavudine solid lipid nanoparticles--from lab to industrial scale. Int. J. Pharm. 2011;416:461–470.

[23] Nowacek A., Gendelman H.E. NanoART, neuroAIDS and CNS drug delivery. Nanomedicine (Lond) 2009;4:557–574.

[24] ICH Q1A(R2)- Stability Testing of New Drug Substances and Products. International Council for Harmonisation of Technical Requirements for Pharmaceuticals for Human Use (ICH); Geneve, Switzerland: 2003.

[25] Tonnesen H.H. Photostability of Drugs and Drug Formulations. CRC Press; New York, NY, USA: 2004.

[26] De Luca M., Ioele G., Spatari C., Ragno G. Photostabilization studies of antihypertensive 1,4-dihydropyridines using polymeric containers. Int. J. Pharm. 2016;505:376–382.

[27] Garg M., Asthana A., Agashe H.B., Agrawal G.P., Jain N.K. Stavudine-loaded mannosylated liposomes: in-vitro anti-HIV-I activity, tissue distribution and pharmacokinetics. J. Pharm. Pharmacol. 2006;58:605–616.

[28] Garg M., Dutta T., Jain N.K. Reduced hepatic toxicity, enhanced cellular uptake and altered pharmacokinetics of stavudine loaded galactosylated liposomes. Eur. J. Pharm. Biopharm. 2007;67:76–85.

[29] Nayak D., Boxi A., Ashe S., Thathapudi N.C., Nayak B. Stavudine loaded gelatin liposomes for HIV therapy: Preparation, characterization and *in vitro* cytotoxic evaluation. Mater. Sci. Eng. C Mater. Biol. Appl. 2017;73:406–416. doi: 10.1016/j.msec.2016.12.073.

[30] Ramana L.N., Sethuraman S., Ranga U., Krishnan U.M. Development of a liposomal nanodelivery system for nevirapine. Int. J. Biomed. Sci. 2010;17:57.

[31] Malik T., Chauhan G., Rath G., Kesarkar R.N., Chowdhary A.S., Goyal A.K. Efaverinz and nano-gold-loaded mannosylated niosomes: a host cell-targeted topical HIV-1 prophylaxis via thermogel system. Artif. Cells Nanomed. Biotechnol. 2018;46:79–90.

[32] Rao M.R.P., Babrekar L.S. Liposomal Drug Delivery for Solubility and Bioavailability Enhancement of Efavirenz. Indian J. Pharm. Sci. 2018;80:1115–1124.

[33] Abdelkader H., Alani A.W., Alany R.G. Recent advances in non-ionic surfactant vesicles (niosomes): self-assembly, fabrication, characterization, drug delivery applications and limitations. Drug Deliv. 2014;21:87–100.

[34] Khan R., Irchhaiya R. Niosomes: a potential tool for novel drug delivery. J. Pharm. Investig. 2016;46:195–204. doi: 10.1007/s40005-016-0249-9

[35] Naseri N., Valizadeh H., Zakeri-Milani P. Solid Lipid Nanoparticles and Nanostructured Lipid Carriers: Structure, Preparation and Application. Adv. Pharm. Bull. 2015;5:305–313.

[36] Joshy K.S., Chandra P.S., Nandakumar K., Sandeep K., Sabu T., Laly A.P. Evaluation of in-vitro cytotoxicity and cellular uptake efficiency of zidovudine-loaded solid lipid nanoparticles modified with Aloe Vera in glioma cells. Mater. Sci. Eng. C Mater. Biol. Appl. 2016;66:40–50.

[37] Freeling J.P., Koehn J., Shu C., Sun J., Ho R.J. Anti-HIV drug-combination nanoparticles enhance plasma drug exposure duration as well as triple-drug combination levels in cells within lymph nodes and blood in primates. AIDS Res. Hum. Retroviruses. 2015;31:107–114.

[38] Mishra N., Mishra M., Padh H. Formulation Development and Optimization of Efavirenz Loaded SLNs and NLCs using Plackett- Burman Design and its Statistical Elucidation. Int. J. Pharm. Res. Health Sci. 2018;6:2379–2388.

[39] Gupta S., Kesarla R., Chotai N., Misra A., Omri A. Systematic Approach for the Formulation and Optimization of Solid Lipid Nanoparticles of Efavirenz by High Pressure Homogenization Using Design of Experiments for Brain Targeting and Enhanced Bioavailability. Biomed. Res. Int. 2017;2017:5984014.

[40] Madhusudhan A., Bhagavanth R.G., Venkatesham M., Veerabhadram G. Design and Evaluation of Efavirenz loaded Solid Lipid Nanoparticles to Improve the Oral Bioavailability. Int. J. Pharm. Pharm. Sci. 2012;2:84–89.

[41] Pardeshi C., Rajput P., Belgamwar V., Tekade A., Patil G., Chaudhary K., Sonje A. Solid lipid based nanocarriers: an overview. Acta Pharm. 2012;62:433–472. doi: 10.2478/v10007-012-0040-z.

[42] Date A.A., Destache C.J. A review of nanotechnological approaches for the prophylaxis of HIV/AIDS. Biomaterials. 2013;34:6202–6228. doi: 10.1016/j.biomaterials.2013.05.012.

[43] Yang X., Yu B., Zhong Z., Guo B.H., Huang Y. Nevirapine-polycaprolactone crystalline inclusion complex as a potential long-acting injectable solid form. Int. J. Pharm. 2018;543:121–129.

[44] Cao S., Woodrow K.A. Nanotechnology approaches to eradicating HIV reservoirs. Eur. J. Pharm. Biopharm. 2018;138:48–63.

[45] Singh L., Kruger H.G., Maguire G.E.M., Govender T., Parboosing R. The role of nanotechnology in the treatment of viral infections. Therap. Adv. Infect. Dis. 2017;4:105–131.

[46] Parboosing R., Maguire G.E., Govender P., Kruger H.G. Nanotechnology and the treatment of HIV infection. Viruses. 2012;4:488–520.

[47] das Neves J., Amiji M.M., Bahia M.F., Sarmento B. Nanotechnology-based systems for the treatment and prevention of HIV/AIDS. Adv. Drug Deliv. Rev. 2010;62:458–477.

[48] Patel B.K., Parikh R.H., Patel N. Targeted delivery of mannosylated-PLGA nanoparticles of antiretroviral drug to brain. Int. J. Nanomed. 2018;13:97–100.

[49] McDonald T.O., Giardiello M., Martin P., Siccardi M., Liptrott N.J., Smith D., Roberts P., Curley P., Schipani A., Khoo S.H., et al. Antiretroviral solid drug nanoparticles with enhanced oral bioavailability: production, characterization, and *in vitro-in vivo* correlation. Adv. Healthc. Mater. 2014;3:400–411.

[50] Marcos-Almaraz M.T., Gref R., Agostoni V., Kreuz C., Clayette P., Serre C., Couvreurb P., Horcajada P. Towards improved HIV-microbicide activity through the co-encapsulation of NRTI drugs in biocompatible metal organic framework nanocarriers. J. Mater. Chem. B. 2017;5:8563–8569.

[51] Chiodo F., Marradi M., Calvo J., Yuste E., Penades S. Glycosystems in nanotechnology: Gold glyconanoparticles as carrier for anti-HIV prodrugs. Beilstein J. Org. Chem. 2014;10:1339–1346.

[52] Peng J., Wu Z., Qi X., Chen Y., Li X. Dendrimers as potential therapeutic tools in HIV inhibition. Molecules. 2013;18:7912–7929.

[53] Ionov M., Ciepluch K., Klajnert B., Glinska S., Gomez-Ramirez R., de la Mata F.J., Munoz-Fernandez M.A., Bryszewska M. Complexation of HIV derived peptides with carbosilane dendrimers. Colloids Surf. B Biointerfaces. 2013;101:236–242.

[54] Garcia-Broncano P., Cena-Diez R., de la Mata F.J., Gomez R., Resino S., Munoz-Fernandez M.A. Efficacy of carbosilane dendrimers with an antiretroviral combination against HIV-1 in the presence of semen-derived enhancer of viral infection. Eur. J. Pharmacol. 2017;811:155–163.

[55] Cena-Diez R., Vacas-Cordoba E., Garcia-Broncano P., de la Mata F.J., Gomez R., Maly M., Munoz-Fernandez M.A. Prevention of vaginal and rectal herpes simplex virus type 2 transmission in mice: mechanism of antiviral action. Int. J. Nanomed. 2016;11:2147–2162.

[56] das Neves J., Amiji M., Bahia M.F., Sarmento B. Assessing the physical-chemical properties and stability of dapivirine-loaded polymeric nanoparticles. Int. J. Pharm. 2013;456:307–314.

[57] Nucleoside Reverse Transcriptase Inhibitors (NRTIs or nukes) [(accessed on 10 April 2019)]; Available online: https://www.hiv.va.gov/patient/treat/nrtis.asp.

[58] Shegokar R., Singh K.K. Stavudine entrapped lipid nanoparticles for targeting lymphatic HIV reservoirs. Pharmazie. 2011;66:264–271.

[59] Kaur C.D., Nahar M., Jain N.K. Lymphatic targeting of zidovudine using surface-engineered liposomes. J. Drug Target. 2008;16:798–805.

[60] Weibull W. A statistical distribution function of wide applicability. J. Appl. Mech. 1951;18:293–297.

[61] Carvalho F.C., Sarmento V.H., Chiavacci L.A., Barbi M.S., Gremiao M.P. Development and *in vitro* evaluation of surfactant systems for controlled release of zidovudine. J. Appl. Mech. 2010;99:2367–2374.

[62] Mainardes R.M., Gremiao M.P., Brunetti I.L., da Fonseca L.M., Khalil N.M. Zidovudine-loaded PLA and PLA-PEG blend nanoparticles: influence of polymer type on phagocytic uptake by polymorphonuclear cells. J. Pharm. Sci. 2009;98:257–267.

[63] Mainardes R.M., Gremiao M.P. Nanoencapsulation and characterization of zidovudine on poly(l-lactide) and poly(l -lactide)-poly(ethylene glycol)-blend nanoparticles. J. Nanosci. Nanotechnol. 2012;12:8513–8521.

[64] Joshy K.S., Susan M.A., Snigdha S., Nandakumar K., Laly A.P., Sabu T. Encapsulation of zidovudine in PF-68 coated alginate conjugate nanoparticles for anti-HIV drug delivery. Int. J. Biol. Macromol. 2018;107:929–937

[65] Dunge A., Sharda N., Singh B., Singh S. Validated specific HPLC method for determination of zidovudine during stability studies. J. Pharm. Biomed. Anal. 2005;37:1109–1114.

[66] Schenfeld E.M., Ribone S.R., Quevedo M.A. Stability and plasmatic protein binding of novel zidovudine prodrugs: Targeting site ii of human serum albumin. Eur. J. Pharm. Sci. 2018;115:109–118.

[67] Perry C.M., Faulds D. Lamivudine. A review of its antiviral activity, pharmacokinetic properties and therapeutic efficacy in the management of HIV infection. Drugs. 1997;53:657–680.

[68] Vogenthaler N.S. Lamivudine and second-line antiretroviral regimens. Clin. Infect. Dis. 2007;44:1387.

[69] Vinogradov S.V., Poluektova L.Y., Makarov E., Gerson T., Senanayake M.T. Nano-NRTIs: efficient inhibitors of HIV type-1 in macrophages with a reduced mitochondrial toxicity. Antivir. Chem. Chemother. 2010;21:1–14.

[70] Bedse G., Kumar V., Singh S. Study of forced decomposition behavior of lamivudine using LC, LC-MS/TOF and MS(n) J. Pharm. Biomed. Anal. 2009;49:55–63.

[71] Konari N.S., Jacob J.T. Stability indicating validated UPLC technique for the simultaneous analysis of raltegravir and lamivudine in pharmaceutical dosage forms. HIV AIDS Rev. 2016;15:161–169.

[72] Kurmi M., Sahu A., Singh D.K., Singh I.P., Singh S. Stability behaviour of antiretroviral drugs and their combinations. 8: Characterization and in-silico toxicity prediction of degradation products of efavirenz. J. Pharm. Biomed. Anal. 2018;148:170–181.

[73] Tamizhrasi S., Shukla A., Shivkumar T., Rathi V., Rathi J.C. Formulation and evaluation of lamivudine loaded polymethacrylic acid nanoparticles. Int. J. Pharmtech Res. 2009;1:411–415.

[74] Bing W., Guan Qun C., Zheng Wei M., Yu Ying Z., Da Hai Y., Chang You G. Preparation and cellular uptake of PLGA particles loaded with lamivudine. Chin. Sci. Bull. 2012;57:3985–3993.

[75] Rajca A., Li Q., Date A., Belshan M., Destache C. Thermosensitive Vaginal Gel Containing PLGA-NRTI conjugated nanoparticles for HIV prophylaxis. NSTI-Nanotech. 2013;3:293–296.

[76] Ramadan E. Transdermal microneedle–mediated delivery of polymeric lamivudine loaded nanoparticles. J. Pharm. Technol. Drug Res. 2016:5. doi: 10.7243/2050-120X-5-1.

[77] Hatami E., Mu Y., Shields D.N., Chauhan S.C., Kumar S., Cory T.J., Yallapu M.M. Mannose-decorated hybrid nanoparticles for enhanced macrophage targeting. Biochem. Biophys. Rep. 2019;17:197–207.

[78] Dev A., Binulal N.S., Anitha A., Nair S.V., Furuike T., Tamura H., Jayakumar R. Preparation of poly(lactic acid)/chitosan nanoparticles for anti-HIV drug delivery applications. Carbohydr. Polym. 2010;80:833–838.

[79] Nesalin J.A.J., Smith A.A. Stability study of chitosan nanoparticles containing some antiretroviral drugs. Res. J. Pharm. Biol. Chem. Sci. 2014;5:193–203.

[80] Deepak M., Nivrati J., Vaibhav R., Ashish K.J. Glycyrrhizin conjugated chitosan nanoparticles for hepatocyte-targeted delivery of lamivudine. J. Pharm. Pharmacol. 2014;66:1082–1093.

[81] Tshweu L., Katata L., Kalombo L., Swai H. Nanoencapsulation of water-soluble drug, lamivudine, using a double emulsion spray-drying technique for improving HIV treatment. J. Nanopart. Res. 2013;15 doi: 10.1007/s11051-013-2040-4.

[82] Oluwaseun O., Namita K., Kahli A.S., Oleg B., Simeon A., Ayele G., Winston A.A., Sergei N., Emmanuel O.A. Antiretroviral Drugs-Loaded Nanoparticles Fabricated by Dispersion Polymerization with Potential for HIV/AIDS Treatment. Inf. Dis. Res. Treat. 2016;9:21–32.

[83] Pravalika R.P., Madhava R.B., Prakash D.J., Latha K., Prashanthi D. Formulation and characterisation of chitosan based lamivudine nanoparticles. Eur. J. Pharm. Med. Res. 2017;4:377–383.

[84] Kumar P., Lakshmi Y.S., C B., Golla K., Kondapi A.K. Improved Safety, Bioavailability and Pharmacokinetics of Zidovudine through Lactoferrin Nanoparticles during Oral Administration in Rats. PLoS ONE. 2015;10:e0140399.

[85] Kumar P., Lakshmi Y.S., Kondapi A.K. Triple Drug Combination of Zidovudine, Efavirenz and Lamivudine Loaded Lactoferrin Nanoparticles: an Effective Nano First-Line Regimen for HIV Therapy. Pharm. Res. 2017;34:257–268.

[86] Shahabadia N., Khorshidia A., Zhalehc H., Kashaniand S. Synthesis, characterization, cytotoxicity and DNA binding studies of Fe3O4@ SiO2 nanoparticles coated by an antiviral drug lamivudine. J. Drug Deliv. Sci. Technol. 2018;46:55–65.

[87] Vasilyeva S.V., Shtil A.A., Petrova A.S., Balakhnin S.M., Achigecheva P.Y., Stetsenko D.A., Silnikov V.N. Conjugates of phosphorylated zalcitabine and lamivudine with SiO2 nanoparticles: Synthesis by CuAAC click chemistry and preliminary assessment of anti-HIV and antiproliferative activity. Bioorg. Med. Chem. 2017;25:1696–1702.

[88] Kumar J.A., Kumar A.N., Arnab D., Debmalya M., Amalesh S. Development of lamivudine containing multiple emulsions stabilizedby gum odina. Future J. Pharm. Sci. 2018;4:71–79.

[89] Suma U.S., Parthiban S., Senthil K.G.P., Tamiz M.T. Effect of span-80 in the formulation lamivudine niosomal gel. Asian J. Res. Biol. Pharm. Sci. 2015;4:35–45.

[90] Godbole M.D., Mathur V. Selection of phospholipid and method of formulation for optimum entrapment and release of lamivudine from liposome. J. Drug Deliv. Ther. 2018;8:175–183.

[91] Wilson B., Paladugu L., Priyadarshini S.R., Jenita J.J. Development of albumin-based nanoparticles for the delivery of abacavir. Int. J. Biol. Macromol. 2015;81:763–767.

[92] Corbo C., Molinaro R., Parodi A., Toledano Furman N.E., Salvatore F., Tasciotti E. The impact of nanoparticle protein corona on cytotoxicity, immunotoxicity and target drug delivery. Nanomedicine (Lond.) 2016;11:81–100.

[93] Lin Z., Gautam N., Alnouti Y., McMillan J., Bade A.N., Gendelman H.E., Edagwa B. ProTide generated long-acting abacavir nanoformulations. Chem. Commun. 2018;54:8371–8374.

[94] Singh G., Pai R.S. Pharmacokinetics and *in vivo* biodistribution of optimized PLGA nanoparticulate drug delivery system for controlled release of emtricitabine. Drug Deliv. 2014;21:627–635.

[95] Singh G., Pai R.S. Optimization (central composite design) and validation of HPLC method for investigation of emtricitabine loaded poly(lactic-co-glycolic acid) nanoparticles: *in vitro* drug release and *in vivo* pharmacokinetic studies. Sci. World J. 2014;2014:583090.

[96] Mandal S., Belshan M., Holec A., Zhou Y., Destache C.J. An Enhanced Emtricitabine-Loaded Long-Acting Nanoformulation for Prevention or Treatment of HIV Infection. Antimicrob. Agents Chemother. 2017:61.

[97] Rao R.N., Vali R.M., Ramachandra B., Raju S.S. Separation and characterization of forced degradation products of abacavir sulphate by LC-MS/MS. J. Pharm. Biomed. Anal. 2011;54:279–285.

[98] Kurmi M., Sahu A., Singh S. Stability behaviour of antiretroviral drugs and their combinations. 5: Characterization of novel degradation products of abacavir sulfate by mass and nuclear magnetic resonance spectrometry. J. Pharm. Biomed. Anal. 2017;134:372–384.

[99] Wang X.J., Youa J., Yub F. Study on the thermal decomposition of emtricitabine. J. Anal. Appl. Pyrolysis. 2015;115:344–352.

[100] Kurmi M., Singh S. Stability behavior of antiretroviral drugs and their combinations. 7: Comparative degradation pathways of lamivudine and emtricitabine and explanation to their differential degradation behavior by density functional theory. J.Pharm. Biomed. Anal. 2017;142:155–161.

[101] Duan J., Freeling J.P., Koehn J., Shu C., Ho R.J. Evaluation of atazanavir and darunavir interactions with lipids for developing pH-responsive anti-HIV drug combination nanoparticles. J. Pharm. Sci. 2014;103:2520–2529.

[102] Freeling J.P., Koehn J., Shu C., Sun J., Ho R.J. Long-acting three-drug combination anti-HIV nanoparticles enhance drug exposure in primate plasma and cells within lymph nodes and blood. Aids. 2014;28:2625–2627.

[103] Peter A.I., Naidu E.C., Akang E., Ogedengbe O.O., Offor U., Rambharose S., Kalhapure R., Chuturgoon A., Govender T., Azu O.O. Investigating Organ Toxicity Profile of Tenofovir and Tenofovir Nanoparticle on the Liver and Kidney: Experimental Animal Study. Toxicol. Res. 2018;34:221–229.

[104] Pokharkar V.B., Jolly M.R., Kumbhar D.D. Engineering of a hybrid polymer-lipid nanocarrier for the nasal delivery of tenofovir disoproxil fumarate: physicochemical, molecular, microstructural, and stability evaluation. Eur. J. Pharm. Sci. 2015;71:99–111.

[105] Ramanathan R., Jiang Y., Read B., Golan-Paz S., Woodrow K.A. Biophysical characterization of small molecule antiviral-loaded nanolipogels for HIV-1 chemoprophylaxis and topical mucosal application. Acta Biomater. 2016;36:122–131.

[106] Jayant R.D., Atluri V.S., Agudelo M., Sagar V., Kaushik A., Nair M. Sustained-release nanoART formulation for the treatment of neuroAIDS. Int. J. Nanomed. 2015;10:1077–1093

[107] Vacas-Cordoba E., Galan M., de la Mata F.J., Gomez R., Pion M., Munoz-Fernandez M.A. Enhanced activity of carbosilane dendrimers against HIV when combined with reverse transcriptase inhibitor drugs: searching for more potent microbicides. Int. J. Nanomed. 2014;9:3591–3600. [PMC free article] [PubMed] [Google Scholar]

[108] Briz V., Sepulveda-Crespo D., Diniz A.R., Borrego P., Rodes B., de la Mata F.J., Gomez R., Taveira N., Munoz-Fernandez M.A. Development of water-soluble polyanionic carbosilane dendrimers as novel and highly potent topical anti-HIV-2 microbicides. Nanoscale. 2015;7:14669–14683.

[109] Sepulveda-Crespo D., Sanchez-Rodriguez J., Serramia M.J., Gomez R., De La Mata F.J., Jimenez J.L., Munoz-Fernandez M.A. Triple combination of carbosilane dendrimers, tenofovir and maraviroc as potential microbicide to prevent HIV-1 sexual transmission. Nanomedicine (Lond) 2015;10:899–914.

[110] Sepulveda-Crespo D., Gomez R., De La Mata F.J., Jimenez J.L., Munoz-Fernandez M.A. Polyanionic carbosilane dendrimer-conjugated antiviral drugs as efficient microbicides: Recent trends and developments in HIV treatment/therapy. Nanomed.- Nanotechnol. Biol. Med. 2015;11:1481–1498.

[111] Agrahari V., Zhang C., Zhang T., Li W., Gounev T.K., Oyler N.A., Youan B.B. Hyaluronidase-sensitive nanoparticle templates for triggered release of HIV/AIDS microbicide *in vitro*. AAPS J. 2014;16:181–193.

[112] Ngo A.N., Ezoulin M.J., Murowchick J.B., Gounev A.D., Youan B.B. Sodium Acetate Coated Tenofovir-Loaded Chitosan Nanoparticles for Improved Physico-Chemical Properties. Pharm. Res. 2016;33:367–383.

[113] Timur S.S., Sahin A., Aytekin E., Ozturk N., Polat K.H., Tezel N., Gursoy R.N., Calis S. Design and *in vitro* evaluation of tenofovir-loaded vaginal gels for the prevention of HIV infections. Pharm. Dev. Technol. 2018;23:301–310.

[114] Shailender J., Ravi P.R., Reddy Sirukuri M., Dalvi A., Keerthi Priya O. Chitosan nanoparticles for the oral delivery of tenofovir disoproxil fumarate: formulation optimization, characterization and ex vivo and *in vivo* evaluation for uptake mechanism in rats. Drug Dev. Ind. Pharm. 2018;44:1109–1119.

[115] Shohani S., Mondanizadeh M., Abdoli A., Khansarinejad B., Salimi-Asl M., Ardestani M.S., Ghanbari M., Haj M.S., Zabihollahi R. Trimethyl Chitosan Improves Anti-HIV Effects of Atripla as a New Nanoformulated Drug. Curr. HIV Res. 2017;15:56–65.

[116] Wu D., Ensinas A., Verrier B., Primard C., Cuvillier A., Champier G., Paul S., Delair T. Zinc-Stabilized Chitosan-Chondroitin Sulfate Nanocomplexes for HIV-1 Infection Inhibition Application. Mol. Pharm. 2016;13:3279–3291.

[117] Meng J., Agrahari V., Ezoulin M.J., Zhang C., Purohit S.S., Molteni A., Dim D., Oyler N.A., Youan B.C. Tenofovir Containing Thiolated Chitosan Core/Shell Nanofibers: *In Vitro* and *in Vivo* Evaluations. Mol. Pharm. 2016;13:4129–4140.

[118] Destache C.J., Mandal S., Yuan Z., Kang G., Date A.A., Lu W., Shibata A., Pham R., Bruck P., Rezich M., et al. Topical Tenofovir Disoproxil Fumarate Nanoparticles Prevent HIV-1 Vaginal Transmission in a Humanized Mouse Model. Antimicrob. Agents Chemother. 2016;60:3633–3639.

[119] Machado A., Cunha-Reis C., Araujo F., Nunes R., Seabra V., Ferreira D., das Neves J., Sarmento B. Development and *in vivo* safety assessment of tenofovir-loaded nanoparticles-in-film as a novel vaginal microbicide delivery system. Acta Biomater. 2016;44:332–340.

[120] Cunha-Reis C., Machado A., Barreiros L., Araujo F., Nunes R., Seabra V., Ferreira D., Segundo M.A., Sarmento B., das Neves J. Nanoparticles-in-film for the combined vaginal delivery of anti-HIV microbicide drugs. J. Control. Release. 2016;243:43–53.

[121] Mandal S., Kang G., Prathipati P.K., Fan W., Li Q., Destache C.J. Long-acting parenteral combination antiretroviral loaded nano-drug delivery system to treat chronic HIV-1 infection: A humanized mouse model study. Antiviral Res. 2018;156:85–91.

[122] Mandal S., Kang G., Prathipati P.K., Zhou Y., Fan W., Li Q., Destache C.J. Nanoencapsulation introduces long-acting phenomenon to tenofovir alafenamide and emtricitabine drug combination: A comparative pre-exposure prophylaxis efficacy study against HIV-1 vaginal transmission. J. Control. Release. 2019;294:216–225.

[123] Mandal S., Prathipati P.K., Kang G., Zhou Y., Yuan Z., Fan W., Li Q., Destache C.J. Tenofovir alafenamide and elvitegravir loaded nanoparticles for long-acting prevention of HIV-1 vaginal transmission. Aids. 2017;31:469–476.

[124] Prathipati P.K., Mandal S., Pon G., Vivekanandan R., Destache C.J. Pharmacokinetic and Tissue Distribution Profile of Long Acting Tenofovir Alafenamide and Elvitegravir Loaded Nanoparticles in Humanized Mice Model. Pharm. Res. 2017;34:2749–2755.

[125] Shailender J., Ravi P.R., Saha P., Dalvi A., Myneni S. Tenofovir disoproxil fumarate loaded PLGA nanoparticles for enhanced oral absorption: Effect of experimental variables and *in vitro*, ex vivo and *in vivo* evaluation. Colloids Surf. B Biointerfaces. 2017;158:610–619.

[126] Cautela M.P., Moshe H., Sosnik A., Sarmento B., das Neves J. Composite films for vaginal delivery of tenofovir disoproxil fumarate and emtricitabine. Eur. J. Pharm. Biopharm. 2018;138:3–10.

[127] Tomitaka A., Arami H., Huang Z., Raymond A., Rodriguez E., Cai Y., Febo M., Takemura Y., Nair M. Hybrid magneto-plasmonic liposomes for multimodal image-guided and brain-targeted HIV treatment. Nanoscale. 2017;10:184–194.

[128] Kraft J.C., McConnachie L.A., Koehn J., Kinman L., Sun J., Collier A.C., Collins C., Shen D.D., Ho R.J.Y. Mechanism-based pharmacokinetic (MBPK) models describe the complex plasma kinetics of three antiretrovirals delivered by a long-acting anti-HIV drug combination nanoparticle formulation. J. Control. Release. 2018;275:229–241.

[129] McConnachie L.A., Kinman L.M., Koehn J., Kraft J.C., Lane S., Lee W., Collier A.C., Ho R.J.Y. Long-Acting Profile of 4 Drugs in 1 Anti-HIV Nanosuspension in Nonhuman Primates for 5 Weeks After a Single Subcutaneous Injection. J. Pharm. Sci. 2018;107:1787–1790.

[130] Koehn J., Iwamoto J.F., Kraft J.C., McConnachie L.A., Collier A.C., Ho R.J.Y. Extended cell and plasma drug levels after one dose of a three-in-one nanosuspension containing lopinavir, efavirenz, and tenofovir in nonhuman primates. Aids. 2018;32:2463–2467.

[131] Perazzolo S., Shireman L.M., Koehn J., McConnachie L.A., Kraft J.C., Shen D.D., Ho R.J.Y. Three HIV Drugs, Atazanavir, Ritonavir, and Tenofovir, Coformulated in Drug-Combination Nanoparticles Exhibit Long-Acting and Lymphocyte-Targeting Properties in Nonhuman Primates. J. Pharm. Sci. 2018;107:3153–3162

[132] Golla V.M., Kurmi M., Shaik K., Singh S. Stability behaviour of antiretroviral drugs and their combinations. 4: Characterization of degradation products of tenofovir alafenamide fumarate and comparison of its degradation and stability behaviour with tenofovir disoproxil fumarate. J. Pharm. Biomed. Anal. 2016;131:146–155.

[133] Kuo Y.C., Lin P.I., Wang C.C. Targeting nevirapine delivery across human brain microvascular endothelial cells using transferrin-grafted poly(lactide-co-glycolide) nanoparticles. Nanomedicine (Lond) 2011;6:1011–1026.

[134] Shegokar R., Singh K.K. Nevirapine nanosuspensions for HIV reservoir targeting. Die Pharmazie. 2011;66:408–415.

[135]S hegokar R., Singh K.K. Surface modified nevirapine nanosuspensions for viral reservoir targeting: *In vitro* and *in vivo* evaluation. Int. J. Pharm. 2011;421:341–352.

[136] Reis N.F., de Assis J.C., Fialho S.L., Pianetti G.A., Fernandes C. Stability-indicating UHPLC method for determination of nevirapine in its bulk form and tablets: identification of impurities and degradation kinetic study. J. Pharm. Biomed. Anal. 2016;126:103–108.

[137] Aungst B.J., Nguyen N.H., Taylor N.J., Bindra D.S. Formulation and food effects on the oral absorption of a poorly water soluble, highly permeable antiretroviral agent. J. Pharm. Sci. 2002;91:1390–1395.

[138] Csajka C., Marzolini C., Fattinger K., Decosterd L.A., Fellay J., Telenti A., Biollaz J., Buclin T. Population pharmacokinetics and effects of efavirenz in patients with human immunodeficiency virus infection. Clin. Pharmacol. Ther. 2003;73:20–30.

[139] Vyas A., Jain A., Hurkat P., Jain A., Jain S.K. Targeting of AIDS related encephalopathy using phenylalanine anchored lipidic nanocarrier. Colloids Surf. B Biointerfaces. 2015;131:155–161.

[140] Makwana V., Jain R., Patel K., Nivsarkar M., Joshi A. Solid lipid nanoparticles (SLN) of Efavirenz as lymph targeting drug delivery system: Elucidation of mechanism of uptake using chylomicron flow blocking approach. Int. J. Pharm. 2015;495:439–446.

[141] Gaur P.K., Mishra S., Bajpai M., Mishra A. Enhanced Oral Bioavailability of Efavirenz by Solid Lipid Nanoparticles: *In Vitro* Drug Release and Pharmacokinetics Studies. BioMed Res. Int. 2014;2014:363404.

[142] Vedha Hari B.N., Dhevendaran K., Narayanan N. Development of Efavirenz nanoparticle for enhanced efficiency of anti-retroviral therapy against HIV and AIDS; Proceedings of the First International Science Symposium on HIV and Infectious Diseases (HIV SCIENCE 2012); Chennai, India. 20–22 January 2012; Heidelberg, Germany: Springer-Verlag GmbH; 2012

[143] Chaowanachan T., Krogstad E., Ball C., Woodrow K.A. Drug synergy of tenofovir and nanoparticle-based antiretrovirals for HIV prophylaxis. PLoS ONE. 2013;8:e61416.

[144] Date A.A., Shibata A., McMullen E., La Bruzzo K., Bruck P., Belshan M., Zhou Y., Destache C.J. Thermosensitive Gel Containing Cellulose Acetate Phthalate-Efavirenz Combination Nanoparticles for Prevention of HIV-1 Infection. J. Biomed. Nanotechnol. 2015;11:416–427.

[145] Roy U., Ding H., Pilakka-Kanthikeel S., Raymond A.D., Atluri V., Yndart A., Kaftanovskaya E.M., Batrakova E., Agudelo M., Nair M. Preparation and characterization of anti-HIV nanodrug targeted to microfold cell of gut-associated lymphoid tissue. Int. J. Nanomed. 2015;10:5819–5835.

[146] Haria V.B.N., Lu C.L., Narayananc N., Wang R.R., Zheng Y.T. Engineered polymeric nanoparticles of Efavirenz: Dissolution enhancement through particle size reduction. Chem. Eng. Sci. 2016;155:366–375.

[147] Hari B.N.V., Narayanan N., Dhevendaran K., Ramyadevi D. Engineered nanoparticles of Efavirenz using methacrylate co-polymer (Eudragit-E100) and its biological effects in-vivo. Mater. Sci. Eng. C. Mater. Biol. Appl. 2016;67:522–532.
[148] Belgamwar A., Khan S., Yeole P. Intranasal chitosan-g-HPbetaCD nanoparticles of efavirenz for the CNS targeting. Artif. Cells Nanomed. Biotechnol. 2018;46:374–386.

[149] Nunes R., Araujo F., Barreiros L., Bartolo I., Segundo M.A., Taveira N., Sarmento B., das Neves J. Noncovalent PEG Coating of Nanoparticle Drug Carriers Improves the Local Pharmacokinetics of Rectal Anti-HIV Microbicides. ACS Appl. Mater. Interfaces. 2018;10:34942–34953.

[150] Martins C., Araújo F., Gomes M.J., Fernandes C., Nunes R., Li W., Santos H.A., Borges F., Sarmento B. Using microfluidic platforms to develop CNS-targeted polymeric nanoparticles for HIV therapy. Eur. J. Pharm. Biopharm. 2018;138:111–124.

[151] Kumar P., Lakshmi Y.S., Kondapi A.K. An oral formulation of efavirenz-loaded lactoferrin nanoparticles with improved biodistribution and pharmacokinetic profile. HIV Med. 2017;18:452–462.

[152] Lakshmi Y.S., Kumar P., Kishore G., Bhaskar C., Kondapi A.K. Triple combination MPT vaginal microbicide using curcumin and efavirenz loaded lactoferrin nanoparticles. Sci. Rep. 2016;6:25479.

[153] Dutta T., Agashe H.B., Garg M., Balakrishnan P., Kabra M., Jain N.K. Poly (propyleneimine) dendrimer based nanocontainers for targeting of efavirenz to human monocytes/macrophages *in vitro*. J. Drug Target. 2007;15:89–98.

[154] Dutta T., Garg M., Jain N.K. Targeting of efavirenz loaded tuftsin conjugated poly(propyleneimine) dendrimers to HIV infected macrophages *in vitro*. Eur. J. Pharm. Sci. 2008;34:181–189.

[155] Hong X., Long L., Guohong F., Xiangfeng C. DFT study of nanotubes as the drug delivery vehicles of Efavirenz. Comput. Theor. Chem. 2018;1131:57–68.

[156] Suvarna V., Thorat S., Nayak U., Sherje A., Murahari M. Host-guest interaction study of Efavirenz with hydroxypropyl-β-cyclodextrin and L-arginine by computational simulation studies: Preparation and characterization of supramolecular complexes. J. Mol. Liq. 2018;259:55–64.

[157]Moura Ramos J.J., Piedade M.F.M., Diogo H.P., Viciosa M.T. Thermal Behavior and Slow Relaxation Dynamics in Amorphous Efavirenz: A Study by DSC, XRPD, TSDC, and DRS. J. Pharm. Sci. 2019;108:1254–1263.

[158] das Neves J., Sarmento B., Amiji M.M., Bahia M.F. Development and validation of a rapid reversed-phase HPLC method for the determination of the non-nucleoside reverse transcriptase inhibitor dapivirine from polymeric nanoparticles. J. Pharm. Biomed. Anal. 2010;52:167–172.

[159] Akil A., Devlin B., Cost M., Rohan L.C. Increased Dapivirine tissue accumulation through vaginal film codelivery of dapivirine and Tenofovir. Mol. Pharm. 2014;11:1533–1541.

[160] das Neves J., Araújo F., Andrade F., Michiels J., Ariën K.K., Vanham G., Amiji M., Bahia M.F., Sarmento B. *In Vitro* and Ex Vivo Evaluation of Polymeric Nanoparticles for Vaginal and Rectal Delivery of the Anti-HIV Drug Dapivirine. Mol. Pharm. 2013;10:2793–2807.

[161] Jiang Y., Cao S., Bright D.K., Bever A.M., Blakney A.K., Suydam I.T., Woodrow K.A. Nanoparticle-Based ARV Drug Combinations for Synergistic Inhibition of Cell-Free and Cell-Cell HIV Transmission. Mol. Pharm. 2015;12:4363–4374.

[162] Krogstad E.A., Ramanathan R., Nhan C., Kraft J.C., Blakney A.K., Cao S., Ho R.J.Y., Woodrow K.A. Nanoparticle-releasing nanofiber composites for enhanced *in vivo* vaginal retention. Biomaterials. 2017;144:1–16.

[163] Goebel F., Yakovlev A., Pozniak A., Vinogradova E., Boogaerts G., Hoetelmans R., de Béthune M.P., Peeters M., Woodfall B. Short-term antiviral activity of TMC278 – a novel NNRTI – in treatment-naive HIV-1-infected subjects. Aids. 2006;20:1721–1726.

[164] Jackson A., McGowan I. Long-acting rilpivirine for HIV prevention. Curr. Opin. HIV AIDS. 2015;10:253–257.

[165] Viciana P. Rilpivirine: The Key for Long-term Success. AIDS Rev. 2017;19:156–166.

[166] Spreen W.R., Margolis D.A., Pottage J.C. Long-acting injectable antiretrovirals for HIV treatment and prevention. Curr. Opin. HIV AIDS. 2013;8:565–571.

[167] Margolis D.A., Boffito M. Long-acting antiviral agents for HIV treatment. Curr. Opin. HIV AIDS. 2015;10:246–252.

[168] Ferretti F., Boffito M. Rilpivirine long-acting for the prevention and treatment of HIV infection. Curr. Opin. HIV AIDS. 2018;13:300–307.

[169] Kovarova M., Council O.D., Date A.A., Long J.M., Nochi T., Belshan M., Shibata A., Vincent H., Baker C.E., Thayer W.O., et al. Nanoformulations of Rilpivirine for Topical Pericoital and Systemic Coitus-Independent Administration Efficiently Prevent HIV Transmission. PLoS Pathog. 2015;11:e1005075.

[170] Ottemann B.M., Helmink A.J., Zhang W., Mukadam I., Woldstad C., Hilaire J.R., Liu Y., McMillan J.M., Edagwa B.J., Mosley R.L., et al. Bioimaging predictors of rilpivirine biodistribution and antiretroviral activities. Biomaterials. 2018;185:174–193.

IV. COMPUTATIONAL APPROACHES FOR THE DISCOVERY OF GPER TARGETING COMPOUNDS

Fedora Grande[1]; Maria Antonietta Occhiuzzi[1]; Rosamaria Lappano [1]; Francesca Cirillo [1,2]; Rita Guzzi [2,3]; Antonio Garofalo [1]; Yves Jacquot [4]; Marcello Maggiolini [1]; Bruno Rizzuti [3].

[1] Department of Pharmacy, Health and Nutritional Sciences, University of Calabria, Rende, Italy.
[2] Department of Physics, University of Calabria, Rende, Italy,
[3] CNR-NANOTEC, Licryl-UOS Cosenza and CEMIF.Cal, Department of Physics, University of Calabria, Rende, Italy.
[4] Cibles Thérapeutiques et Conception de Médicaments (CiTCoM), CNRS UMR 8038, INSERM U1268, Faculté de Pharmacie de Paris, Université de Paris, Paris, France.

Estrogens exert a panel of biological activities mainly through the estrogen receptors α and β, which belong to the nuclear receptor superfamily. Diverse studies have shown that the G protein-coupled estrogen receptor 1 (GPER, previously known as GPR30) also mediates the multifaceted effects of estrogens in numerous pathophysiological events, including neurodegenerative, immune, metabolic, and cardiovascular disorders and the progression of different types of cancer. In particular, GPER is implicated in hormone-sensitive tumors, albeit diverse issues remain to be deeply investigated. As such, this receptor may represent an appealing target for therapeutics in different diseases. The yet unavailable complete GPER crystallographic structure, and its relatively low sequence similarity with the other members of the G protein-coupled receptor (GPCR) family, hamper the possibility to discover compounds able to modulate GPER activity. Consequently, a reliable molecular model of this receptor is required for the design of suitable ligands. To date, convergent approaches involving structure-based drug design and virtual ligand screening have led to the identification of several GPER selective ligands, thus providing important information regarding its mode of action and function. In this survey, we summarize results obtained through computer-aided techniques devoted to the assessment of GPER ligands toward their usefulness in innovative treatments of different diseases.

1. Introduction

The multifaceted responses to estrogens are principally mediated by the estrogen receptors (ERs) α and β, which act as transcription factors by binding to estrogen response elements (EREs) located in the promoter regions of target genes [1]. Recently, a seven-transmembrane G protein-coupled receptor, known as G protein estrogen receptor (GPER), has attracted the attention of several researcher groups working on the identification of the intricate estrogen routes in different biological systems. A panel of experiences has highlighted the involvement of GPER in various pathophysiological processes. For instance, its role in hormone-dependent cancers has been addressed in several studies, providing a better understanding of the related gene landscape and transduction pathways. In particular, GPER modulates signaling processes leading to the transcription of genes promoting tumor growth *in vitro* and *in vivo*, such as calcium mobilization, cAMP synthesis, the cleavage of matrix metalloproteinases, the transactivation of epidermal growth factor receptor (EGFR) and the activation of PI3K and MAPK transduction pathways [2–11]. To date, GPER expression has been correlated with negative cancer features including increased tumor size, distant

metastasis and tumor recurrence [12–14]. In addition, a bioinformatic analysis of large cohorts of patients has recently demonstrated that GPER expression is correlated with the expression of pro-metastatic genes in ER-negative breast tumors [15]. On the basis of the aforementioned findings, this receptor might be considered as a promising therapeutic target for the treatment of diverse types of tumors, including breast cancer. Nevertheless, other studies reached different conclusions [16], therefore indicating that further investigations are required to better appreciate the role exerted by GPER in cancer.

Most estrogens and anti-estrogens are able to bind to GPER and ERs, albeit with a different affinity and even with an opposite action (i.e., agonism vs. antagonism) [10, 17, 18]. Considering the interest to identify specific GPER ligands to decipher its unique potential, several successful efforts have been made during the last few years [19–25]. In this context, it should be mentioned the intriguing discovery of the indole derivative MIBE, which has the property of binding to and antagonizing the effects of both GPER and ER, thus representing a useful tool toward more comprehensive approaches in estrogen-dependent tumors [22].

The overall structural heterogeneity among agents targeting these receptors constitutes an obstacle to identify agonists or antagonists and to predict their effects. Thus, the design of potent selective GPER ligands and dual ER/GPER inhibitors is still challenging. While the crystallographic structure of the ER ligand-binding domain is available, the detailed structure of GPER remains yet unsolved due to the well-known difficulties in fully characterizing membrane proteins. Nevertheless, a homology model of GPER can be obtained with the help of computational techniques (Figure 1), allowing access to relevant structural information. More importantly, virtual ligand screening approaches and structure-based drug design methods can support experiments aiming to identify new GPER ligands. The results obtained by application of computational techniques are herein summarized toward their adoption as starting point for the design and development of novel active agents.
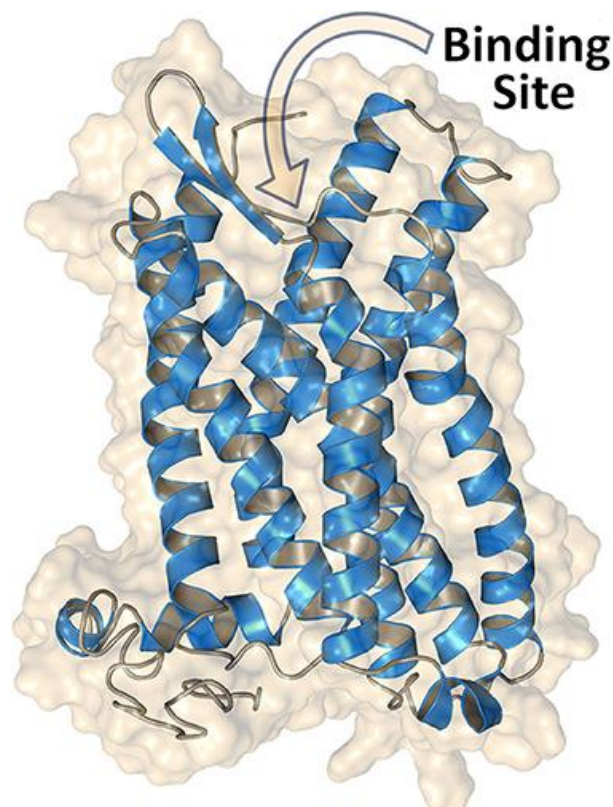
Figure 1. *Structure of GPER obtained through homology modeling by using the web server GPCR-I-TASSER [26]. The extracellular N-terminal region (residues 1–50) is omitted, and access to the binding site for the ligands is indicated.*

2. The early age of ligand-based design for targeting GPER

With respect to the computational design of GPER ligands, one of the earliest achievements is indisputably the synthesis of the quinoline G-1 [19]. To this aim, a library of 10,000 candidate molecules has been analyzed by combining their structural features in common with the archetypal ligand 17β-estradiol (E2). Three distinct categories of criteria were defined: (i) 2D structural patterns, including both symmetric and asymmetric features, (ii) 3D shape analogies and metrics and (iii) pharmacophore-based motifs, including hydrogen-bond donors/acceptors and the possibility of forming hydrophobic interactions. The resulting computational analysis was completed with an *in vitro* biomolecular screening to validate the occurrence of a competitive ligand binding. The molecule G-1 (for the chemical structure of this compound and all the other mentioned throughout the text, see Figure 2) has emerged from this screening funnel as the first GPER-specific agonist able to activate the receptor in cells expressing both GPER and ERs. A similar virtual screening methodology, applied on a larger library with more than 140,000 compounds, led successively to the identification of a high-affinity GPER ligand named G-15, a G-1 analog acting as a selective antagonist [20]. The success of these original ligand-based virtual screenings was facilitated by the limited number of internal degrees of freedom of the studied compounds. These observations referred also to the conformational space of the ligand-binding pocket of the different steroid hormone receptors [27]. In the absence of a model for the GPER tertiary structure, the previous works were, therefore, expanded to an "indirect" structure-based approach consisting in the analysis into deeper details of the ERα and ERβ binding sites. In fact, the main concern was to focus on the acetyl moiety of the ER agonist G-1, which is lacking in

the antagonist G-15 [21]. Molecular docking was then performed to explore the possibility to increase steric clashes within the binding pocket of the ERs through an isopropyl moiety instead of the acetyl group. The resulting compound, named G-36, showed an enhanced selectivity with an antagonist effect toward GPER, and a low-affinity cross-reactivity toward ERα.
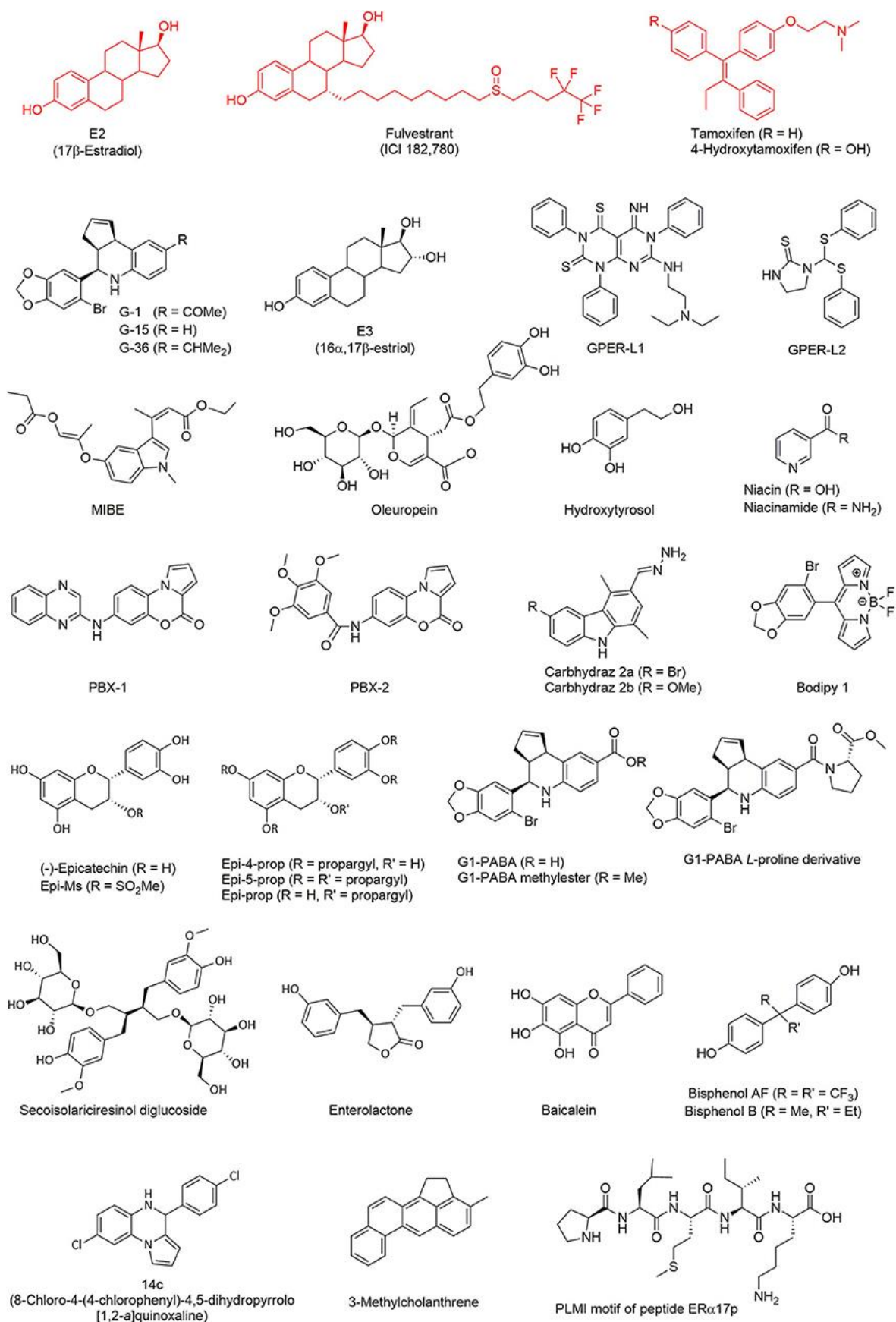
Figure 2. *GPER ligands investigated by computational methods. Typical ligands (represented in red), including E2, fulvestrant, and tamoxifen, have been extensively tested in simulation as*

3. Homology modeling for predicting the structure of GPER

The possibility of investigating in simple and accurate ways the binding location and the affinity of molecules to GPER is intimately linked with the availability of a correct molecular description of the protein structure. The first crude GPER model was built to predict ligand binding, through computational approaches [28]. A more accurate structure of GPER was later used as a support to elucidate a number of "wet-lab" experiments [18, 22, 29]. In all cases, a special emphasis was put on providing details about the topology of the putative binding-site of the protein, rather than the whole protein tertiary structure. The 3D structure of GPER was constructed through homology modeling [30, 31], by using the crystal structure of bovine rhodopsin [32] as a template.

Subsequent efforts were devoted on the improvement of the molecular description of the protein structure, with a broader emphasis on the description of the overall protein architecture. Consistent results were achieved by using as a template the X-ray structure of the β2-adrenergic receptor, which was found to possess a higher degree of homology with GPER, when compared to bovine rhodopsin. The crystal structures of both the active and inactive states of the β2-adrenergic receptor were available [33, 34], allowing to model different conformations of GPER in complex with agonists or antagonists [35].

Alternatively, GPER has been modeled [36] by using as a template the crystallographic structure of the chemokine receptor CXCR4 [37]. It was also possible to identify some structural differences between agonists and antagonists, depending on their ability to form hydrogen bonds with key residues located in specific transmembrane helices. The quality level of this new GPER model was further improved through molecular dynamics (MD) simulations [36, 38, 39], which were helpful to take into account the internal dynamics of the protein, concomitantly to the contribution of the surrounding lipid matrix.

A more comprehensive view of the 3D structure of GPER has been recently obtained by using the web server GPCR-I-TASSER [26, 40], which is a computational suite derived from the parent I-TASSER package [41], one of the most popular on-line resources for protein structure prediction and refinement. A major strength of the algorithm used in GPCR-I-TASSER is that it was specifically devised for the prediction of GPCRs and, as such, it works with a dedicated knowledge-based force field as a guide for an accurate assembly of the receptor structure. A number of works [25, 38, 42, 43] have adopted this computational tool to design high-quality GPER models (see again Figure 1). High-quality and tailored software, together with the growing number of experimentally-determined GPCR structures that can be used as GPER templates, are contributing to make homology modeling algorithms more accurate in predicting the receptor structure.

4. The beginning of structure-based design of ligands for GPER

In the last decade, one of the major aims of our research group has been the identification of novel GPER ligands supported by computational drug discovery approaches. A first result (18) was the identification of 16α,17β-estriol (E3) as a GPER antagonist (see Figure 2). This compound, which corresponds to a final metabolite of E2 [44], is one of the three natural estrogens produced by the human body (i.e., estradiol, estrone, and estriol). It is of note that E3 can also be biosynthesized from estrone sulfate as well as from testosterone and androstenedione [44].

A computational analysis also allowed the discovery of two new molecules [22], named GPER-L1 and GPER-L2, both acting on GPER as selective agonists but unable to bind and activate ERs. These two ligands were selected through a typical process of virtual screening starting from a chemical library including more than 300 molecules. Despite strong differences in their chemical structure, they share some crucial features such as the ability of exposing a phenyl ring into a hydrophobic protein pocket and, thereby, of forming stabilizing π-π stacking interactions. Due to their selectivity, these molecules contribute to increase our understanding of the function of various cancer phenotypes, through different estrogen-targeted receptors.

In sharp contrast, MIBE was identified as a unique case of dual antagonist for both GPER and ERα [29], by using molecular docking. The possibility of targeting simultaneously GPER and ERα is particularly interesting from a pharmacological point of view, because active compounds antagonizing both proteins could be useful in tackling breast carcinomas at the initial stage or during their progression. In a subsequent work [45], it was demonstrated that oleuropein and hydroxytyrosol, two natural phenols, were able to bind GPER. Flexible molecular docking calculations were performed with these two molecules, considering free rotation of seven bulky side chains in the binding site of the receptor, which was especially required to accommodate the relatively large molecular structure of oleuropein. The following experiments demonstrated that both ligands act as GPER inverse agonists in ER-negative and GPER-positive SkBr3 breast cancer cells, as recently found with the peptide ERα17p [25].

A virtual screening campaign on a library of chemical fragments demonstrated the binding of niacin (also known as nicotinic acid, vitamin B3, or vitamin PP) and of its amide form niacinamide (or nicotinamide) to GPER and niacin receptor GPR109A/HCA2 [46]. The latter is a subtype of the receptor GPR109 that mainly, although not exclusively, mediates the action of niacin (but not of niacinamide). Sequence alignment revealed a lack of homology between GPER and GPR109A, at least in their ligand-binding sites, thus the anchoring of these two molecules to both GPER and GPR109A was not obvious. Nevertheless, molecular docking suggested some similarities in the binding mode of the pyridine ring of both compounds. The presence of two important arginine residues able to form hydrogen bonds with the carboxylic acid moiety of niacin, allowing GPR109A specificity, were also highlighted. Both niacin and niacinamide were demonstrated to exert an agonist activity toward GPER in the successive experiments.

Computational techniques further helped to design two novel benzopyrroloxazines [24] acting as selective GPER antagonists. The starting point was the virtual screening of a compound library and the identification of a rigid molecular structure closely resembling the chemical skeleton of other known GPER ligands. This structure was used as a template and two derivatives, named PBX1 and PBX2, were demonstrated to bind to GPER. To this aim, flexible molecular docking was performed by allowing the rotation of the dihedral angles in the side chain of eight residues within the protein-binding site.

In a separate study [23], two novel carbazole derivatives were synthesized. While both of them did not activate the classical ERα, one of them, abbreviated as carbhydraz 2a, showed a favorable affinity for GPER, as shown by docking assays with seven flexible residues. This compound was then shown to display an agonistic response on GPER.

As a final example, a rational design has been completed with the first GPER selective fluorescent organoboron probe [47], which consists in a boron-dipyrromethene difluoride derivative. In this case, the starting molecular template was a bromobenzodioxolyl substituent, which is also present in the structure of G-1 and constitutes a key motif for GPER binding. Using molecular docking, the obtained compound, named Bodipy 1, was predicted to share a binding mode similar to G-1, by interacting with the key protein residue Phe-208

and by forming π-π stacking with its bromobenzodioxole moiety. Bodipy 1 was later demonstrated to compete with niacin in ER-negative and GPER-positive SkBr3 breast cancer cells.

5. The current area of computational methods for studying GPER

The study of GPER through theoretical modeling approaches has lately benefited from a number of improvements, including the use of targeted simulations to capture important aspects of the protein dynamics. Molecular docking on GPER structures extracted from all-atom MD has demonstrated [48] that the natural polyphenol (–)-epicatechin (see Figure 2) has the ability to anchor to this receptor with a binding mode similar to the agonist G-1. It is interesting to note that flavonoids sharing structural similarities to estrogens, such as genistein and other phytoestrogens [49–51], not only bind but also activate the classical receptors ERα and ERβ. In contrast, and in spite of its evident structural analogies to these phytochemicals, (–)-epicatechin fails to bind ERα and ERβ. Since (–)-epicatechin can associate within the GPER binding pocket, an important role of this receptor on cardiovascular system protection seems likely. In a subsequent study [52], (–)-epicatechin derivatives were obtained where the phenol and alcohol groups are functionalized with a propargyl or a mesyl group. The resulting compounds, i.e., Epi-4-prop, Epi-5-prop, Epi-prop and Epi-Ms, were investigated by docking methods on the GPER structures obtained through MD. Strikingly, it was observed that the alkyne function of the propargyl was prone to generate additional interactions in the receptor-binding site and to enhance the GPER agonistic activity, when compared to the parent compound. Later, MD simulations showed that Epi-4-prop and Epi-5-prop share with (–)-epicatechin similar interactions at the GPER binding site [53].

A number of additional GPER binders have also been identified using theoretical modeling calculations. It is the case of G1-PABA [54], a compound part of a small series of G1 analogs, in which the acetyl moiety is replaced with a carboxyl group. The same pharmacophore core was further used to obtain a G1-PABA methylester and L-proline derivative, with similar structural and energetic binding properties [55]. All these newly synthesized compounds were validated *in vitro* in experimental assays using breast cancer cell lines. Another example is secoisolariciresinol diglucoside, a phytoestrogen extracted from flaxseed and able to suppress benign prostatic hyperplasia [56], which was indirectly investigated through molecular docking of its mammalian metabolite enterolactone [57]. Similarly, the binding mode to both GPER and ERα of baicalein, a flavonoid derived from the roots of a medicinal herb, has been extensively studied [58]. Molecular docking analysis was especially focused on the hydrogen-bond network favoring the ligand binding. The observation that GPER appeared to mediate the estrogenic effects of some bisphenol A analogs was the starting point of another computational study [59], which predicted a favorable binding of bisphenol AF and bisphenol B. Experimental assays have confirmed the agonistic activity of these compounds, supporting the hypothesis of their disrupting action on the GPER-mediated pathway. These observations clearly highlight the lack of selectivity of phytoestrogens [60].

Similarly, to G-15, theoretical methods have also been used to identify new compounds [61] with a selective anti-proliferative activity against GPER-expressing breast cancer cells. A virtual screening campaign was carried out on a chemical library of about 1,000 compounds, in search of molecules showing a binding mode close to G-15 and G-36. They were selected on the basis of their binding score and by visual inspection, as well as their ability to form polar contacts with previously identified GPER residues. Four different chemical scaffolds

were found. A particularly promising compound, named 14c and based on one of these scaffolds, has been proposed as a starting point for a future hit-to-lead optimization process. By using combined docking and MD simulations approach, the association of the chemical carcinogen 3-methylcholanthrene with GPER has been recently studied [43]. This environmental pollutant, which is generated by incomplete combustion processes including cigarette smoke, was known to bind to both ERα and the aryl hydrocarbon receptor (AhR), stimulating thereby a functional interaction between these two receptors. The results pointed out to a functional crosstalk and a cross-stimulation between GPER and AhR. Computational methods have also been used to investigate the binding to GPER of the peptide ERα17p, which encompasses a part of the hinge region/AF2 domain of the human ERα [25, 62]. This peptide acts as a GPER inverse agonist and shows anti-proliferative effects in breast cancer cells and a decrease in the volume of breast tumors in xenografted mice [63]. The N-terminal PLMI motif of this peptide presents some chemical analogies with the GPER antagonist PBX1 and exerts the same anti-proliferative potency as the whole length peptide [25, 62], suggesting strongly that this region corresponds to the active motif. Due to the large number of rotatable bonds in ERα17p, MD simulations were necessary to map the conformational landscape of the receptor-peptide molecular system. The fact that a specific amino acid drives the anchoring of ERα17p opens the way to the possibility of modulating GPER by using peptide-based compounds. It is particularly notable that ERα17p is, to the best of our knowledge, the first peptidic GPER modulator.

6. Conclusions

GPER is increasingly recognized as a mediator of different estrogen-dependent pathophysiological responses, such as those that characterize cancer progression. The persistent difficulty in obtaining an experimental structure of the native structure of this membrane receptor, let alone in complex with any endogenous or exogenous ligands, has prompted an abundance of theoretical studies to clarify its conformation and binding properties. In this context, molecular modeling of GPER ligands has demonstrated that targeting this receptor with computational methods is feasible. Accordingly, a number of compounds has been defined toward the development of innovative molecular modulators of GPER action in different biological systems. In particular, the first identified GPER agonist, G-1, is currently undergoing phase 1 clinical trials for its immunomodulatory and antineoplastic properties. In this respect, the findings recapitulated and discussed herein could be useful in order to clarify the potential role of GPER in cancer and other diseases, and the advantages of computational approaches to drive drug discovery for this target.

Abbreviations
AhR, aryl hydrocarbon receptor; E2, 17β-estradiol; E3, 16α 17β-estriol; EGFR, epidermal growth factor receptor; ER, estrogen receptor; ERE, estrogen response element; GPCR, G protein-coupled receptor; GPER (or GPR30), G protein-coupled estrogen receptor 1; MD, molecular dynamics.

References

[1] Geserick C, Meyer HA, Haendler B. The role of DNA response elements as allosteric modulators of steroid receptor function. Mol Cell Endocrinol. (2005) 236:1–7.

[2] Barton M, Filardo EJ, Lolait SJ, Thomas P, Maggiolini M, Prossnitz ER. Twenty years of the G protein-coupled estrogen receptor GPER: historical and personal perspectives. *J Steroid Biochem Mol Biol.* (2018) 176:4–15

[3] Pandey DP, Lappano R, Albanito L, Madeo A, Maggiolini M, Picard D. Estrogenic GPR30 signalling induces proliferation and migration of breast cancer cells through CTGF. *EMBO J.* (2009) 28:523–32.

[4] De Francesco EM, Pellegrino M, Santolla MF, Lappano R, Ricchio E, Abonante S, et al. GPER mediates activation of HIF1α/VEGF signaling by estrogens. *Cancer Res.* (2014) 74:4053–64

[5] De Marco P, Lappano R, De Francesco EM, Cirillo F, Pupo M, Avino S, et al. GPER signalling in both cancer-associated fibroblasts and breast cancer cells mediates a feedforward IL1β/IL1R1 response. *Sci Rep.* (2016) 6:24354.

[6] Rigiracciolo DC, Santolla MF, Lappano R, Vivacqua A, Cirillo F, Galli GR, et al. Focal adhesion kinase (FAK) activation by estrogens involves GPER in triple-negative breast cancer cells. *J Exp Clin Cancer Res.* (2019) 38:58.

[7] Lappano R, Pisano A, Maggiolini M. GPER function in breast cancer: an overview. *Front Endocrinol.* (2014) 5:66.

[8] Santolla MF, Vivacqua A, Lappano R, Rigiracciolo DC, Cirillo F, Galli GR, et al. GPER mediates a feedforward FGF2/FGFR1 paracrine activation coupling CAFs to cancer cells toward breast tumor progression. *Cells.* (2019) 8:223.

[9] Cirillo F, Pellegrino M, Malivindi R, Rago V, Avino S, Muto L, et al. GPER is involved in the regulation of the estrogen-metabolizing CYP1B1 enzyme in breast cancer. *Oncotarget.* (2017) 8:106608–24.

[10] Filardo EJ, Quinn JA, Bland KI, Frackelton AR Jr. Estrogen-induced activation of Erk-1 and Erk-2 requires the G protein-coupled receptor homolog, GPR30, and occurs via trans-activation of the epidermal growth factor receptor through release of HB-EGF. *Mol Endocrinol.* (2000) 14:1649–60.

[11] Marjon NA, Hu C, Hathaway HJ, Prossnitz ER. G protein-coupled estrogen receptor regulates mammary tumorigenesis and metastasis. *Mol Cancer Res.* (2014) 12:1644–54.

[12] Filardo EJ, Graeber CT, Quinn JA, Resnick MB, Giri D, DeLellis RA, et al. Distribution of GPR30, a seven membrane-spanning estrogen receptor, in primary breast cancer and its association with clinicopathologic determinants of tumor progression. *Clin Cancer Res.* (2006) 12:6359–66.

[13] Smith HO, Leslie KK, Singh M, Qualls CR, Revankar CM, Joste NE, et al. GPR30: a novel indicator of poor survival for endometrial carcinoma. *Am J Obstet Gynecol.* (2007) 196:386.e1.

[14] Smith HO, Arias-Pulido H, Kuo DY, Howard T, Qualls CR, Lee SJ, et al. GPR30 predicts poor survival for ovarian cancer. *Gynecol Oncol.* (2009) 114:465–71.

[15] Talia M, De Francesco EM, Rigiracciolo DC, Muoio MG, Muglia L, Belfiore A, et al. The G protein-coupled estrogen receptor (GPER) expression correlates with pro-metastatic pathways in ER-negative breast cancer: a bioinformatics analysis. *Cells.* (2020) 9:622.

[16] Martin SG, Lebot MN, Sukkarn B, Ball G, Green AR, Rakha EA, et al. Low expression of G protein-coupled oestrogen receptor 1 (GPER) is associated with adverse survival of breast cancer patients. *Oncotarget.* (2018) 9:25946–56.

[17] Thomas P, Pang Y, Filardo EJ, Dong J. Identity of an estrogen membrane receptor coupled to a G protein in human breast cancer cells. *Endocrinology.* (2005) 146:624–32.

[18] Lappano R, Rosano C, De Marco P, De Francesco EM, Pezzi V, Maggiolini M. Estriol acts as a GPR30 antagonist in estrogen receptor-negative breast cancer cells. *Mol Cell Endocrinol.* (2010) 320:162–70.

[19] Bologa CG, Revankar CM, Young SM, Edwards BS, Arterburn JB, Kiselyov AS, et al. Virtual and biomolecular screening converge on a selective agonist for GPR30. *Nat Chem Biol.* (2006) 2:207–12.

[20] Dennis MK, Burai R, Ramesh C, Petrie WK, Alcon SN, Nayak TK, et al. *In vivo* effects of a GPR30 antagonist. *Nat Chem Biol.* (2009) 5:421–7.

[21] Dennis MK, Field AS, Burai R, Ramesh C, Petrie WK, Bologa CG, et al. Identification of a GPER/GPR30 antagonist with improved estrogen receptor counterselectivity. *J Steroid Biochem Mol Biol.* (2011) 127:358–66.

[22] Lappano R, Rosano C, Santolla M. F, Pupo M, De Francesco E.M, De Marco P, et al. Two novel GPER agonists induce gene expression changes and growth effects in cancer cells. *Curr Cancer Drug Targets.* (2012) 12:531–42.

[23] Sinicropi MS, Lappano R, Caruso A, Santolla MF, Pisano A, Rosano C, et al. (6-bromo-1,4-dimethyl-9H-carbazol-3-yl-methylene)-hydrazine (carbhydraz) acts as a GPER agonist in breast cancer cells. *Curr Top Med Chem.* (2015) 15:1035–42.

[24] Maggiolini M, Santolla MF, Avino S, Aiello F, Rosano C, Garofalo A, et al. Identification of two benzopyrroloxazines acting as selective GPER antagonists in breast cancer cells and cancer-associated fibroblasts. *Future Med Chem.* (2015) 7:437–48.

[25] Lappano R, Mallet C, Rizzuti B, Grande F, Galli GR, Byrne C, et al. The peptide ERα17p is a GPER inverse agonist that exerts antiproliferative effects in breast cancer cells. *Cells.* (2019) 8:590.

[26] Zhang J, Zhang Y. GPCRRD: G protein-coupled receptor spatial restraint database for 3D structure modeling and function annotation. *Bioinformatics.* (2010) 26:3004–5.

[27] Prossnitz ER, Maggiolini M. Mechanisms of estrogen signaling and gene expression via GPR30. *Mol Cell Endocrinol.* (2009) 308:32–8.

[28] Hamza A, Sarma MH, Sarma RH. Plausible interaction of an alpha-fetoprotein cyclopeptide with the G-protein-coupled receptor model GPR30: docking study by molecular dynamics simulated annealing. *J Biomol Struct Dyn.* (2003) 20:751–8.

[29] Lappano R, Santolla MF, Pupo M, Sinicropi MS, Caruso A, Rosano C, et al. MIBE acts as antagonist ligand of both estrogen receptor α and GPER in breast cancer cells. *Breast Cancer Res.* (2012) 14:R12.

[30] Rosano C, Lappano R, Santolla MF, Ponassi M, Donadini A, Maggiolini M. Recent advances in the rationale design of GPER ligands. *Curr Med Chem.* (2012) 19:6199–206.

[31] Rosano C, Ponassi M, Santolla MF, Pisano A, Felli L, Vivacqua A, et al. Macromolecular modelling and docking simulations for the discovery of selective GPER ligands. *AAPS J.* (2016) 18:41–6.

[32] Okada T, Sugihara M, Bondar AN, Elstner M, Entel P, Buss V. The retinal conformation and its environment in rhodopsin in light of a new 2.2 Å crystal structure. *J Mol Biol.* (2004) 342:571–83.

[33] Cherezov V, Rosenbaum DM, Hanson MA, Rasmussen SG, Thian FS, Kobilka TS, et al. High-resolution crystal structure of an engineered human β2-adrenergic G protein-coupled receptor. *Science.* (2007) 318:1258–65.

[34] Rasmussen SG, DeVree BT, Zou Y, Kruse AC, Chung KY, Kobilka TS, et al. Crystal structure of the β2 adrenergic receptor-Gs protein complex. *Nature.* (2011) 477:549–55.

[35] Arnatt CK, Zhang Y. G Protein-coupled estrogen receptor (GPER) agonist dual binding mode analyses toward understanding of its activation mechanism: a comparative homology modeling approach. *Mol Inform.* (2013) 32:647–58.

[36] Bruno A, Aiello F, Costantino G, Radi M. Homology modeling, validation and dynamics of the G protein-coupled estrogen receptor 1 (GPER-1). *Mol Inform.* (2016) 35:333–9.

[37] Wu B, Chien EY, Mol CD, Fenalti G, Liu W, Katritch V, et al. Structures of the CXCR4 chemokine GPCR with small-molecule and cyclic peptide antagonists. *Science.* (2010) 330:1066–71.

[38] Méndez-Luna D, Martínez-Archundia M, Maroun RC, Ceballos-Reyes G, Fragoso-Vázquez MJ, González-Juárez DE, et al. Deciphering the GPER/GPR30-agonist and antagonists interactions using molecular modeling studies, molecular dynamics, and docking simulations. *J Biomol Struct Dyn.* (2015) 33:2161–72.

[39] Méndez-Luna D, Bello M, Correa-Basurto J. Understanding the molecular basis of agonist/antagonist mechanism of GPER1/GPR30 through structural and energetic analyses. *J Steroid Biochem Mol Biol.* (2016) 158:104–16.

[40] Zhang J, Yang J, Jang R, Zhang Y. GPCR-I-TASSER: a hybrid approach to G protein-coupled receptor structure modeling and the application to the human genome. *Structure.* (2015) 23:1538–49.

[41] Roy A, Kucukural A, Zhang Y. I-TASSER: a unified platform for automated protein structure and function prediction. *Nat Protoc.* (2010) 5:725–38.

[42] Vidad AR, Macaspac S, Ng H-L. Locating ligand binding sites in G-protein coupled receptors using combined information from docking and sequence conservation. *bioRxiv [Preprint].* (2019).

[43] Cirillo F, Lappano R, Bruno L, Rizzuti B, Grande F, Guzzi R, et al. AHR and GPER mediate the stimulatory effects induced by 3-methylcholanthrene in breast cancer cells and cancer-associated fibroblasts (CAFs). *J Exp Clin Cancer Res.* (2019) 38:335.

[44] Thomas MP, Potter BV. The structural biology of oestrogen metabolism. *J Steroid Biochem Mol Biol.* (2013) 137:27–49.

[45] Chimento A, Casaburi I, Rosano C, Avena P, De Luca A, Campana C, et al. Oleuropein and hydroxytyrosol activate GPER/ GPR30-dependent pathways leading to apoptosis of ER-negative SKBR3 breast cancer cells. *Mol Nutr Food Res.* (2014) 58:478–89.

[46] Santolla MF, De Francesco EM, Lappano R, Rosano C, Abonante S, Maggiolini M. Niacin activates the G protein estrogen receptor (GPER)-mediated signalling. *Cell Signal.* (2014) 26:1466–75.

[47] Papalia T, Lappano R, Barattucci A, Pisano A, Bruno G, Santolla MF, et al. Bodipy as a luminescent probe for detection of the G protein estrogen receptor (GPER). *Org Biomol Chem.* (2015) 13:10437–41.

[48] Moreno-Ulloa A, Mendez-Luna D, Beltran-Partida E, Castillo C, Guevara G, Ramirez-Sanchez I, et al. The effects of (–)-epicatechin on endothelial cells involve the G protein-coupled estrogen receptor (GPER). *Pharmacol Res.* (2015) 100:309–20.

[49] Kuiper GG, Lemmen JG, Carlsson B, Corton JC, Safe SH, van der Saag PT, et al. Interaction of estrogenic chemicals and phytoestrogens with estrogen receptor β. *Endocrinology.* (1998) 139:4252–63.

[50] Grande F, Rizzuti B, Occhiuzzi MA, Ioele G, Casacchia T, Gelmini F, et al. Identification by molecular docking of homoisoflavones from *Leopoldia comosa* as ligands of estrogen receptors. *Molecules.* (2018) 23:894.

[51] Puranik NV, Srivastava P, Bhatt G, John Mary DJS, Limaye AM, Sivaraman J. Determination and analysis of agonist and antagonist potential of naturally occurring flavonoids for estrogen receptor (ERα) by various parameters and molecular modelling approach. *Sci Rep.* (2019) 9:7450. doi: 10.1038/s41598-019-43768-5

[52] Sarmiento V, Ramirez-Sanchez I, Moreno-Ulloa A, Romero-Perez D, Chavez D, Ortiz M, et al. Synthesis of novel (–)-epicatechin derivatives as potential endothelial GPER agonists: evaluation of biological effects. *Bioorg Med Chem Lett.* (2018) 28:658–63.

[53] Bello M, Méndez-Luna D, Sarmiento V, Correa Basurto J, Najera N, Villarreal F, et al. Structural and energetic basis for novel epicatechin derivatives acting as GPER agonists through the MMGBSA method. *J Steroid Biochem Mol Biol.* (2019) 189:176–86.

[54] Martínez-Muñoz A, Prestegui-Martel B, Méndez-Luna D, Fragoso-Vázquez MJ, García-Sánchez JR, Bello M, et al. Selection of a GPER1 ligand via ligand-based virtual screening coupled to molecular dynamics simulations and its anti-proliferative effects on breast cancer cells. *Anticancer Agents Med Chem.* (2018) 18:1629–38.

[55] Zacarías-Lara OJ, Méndez-Luna D, Martínez-Ruíz G, García-Sanchéz JR, Fragoso-Vázquez MJ, Bello M, et al. Synthesis and *in vitro* evaluation of tetrahydroquinoline derivatives as antiproliferative compounds of breast cancer via targeting the GPER. *Anticancer Agents Med Chem.* (2019) 19:760–71.

[56] Kezimana P, Dmitriev AA, Kudryavtseva AV, Romanova EV, Melnikova NV. Secoisolariciresinol diglucoside of flaxseed and its metabolites: Biosynthesis and potential for nutraceuticals. *Front Genet.* (2018) 9:641.

[57] Ren GY, Chen CY, Chen WG, Huang Y, Qin LQ, Chen LH. The treatment effects of flaxseed-derived secoisolariciresinol diglycoside and its metabolite enterolactone on benign prostatic hyperplasia involve the G protein-coupled estrogen receptor 1. *Appl Physiol Nutr Metab.* (2016) 41:1303–10.

[58] Chen Y, Wang J, Hong DY, Chen L, Zhang YY, Xu YN, et al. Baicalein has protective effects on the 17β-estradiol-induced transformation of breast epithelial cells. *Oncotarget.* (2017) 8:10470–84.

[59] Cao LY, Ren XM, Li CH, Zhang J, Qin WP, Yang Y, et al. Bisphenol AF and bisphenol B exert higher estrogenic effects than bisphenol A via G protein-coupled estrogen receptor pathway. *Environ Sci Technol.* (2017) 51:11423–30.

[60] Leclercq G, de Cremoux P, This P, Jacquot Y. Lack of sufficient information on the specificity and selectivity of commercial phytoestrogens preparations for therapeutic purposes. *Maturitas.* (2011) 68:56–64.

[61] Aiello F, Carullo G, Giordano F, Spina E, Nigro A, Garofalo A, et al. Identification of breast cancer inhibitors specific for G protein-coupled estrogen receptor (GPER)-expressing cells. *ChemMedChem.* (2017) 12:1279–85.

[62] Trichet M, Lappano R, Belnou M, Salazar Vazquez LS, Alves I, Ravault D, et al. Interaction of the anti-proliferative GPER inverse agonist ERα17p with the breast cancer cell plasma membrane: from biophysics to biology. *Cells.* (2020) 9:447.

[63] Pelekanou V, Kampa M, Gallo D, Notas G, Troullinaki M, Duvillier H, et al. The estrogen receptor α-derived peptide ERα17p (P_{295}-T_{311}) exerts pro-apoptotic actions in breast cancer cells *in vitro* and *in vivo*, independently from their ERα status. *Mol Oncol.* (2011) 5:36–47.

V. BENZOPYRROLOXAZINES CONTAINING A BRIDGEHEAD NITROGEN ATOM AS PROMISING SCAFFOLDS FOR THE ACHIEVEMENT OF BIOLOGICALLY ACTIVE AGENTS

Fedora Grande, Maria A. Occhiuzzi, Giuseppina Ioele, Gaetano Ragno, Antonio Garofalo

Department of Pharmacy, Health and Nutritional Sciences, University of Calabria, Via P. Bucci, 87036, Rende (CS), Italy

Abstract:

The present review lists the papers and patents dealing with the class of polycondensed heterocycles called benzopyrroloxazines published in the last decades. The survey is limited to substances characterized by the presence of a bridgehead N atom, which means that the present N atom serves to connect different rings within the same molecule. In the case of benzopyrroloxazines, the bridgehead N atom belongs at the same time to the pyrrole and oxazine rings. All other compounds not possessing this feature were kept out accordingly. Relevant synthetic methods to such compounds have been outlined. Many different biological properties have been attributed to several functionalized derivatives of these heterocycles and cited within the review.

Keywords: Polycondensed heterocycles; Oxazinoindoles; Biological activity; Synthetic methods.

1. Introduction

Benzopyrroloxazines are tricyclic systems deriving from the fusion of a two-ring (bicyclic) benzoxazine moiety with a pyrrole ring and represent interesting scaffolds for the pursuit of new biologically active compounds. Several combinations for the condensation of the three rings are possible thus generating a number of isomers. We herein report on benzopyrroloxazines characterized by the presence of a bridgehead N atom into the structure. This way, six different isomeric basic structures can be drawn all showing the empirical formula $C_{11}H_9NO$. In particular, two linear (**A**,**B**) and four angular (**C**-**F**) annelations are feasible. Three more structures (G-I) deriving from the peri-fusion of pyrrole with the benzo and the oxazine rings could be considered as members of this same chemical family and therefore herein included, although they are commonly known as oxazinoindoles (Figure 1). Three out of the nine mentioned structures (**B**, **F**, **I**) have not been described yet, while the six known structures are compiled herein. However, the annelation of additional rings to the basic tricyclic systems generates compounds, which could be included in more than one group.

The majority of the papers so far appeared in the literature dealing with these subjects refers on a benzopyrroloxazine system embedded in larger fused structures with the pyrrole ring often lacking aromaticity or condensed with an extra benzo-fused ring participating in this case to the formation of an indole nucleus. Derivatives of these heterocyclic systems have been isolated either from natural sources, although in a few cases, or after synthetic investigations and their biological activities, when present, are mentioned in this survey.

9*H*-benzo[*e*]pyrrolo[2,1-*b*][1,3]oxazine
A

10*H*-benzo[*e*]pyrrolo[1,2-*b*][1,2]oxazine
B

4*H*-benzo[*b*]pyrrolo[1,2-*d*][1,4]oxazine
C

5*H*-benzo[*e*]pyrrolo[1,2-*c*][1,3]oxazine
D

5*H*-benzo[*d*]pyrrolo[2,1-*b*][1,3]oxazine
E

6*H*-benzo[*d*]pyrrolo[1,2-*b*][1,2]oxazine
F

[1,4]oxazino[2,3,4-*hi*]indole
G

1,3-dihydro-[1,3]oxazino[5,4,3-*hi*]indole
H

[1,2]oxazino[4,3,2-*hi*]indole
I
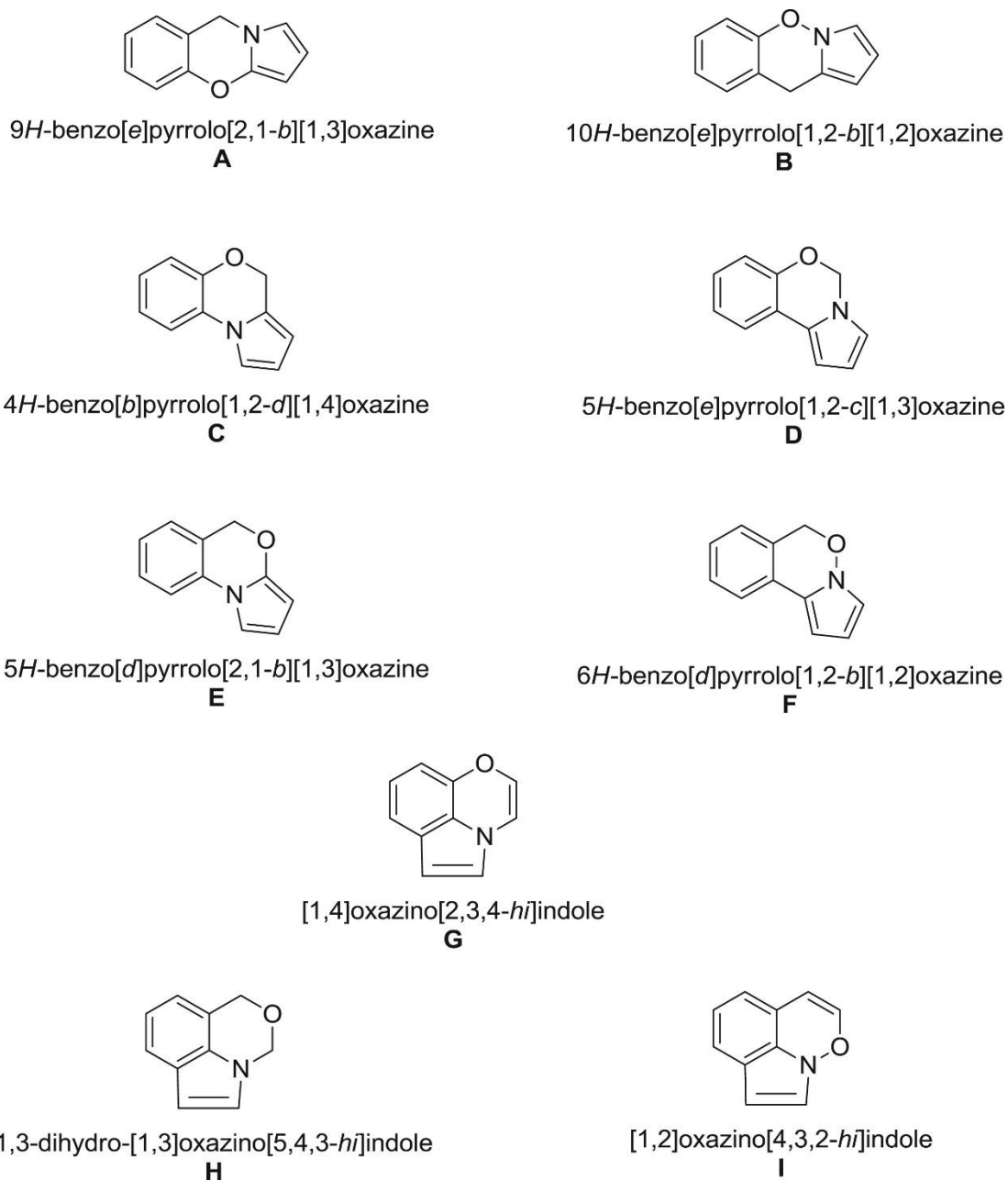
Figure 1. *Benzopyrroloxazines with a bridgehead N atom.*

2. 9*H*-Benzo[e]pyrrolo[2,1-b][1,3]oxazine A

The unique linear benzopyrroloxazine known in the literature is 9H-benzo[*e*]pyrrolo[2,1-b][1,3]oxazine **A**. The first paper reporting the formation of 5a,10-dihydro-5a-methyl-12H-isoindolo[1,2-b][1,3]benzoxazine-10,12-dione (1) (Figure 2), a derivative of the title system, is dated 1971 [1]. This compound was prepared by the reaction of methyl or ethyl o-acetylbenzoate and salicylamide.

233
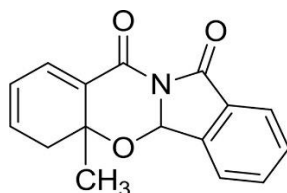
Figure 2. Structure of compound **1**.

A patent application reported a number of derivatives of the title system that were demonstrated to possess antibacterial and antifungal properties. Such compounds were isolated from cultures of Streptomices and chemically modified. The most promising example, 2-chloro-6,8-dihydroxy-7-propyl-9H-benzo [*e*]pyrrolo[2,1-b][1,3]oxazin-9-one (**2a**) (Figure 3, **A**), proved to possess activity against a panel of microorganisms at 0.1 mg/mL concentration [2]. Subsequently, the structure of this compound, named Streptopyrrole, was fully elucidated by extensive NMR experiments [3].

In a second patent application, the same compound showed a minimal inhibitory concentration (MIC) of 0.20–0.78 µg/mL against different strains of *Staphylococcus* [4]. American researchers reported in a patent application and in a subsequent paper the corresponding dechlorinated derivative **2b**. This latter was obtained either by catalytic hydrogenation of compound **2a** or by total synthesis, as outlined in Figure 3, **B**. Fully methoxymethyl-protected benzene-1,3,5-triol (**3**) was acylated with 1H-pyrrole-1-carboxylic anhydride to give compound **4**. After deprotection of **4**, an oxidative cyclization to the 2-position of the pyrrole using Pd(OAc)$_2$ gave 6,8-dihydroxy-9*H*-benzo [*e*]pyrrolo[2,1-b][1,3]oxazin-9-one (**5**). This reaction represents the key step of the entire synthetic pathway. Subsequent reaction with allyl bromide followed by ZnCl2-promoted allyl group migration, gave compound **6**, which was subjected to O-dealkylation to 7-allyl-6,8-dihydroxy-9H-benzo [*e*]pyrrolo[2,1-b][1,3]oxazin-9-one (**7**). Final hydrogenation led to compound **2b**, which showed antibacterial activity with a MIC of 2.0 µg/mL against *S. aureus* and *E. coli* [5,6].
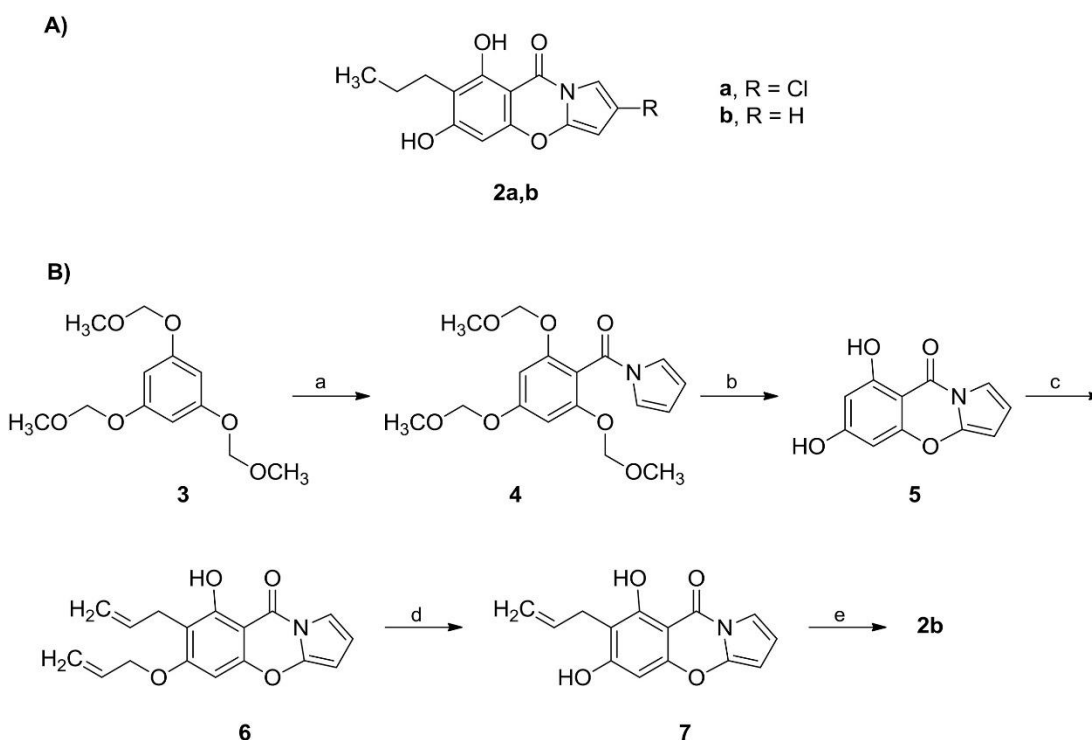
A)

a, R = Cl
b, R = H

2a,b

B)

Compound **2a** along with a series of halogenated analogues **8–15**, (Figure 4) have been isolated from *S. rimosus* cultures, after introduction of saline additives into the culture media, and fully characterized by spectroscopic methods. The most promising derivative remained compound **2a**, which exhibited activity in a panel of antimicrobic and antifungal tests. The efficacy of this compound seemed attributable to its ability in inhibiting the nitrogen regulator II (NRII) histidine kinase, a member of a large family of proteins that are part of the signal transduction systems with an IC_{50} of 20 μM. NRII is a homodimeric signal-transducing protein responsible for the transcriptional function in *E. coli*. Moreover, the same compound showed activity against selected human cancer cell lines [7].

8,	R_1 = Cl, R_2 = H, R_3 = Et, R_4 = OH
9,	R_1 = R_2 = Cl, R_3 = Pr, R_4 = OCH$_3$
10,	R_1 = Cl, R_2 = H, R_3 = Pr, R_4 = OCH$_3$
11,	R_1 = Cl, R_2 = H, R_3 = Bu, R_4 = OH
12,	R_1 = Cl, R_2 = H, R_3 = Et, R_4 = OCH$_3$
13,	R_1 = R_2 = Cl, R_3 = Pr, R_4 = OCH$_3$
14,	R_1 = Br, R_2 = H, R_3 = Pr, R_4 = OH
15,	R_1 = R_2 = Cl, R_3 = Et, R_4 = OH

Figure 4. Chemical structures of compounds 8–15.

Four polycyclic compounds based on a 9*H*-benzo[*e*]pyrrolo[2,1-b][1,3]oxazine moiety have been obtained by reaction between the Betti base or equivalents (i.e. 1-(aminomethyl)naphthalen-2-ol, 16) with 2-formylbenzoic acid **17** or levulinic acid. Compounds **18–21** were obtained following the route below described representatively for compound 18 (Figure 5) [8].
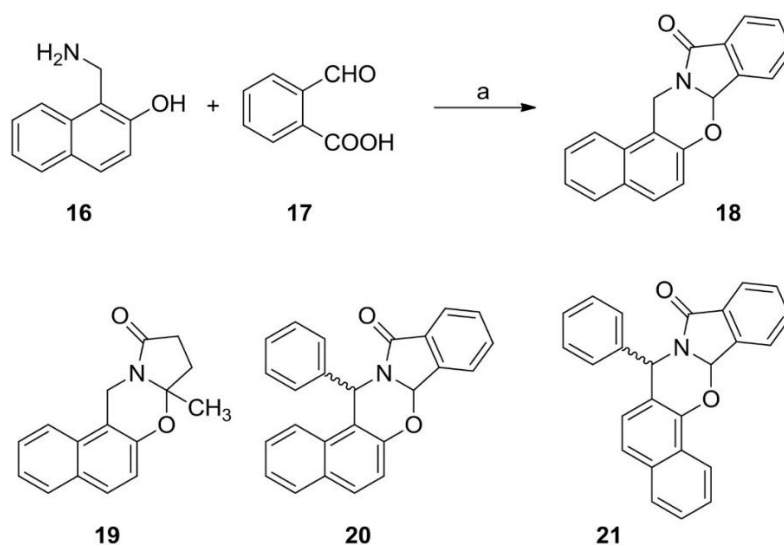
Figure 5. Synthesis of compound 18 and structure of analogs 19–21. Reagents and conditions: (a) toluene, rt.

Derivatives of the previously unknown indolo[2,1-b][1,3]benzoxazine system were obtained by condensation of iodomethilates of 2-[(dimethylamino)methylphenols] and 2-

bromomelatonin, in boiling DMF in the presence of K$_2$CO$_3$. As a representative example the reaction of 1-(2-hydroxy-5-methoxyphenyl)-N,N,N-trimethylmethanaminium iodide (**22**) with N-(2-(2-bromo-5-methoxy-1H-indol-3-yl)ethyl)acetamide (**23**) to give N-(2-(2,8-dimethoxy-12H-benzo[5,6][1,3]oxazino[3,2-a]indol-6-yl)ethyl)acetamide (**24**) is outlined in Figure 6 [9].
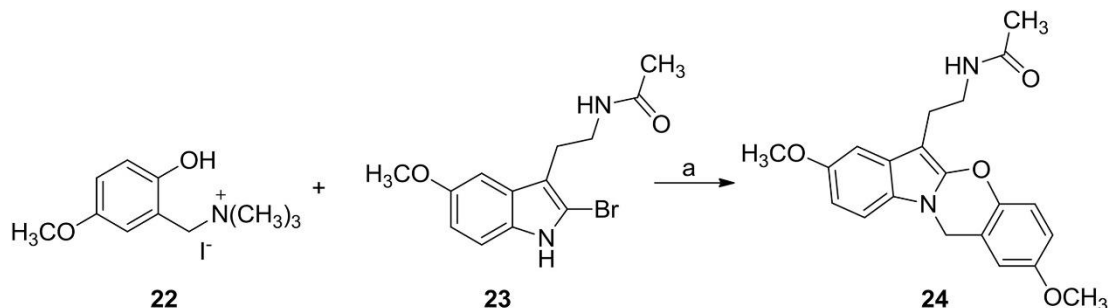
Figure 6. Synthesis of compound 24. Reagents and conditions: (a) DMF, K$_2$CO$_3$, reflux.

Substituted isomeric 4b*H*-benzo[5,6][1,3]oxazino[2,3-*a*]isoindol-12(10*H*)-one and 5*H*-benzo[4,5][1,3]oxazino[2,3-*a*]isoindol-11 (6a*H*)-one were obtained by a tandem heterocyclization of 2-formylbenzoic acid **17** with 2-(1-aminoalkyl)phenols or 2-aminophenilcarbinols. The basic skeletons **25** and **26** of such tetracyclic compounds are reported in Figure 7 [10].
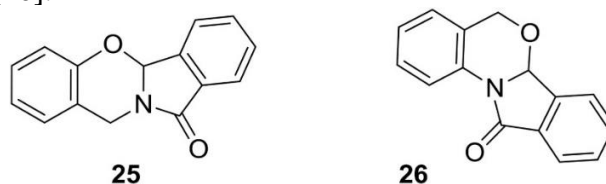
Figure 7. Structure of compound 25 and 26.

Cu$_2$O-catalyzed intramolecular domino bond formation on an easily available *gem*-dibromovinylic precursor **27** gave rise to 12*H*-benzo[5,6][1,3]oxazino[3,2-*a*]indol-12-one (**28**) (Figure 8) [11].
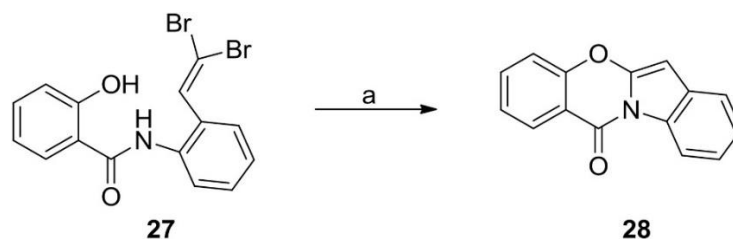
Figure 8. Synthesis of compound 28. Reagents and conditions: (a) Cu$_2$O, DMEDA, K$_2$CO$_3$, toluene, 100 °C.

Further derivatives of this same heterocyclic system were achieved accidentally after an intramolecular dehydrohalide coupling on a 1-(2-bromobenzyl)indolin-2-one (**29a,b**) promoted by *t*-BuOK, in an unusual *O*-arylation fashion, to give compounds **30a,b** (Figure 9) [12,13].
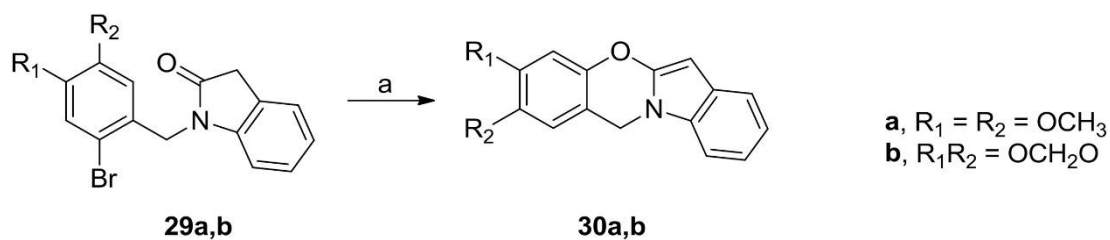
Figure 9. *Intramolecular cyclization to **30a,b**. Reagents and conditions: (a) t-BuOK, sealed tube, 100 °C.*

Recently, the one-step reaction between salicylaldheydes (**31a,b**) and *L*-4-hydroxyproline (**32**) *via* iodine-mediated electrophilic cyclization catalyzed by 1-butyl-3-methylimidazolium bromide, under MW irradiation, gave substituted derivatives of the basic tricyclic system **33a,b** (Figure 10) [14].
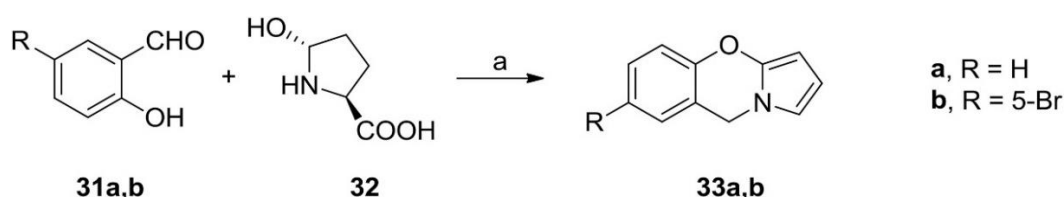
Figure 10. *Synthesis of 9H-benzo [e]pyrrolo[2,1-b][1,3]oxazines **33a,b**. Reagents and conditions: (a) 1-butyl-3-methylimidazolium bromide, MW.*

3. 4*H*-Benzo[*b*]pyrrolo[1,2-*d*][1,4]oxazine C

A first report on the synthesis of derivatives of his heterocyclic system appeared in 1961 by a Japanese author. The described compounds were obtained starting from *o*-aminophenol (**34**) and diethyl-α-oxoglutarate (**35**) to give a benzoxazine intermediate **36**, which was in turn converted into 1-ethoxy-4-oxo-3a,4-dihydro-3*H*-benzo [*b*]pyrrolo[1,2-d][1,4]oxazine-2,3-dicarbaldehyde (**37**) by reaction with POCl$_3$/DMF (Figure 11). Then, reactive groups on the pyrrole ring of this latter compound were further elaborated [15].
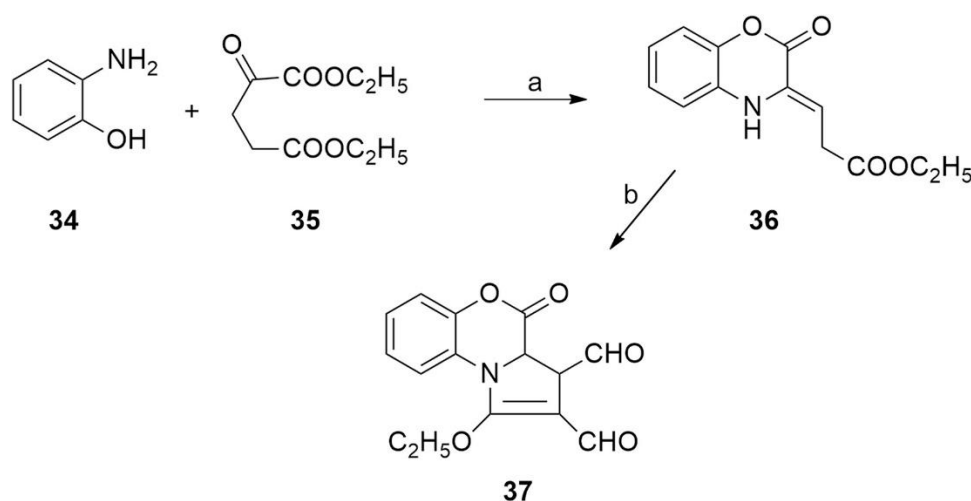
Figure 11. *Synthesis of the benzopyrroloxazine **37**. Reagents and conditions: (a) EtOH, reflux, 4h; (b) POCl$_3$, DMF, reflux, 4h.*

The basic tricylic system **C** was obtained by treating 2-(1*H*-pyrrol-1-yl)phenol (**38**) with formaldehyde and dimethylamine to give 2-(2-((dimethylamino)methyl)-1*H*-pyrrol-1-yl)phenol (**39**), which, after transformation into the methiodide salt, was subjected to cyclization to 4*H*-benzo[*b*]pyrrolo[1,2-d][1,4]oxazine **C**, by the action of sodium ethoxide (Fig. 12). In the same report, it was described that the starting material **38** was first transformed into the corresponding ethyl carbonate **40** and this latter was subjected to intramolecular cyclization with zinc chloride to give the 4-oxo analog **41** (Figure 12) [16]. The same synthetic approach was also adopted by another research group for the preparation of halogen-substituted analogs of **41** [17]. Compound **38** was also used for the preparation of a series of 4-substituted derivatives of basic system **C** by acid catalyzed condensation with carbonyl components. As an example, compound **38** was condensed with acetone to give 4,4-dimethyl-4*H*-benzo [*b*]pyrrolo[1,2-d][1,4]oxazine (**42**) (Figure 12) [18]. The application of this synthetic pathway led to a number of 4,4-disubstituted derivatives patented as antihypertensive and SNC active agents [19].
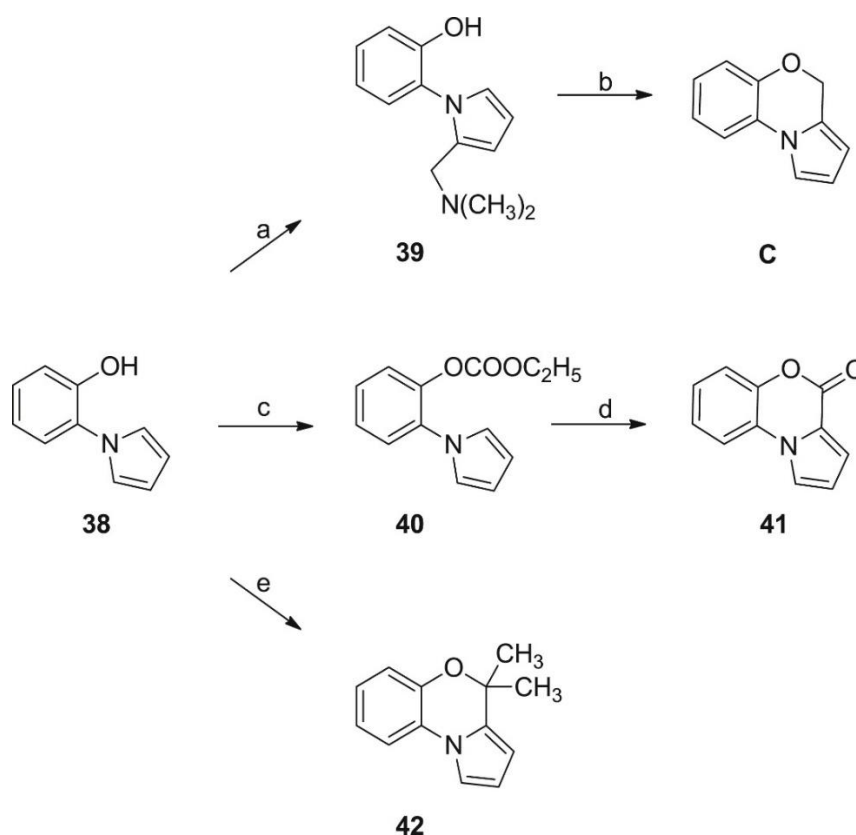
Figure 12. *Synthesis of 4H-benzo [b]pyrrolo[1,2-d][1,4]oxazine **C** and its analogs **41** and **42**, starting from 2-(1H-pyrrol-1-yl)phenol **38**. Reagents and conditions: (a) CH₂O, NHMe₂, AcOH, rt, 40h; (b) CH₃I, THF, rt, 3h, then EtONa, EtOH, reflux, 16h; (c) EtONa, ClCOOEt, THF, rt, 2h; (d) ZnCl₂, o-dichlorobenzene, reflux, 1h; (e) acetone, PTSA, reflux, 15h.*

In a paper appeared in 1972, was reported the synthesis of 1,2,3,3a-tetrahydro-4*H*-pyrrolo[2,1-*c*][1,4]benzoxazine (**43**) starting from a preformed benzoxazine, in a multi-step fashion (Figure 13) [20].
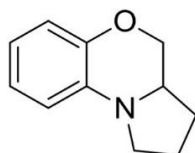
Figure 13. Chemical structure of compound 43.

During the search for anticancer substances related to Mitomycin C, 1-(2,5-dimethoxyphenyl)-1*H*-pyrrole-2-carbonyl chloride (**44**) was converted into tricyclic derivative **45** under Friedel-Crafts conditions in the absence of oxygen (Figure 14). 5-Substituted derivatives of compound **45** inhibited bladder cancer cell growth in the low micromolar range [21].
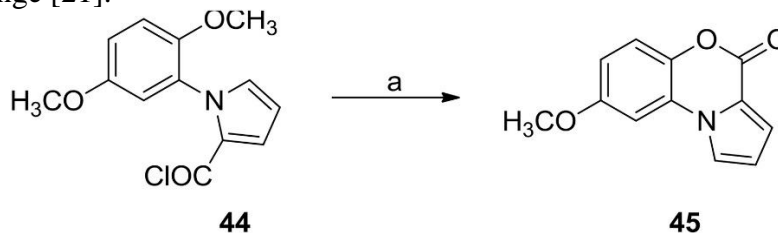
Figure 14. Synthesis of 8-methoxy-4H-benzo [b]pyrrolo[1,2-d][1,4]oxazin-4-one 45. Reagents and conditions: (a) Friedel-Crafts <u>cyclization</u>, N₂.

In a study aimed at transforming derivatives of the 4*H*-benzo[*b*]pyrrolo[1,2-d][1,4]oxazin-4-one nucleus into fluorazone derivatives, sequential nitration/reduction of 7-methoxy-6-methyl-4*H*-benzo [*b*]pyrrolo[1,2-*d*][1,4]oxazin-4-one (**46**) furnished the corresponding amino derivative **47**, which was subjected to photo-irradiation with the achievement of the expected results (Figure 15) [22]. The application of this synthetic strategy is potentially useful in the Mitomycin synthesis [23].
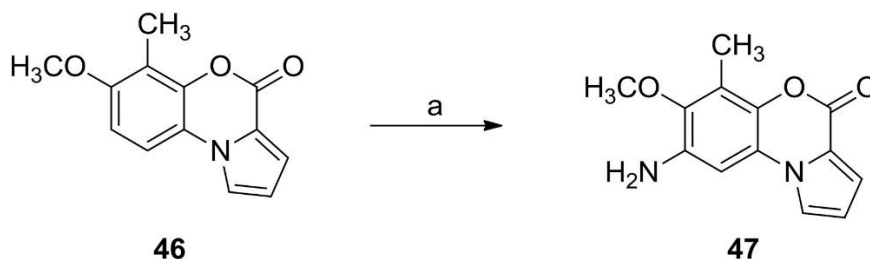
Figure 15. Synthesis of 8-amino-7-methoxy-6-methyl-4H-benzo [b]pyrrolo[1,2-d][1,4]oxazin-4-one 47. Reagents and conditions: (a) HNO₃, H₂SO₄, then H₂, Pd(C).

Starting from (un)substituted *o*-aminophenols, several benzo [*b*]pyrrolo[1,2-*d*][1,4]oxazines were obtained in refluxing dioxane by action of methyl acetylenedicarboxylate [24]. Successively, this method was applied for a three-component one-pot reaction adding nitrostyrene to the two above starting reagents to give substituted 2-aryl derivatives. The structures of the prototype products **48** and **49**, respectively, are depicted in Figure 16 [25].
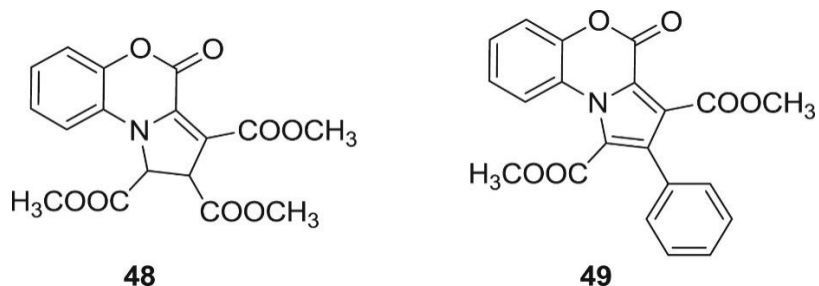
Figure 16. Chemical structure of trimethyl 4-oxo-2,4-dihydro-1H-*benzo [b]pyrrolo[1,2-d][1,4]oxazine-1,2,3-tricarboxylate **48** and dimethyl 4-oxo-2-phenyl-4H-benzo [b]pyrrolo[1,2-d][1,4]oxazine-1,3-dicarboxylate **49**.*

Starting from 10*H*-phenoxazine (**50**), pyrrolo [3,2,1-*kl*]phenoxazin-1(2*H*)-one (**51**) was obtained by action of 2-chloroacetyl chloride and AlCl$_3$. This latter compound was used as starting point for the preparation of several potent dual inhibitors of cyclooxygenase and 5-lipoxygenase in the arachidonic acid metabolism pathway with *in vivo* anti-inflammatory activity. In particular compound **52** (Figure 17) showed IC$_{50}$ value of 0.02 and 1.5 μM against rat cyclooxygenase and 5-lipooxigenase, respectively [26,27].
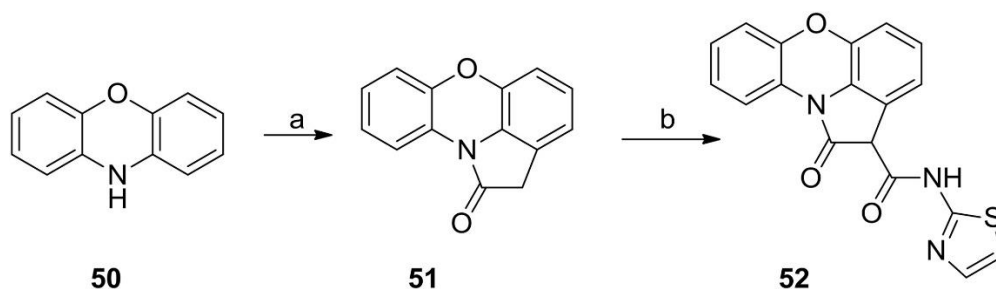
Figure 17. *Schematic synthetic pathway to 1-oxo-N-(thiazol-2-yl)-1,2-dihydropyrrolo [3,2,1-kl]phenoxazine-2-carboxamide **52**. Reagents and conditions: (a) ClCH$_2$COCl, then AlCl$_3$, benzene; (b) EtONa, EtOH, (MeO)$_2$CO, reflux, 3h, then 2-aminothiazole, toluene, reflux.*

A patent by Japanese authors described a series of pyrrolobenzoxazines showing activity on 5-HT receptors. Their preparation was achieved by reaction of ethyl 3-hydroxy-2-(1*H*-pyrrol-1-yl)benzoate or its 5-chloro derivative **53** with acetone and *p*-toluensulfonic acid to give substituted pyrrolobenzoxazines. These latter were then saponified and amidated to give a number of amide derivatives. As an example, the reaction of **53** with acetone give rise to ester **54**, which was transformed into 7-chloro-4,4-dimethyl-*N*-(quinuclidin-3-yl)-4*H*-benzo[*b*]pyrrolo[1,2-*d*][1,4]oxazine-9-carboxamide (**55**) after hydrolysis (Figure 18). This last compound showed 68% inhibition at 3.2 μg/kg in the Benzold-Jarisch reflex test [28]. The same authors reported in a separate paper the structure-activity relationships (SAR) of such derivatives tested against the 5-HT$_3$ receptor and found that the previously reported amide **55** was 40-fold more potent than ondansetron, a well known antiemetic agent [29].
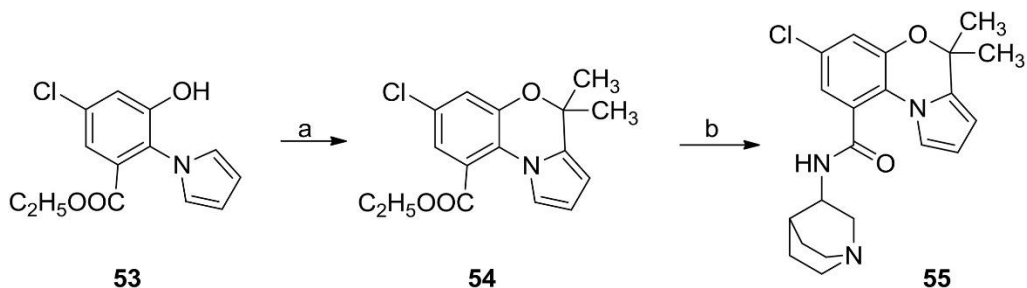
Figure 18. *Schematic synthetic pathway to compound* ***55***. *Reagents and conditions: (a) acetone, PTSA, benzene; NaOH, H₂O, EtOH; (b) DCC, HOBT, quinuclidin-3-amine, DMF.*

A patent dealing with the discovery of inhibitors of sodium/hydrogen cellular exchange reported a significant activity for a series of polysubstituted 4*H*-benzo [*b*]pyrrolo[1,2-*d*][1,4]oxazine bearing a guanidine residue and for several other guanidine derivatives. The compounds were proposed as useful tools for the treatment of cardiovascular diseases. The structure of the lead derivative **56** is reported in Figure 19 [30].
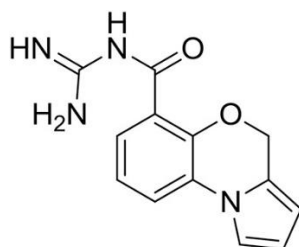
Figure 19. *Chemical structure of* N-*carbamimidoyl-4*H-*benzo [*b*]pyrrolo[1,2-*d*]*[1,4]oxazine-6-carboxamide* ***56***.

Benzopyrroloxazine and benzopyrrolothiazine derivatives were also described for their use as potential calcium channel blockers related to Diltiazem, a well known antihypertensive agent. The preparation route started from (1-(2-fluorophenyl)-1*H*-pyrrol-2-yl) (4-methoxyphenyl)methanol (**57a**) which was subjected to intramolecular nucleophilic displacement by action of a strong base to give the tricyclic derivative **58** further functionalized to 1-(4-(4-methoxyphenyl)-4*H*-benzo[*b*]pyrrolo[1,2-*d*][1,4]oxazin-1-yl)-*N*,*N*-dimethylmethanamine (**59**) with formaldehyde/dimethyl amine (Figure 20). This compound resulted however 15-fold less active than the corresponding benzopyrrolothiazine analogue in a guinea pig aorta strip binding affinity assay [31]. A similar synthetic approach, starting from 2-fluoroaniline and 2,5-dimethoxytetrahydrofuran and a final Mannich pyrrole aminoalkylation, led to several 4*H*-benzo [*b*]pyrrolo[1,2-*d*][1,4]oxazine analogs of compound **59** [32]. The same authors reported in a successive paper the oxidation of the sulfide **60**, obtained after the same synthetic pathway from compound **57b**, to give the sulfone **61** (Figure 20). This compound showed a moderate COX-1 and COX-2 inhibitory activity as well as an antiproliferative effect on a panel of human cancer cell lines [33].
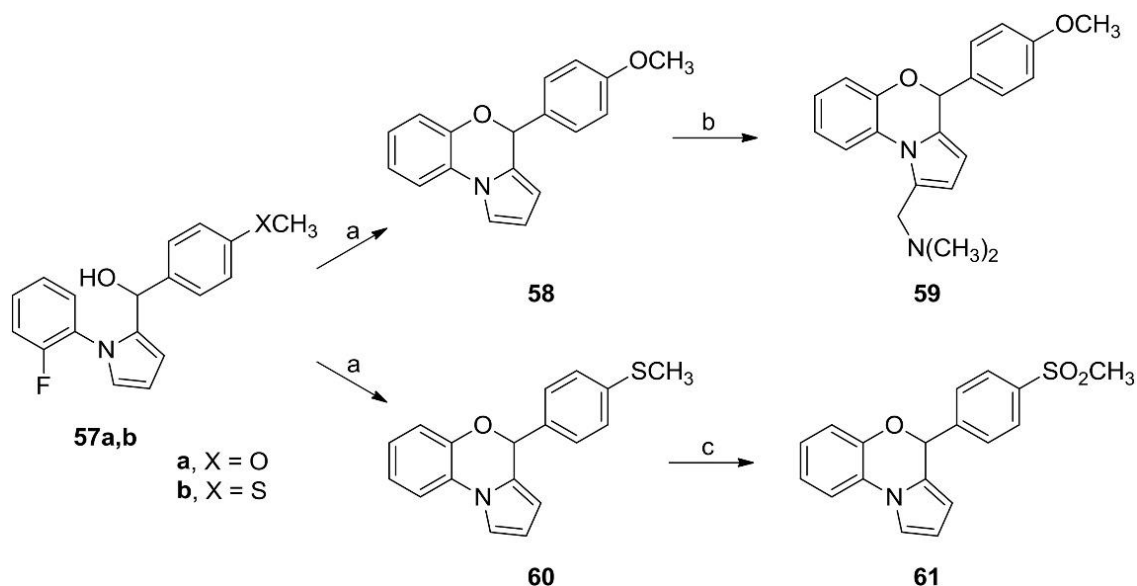
Figure 20. *Schematic synthetic pathway to compound **59** and **61**. Reagents and conditions: (a) NaH, benzene, DMF, 80 °C, 6h; (b) CH₂O, NH(CH₃)₂, AcOH, rt, 3h; (c) m-CPBA, DCM, 0 °C, 4h.*

More recently the first pyrrolation step on aniline derivatives has been more conveniently carried out in aqueous media in the presence of mesoporous hydrogen sulfated MCM-41 (MCM-41-SO3H) [34].

In a patent dealing with the identification of antimicrobial agents, starting from 2-(2-hydroxymethyl-pyrrol-1-yl)-5-nitrophenol (**62**), 7-nitro-4*H*-benzo[*b*]pyrrolo[1,2-*d*][1,4]oxazine (**63**) was obtained under Mitsunobu conditions. This latter compound was subjected to nitro group reduction and the corresponding amino derivative **64** was in turn converted into the oxazolidinone derivative **65** in two steps (Figure 21) [35].
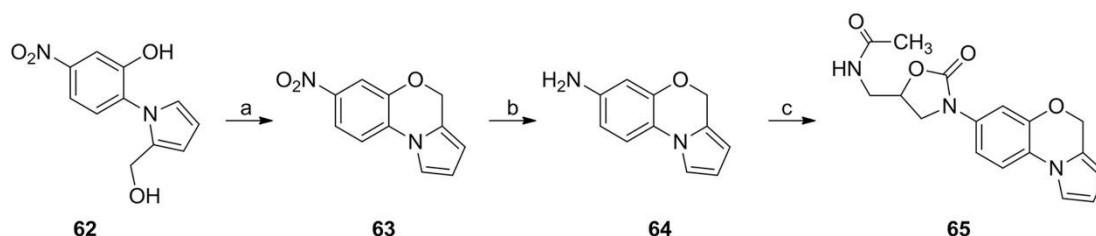
Figure 21. *Synthesis of N-((3-(4H-benzo [b]pyrrolo [1,2-d] [1,4]oxazin-7-yl)-2-oxooxazolidin-5-yl)methyl)acetamide **65**. Reagents and conditions: (a) DEAD, Ph₃P, THF, rt, 14h; (b) H₂, Pd(C), 3h; (c) acetyl-aminomethyl-oxirane, CHCl₃, silica gel, DCM, then CDI, 1,4-dioxane, reflux, 12h.*

Russian authors described a convenient preparation of benzoyl-, furoyl- and thienoyl-benzopyrroloxazinetriones by the reaction of 2,4-dioxo-4-phenylbutanoic acid (**66a**) or 4-(furan-2-yl)-2,4-dioxobutanoic acid (**66b**) or 2,4-dioxo-4-(thiophen-2-yl)butanoic acid (**66c**) and 2-aminophenol (**34**). The resulting benzoxazine derivatives **67a-c** were treated with oxalyl chloride to give the benzopyrroloxazines. **68a-c**, which were used as intermediates for the preparation of various poly-heterocyclic derivatives [36,37]. This convenient synthetic approach to pyrrolobenzoxazinetriones was exploited by a second Russian research group. In this case, the above reaction with oxalyl chloride gave rise to trione derivatives along with small amount of by-products of formula **69a-c** deriving from the addition of a molecule of water [38]. The same authors reported the reaction of previously obtained 3-benzoyl-1*H*-benzo [*b*]pyrrolo[1,2-*d*][1,4]oxazine-1,2,4-trione (**68a**) with 2-

242

hydrazinylbenzoic acid that led to (Z)-2-(2-(3-benzoyl-1,4-dioxo-1H-benzo [b]pyrrolo[1,2-d][1,4]oxazin-2(4H)-ylidene)hydrazinyl)benzoic acid (**70**) in 47% yield (Figure 22) [39].
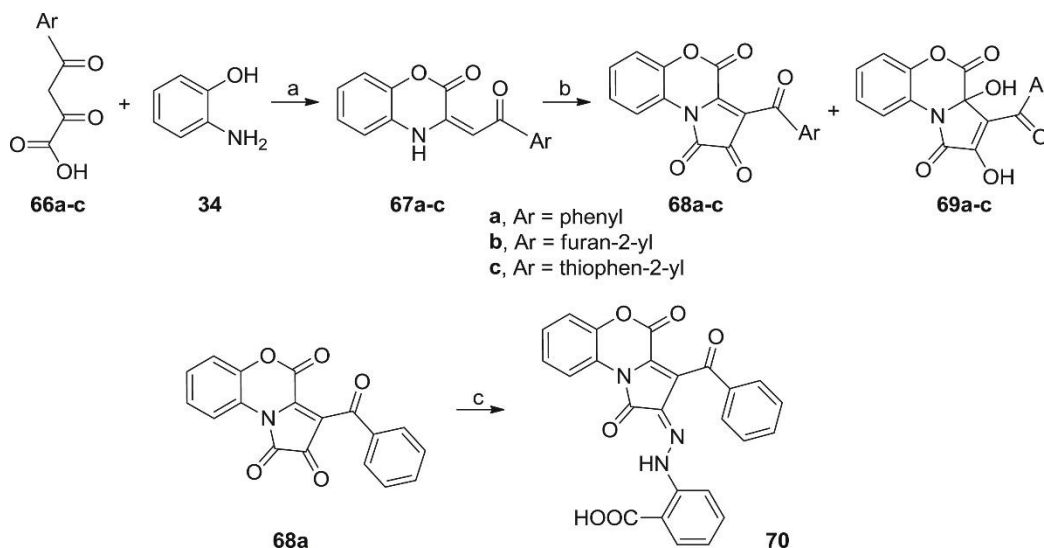
Figure 22. *Synthesis of 3-benzoyl-, 3-(furan-2-carbonyl)- and 3-(thiophene-2-carbonyl)-1H-benzo [b]pyrrolo[1,2-d][1,4]oxazine-1,2,4-trione **68a-c**, the by-products **69a-c** and the derivative **70**. Results and conditions: (a) 1,4-dioxane, reflux; (b) (COCl)₂, DCM, reflux; (c) phenylhydrazine, MeCN, reflux.*

Flash vacuum pyrolysis of methyl 3-(1-(2-(benzyloxy)phenyl)-1H-pyrrol-2-yl)acrylate (**71**) was reported to give a mixture of methyl 4H-benzo [b]pyrrolo[1,2-d][1,4]oxazine-4-carboxylate (**72**) and methyl 3-(1-(2-hydroxyphenyl)-1H-pyrrol-2-yl)acrylate (**73**), in 34 and 27% yield respectively (Figure 23). The result of this reaction was confirmed by an independent synthetic strategy [40].
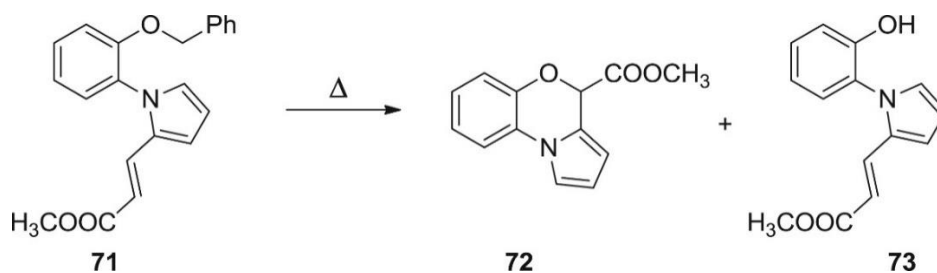
Figure 23. *Pyrolysis of compound **71**.*

In a patent dealing with the identification of protein kinase C (PKC) inhibitors, potentially useful as anticancer agents, variously substituted active derivatives were obtained by coupling 4H-benzo [b]pyrrolo[1,2-d][1,4]oxazin-8-amine (**74**) with appropriately substituted 2-chloro-5-fluoropyrimidines **75a,b**. Compounds **76a,b** (Figure 24) were so obtained and showed remarkable activity with IC$_{50}$ ranging from 0.25 to 5 μM in an *in vitro* inhibitory assay [41].
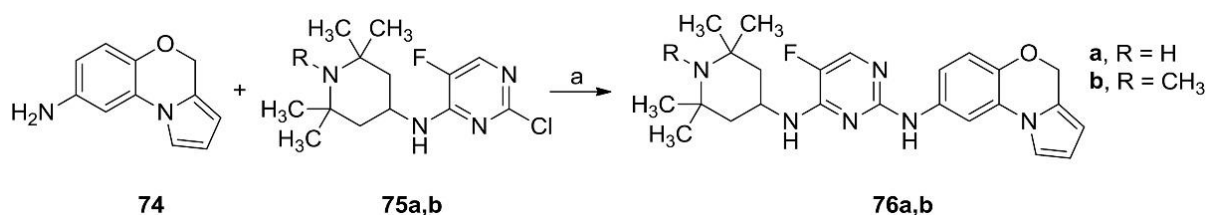
Figure 24. *Synthesis of compounds **76a,b**. Reagents and conditions: (a) TFA, 2-propanol, 100 °C.*

The 4*H*-benzo[*b*]pyrrolo[1,2-*d*][1,4]oxazine moiety embedded into a tetracyclic azaindolo[2,1-*c*][1,4]benzoxazine system was also obtained by reaction of di-lithiated 2-butoxycarbonylamino-3-methylpyridine (**77**) and Weinreb amide of 2-(2,4-difluorophenoxy)-2,2-dimethylacetic acid (**78**) followed by TFA treatment to give compound **79** [42]. Successively, the same research group published an in depth study on this reaction by which they obtained several compounds likely through an unusual N→C [1,4] Boc migration. In this way a series of carboxyl functionalized 7-azaindolo[2,1-*c*][1,4]benzoxazines were obtained. Two examples of this type of compounds are reported in Figure 25 (compound **80** and **81**) [43].
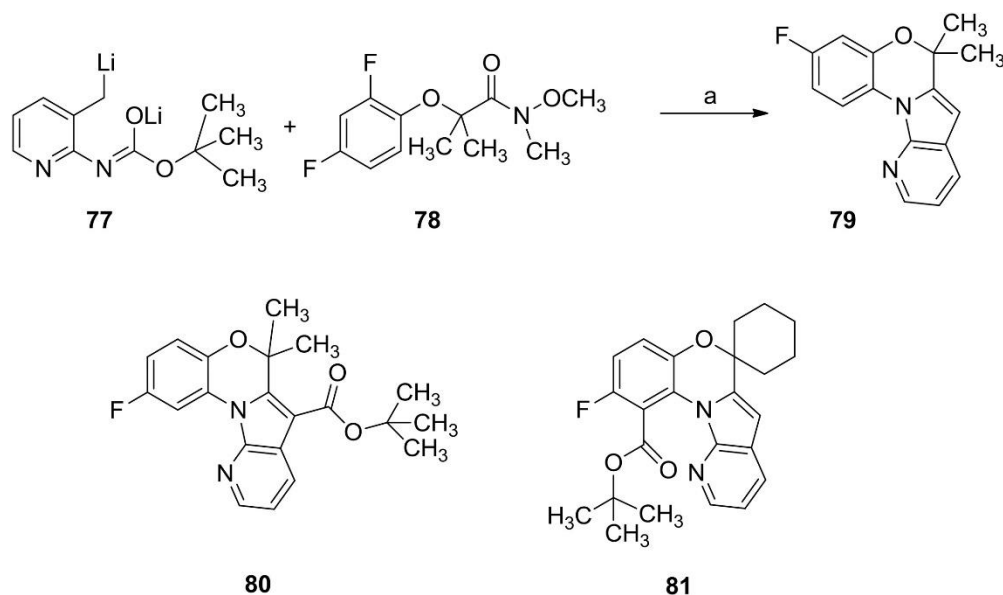
Figure 25. *Synthesis of 3-fluoro-6,6-dimethyl-6*H-*benzo [*b*]pyrido [3',2':4,5]pyrrolo[1,2-*d*][1,4]oxazine **79** and structure of compounds **80** and **81**. Reagents and conditions: (a) THF, −15 °C to rt, 1.5h, then TFA, DCM, 0 °C to rt, 0.5h.*

The 4*H*-benzo [*b*]pyrrolo[1,2-*d*][1,4]oxazine and the corresponding indole analog were obtained from pyrrole or indole carboxylate, respectively, linked to a pendant haloarene, by an intramolecular copper-catalyzed arylation promoted by MW irradiation. As an example, cyclization of 2-iodophenyl 1*H*-pyrrole-1-carboxylate (**82**) in the presence of CuI, *L*-proline and NaH gave compound **41**. Similarly, the reaction of indole analog **83** gave *6H*-benzo[5,6][1,4]oxazino [4,3-*a*]indol-6-one (**84**) (Figure 26) [44].
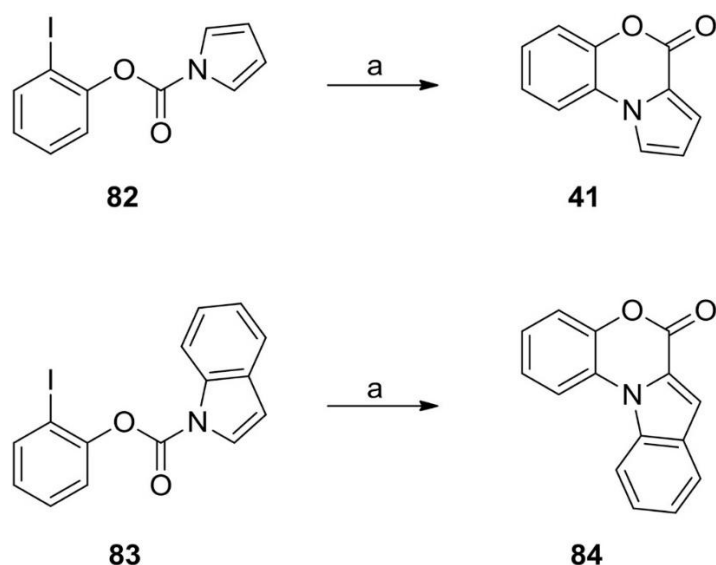
Figure 26. *Synthesis of compounds 41 and 84. Reagents and conditions: (a) CuI, L-proline, NaH, DMF.*

The tricyclic moiety of 4*H*-benzo [*b*]pyrrolo[1,2-*d*][1,4]oxazine could be also single out in a series of potent and metabolically stable benzopyrimido-pyrrolo-oxazinediones active as cystic fibrosis transmembrane conductance regulator (CFTR) inhibitors. These compounds were synthesized starting from a substituted 2-(1*H*-pyrrol-1-yl)phenol by a TFA catalyzed reaction with a furfural derivative. The most active compound was prepared starting from ethyl 3-(1,3-dimethyl-2,4-dioxo-5-phenyl-3,4-dihydro-1*H*-pyrrolo[3,4-*d*]pyrimidin-6(2*H*)-yl)-4-hydroxybenzoate (**85**) to give the cyclized product **86**, in a two-step procedure (Figure 27). This compound completely inhibited CFTR with an IC_{50} value of 8 nM and prevented cyst growth with IC_{50} of 100 nM in an embryonic kidney culture model [45,46].
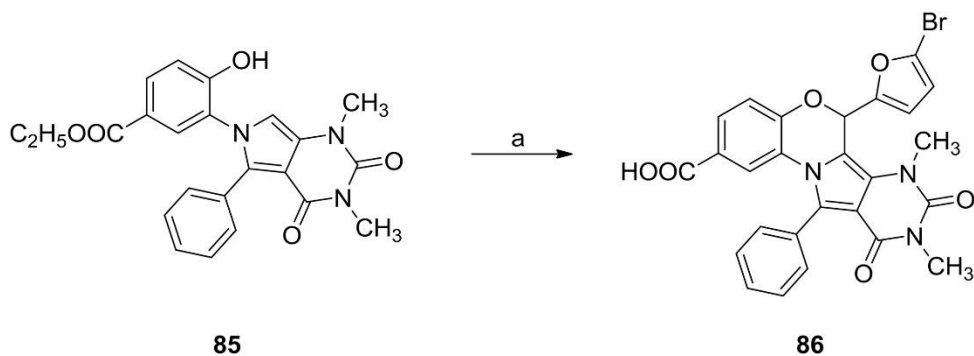
Figure 27. *Synthesis of 6-(5-bromofuran-2-yl)-7,9-dimethyl-8,10-dioxo-11-phenyl-7,8,9,10-tetrahydro-6H-benzo [*b*]pyrimido [4',5':3,4]pyrrolo[1,2-*d*][1,4]oxazine-2-carboxylic acid 86. Reagents and conditions: (a) 5-bromofurfural, TFA, CHCl₃, 150 °C, then KOH, THF/H₂O, then HCl workup.*

A large series of spiro [chromene-piperidine] derivatives including the tricyclic basic system and their channel modulatory activity measurements has been reported in a patent. A noteworthy activity towards Nav1.7 ion channel cell line was found for 1'-(3-hydroxy-2-methoxybenzoyl)spiro[benzo[*b*]pyrrolo[1,2-*d*][1,4]oxazine-4,4'-piperidine]-1-carbonitrile (**87**) (IC_{50} < 2 μM) [47,48]. Nav1.7 ion channel have been shown to be involved in pain transmission. In a recent patent dealing with tricyclic sulfonamide derivatives claimed as methionyl aminopeptidase 2 modulators, thus potentially useful in cancer and rheumatoid

arthritis treatment, several 4*H*-benzo[*b*]pyrrolo[1,2-*d*][1,4]oxazines were prepared. The most interesting compound (*Z*)-7-(2-(3-(diethylamino)prop-1-en-1-yl)-4-fluorophenylsulfonamido)-4*H*-benzo[*b*]pyrrolo[1,2-*d*][1,4]oxazine-6-carboxylic acid (**88**) was tested in a recombinant human assay showing IC$_{50}$ value < 0.05 µM [49]. A derivative of the title tricyclic system, namely 1-amino-2-(1*H*-benzo[*d*]rimethyl-2-yl)-8-methyl-3a,4-dihydro-3*H*-benzo[*b*]pyrrolo[1,2-*d*][1,4]oxazin-3-one (**89**) was reported in a patent dealing with the identification of opioid receptors modulators [50]. The reaction of above mentioned amine derivative **64** with 2-chloroquinoxaline or 3,4,5-trimethoxybenzoyl chloride gave compounds **90** and **91**, respectively. Both compounds were demonstrated active as selective G-protein coupled estrogen receptor antagonists and thus useful as potential agents for breast cancer treatment. The structures of this series of compounds are reported in Figure 28 [51].
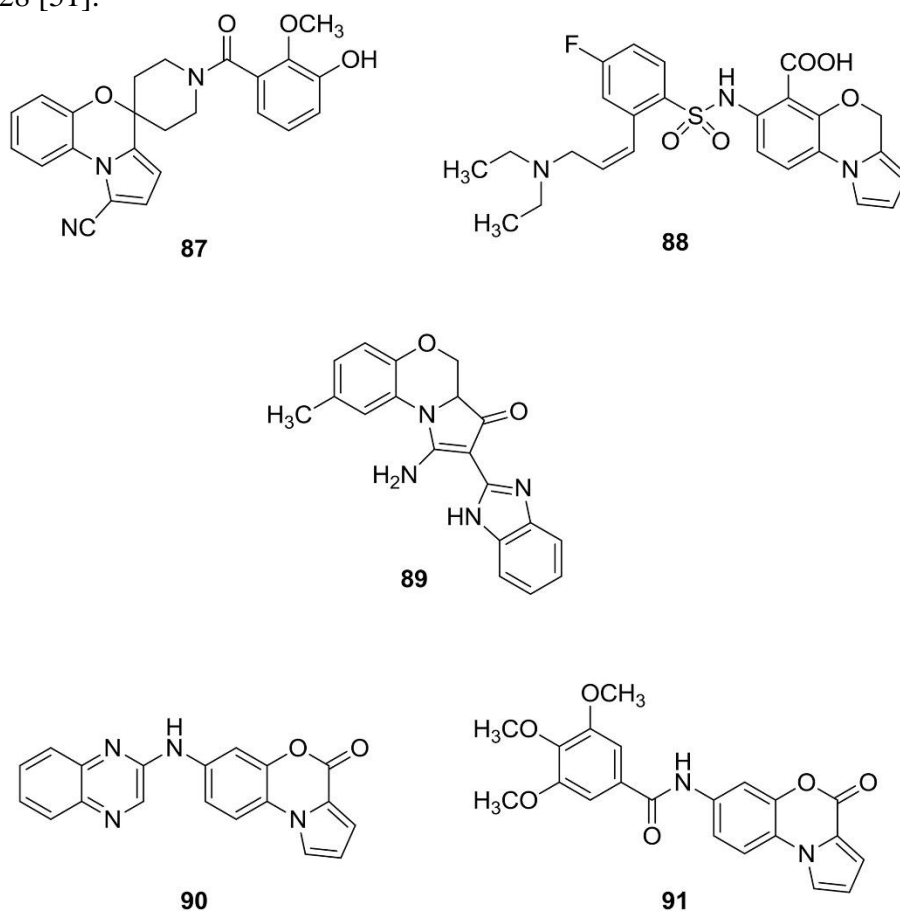
Figure 28. *Structure of compounds 87–91.*

4. 5*H*-Benzo[*e*]pyrrolo[1,2-*c*][1,3]oxazine D

A first paper dealing with the synthesis of nitrogen heterocyclic analogs of cannabinoids (CB) reported the cyclization of 2-(1*H*-indol-2-yl)phenol (**92**) with acetone in the presence of *p*-toluensulphonyl chloride to give the title heterocyclic skeleton, although comprised in the tetracylic system of compound **93** (Figure 29). Several substituted analogs described in successive papers were obtained following the same procedure [52-54]. Such derivatives could result useful for the treatment of several auto-immune pathologies as well as chronic pain and cancer.
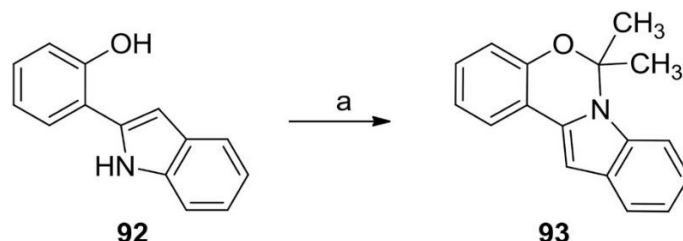
Figure 29. *Synthesis of 6,6-dimethyl-6H-benzo[5,6][1,3]oxazino [3,4-a]indole 93. Reagents and conditions: (a) acetone, tosyl chloride, reflux, 50h.*

Thermal rearrangement of ethyl 1a,1b,6b,6c-tetrahydro-1*H*-benzofuro [2′,3′:3,4] cyclobuta [1,2-*b*]azirine-1-carboxylates **94a-c** gave the corresponding 4-oxo derivatives of the title tricyclic system **95a-c** (Fig. 30) together with some related derivatives [55].
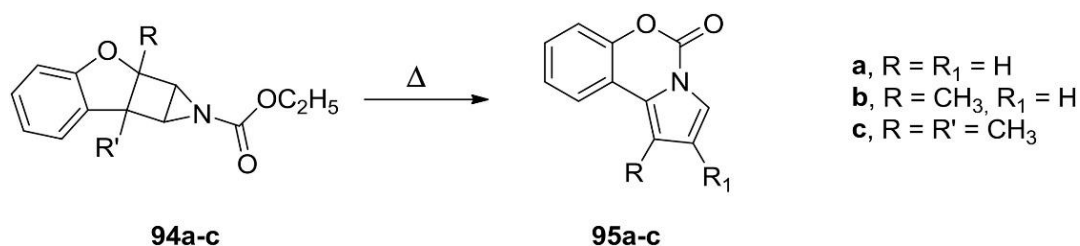
Figure 30. *Thermal rearrangement to 4H-benzo[b]pyrrolo[1,2-d][1,4]oxazin-4-ones 95a-c.*

The **D** tricyclic skeleton embedded in a tetracyclic system was obtained by a synthetic strategy involving a trifluoroacetic acid catalyzed cyclization of an opportunely *N*-substituted 3-hydroxyisoindolin-1-one as a key step. Representatively, reaction of *N*-(chloromethyl)phthalimide (**96**) with phenol gave 2-(phenoxymethyl)isoindoline-1,3-dione (**97**) which was subjected to reduction to give carbinol **98** in turn cyclized to compound **99** (Figure 31). Several substituted derivatives were then obtained by use of variously substituted phenols [56]. Another research group achieved a similar cyclization acting on the acetyl ester of **98** by the action of Bi(OTf)$_3$ as the catalyst [57].
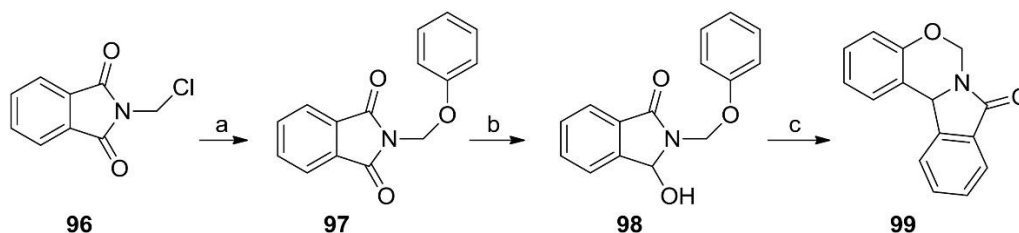
Figure 31. *Synthesis of 6H-benzo[5,6][1,3]oxazino [4,3-a]isoindol-8 (12bH)-one 99. Reagents and conditions: (a) phenol, MeONa, DMF, rt, 12h; (b) NaBH₄, MeOH, 0–5 °C, 1h; (c) TFA, rt, 12h.*

The cyclization of an indole precursor **100** led to the tetracyclic derivative **101**, containing the title system. Compound **101** showed a moderate activity as hepatitis C virus (HCV) NS5B RNA polymerase inhibitor (IC$_{50}$ = 0.14 μM) [58]. A similar activity was detected for a series of thienopyrrole derivatives structurally related to previously cited tetracyclic indoles. During this search, 11-cyclohexyl-8-methyl-6*H*-benzo [*e*]thieno [2′,3′:4,5]pyrrolo[1,2-*c*][1,3]oxazine-9-carboxylic acid (**102**) was obtained as a by-product (Figure 32) [59].
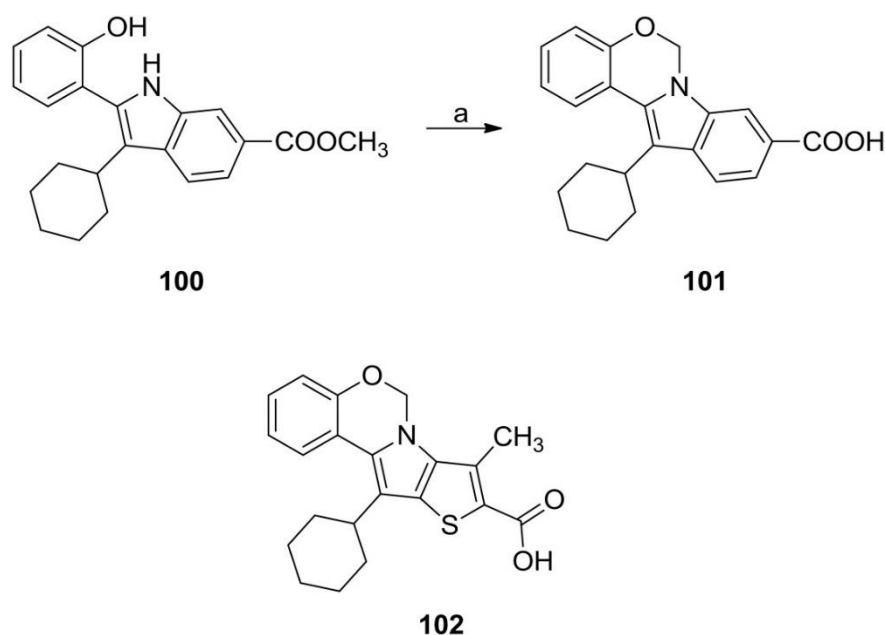
Figure 32. *Synthesis of 12-cyclohexyl-6H-benzo[5,6][1,3]oxazino [3,4-a]indole-9-carboxylic acid **101** and structure of analog **102**. Reagents and conditions: (a) CH$_2$Br$_2$, K$_2$CO$_3$, <u>acetone</u>, then NaOH, THF/H$_2$O.*

A number of indole derivatives, comprising the title tricyclic scaffold, in which a tetracyclic system acts as a tether linking two symmetric chains containing a valine residue in turn linked to an imidazole-pyrrolidine moiety was described in several patents and tested as HCV NS5B RNA polymerase inhibitors. Representatively, 5-bromo-2-(5-bromo-3-fluoro-1*H*-indol-2-yl)phenol (**103**) was cyclized to give the tetracyclic derivative **104**, in turn converted into the final compound **105**, which showed an IC$_{50}$ value of 0.001 nM [60-68]. In a successive paper, following a similar synthetic approach, compound MK-8742 (Elbasvir) **106** was prepared and recognized as a direct-acting antiviral agent, able to prevent viral replication in several HCV genotypes [69-71]. Intensive SAR studies have been carried out in order to identify more potent analogs against resistant HCV variants [72-74]. In a number of papers produced by the same research group, several active derivatives with a similar structural architecture have been described and deeply investigated for their antiviral activity. A novel series of chromane containing NS5A inhibitors have been accordingly identified. The most active compounds **107** and **108** showed EC$_{90}$ values ranging from 0.003 to 0.5 nM [75]. The best result was finally reached with the identification of 2-cyclopropylthiazole derivative **109** (Ruzasvir, MK-8408, EC$_{90}$ from 0.003 to 0.067 nM) which is presently undergoing clinical trials (Figure 33) [76].
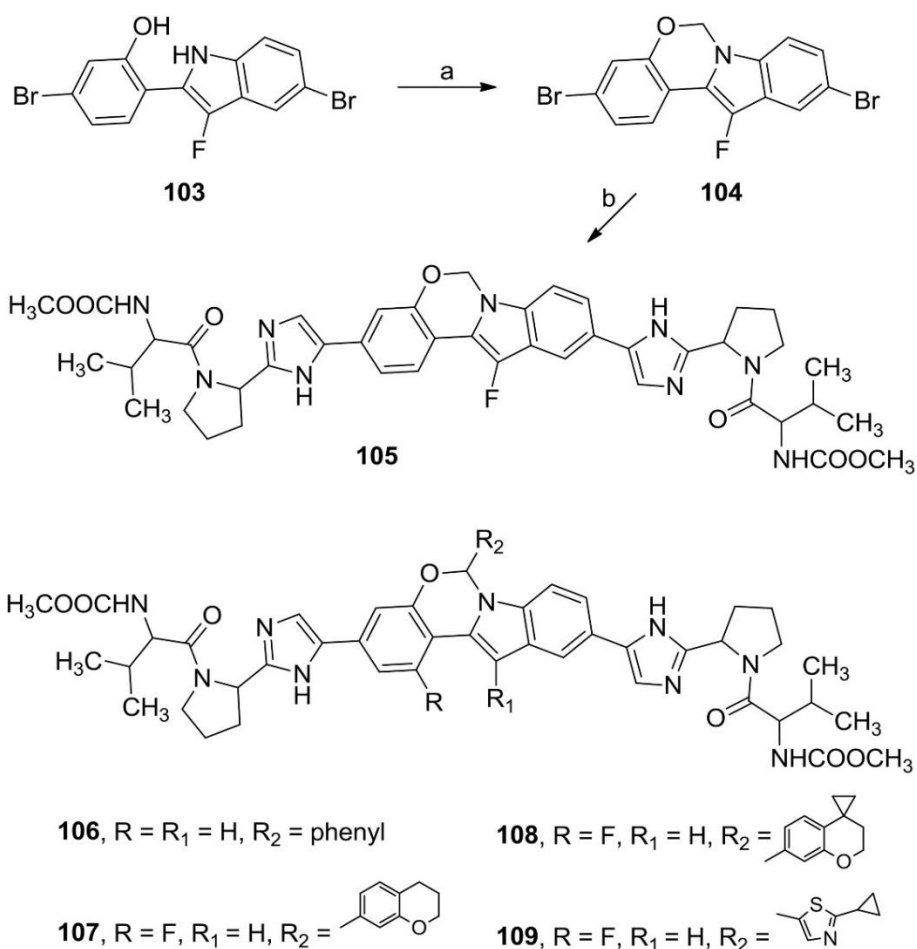
Figure 33. *Synthesis of dimethyl ((2,2'-(5,5'-(12-fluoro-6H-benzo[5,6][1,3]oxazino [3,4-a]indole-3,10-diyl)bis (1H-imidazole-5,2-diyl))bis (pyrrolidine-2,1-diyl))bis(3-methyl-1-oxobutane-2,1-diyl))dicarbamate **105** and structure of analogs **106–109**. Reagents and conditions: (a) CH₂Br₂, K₂CO₃, DMF, 80 °C, 5h; (b) pinacol borate, Pd (dppf)Cl₂, AcOK, 1,4-dioxane, 80 °C, 3h, then t-butyl 2-(2-bromo-1H-imidazol-5-yl)pyrrolidin-1-carboxylate, Pd (dppf)Cl₂, Na₂CO₃, THF/H₂O, 75 °C, 12h; then HCl, MeOH; then 2-(methoxycarbonylamino)-3-methylbutanoic acid, DIPEA, MeCN, BOP, rt.*

In a further series of patents the same tetracyclic system was appended to a variously substituted benzofuran to obtain a large number of antiviral agents acting on the same enzyme, although at higher concentrations than preceding derivatives. The structure of two representative analogs **110** and **111** are reported in Figure 34 [77-79].

110, R = R₁ = H, R₂ = 2-oxopyrrolidin-1-yl
111, R = Cl, R₁ = cyclopropyl, R₂ = N(CH₃)SO₂CH₃
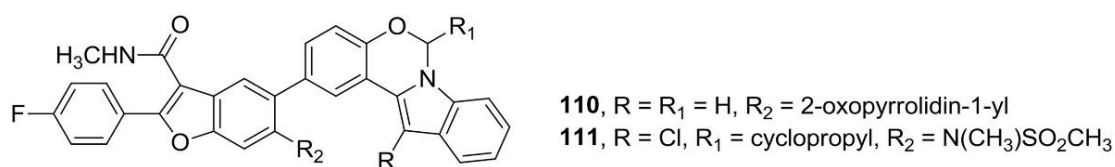
Figure 34. *Structure of derivatives 110 and 111.*

Cyclization of *N*-benzyloxymethylindolylmaleimide (**112**), bearing a fully protected glucosyl moiety attached to the indole nitrogen, with *p*-benzoquinone gave the spiro intermediate **113** referable to a 5*H*-benzo [*e*]pyrrolo[1,2-*c*][1,3]oxazine skeleton. This latter was deprotected to give compound **114**, which showed a checkpoint kinase 1 inhibitory property with an IC_{50} value of 1.92 μM, together with a moderate *in vitro* antiproliferative activity (Figure 35) [80].
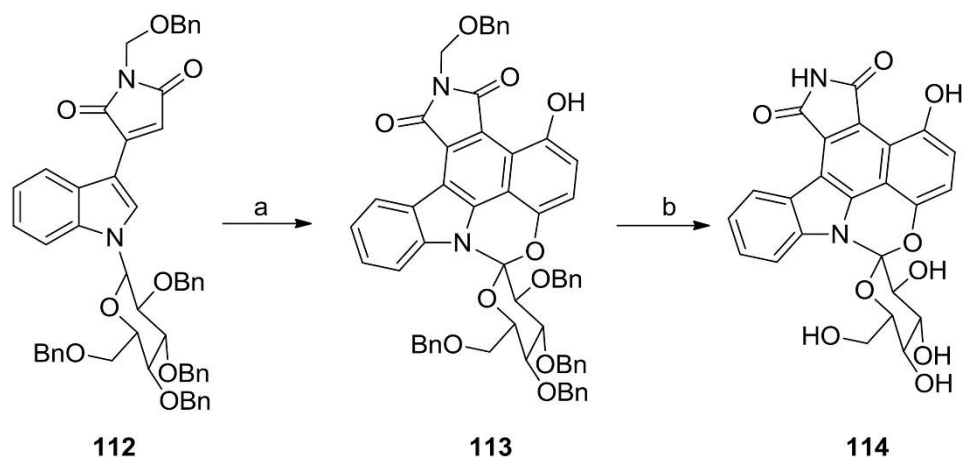
Figure 35. Synthesis of (2′R,3′S,4′R,5′R, 6′S)-3′,4,4′,5′-tetrahydroxy-6'-(hydroxymethyl)-3′,4′,5′,6′-tetrahydro-1*H*-spiro[7-oxa-2,8a-diazabenzo[*cd*]cyclopenta [*a*]fluoranthene-8,2′-pyran]-1,3(2*H*)-dione **114**. Reagents and conditions: (a) *p*-benzoquinone, toluene; (b) H2, Pd(OH)2, then NH4OH, THF/MeOH, rt, 12h.

5. 5*H*-Benzo[*d*]pyrrolo[2,1-*b*][1,3]oxazine E

A first publication reporting a lactone derived from the title system appeared in 1933. Prolonged heating of 2-(2-carboxyphenyl)-1-hydroxy-3-oxoisoindoline-1-carboxylic acid (**115**) resulted in the cyclization to compound **116**, the structure of which was elucidated by chemical proofs (Figure 36). This last compound was obtained in a separate study and its structure was accordingly confirmed [81,82]. More recently, the same lactone was successfully synthesized by condensation of 2-formylbenzoic acid (**17**) with 2-aminobenzoic acid (**117**) [83].
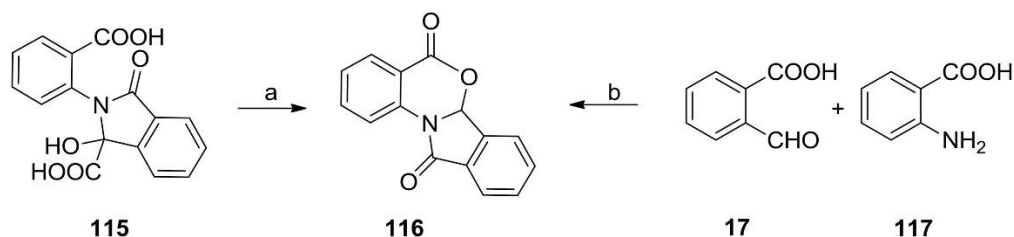
Figure 36. *Synthetic approaches to 5*H-*benzo[4,5][1,3]oxazino [2,3-*a*]isoindole-5,11 (6a*H*)-dione **116**. Reagents and conditions: (a) 170–190 °C; (b) EtOH, reflux.*

Starting from 2-(1*H*-pyrrol-1-yl)benzoic acid (**118**) the tricyclic lactone 1*H*-benzo[*d*]pyrrolo[2,1-*b*][1,3]oxazine-1,5(3a*H*)-dione (**119**) was obtained by treatment with singlet oxygen, during studies aimed to the synthesis of antitumoral Mitomycin antibiotics. Successive hydrogenation gave rise to the saturated analog **120** [84]. Successively, the same research group attempted photooxydation of (3,5-

dimethoxy-2-(1*H*-pyrrol-1-yl)phenyl)methanol (**121**) to obtain the corresponding tricyclic derivative **122** preserving the pyrrole aromaticity (Figure 37) [85].
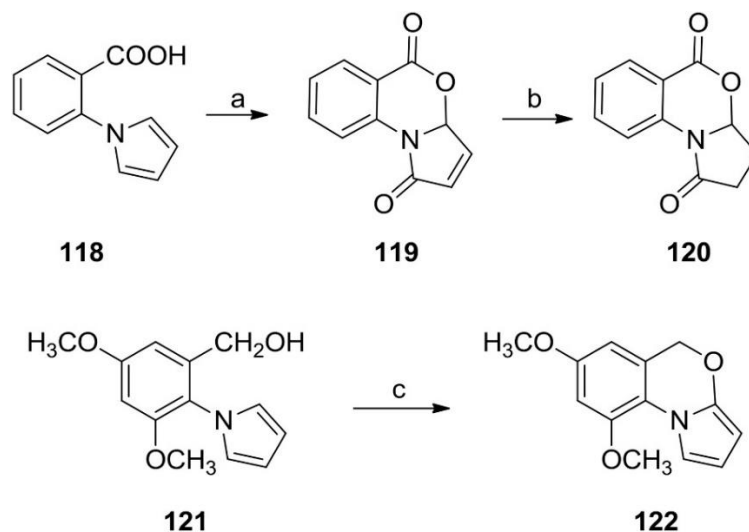

Figure 37. *Synthesis of 3,3a-dihydro-1H-benzo[d]pyrrolo[2,1-b][1,3]oxazine-1,5(2H)-dione 120 and 7,9-dimethoxy-5H-benzo[d]pyrrolo[2,1-b][1,3]oxazine 122. Reagents and conditions: (a) irradiation, $^1O_2$, DCM; (b) Pd(C), acetone, 20min; (c) irradiation, $^1O_2$, MeOH.*

Chlorination of 2-(2-carboxybenzamido)benzoic acid (**123**) with $SOCl_2$ followed by treatment with methanol gave the cyclization to 6a-methoxy-5*H*-benzo[4,5][1,3]oxazino[2,3-*a*]isoindole-5,11(6a*H*)-dione (**124**), a tetracyclic derivative of the title system (Figure 38). Further elaboration of compound **123** gave the demethoxy analog **116** [86].
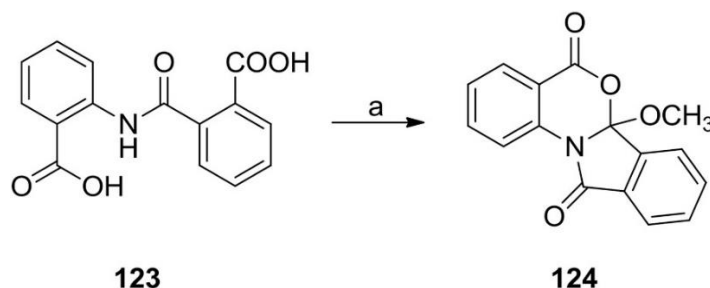
Figure 38. *Synthesis of compound 124. Reagents and conditions: (a) SOCl$_2$, then MeOH.*

In a representative synthetic pathway, double cyclization of 2-(*N*-(carboxymethyl)acetamido)benzoic acid (**125**) with acetic anhydride led to tricyclic compound **126**, which was subjected to selective hydrolysis with acetic acid to give compound **127** (Figure 39). These compounds were studied for both synthetic purposes and thermodynamic analysis applications [87-91].
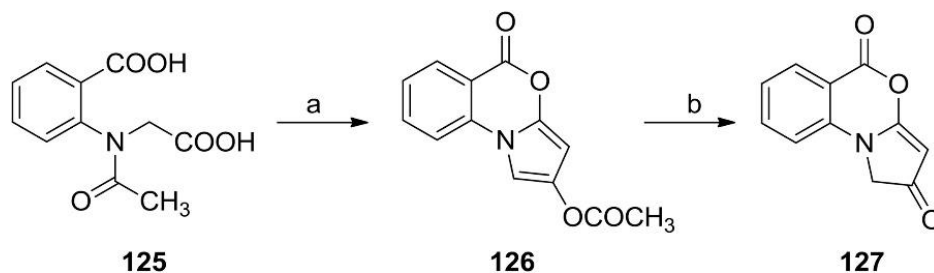
Figure 39. Synthesis of 5-oxo-5H-benzo [d]pyrrolo[2,1-b][1,3]oxazin-2-yl acetate **126** and 1H-benzo [d]pyrrolo [2,1-b] [1,3]oxazine-2,5-dione **127**. Reagents and conditions: (a) Ac₂O, reflux; (b) AcOH.

In a study aimed to the preparation of sulfone-containing heterocycles, one-pot reaction of diethyl 2-(2-bromo-1-phenyl-2-(phenylsulfonyl)ethylidene)malonate (**128a**) and anthranilonitrile (**129**) in dioxane/triethylamine solution led to the corresponding tricyclic derivative **130a** (Figure 40). The corresponding 2-(4-chlorophenyl) derivative **130b** was obtained in the same way starting from chloro derivative **128b** [92,93]. A similar approach was also described in separate studies [94-96].
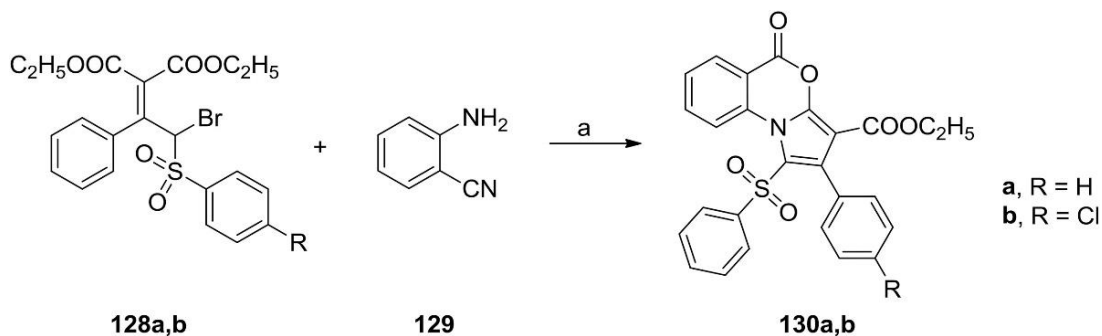
Figure 40. Synthesis of ethyl 5-oxo-2-phenyl-1-(phenylsulfonyl)-5H-benzo[d]pyrrolo[2,1-b][1,3]oxazine-3-carboxylate **130a** and its chloro derivative **130b**. Reagents and conditions: (a) Et₃N, 1,4-dioxane, reflux, 3h, then dil. HCl.

Acid catalyzed cyclization of 3-hydroxy-2-(2-(hydroxymethyl)phenyl)isoindolin-1-one (**131**) led to tetracyclic compound **132**, containing the skeleton of the title system (Figure 41). The synthetic method was applied to the synthesis of some substituted diastereoisomeric derivatives [97].
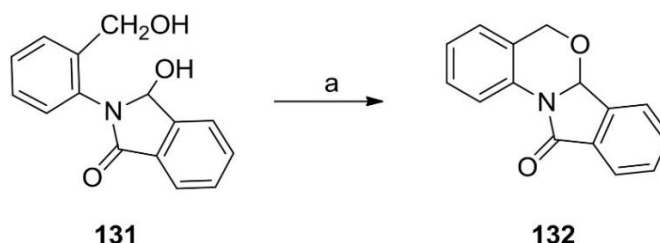
Figure 41. Synthesis of 5H-benzo[4,5][1,3]oxazino [2,3-a]isoindol-11(6aH)-one **132**. Reagents and conditions: (a) PTSA, DCM.

Terresoxazine (**133**) (Figure 42), a compound with an **E** skeleton, was isolated from the plant *Tribulus terrestris*, used for a long time in the treatment of a number of diseases in Chinese folk medicine. Its structure was elucidated by crystallographic analysis [98,99].
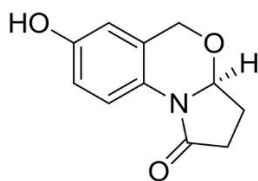
Figure 42. *Structure of Terresoxazine, (S)-7-Hydroxy-2,3,3a,5-tetrahydro-1H-benzo [d]pyrrolo[2,1-b][1,3]oxazin-1-one **133**.*

Reaction of 2-aminobenzoic acid (**117**) with maleic anhydride (**134**) gave 1,5-dioxo-3a,5-dihydro-1*H*-benzo [*d*]pyrrolo[2,1-*b*][1,3]oxazin-3a-yl acetate (**135**) in a two-step fashion with very good yield (Figure 43). The tricyclic derivative showed activity as acetylcholinesterase inhibitor with a Ki value of 4.7 µM, with a therapeutic potential in the management of neuro-degenerative diseases [100].
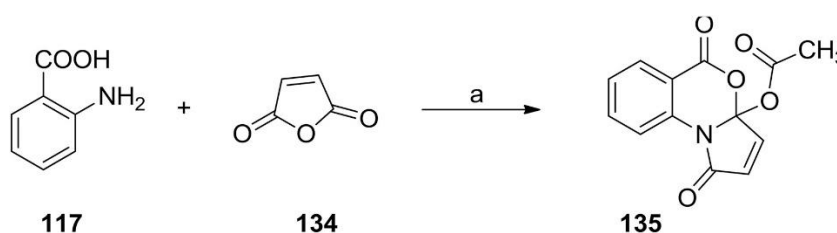
Figure 43. *Synthesis of compound **135**. Reagents and conditions: (a) rt, 2h, then Ac₂O, AcONa, 60 °C, 3h.*

During a research project on the identification of DNA gyrase inhibitors with antibacterial properties, the reaction of salicylic aldehydes and a proper aniline derivative gave a small series of tetracyclic compounds based on the title system. The most active compound **136** showed a moderate activity in an *in vitro E. coli* DNA gyrase supercoiling assay with a maximal non-effective concentration value of 0.5 µg/mL and activity in a panel of bacterial assays with MIC ranging from 2 to 8 µg/mL [101]. Structurally similar isoindolobenzoxazinones were synthesized by reaction of substituted 2-formyl benzoic acids with 2-aminophenyl carbinol derivatives, as already mentioned. One of the compounds obtained **137** (Figure 44) showed protective properties against action of herbicides on plants [10,102].
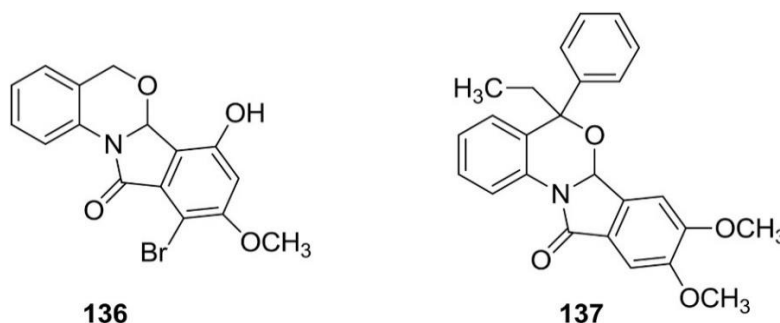

Figure 44. *Structure of 10-bromo-7-hydroxy-9-methoxy-5H-benzo[4,5][1,3]oxazino[2,3-a]isoindol-11 (6aH)-one **136** and its structural analog **137**.*

The acid **118** was subjected to direct cyclization by action of activated MnO₂, to directly give lactone **138** in good yield. The same procedure was applied to several substituted derivatives, including acid **139**, which gave indole analog **140** (Figure 45). Some

derivatives of these systems have been successively tested for their anti-proliferative activity [103].
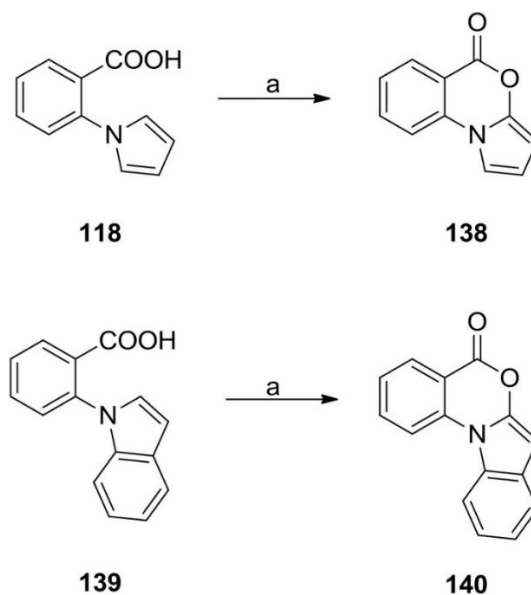

118 → **138**

139 → **140**

Figure 45. *Synthesis of 5*H-*benzo [*d*]pyrrolo[2,1-*b*][1,3]oxazin-5-one **138** and 5H-benzo[4,5][1,3]oxazino [3,2-*a*]indol-5-one **140**. Reagents and conditions: (a) MnO₂, toluene, reflux.*

6. [1,4]Oxazino[2,3,4-*hi*]indole G

Derivatives of the title heterocyclic system, although comprised in a larger structure, were reported first in a patent of 1977 focusing on the discovery of sedative agents. 5-Methyl-1,2,7,8,9,10-hexahydro-[1,4]oxazino[2,3,4-*hi*]pyrido[4,3-*b*]indole (**141**) (Fig. 46), a representative example of this series of compounds, showed a sedative *in vivo* effect with a minimal effective dose of 1 mg/kg in mice [104].
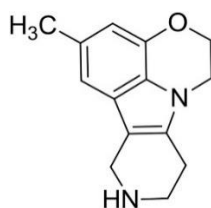

Figure 46. *Structure of compound **141**.*

A French patent appeared in 1986 reported the synthesis of derivatives of the title system endowed with antidepressant activity. As an example, the reaction of 4-amino-3,4-dihydro-2*H*-1,4-benzoxazine (**142**) with ethyl 2-oxopropanoate (**143**) gave ethyl 2,3-dihydro-[1,4]oxazino[2,3,4-*hi*]indole-5-carboxylate (**144**), which was in turn converted into the derivative **145** (Fig. 47) [105].
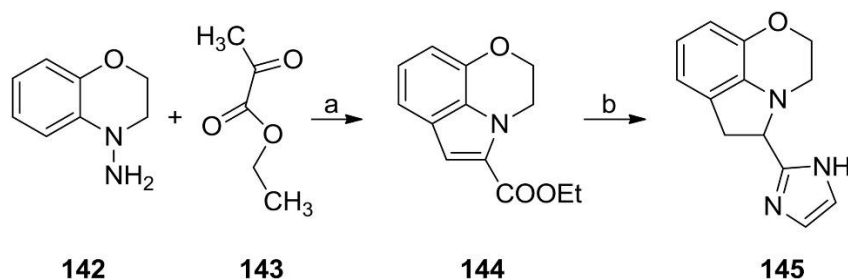
Figure 47. *Synthesis of 5-(1H-imidazol-2-yl)-2,3,5,6-tetrahydro-[1,4]oxazino[2,3,4-hi]indole 145. Reagents and conditions: (a) EtOH, reflux, then dry HCl; (b) H₂, Sn, dry HCl, EtOH, −50 °C, then Me₃Al, ethylenediamine, toluene, 5 min.*

The ester **144** was also utilized as intermediate for the preparation of several derivatives endowed with different pharmacological activities [106]. A series of potent CB1 receptor agonists was obtained from a derivative of above ester bearing a cyclohexyl moiety at position 3 of the tricyclic system. Some compounds showed promising therapeutic potential for the treatment of neuropathic pain and autoimmune disorders. The most representative compound (*R*)-(3-cyclohexyl-2,3-dihydro-[1,4]oxazino[2,3,4-*hi*]indol-6-yl)(4-ethylpiperazin-1-yl)methanone (**146**) and its analogs **147**–**149** resulted active with EC_{50} values ranging from 7.5 to 8.3 on a CB1 binding assay [107-109]. A similar synthetic approach was expanded to the synthesis of potent inhibitors of myeloid cell leukemia-1 (Mcl-1), potentially useful anticancer agents. The most representative compound 9-chloro-6-(3-(4-chloro-3,5-dimethylphenoxy)propyl)-2,3-dihydro[1,4]oxazino [2,3,4-*hi*]indole-5-carboxylic acid (**150**) showed a Ki of 9 nM in a Mcl-1 binding assay [110]. A series of spiro derivatives with the tetracyclic skeleton **151**, comprising the title system, were prepared and claimed as aldose reductase inhibitors, then useful for reduction and prevention of chronic diabetic complications (Figure 48) [111].
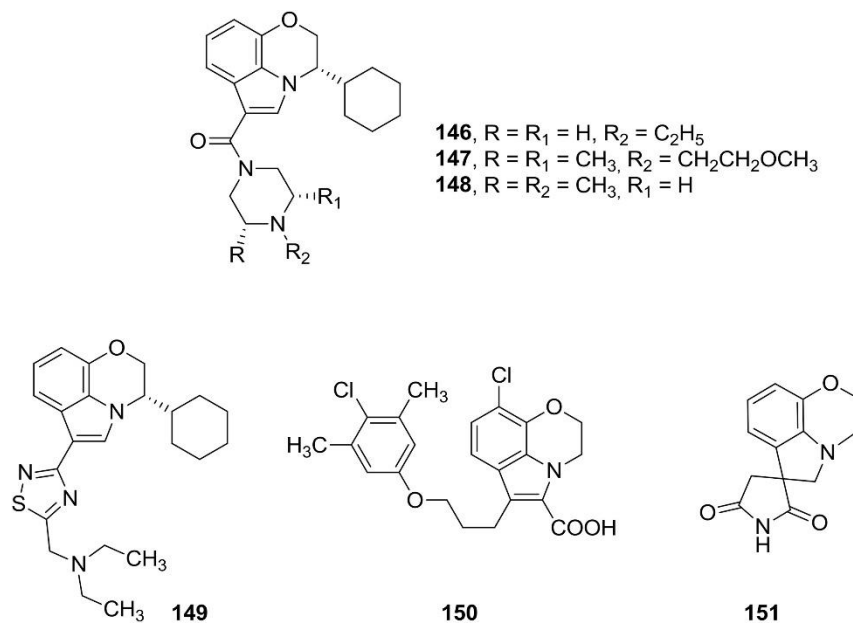

Figure 48. *Structure of [1,4]oxazino[2,3,4-*hi*]indoles **146**–**151**.*

A series of tetracyclic derivatives, comprising the title system, and bearing an imidazole side-chain were prepared and claimed as potent 5-HT$_3$ receptor antagonists. The general structure **152** is reported in Figure 49 [112].
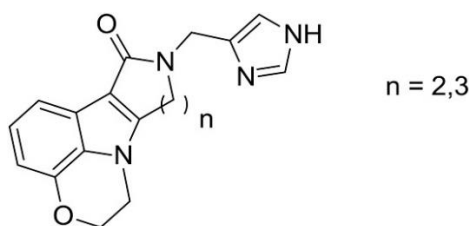

Figure 49. Scaffold of 5-HT$_3$ receptor antagonists 152.

An interesting anti-inflammatory compound **153** based on a [1,4]oxazino[2,3,4-*hi*]indole scaffold was obtained after a multistep synthetic strategy. This compound showed an ED$_{50}$ of 3.5 mg/kg in the acetic acid-induced writhing assay in rats [113]. In a search aimed to the identification of inhibitors of platelet activating-factor (PAF) induced aggregation, a number of α-(piperazinylalkyl)indoles was described in a German patent appeared in 1993 aimed to the discovery of anticoagulant agents. A significant example is represented by 5-methyl-6-(2-(4-(4-methylpyridin-2-yl)piperazin-1-yl)ethyl)-2,3-dihydro[1,4]oxazino[2,3,4-*hi*]indole (**154**) reported in Fig. 50 [114]. The same authors described, in a separate patent and in a paper, several analogs bearing the piperazin-containing chain linked to a different position of the tricyclic system. These compounds were tested as PAF activity antagonists as well as leukotriene synthesis inhibitors *in vitro* and as antihistaminic agents *in vivo*. The structure of the most representative compounds **155**–**156** are depicted in Figure 50 [115,116].
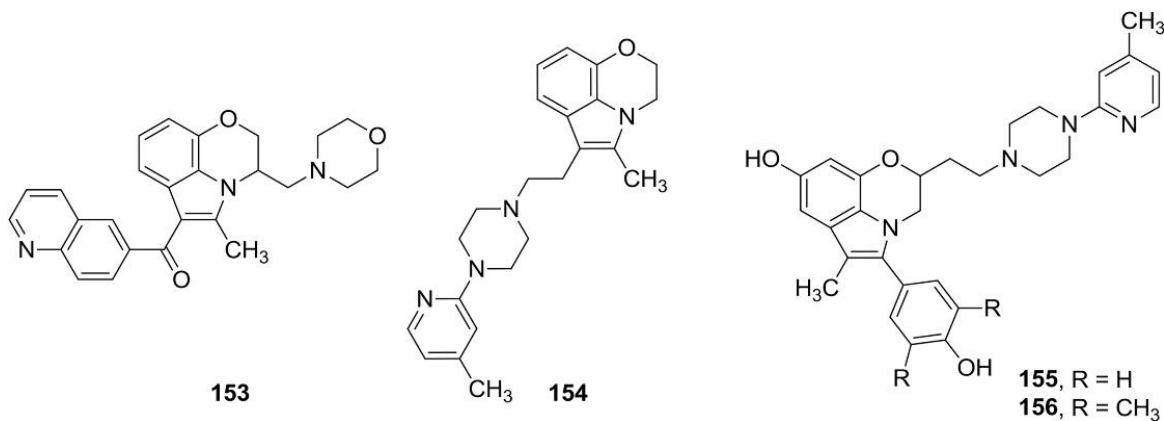

Figure 50. Structure of compounds 153–156.

Starting from 10*H*-phenoxazine (**50**), an intermediate pyrrolo[3,2,1-*kl*]phenoxazine-1,2-dione (**157**), containing the [1,4]oxazino[2,3,4-*hi*]indole skeleton, was obtained by action of oxalyl chloride. This latter compound was converted into the basic tetracyclic system **158** *via* borane reduction [117]. The same intermediate **157** led to a number of derivatives included in a patent dealing with the identification of agents useful for the treatment of cognitive and neurological disorders. Representative examples of such compounds are reported below (Figure 51, compounds **159** and **160**) [118].
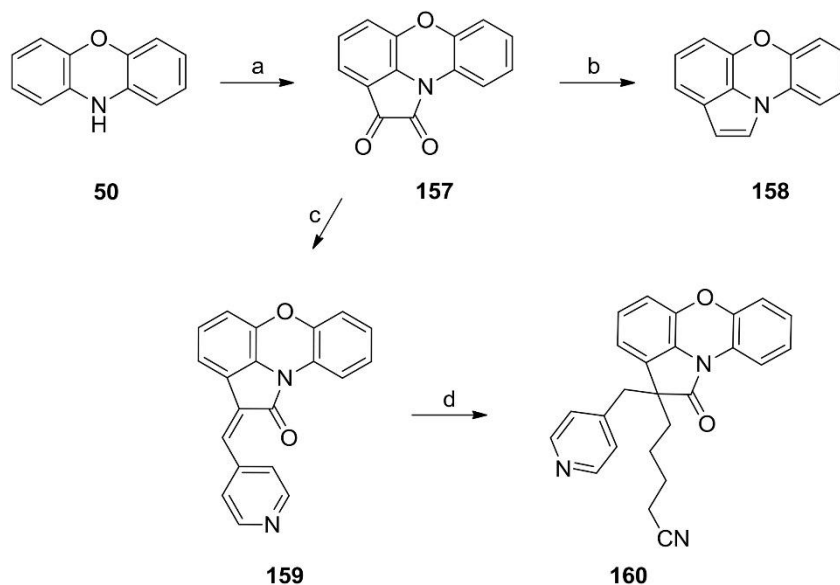
Figure 51. *Synthesis of pyrrolo[3,2,1-*kl*]phenoxazines **158–160**. Reagents and conditions: (a) (COCl)₂, THF, then AlCl₃, CS₂; (b) BH₃/THF, 0 °C, 24h; (c) 4-picoline, Ac₂O, AcOH, 110 °C, 45 min; (d) 5-bromovaleronitrile, NaH, THF, rt, 3 days.*

During the course of a research aimed to the identification of Na^+/H^+ exchange transport system inhibitors, compound **161** was described as an analog of 4*H*-pyrrolo[3,2,1-*ij*]quinolin-6(5*H*)-one system **162** (Figure 52) and showed remarkable activity [119].
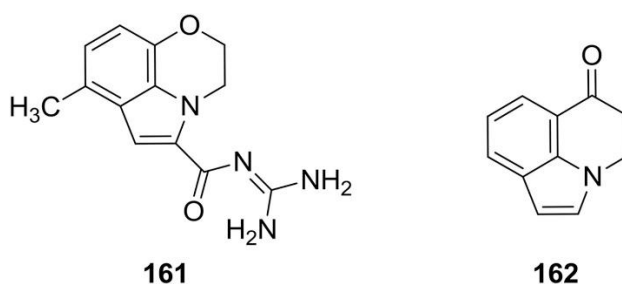

Figure 52. *Structures of* N-*(diaminomethylene)-7-methyl-2,3-dihydro[1,4]oxazino[2,3,4-*hi*]indole-5-carboxamide **161** and yrroloquinolinone **162**.*

In a study focusing on cannabimimetic aminoalkylindole derivatives, (*R*)-(5-methyl-3-(morpholinomethyl)-2,3-dihydro-[1,4]oxazino[2,3,4-*hi*]indol-6-yl)   (naphthalen-1-yl) methanone (**163**), named (+)-**WIN55212**, previously described as a potent agonist for the CB1 receptor, was used as comparison for the test of structurally simpler indole derivatives [120-122]. Moreover, the 5,7-ditritiated derivative of **163** was designed as CB1 receptor radioligand [123]. In the course of a separate research study on similarly active compounds, the diastereoisomers **164a** and **164b** were isolated and tested for their agonistic activity (Figure 53) [124].
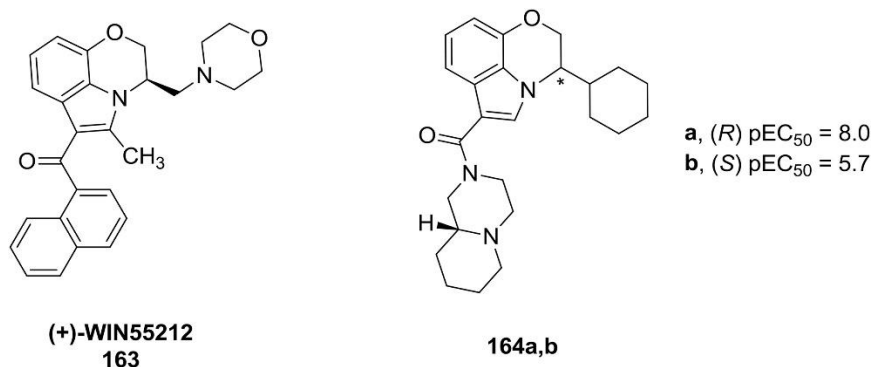
Figure 53. *Structure of (+)-WIN55212 **163** and derivatives **164a**,b.*

In a French patent application, the 2,3-dihydropyrrolo[1,2,3-*de*]-1,4-benzoxazine-5,6-dione (**165**) (Figure 54) was used as starting reagent for the preparation of 1,4-benzoxazines derivatives claimed as 5HT$_4$ receptor selective ligands [125]. Derivatives of the same starting material were used as intermediates for the synthesis of antibacterial agents related to ciprofloxacin [126].
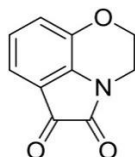

Figure 54. *Structure of compound **165**.*

Reaction of indolin-7-ol (**166**) and ethyl 2,3-dibromopropanoate (**167**) gave ethyl 2,3,5,6-tetrahydro-[1,4]oxazino[2,3,4-*hi*]indole-2-carboxylate (**168**), which was in turn converted into imidazoline derivative **169**. Dehydrogenation of compound **168** gave the corresponding 2,3-dihydro derivative **170**, similarly transformed into the analog **171** (Figure 55). Final compounds showed α-adrenergic receptor antagonistic activity in *in vitro* and *in vivo* assays, thus potentially useful as antihypertensive agents [127-129].
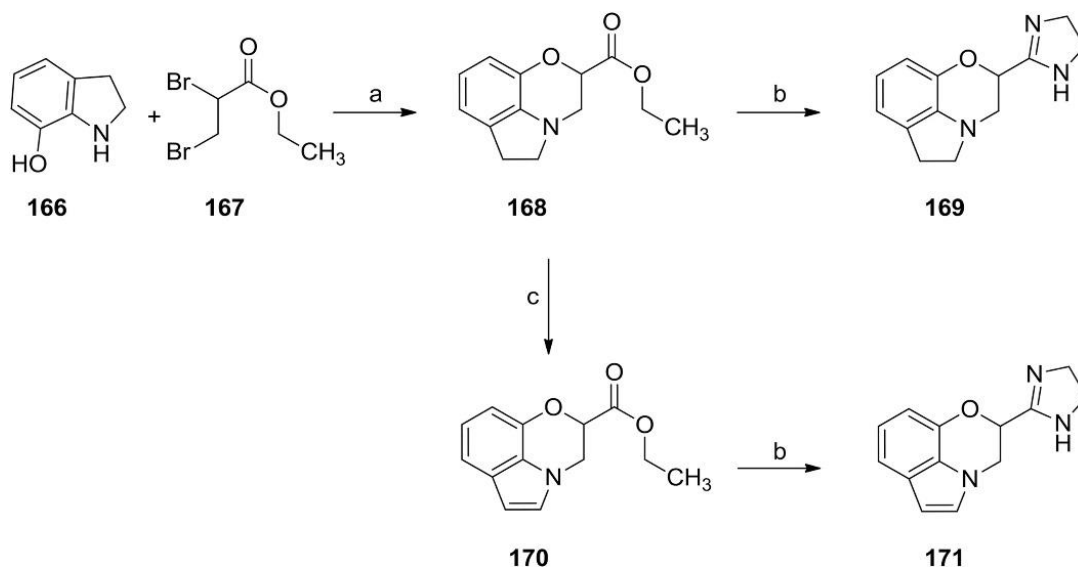

Figure 55. *Synthesis of α-adrenergic receptor antagonist 2-(4,5-dihydro-1H-imidazol-2-yl)-2,3,5,6-tetrahydro-[1,4]oxazino[2,3,4-hi]indole **169** and the corresponding 2,3-dihydro analog **171**. Reagents and conditions: (a) K$_2$CO$_3$, acetone; (b) Me$_3$Al, ethylenediamine, toluene, reflux; (c) DDQ, toluene, 0 °C.*

A series of azepinoindoles based on the tetracyclic skeleton 2,7,8,9,10,11-hexahydro-1*H*-azepino[4,5-*b*][1,4]oxazino[2,3,4-*hi*]indole (**172**), embedding the title tricyclic system, were described in two patents dealing with the identification of 5HT receptor ligands [130,131]. Similarly, a patent appeared in 2011 described the preparation and the activity on several SNC receptors of pyrido-indole tetracyclic analogs. Two examples **173** and **174** are reported below [132]. These compounds could result useful in the treatment of a variety of SNC disorders. Similar compounds bearing a substituted benzo fused ring instead of the azepine moiety were synthesized and tested as 5HT$_6$ receptor modulators. Among these compounds, (*R*)-2-[(1-phenyl-1,2-dihydro-1,4-oxazino[2,3,4-*jk*]carbazol-7-yl)oxy] ethanamine (**175**) and (*R*)-2-((2-((1-phenyl-1,2-dihydro- [1,4]oxazino[2,3,4-*jk*]carbazol-7-yl)oxy)ethyl)amino)ethanol (**176**) resulted as the most promising derivatives with a Ki of 1.8 and 3.0 nM, respectively, in a binding assay. Some aminoalkoxyindoles were studied for a similar application [133-135]. The two enantiomers relative to formula 177 were described during a search for novel, potent and selective 5-HT$_{2A}$/D$_2$ receptors antagonists with a potential atypical antipsychotic application (Figure 56) [136].
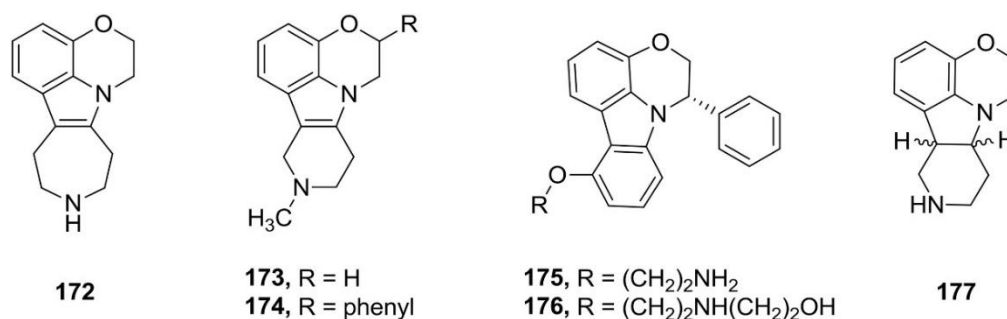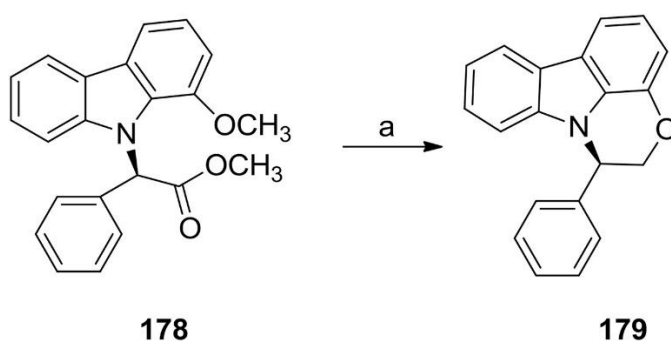

Figure 56. *Structure of azepine **172** and its SNC active analogs **173**–**177**.*

DIBAL-H reduction of (*R*)-methyl 2-(1-methoxy-9*H*-carbazol-9-yl)-2-phenylacetate (**178**) followed by the alcohol mesylation and one-step thermal cyclization/dealkylation gave tetracyclic compound **179** (Figure 57), which represents the structural core of a series of 5-HT$_6$ receptor antagonists [137].

Figure 57. *Synthesis of (*R*)-1-phenyl-1,2-dihydro-[1,4]oxazino[2,3,4-*jk*]carbazole **179**. Reagents and conditions: (a) DIBAL-H, then MsCl, Et$_3$N, then DMF, 155 °C.*

The pentacyclic compound **180** was isolated as the major product after an unwanted intramolecular cyclization reaction, during a search aimed to the discovery of anticancer agents related to Adriamycin [138]. A number of methanamine derivatives of the title tricyclic system was prepared and tested as 5HT receptors ligands potentially useful for the treatment of diseases in which such a receptor seems to be involved. The most representative

compound (8-(2,4-dichlorophenyl)-2,3,5,6-tetrahydro-[1,4]oxazino[2,3,4-*hi*]indol-6-yl) methanamine (**181**) is reported in Fig. 58 [139]. The installation of a proper side chain on the title tricyclic system and some of its analogs led to a class of potent and highly selective human β_3-adrenergic receptor agonists, with high cell permeability. A representative derivative **182** showing an EC_{50} of 0.92 nM and a good selectivity on β_3-receptor is reported below [140]. In two separate papers the synthesis of 1-oxo-1,2-dihydro-1,4-oxazino[2,3,4-*jk*]carbazole-4-carbaldehyde (**183**), a tetracyclic derivative of the title system, was easily obtained from 1-hydroxy-carbazole-2-carbaldehyde. The compound was then subjected to extensive crystallographic studies [38,141]. A patent application appeared in 2008 reported the synthesis of several derivatives of the title system characterized by a substituted carboxamide side chain. These compounds showed activity as antiviral agents and the most promising analog, namely 6-cyclohexyl-*N*-(*N*,*N*-dimethylsulfamoyl)-5-phenyl-2,3-dihydro-[1,4]oxazino[2,3,4-*hi*]indole-9-carboxamide (**184**) (Figure 58), presented an IC_{50} value lower than 10 µM in a HCV NS5B assay [142].
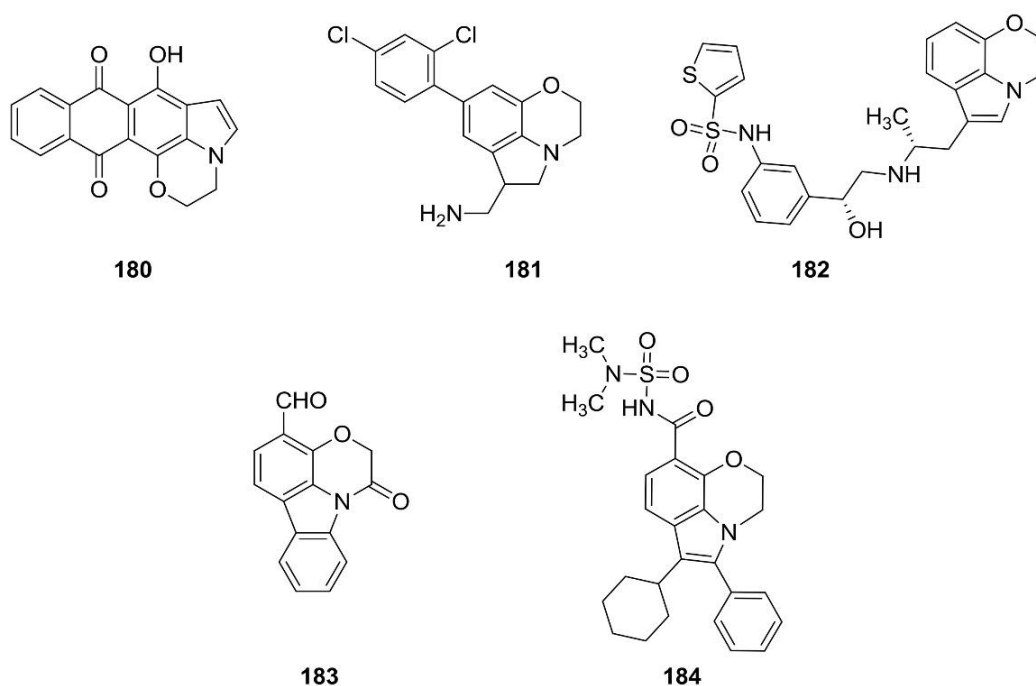
Figure 58. *Structure of 7-hydroxy-2,3-dihydronaphtho[2,3-*f*][1,4]oxazino[2,3,4-*hi]indole-8,13-dione **180** and derivatives **181**–**184**.*

A natural product of formula 185 (Fig. 59), a *seco* derivative of alkaloid Dichotine [143], based on the tricyclic title framework, was identified as a component of the crude extract of *Acanthopanax senticosus* studied for its anti-fatigue activity. The same compound was isolated successively from African breadfruit *Treculia africana* seed oil [144,145].

Figure 59. *General structure 185.*

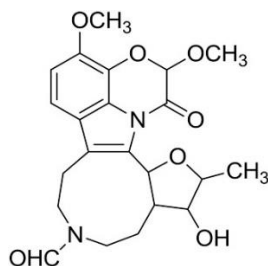Compounds assembled by linking two indolephenoxazine pentacyclic nuclei, containing the title system, by a simple bond or an aromatic tether were described as useful tools for electrochemical applications. The general basic formula 186 is reported below (Figure 60) [146].
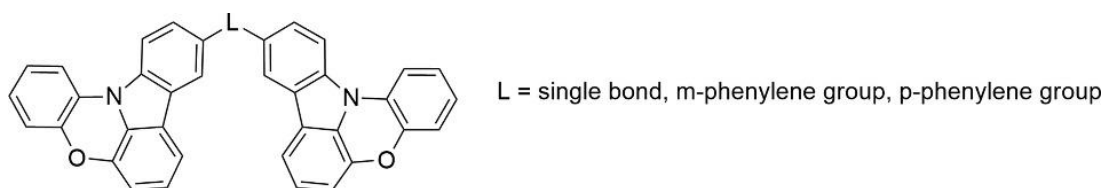

L = single bond, m-phenylene group, p-phenylene group

Figure 60. General structure 186.

The preparation of [1,4]oxazino[2,3,4-*jk*]carbazole-1,2-diones, the general formula **187** of which is reported below (Figure 61), starting from the corresponding 1-hydroxycarbazoles by action of oxalyl chloride was described in a paper dealing with the synthesis of substituted furo- and pyrano-carbazoles [147].
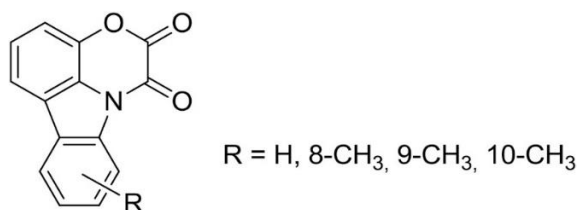

R = H, 8-CH$_3$, 9-CH$_3$, 10-CH$_3$

Figure 61. General structure 187.

Compounds based on a [1,4]oxazino[2,3,4-*hi*]indole core embedded into a tetracyclic system, analogously to previously described tetracyclic derivatives **103**, **106**–**109**, were reported as promising antiviral agents in two patents. Noteworthy, the derivative **188** (Figure 62) showed an EC$_{50}$ value of 0.01 in a HCV cell-based assay [148,149].
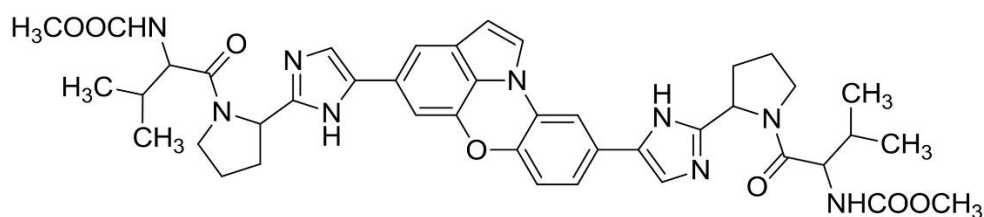
Figure 62. Structure of anti HCV agent 188.

Multifunctionalized derivatives of the title system, showing the general formula **189** and **190** (Figure 63), were obtained by a synthetic domino approach using MW irradiation [141]. A series of tricyclic indole derivatives were prepared and tested for activity on cell surface lipase using cells expressing human endothelial lipase. 5-Phenethyl-6-(trifluoromethyl)-2,3-dihydro-[1,4]oxazino[2,3,4-*hi*]indole (**191**), a derivative of the title system, showed IC$_{50}$ values of 0.039 and 0.031 μM on human and mouse cells, respectively [150]. These compounds could result useful during the treatment of metabolic disorders. In a recent study, C3-fluorinated oxindoles were synthesized through a reagent-free cross-dehydrogenative coupling. Among these compounds, methyl 6-fluoro-5-oxo-2,3,5,6-tetrahydro[1,4]oxazino[2,3,4-*hi*]indole-6-carboxylate (**192**), based on the tricyclic title system, was obtained in 72% yield (Figure 63) [151].
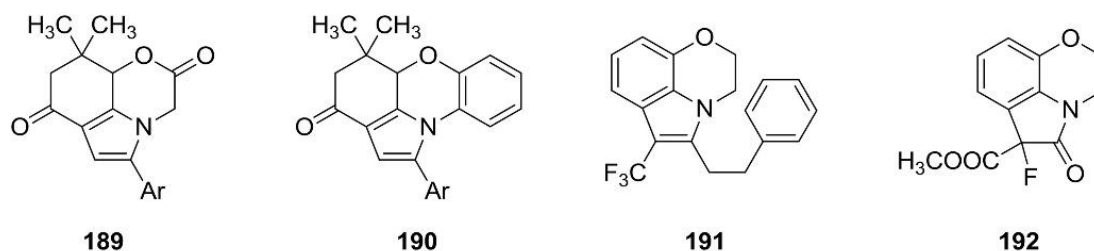
Ar = mono- or di-subsituted phenyl, 4-tolyl,
benzo[d][1,3]dioxol-6-yl.

Figure 63. General structures 189–192.

Very recently several patents from Asian researchers reported a number of polycyclic derivatives of [1,4]oxazino[2,3,4-*hi*]indole useful during various electrochemical applications [152-154].

7. *H*-Benzo[*d*]pyrrolo[2,1-b][1,3]oxazine H

The first example of a derivative of the tricyclic system, compound **193** (Figure 64), was described in a paper appeared in 1986. This compound was synthesized from *N*-acetylindoline in a multistep procedure [155].
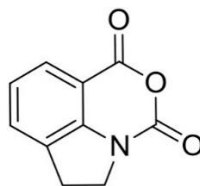
*Figure 64. Structure of 5,6-dihydro[1,3]oxazino[5,4,3-*hi*]indole-1,3-dione 193.*

The cyclization of 11*H*-benzo[*a*]carbazole-1,4-diol (**194**) with acetone was described to give rise to 5,5-dimethyl-5*H*-4-oxa-5a-azabenzo[*cd*]fluoranthen-1-ol (**195**), a pentacyclic derivative of the title system [156]. In a study focusing on cytotoxic compounds active in human lung cancer, treatment of carbinol **196** with methyl isocyanate gave the pentacyclic 7-methoxy-9-methyl-3-(methylamino)-1,3-dihydro-[1,3]oxazino [3,4,5-*lm*]pyrido [4,3-*b*]carbazol-3-ol (**197**), embedding the title tricyclic system (Figure 65) [157].
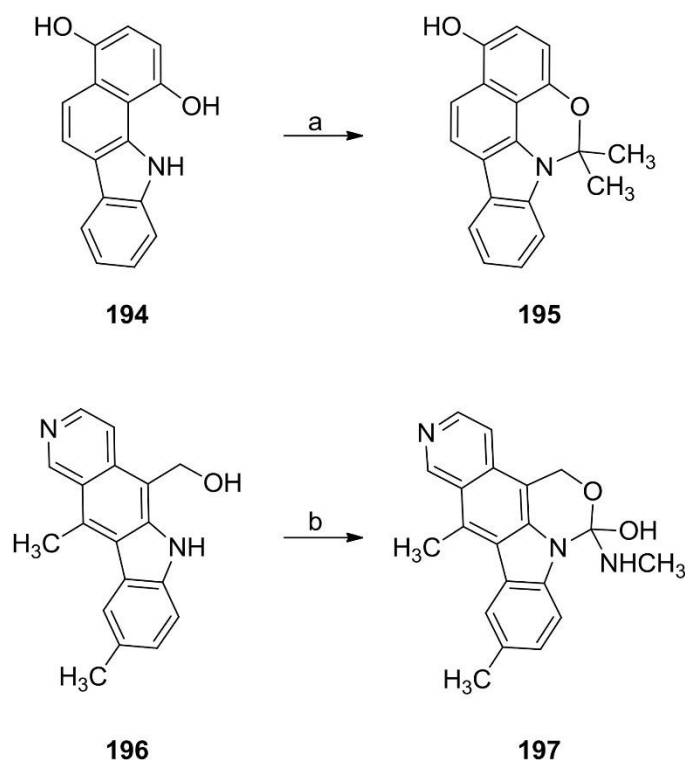
Figure 65. *Synthesis of compound **195** and **197**. Reagents and conditions:*
(a) acetone, tosyl chloride; (b) MeNCO.

Lithiation of *N*-Boc indoline (**198**) followed by reaction with a proper electrophile gave 1-ethyl-5,6-dihydro[1,3]oxazino[5,4,3-*hi*]indol-3(1*H*)-one (**199a**) or its *p*-methoxyphenyl analog **199b** [158]. In a paper dealing with the catalyst-free synthesis of 2-halo-3-carboxyidoles, 7-(2,2-dibromovinyl)indoline (**200**) gave the tricyclic (*Z*)-1-(bromomethylene)-5,6-dihydro-[1,3]oxazino[5,4,3-*hi*]indol-3(1*H*)-one (**201**), by action of cesium carbonate (Figure 66) [159].
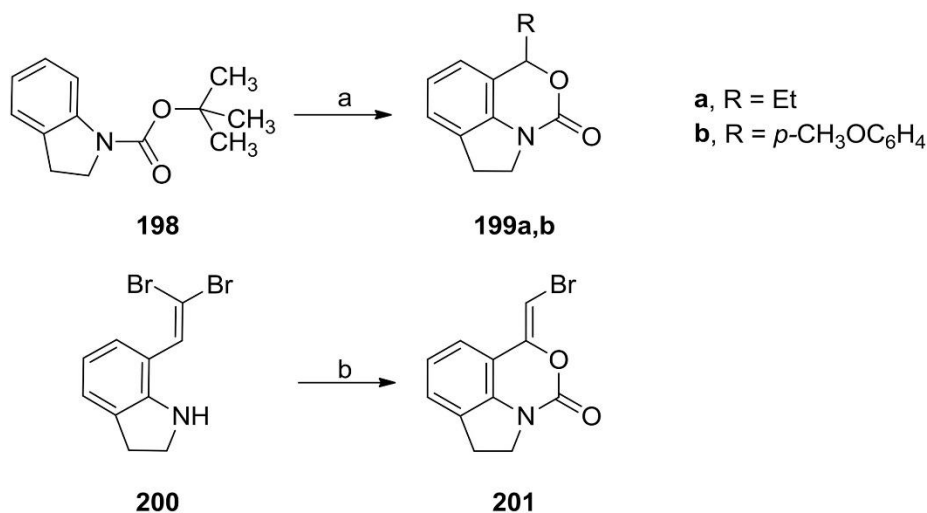
Figure 66. *Synthesis of compounds **199a,b** and **201**. Reagents and conditions: (a)* s-*BuLi-TMEDA, THF, −78 °C, then electrophile; (b) Cs$_2$CO$_3$, DMSO, sealed tube, 120 °C, then HCl workup.*

In a patent application, 6-(2-(phenylamino)ethyl)-[1,3]oxazino[5,4,3-*hi*]indol-3(1*H*)-one (**202**) (Fig. 67), and some of its substituted derivatives, were hydrolyzed to generate indole based compounds endowed with anticancer activity [160].
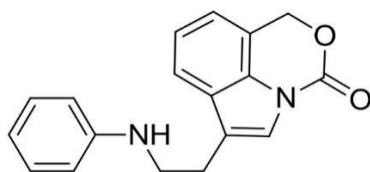
Figure 67. *Structure of compound **202**.*

8. Conclusion

Compounds deriving from all possible annulation of pyrrole to various benzoxazine systems, but keeping the bridgehead N atom, have been reviewed herein. Three out of the nine possible combinations are not yet been described in the literature. Among the six known classes, only two examples of naturally occurring derivatives have been so far reported: a dichotine derivative with anti-fatigue properties and a component of fruit used in formulation of traditional eastern medicinal remedies. On the other hand, several approaches have been carried out to the preparation of a large number of synthetic analogs. The majority of the synthetic work done have dealt with derivatives of system **C** and **G**, both derived from the 4*H*-benzo[*b*][1,4]oxazine bicyclic moiety, while only few reports focused on derivatives of system **H**. However, many suitable synthetic approaches initially conceived have been improved over the years. The interest of all these classes of compounds resides in their possible application in many research fields such as photochemistry, thermodynamics and drug discovery. Regarding this last point, pursued by the identification of biologically active derivatives, a wide range of properties were accordingly found, the most intriguing of which occur in the field of SNC, antiviral and anticancer agents. Effective SNC agents belong to all the six family described. In particular, serotonin receptors modulators, meriting further in-depth investigation towards the discovery of therapeutic useful agents, have been identified. Another class of active compounds derivaed from systems **D** and **G** showed a peculiar profile as CB receptors agonists, after the identification of (+)-**WIN55212**, **163**, a "**G**" derivative used as a reference for the evaluation of their activity. An almost homogeneous class of interesting derivatives of same systems **D** and **G**, showed a remarkable activity as HCV NS5B RNA polymerase inhibitors. For the majority of them, however, the polycyclic scaffolds seem to confer only a correct geometry for such molecules to approach the target, while the effective interactions should be due to the two highly functionalized symmetric side chains. The anticancer activity of several derivatives was attributable to specific interference with targets involved in cancer emergence and progression. In particular, remarkable activity was found for a number of compounds belonging to all above series with, however, distinct molecular targets. Compounds active with different mode of action have been identified and the most promising agents were shown to be active as kinases inhibitors with anti-proliferative effects.
Regarding antibacterial activity found for some benzopyrroloxazines, it should be noted that only early reports have dealt with these topics, and, in general, this research field was soon abandoned probably due to the impossibility of developing more powerful derivatives not susceptible to resistance onset. Finally, a research field initially showing a promising potential was the inhibition of enzymes such as cyclooxygenase, lipoxygenase and PAF involved in inflammatory pathologies.
Despite the initial promising results, researches in this field did not produce results worthy of further investigation.

Taking into consideration the collected data on all these derivatives, it could be deducted that an in-depth investigation of selected classes as well as an optimization of known agents could be desirable in order to identified drug candidates to be developed for clinical application.

References

[1] A.O. Fitton, M.P. Ward, 3,4-Dihydro-4-oxo-2H-1,3-benzoxazine carboxylic acids, Journal of the Chemical Society [Section] C: Organ 1 (1971) 146e149.

[2] H. Demuth, J. Breinholt, S.E. Nielsen, H. Gurtler, Active Bio-compounds Manufacture with Streptomyces, 1997 in WO 9723486 A1.

[3] J. Breinholt, H. Gurtler, A. Kjaer, S.E. Nielsen, C.E. Olsen, Streptopyrrole: an antimicrobial metabolite from Streptomyces armeniacus, Acta Chem. Scand. 52 (1998) 1040e1044.

[4] E. Olson, S.J. Trew, S.K. Wrigley, L. Pairet, M.A. Hayes, S. Martin, D.A. Kau, Microorganism Capable of Producing Compounds where Pyrrole Is Fused with 4-oxo-1,3-benzoxazine and Method of Use as Antibacterial and Antifungal, 1998 in WO 9825931 A1.

[5] J.M. Domagala, E.L. Ellsworth, M.A. Stier, L. Huang, R.G. Micetich, R. Singh, S.K. Wrigley, S. Wang, Preparation of Pyrrolo[2,1-b][1,3]benzoxazines as Antibacterial Agents, in US 1997022356, 1998.

[6] L.R. Huang, E.L. Ellsworth, S. Randhawa, M.A. Stier, Y.T. Huang, P. Bird, M. Lebedev, K. Wu, R.G. Micetich, J.M. Domagala, R. Singh, N.L. Colbry, Synthesis of the novel antibacterial 6,8-dihydroxy-7-propyl-9H-pyrrolo[1,2-b] [1,3]-benzoxazin-9-one, Tetrahedron Lett. 41 (2000) 4061e4064.

[7] S.J. Trew, S.K. Wrigley, L. Pairet, J. Sohal, P. Shanu-Wilson, M.A. Hayes, S.M. Martin, R.N. Manohar, M.I. Chicarelli-Robinson, D.A. Kau, C.V. Byrne, E.M.H. Wellington, J.M. Moloney, J. Howard, D. Hupe, E.R. Olson, Novel streptopyrroles from Streptomyces rimosus with bacterial protein histidine kinase inhibitory and antimicrobial activities, J. Antibiot. 53 (2000) 1e11.

[8] I. Szatmari, A. Hetenyi, L. Lazar, F. Fulop, Transformation reactions of the Betti base analog aminonaphthols, J. Heterocycl. Chem. 41 (2004) 367e373.

[9] V.A. Osyanin, Y.N. Klimochkin, Synthesis of the new heterocyclic system, indolo[2,1-b]benzoxazine, Chem. Heterocycl. Comp. 45 (2009) 833e836.

[10] E.V. Gromachevskaya, A.S. Pilipenko, A.V. Butin, V.E. Zavodnik, G.D. Krapivin, Investigations in the Field of Benzoxazines. 15. Tandem heterocyclizations with the participion of 2-formylbenzoic acid. the synthesis of isoindolo[1,2- b][1,3]- and [2,1-a][3,1]benzoxazinones, Chem. Heterocycl. Comp. 46 (2010) 106e116.

[11] Z.M. Xia, K. Wang, J.N. Zheng, Z.Y. Ma, Z.G. Jiang, X.X. Wang, X. Lv, Coppercatalyzed domino intramolecular cyclization: a facile and efficient approach to polycyclic indole derivatives, Org. Biomol. Chem. 10 (2012) 1602e1611.

[12] S. De, S. Ghosh, S. Bhunia, J.A. Sheikh, A. Bisai, Intramolecular direct dehydrohalide coupling promoted by (KOBu)-Bu-t: total synthesis of amaryllidaceae alkaloids anhydrolycorinone and oxoassoanine, Org. Lett. 14 (2012) 4466e4469.

[13] S. De, S. Mishra, B.N. Kakde, D. Dey, A. Bisai, Expeditious approach to pyrrolophenanthridones, phenanthridines, and benzo[c]phenanthridines via organocatalytic direct biaryl-coupling promoted by potassium tert-butoxide, J. Org. Chem. 78 (2013) 7823e7844.

[14] V.D. Yadav, S.U. Dighe, S. Batra, Synthesis of N-alkyl pyrroles via decarboxylation/ dehydration in neutral ionic liquid under catalyst-free conditions, RSC Adv. 4 (2014) 57587e57590.

[15] I. Kumashiro, The synthesis of the derivatives of pyrrolo[2,1-c][1,4]benzoxazine, Nippon O Kagaku Zasshi 82 (1961) 1072e1075.

[16] M. Artico, G.C. Porretta, G. De Martino, Synthesis of 4H-pyrrolo[2,1-c][1,4] benzoxazine, J. Heterocycl. Chem. 8 (1971) 283e287.

[17] G.W.H. Cheeseman, M. Rafiq, P.D. Roy, C.J. Turner, G.V. Boyd, Synthesis and reactions of pyrrolo[2,1-c][1,2,4]benzotriazine and 4-oxo-4H-pyrrolo[2,1-c][1,4]benzoxazine, Journal of the Chemical Society [Section] C: Organ 10 (1971) 2018e2022.

[18] I. Jirkovsky, L.G. Humber, R. Baudy, 4-Substituted 4H-pyrrolo[2,1-c][1,4]- benzoxazines, J. Heterocycl. Chem. 13 (1976) 311e316.

[19] I.L. Jirkovsky, L.G. Humber, Pyrrolobenzoxazines and Pyrrolobenzothiazines, 1977 in US 4035495 A1.

[20] H. Techer, M. Kryvenko, M. Pesson, 1,2,3,3a-Tetrahydro-4H-pyrrolo[2,1-c] [1,4]benzoxazine and derivatives, Comptes Rendus des Seances de l'Academie des Sciences, Serie C: Sciences Chimiques 274 (1972) 1081e1083.

[21] R. Giuliano, G.C. Porretta, M. Scalzo, S. Vomero, M. Artico, E. Dolfini, L. Morasca, Antiblastic substances. XLVII. Synthesis and cytostatic activity of 1-(2,5-dimethoxyphenyl)pyrrole derivatives, Farmaco, Edizione Scientifica 27 (1972) 908e917.

[22] G.J. Siuta, R.W. Franck, A.A. Ozorio, Meta-photo-Fries reaction, J. Chem. Soc., Chem. Commun. 21 (1974) 910.

[23] D.R. Crump, R.W. Franck, R. Gruska, A.A. Ozorio, M. Pagnotta, G.J. Siuta, J.G. White, Approaches to the mitomycins. A meta photo-Fries reaction, J. Org. Chem. 42 (1977) 105e108.

[24] N. Kawahara, T. Shimamori, T. Itoh, H. Ogura, Thermal reactions of o-aminophenols and dimethyl acetylenedicarboxylate, Heterocycles 24 (1986) 2803e2807.

[25] M.L.,M. Piltan, H. Rostami, One-pot synthesis of novel pyrrolo-1,4- benzoxazines via a three-component reaction of 2-amino phenols, acetylenic esters and nitrostyrene derivatives, Chin. Chem. Lett. 25 (2014) 123e126.

[26] B.L. Mylari, T.J. Carty, P.F. Moore, W.J. Zembrowski, 1,2-Dihydro-1- oxopyrrolo[3,2,1-kl]phenothiazine-2-carboxamides and congeners, dual Cyclooxygenase 5-Lipoxygenase inhibitors with antiinflammatory activity, J. Med. Chem. 33 (1990) 2019e2024.

[27] B.L. Mylari, J.M. McManus, J.G. Lombardino, Pyrroloquinoline- and Pyrrolophenothiazine, and Pyrrolophenoxazinecarboxamides as Inflammation Inhibitors, 1989 in EP 332364.

[28] M. Kato, S. Nishino, H. Takasugi, Pyrrolobenzoxazine Derivatives as 5-HT Agonists and Antagonists, 1993 in WO 9306108 A1.

[29] M. Kato, S. Nishino, K. Ito, H. Yamakuni, H. Takasugi, New 5-HT3 (serotonin- 3) receptor antagonists .5. Synthesis and structure-activity relationships of pyrrolo[2,1-c][1,4]benzoxazine-6-carboxamides, Chem. Pharm. Bull. 43 (1995) 1358e1363.

[30] A. Kuno, Y. Inoue, H. Takasugi, H. Mizuno, K. Yamasaki, Guanidine Derivatives as Inhibitors of Naþ/Hþ Exchange in Cells, 1994 in WO 9426709 A1.

[31] G. Campiani, A. Garofalo, I. Fiorini, M. Betta, V. Nacci, A. Tafi, A. Chiarini, R. Budriesi, G. Bruni, M.R. Romeo, Pyrrolo[2,1-c][1,4]benzothiazines - synthesis, structure-activity relationships, Molecular Modeling studies, and cardiovascular activity, J. Med. Chem. 38 (1995) 4393e4410.

[32] I. Sanchez, M.D. Pujol, A convenient synthesis of pyrrolo[2,1-c][1,4]benzoxazines, Tetrahedron 55 (1999) 5593e5598.

[33] Y. Harrak, G. Casula, J. Basset, G. Rosell, S. Plescia, D. Raffa, M.G. Cusimano, R. Pouplana, M.D. Pujol, Synthesis, anti-inflammatory activity, and *in vitro* antitumor effect of a novel class of cyclooxygenase inhibitors: 4-(aryloyl) phenyl methyl sulfones, J. Med. Chem. 53 (2010) 6560e6571.

[34] H. Ghafuri, A. Emami, M.G. Dekamin, Nano-ordered MCM-41-SO3H an efficient catalyst for the synthesis of N-substituted pyrroles in water, Sci. Iran. 23 (2016) 1102e1110.

[35] S. Raddatz, S. Bartel, W. Guarnieri, U. Rosentreter, M. Ruppelt, H. Wild, R. Endermann, H.P. Kroll, K. Henninger, Preparation of New Oxazolidinones with Azo-containing Tricycles as Antimicrobial Agents, in WO 9940094 A1, 1999.

[36] I.A. Tolmacheva, I.V. Mashevskaya, A.N. Maslivets, Recyclization of 3- heteroylpyrrolo[2.1-c][1.4]benzoxazine-1,2,4-triones at treatment with ophenylenediamine, Russ. J. Org. Chem. 37 (2001) 596e597.

[37] I.V. Mashevskaya, A.V. Duvalov, I.A. Tolmacheva, Z.G. Aliev, A.N. Maslivets, Five-membered 2,3-dioxo heterocycles: XLVIII. Reaction of 3-aroyl- and 3- heteroyl-2,4-dihydro-1H-pyrrolo[2,1-c][1,4]-benzoxazine-1,2,4-triones with 3-amino-5,5-dimethyl-2-cyclohexenone, Russ. J. Org. Chem. 40 (2004) 1359e1363.

[38] T.D. Semenova, O.P. Krasnykh, Chemistry of Acyl(imidoyl)ketenes: Part IX. Synthesis and thermolysis of 3-aroyl-8-chloro-1,2-dihydro-4Hpyrrolo[2,1-c] [1,4]benzoxazine-1,2,4-triones, Russ. J. Org. Chem. 41 (2005) 1222e1227.

[39] L.V. Kuslina, I.V. Mashevskaya, P.A. Slepukhin, A.N. Maslivets, New pathway of the reaction of hetareno[a]pyrrole-2,3-diones with NH nucleophiles, Russ. J. Org. Chem. 48 (2012) 145e146.

[40] J.I. Cadogan, C.M. Hewage, H. McNab, A.D. Macpherson, I.S. Nicolson, D. Reed, I.H. Sadler, Generation and contrasting gas-phase reactivity of 2-(2- alkenylpyrrol-1-yl)phenoxyl and thiophenoxyl radicals, Org. Biomol. Chem. 4 (2006) 2446e2451.

[41] H. Zhao, R. Kolluri, C. Valdez, K. Tso, R. Singh, J. Ramphal, 2,6-Bis(heterocyclylamino)pyrimidine Derivatives as Protein Kinase C Inhibitors, and Their Preparation and Use for the Treatment of Disorders Mediated or Sustained through a PKC Activity, in WO 2010083207 A2, 2010.

[42] S. Kurhade, R.D. Kaduskar, B. Dave, P.A. Ramaiah, V.P. Palle, D. Bhuniya, Synthesis of a novel tetracyclic azaindolo[2,1-c][1,4]benzoxazine ring system, Tetrahedron Lett. 52 (2011) 1874e1877.

[43] S. Kurhade, P.A. Ramaiah, P. Prathipati, D. Bhuniya, Unprecedented N -> C [1,4] Boc migration: synthesis of 3-carboxyl functionalized 7-azaindolo[2,1- c][1,4]benzoxazine ring system, Tetrahedron 69 (2013) 1354e1362.

[44] V.A. Vaillard, R.A. Rossi, S.E. Martin, Synthesis of pyrrole and indole quinoxalinone and oxazinone derivatives by intramolecular copper-catalyzed reactions, Org. Biomol. Chem. 9 (2011) 4927e4935.

[45] D.S. Snyder, L. Tradtrantip, C.J. Yao, M.J. Kurth, A.S. Verkman, Potent, metabolically stable benzopyrimido-pyrrolo-oxazine-dione (BPO) CFTR inhibitors for polycystic kidney disease, J. Med. Chem. 54 (2011) 5468e5477.

[46] A.S. Verkman, D.S. Snyder, Preparation of Pyrimidopyrrolo Derivatives as CFTR Inhibitors and Uses Therefor, in WO 2012166658 A1, 2012.

[47] S.S. Hadida-Ruah, E.A. Kallel, M.T. Miller, J. Pontillo, C. Anderson, M. Numa, E. al, Heterocyclic-fused spiro[chromene-piperidine] Derivatives and Related Compounds as Modulators of Ion Channels and Their Preparation and Use for the Treatment of Diseases, in WO 2011140425 A1, 2011.

[48] S.S. Hadida-Ruah, P.D.J. Grootenhuis, M.T. Miller, C. Anderson, J. Pontillo, E.A. Kallel, E. al, Preparation of spiro Benzoxazine Derivatives as Modulators of Ion Channels, in WO 2013067248 A1, 2013.

[49] S.M. Cramp, H.J. Dyke, T.D. Pallin, R. Zahler, Preparation of Tricyclic Pyrazole Sulfonamide Derivatives for Use as Methionyl Aminopeptidase 2Modulators, in WO 2012154679 A1, 2012.

[50] C. Bowen, S. Malcolm, L. Melnick, L. Xie, Preparation of Benzimidazolyl Substituted Pyrrole and Pyrazole Derivatives as Modulators of Opioid Receptors, in WO 2013070659 A1, 2013.

[51] M. Maggiolini, M.F. Santolla, S. Avino, F. Aiello, C. Rosano, A. Garofalo, F. Grande, Identification of two benzopyrroloxazines acting as selective GPER antagonists in breast cancer cells and cancer-associated fibroblasts, Future Medicinal Chemistry 7 (2015) 437e448.

[52] V.K. Mahesh, M. Maheswari, R. Sharma, R. Sharma, Analogs of cannabinoids - synthesis of some 7H-indolo[1,2-c][1,3]benzoxazine, 5H-imidazolo[1,2-c] [1,3]benzoxazine, 7H-benzimidazolo[1,2-c][1,3]benzoxazine novel ring-systems, Can. J. Chem. 63 (1985) 632e635.

[53] V.K. Mahesh, M. Maheshwari, R. Sharma, Compounds analogous to cannabinoids: synthesis of 7H-indolo[1,2-c][1,2]benzoxazine and 5H-imidazolo [1,2-c][1,3]benzoxazine systems, Chem. Ind. (Lond.) 5 (1980) 200.

[54] S.C. Sharma, M.P. Swami, R.C. Sharma, Nitrogen heterocyclic analogs of cannabinoids. Part I: synthesis of 6H-indolo[1,2-c][1,3]benzoxazine systems and evaluation of their biological activities, J. Indian Chem. Soc. 60 (1983) 1002e1004.

[55] J. Kurita, H. Sakai, S. Yamada, T. Tsuchiya, Novel thermal rearrangements of tetrahydro-azirinocyclobutabenzofuran derivatives, J. Chem. Soc., Chem. Commun. (1987) 285e286.

[56] N. Hucher, A. Daich, B. Decroix, Synthesis of isoindolo[1,3]benzoxazine derivatives through intramolecular arylation of N-acyliminium ions, J. Heterocycl. Chem. 35 (1998) 1477e1483.

[57] F. Pin, S. Comesse, B. Garrigues, S. Marchalin, A. Daich, Intermolecular and intramolecular alpha-amidoalkylation reactions using bismuth triflate as the catalyst, J. Org. Chem. 72 (2007) 1181e1191.

[58] K. Ikegashira, T. Oka, S. Hirashima, S. Noji, H. Yamanaka, Y. Hara, T. Adachi, J.I. Tsuruha, S. Doi, Y. Hase, T. Noguchi, I. Ando, N. Ogura, S. Ikeda, H. Hashimoto, Discovery of conformationally constrained tetracyclic compounds as potent hepatitis C virus NS5B RNA polymerase inhibitors, J. Med. Chem. 49 (2006) 6950e6953.

[59] S. Colarusso, J. Habermann, F. Narjes, S. Ponzi, R.F. M, Preparation of Thienopyrrolobenzodiazocinecarboxylates as Antiviral Agents, in WO 2006119975 A1, 2006.

[60] C.A. Coburn, J.A. McCauley, S.W. Ludmerer, K. Liu, J.P. Vacca, H. Wu, E. al, Preparation of L-prolinamide Derivatives as Inhibitors of Protein NS5A of Hepatitis C Virus, in WO 2010111483 A1, 2010.

[61] J.A. Kozlowski, S.B. Rosenblum, C.A. Coburn, B.B. Shankar, G.N. Anilkumar, L. Chen, E. al, Preparation of Tetracyclicindole Derivatives and Analogs for Use in Treatment of Hepatitis C Virus Infection, in WO 2012041014, 2012.

[62] J.A. Kozlowski, S.B. Rosenblum, C.A. Coburn, B.B. Shankar, G.N. Anilkumar, L. Chen, E. al, Preparation of Tetracyclic Indole Derivatives for Treatment of HCV Infection, in WO 2012040923 A1, 2012.

[63] J.P. Vacca, C.A. Coburn, D.B. Olsen, J.A. Kozlowski, S.B. Rosenblum, Polycyclic Heterocycle Derivatives and Methods of Use Thereof for the Treatment of Viral Diseases, in WO 2012050850 A1, 2012.

[64] V. Girijavallabhan, F.G. Njoroge, S. Bogen, V. Verma, F. Bennett, A. Kerekes, A. Arasappan, E. al, Preparation of 2'-substituted Nucleoside Derivatives and Methods of Use Thereof for the Treatment of Viral Diseases, in WO 2012142085 A1, 2012.

[65] V. Girijavallabhan, F.G. Njoroge, S. Bogen, F. Bennett, V. Verma, A. Arasappan, E. al, Preparation of 2'-substituted Nucleoside Derivatives and Methods of Use Thereof for the Treatment of Viral Diseases, in WO 2012142075 A1, 2012.

[66] L. Tong, W. Yu, J.A. Kozlowski, L. Chen, O. Selyutin, S.H. Kim, E. al, Thiophene- Substituted Tetracyclic Compounds and Methods of Use Thereof for the Treatment of Viral Diseases in WO2014110688 A1, 2014.

[67] L. Tong, W. Yu, J.A. Kozlowski, L. Chen, O. Selyutin, S.H. Kim, E. al, Thiophenesubstituted Tetracyclic Compounds and Methods of Use Thereof for Treatment
of Viral Diseases in WO 2014110706 A1, 2014.

[68] J.A. Kozlowski, W. Yu, Silane-containing Heterocyclic Compounds and Methods of Use Thereof for the Treatment of Viral Diseases in WO 2017112531 A1, 2017.

[69] I.K. Mangion, C.Y. Chen, H. Li, P. Maligres, Y. Chen, M. Christensen, R. Cohen, I. Jeon, A. Klapars, S. Krska, H. Nguyen, R.A. Reamer, B.D. Sherry, I. Zavialov, Enantioselective synthesis of an HCV NS5a antagonist, Org. Lett. 16 (2014) 2310e2313.

[70] C.A. Coburn, P.T. Meinke, W. Chang, C.M. Fandozzi, D.J. Graham, B. Hu, Q. Huang, S. Kargman, J. Kozlowski, R. Liu, J.A. McCauley, A.A. Nomeir, R.M. Soll, J.P. Vacca, D. Wang, H. Wu, B. Zhong, D.B. Olsen, S.W. Ludmerer, Discovery of MK-8742: an HCV NS5A inhibitor with broad genotype activity, ChemMedChem 8 (2013) 1930e1940.

[71] M.P. Dwyer, K.M. Keertikar, L. Chen, L. Tong, O. Selyutin, A.G. Nair, W. Yu, G. Zhou, B.J. Lavey, D.Y. Yang, M. Wong, S.H. Kim, C.A. Coburn, S.B. Rosenblum, Q. Zeng, Y. Jiang, B.B.

Shankar, R. Rizvi, A.A. Nomeir, R. Liu, S. Agrawal, E. Xia, R. Kong, Y. Zhai, P. Ingravallo, E. Asante-Appiah, J.A. Kozlowski, Matched and mixed cap derivatives in the tetracyclic indole class of HCV NS5A inhibitors, Bioorg. Med. Chem. Lett 26 (2016) 4106e4111.

[72] L. Tong, W. Yu, C.A. Coburn, L. Chen, O. Selyutin, Q. Zeng, M.P. Dwyer, A.G. Nair, B.B. Shankar, S.H. Kim, D.Y. Yang, S.B. Rosenblum, R.T. Ruck, I.W. Davies, B. Hu, B. Zhong, J. Hao, T. Ji, S. Zan, R. Liu, S. Agrawal, D. Carr, S. Curry, P. McMonagle, K. Bystol, F. Lahser, P. Ingravallo, S. Chen, E. Asante- Appiah, J.A. Kozlowski, Structure-activity relationships of proline modifications around the tetracyclic-indole class of NS5A inhibitors, Bioorg. Med. Chem. Lett 26 (2016) 5354e5360.

[73] W. Yu, G. Zhou, C.A. Coburn, Q. Zeng, L. Tong, M.P. Dwyer, B. Hu, B. Zhong, J. Hao, T. Ji, S. Zan, L. Chen, R. Mazzola, J.H. Kim, D. Sha, O. Selyutin, S.B. Rosenblum, B. Lavey, A.G. Nair, S. Heon Kim, K.M. Keertikar, L. Rokosz S. Agrawal, R. Liu, E. Xia, Y. Zhai, S. Curry, P. McMonagle, P. Ingravallo, E. Asante-Appiah, S. Chen, J.A. Kozlowski, Substituted tetracyclic indole core derivatives of HCV NS5A inhibitor MK-8742, Bioorg. Med. Chem. Lett 26 (2016) 4851e4856.

[74] W. Yu, B. Vibulbhan, S.B. Rosenblum, G.S. Martin, A.S. Vellekoop, C.L. Holst, C.A. Coburn, M. Wong, O. Selyutin, T. Ji, B. Zhong, B. Hu, L. Chen, M.P. Dwyer, Y. Jiang, A.G. Nair, L. Tong, Q. Zeng, S. Agrawal, D. Carr, L. Rokosz, R. Liu, S. Curry, P. McMonagle, P. Ingravallo, F. Lahser, E. Asante-Appiah, J. Fells, J.A. Kozlowski, Discovery of potent macrocyclic HCV NS5A inhibitors, Bioorg. Med. Chem. Lett 26 (2016) 3793e3799.

[75] W. Yu, L. Tong, B. Hu, B. Zhong, J. Hao, T. Ji, S. Zan, C.A. Coburn, O. Selyutin, L. Chen, L. Rokosz, S. Agrawal, R. Liu, S. Curry, P. McMonagle, P. Ingravallo, E. Asante-Appiah, S. Chen, J.A. Kozlowski, Discovery of chromane containing Hepatitis C Virus (HCV) NS5A inhibitors with improved potency against resistance-associated variants, J. Med. Chem. 59 (2016) 10228e10243.

[76] L. Tong, W. Yu, L. Chen, O. Selyutin, M.P. Dwyer, A.G. Nair, R. Mazzola, J.H. Kim, D. Sha, J. Yin, R.T. Ruck, I.W. Davies, B. Hu, B. Zhong, J. Hao, T. Ji, S. Zan, R. Liu, S. Agrawal, E. Xia, S. Curry, P. McMonagle, K. Bystol, F. Lahser, D. Carr, L. Rokosz, P. Ingravallo, S. Chen, K.I. Feng, M. Cartwright, E. Asante- Appiah, J.A. Kozlowski, Discovery of Ruzasvir (MK-8408): a potent, pangenotype HCV NS5A inhibitor with optimized activity against common resistance-associated polymorphisms, J. Med. Chem. 60 (2017) 290e306.

[77] C.C. McComas, N.J. Liverton, R.M. Soll, P. Li, X. Peng, H. Wu, E. al, Preparation of Substituted 2-phenylbenzofurancarboxamides as Inhibitors of Hepatitis C Virus NS5B Polymerase, in WO 2011106992 A1, 2011.

[78] C.C. McComas, N.J. Liverton, J. Habermann, U. Koch, F. Narjes, P. Li, E. al, Preparation of Tetracyclic Heterocycle Compounds for the Treatment of HCV Infection, in WO 2013033900 A1, 2013.

[79] C.C. McComas, N.J. Liverton, J. Habermann, U. Koch, F. Narjes, P. Li, E. al, Preparation of Pyridooxazinoindole Derivatives and Analogs for Use as Antiviral Agents, in WO 2013033971 A1, 2013.

[80] E. Conchon, F. Anizon, B. Aboab, R.M. Golsteyn, S. Leonce, B. Pfeiffer, M. Prudhomme, Synthesis, checkpoint kinase 1 inhibitory properties and *in vitro* antiproliferative activities of new pyrrolocarbazoles, Bioorg. Med. Chem. 16 (2008) 4419e4430.

[81] E. Hope, R.W.R. Kersey, D. Richter, Benzoyl derivatives of indigotin, Journal of the Chemical Society [Section] C: Organ (1933) 1000e1003.

[82] H. Diesbach, E. Heppner, I. Siegwart, Benzoyl derivatives of indigo. VIII, Helv. Chim. Acta 31 (1948) 724e735.

[83] V. Pestellini, M. Ghelardoni, C. Bianchini, A. Liquori, Fused ring compounds derived from phtalaldehydic acid, Boll. Chim. Farm. 117 (1978) 54e60.

[84] R.W. Franck, J. Auerbach, Singlet oxygen oxidation of N-phenylpyrroles. Its application to the synthesis of a model mitomycin, J. Org. Chem. 36 (1971) 31e36.

[85] F.Z. Basha, R.W. Franck, Approaches to the mitomycins: a novel pyrrole photooxidation product, J. Org. Chem. 43 (1978) 3415e3417.

[86] I. Butula, G. Bacic, R. Arneri, M. Lacan, Synthesis and hydrogenolysis of 6asubstituted 6a,11-dihydro-5H-isoindolo[2,1-a][3,1]benzoxazine-5,11-diones and related compounds, Croat. Chem. Acta 48 (1976) 53e58.

[87] E. Tighineanu, F. Chiraleu, D. Raileanu, New stable mesoionic oxazolones by the double cyclization of phenylglycine-o-carboxylic acid, Tetrahedron Lett. (1978) 1887e1890.

[88] E. Tighineanu, F. Chiraleu, D. Raileanu, Double cyclization of phenylglycineo- carboxylic acids. I. New stable mesoionic oxazolones, Tetrahedron Lett. 36 (1980) 1385e1397.

[89] I. Ciocazanu, E. Tighineanu, Thermodynamic study of some substituted derivatives of pyrrolobenzoxazinone, Calorim. Anal. Therm. 27 (1996) 122e126.

[90] E. Tighineanu, D. Raileanu, Double cyclization of phenylglycine-o-carboxylic acids .2. Michael-type adducts of mesoionic oxazolones, Rev. Roum. Chem. 37 (1992) 1307e1314.

[91] E. Tighineanu, D. Raileanu, Y. Simonov, P. Bouros, 5H-Pyrrolo[1,2-a][3,1] benzoxazin-5-ones - reconsideration of the double cyclisation of o-carboxyphenylglycine, Tetrahedron 52 (1996) 12475e12482.

[92] A.W. Erian, Y.A.E. Issac, M.S.A. Sherif, F.F. Mahmoud, Heterocyclic sulfones. Part IV. A novel synthesis of pyrrole and fused heterocyclic sulfones, J Chem Soc Perk T 1 (2000) 3686e3691.

[93] F.F. Mahmoud, N.R. Mohamed, S.M. Sherif, A.W. Erian, Heterocyclic sulfones IV: a novel synthesis of pyrrole and fused heterocyclic sulfones, Phosphorus Sulfur 167 (2000) 133e149.

[94] S.M. Batterjee, A novel synthesis of fused heterocyclic sulfones, J Chin Chem Soc-Taip 52 (2005) 97e102.

[95] Y.M. Elkholy, Studies with phenylsulfone derivatives: synthesis of pyrrole, thiophene and their fused derivatives, J. Heterocycl. Chem. 45 (2008) 1237e1241.

[96] Y.M. Elkholy, Studies with phenylsulfone derivatives: synthesis of pyrrole, thiophene and their fused derivatives, Trends Heterocycl. Chem. 12 (2007) 75e82.

[97] P. Pigeon, J. Sikoraiova, S. Marchalin, B. Decroix, Intramolecular addition of a hydroxyl to a N-acyliminium system. Application to the synthesis of isoindolo[2,1-a][3,1]benzoxazine and isoindolo[1,2-c][2,4] benzoxazepine derivatives, Heterocycles 56 (2002) 129e138.

[98] J.W. Huang, C.H. Tan, S.H. Jiang, D.Y. Zhu, Terresoxazine, A novel compound with benzoxazine skeleton from Tribulus terrestris, Chin. Chem. Lett. 15 (2004) 305e306.

[99] Z.-D. Yang, T. Li, C. Peng, Isolation and identification of chemical constituents in Hemerocallis fulva (II), Chin. Tradit. Herb. Drugs 39 (2008) 1288e1290.

[100] J. Correa-Basurto, J. Espinosa-Raya, M. Gonzalez-May, L.M. Espinoza-Fonseca, I. Vazquez-Alcantara, J. Trujillo-Ferrara, Inhibition of acetylcholinesterase by two arylderivatives: 3a-Acetoxy-5H-pyrrolo (1,2-a) (3, 1)benzoxazin- 1,5- (3aH)-dione and cis-N-p-Acetoxy-phenylisomaleimide, J. Enzym. Inhib. Med. Chem. 21 (2006) 133e138.

[101] T. Lubbers, P. Angehrn, H. Gmunder, S. Herzig, Design, synthesis, and structure-activity relationship studies of new phenolic DNA gyrase inhibitors, Bioorg. Med. Chem. Lett 17 (2007) 4708e4714.

[102] E.V. Gromachevskaya, A.V. Butin, A.S. Pilipenko, G.V. Krapivin, A.A. Borodavko, L.I. Isaeva, V.D. Strelkov, Preparation of Substituted 6a,11- dihydro-5H-benzo[4,5][1,3]oxazino[2,3-a]isoindol-11-ones as Herbicide Antidotes for the Hormonal Action of 2,4-dichlorophenoxyacetic Acid and Process for Their Preparation, in RU 2345083 C1, 2009.

[103] M. Badolato, G. Carullo, B. Armentano, S. Panza, R. Malivindi, F. Aiello, Synthesis and anti-proliferative activity of a small library of 7-substituted 5Hpyrrole [1,2-a][3,1]benzoxazin-5-one derivatives, Bioorg. Med. Chem. Lett 27 (2017) 3092e3095.

[104] P. Rajagopalan, Pyridopyrrolobenzoxazine, in US 4013652 A, 1977.

[105] D. Bigg, J. Menin, C. Maloizel, J.P. Merly, Pyrrolo[1,2,3-de][1,4]benzoxazines, in FR 2567126 A1, 1986.

[106] K. Masahumi, O. Naohito, Substituted Guanidine Derivatives, Process for Production Thereof, and Pharmaceutical Uses Thereof in US5834454 a, 1998.

[107] J. Adam-Worrall, Preparation of Tricyclic 1-[(3-indol-3-yl)carbonyl]piperazine Derivatives as Cannabinoid CB1 Receptor Agonists, in WO 2005058327

[108] J. Adam-Worrall, A.J. Morrison, G. Wishart, T. Kiyoi, D.R. McArthur, Preparation of (Indol-3-yl)-heterocycle Derivatives as Agonists of the Cannabinoid CB1 Receptor, in WO 2005089754 A1, 2005.

[109] T. Kiyoi, M. York, S. Francis, D. Edwards, G. Walker, A.K. Houghton, J.E. Cottney, J. Baker, J.M. Adam, Design, synthesis, and structure-activity relationship study of conformationally constrained analogs of indole-3- carboxamides as novel CB1 cannabinoid receptor agonists, Bioorg. Med. Chem. Lett 20 (2010) 4918e4921.

[110] J.P. Burke, Z. Bian, S. Shaw, B. Zhao, C.M. Goodwin, J. Belmar, C.F. Browning, D. Vigil, A. Friberg, D.V. Camper, O.W. Rossanese, T. Lee, E.T. Olejniczak, S.W. Fesik, Discovery of tricyclic indoles that potently inhibit Mcl-1 using fragment-based methods and structure-based design, J. Med. Chem. 58 (2015) 3794e3805.

[111] K. Masuzawa, K. Okamura, S. Fujimori, S. Kinoshita, H. Matsukubo, Improved Preparation of Spiropyrrolidinepyrrolobenzoxazinetriones Useful as Aldose Reductase Inhibitors, in EP 254149 A2, 1988.

[112] D.E. Bays, I.H. Coates, A.W. Oxford, P.C. North, Preparation and Formulation of (Imidazolylmethyl)pyridopyrroloquinolinones and Analogs as Serotonin Antagonists, in EP 357417 A1, 1990.

[113] T.E. D'Ambra, M.R. Bell, Preparation of 2- and 3-aminomethyl-6- arylcarbonyl-2,3-dihydropyrrolo[1,2,3-de]-1,4-benzoxazines as analgesics, in US 4939138 A, 1990.

[114] D. Jasserand, D. Paris, P. Demonchaux, M. Cottin, F. Floc'h, P. Dupassieux, R. White, Preparation of Annellated a-(piperazinylakyl)indoles and Related Compounds as Drugs, in DE 4128015 A1, 1993.

[115] P. Demonchaux, P. Lenoir, G. Augert, P. Dupassieux, Design of pyrrolo-1,4- benzoxazine derivatives as inhibitors of 5-Lipoxygenase and Paf antagonists with antihistaminic properties, Bioorg. Med. Chem. Lett 4 (1994) 2383e2388.

[116] P. Demonchaux, P. Lenoir, Preparation of 5-phenylpyrrolo[1,2,3-de][1,4] benzoxazine and -thiazine derivatives as antiinflammatories and allergy inhibitors, in DE 4304806 A1, 1994.

[117] L.C. Sequeira, A.L. Pereira, A.C. Pinto, Synthesis of new tetracyclic derivatives of 10H-phenoxazine, 10,11-dihydro-5H-dibenzo[b,f]azepine, and (9)10Hacridinone through isatinic intermediates, J. Braz. Chem. Soc. 4 (1993) 34e39.

[118] R.A. Earl, M.J. Myers, Preparation of 3,3-disubstituted Tri- and Tetracyclic Indolin-2-ones Useful for the Treatment of Cognitive Disorders, in WO 9409009 A1, 1994.

[119] M. Kitano, N. Ohashi, Preparation of Pyrroloquinolinecarbonyl- and Azepinoindolecarbonyl-Substituted Guanidines as Inhibitors of Sodium/ Proton Exchange Transport System, in EP 787728 A1, 1997.

[120] A.K. Dutta, W. Ryan, B.F. Thomas, M. Singer, D.R. Compton, B.R. Martin, R.K. Razdan, Synthesis, pharmacology, and molecular modeling of novel 4- alkyloxy indole derivatives related to cannabimimetic aminoalkyl indoles (AAIs), Bioorg. Med. Chem. 5 (1997) 1591e1600.

[121] D.R. Compton, L.H. Gold, S.J. Ward, R.L. Balster, B.R. Martin, Aminoalkylindole analogs: cannabimimetic activity of a class of compounds structurally distinct from delta 9-tetrahydrocannabinol, J. Pharmacol. Exp. Therapeut. 263 (1992) 1118e1126.

[122] B.R. Martin, D.R. Compton, B.F. Thomas, W.R. Prescott, P.J. Little, R.K. Razdan, M.R. Johnson, L.S. Melvin, R. Mechoulam, S.J. Ward, Behavioral, biochemical, and molecular modeling evaluations of cannabinoid analogs, Pharmacol. Biochem. Behav. 40 (1991) 471e478.
[123] R.J. Seguin, C.N. Filer, Synthesis and characterization of the potent cannabinoid agonist [naphthyl-H-3] WIN 55212-2 at high specific activity, J. Labelled Comp. Rad. 46 (2003) 67e71.

[124] E.M. Moir, K. Yoshiizumi, J. Cairns, P. Cowley, M. Ferguson, F. Jeremiah, T. Kiyoi, R. Morphy, J. Tierney, G. Wishart, M. York, J. Baker, J.E. Cottney, A.K. Houghton, P. McPhail, A. Osprey, G. Walker, J.M. Adam, Design, synthesis, and structure-activity relationship study of bicyclic piperazine analogs of indole-3-carboxamides as novel cannabinoid CB1 receptor agonists, Bioorg. Med. Chem. Lett 20 (2010) 7327e7330.

[125] S. Jegham, A. Lochead, A. Nedelec, A. Solignac, Preparation of 5-(2,3-dihydro- 1,4-benzoxazin-5-yl)-3-(piperidin-4-yl)-1,3,4-oxadiazol-2(3H)-one Derivatives and Their Therapeutic Application as 5-HT4 Agonists or Antagonists, in FR 2759699 A1, 1998.

[126] P. Bird, E.L. Ellsworth, D.Q. Nguyen, J.P. Sanchez, H.D.H. Showalter, R. Singh, M.A. Stier, Preparation of 3-aminoquinazoline-2,4-dione Antibacterial Agents, in WO 2001053273 A1, 2001.

[127] F. Touzeau, A. Arrault, G. Guillaumet, E. Scalbert, B. Pfeiffer, M.C. Rettori, P. Renard, J.Y. Merour, Synthesis and biological evaluation of new 2-(4,5- dihydro-1H-imidazol-2-yl)-3,4-dihydro-2H-1,4-benzoxazine derivatives, J. Med. Chem. 46 (2003) 1962e1979.

[128] S. Mayer, A. Arrault, G. Guillaumet, J.Y. Merour, Attempted synthesis of ethyl 3,4-dihydro-2H-1,4-benzoxazine-3-carboxylate and 3-acetate derivatives, J. Heterocycl. Chem. 38 (2001) 221e225.

[129] G. Guillaumet, J.Y. Merour, F. Touzeau, B. Pfeiffer, P. Renard, E. Scalbert, Preparation of Imidazolinylbenzoxazines and Analogs as Imidazoline Receptor Ligands, in EP 894796 A1, 1999.

[130] J.B.J. Hester, B.N. Rogers, E.J. Jacobsen, M.D. Ennis, B.A. Acker, V.V. S. L, Preparation of Tetracyclic Azepinoindoles as 5-HT Receptor Ligands, in WO 2000064899 A1, 2000.

[131] J.B.J. Hester, B.N. Rogers, E.J. Jacobsen, M.D. Ennis, B.A. Acker, S.L. Vander Velde, K.E. Frank, Preparation of Tetracyclic Azepinoindoles as 5-HT Receptor Ligands for Treatment of CNS Disorders, in US 6407092 B1, 2002.

[132] S. Chakravarty, B.P. Hart, R.P. Jain, Fused Tetracyclic Pyrido[4,3-b]indole and Pyrido[3,4-b]indole Derivatives as Histamine Receptor Modulators and Their Preparation and Use in the Treatment of Diseases, in US 6407092 B1, 2011.

[133] R.E. TenBrink, Oxazinocarbazoles for the Treatment of CNS Diseases in US 6821970 B2, 2004.

[134] R.E. TenBrink, Preparation of Oxazinocarbazoles as 5-HT6 Serotonin Receptor modulators., in WO 2001009142 A1, 2001.

[135] S.H. Zhao, Preparation of Aminoalkoxyindoles as 5-HT6-receptor Ligands, in Particular Selective 5-HT6 Antagonists, for Treating CNS Disorders, in WO 2010083207 A2, 2004.

[136] T. Lee, A.J. Robichaud, K.E. Boyle, Y.M. Lu, D.W. Robertson, K.J. Miller, L.W. Fitzgerald, J.F. McElroy, B.L. Largent, Novel, highly potent, selective 5- HT2A/D-2 receptor antagonists as potential atypical antipsychotics, Bioorg. Med. Chem. Lett 13 (2003) 767e770.

[137] V. Arredondo, S.C. Hiew, E.S. Gutman, I.D.U.A. Premachandra, D.L. Van Vranken, Enantioselective palladium-catalyzed carbene insertion into the NH bonds of aromatic heterocycles, Angew. Chem. Int. Ed. 56 (2017) 4156e4159.

[138] A.E. Shchekotikhin, V.N. Buyanov, M.N. Preobrazhenskaya, Synthesis of 1- (omega-aminoalkyl)naphthoindolediones with antiproliferative properties, Bioorg. Med. Chem. 12 (2004) 3923e3930.

[139] J.M. Fu, Preparation of Tetrahydrooxazinoindolylmethanamines and Analogs as Therapeutic 5-HT Ligand Compounds, in WO 2003024976 A2, 2003.

[140] K. Mizuno, M. Sawa, H. Harada, I. Taoka, H. Yamashita, M. Oue, H. Tsujiuchi, Y. Arai, S. Suzuki, Y. Furutani, S. Kato, Discovery of 1,7-cyclized indoles as a new class of potent and highly selective human beta3-adrenergic receptor agonists with high cell permeability, Bioorg. Med. Chem. 13 (2005) 855e868.

[141] B. Jiang, Q.Y. Li, H. Zhang, S.J. Tu, S. Pindi, G.G. Li, Efficient domino approaches to multifunctionalized fused pyrroles and dibenzo[b,e][1,4]diazepin-1-ones, Org. Lett. 14 (2012) 700e703.

[142] K.S. Yeung, J.F. Kadow, Preparation of (1,4-oxazino[2,3,4-hi]indol-9-yl)carboxamides and Similar Compounds as HCV NS5B Inhibitors, in US 20080221090 A1, 2008.

[143] N.C. Ling, C. Djerassi, P.G. Simpson Alkaloid Studies. LXII.' X-Ray crystallographic structure determination of dichotine hydrobromide, J Amer. Chem soc 92 (1970) 222e223.

[144] L.Z. Huang, B.K. Huang, J. Liang, C.J. Zheng, T. Han, Q.Y. Zhang, L.P. Qin, Antifatigue activity of the liposoluble fraction from Acanthopanax senticosus, Phytother Res. 25 (2011) 940e943.

[145] T.U. Nwabueze, A.G. Emenonye, Processing Effect on the physicochemical and volatile fatty acid profile of african breadfruit (treculia africana) seed oil, Food Nutr. Sci. 7 (2016) 627e635.

[146] T. Kosuge, J. Kamatani, S. Abe, K. Kishino, Indolophenoxazine Compounds for Organic Light Emitting Devices, in WO 2012077582 A1, 2012.

[147] K. Prabakaran, K.J.R. Prasad, Facile synthesis of substituted furo- and pyranocarbazoles, Synth. Commun. 42 (2012) 2966e2980.

[148] C.A. Coburn, S.B. Rosenblum, J.A. Kozlowski, R. Soll, H. Wu, B. Hu, E. al, Preparation of Tetracyclic xanthene Amino Acid Derivatives for Treatment of Viral Diseases, in WO 2012125926 A2, 2012.

[149] C.A. Coburn, S.B. Rosenblum, J.A. Kozlowski, R. Soll, H. Wu, B. Hu, E. al, Preparation of Tetracyclic Xanthene Amino Acid Derivatives for Treatment of Viral Diseases, in WO2012006055A2, 2012.

[150] M.A. Connelly, M. Greco, H. Ye, Preparation of Tricyclic Indole Derivatives Useful as Endothelial Lipase Inhibitors, in US 20130210806 A1, 2013.

[151] Z.J. Wu, H.C. Xu, Synthesis of C3-Fluorinated Oxindoles through reagent-free cross-dehydrogenative coupling, Angew. Chem. Int. Ed. 56 (2017) 4734e4738.

[152] A. Hayer, D. Joosten, H. Heil, R.M. Anemian, C. De Nonancourt, Polycyclic Phenylpyridine Iridium Complexes and Derivatives Thereof for Oleds in WO2015039723 A1, 2015.

[153] T. Kosuge, J. Kamatani, S. Abe, K. Kishino, Indolophenoxazine Compound and Organic Light Emitting Device Using the Same in US 9515270 B2, 2016.

[154] J. Xu, S. Mo, Isoindolinone Formamide Skeleton-containing boron Bifluoride Complex and Preparing Method Thereof in CN105566369 a, 2016.

[155] G.M. Coppola, S. Palermo, Novel heterocycles .13. Synthesis of 5,6-dihydro- 1H-3H-pyrrolo[3,2,1-ij][3,1]benzoxazine-1,3-dione, J. Heterocycl. Chem. 23 (1986) 971e972.

[156] S.C. Sharma, Nitrogen heterocyclic analogs of cannabinoids. Part III. Synthesis of 10a-11-etheno-6H-indolo[1,2-c][1,3]benzoxazine system and studies of antibacterial, antifungal, and toxicological activities, Orient. J. Chem. 2 (1986) 58e61.

[157] S.P. Modi, T. Mccomb, A. Zayed, R.C. Oglesby, S. Archer, Synthesis of 6Hpyrido[4,3-b]carbazoles, Tetrahedron 46 (1990) 5555e5562.

[158] M. Iwao, T. Kuraishi, Directed Lithiation of 1-(tert-butoxycarbonyl)indolines - a convenient route to 7-substituted indolines, Heterocycles 34 (1992) 1031e1038.

[159] A.R. Kunzer, M.D. Wendt, Rapid, robust, clean, catalyst-free synthesis of 2- halo-3-carboxyindoles, Tetrahedron Lett. 52 (2011) 1815e1818.

[160] B. Schoentjes, S. Descamps, N.C.I. Amblard, Preparation of Indole Derivatives as Anticancer Agents, in WO 2010089327 A2, 2010.

CONCLUSIONS

Although remarkable progress has been made during the past decade in almost all the areas concerning drug design and discovery, there is still a clear need to develop new effective drugs for the treatment of several diseases. In this contest, the doctoral course in "Translational Medicine" characterized by a multidisciplinary approach aims to the design of novel drugs or innovative therapeutic approaches useful for diagnostic and clinical applications.

During the three years PhD course, the main topics of my research work have been:

- application of advanced computational techniques toward the identification of new drugs;
- study of compounds both of natural or synthetic origin as drug candidates;
- design and synthesis of NSAIDs analogs and dihydropiridines derivatives;
- photodegradation studies and development of innovative photoprotective delivery systems for topical use of drugs.

Computational studies focused on the capability of different series of compounds of natural origin such as homoisoflavones, flavones and tanshinones derivatives to bind the active site of macromolecules involved in different diseases including cancer and metabolic disorders. The interactions mode of newly synthesized compounds with the active site of enzymes involved in cancer emergence and development or cardiovascular pathologies were investigated as well.

The availability of crystallographic structures of different target proteins involved in various diseases as well as the results of previously published papers spurred the design and the synthesis of several compounds as potential ligands.

Some of the synthesized compounds showed sensitivity to light, thus, their photodegradation profile was investigated under different conditions, according to the international rules.

In particular, the attention was focused on both newly synthesized compounds and known drugs endowed with anti-inflammatory activity or potentially usable in neuropathic pain, formulated in solution or in gel and included into supramolecular systems such as cyclodextrin matrices or pluronic surfactants.

Furthermore, in order to discover novel lead compounds and better understand the mechanism of action of new drugs or the responses of macromolecule targets to ligand interactions, different series of compounds reported in literature have been explored.